



HAL
open science

Methodological development in FT-ICR MS for the analysis of bio-oils produced by pyrolysis of lignocellulosic biomass

Anthony Abou Dib

► **To cite this version:**

Anthony Abou Dib. Methodological development in FT-ICR MS for the analysis of bio-oils produced by pyrolysis of lignocellulosic biomass. Analytical chemistry. Université de Lorraine, 2023. English. NNT: 2023LORR0060 . tel-04411478

HAL Id: tel-04411478

<https://theses.hal.science/tel-04411478v1>

Submitted on 23 Jan 2024

HAL is a multi-disciplinary open access archive for the deposit and dissemination of scientific research documents, whether they are published or not. The documents may come from teaching and research institutions in France or abroad, or from public or private research centers.

L'archive ouverte pluridisciplinaire **HAL**, est destinée au dépôt et à la diffusion de documents scientifiques de niveau recherche, publiés ou non, émanant des établissements d'enseignement et de recherche français ou étrangers, des laboratoires publics ou privés.



**UNIVERSITÉ
DE LORRAINE**

**BIBLIOTHÈQUES
UNIVERSITAIRES**

AVERTISSEMENT

Ce document est le fruit d'un long travail approuvé par le jury de soutenance et mis à disposition de l'ensemble de la communauté universitaire élargie.

Il est soumis à la propriété intellectuelle de l'auteur. Ceci implique une obligation de citation et de référencement lors de l'utilisation de ce document.

D'autre part, toute contrefaçon, plagiat, reproduction illicite encourt une poursuite pénale.

Contact bibliothèque : ddoc-theses-contact@univ-lorraine.fr
(Cette adresse ne permet pas de contacter les auteurs)

LIENS

Code de la Propriété Intellectuelle. articles L 122. 4

Code de la Propriété Intellectuelle. articles L 335.2- L 335.10

http://www.cfcopies.com/V2/leg/leg_droi.php

<http://www.culture.gouv.fr/culture/infos-pratiques/droits/protection.htm>

PhD Thesis

Presented and defended publicly for obtaining the title of

DOCTOR OF THE UNIVERSITY OF LORRAINE

Grad: Chemistry

by **Anthony N. ABOU DIB**

Under the supervision of Pr. Frédéric AUBRIET and Dr. Vincent CARRÉ

**Methodological development in FT-ICR MS for the analysis of bio-oils
produced by pyrolysis of lignocellulosic biomass**

03 May 2023 in Metz

Jury Members:

Thesis directors:	Pr. Frédéric AUBRIET	Professor, LCP-A2MC, University of Lorraine
	Dr. Vincent CARRÉ	Maître de conférences, LCP-A2MC, University of Lorraine
Jury President:	Pr. Stephanie HESSE	Professor, LCP-A2MC, University of Lorraine
Rapporteur:	Pr. Laurence CHARLES	Professor, ICR, University of Aix-Marseille
	Dr. Nadège CHARON	Research Engineer, IPF Energies Nouvelles
Examiners:	Dr. Marie HUBERT-ROUX	Research Engineer, COBRA, University of Rouen
	Pr. Guillaume VAN DER REST	Professor, ICP, University Paris Saclay
	Dr. Yann LE BRECH	Maître de conférences, LRGP, University of Lorraine

*Dedicated to my family and to my
father's soul, my guardian angel in
God's hand.*

« Everything will get better. Try to find the positive in every bad situation. There will always be light in the end of the tunnel. »

“You become what you believe. You are where you are today in your life based on everything you have believed.”

~Oprah WINFREY

ACKNOWLEDGEMENTS

When you start your journey with a firm footing to stop at a peak, it seems like you must carry yourself to that peak. Once you have completed your journey and landed on this peak, you realize that if it hadn't been for the strong support and friendly push from people throughout the journey, it would have been a dream. It is not possible to abuse the support and faith of people who have been shown to me, but God has given me this small opportunity to express my overloaded string harmony with feelings of gratitude to all who have guided and raised me to this summit. It's only a small opportunity compared to the goodwill people have shown me. Several people have contributed to making this thesis possible and I take this opportunity to thank them all for their valuable contributions.

Before I begin to express my gratitude to everyone who has surrounded me over the past three years, I would like to sincerely thank the jury members who took the time and do me the honor of evaluating my thesis work: **Pr. Stéphanie HESSE, Dr. Nadège CHARON, Pr. Guillaume VAN DER REST, Dr. Marie HUBERT-ROUX, and Pr. Laurence CHARLES**. I would like also to express my thanks to the GREENER group at LRGP, Nancy and especially **Dr. Yann LE BRECH** for being an examiner to my thesis.

And let's not forget to thank all the people and institutions involved in the RESEX project which notably financed my thesis.

Here we are!! Let's talk about everyone who supported me for the past three years and has helped make the journey of thousands of miles achievable.

First and foremost, I feel expressionless and I lack words to overstate my gratitude and my debt of heart towards my thesis supervisors: **Pr. Frédéric AUBRIET** and **Dr. Vincent CARRÉ**. I count myself among the luckiest students to have you both as mentors. You both helped me, guided me to the best of your abilities whenever I was in a difficult situation. Your encouraging words, and support, your inspiration, your perseverance and your solid knowledge have contributed enormously to the realization of this work. I have acquired a lot of knowledge by your side, and if these three years have allowed me to develop both professionally and personally, it is mainly thanks to you. Thank you both for always pushing me forward and believing in me from day one. Once again, thank you for everything!!

Regarding my two thesis supervisors, I would like to thank each member at my host laboratory "le Laboratoire de Chimie et Physique – Approches Multi-échelles des Milieux Complexes (LCP-A2MC)", and especially my group colleagues. My earnest and honest thanks to **Pr. Patrick CHAIMBALUT, Dr. Sébastien SCHRAMM, Dr. Lionel VERNEX-LOSSET, Dr. Gabriel KRIER** and **Dr. Jasmine HERTZOG** for providing me indispensable suggestions and scientific discussions as well as their technical and administrative support. I gratefully and admirably

acknowledge all your help in successful completion of this thesis and I also thank you for all the non-scientific discussions we had and your friendship. And let's not forget **Dr. Sandrine RUP-JACQUES** for all her support, her suggestions, her help, and for her scientific and technical contribution in NMR. I am also grateful to **Pr. Amadou DICKO**, and **Dr. Michèle SINDT** for all their scientific organics discussions. It was a great privilege and honor to work with all of you.

I would like to thank **Pr. Peter O'CONNOR** and **Pr. Mark BARROW** for having done me the honor of visiting their laboratory at the University of Warwick - United Kingdom to develop a fruitful collaboration between our laboratories and to do new research work, thanks to the DrEAMS grant from the University of Lorraine. I would also like to thank them for their guidance and discussions.

Mes remerciements vont également à **Cathy AUBERT** « la reine des TP de chimie des solutions » pour son support et pour sa gentillesse, son aide surtout durant les séances de cours de TP.

I was lucky to have after about a year of loneliness in the office, the best office/laboratory colleagues with whom I not only shared the office, but I also laughed and shared my daily life.

To **Clarisse GOSSET-ERRARD**: Do you remember the first day we met and when I started asking you a lot of questions about the thesis? From that day on, I knew you weren't just a co-worker but also a friend I can grumble with and share my weirdness with. You were also my partner of the doctoral student representatives on the laboratory council. Thank you for always being there for me, for your support and for your help. Thank you for the trust you gave me by being your mail keeper. It was an honor for me to meet someone like you. And even if our paths do not cross, you will always have me as a loyal friend ready to support you. Once again, thank you very much for making these three years memorable.

To **Marisa MAIA**: Hello my friend! Even though I'm sometimes mean to you, that doesn't mean you're not the funniest and loveliest person I've met. We met during my last year of thesis and you made it so special. The office wouldn't have been the same without your presence, the positive vibes, your critics and the Portuguese chocolates. Thank you for the good times we shared that made me an alcoholic (more than I was). Your constant moral support was like the driving force behind achieving my goal. We made so many memories together, and I hope you won't forget any of them (even though I didn't mention them). Carry on with your very good sense of humor and whenever you come into the office, just remember me next to you with my little message "YOU LOOK SO BEAUTIFUL TODAY". **EU TE AMO MEU AMIGA.**

To **Farès SLIMANI**: Hello T.J Detweiler! I would like to apologize for the Lindt chocolate but after all I am your BUDDY. Thank you for the good times of laughter that we shared and

especially the conversations of our Microsoft teams. Don't forget the handsome friend who sat behind you and our weird gaze when we're bored. By the way "EHEINN".

To **Théo VOELLINGER**: I have known you since my first year of thesis and it was a pleasure. Thank you for all the scientific and non-scientific discussions we had and for being my bio-oils partner. Thank you for being our IT guy in the office who finds us the solution to every problem that arises on our PCs (my PC is afraid of you). Keep up that good sense of humor.

To **Pierre PACHOLSKY**: The calmest person I have ever known. We didn't have a lot of scientific discussions, but you always helped me with any problem and gave me some suggestions. Thank you so much for being the guy who cared a lot about us and about the power consumption.

My sincere thanks to all of you who have always had a free hand to help me, encourage me and maintain a pleasant working environment. It was an amazing experience working with all of you.

I would like to extend my acknowledgements to the former ATER member: **Dr. Ali ZAITER**, and **Dr. Julien COMEL** for their help and support. I also express my gratitude to the students, doctoral students, post-doctoral students and permanent staff of the UFR SciFA and the ICPM that I had the pleasure of meeting, especially: **Pauline GASCHT**, **Dyhia AIT-ABDALLAH**, **Ophélie FERRARA**, **Tugba KASARUVAN**, **Arthur JULLIOT**, **Max THACKERAY**, **Kahine TAZEKRITT**, **Julia EKOUTOU**, and **Omar SOLH**. I want to thank everyone for the positive energy you provided to the lab for a few months.

I am grateful to everyone I've collaborated with externally especially at the University of Warwick. Thank you all for your help, support, and friendship.

At the University of Warwick, my experience was amazing, thanks to **Dr. Bryan MARZULLO**, **Dr. Diana Catalina PALACIO LOZANO** and **Dr. Hugh JONES** who made my journey so special. It was an honor for me to meet such beautiful people inside out. On a professional level, thank you for guiding me, supporting me and helping me. Thank you for the most valuable scientific discussion we have had. Thank you for welcoming me with open arms on my first day at Warwick and making me feel at home. On a personal level, thank you for being the friends everyone wishes they had and for always caring about me. I will never be able to forget your wonderful company, drinking a lot of beer and always checking on me. Your friendship and support have added so much to my life. And also, to Bryan, no words can describe how grateful I am for everything you've done for me and you've always been there to help me even though there's a lot going on with you. I am grateful for your friendship.

To all of you, thank you for this beautiful collaboration that turned into friendship!

Throughout my life, I have had the chance to meet other wonderful people who have inspired me, helped me, made me grow, learned a lot... All these people have indirectly contributed to the success of this thesis, they therefore deserve a place in these acknowledgments!

I would like to thank **Dr. Elias HADDAD**. Thank you for having confidence in being my M2 internship supervisor and for believing in me. I take this opportunity to also thank **Dr. Eddy SOUAID** for always pushing me towards the realization of my dreams and for always being present in all the successes I have had during my professional and personal life.

A life without friends is like a Tree without leaves. And here, we are! This part of the acknowledgements will be dedicated to those that I am proud to call **F.R.I.E.N.D.S.**

I would like to start by thanking my former roommate in Lebanon, **Farid MAHFOUD** who is now in Strasbourg, and **Gilbert MANSOUR**, my friend from Mulhouse. You have never failed to make me happy, and whenever I am in trouble, you have always been there for me. Thank you for all the memories we made together and many more to come. Farid, there's always light at the end of the PhD tunnel.

Thank you also **Andy ARIDA** to whom I cannot express my grateful for her unwavering encouragement and support.

I would also like to extend the list to the Lebanese that I have met here in Metz and who have become friends, in particular: **Tony AL HADDAD, Joe BOUSTANY, Maroun CHALHOUB, Jack FADLLALAH, Valérie KHALIL, Farah SAHYOUNI, Hanna OBEID, Christy FADEL, Alain CHAAYA, Mitchael SAADE, Amale KHATIB, Léa BITAR, and Charbel AKOURY.** You have all made life in Metz better and special. Thank you all!

Next, I would like to thank five people who have marked my life: **Antoine ZAATAR, Paula ACHKAR, Nathalie SALAMEH, Ghiwa KARAM** and **Ghiwa ZOGHBY**. No words can describe how lucky I am to have you all in my life. Throughout my journey, you have never failed to bring a spark of hope to everything I have been through. I am grateful to have you in my life and I look forward to seeing you all. Nathalie, you once told me "Distance doesn't matter", and from that day "pinky swear my friend".

My gratitude also goes to **Lara MOUSSA**. Among many things for which I am grateful, our paths crossed during the masters are part of it. I'm proud of the person you've become and proud to call you best friend. Thank you for everything and thank you for your friendship that will never end.

I would like to thank also: **Monica AWAD, Monica KASSOUF, Charbel CHIBANI, Elia MOARBESS, Elias SARKIS, Elie ANDOS, Eghnatios EL ALAM, Jean-Mark RIACHY** and **Mikel SADER** for their friendship and support.

The last part of the acknowledgment as well as my thesis will be dedicated to the most important part of my life: my family.

To my mother **Mireille** and my brother **Charbel**, I take this opportunity to thank you for your selfless help and constant and endless support. Your prayer for me has been what has sustained me this far.

To my father **Najib** who never saw this adventure, I wish you were here to see my success. You who always said, "go conquer the world and let your success make noise", I wish you were here today, with me, with us, the day you dreamed of. You always planned to celebrate this day together. But guess what, you're here as my guardian angel. I miss you and love you so much. Thank you so much for believing in me every day and I hope I have made you proud.

Thanks to my uncles, aunts, cousins... who I miss so much! From the bottom of my heart, I would like to say a big thank you to: my sister-in-law **Jennifer BEAINY ABOUDIB**, **Laura ABOUDIB** (for your candles, and love like no other), **André BARMAKI**, and my cousins **Maya KHAZAKA**, **Moni**, and **Michael KASSOUF**. And let's not forget my grandparents **Najat** and **Joseph** as well as those who left us **Georgette** and **Georges** who always blessed me with their prayers.

Without all of you, I wouldn't have made it this far... For all of you, just a simple "thank you for everything" will never be enough.

Thank you from the bottom of my heart!

~Anthony N. ABOU DIB

A handwritten signature in black ink, appearing to be 'Anthony N. ABOU DIB', with a long horizontal stroke extending to the right.

TABLE OF CONTENT

Acknowledgements	1
Table of content	7
Abbreviation List	10
List of figures	15
List of tables	23
General introduction	27
References	29
PART I : State of the art	33
CHAPTER 1 : State of the art	35
Preamble.....	35
1.1. Review: Next Challenges for the Comprehensive Molecular Characterization of Complex Organic Mixtures in the Field of Sustainable Energy.....	35
1.2. Introduction	36
1.3. Biomass	36
1.4. First to third generation biofuels.....	44
1.5. Bio-oil characterization using analytical methods.....	68
1.6. Conclusion.....	104
1.7. References	105
PART II : Mass spectrometry and application	134
CHAPTER 2 : Materials and Methods	136
2.1. Introduction	136
2.2. Bio-oils produced by pyrolysis	137
2.3. Petroleomic' methods for characterizing the pyrolysis bio-oils.....	138
2.4. Ionization sources	140
2.5. Mass analyzer	156
2.6. Data Acquisition.....	173
2.7. - Data Treatment	175
2.8. – Graphical Representations	178

2.9. Tandem Mass Spectrometry.....	180
2.10. Conclusion.....	185
2.11. References	185
PART III : Specific derivatization of chemical functional group.....	199
CHAPTER 3 : Characterization of bio-oil at molecular level: specific derivatization of chemical functional group	201
3.1. Publication: Characterization of bio-oil at molecular level: specific derivatization of chemical functional group	201
3.2. Introduction	201
3.3. Materials and Methods	205
3.4. Results and Discussion	207
3.5. Application to Bio-oils.....	218
3.6. Conclusion.....	231
3.7. References	231
PART IV : Tandem mass spectrometry: Structural analysis of chemical functional groups	236
CHAPTER 4 : UVPD vs CID: Potential tool for structural analysis of bio-oils components	238
4.1. Publication: UVPD vs CID potential tool for structural analysis of bio-oil components.....	238
4.2. Abstract.....	238
4.3. Introduction	239
4.4. Materials and methods.....	241
4.5. Results and discussion	242
4.6. Conclusion.....	269
4.7. References	270
CHAPTER 5 : Principle of the two-dimensional mass spectrometry 2D FTMS and application on bio-oil	276
5.1. Introduction	276
5.2. 2D-FTMS principle.....	276
5.3. Data processing and representation	279
5.4. 2D-FTMS advantages	281
5.1. Application on bio-oil.....	282

5.2. References	299
General conclusion and perspectives	305
List of publications and communications.....	310
Publications	310
Oral communications	310
Poster Communications	311
Awards	312
Collaboration and scholarship	312
Teaching Missions	312
Lab Responsibilities.....	312
Résumé en Français de la thèse.....	314
Introduction.....	316
Principe de l'approche pétroléomique	319
La FT-ICR MS	321
Les sources d'ionisation.....	322
Matériels et méthodes	325
Spectromètres de masse à résonance cyclotronique de ions à transformée de Fourier.....	325
Production du bio-huile	325
Première approche : Dérivation Spécifique Des Fonctions Chimiques.....	327
Deuxième Approche : Spectrométrie De Masse En Tandem : Analyse Structurale....	330
La spectrométrie de masse en tandem	330
La spectrométrie de masse bidimensionnelle 2D FTMS.....	331
CID vs UVPD	333
La spectrométrie de masse bidimensionnelle	335
Conclusion	337
CHAPTER 6 : Références	338

ABBREVIATION LIST

1DMS: One-dimensional mass spectrometry

1G: First generation

2D-GC: Two-dimensional gas chromatography

2D-LC: Two-dimensional liquid chromatography

2DMS: Two-dimensional mass spectrometry

2G: Second generation

3G: Third generation

APCI: Atmospheric pressure chemical ionization

APPI: Atmospheric pressure photo-ionization

ASAP: Atmospheric solid analysis probe

CID: Collision induced dissociation

cIMS: Cyclic ion mobility high-resolution mass spectrometry

CIA: Chloroaniline

CPC: Centrifugal partition chromatography

CPWR: pyrolysis of wood and rubber

CSS: Collision Cross-Section

DBE: Double bond equivalent

DI: Direct injection

DIA: Data independent analysis

DMF: Dimethylformamide

DPF: Distillation, Precipitation and Fractionation

ECD: Electron capture dissociation

E-SARA: Extended Saturate Aromatic Resin Asphaltene

ESI: Electrospray Ionization

ETD: Electron transfer dissociation

FAIMS: High Field Asymmetric Waveform Ion Mobility Spectrometry

FFA: Free fatty acids

F-T: Fischer Tropsch

FT-ICR MS: Fourier transform ion cyclotron resonance mass spectrometry

FT-IR: Fourier Transform infrared

FWHM: Full width at half maximum

GC: Gas chromatography

GPC: Gel permeation chromatography

HDO: Hydrodeoxygenation

HDX: H/D exchange

HESI: Heated electrospray

HHV: High heating value

HPTLC: High-performance thin-layer chromatography

HPTLC: High-performance thin-layer chromatography

HRMS: High-resolution mass spectrometry

HTL: Hydrothermal liquefaction

IM: Ion mobility

IRMPD: Infrared multi-photon dissociation.

LC: Liquid Chromatography

LDI: Laser Desorption/ionization

MALDI: Matrix-assisted laser Desorption/ionization

MAPS: Modified aminopropyl silica

MLR: Multiple linear regression

MS: Mass spectrometry

NCD: Nitrogen chemiluminescent detection

NMR: Nuclear magnetic resonance

PAH: Polycyclic aromatic hydrocarbons

PASH: Polycyclic aromatic sulfur heterocycles

PFP: Pentafluoropyridine

PW: Pyrolysis wood

QcIMS: Quadrupole-selected cyclic ion mobility mass spectrometry

Q-TOF: Quadrupole Time of Flight

RPLC: Reversed phase liquid chromatography

SARA: Saturate Aromatic Resin Asphaltene

SEC: Size exclusion chromatography

SFC: Supercritical fluid chromatography

SPE: Solid phase extraction

TAN: Total acid number

TG: Triglyceride

THF: Tetrahydrofuran

THF: Tetrahydrofuran

Tof: Time of flight

TOF-MS: Time of flight mass spectrometry

TWIMS: Traveling Wave Ion Mobility Spectrometry

UHPLC: Ultra-high-performance liquid chromatography

UV: Ultra-violet

UVPD : Ultraviolet photodissociation

VGO : Vacuum gasoline

 LIST OF FIGURES

Part I – State of the Art
Chapter 1:

Figure 1-1: The life cycle of biodiesel incorporating CO ₂ . ⁹	37
Figure 1-2: Molecular to cell membrane-level structural compositions of biomass. The main components are cellulose, hemicellulose, and lignin. ¹²⁻¹⁴	40
Figure 1-3: Main mono-aromatic groups of lignin. ¹⁵	41
Figure 1-4: Molecular Structure of Cellulose. ¹⁵	42
Figure 1-5 : Main constituents of hemicellulose. ³⁶	43
Figure 1-6: Structure of one triglyceride. ⁴²	43
Figure 1-7: The different biofuels generations. ⁵⁰	45
Figure 1-8: The ethanol sector for first generation biofuels. ⁵⁶	46
Figure 1-9: Structure of the sucrose molecule.....	46
Figure 1-10: Production of biodiesel from vegetable oils. ⁶⁹	48
Figure 1-11: Conversion of triglycerides into glycerol and fatty acid alkyl esters by transesterification. ⁷³	49
Figure 1-12: Biofuels from microalgae. ⁹⁵	51
Figure 1-13: Lignin, cellulose, and hemicellulose are graphically represented in a plant cell. ¹⁰⁶	51
Figure 1-14: Technologies for Thermochemical Conversion of Biomass. ¹⁰⁷	52
Figure 1-15: Process of gasifying biomass and the ultimate use of syngas are shown schematically. ¹¹⁸	54
Figure 1-16: Impact of the interactions between the constituents of basic biomass on the yield of pyrolysis products. ¹³⁸	56
Figure 1-17: Main products obtained from lignin pyrolysis. ¹³⁹	59
Figure 1-18: Main products obtained from cellulose pyrolysis. ¹³⁹	60
Figure 1-19: Main products obtained from hemicellulose pyrolysis. ¹³⁹	61
Figure 1-20: Liquefaction of biomass by hydrothermal processes. ¹⁴⁹	62
Figure 1-21: Pyrolysis bio-oil applications. ¹⁶¹	64
Figure 1-22: 4-(trifluoromethyl)phenylhydrazine used for the derivatization of carbonyl group. ²⁰²	69
Figure 1-23: Typical petroleomic workflow: (A) acquisition of mass spectrum in high resolution mode (here LDI of coal-type sample); (B) distribution of mass measurement errors of assigned peaks after internal calibration of HR mass spectrum—the histogram is used to verify the normality of the error distribution; and (C) description of sample composition by various visualization tools.....	71

Figure 1-24: New methodologies in petroleomics that contribute to the chemical characterization of bio-oil at the molecular level.	73
Figure 1-25: Venn diagram (left) and DBE vs. #O (right) of the CHO formulae obtained from ESI, APPI, and LDI FT-ICR MS analyses. ²⁵⁶	79
Figure 1-26: Schematic of Crude Oil Saturate, Aromatic, Resin, and Asphaltene (SARA) Fractionation.	81
Figure 1-27: Comparison of extended-SARA (E-SARA) analysis with conventional SARA. ²⁸⁴ .	83
Figure 1-28: DPF fractionation steps adapted from Yerabolu et al. ²⁸⁶	84
Figure 1-29: Scheme of the experimental workflow from sample fractionation to gravimetric analysis and molecular characterization. The diagram was reprinted with permission from Ref. ²⁹²	86
Figure 1-30: Scheme for fractionating bio-oil by polarity (using water-based) LLE. ³⁰²	88
Figure 1-31: Use of solid phase extraction application scheme. ³⁰⁷	89
Figure 1-32: 2D TIMS-FT-ICR-MS survey spectra of the Athabasca asphaltene. Reprinted with permission from Ref. ³¹⁴ . 2021, Carlos Afonso.....	91
Figure 1-33: Main publications of IM-MS petroleomics. ^{309,314–323}	92
Figure 1-34: Advantages of the different of IMS technology ^{312,325–327} ..	93
Figure 1-35: The outline for the isotope labelling.	102

Part II – Mass spectrometry and applications

Chapter 2: Materials and methods

Figure 2-1: Diagram of the bio-oil collection system and microfluidized bed reactor ¹	137
Figure 2-2: Change of the solvent's shape at the output of the capillary in respect with the applied electric field. ³²	141
Figure 2-3: The electrospray ionization (ESI) method is represented. ^{34–37}	141
Figure 2-4: Ion ejection model (IEM), charge residue model (CRM), and chain ejection model are shown schematically as part of the ESI ionization process (CEM). ⁴⁰	143
Figure 2-5 : Bruker Solarix ESI source configuration. Adapted from Bruker's FTMS Library.	144
Figure 2-6 : An illustration of a nESI setup design. ⁵¹	145
Figure 2-7: A microscopic picture of the nanoESI capillary spray is presented. ⁵²	146
Figure 2-8: Relationship between the ionization energies of common chemicals and the photon energy of UV lamps used for APPI. ^{47,57}	147
Figure 2-9 : Diagram of the UV light and APPI source. ⁵⁷	150
Figure 2-10: (Top) APPI II source components (source housing removed), (Bottom) Interior part of the source. Adapted from Bruker's FTMS Library.	151
Figure 2-11: APCI source diagram. ⁷³	152
Figure 2-12: Bruker Solarix APCI source configuration. Adapted from Bruker's FTMS Library.	155

Figure 2-13: Ions moving in a circle in a magnetic field. Positive ions move in a counterclockwise manner when seen along the magnetic field's direction (left), whereas negative ions move in a clockwise direction (right). ⁹³	157
Figure 2-14: Correlation between the mass-to-charge ratio m/z and the ion orbital radius r for various magnetic field B_0 values. ⁷⁸	159
Figure 2-15: At magnetic field strengths between 3.0 and 9.4 T, the orbital radius and the kinetic energy of m/z 100 ions in an ICR cell are shown. ⁹⁴	159
Figure 2-16: Schematic diagram of part of the FTICR mass spectrometry. Ions are contained in an ICR cell, where they are trapped under a magnetic and radio frequency electrostatic field. Adapted from Bruker FTMS Library.	160
Figure 2-17: Diagram showing the motion of a magnetron and cyclotron within an ICR cell in the absence (A) and presence (B) of collision gas. ⁸⁸	162
Figure 2-18: (A) representation of the individual ion movements within an ICR cell, and (B) representation of the total ion motion that results. ^{94,95}	163
Figure 2-19: The steps involved in ICR-MS's excitation and image current detection. The ion cloud's spiral trajectory is shown in figure (a), which was caused by the ions being excited by an RF electric field that oscillated at the cyclotron resonance frequency. However, the frequency f_c of circulation is not a function of ion velocity, and the radius is constant throughout detection. ⁸⁸	164
Figure 2-20: Time-domain (left) and frequency-domain (right) excitation waveforms: (a, b) rectangular pulses yield inhomogeneous and rather narrow excitation windows; (c) "chirp" excitation; (d, e) SWIFT excitations, with (e) designed to eject a certain mass range from the cell. ⁹⁴	166
Figure 2-21: The procedure of turning an ion's cyclotron motion into a mass spectrum. ¹¹⁶	167
Figure 2-22: Various input signals and how Fourier transformations affect them. (a) A step function is converted to sinc (x), (b) a fully dampened transient signal containing only one frequency yields a single Lorentzian curve, and (c) when a transient signal is shortened, it may be seen as a mixture of (a) and (b) and produces a Lorentzian curve with "wiggles."	168
Figure 2-23: Important ICR cell types; A) Cubic cell, B) open-ended cylindrical cell, C) and D) open-ended cylindrical cells with compensation electrodes, E) capped cylindrical cell, F) Infinity cell, and G) dynamically harmonized capped cylindrical cell. The individual electrodes are labelled: excite (E), detect (D), trap (T), and compensation electrode (C). ¹²²	169
Figure 2-24: Dynamically harmonized ICR cell. (a) Axial cross section showing the segmented cell walls and the hyperbolic trapping potential experienced by ions on average per full cycle. (b) Division into four 90° sections to accomplish excitation and detection plus detail of a trapping plate. (c) Photograph of the Paracell; gold plating is used to minimize electrode oxidation. ¹²⁴	170
Figure 2-25: Determining a peak's resolution using its peak width and peak center of Oak bio-oil analyzed in (+) ESI FT-ICR MS.	172
Figure 2-26: Performance of FT-ICR mass spectrometers as a function of magnetic field strength. ⁹⁴	173

Figure 2-27: Schematic of the 7 T 2 ω Bruker Solarix used for the work presented in this thesis. The numbered sections are referred to in the next section. Adapted from Bruker's Instrument diagram.....	174
Figure 2-28 : (Right) Mass error (in ppm) vs. m/z for C _x H _y O _z compounds of an Oak pyrolysis bio-oil analysed in (-) ESI FT-ICR MS, (Left) Normal probability plot.	177
Figure 2-29: (-) ESI FT-ICR mass spectrum of Oak pyrolysis bio-oil.....	177
Figure 2-30: Van Krevelen diagram shows certain significant biomolecular parts arranged in various areas. ¹³³	178
Figure 2-31: Kendrick's map of C _x H _y O _z compound family from Oak pyrolysis bio-oil analysed in (-) ESI FT-ICR MS.	179
Figure 2-32: Global composition description of an Oak bio-oil by (+) ESI FT-ICR MS analysis. DBE versus oxygen number (right), and relative distribution in respect with the oxygen atom count (left).....	180
Figure 2-33: Typical steps for performing a tandem MS experiment.....	181
Figure 2-34: A collision cell's representation of the CID fragmentation of precursor ions. ...	182
Figure 2-35: UVPD configuration for FT-ICR-MS. Through the center hole of the indirectly heated ring dispenser cathode affixed to the rear trapping plate of an ICR cell, the IR laser is delivered into the cell. ¹⁶⁰	183
Figure 2-36: Illustration of energy deposition by different fragmentation techniques (CID, IRMPD, and UVPD). ¹⁶⁹	184
Figure 2-37 : UVPD in FT-ICR MS Solarix.....	184

Part III – Specific derivatization of chemical functional groups

Chapter 3: Characterization of bio-oil at molecular level: specific derivatization of chemical functional group

Figure 3-1: Scheme of the experimental workflow from sample fractionation to derivatization and functional characterization.	207
Figure 3-2: Mechanism of the reaction leading to the Schiff base formation from primary amine.....	209
Figure 3-3: Mechanism of the reaction leading to the tetrafluoropyridyl bi-aryl ether formation from the reaction between phenol and pentafluoropyridine.	210
Figure 3-4: Structure of the butyrophenone obtained in fraction 1 and its corresponding derivatization using the primary amine.	211
Figure 3-5: Structure of the four compounds obtained in fraction 2 after derivatization using the PFP and the primary amine.....	213
Figure 3-6: ¹⁹ F NMR spectrum (Top) ¹⁹ F NMR of the obtained product "Tetrafluoropyridyl bi-aryl ether" after derivatization of the standard phenol on the SPE cartridge. Fa corresponds to the fluorine in the meta position and Fb corresponds to that the fluorine in the ortho position. (Bottom) ¹⁹ F NMR of the pentafluoropyridine	215

Figure 3-7: Structure of the four compounds obtained in fraction 3 and its corresponding derivatization using the PFP.....	217
Figure 3-8: Van Krevelen diagrams of Oak raw bio-oil analyzed by FT ICR-MS with (+) ESI (A), (-) ESI (B), (+) APPI (C), and (+) APCI (D). Representations done using the in-house “Punc’data” data treatment software.....	219
Figure 3-9: Mass spectrum obtained after the analysis of each fraction. (Top left) Mass spectrum of the fraction 1 before adding the primary amine, (Top right) Mass spectrum of the fraction 1- CIA after adding the primary amine, (Middle left) Mass spectrum of the fraction 2 before adding the primary amine, (Middle right) Mass spectrum of the fraction2- CIA after adding the primary amine, and (Bottom) Mass spectrum of the fraction 3.	220
Figure 3-10: Van Krevelen diagram of: A- fraction 1 analyzed by (+) APCI FT-ICR MS B,C,D- fraction 1 – CIA analyzed by (+) ESI FT-ICR MS for compounds that remain non-derivatized (B), are derivatized once (C), and are derivatized twice (D) by 3-chloroaniline.....	221
Figure 3-11: Relative distribution in respect with the carbon atom count (left) and with the oxygen atom count (right) for the fraction 1 after adding the 3-chloroaniline.....	222
Figure 3-12: DBE versus #C and #O for the fraction 1 CIA, (blue) not derivatized by the 3-chloroaniline, (red) derived once, and (green) derived twice with PFP.	223
Figure 3-13: (Top Left) Van Krevelen diagram of the fraction 2 derived once with PFP, (Top right) Van Krevelen diagram of the fraction 2 derived twice with PFP, and (Bottom left) Van Krevelen diagram of the fraction 2 derived thrice with PFP.....	224
Figure 3-14: (Left) Van Krevelen diagram of the fraction 2 CIA derived once with PFP and the primary amine, and (Right) Van Krevelen diagram of the fraction 2 CIA derived only once with PFP.....	225
Figure 3-15: DBE versus #C for the compounds obtained in fraction 2 after subtraction of the derivatization reagent. (Upper left, A) DBE versus #C for the compounds once derived with the PFP, (Upper right, B) DBE versus #C for the compounds twice derived with the PFP, and (Bottom C) DBE versus #C for the compounds derived thrice with the PFP.	226
Figure 3-16: Relative distribution in respect with the carbon atom count (left) and with the oxygen atom count (right) for the different compounds obtained in fraction 2.....	226
Figure 3-17: DBE versus #C for the compounds obtained in fraction 2 – CIA after subtraction of the derivatization reagent. (Left, A) DBE versus #C for the compounds once derived with the PFP and once with the primary amine, (Right, B) DBE versus #C for the compounds derived only with PFP and not derived with primary amine.....	227
Figure 3-18: Van Krevelen of the fraction 3, (left, A) not derived by the pentafluoropyridine, (middle, B) derived once by the pentafluoropyridine, and (right, C) derived twice by the pentafluoropyridine.	228
Figure 3-19: The density of molecules distributed along the H/C and O/C ratio for the fraction 3.....	228
Figure 3-20: DBE versus carbon number of the compounds obtained in fraction 3, (top) not derived, (middle) derived once, and (bottom) derived twice.....	229

Figure 3-21: Relative distribution in respect with the carbon atom count (left) and with the oxygen atom count (right) for the different compounds obtained in fraction 3.....	229
Figure 3-22: m/z ratio versus H/C ratio showing that the derivatized compounds in the fraction 3.	230

Part IV – Tandem mass spectrometry: Structural analysis of chemical functional groups

Chapter 4: UVPD vs CID: Potential tool for structural analysis of bio-oils components

Figure 4-1: Structures of the six bio-oils standards that were investigated in this study. The various moieties in each compound are highlighted by the color coding of the structures.	242
Figure 4-2: Proposed mechanism of CID (black) and UVPD (black and red) fragmentation of 2.5 dihydroxy benzoic acid.....	243
Figure 4-3: (Top) CID MS/MS spectrum of the deprotonated vanillin molecule, along with its corresponding cleavage diagram. (Bottom) UVPD MS/MS spectrum of coniferyl alcohol along with its cleavage diagram.....	245
Figure 4-4: (Top) Proposed mechanism of CID fragmentation of vanillin, (Bottom) Proposed mechanism of UVPD fragmentation of vanillin.....	247
Figure 4-5: (Top) CID MS/MS spectrum of the deprotonated coniferyl alcohol molecule, along with its corresponding cleavage diagram. (Bottom) UVPD MS/MS spectrum of coniferyl alcohol along with its cleavage diagram.....	248
Figure 4-6: (Top) CID MS/MS spectrum of the deprotonated sinapyl alcohol molecule, along with its corresponding cleavage diagram. (Bottom) UVPD MS/MS spectrum of sinapyl alcohol along with its cleavage diagram.....	249
Figure 4-7: (Top) Proposed mechanism of CID fragmentation of coniferyl alcohol, (Bottom) Proposed mechanism of UVPD fragmentation of coniferyl alcohol.	252
Figure 4-8: Proposed mechanism of CID fragmentation of sinapyl alcohol.	254
Figure 4-9: Proposed mechanism of UVPD fragmentation of sinapyl alcohol	255
Figure 4-10: Phenoxide/ quinone methide conversion. ⁶² Two pathways should be considered: (1) anion/neutral complex-mediated proton abstraction leading to the loss of the H ₂ O in β -O-4 linkage, (2) secondary fragmentation leading to a charge-driven cleavage except H ₂ O...	256
Figure 4-11: (Top) CID MS/MS spectrum of the deprotonated pinoresinol molecule, along with its corresponding cleavage diagram. (Bottom) UVPD MS/MS spectrum of the deprotonated pinoresinol molecule along with its cleavage diagram.	257
Figure 4-12: Proposed mechanism of CID fragmentation of pinoresinol.....	260
Figure 4-13: Proposed mechanism of UVPD fragmentation of pinoresinol.	261
Figure 4-14: (Top) CID MS/MS spectrum of the deprotonated GGE molecule, along with its corresponding cleavage diagram. (Bottom) UVPD MS/MS spectrum of GGE along with its cleavage diagram.....	262
Figure 4-15: Proposed mechanism of CID fragmentation of GGE.	265

Figure 4-16: Proposed mechanism of UVPD fragmentation of GGE.	266
Figure 4-17: DBE versus number of carbons of CID (dark blue) and UVPD (light purple) for the six bio-oil standards. The precursor ion is in light blue. (A) DHB, (B) Vanillin, (C) Coniferyl alcohol, (D) Sinapyl alcohol, (E) Pinoresinol, and (F) GGE.....	268

Chapter 5: Principal of the two-dimensional mass spectrometry 2D FTMS and application on bio-oil

Figure 5-1: A common Gäumann FT-ICR 2DMS pulse sequence is shown in (A). (B) How the pulse sequence affected the ions' orbital radii. (C) The impact of the ion's circling radius on fragmentation efficiency. It is important to keep in mind that the ion is totally in-phase with the second excitation pulse for $\Delta\phi = 0^\circ$, while it is fully out-of-phase for $\Delta\phi = 180^\circ$. Most ions will settle within these two limits in the majority of scans. Ions with lower orbital energies will fragment more easily than ions with greater radii (orange line) (red and purple). ^{4,5}	278
Figure 5-2: Graph showing the fluctuation in intensity between the precursor ions (black) and matching fragment ions (red and blue). ⁵	279
Figure 5-3: A 2DMS contour plot is represented and labelled with the numerous lines that may be seen to analyze the data. ⁵	280
Figure 5-4: Structures of the three lignin standards employed in this study. The various moieties found in each compound are highlighted by the color-coding of the structures... ..	285
Figure 5-5: (A) 2D-UVPD-MS map for the three standards mixtures, (B) the extracted autocorrelation line, (C) the extracted neutral loss line of $m/z124$ (guaiacol), and (D) the extracted horizontal line at $m/z357$	287
Figure 5-6: UV spectrums of the used three standards with a concentration of 1 mg.mL^{-1} in methanol. The UV analysis was conducted at the chemistry department of the University of Lorraine in Metz. A UV/Vis thermo scientific Evolution 201 was the used spectrophotometer and the data were obtained using thermo insight software.	291
Figure 5-7: 2D contour plot of a bio-oil. (Left) 2D contour plot with a de-noise rank 25, (Right) 2D contour plot without de-noise. (C) Mass spectrum corresponding to the autocorrelation line extracted from the 2D map at a low m/z value, and (D) Mass spectrum corresponding to the autocorrelation line extracted from the 2D map at a high m/z value.	293
Figure 5-8: (A) Mass spectrum corresponding to the autocorrelation line extracted from the 2D map with a denoise rank of 25, (B) Mass spectrum of a raw bio-oil analyzed by negative electrospray (C) Venn Diagram highlighting that no significant loss between 2DMS on bio-oil and the FTMS analysis of raw bi-oil in (-) ESI.	295
Figure 5-9: (A) Van Krevelen diagram of the extracted autocorrelation line from the 2D map in negative ESI, (B) DBE versus the number of carbons of the precursor present in the autocorrelation line. The graphical representation was done by using in house developed software.....	296

 LIST OF TABLES

Part I: State of the art
Chapter 1: State of the art

Table 1-1: Nature of the biomass used to produce alternatives fuel. ¹¹	38
Table 1-2: Typical component analysis of some plant biomass samples. ^{109,110}	53
Table 1-3: Methods of pyrolysis and its main characteristics. ¹¹⁹⁻¹²³	55
Table 1-4: Typical physicochemical properties of heavy, 2G pyrolysis, 2G liquefaction, and 3G oil. ¹⁶⁵⁻¹⁶⁷	65
Table 1-5: Bio-oil's Chemical Composition. ¹⁶⁹	66
Table 1-6: Performances of several HRMS instruments (manufacturer's specification sheet). An asterisk (*) indicates maximum resolving power (the resolution decreases as the acquisition measurement rate increases). (ND: No Data.)	72
Table 1-7: Sheath and auxiliary gas and solvents used for the analysis of DPF fractions by positive ion APCI. ²⁸⁹	85
Table 1-8: Examples of derivatization reagents used to study oxygenated functional groups in bio-oils.	98

Part III – Specific derivatization of chemical functional groups
Chapter 3: Characterization of bio-oil at molecular level: specific derivatization of chemical functional group

Table 3-1: Structure and molecular weight of standards compounds and their derivatization reagent.	203
Table 3-2: Tandem mass spectrometry analysis of the butyrophenone and its corresponding imine compound.	212
Table 3-3: Tandem mass spectrometry analysis of the derivatized standard eluted using the pentafluoropyridine PFP as derivatization agent.....	216
Table 3-4: Tandem mass spectrometry analysis of the derivatized standard eluted using the formic acid after derivatization by pentafluoropyridine.	218

Part IV – Tandem mass spectrometry: Structural analysis of chemical functional groups

Chapter 4: UVPD vs CID: Potential tool for structural analysis of bio-oils components

Table 4-1: Peak list and relative intensity of the fragments from CID and UVP of 2.5 DHB..	243
Table 4-2: Peak list and relative intensity of the fragments from the CID and UVPD of vanillin.	246
Table 4-3: Peak list, relative intensity of the fragments, and assignments from the CID and UVP of coniferyl alcohol.	250
Table 4-4: Peak list, relative intensity of the fragments, and assignment from the CID and UVP of sinapyl alcohol.	251
Table 4-5: Peak list, relative intensity of the fragments, and assignment from the CID and UVPD of Pinoresinol.	259
Table 4-6: Peak list, relative intensity of the fragments, and assignment from the CID and UVPD of GGE.	264
Table 4-7: For each bio-oil standard, moieties found by the two fragmentation techniques.	267

Chapter 5: Principal of the two-dimensional mass spectrometry 2D FTMS and application on bio-oil

Table 5-1: Fragmentation efficiency percentages (FE (%)) and moiety coverage (%) in the 1D and 2D experiments for each Investigated lignin standard.	287
Table 5-2: Peak list, relative intensity of the fragment, and assignment from the 1DMS of the standard coniferyl alcohol.	288
Table 5-3: Peak list, relative intensity of the fragment, and assignment from the 2DMS of coniferyl alcohol in the standard mixture after a denoise rank of 25.	288
Table 5-4: Peak list, relative intensity of the fragment, and assignment from the 1DMS of the standard pinoresinol.	289
Table 5-5: Peak list, relative intensity of the fragment, and assignment from the 2DMS of pinoresinol in the standard mixture after a denoise rank of 25.	289
Table 5-6: Peak list, relative intensity of the fragment, and assignment from the 1DMS of the standard GGE.	290
Table 5-7: Peak list, relative intensity of the fragment, and assignment from the 2DMS of GGE in the standard mixture after a denoise rank of 25.	290
Table 5-8: Different fragment ions collected from 1D and 2D-UPVD-MS of the standard mixture were distributed between odd and even-electron ion.	292
Table 5-9: Classification of functional groups and lignin monomers by neutral loss masses and percentage of precursors. ^{29,40}	296
Table 5-10: Peak list, relative intensity of the fragment, and assignment from the 2DMS of the candidate compound at m/z 179, 357, and 319 in bio-oil after a denoise rank of 25.	298

Table 5-13: Fragmentation efficiency percentages (FE (%)) and moiety coverage (%) in 2D experiments on bio-oils..... 299

GENERAL INTRODUCTION

Due to the increase in the world's population and the demand for energy, the use of fossil fuels such as oil, coal and gas, which have been stored for several million years, poses several problems related to their availability and their impact on the environment. The decreasing availability of these resources is at the root of some of the current geopolitical and economic crises. The use of fossil fuels is also causing increasing environmental and ecological problems in connection with global warming. It is therefore necessary to find alternatives to the use of fossil resources that are more sustainable and environmentally friendly.¹

Plastics and biomass can be some of these alternatives as their transformation can lead to high value-added compounds. Biomass is defined as the organic matter produced by all plants and animals.^{2,3} It is the main source of renewable energy that can be converted into fuels. It is widely available and comes from the agricultural and forestry sectors.⁴

The nature of the biofuels and high-value compounds that can be produced depends on the nature of the biomass used and the conversion/transformation processes that are employed.^{5,6} Biodiesel, bioethanol and biogas are the most widely used first generation biofuels.⁷ Transesterification of vegetable oils and fats produces biodiesel, while fermentation of sugars and starches produces bioethanol. Biogas is produced from the anaerobic digestion of animal or plant waste, but also from dedicated crops. The liquid manure that is also produced during this process is used as agricultural fertilizer.⁷

The major problem with first-generation biofuels is the use of edible products by humans or animals whose production requires dedicated crops. To overcome this problem, second-generation biofuels are being developed and differ from the former in that the nature of the feedstock used does not interfere with the food or feed sectors.⁸ These biofuels are produced using lignocellulosic biomass from wood and agricultural residues such as straw.^{8,9} The main constituents of lignocellulosic biomass, cellulose, hemicellulose, and lignin,^{10,11} lead to the production of second-generation biofuels through two main conversion routes. The first route is biochemical and involves converting cellulose, hemicellulose, and eventually starch from biomass into simple sugars using enzymes and microorganisms and then being transformed into alcohol by fermentation.¹² The second is thermochemical conversion, which involves pyrolysis, liquefaction, or gasification of all components of the lignocellulosic biomass.^{13,14,15} In these processes, biomass is converted, at high temperatures (pyrolysis/gasification) or high pressures (liquefaction), in the presence or absence of oxygen, into biogas, biochar, and bio-oils.¹⁶ There is a growing interest in bio-oils, as their potential for valorization and their molecular composition are very complex, sometimes leading to being called "green oil".¹⁷ The bio-oils obtained have a high oxygen content, which gives them a high acidity and high reactivity, so their direct use is impossible (problems of corrosivity and

storage).^{18,19} To overcome these issues, it is necessary to develop catalytic hydrodeoxygenation up-grading treatments to reduce the oxygen amounts.^{20,21} These catalytic processes must also allow the catalytic cracking of the heaviest compounds.²¹

To determine which catalytic treatments are most suitable and optimize bio-oil production, it is necessary to know the composition of these bio-oils as precisely as possible. Works have been carried out on the characterization of bio-oils using different analytical techniques (GC/MS, 2D GC/MS, HPLC, HPLC/MS, FTIR, and NMR). Still, these methods have yet to allow for finely characterizing the molecular composition of the bio-oils.^{22,23} The combination of several techniques is necessary to achieve this objective. Two approaches are generally used to investigate complex mixtures. The first is based on research and quantification of known compounds using specific analytical techniques. It is called “targeted analysis.” For this purpose, infrared and nuclear magnetic resonance spectroscopy can be used,^{19,22} as gas and liquid chromatography coupled to mass spectrometry. The main drawback of the targeted techniques is that only a pre-established list of compounds, usually of low molecular weight, are detected representing only a tiny fraction of bio-oils components.^{22,24} Marshall et al. developed a non-target approach by initially applying it to the study of crude oil to study the thousands of components of an oil or bio-oil over a broader mass range.²⁵ This approach is typically based on the direct infusion of the oil or bio-oil sample into the ionization source of the mass spectrometer. This non-targeted approach is called “petroleomics” and intended to describe all oil components detected at the molecular level.^{25,26} Due to the high molecular complexity of crude oil and bio-oil samples, a high-resolution mass spectrometer (HRMS), such as the Fourier-transform ion cyclotron resonance mass spectrometer (FT-ICR MS) is required.^{27,28} This instrument can identify thousands of species with high mass measurement accuracy and ensures the unambiguously assignment of a single formula to all mass spectrum peaks. In addition, the use of different sources ionization can be an advantage for exploring bio-oils in depth.²⁹ This approach does not allow quantitative information or separation of isomers.

To obtain structural information on the more than six thousand species that have already been identified in bio-oils, two approaches have been developed in this Ph.D. thesis using high-resolution mass spectrometry FT-ICR MS. The first used specific derivation and fractionation procedures, and the second used tandem mass spectrometry.

The composition of biomass and the different types of biofuels that result from its conversion will be discussed in the first chapter. Emphasis will be placed on the production processes of second-generation biofuels, methods for their up-grading, and their sustainability potential. This second section of this chapter will be devoted to the different analytical methods that could be used to characterize these bio-oils.

The second chapter will describe the production method by pyrolysis of the bio-oil studied in this thesis. These ionization methods were used, as well as the principle of mass

spectrometry FT-ICR MS and used in this work. The principle of petroleomic analysis will also be presented. The last section of this chapter will introduce the principle of tandem mass spectrometry used for the structural investigation of bio-oil components.

In the third chapter, the development of the fractionation-derivatization method will be described. Throughout this chapter, the different operating conditions used, as well as the different derivatization reagents used to identify functional groups within the constituents of the bio-oils will be presented.

The fourth chapter will introduce the structural analysis of bio-oil compounds by tandem mass spectrometry. The differences between collision-induced dissociation (CID) and ultraviolet photodissociation (UVPD) will be extensively discussed by considering six standard bio-oil compounds.

Chapter five will be devoted to UVPD two-dimensional mass spectrometry analysis of bio-oils. This recent technique, currently applied to the study of peptides ionized by ESI, has the particularity of not resorting to a classic selection of the precursor ion. It is thus possible to produce in a reasonable time, of the order of a few tens of minutes to a few hours, all the fragmentation spectra of the thousands of ions observed on a mass spectrum associated with studying a complex mixture like a bio-oil.

Combination the 2D FTMS approach and the directed non-targeted approach (fractionation/derivatization) will ultimately make obtaining relevant structural information on bio-oil components possible. Finally, all the methodologies put in place have been applied to studying crude bio-oils.

References

- (1) Bracmort, K. Biomass: Comparison of Definitions in Legislation. 20.
- (2) Perea-Moreno, M.-A.; Samerón-Manzano, E.; Perea-Moreno, A.-J. Biomass as Renewable Energy: Worldwide Research Trends. *Sustainability* **2019**, *11* (3), 863. <https://doi.org/10.3390/su11030863>.
- (3) Contescu, C.; Adhikari, S.; Gallego, N.; Evans, N.; Biss, B. Activated Carbons Derived from High-Temperature Pyrolysis of Lignocellulosic Biomass. *C* **2018**, *4* (3), 51. <https://doi.org/10.3390/c4030051>.
- (4) Li, Y.; Rezgui, Y.; Zhu, H. District Heating and Cooling Optimization and Enhancement – Towards Integration of Renewables, Storage and Smart Grid. *Renew. Sustain. Energy Rev.* **2017**, *72*, 281–294. <https://doi.org/10.1016/j.rser.2017.01.061>.
- (5) McKendry, P. Energy Production from Biomass (Part 2): Conversion Technologies. *Bioresour. Technol.* **2002**, *83* (1), 47–54. [https://doi.org/10.1016/S0960-8524\(01\)00119-5](https://doi.org/10.1016/S0960-8524(01)00119-5).
- (6) Huber, G. W.; Iborra, S.; Corma, A. Synthesis of Transportation Fuels from Biomass: Chemistry, Catalysts, and Engineering. *Chem. Rev.* **2006**, *106* (9), 4044–4098. <https://doi.org/10.1021/cr068360d>.

- (7) Naik, S. N.; Goud, V. V.; Rout, P. K.; Dalai, A. K. Production of First and Second Generation Biofuels: A Comprehensive Review. *Renew. Sustain. Energy Rev.* **2010**, *14* (2), 578–597. <https://doi.org/10.1016/j.rser.2009.10.003>.
- (8) Callegari, A.; Bolognesi, S.; Cecconet, D.; Capodaglio, A. G. Production Technologies, Current Role, and Future Prospects of Biofuels Feedstocks: A State-of-the-Art Review. *Crit. Rev. Environ. Sci. Technol.* **2020**, *50* (4), 384–436. <https://doi.org/10.1080/10643389.2019.1629801>.
- (9) Dutta, K.; Daverey, A.; Lin, J.-G. Evolution Retrospective for Alternative Fuels: First to Fourth Generation. *Renew. Energy* **2014**, *69*, 114–122. <https://doi.org/10.1016/j.renene.2014.02.044>.
- (10) Demirbaş, A. Calculation of Higher Heating Values of Biomass Fuels. *Fuel* **1997**, *76* (5), 431–434. [https://doi.org/10.1016/S0016-2361\(97\)85520-2](https://doi.org/10.1016/S0016-2361(97)85520-2).
- (11) Shahzadi, T.; Mehmood, S.; Irshad, M.; Anwar, Z.; Afroz, A.; Zeeshan, N.; Rashid, U.; Sughra, K. Advances in Lignocellulosic Biotechnology: A Brief Review on Lignocellulosic Biomass and Cellulases. *Adv. Biosci. Biotechnol.* **2014**, *2014*. <https://doi.org/10.4236/abb.2014.53031>.
- (12) Sivamohan Reddy, N. Pathways of Lignocellulosic Biomass Conversion to Renewable Fuels. *Biomass Convers. Biorefinery* **2013**.
- (13) Dhyan, V.; Bhaskar, T. A Comprehensive Review on the Pyrolysis of Lignocellulosic Biomass. *Renew. Energy* **2018**, *129*, 695–716. <https://doi.org/10.1016/j.renene.2017.04.035>.
- (14) van Rossum, G.; Zhao, W.; Castellvi Barnes, M.; Lange, J.-P.; Kersten, S. R. A. Liquefaction of Lignocellulosic Biomass: Solvent, Process Parameter, and Recycle Oil Screening. *ChemSusChem* **2014**, *7* (1), 253–259. <https://doi.org/10.1002/cssc.201300297>.
- (15) Jindal, M. K.; Jha, M. K. Hydrothermal Liquefaction of Wood: A Critical Review. *Rev. Chem. Eng.* **2016**, *32* (4), 459–488. <https://doi.org/10.1515/revce-2015-0055>.
- (16) Wu, Y.; Wang, H.; Li, H.; Han, X.; Zhang, M.; Sun, Y.; Fan, X.; Tu, R.; Zeng, Y.; Xu, C. C.; Xu, X. Applications of Catalysts in Thermochemical Conversion of Biomass (Pyrolysis, Hydrothermal Liquefaction and Gasification): A Critical Review. *Renew. Energy* **2022**, *196*, 462–481. <https://doi.org/10.1016/j.renene.2022.07.031>.
- (17) No, S.-Y. Application of Bio-Oils from Lignocellulosic Biomass to Transportation, Heat and Power Generation—A Review. *Renew. Sustain. Energy Rev.* **2014**, *40*, 1108–1125. <https://doi.org/10.1016/j.rser.2014.07.127>.
- (18) Stöcker, M. Biofuels and Biomass-To-Liquid Fuels in the Biorefinery: Catalytic Conversion of Lignocellulosic Biomass Using Porous Materials. *Angew. Chem. Int. Ed.* **2008**, *47* (48), 9200–9211. <https://doi.org/10.1002/anie.200801476>.
- (19) Staš, M.; Auersvald, M.; Kejla, L.; Vrtiška, D.; Kroufek, J.; Kubička, D. Quantitative Analysis of Pyrolysis Bio-Oils: A Review. *TrAC Trends Anal. Chem.* **2020**, *126*, 115857. <https://doi.org/10.1016/j.trac.2020.115857>.
- (20) Xiu, S.; Shahbazi, A. Bio-Oil Production and Upgrading Research: A Review. *Renew. Sustain. Energy Rev.* **2012**, *16* (7), 4406–4414. <https://doi.org/10.1016/j.rser.2012.04.028>.
- (21) Lian, X.; Xue, Y.; Zhao, Z.; Xu, G.; Han, S.; Yu, H. Progress on Upgrading Methods of Bio-Oil: A Review: Upgrading Progress of Bio-Oil. *Int. J. Energy Res.* **2017**, *41* (13), 1798–1816. <https://doi.org/10.1002/er.3726>.

- (22) Michailof, C. M.; Kalogiannis, K. G.; Sfetsas, T.; Patiaka, D. T.; Lappas, A. A. Advanced Analytical Techniques for Bio-Oil Characterization. *WIREs Energy Environ.* **2016**, *5* (6), 614–639. <https://doi.org/10.1002/wene.208>.
- (23) Wang, Y.; Han, Y.; Hu, W.; Fu, D.; Wang, G. Analytical Strategies for Chemical Characterization of Bio-Oil. *J. Sep. Sci.* **2020**, *43* (1), 360–371. <https://doi.org/10.1002/jssc.201901014>.
- (24) Djokic, M. R.; Dijkmans, T.; Yildiz, G.; Prins, W.; Van Geem, K. M. Quantitative Analysis of Crude and Stabilized Bio-Oils by Comprehensive Two-Dimensional Gas-Chromatography. *J. Chromatogr. A* **2012**, *1257*, 131–140. <https://doi.org/10.1016/j.chroma.2012.07.035>.
- (25) Marshall, A. G.; Rodgers, R. P. Petroleomics: The Next Grand Challenge for Chemical Analysis. *Acc. Chem. Res.* **2004**, *37* (1), 53–59. <https://doi.org/10.1021/ar020177t>.
- (26) Marshall, A. G.; Rodgers, R. P. Petroleomics: Chemistry of the Underworld. *Proc. Natl. Acad. Sci.* **2008**, *105* (47), 18090–18095. <https://doi.org/10.1073/pnas.0805069105>.
- (27) Marshall, A. G.; Rodgers, R. P. Petroleomics: The Next Grand Challenge for Chemical Analysis. *Acc. Chem. Res.* **2004**, *37* (1), 53–59. <https://doi.org/10.1021/ar020177t>.
- (28) Abdelnur, P. V.; Vaz, B. G.; Rocha, J. D.; de Almeida, M. B. B.; Teixeira, M. A. G.; Pereira, R. C. L. Characterization of Bio-Oils from Different Pyrolysis Process Steps and Biomass Using High-Resolution Mass Spectrometry. *Energy Fuels* **2013**, *27* (11), 6646–6654. <https://doi.org/10.1021/ef400788v>.
- (29) Cho, Y.; Ahmed, A.; Islam, A.; Kim, S. Developments in FT-ICR MS Instrumentation, Ionization Techniques, and Data Interpretation Methods for Petroleomics: METHODS FOR PETROLEOMICS. *Mass Spectrom. Rev.* **2015**, *34* (2), 248–263. <https://doi.org/10.1002/mas.21438>.

PART I : STATE OF THE ART

CHAPTER 1 : STATE OF THE ART

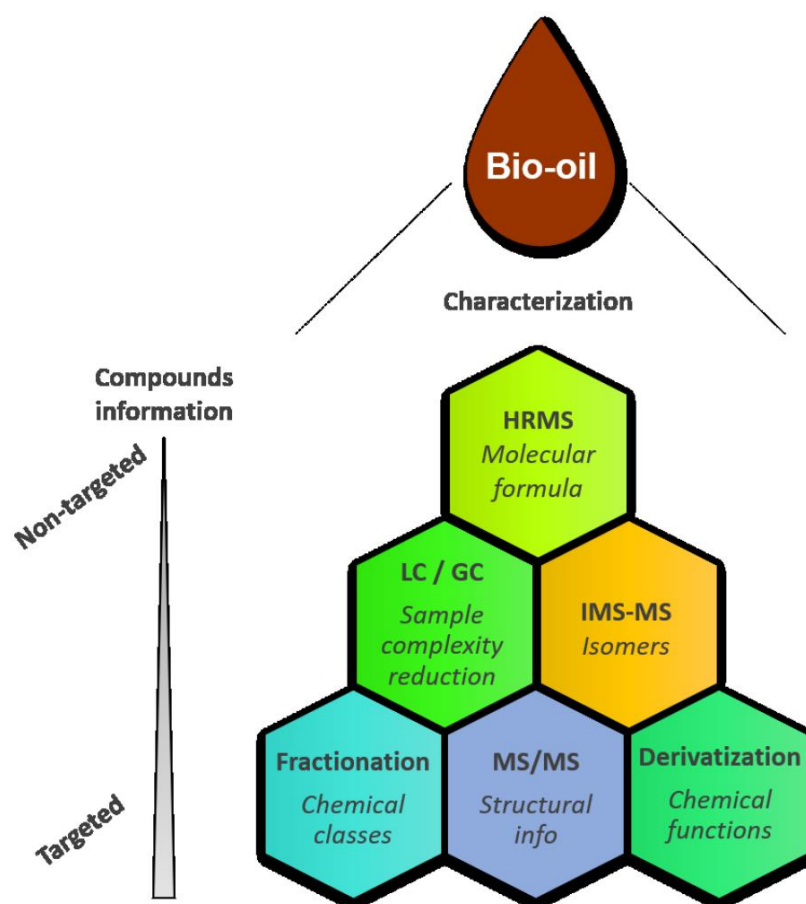
Preamble

The last sections of this state-of-the-art chapter were written based on the review published in 2023 in *Molecules*. However, this is not a strict reproduction of its contents but an expanded version with additional information and a slightly different organization.

1.1. Review: Next Challenges for the Comprehensive Molecular Characterization of Complex Organic Mixtures in the Field of Sustainable Energy

Anthony Abou-Dib, Frédéric Aubriet, Jasmine Hertzog, Lionel Vernex-Loiset, Sébastien Schramm and Vincent Carré.

Published in *Molecules* journal, DOI: 10.3390/molecules27248889



1.2. Introduction

The increasing world population and energy demand have caused the urgent need to develop alternative energy sources that are clean, new, greener, and more sustainable. Utilizing lignocellulosic biomass resources may be required to solve the issues of severe environmental issues and the lack of fossil fuels.¹⁻³ Added-value molecules can be produced by the conversion of biomass using enzymatic, chemical, hydrothermal or thermal processes.

In this chapter, the composition of the lignocellulosic biomass will be detailed as part of processes (pyrolysis and liquefaction) used to its conversion into added-value compounds and more specifically of bio fuels. The specificities of primary, secondary, and third generation bio-carburant will be also discussed.

The conversion of lignocellulosic biomass by pyrolysis or liquefaction leads to biogas, biochar, and bio-oil production. This latter corresponds to the condensation of part of the gaseous compounds during the conversion process and presents a complexity, some properties, and potential valorization close to those of petroleum. The valorization and the up-grading of bio-oils require a comprehensive description of their molecular description. Indeed, in-depth information is important to finely adapt the catalytic treatments of crude bio-oils necessary for their up-grading as well as the conversion processes used for their production. Consequently, the analytical techniques required for such characterization will be developed in this chapter. They include targeted and non-targeted approaches, and fractionation/derivatization methodologies to focus on specific functional groups.

1.3. Biomass

1.3.1. Definition

Biomass is the second largest source of renewable energy in the world. This energy comes mainly from its combustion. This study is mainly dedicated to the potential of lignocellulosic biomass since it is the only sustainable, abundant, and non-food source of organic carbon.⁴

Geographical specificities, resource availability, biodiversity, technology advancements, and economic factors can impact biomass production and its potential to be converted into sustainable bioenergy.⁵ The lignocellulosic biomass undergoes different conversion processes to produce bio-oils (a source of biofuels),^{6,7} as well as molecules with enhanced applications in the chemical industry.

The CO₂ released into the atmosphere because of this transformation and the use of the bio-fuel produced corresponds at most to the amount of CO₂ absorbed by plants during their growth. Therefore, the carbon impact on the atmosphere from burning biofuels is particularly low (event negative due to the formation of biochar during conversion) compared to petroleum-based fuels (Figure 1.1).⁸

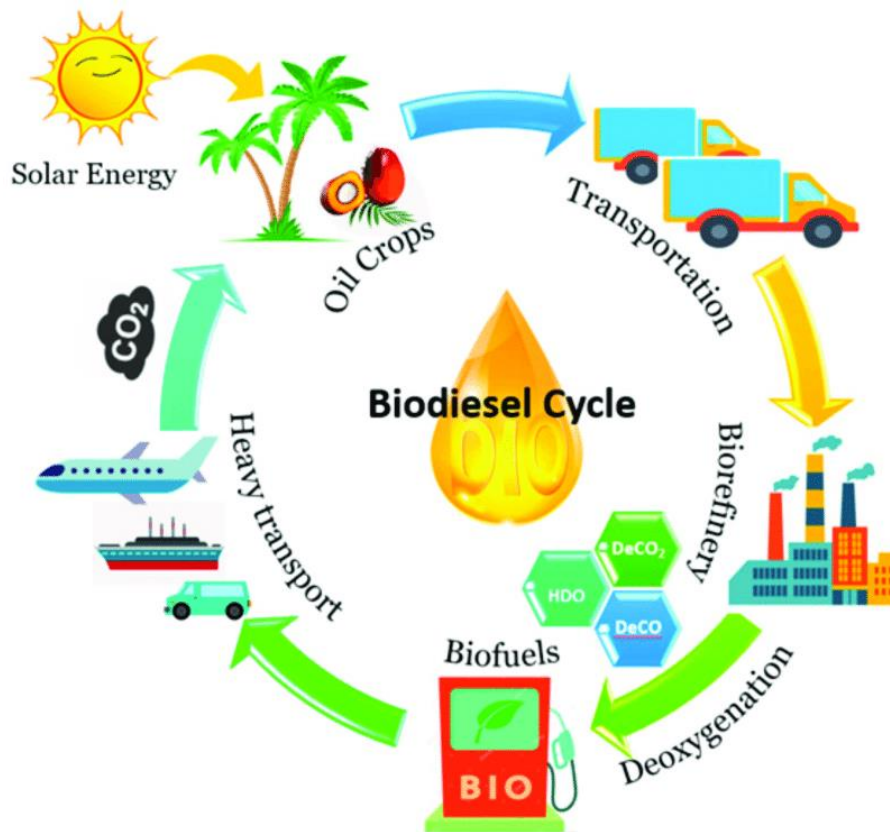


Figure 1-1: The life cycle of biodiesel incorporating CO₂.⁹

However, the processes used to produce biofuels are not entirely carbon neutral, they must be improved to be more sustainable.¹⁰ Currently, a variety of biofuels are produced and classified based on the raw material. Table 1.1 presents a non-exhaustive description of the used biomass raw material.

Table 1-1: Nature of the biomass used to produce alternatives fuel.¹¹

Biomass	Subgroups, species, and variants of biomass
Wood and woody biomass	Coniferous or deciduous, angiospermous or gymnospermous and soft or hard such as stems, barks, branches (twigs), leaves (foliage), bushes (shrubs), chips, lumps, pellets, briquettes, sawdust, sawmill and others from various wood species.
Herbaceous and agricultural biomass	<p>Annual or perennial, arable or non-arable and field-based or processed-based biomass from various species such as:</p> <p style="padding-left: 40px;">Grasses and flowers (alfalfa, arundo, bamboo, bana, cane, miscanthus, reed canary, ryegrass, switchgrass, timothy, others)</p> <p>Straws (barley, bean, corn, flax, mint, oat, paddy, rape, rice, rye, sesame, sunflower, triticale, wheat, others)</p> <p>Stalks (alfalfa, arhar, arundo, bean, corn, cotton, kenaf, mustard, oreganum, sesame, sunflower, thistle, tobacco, others)</p> <p style="padding-left: 40px;">Fibers (coconut coir, flax, jute bast, kenaf bast, palm, others)</p> <p>Shells and husks (almond, cashewnut, coconut, coffee, cotton, hazelnut, millet, olive, peanut, rice, sunflower, walnut, others)</p> <p style="padding-left: 40px;">Pits (apricot, cherry, olive, peach, plum, others)</p> <p>Other residues (fruits, pips, grains, seeds, coir, cobs, bagasse, food, fodder, marc, pulps, cakes, others) from various species</p>
Aquatic biomass	Marine or freshwater, macroalgae or microalgae and multicellular or unicellular species (blue, blue-green, brown, golden, green and red algae; diatoms, duckweed, giant brown kelp, kelp, salvinia, seaweed, sweet-water weeds, water hyacinth, others)

Animal and human biomass wastes	Bones, chicken litter, meat-bone meal, sponges, various manures, others
Contaminated biomass and industrial biomass wastes (semi-biomass)	Municipal solid waste, demolition wood, refuse-derived fuel, sewage sludge, hospital waste, paper-pulp sludge, waste papers, paperboard waste, chipboard, fibreboard, plywood, wood pallets and boxes, railway sleepers, tannery waste, others
Biomass mixtures	Blends from the above varieties

1.3.2. Composition of the lignocellulosic biomass

The basic components of biomass include cellulose (40 to 50 % weight), hemicelluloses (25 to 35 % weight), lignin (15 to 20 % weight), triglycerides, proteins, and terpenes.^{12–15} The most prevalent components in biomass are cellulose, hemicellulose, and lignin, which together make up the cell membrane (Figure 1-2). However, their amounts vary depending on the nature of the biomass. The biomass conversion processes leading to the production of bio-oil will be described in the 1.4 section, but it is interesting to state now that cellulose and hemicellulose lead to the formation of carbohydrates while lignin, an aromatic heteropolymer, mainly forms phenolic compounds.¹⁶

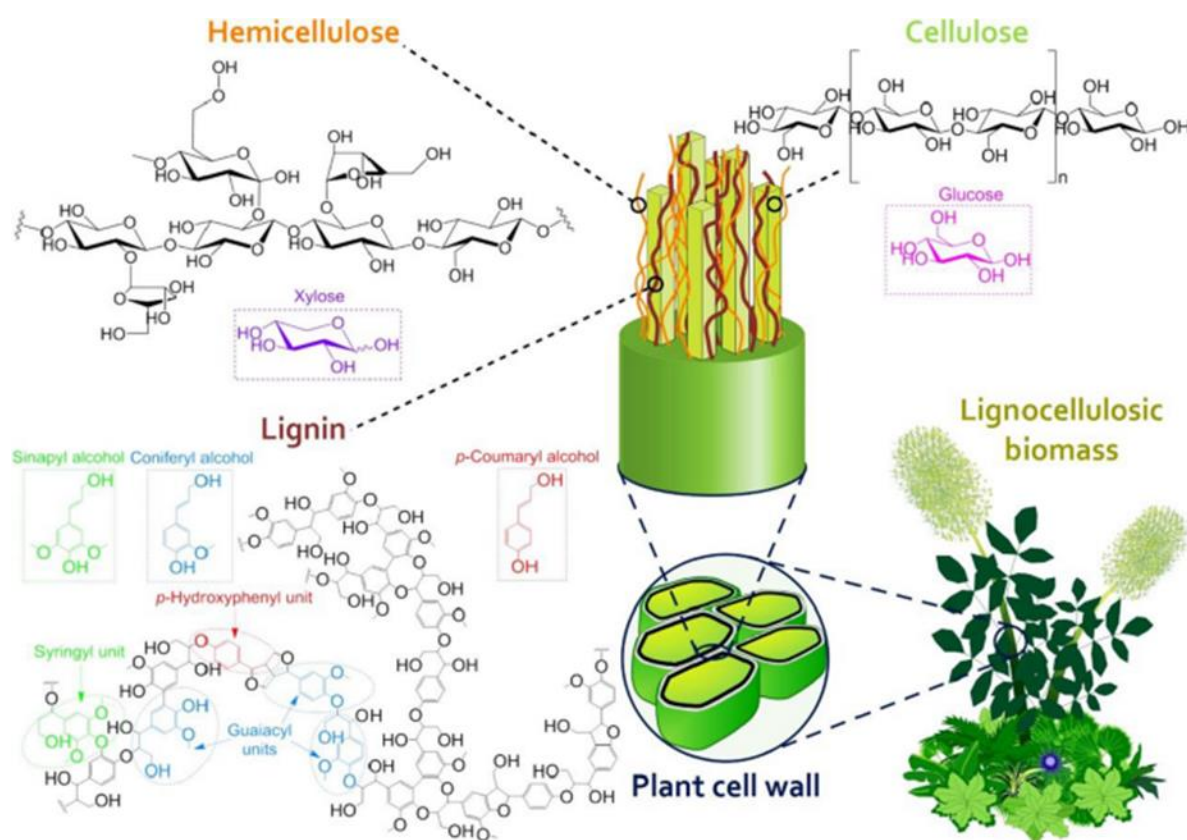


Figure 1-2: Molecular to cell membrane-level structural compositions of biomass.^{12–14}

1.3.2.1. Lignin

The relative amount of lignin in the biomass ranges from 10 to 35%.^{17,18} It is a three-dimensional polyphenolic polymer that gives plant biomass, particularly that of woody species, rigidity. It is an amorphous heteropolymer composed of aromatic units that are bonded together. Typically, phenolic aromatic groups are connected to a three-carbon chain with or without the inclusion of one or two methoxy groups. The p-hydroxyphenyl units that constitute this aromatic heteropolymer are joined by C-C or C-O-C bonds.^{18,19}

P-hydroxyphenyl (H), guaiacyl (G), and syringyl (S), respectively, are the produced corresponding phenylpropanoid moieties that are present in the lignin.^{18,20}

The structure of these phenylpropanoids is present in Figure 1-3:

- p-coumaryl alcohol, unit H (hydroxyphenyl)
- Coniferyl alcohol, unit G (guaiacyl)
- Sinapyl alcohol, unit S (syringyl)

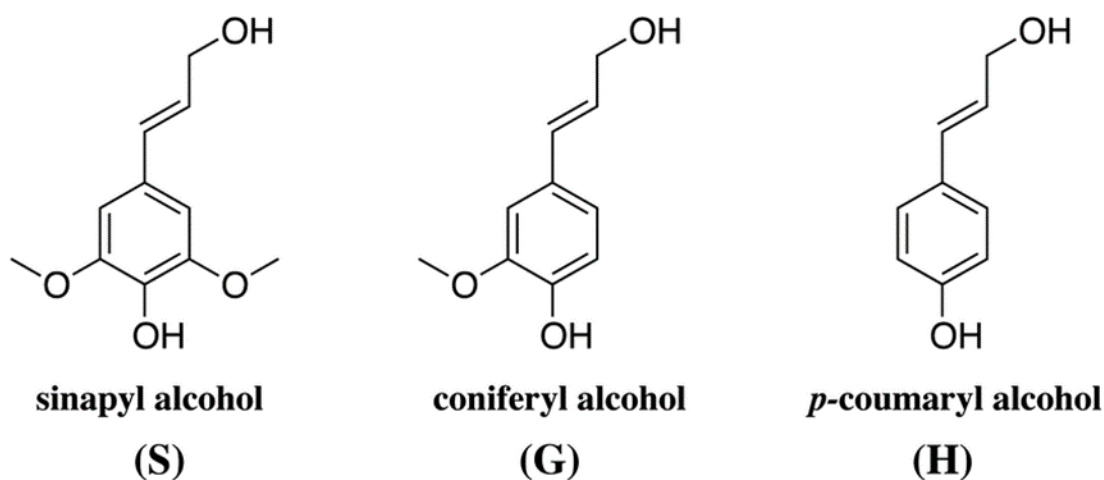


Figure 1-3: Main mono-aromatic groups of lignin.¹⁵

The structure of the lignin varies depending on the proportion of S and G subunits. Guaiacyl moieties from coniferyl units are the major component of the softwood-lignin (spruce and pine). While the lignin of eucalyptus, oak, and other hardwood species includes an equal mixture of sinapyl (S) and coniferyl (G) monomers. In addition, grass plants have relatively small quantities of p-hydroxyphenyl and comparable amounts of guaiacyl and syringyl units.²¹

The pulp and paper industries produce huge quantities of lignin as a by-product, which is employed as a low-grade fuel. The valorization of this industrial by-product by pyrolysis or liquefaction into phenolic compounds is carried out by breaking the ether or carbon-carbon bonds.^{22,23} The resulting compounds may be transformed into fuel and value-added chemicals.^{24,25}

1.3.2.2. Cellulose

The cellulose (a glucose polymer) is the most abundant organic homopolymer on Earth and, represents for 40 to 80% of biomass.^{26,27} It is crystalline, has a very high average molecular weight, and is composed of one linear chain of "D-glucopyranose" monomers connected by β -1,4 glycosidic linkages (Figure 1-4). Starch-based plants like corn and wheat contain and other glucose polymer.²⁸ The α -1,4 and α -1,6 connections give the starch an amorphous form at the cellulose-starch interface.

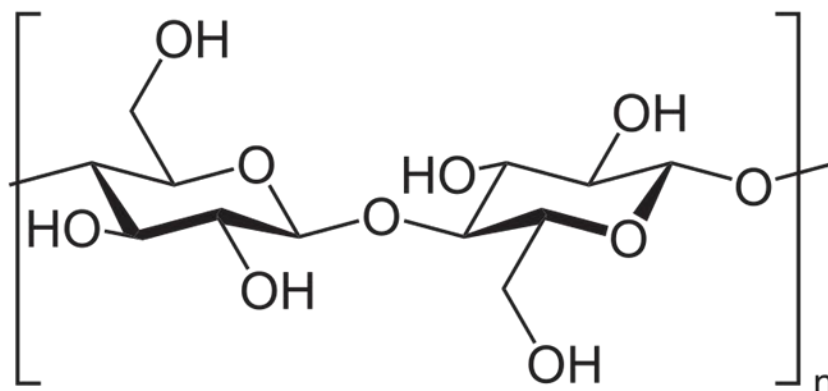


Figure 1-4: Molecular structure of cellulose.¹⁵

The intra- and intermolecular H bonds provide cohesion of the 3D-network remains in place. Cellulose is insoluble in water and significantly resistant to enzyme attacks and thermal decompositions due to these hydrogen bonds.

Moreover, chemical or enzymatic conversion of cellulose or starch into glucose units is a source of bioethanol after a fermentation process.²⁹⁻³¹

1.3.2.3. Hemicellulose

This polymer is the second most abundant (15–30%) and has a more complicated structure than cellulose. Indeed, this polysaccharide is constituted of different pentose and hexose units. It includes C₅-sugars (xylose and arabinose) and C₆-sugars (glucose, galactose, and mannose) (Figure 1-5).³²

The C₅- and C₆-sugars obtained when the hemicellulose is depolymerized may be utilized after upgrading processes for the synthesis of polymers, or transformed into gasoline or jet fuel.^{12,33-35}

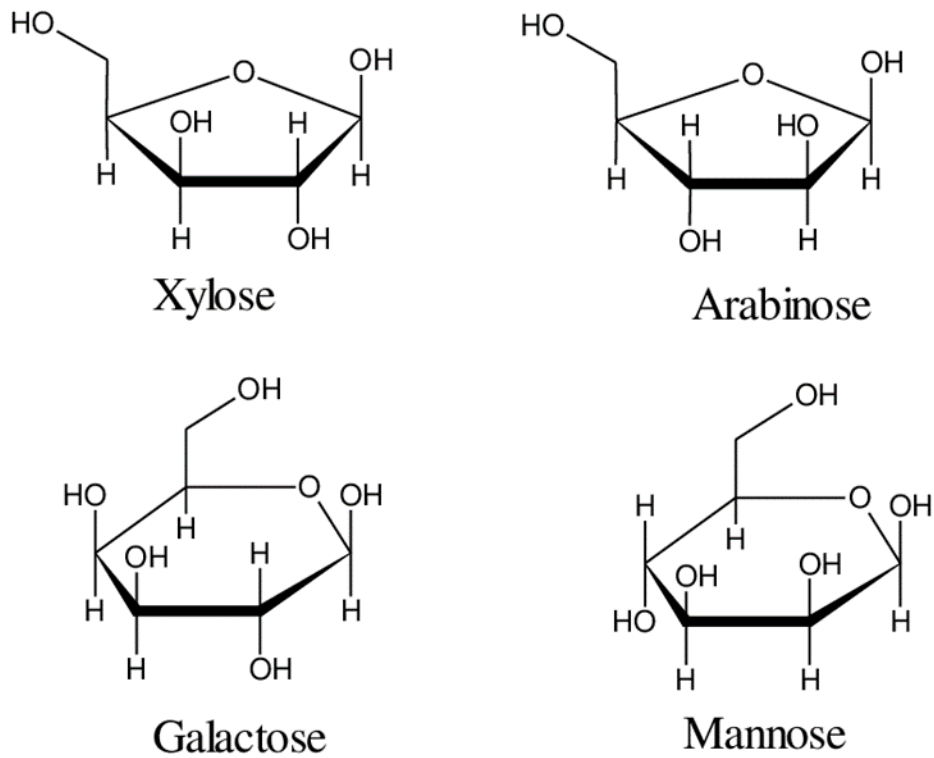


Figure 1-5 : Main constituents of hemicellulose.³⁶

1.3.2.4. Other biomass constituents

Lipids

Lipids are also constituents of the biomass and are found in very diverse forms as mono-, di- and triglycerides in seeds of oil plant (rapeseed, sunflower, soy, cotton ...).^{37,38} These triglycerides (vegetable oils Figure 1-6) present a great potential to produce biodiesels by transesterification.³⁹ Following the glycerol co-product can be up-graded in different ways and represents a promising raw material.^{40,41}

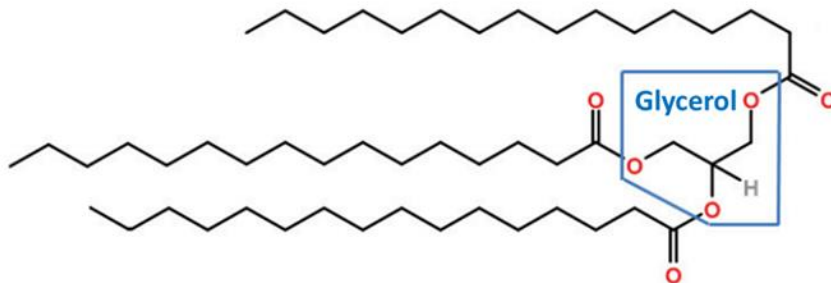


Figure 1-6: Structure of one triglyceride.⁴²

The proteins

In respect with the nature of the biomass the amounts of proteins may be low (plant) or more significant (animal, algae). They are mainly used as pet food and their conversion into value-added chemicals yields peptides and amino acids.^{43,44}

The bio-oils produced by conversion of protein-rich biomass, contain important amounts of nitrogenated compounds which may limit their use.^{42,45} Indeed, their combustion leads to the release of nitrogen oxides into the atmosphere and their catalytic up-grading is complicated by the nitrogen poisoning of catalysts.

Terpenes

A very small percentage of plant biomass is made up of terpenes. Indeed, some plant species transform their carbohydrates into terpenes, which are polymers of isoprene units. The most well-known naturally occurring isoprene-based substance is latex, a rubber made by the heave tree.^{46,47}

Minerals and extractable organic compounds

Biomass also contains inorganic compounds in very low amounts (<1% by weight). The main mineral components are: potassium, sodium, phosphorus, magnesium and calcium as well as extractable organic compounds such as compounds of fats, pectin, and resins.⁴⁸

1.4. First to third generation biofuels

Biofuels are produced by transforming raw plant- or animal-based materials. Different generations of biofuels must be considered depending on the raw material, the conversion process, and the final products. The three first generation biofuels result from the conversion of non-modified biomass: edible biomass, non-edible biomass, and algal biomass. The fourth-generation biofuel has been recently introduced and is the amalgamation of genomically prepared microorganisms and genetically engineered feedstock (Figure 1-7).⁴⁹ This study focusses on second-generation biofuel, therefore, the first- and third-generation biofuels will be examined first.

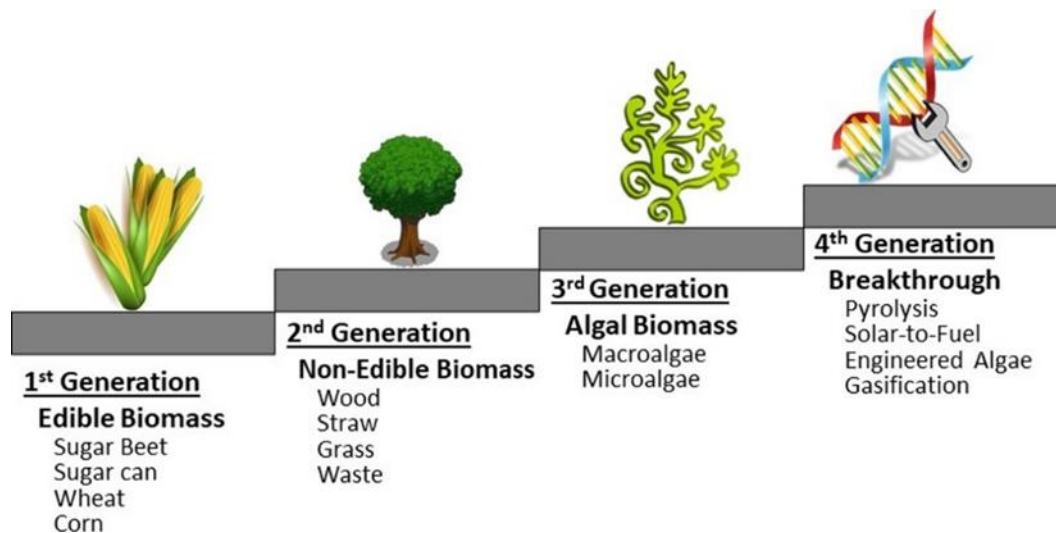


Figure 1-7: The different biofuels generations.⁵⁰

1.4.1. First generation biofuels

These biofuels come from agricultural (edible) products (beet, potato, sugar cane, wheat, etc.) transform into fuel by various processes. Two first-generation biofuels must be considered: bioethanol and biodiesel.

1.4.1.1. Bioethanol

Bioethanol is the only liquid fuel for gasoline engines that is both renewable and widely available.^{51,52} The yearly production of bioethanol was reported at 10¹⁰ L in 2016 according to the Renewable Fuels Association.⁵³ Beets, sugar cane, corn, wheat, and other crops are utilized to make bioethanol. These plants thrive by absorbing CO₂ from the atmosphere, which is converted into carbohydrates by photosynthesis. After fermentation, these carbohydrates yield bioethanol (Figure 1-8). The amounts of CO₂ absorbed during biomass growth and the amounts of CO₂ emitted into the atmosphere when the engine is running are comparable.⁵⁴

Depending on the complexity of the carbohydrates, two classes of plants must be considered: the sugar (sugar cane, beet, ...) and the starchy (corn, rice, ...) plants.⁵⁵

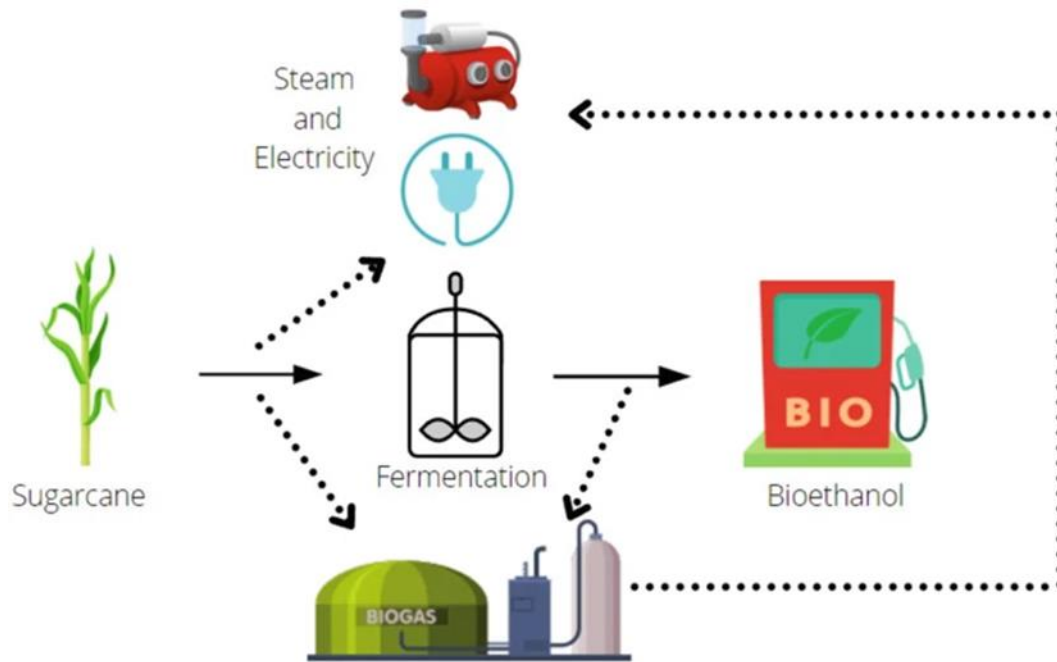


Figure 1-8: The ethanol sector for first generation biofuels.⁵⁶

Bioethanol from sugar plants

The largest part of bioethanol is from sugar plants, particularly those that are sucrose-rich (30% by weight for sugar cane)(Figure 1-9).^{57,58}

Sucrose is a disaccharide of glucose and fructose; whose standardized name is α -D-glucopyranosyl- (1 \leftrightarrow 2) - β -D-fructofuranoside.

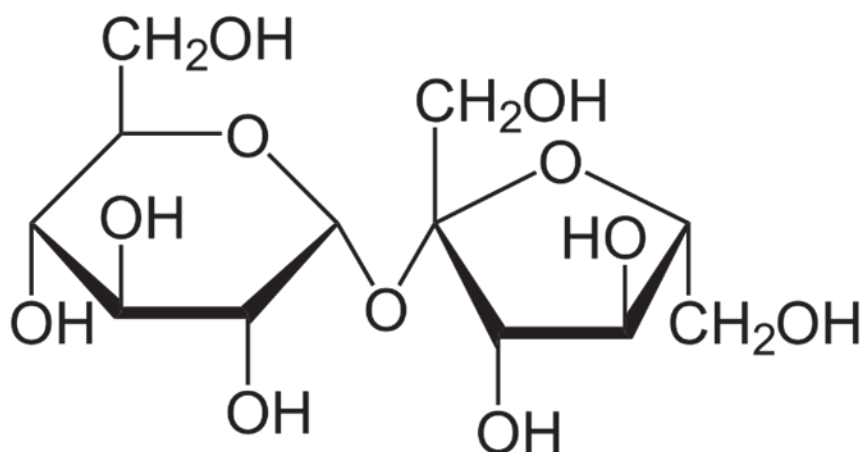
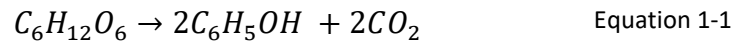


Figure 1-9: Structure of the sucrose molecule.

Bacteria and yeast are able to hydrolyze sucrose into glucose and fructose and to convert them into ethanol by fermentation. The sugar plant must first be ground to separate the insoluble lignocellulosic fraction from the juice containing sucrose.⁵⁹

The fermentation reaction takes place according to the following equation:



Bioethanol from species containing starch

Starch is an amorphous glucose/maltose $(C_6H_{10}O_5)_n$ polymer, which has to be converted first into simple carbohydrates before to produce bioethanol by fermentation. Two processes are used:

The wet-milling process is the oldest one.^{60,61} The seed of starchy plants are ground before water is added to produce a mash containing 15-20% starch. The mash is then treated at a high temperature (90–100 °C), and two separate enzymes are successively introduced. The first one (α -amylase) hydrolyzes starch enzyme to produce short chains of glucose (dextran). This is catalyzed by acidic conditions. The second is glucoseamylase breaks down the dextrans into glucose and maltose.

The dry grinding does not require the presence of water prior to the both amylases' hydrolysis.^{62,63} Finally, a particular bacterium ferment allows the glucose and maltose conversion into bioethanol.⁵⁹

The use of bioethanol

Bioethanol from biomass can be used in different ways. In the presence of isobutene, it is transformed into ETBE (Ethyl tertio butyl ether),⁶⁴ which is mixed with conventional gasoline in a proportion of 15%. This derivative currently uses most of the production of bioethanol but it is also the most polluting.⁶⁵ Bioethanol is also incorporated in the E85 fuel, which is a mixture of 85% bioethanol and 15% unleaded 95 fuel. E85 is considered the most ecological fuel from a consumption point of view.⁶⁶

1.4.1.2. Biodiesel

This biofuel, also named “bio-ester” comes mainly from vegetable oils and is used by diesel engines. The European Union produced 10^6 tons of biodiesel in 2003, accounting for 82% of the global production of biofuels.⁶⁷ Biodiesel is intended to partially replace diesel fuel and does not need to be blended with petroleum-based diesel. In reality, biodiesel is blended up to 20 vol.% with conventional diesel fuel to respond to the present huge diesel fuel demand.

Biodiesel is obtained by transesterification of hydrotreated vegetable oils (HVO) produced from seeds of rapeseed, sunflower, palm, ... (Figure 1-10).⁶⁸

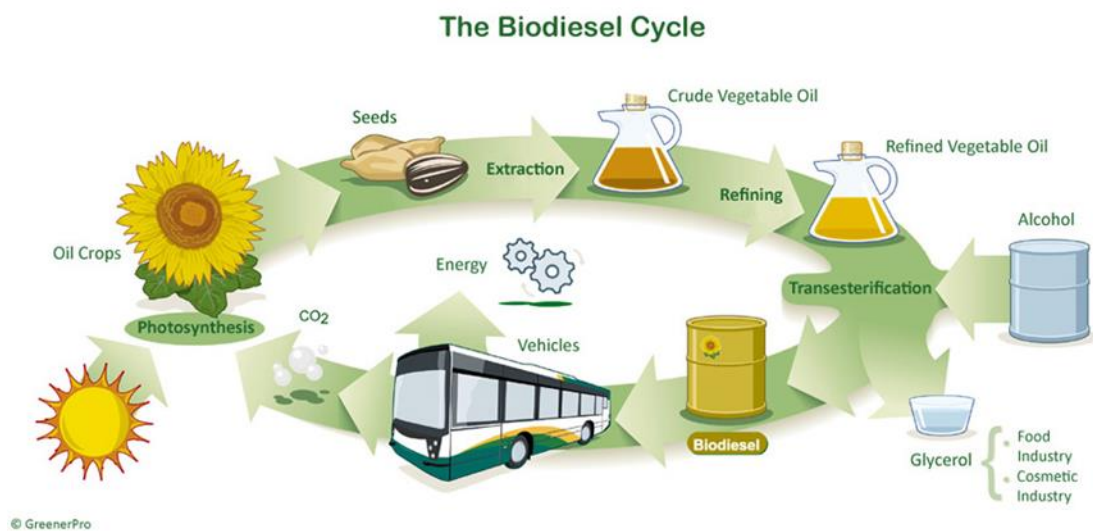


Figure 1-10: Production of biodiesel from vegetable oils.⁶⁹

HVO are triglycerides (esters of three fatty acid and one glycerol molecule). Once the transesterification reaction takes place, a reaction between the acid group of the triglyceride (TG) and the three hydroxyl groups of glycerol, fatty alkyl (mainly methyl) esters are formed. This reaction must be activated by homogeneous or heterogeneous catalysts.⁷⁰

The homogeneous catalyst

Transesterification leading to the final production of glycerol and fatty esters is a reversible step-by-step process (Figure 1-11).^{71,72} The intermediary products are di- and mono-glycerides.

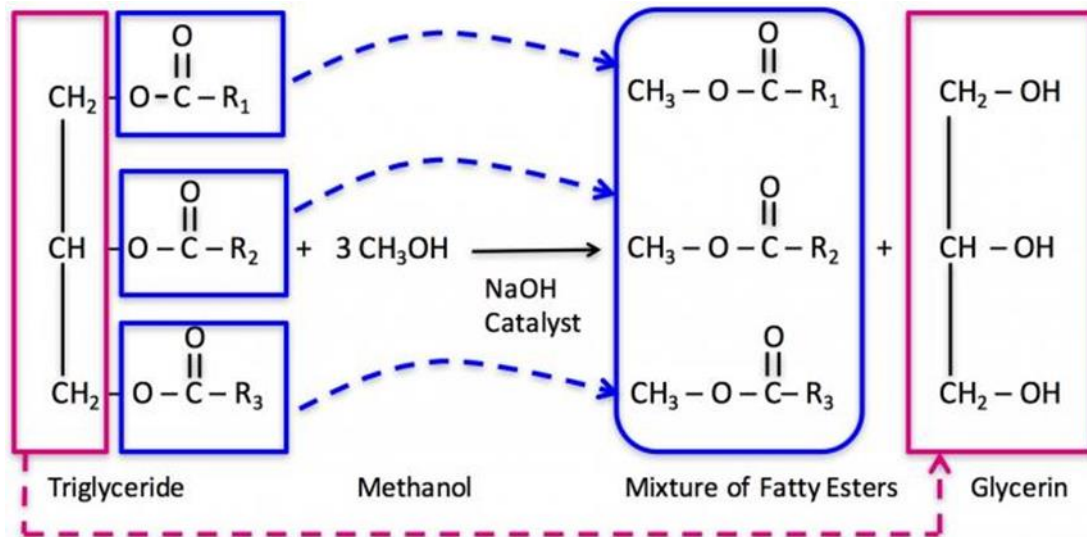


Figure 1-11: Conversion of triglycerides into glycerol and fatty acid alkyl esters by transesterification.⁷³

There are several factors, which affect the displacement of the equilibria:

- The molar alcohol to TG ratio. A greater alcohol concentration results in a more thorough transesterification process.^{74,75} Methanol is one of the most widely utilized alcohols because it is inexpensive, produced fatty acid methyl esters (FAME), and may be bio-sourced. 1-butanol or ethanol are also used.⁷⁶
- The presence of an acid or an alkali catalyst in the solution. Alkaline compounds (sodium methoxide and sodium hydroxide)^{75,77,78} are more active and contribute significantly to lowering corrosion issues.^{75,79} Sulfuric, phosphoric and hydrochloric acids^{75,78} are better suited for fats with a high concentration of free fatty acids FFA (frying oil, for instance).⁸⁰
- Because it combines with the various esters to create FFA, water concentration has to be low in the treated HVO.^{75,77,80,81}
- The addition of tetrahydrofuran speed up the reaction.⁸²
- The temperature and reaction time affect the reaction yield.^{75,77,83}

Traditionally low temperatures, and very effective catalysts (bases or strong acids) are used. Homogeneous catalysis ultimately requires the removal of acid or alkaline catalyst. Therefore, heterogeneous catalysis is preferred.

The heterogeneous catalyst

This kind of catalyst has the advantage of being simple to remove and recycle. They are supported on alumina, zirconia, or activated carbon surfaces.^{84–86}

Heterogeneous acid catalysts are utilized to convert vegetable oils with a high FFA concentration. The simultaneous esterification of the FFA and transesterification of the TG (yield of 77%) occur.⁸⁷ When FFA is present, alkali-catalyzed transesterification results in the creation of soap, which alter the catalyst. If such a catalyst is used, FFA must be eliminated before transesterification reaction.⁸⁸

1.4.1.3. Conclusion

Despite its reduced carbon impact, first-generation biofuels are not sustainable. In reality, several issues relating to their production interfere with their sustainability. Indeed, their production requires edible feedstocks with a dedicated crop (use of fertilizers, phytosanitary treatments, and large agricultural areas often the result of deforestation) and competes with human and animal food. Therefore, second- and third-generation biofuels have been developed.⁸⁹

1.4.2. Third generation biofuels

Micro and macro oil-rich algae are the primary sources of third-generation biofuels, offering the advantages of not competing with animal and human food and having the ability to grow quickly and reproduce in harsh conditions.⁹⁰ This biofuel is the latest and is still under development.⁹¹

Solar energy, water, and large concentrations of CO₂ ensure the growth of algae, which present the benefit to can trap the carbon dioxide emitted by power plants and industries, and thus reduces the carbon footprint of the human activities.⁹⁰

TG and cellulose are present in significant quantities in algae. The TG is transformed into biodiesel by a transesterification reaction, while the cellulose will be transformed into bioethanol through enzymatic and acidic hydrolysis followed by fermentation reactions (Figure 1-12).^{92–94} Microalgae may also go through a variety of thermochemical processes to yield biofuel.⁹⁰

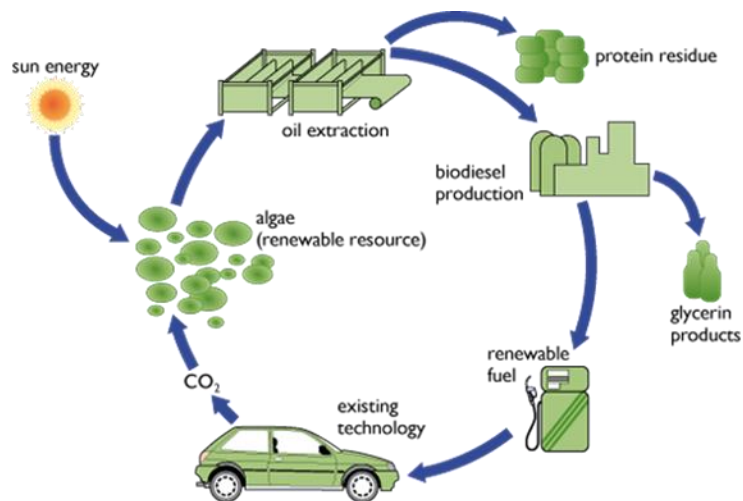


Figure 1-12: Biofuels from microalgae.⁹⁵

1.4.3. Second generation biofuels

1.4.3.1. Advantages

The production of second-generation biofuel relies solely on the use of agricultural waste and inedible plant components. As previously indicated, biomass is separated into two parts: a small portion that is used for animal and human food, and a large portion (10^{11} tons) that may be considered waste, which can be used to produce high-added-value compounds.⁹⁶ Thus, different non-food crops and agricultural byproducts, including cereal straw, wheat stalk, corn, and wood, are frequently used (Figure 1-13) as feedstock to produce bio-oil.^{97–99} Similarly, liquid biofuels may be produced from wood shavings.^{100,101} Because of their rapid growth, some plants that are of significant interest. The poplar, commonly known as eucalyptus (short rotation forest crops), and the perennial grass.

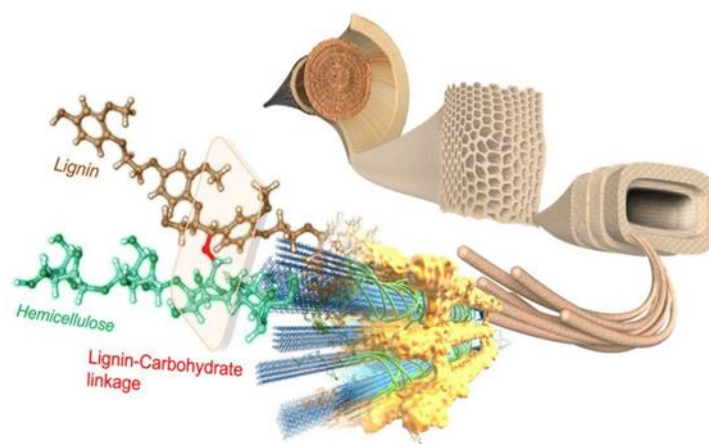


Figure 1-13: Lignin, cellulose, and hemicellulose are graphically represented in a plant cell.¹⁰⁶

"Miscanthus" is another interesting example.^{102–104} The miscanthus has the advantage of being cultivated on abandoned industrial land and therefore not compete with agricultural fields.¹⁰⁵ Compared to the first-generation biofuels, it is the whole plant that is used as feedstock. Additionally, ethanol made from wheat or beet only decreases CO₂ levels by 60% compared to conventional oil, whereas cellulosic ethanol (generated from grasses, wood, algae, etc.) generates 75% less CO₂.^{51,89}

Since they do not compete with food or animal feed, these feedstocks do not raise ethical concerns. In addition, they are greener than first-generation biofuels. Both phytosanitary measures and fertilizer are not necessary. They are affordable materials from an economic standpoint. Therefore, it may be said that these biofuels are more eco sustainable than those of the first generation.^{51,89}

Due to the fact that this second generation of biofuels is produced using lignocellulosic sources, which are plant-based and not food-related, an issue with the first generation has been resolved. Cellulose, hemicellulose, and lignin are all present in significant amounts in this source.

1.4.3.2. Biomass conversion

Lignocellulosic biomass contains (Table 1-2) cellulose which is insoluble in water, hemicellulose and lignin which form a protective envelope around cellulose, protecting it from enzymatic attack.

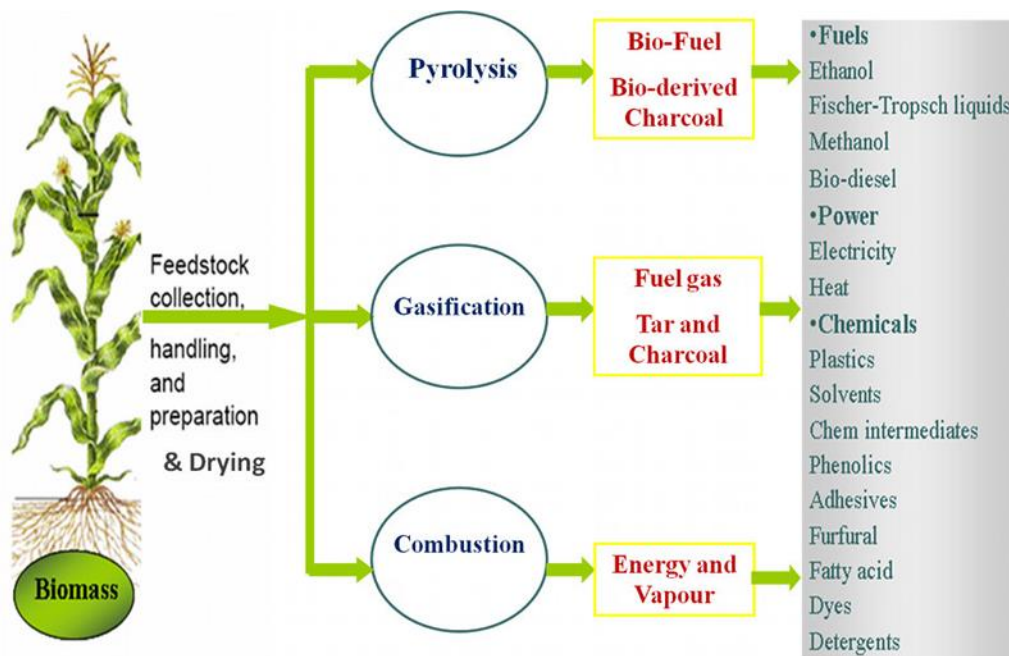


Figure 1-14: Technologies for thermochemical conversion of biomass.¹⁰⁷

Therefore, in order to transform this type of biomass, it is required to submit it to severe treatments. Conversion is the name given to these processes (Figure 1-14). The two distinct paths are as follows¹⁰⁸:

- Route 1 is a biochemical processing via catalytic hydrolysis and fermentation of certain biomass constituents.
- Route 2 involves thermochemical treatment, in which the biomass is heated and transformed into a wide variety of products. These conversion processes include pyrolysis, liquefaction, and gasification.

From the pyrolysis and liquefaction of biomass, two distinct products are generated: refined products like bioethanol and biodiesel, and unrefined products like bio-oils. Several conversion procedures will be in-depth described in following paragraphs, with an emphasis on the biomass-to-liquid (BTL) procedures.

Table 1-2: Typical component analysis of some plant biomass samples.^{109,110}

Lignocellulosic Biomass	% Cellulose	% Hemicellulose	% Lignin
Sugare cane bagasse	42	25	20
Hardwood	40-55	24-40	18-25
Softwood	45-50	25-35	25-35
Rice straw	32	24	18
Wheat Straw	29-35	26-32	16-21
Banana waste	13	~15	14
Corn cobs	45	35	15

1.4.3.3. Biochemical treatment

The use of the two primary procedures—enzymatic hydrolysis and fermentation—enables the conversion of polysaccharides, or "starch" from lignocellulosic biomass into second generation bioethanol. Despite being more complicated, this procedure is similar to the first-generation bioethanol production. The separation of the different lignocellulosic biomass components (cellulose from hemicellulose and lignin) also necessitates a pretreatment step.^{111,112,113}

1.4.3.4. Thermochemical Treatment

Gasification

Gasification, a thermochemical process that belongs to the gas-to-liquid processes, is the conversion of the biomass by heating at temperatures between 850 and 1100°C in the presence of air or water vapor. Synthesis gas, commonly known as "syngas," is a combination of CO, H₂, CO₂, CH₄, and N₂ (Figure 1-15). For its use in diesel and gasoline engines, Fischer-Tropsch synthesis transforms it into hydrocarbons.^{114–116} Drying, pyrolysis, oxidation, and carbon reduction are the four fundamental phases in the gasification process. Nevertheless, this conversion present advantages and drawbacks:

- The benefit of this technique is that it does not rely on the type of feedstock.
- The primary limitations of this approach are the sensitivity of the gasification processes to the water present in the biomass and to the contaminants present in the generated biogas.¹¹⁷

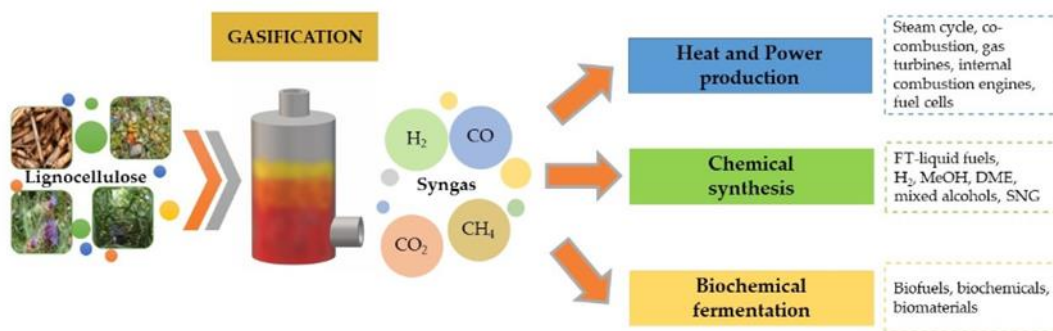


Figure 1-15: Process of gasifying biomass and the ultimate use of syngas are shown schematically.¹¹⁸

Pyrolysis

Pyrolysis consists of heating biomass with low moisture content (<10%), at moderate temperatures in an inert environment, in the absence of oxygen, at a small residence time and at a pressure ranging from 1 to 5 atm. And so, the biomass will be broken down into different phases depending on the operating parameters:

1. Solid: biochar or charcoal,
2. Liquid: bio-oil,
3. Gas: syngas.

Table 1-3: Methods of pyrolysis and its main characteristics.¹¹⁹⁻¹²³

Pyrolysis type	Temperature °C	Heating	Residence Time (s)	Feedstock size
Slow	300-700	Low	300-1800	Massive
Flash	600-1000	Very High	Few seconds	Very Fine <0,2 mm
Fast		High	0,5-10	Fine <1 mm

Specifically, the biomass pyrolysis generates vapors containing thousands of compounds that are condensed by cooling and gives the so-called bio-oil.¹²⁴

Table 1-13 shows the dependence of the distribution of the pyrolysis products in respect with the heating rate and the residence time.^{119,120,125,126}

Fast pyrolysis

Due to the extremely rapid heating and heat transfer rates of this form of pyrolysis, it is feasible to treat very dry biomass (humidity level <10%) and finely powdered biomass with a diameter ranging from 0.5 to 5 millimeters. This pyrolysis is conducted with a residence period of a few seconds at a low temperature of 500 ° C.

In order to produce pyrolysis oil (70 to 80 wt%), the steam must be quickly cooled. Charcoal (15-25 wt%) and incondensable gas (10-20 wt%) are two by-products.^{123,127-129}

Slow pyrolysis

Often known as carbonization or ordinary pyrolysis, this kind of pyrolysis occurs over a long period of time at a temperature of 500 °C and a slow heating rate 10 °C/s. It is called "carbonization" because at the reactor's level, the vapors that are produced do not quickly escape, allowing the compounds to interact and form carbonized compounds, ultimately charcoal (30–50 wt%). The weight percentages of bio-oil and gas are 35-50 and 10-30, respectively.¹³⁰⁻¹³³

Flash pyrolysis

The majority of bio-oil production processes uses flash pyrolysis. As a result, high temperatures are used to heat the biomass in the absence of air during a few seconds.¹³⁴ After condensation, a bio-oil is produced.

The following factors affect necessary the yield of bio-oil production:^{134,135}

1. A temperature carefully regulated to be below 500 ° C to reduce the amount of coal produced,
2. A minimal contact time,
3. An excellent coefficient of heat transmission,
4. A quick cooling of the pyrolysis vapor,

As the temperature increases, the proportion of biochar decreases while the amounts of gas increases. In general, 475 °C is the ideal temperature for producing the most bio-oil and avoid secondary cracking. With an increase in pyrolysis temperature, the production of bio-oil drops. Up to 70% of the biomass can be turned into bio-oil under ideal conditions.^{134–136}

Interaction between pyrolysis product

Interactions between the biomass components and the pyrolysis products that are formed throughout the heating process are unavoidable and are both present regardless the type of used pyrolysis (Figure 1-16).¹³⁷ For instance, when volatile products from cellulose interact with tar and char from lignin, the production of tar from cellulose and lignin as well as the yield of gaseous products increases, while the yield of char from cellulose and lignin decreases. The yield of levoglucosan, and the composition of pyrolysis products are affected by the presence of hemicelluloses as well as by the inorganics in the biomass.¹³⁸

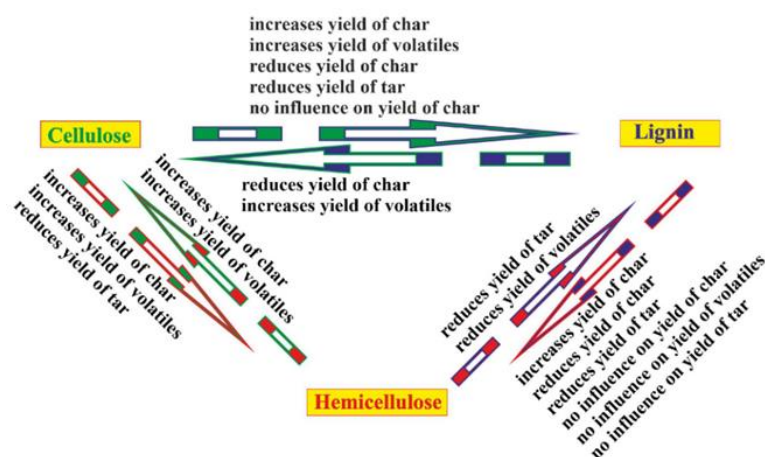


Figure 1-16: Impact of the interactions between the constituents of basic biomass on the yield of pyrolysis products.¹³⁸

Composition of the bio-oil obtained from the pyrolysis of lignocellulosic biomass.

The conversion of lignocellulosic biomass by pyrolysis leads to the formation of bio-oil which are essentially formed by the pyrolysis products of lignin, cellulose and hemicellulose. The decomposition of hemicelluloses occurs between 200 and 300 ° C, cellulose between 300 and 400 ° C and that of lignin in a wider range, between 250 and 500 ° C. The figures 1-17, 1-18 and 1-19 report the main products formed by the pyrolysis of lignin, cellulose and hemicellulose, respectively. The composition of bio-oil obtained from the pyrolysis of lignocellulosic biomass can vary depending on several factors such as the type of biomass, pyrolysis conditions, and the specific pyrolysis process used. However, bio-oil typically consists of a complex mixture of organic compounds, including the following components:

Lignin-derived compounds commonly found in bio-oil include (Figure 1-17)¹³⁹:

- Phenols: Bio-oil often contains various phenolic compounds derived from lignin, such as guaiacol, syringol, and catechol. These compounds contribute to the characteristic aroma and flavor of bio-oil.
- Furanic compounds: Bio-oil may contain furanic compounds like furfural and hydroxymethylfurfural (HMF). These compounds can be produced during the pyrolysis process of lignin.
- Methoxyphenols: Lignin-derived methoxyphenols, such as eugenol and vanillin, are commonly present in bio-oil. They give a distinct scent and can have potential applications in flavoring and fragrance industries.
- Polyaromatic hydrocarbons (PAHs): PAHs can form during the pyrolysis of lignin and are often found in bio-oil. PAHs are a class of organic compounds with multiple aromatic rings and can have implications for environmental and health considerations.

Cellulose-derived compounds commonly found in bio-oil include (Figure 1-18)¹³⁹:

- Levoglucosan: It is one of the most abundant cellulose-derived compounds in bio-oil. Levoglucosan is a cyclic molecule formed during the pyrolysis of cellulose and serves as a marker compound for cellulose degradation.
- Anhydro-sugars: Bio-oil often contains anhydro-sugar compounds like anhydroglucose, anhydromannose, and anhydroxylose. These compounds are formed when the cellulose molecules undergo dehydration during pyrolysis.
- Furans: Cellulose pyrolysis also produces furanic compounds in bio-oil, including 5-hydroxymethylfurfural (HMF) and furfural. These furans contribute to the overall composition and properties of the bio-oil.
- Acids: Bio-oil derived from cellulose may contain organic acids such as formic acid, acetic acid, and levulinic acid. These acids can be formed as a result of cellulose degradation and contribute to the acidity of the bio-oil.

Hemicellulose-derived compounds commonly found in bio-oil include (Figure 1-19)¹³⁹:

- **Xylose:** Xylose is a sugar derived from hemicellulose and is often present in bio-oil. It can be used as a precursor for the production of various chemicals and fuels.
- **Furanic compounds:** Similar to cellulose, hemicellulose pyrolysis produces furanic compounds in bio-oil. These include furfural and its derivatives, which contribute to the overall composition and characteristics of the bio-oil.
- **Acids:** Hemicellulose degradation during pyrolysis can yield organic acids like acetic acid, formic acid, and levulinic acid. These acids are commonly found in bio-oil derived from hemicellulosic feedstocks.
- **Sugar derivatives:** Hemicellulose-derived bio-oil may contain other sugar derivatives such as arabinose, galactose, and mannose. These compounds can serve as valuable feedstocks for various chemical processes.

It's important to note that the composition of bio-oil can vary depending on the feedstock and the specific pyrolysis conditions used, so for example, the exact lignin-derived products may vary from one bio-oil sample to another. The exact composition and distribution of these components can vary depending on the specific feedstock used, the pyrolysis process conditions (temperature, heating rate, residence time, etc.), and any subsequent treatments applied to the bio-oil. Analytical techniques such as gas chromatography-mass spectrometry (GC-MS) are commonly used to determine the precise composition of bio-oil samples.

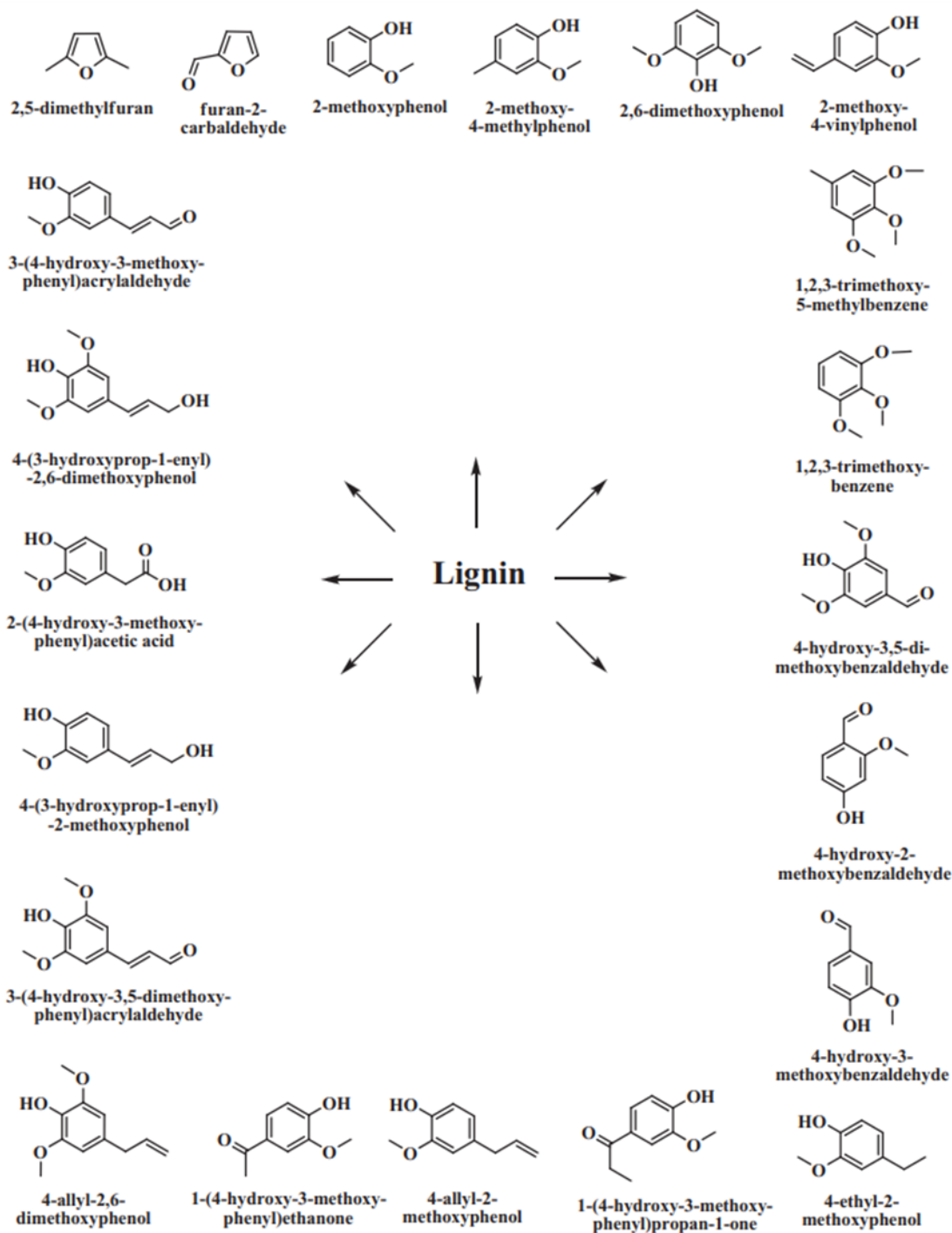


Figure 1-17: Main products obtained from lignin pyrolysis.¹³⁹

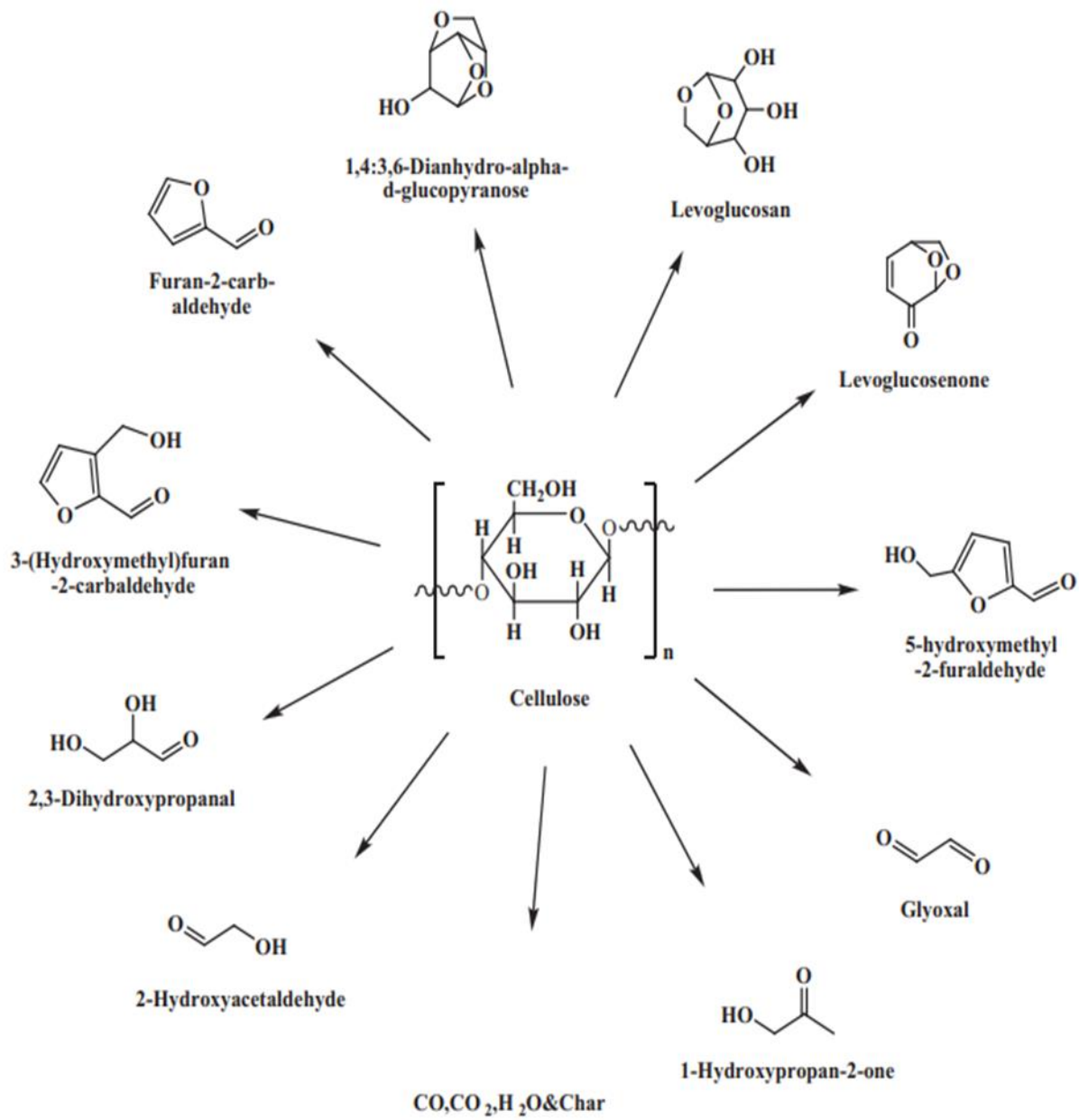


Figure 1-18: Main products obtained from cellulose pyrolysis.¹³⁹

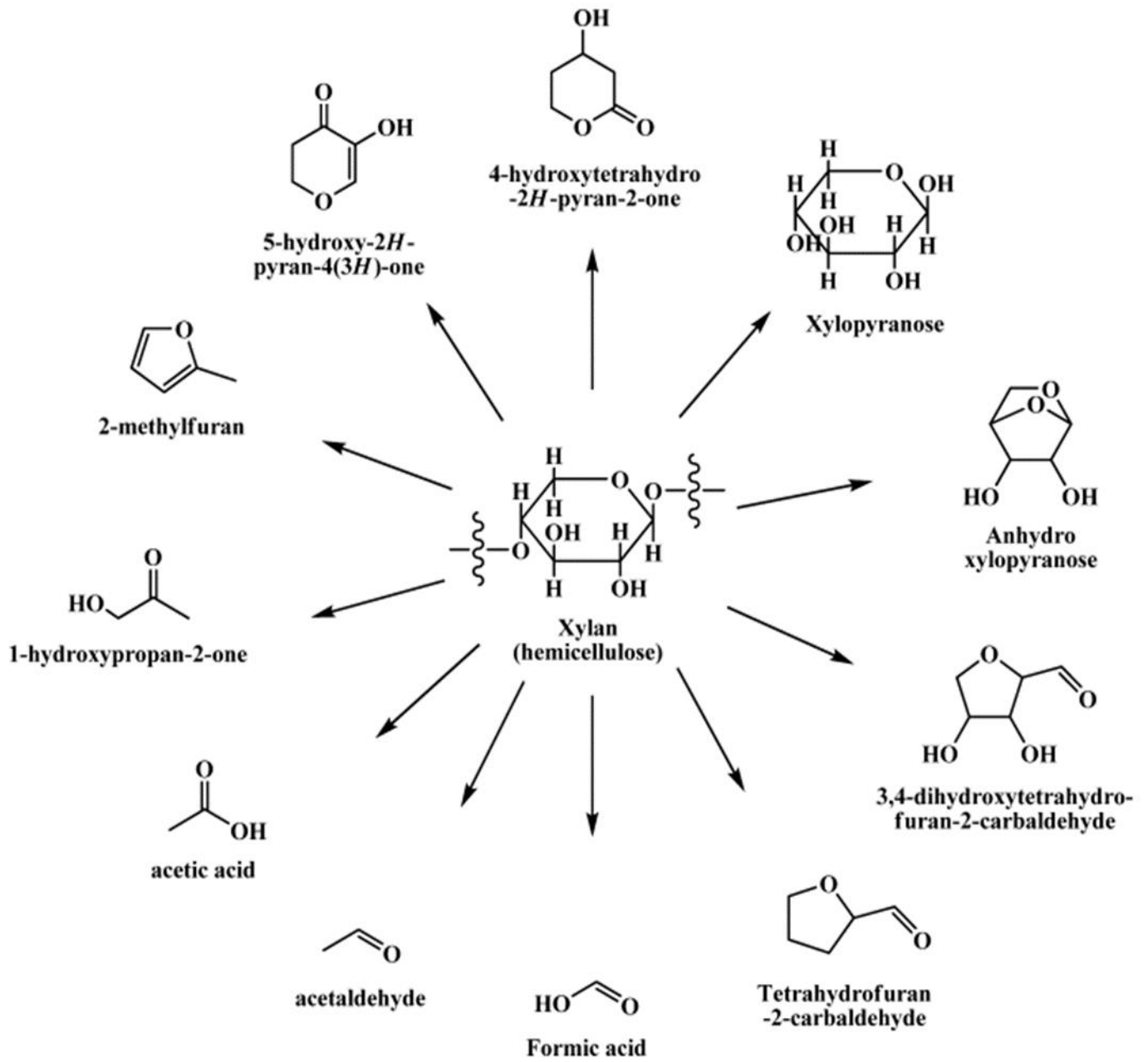


Figure 1-19: Main products obtained from hemicellulose pyrolysis.¹³⁹

1.4.3.4.1. Liquefaction

Liquefaction (Figure 1-20) requires a temperature of 200 to 450 °C, a very high pressure of 5 to 30 MPa (expensive system), and a time period ranging from 30 minutes to four hours.^{140,141} Compared to pyrolysis, the biomass not required to be dried.^{142,143}

Depending on the nature of the medium, there are three different liquefaction processes:

1. **Hydropyrolysis** (without a liquid solvent). This process involves heating lignocellulosic biomass in a reactor vessel containing H₂, at a high pressure, and in presence of a solid catalyst, which ensures deoxygenation reaction.^{144,145}
2. **Hydrothermal liquefaction (HTL)** happens when a solvent under supercritical or subcritical condition is in contact with biomass. Physical and chemical changes occur, which lead to the production of a liquid.^{142,146} Due to its low cost, high availability, minimal hazard, and low toxicity, water is the most widely utilized solvent. HTL can convert both wet and dry biomass.
3. **Solvolyis**: this process result from reaction between the lignocellulosic raw molecules and a reactive solvent as ethanol or acetone.^{147,148}

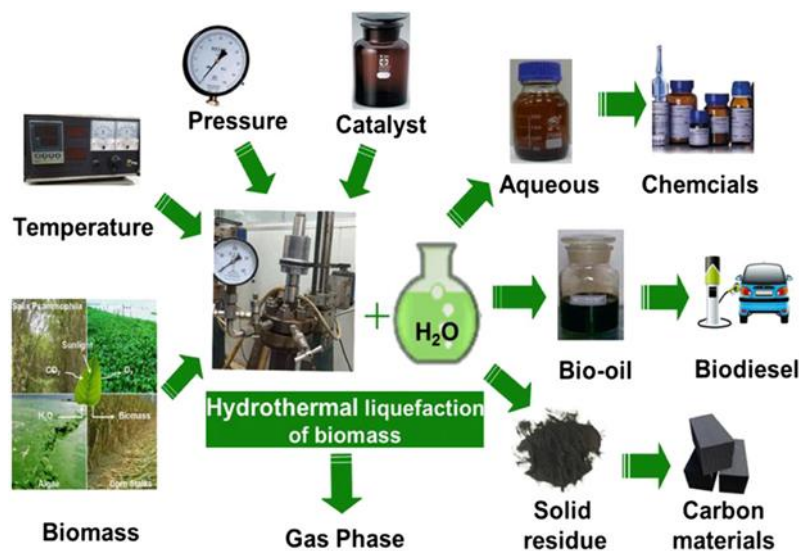


Figure 1-20: Liquefaction of biomass by hydrothermal processes.¹⁴⁹

The components of the biomass are first hydrolyzed into monomers and undergo dehydration, dehydrogenation, decarbonylation, or decarboxylation.^{150,151}

Depending on the liquefaction method employed, the yield of the final products varies. Like all other conversion processes, the liquefaction typically produces three different types of compounds: bio-oils with a weight percentage of about 75% (with a little quantity of water), biochar (solid residue), and biogas with a weight percentage of around 10–20% each.^{152–154}

Different factors affect the effectiveness of the liquefaction process.^{152,155,156} Temperatures above 250–350 °C lead to an increase of gas and char production. Another crucial parameter is the residence time. The production of bio-oil decreases at high retention duration. The nature of the solvent and the used pressure also affect the yield of conversion and the relative distribution of gas, liquid and char. The liquefaction products are stabilized, and the yield of bio-oil is increased by using reducing gases (H₂ and CO). The yield of the cellulose and hemicellulose hydrolysis is increased by homogeneous catalysis using alkali salts like sodium or potassium carbonate.^{156,157}

1.4.4. Biofuel technologies and sustainable development – Final comments

The second-generation biofuels offer a number of benefits in terms of feedstock and effects on the economy and the environment.^{89,158} Their production don't need extraction pretreatment, unlike the biochemical method. This has an advantage on lowering the price of bio-oil production.

Gasification, pyrolysis, or liquefaction are the three main way of biomass conversion to produce biofuels regardless of the employed feedstock.¹⁵⁹ The fast pyrolysis technique is the least expensive.¹⁶⁰ The primary outcome of the pyrolysis process is bio-oil. Many kinds of study are presently being conducted all over the world to maximize and enhance the quantity and quality of bio-oil generated. Researchers' focus is on reactor designs to produce bio-oils of a higher grade. The bio-oil products (Figure 1-20) have a variety of employment. They may use, after up-grading processes, as chemicals, transportation fuels or to produce energy and heat.¹⁶¹

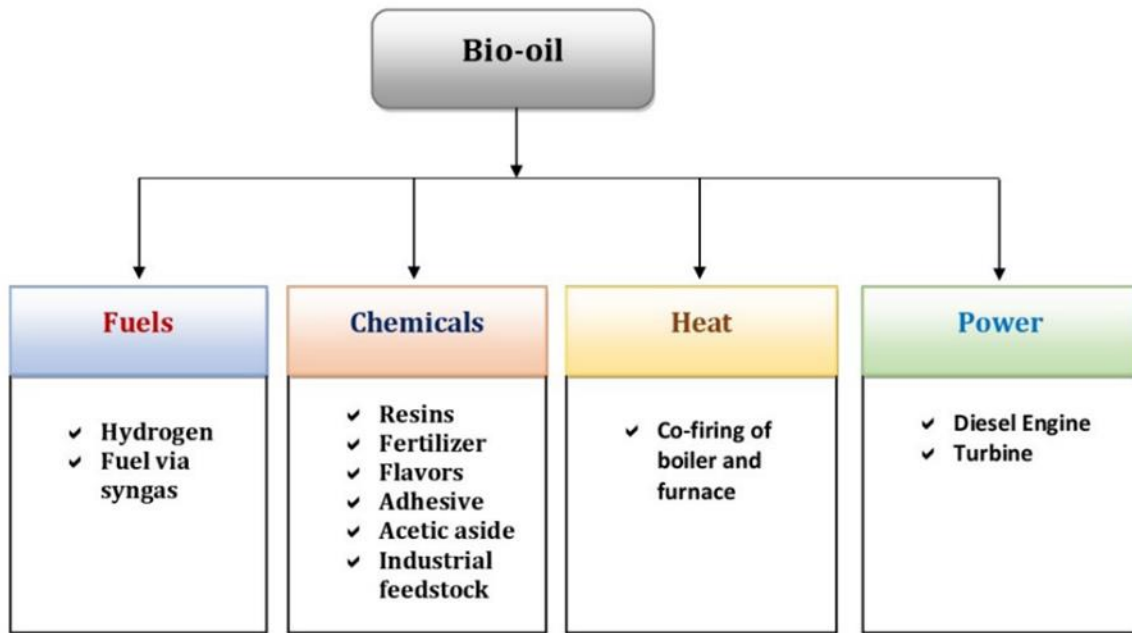


Figure 1-21: Pyrolysis bio-oil applications.¹⁶¹

The isolation of some desired molecules is mainly ensured by liquid-liquid fractionation techniques. Depending on how soluble they are in water, the bio-oils can be fractionated to access different components. Due to their organoleptic qualities, several aldehydes and phenolic compounds from the bio-oil aqueous fraction are employed in the food industry.¹⁶² Different lignin derivatives (water-insoluble fraction) may be utilized in polymer chemistry to produce resin. Levoglucosan, a product of cellulose's heat degradation, may be converted into drugs, polymers, and surfactants.¹⁶³

In conclusion, the bio-oil product offers a wide range of uses and merits significant research investment.

1.4.5. Bio-oils properties

1.4.5.1. Physicochemical properties

As detailed in previous section, the bio-oils may be produced by extraction and conversion of the lipids from algae, by thermal activation (pyrolysis) or hydrothermal liquefaction (HTL) of lignocellulosic biomass and algae¹⁶⁴. These materials are very complex organic matrices. Independently of the fuel origin, crude oil or biomass, all these matrices require different upgrading treatments in order to be suitable for engines, with the appropriate physicochemical properties. Indeed, as shown in Table

1-4, second (2G) and third (3G) generation bio-oils obtained from the thermochemical conversion of biomass present higher oxygen amount than crude oils, which is notably responsible for lower energetic density.^{165–168}

Table 1-4: Typical physicochemical properties of heavy, 2G pyrolysis, 2G liquefaction, and 3G oil.^{165–167}

Properties	Heavy oil	Pyrolysis bio-oil		Liquefaction oil (corn straw, 2G)	Pyrolysis of Aegle marmelos (3G)
		Wood (2G)	Straw (2G)		
<i>C</i>	85	54-58	48.9	44.57	40.0
<i>H</i>	11	5.5-7.0	6.5	5.53	6.1
<i>O</i>	1	35-40	42.6	33.70	52.3
<i>N</i>	0.3	0-0.02	1.1	0.93	1.5
<i>S</i>	1.0-1.8	0.0-0.02	0.0-0.06	0.10	0.0005
<i>Ash</i>	0.1	0-0.2	5.5	7	2.2
Water content, wt. %	0.1	15-30	6.5	7-15	3.0
pH	-	2.5	-	-	-
Viscosity, cP	180	40-100 (at 50 °C)	140	-	-
Higher heating value, MJ.kg⁻¹	40	16-19	18.0-23.3	16.96	20.2
Distillation residue, wt. %	1	up to 50	-	-	-
Solids, wt. %	1	0.2-1	-	-	-

1.4.5.1.1. Chemical composition of bio-oils from pyrolysis

The Table 1-5 lists the several chemical classes that make up a pyrolysis bio-oil. At least one oxygenated chemical function is found in the majority of the bio-oil components. These oxygenated organic compounds come in a variety of molecular weights and concentrations.

Table 1-5: Bio-oil's Chemical Composition.¹⁶⁹

Functional group	Bio-oil (wt, %)
Alcohol	3.97
Carboxylic acids	32.91
Phenol	18.24
Ester	7.10
Furan	6.17
Ketone	13.87
Olefins	4.62
Others (water, carbonyls, ethers...)	13.12

1.4.5.1.1.1. pH:

The total acid number (TAN) approach is used to assess the acidity of bio-oils. By using an acid-base titration, it may be calculated and is expressed as mg KOH/g of bio-oil.^{170–172} It was evidenced that the acids, whose pKa values are the lowest of all the bio-oil components, account for 60–70% of the acidity of fast pyrolysis bio-oils. Due to the high concentration of carboxylic acids, the bio-oil causes corrosiveness challenges and, as a result, storage difficulties.^{172,173}

Fatty and resin acids (5%), and phenolic compounds (5–10%) are two more classes of chemicals that also significantly affect the acidity of bio-oil. The "sugar" fraction's acidity, which is mostly caused by hydroxy acids, accounts for around 20% of the total acidity.

1.4.5.1.1.2. Water:

Water makes up a very minor portion of the weight. Both negative and beneficial impacts on the characteristics of the oil result from the presence of water. It is obvious that water reduces the heating value, extends ignition delay, and slows combustion rate. However, water enhances bio-oil flow properties (reduces oil viscosity), which is advantageous for combustion.¹⁷²

1.4.5.1.1.3. Aging:

A bio-oil is not thermodynamically stable.¹⁷⁴ As organic chemicals in bio-oil samples are stored, they can continue to interact to produce heavier molecules that can increase viscosity and water content (condensation reaction).¹⁷⁵ Indeed, water can be produced by etherification and esterification between components including hydroxyl, carbonyl, and carboxyl groups.^{172,176} Due to the instability of some compounds, polymerization reaction may occur (unsaturated bio-oil components). These reactions become more efficient as the temperature and duration increase and induce significant modification of the bio-oil properties.¹⁷⁵

1.4.5.1.2. Bio-oil from liquefaction

The liquefaction bio-oils have a greater energy density (HHV), a lower oxygen concentration, and a lower moisture content than pyrolysis bio-oils (Table 1-4) but a lower HHV and a greater oxygen concentration than traditional fuels. Such a bio-oil contains phenolic, carboxylic, aldehydic, ketonic, alcoholic, and nitrogen compound-based compounds that are insoluble in water.¹⁷⁷⁻¹⁸⁰ The aging also affects the composition and the properties of this type of bio-oil.^{178,180-182} Similar to pyrolysis bio-oil, some upgrading procedures utilizing heterogeneous catalysis are required to get rid of oxygen, minimize the TAN and viscosity, and raise the HHV.

1.4.5.2. Upgrading of the bio-oils

The presence of water, acids, and aldehydes in bio-oil is the primary cause of its poor quality, which results in bio-oil's low HHV, instability, and high corrosiveness.¹⁸³ The removal of water, acid, and unstable components can enhance the bio-oil's quality.¹⁸³ As a result, many physical and chemical processes have been used for improving bio-oil. In general, there are three basic ways to upgrade the pyrolysis bio-oil: physically, chemically, and catalytically. Three different physical

upgrading techniques are used and include emulsification,^{184–186} solvent extraction,¹⁸⁷ and supercritical fluids.^{188,189} Zeolite cracking^{190–193}, hydrodeoxygenation (HDO)^{194–197}, and steam reforming are examples of catalytic upgrading methods whereas esterification is mostly used for chemical upgrading. However, some treatments, such as hydro-pyrolysis and catalytic fast pyrolysis, could be carried out during the actual synthesis of bio-oil.^{198,199}

1.4.6. Conclusion

Renewable energy sources include biomass-derived biofuels. More specifically, second generation biofuels are eco-friendlier. To make liquid fuel from these feedstocks, thermochemical processes like liquefaction and pyrolysis are required. The bio-oil that was initially produced, however, cannot be used directly as motor vehicle fuel due to its physicochemical properties. As a result, specific upgrading methods have been developed. Among these, HDO and catalysis on zeolite shown the greatest abilities. Liquid with properties resembling those of petroleum is created by these catalytic processes.

A thorough description of the bio-oil is required to increase the bio-oil output and the catalyst efficiency. This might be accomplished by different analytical workflows. The final section of this chapter will outline the different strategies that might be used.

1.5. Bio-oil characterization using analytical methods

The final product of the biomass pyrolysis process is biomass crude oil, which is a dark brown, freely flowing liquid with a spicy or smoky odor.²⁰⁰ It is significant to remember that the depolymerization of cellulose, hemicellulose, and lignin produce a highly complex mixture of chemicals. It's necessary to have thorough understanding of many substances. The tens of thousands of species that constitute this material cover a wide variety of polarity and molecular weights. As a result, based on the class of the substances analyzed, several analytical techniques are employed. The next paragraphs will cover these complementary techniques primarily focused on sample preparation, chromatographic, and spectroscopic methods in the petroleomic field and their possible or still implemented applications to investigate bio-oils.

1.5.1. Nuclear magnetic resonance spectroscopy NMR: ^{19}F

Nuclear magnetic resonance spectroscopy takes advantage of the magnetic characteristics of certain atomic nuclei. This method is often used to analyze the composition of oil and the structural characterization of certain petroleum components. It is possible to differentiate and quantify aromatics and aliphatics by ^1H and ^{13}C NMR. Bio-oil components can be characterized using one-dimensional (1D) and two-dimensional (2D) NMR. Other nuclei like ^{19}F can also be used.

It is effective to characterize carbonyl functional groups using ^{19}F NMR. Aldehydes and ketones are derivatized with 4-(trifluoromethyl) phenylhydrazine before NMR analysis (Figure 1-22) to be quantified, and consequently to evaluate the effectiveness of the different bio-oil upgrading processes. This method was employed by Huang *et al.*²⁰¹

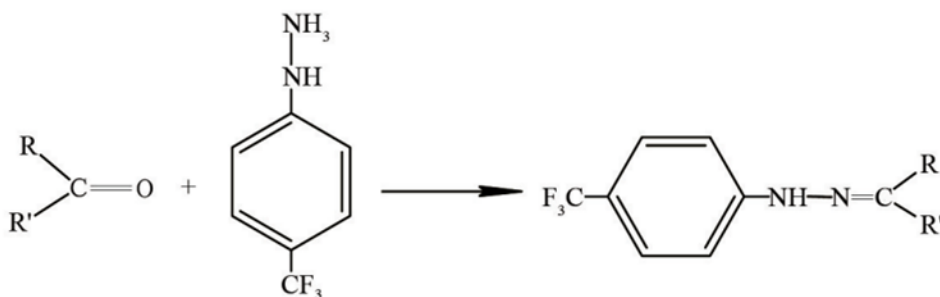


Figure 1-22: 4-(trifluoromethyl)phenylhydrazine used for the derivatization of carbonyl group.²⁰²

The same protocol was recently used by Mondal *et al.* to measure the carbonyl functional groups in pyrolysis oil with and without the use of zeolites as a catalyst and evaluated the up-grading efficiency.

The ^{19}F NMR not only made it possible to quantify the carbonyl functional group but also to investigate the effect of adding ethanol in HTL process on hydroxylated and carbonyl compounds. According to ^{19}F NMR results, adding ethanol had a considerable impact on the bio-oils' total hydroxyl and carbonyl concentrations. The addition of ethanol was observed to enhance the total hydroxyl number (OHN) and aliphatic type OH, while decreasing the concentration of phenolic OH. A decrease in carbonyl content was also evidenced.²⁰³

1.5.2. *Petroleomic approach*

1.5.2.1. *Introduction*

One of the main preferred characterization ways of complex mixture is high resolution mass spectrometry (HRMS), which, in application to the non-targeted analysis of petroleum, is called petroleomics. HRMS instruments comprise Q-TOF, Orbitrap, and Fourier transform ion cyclotron resonance mass spectrometer (FT-ICR MS), whose capabilities are described in chapter II. Both Orbitrap and FT-ICR analyzers are Fourier Transform Mass Spectrometry (FTMS) instruments.²⁰⁴ Alan Marshall is a pioneer in petroleum analysis by HRMS and, more specifically, by Fourier transform ion cyclotron resonance mass spectrometry (FT-ICR MS). In association with Ryan Rodgers, he coined the term “petroleomics” to determine petroleum properties and behavior based on description of all detected petroleum components at the molecular level^{205,206}. Nowadays, this non-targeted approach is also applied to bio-oils.²⁰⁷

Due to the high molecular complexity of crude oil and bio-oil samples, HRMS is required with or without using an upstream separative method, such as chromatography. Petroleomic studies and principles regarding crude oil and bio-oils were reported in different recently-published reviews^{208–215}. The high mass resolution and accuracy (Figure 1-23 A, B) allow the technique, respectively, to detect and assign hundreds of thousands of molecular formulae. As an example, atmospheric pressure photo-ionization (APPI) FT-ICR MS analysis of a volcanic asphalt sample demonstrated the ability to assign more than 126,000 chemical formulae.²¹⁶ The great amount of generated data requires a graphical representation to facilitate both the sample description and its comparison with another investigated sample. As illustrated in Figure 1-23 C, the molecular assignments can be represented according to the heteroatom class (CH, CHO, CHON...), the double bond equivalent number (DBE) (i.e., the number of unsaturation, vs. the carbon number), and also on the van Krevelen diagram. This latter graph was historically used for coal, petroleum, and kerogen samples but it is now applied to a large range of matrices.^{217,218} For instance, the H/C vs. O/C van Krevelen diagram allows the distinguishing of chemical families such as lipids, unsaturated hydrocarbons, phenolics, and carbohydrates.²¹⁷ This diagram represents the different compounds by dots whose x and y coordinates are the ratios O/C and H/C, respectively. Thus, lipids are characterized by low O/C ratio and H/C ratio close to 2, carbohydrate derivatives by high O/C and H/C ratios, and lignin pyrolytic products by H/C value close to 1 and O/C ratio in the 0.2 to 0.6 range. For compounds

containing nitrogen and/or sulfur atoms, N/C and S/C ratios can also be used to draw similar diagrams.²¹⁹ Regarding Kendrick's maps, the method consists of using the mass defects in modifying the mass scale by taking, for example, CH₂ as the new mass scale reference.

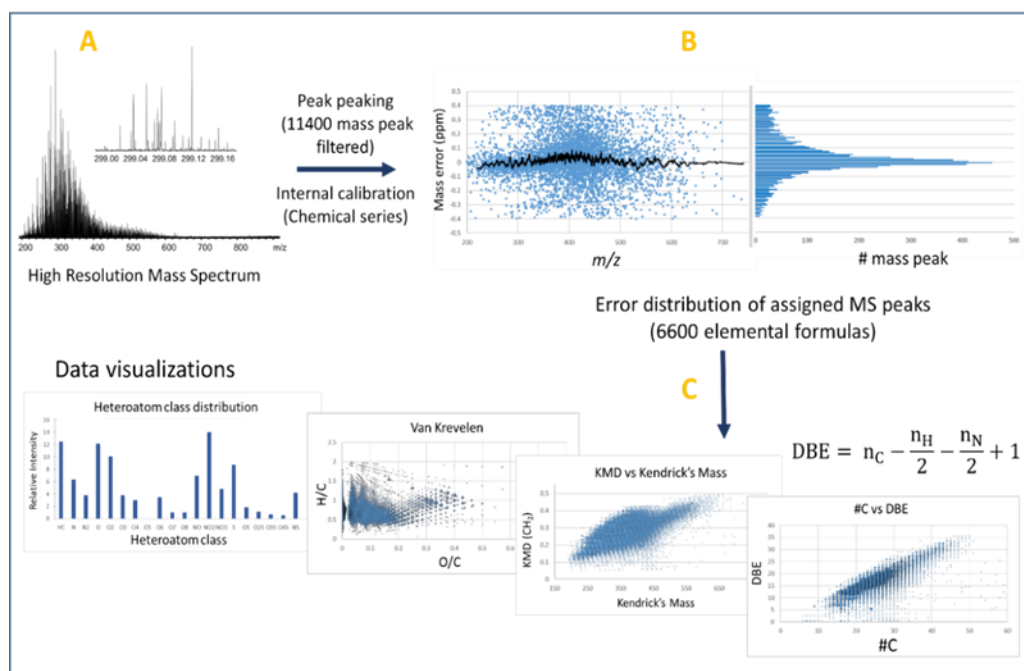


Figure 1-23: Typical petroleomic workflow: (A) acquisition of mass spectrum in high resolution mode (here LDI of coal-type sample); (B) distribution of mass measurement errors of assigned peaks after internal calibration of HR mass spectrum—the histogram is used to verify the normality of the error distribution; and (C) description of sample composition by various visualization tools.

Each signal associated with this new so-called Kendrick mass (KM(CH₂)) is plotted as a function of its Kendrick mass defect relative to its nominal mass. Thus, compounds differing by one or more CH₂ units have the same Kendrick mass defect (Figure 1-23 C), so they all line up on a horizontal line.²²⁰ Such graphs were helpful to follow-up oil or bio-oil upgrading treatment (elimination of oxygen, nitrogen, or sulfur by hydrotreatment or cracking).^{221,222} As reported in the different reviews^{208–215}, most of the HRMS analyses are performed in direct infusion (DI) mode, which may be responsible for ion suppression phenomenon,²²³ especially in electrospray ionization mode. In addition, the majority of the analyses are carried out by FT-ICR MS due to its greatest capabilities in terms of resolution power and mass accuracy measurement (Table 1-6).²²⁴ The petroleomic approach, in DI mode, shows some limitations, as only the isobaric level is well described whereas quantitative, isomeric, chemical functions, and structural information is missing. Although only a small number of research

Chapter I – State of the Art

projects, mostly in the petroleum industry, have been reported, it has been demonstrated that these various characteristics are important for understanding catalytic treatments.^{225,226} New analytical methodologies are needed, and some of them are already under development, to achieve a more complete molecular description of bio-oils (Figure 1-24).

Table 1-6: Performances of several HRMS instruments (manufacturer's specification sheet). An asterisk (*) indicates maximum resolving power (the resolution decreases as the acquisition measurement rate increases). (ND: No Data.)

Instrument	Resolution	Error (ppm, Internal Calibration)	Sensitivity (ESI)	Typical Measurement rate	Mass Range (m/z)	Instrument Model
Orbitrap	1 M * at m/z200	<1 ppm	100 fg reserpine (S/N: 100:1)	1 Hz	50–8000	Eclipse tribrid ThermoFisher Scientific
FTICR	>20 M * at m/z400	<600 ppb	100 amol Ubiquitin (S/N > 20:1)	0.5 Hz	100–10,000	7 Tesla 2XR Bruker
Q-TOF	60 000 at m/z1222	<800 ppb	100 fg reserpine (S/N: 100:1)	50 Hz	20–40,000	Impact II Bruker
timsTOF	60,000 at m/z1222	<800 ppb	100 fg reserpine (S/N: 100:1)	50 Hz	20– 20,000	timsTOF Pro 2 Bruker
Q-Tof MRT	>200,000	<500 ppb	ND	10 Hz	50– 3000	Select Series MRT Waters

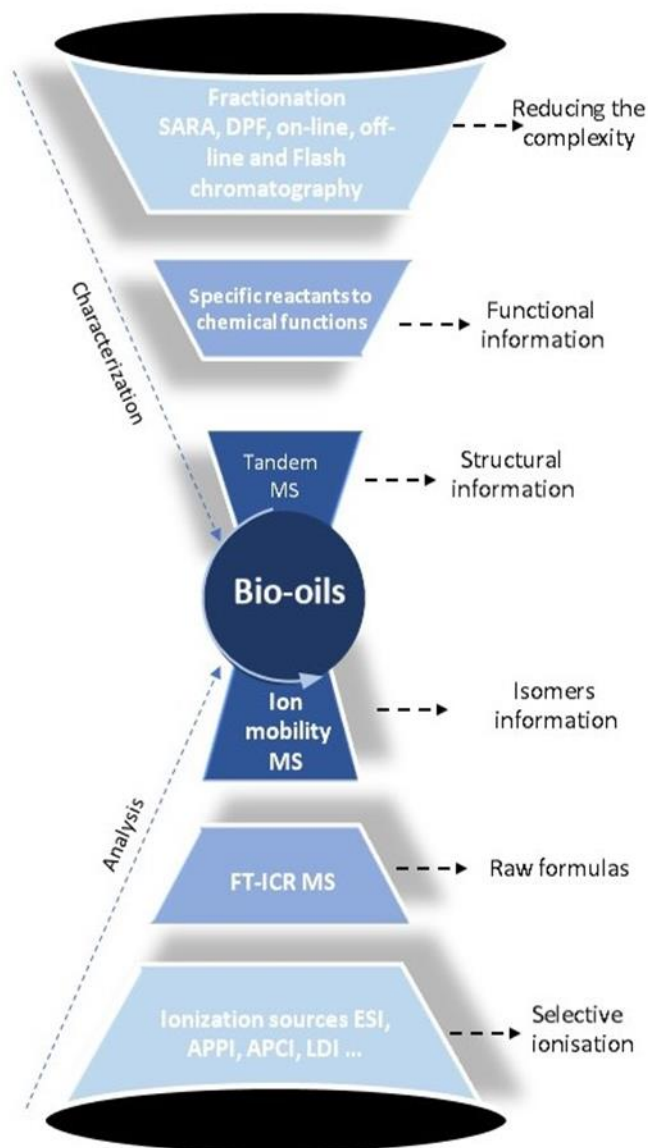


Figure 1-24: New methodologies in petroleomics that contribute to the chemical characterization of bio-oil at the molecular level.

1.5.2.2. Ion sources used in petroleomics and relation with the compound properties

Several ion sources are commonly used to study oil and bio-oil samples by HRMS: electrospray ionization (ESI), atmospheric pressure chemical ionization (APCI) and photoionization (APPI) and, laser desorption/ionization (LDI).^{227,228} The specificities of each of these ionization sources led to suggest the potential functional characteristics of the detected compounds, which provide additional information.

1.5.2.2.1. Electrospray ionization: ESI

ESI is the main ionization source in petroleomics^{206,207,216} and it can be operated in positive or negative mode. It is mainly used to ionize and detect polar compounds. In positive-ion mode, basic compounds are specifically detected, especially using acids (formic acid, acetic acid) as additives²²⁹ to promote the formation of protonated molecular ions $[M+H]^+$. The negative detection mode is more adapted to the detection of acidic or neutral species by deprotonation using dopants as ammonium hydroxide to form $[M-H]^-$ ions.^{207,223,230,231}

Other additives could also be used to enhance the ionization. Hertzog et al. used sodium acetate (AcONa) to promote the cationization of carbohydrate-like compounds (molecules containing a great oxygen content >5) in Miscanthus pyrolysis bio-oils by Lewis's acid-base reaction between Na^+ and the lone pair of the oxygen atoms.²⁰⁷ The formation of such cationic adducts allows access to an extended composition description of a lignocellulosic bio-oil whereas formic acid and ammonium salts mainly promote the ionization of basic nitrogen-containing species.²⁰⁷ The same methodology was used to investigate fast pyrolysis of oak bio-oil in positive ion ESI.^{232,233} With AcONa, the oak sugar derivatives were sensitively evidenced by (+) ESI.²³³ Mase et al. applied the same strategy to successfully investigate pinewood bio-oils by (+) ESI FT-ICR MS.²³²

Alternatively, Alsbou and Helleur studied bio-oils produced from forest residue, cellulose, and hardwood lignin (the last two were considered as reference bio-oils) by ESI-Ion-Trap MS. They used NaCl, NH_4Cl , and formic acid for positive ion ESI and NaOH, and NH_4Cl for negative ESI analysis.²³⁴ According to these authors, adding NH_4Cl can help to distinguish carbohydrate-derived products from other bio-oils components. These authors demonstrated a significant sensitivity increase by using NaOH and NaCl additives to promote the detection of deprotonated or sodium adducts, by (-) ESI and positive ion (+) ESI, respectively.²³⁴

Other dopants were employed to analyze crude oils in greater depth, substances which could be relevant to the investigation of bio-oils. Tetramethylammonium hydroxide (TMAH) has a stronger basicity than ammonium hydroxide NH_4OH ; this is why it is preferably used as a reagent to promote deprotonation processes to ensure (-) ESI-MS measurements.²³⁵ Indeed, TMAH ensured the detection and the assignment of more than 30 000 elemental compositions by (-) ESI FT-ICR MS of a South American crude oil (HC, NOS, NS_2 , S_2

classes). Compared to the use of NH_4OH , the additional detected features (close to 25 000) are related to the weak acidic compounds. Indeed, NH_4OH ensures the efficient deprotonation of the most acidic compound classes, such as O_2 and SO_2 (naphthenic and sulfonic acid), whereas TMAH also allows the O_1 (phenol), thiols or the poorly acidic N_1 , N_1S_1 , NO , NS_2 and SO classes of compounds to be detected by (-) ESI²³⁵. The main difference between NH_4OH and TMAH reagents relates to the detection of hydrocarbon class (HC) compounds, which are not ionized by using NH_4OH .^{235,236} The fact that TMAH, unlike ammonia, does not react with carbonyls to generate imine derivatives during the ESI process is another reason for its relevance in investigating bio-oils.²³⁷

Furthermore, silver trifluoromethylsulfonate (AgOTf) could be used as a dopant in (+) ESI analysis. Lobodin et al. suggested its interest to favor the detection of aromatic and heteroaromatic hydrocarbons in four petroleum samples from different origins.²³⁸ Thus, the aromatic hydrocarbon (HC) and the non-to-poor polar (S_{1-2} and S_1O_1) sulfur-containing classes were observed as cations. The use of formic acid dopant only ensured the detection of N_1 and N_1S_1 classes. The cationization by Ag^+ of aromatic HC, S_{1-2} , and S_1O_1 species is the result of the interaction of the π electrons with the silver Lewis acid cation to form a charge transfer complex.²³⁸ AgOTf may present a significant interest to promote the ionization of the low polar lignin-linked bio-oil components.^{238,239}

1.5.2.2.2. Atmospheric pressure photoionization and chemical ionization: APPI and APCI

To characterize a wider range of compounds, more specifically those of lower polarity, APCI and APPI have been used.^{240–243} Even if the involved ionization processes are quite different, these techniques ensure the efficient ionization of poorly polar aromatic (APPI and APCI) and poorly polar aliphatic (APCI) compounds, amounts of which may be significant in bio-oils, especially after catalytic upgrading treatments. APPI can ionize a large range of aromatics, usually using a dopant (toluene or acetone), to promote proton-transfer or charge exchange reactions²⁴⁴. Both protonated and radical ions are formed, which significantly increases the number of detected m/z signals.^{207,229,245} As a consequence, it is necessary to achieve very high MS performances in terms of mass resolution to resolve all contributions present on an APPI or APCI mass spectrum. Besides, APPI is a less selective ionization source compared to ESI. Ware et al. used APPI for the analysis of bio-oils obtained from pine

fast pyrolysis using toluene as a dopant in positive-ion mode. The results showed more aromatic and higher fractions for polar species.²⁴⁶ Indeed, bio-oil components derived from lignin were selectively ionized by APPI. Other types of bio-oils were also analyzed by positive ion APPI such as softwood and esterified softwood bio-oils using 1% of formic acid. High oxygen species with low DBE highlighted the presence of alcohols and ethers. This method allowed not only the detection of compounds with N₁ heteroatom but also the detection of compounds including boron heteroatom that was evidenced in ESI negative analysis by Javis et al. using negative ESI on bio-oils produced from the fast pyrolysis of woody biomass.^{229,247}

As for APCI, Stas et al. used positive and negative ion modes for the analysis of bio-oils from spruce wood, beech wood, poplar wood, and Miscanthus produced by fast pyrolysis and ablative flash pyrolysis.²⁴⁸ Compounds with one to twelve oxygen atoms and high DBE values (up to 22) were detected. The negative APCI was more sensitive to lignin degradation products than positive ion APCI and showed a high abundance of compounds with two to four oxygen atoms and DBE ranging from 5 to 7. With APCI, these authors were able to detect high mass and more unsaturated species.²⁴⁸ Thus, APCI provides more comprehensive information as the features detected by APCI were also observed by combining ESI and APPI results. Indeed, aromatic and aliphatic molecules were efficiently ionized by APCI.^{247,248} Similar behavior was recently reported by Mase et al. in the study of a bio-oil produced by pinewood residue pellets fast pyrolysis.²³² The components of the bio-oil produced from cellulose and hemicellulose were visible under both ESI conditions utilized (with formic acid or sodium acetate dopants) while the lignin derivatives were selectively ionized by APPI. Additionally, APCI provided the ability to identify aromatic and aliphatic compounds and allowed the ionization of the molecule families that were also recognized with ESI and APPI.²³²

1.5.2.2.3. Laser desorption-ionization: LDI

LDI is a suitable source for a solid analysis. Briefly, in LDI, the key parameter is the absorption efficiency of the photon by the investigated sample. Therefore, the species which can be easily ionized have to present a significant absorption at the wavelength of the used laser, which ensures the absorption of one or more, generally two photons.^{247,248} Alternatively, the ionization may occur in the gas phase by interaction (charge or proton transfer) between co-desorbed ions and neutrals. Such a process is close to what is observed in well-known MALDI experiments. Part of the

lignin-derivates, the structure of which is close to those of common MALDI matrices, assist the desorption and the ionization of the bio-oil components not absorbing at the wavelength of the laser.²⁴⁵ Hertzog et al. applied positive and negative ion LDI for the analysis of bio-oils.²⁰⁷ In positive ion LDI, both pyrolytic lignin and carbohydrate compounds were detected. By negative LDI, a specific distribution of pyrolytic lignin compounds was evidenced.²⁰⁷ The inability of non-aromatic pyrolysis products of cellulose to absorb the laser light causes LDI to suffer from several limitations (lower sensitivity toward carbohydrate-like components, fragmentation and recombination reactions due to laser-matter interaction that leads to artefact compounds) to analyze bio-oils.²⁴⁹ To overcome these limitations, several authors investigated matrix-assisted LDI (MALDI) for studying bio-oils. Compared to LDI analysis, Smith et al.²⁵⁰ observed a slight improvement in signal (increase of the S/N ratio) when they used colloidal graphite as a matrix. Other MALDI matrices were also investigated without significant improvement of the S/N ratio compared to LDI results.²⁵⁰ Nevertheless, Qi and Volmer demonstrated the usefulness of some MALDI matrices to investigate lignin degradation products.²⁴⁵ Whereas DCTB led to close results to LDI and CHCA to ion suppression phenomenon, 2,5 DHB promoted the ionization of high mass and Sox compounds. In the investigation of vanadyl porphyrins from crude oils, Giraldo-Dávila et al.²⁵¹ used cyanophenylenevinylene (CNPV-CH₃) as a matrix. This matrix ensured the sensitive ionization of polyaromatics, porphyrin-like compounds by electron transfer (ET). The so-called electron transfer ionization MALDI (ET-MALDI) was successfully applied to the investigation, after extraction, of vanadyl porphyrins from two heavy South American crude oils.²⁵¹ The results obtained by CNPV-CH₃ ET-MALDI were compared with those obtained by LDI and by MALDI using 3-(4-tert-butylphenyl)-2-methyl-2-propenylidene malonotrile (DCTB). CNPV-CH₃ demonstrated an impressive selectivity to porphyrin-like compounds. ET-MALDI with CNPV-CH₃ may be of significant interest in investigating third-generation bio fuel produced from algae to evidence chlorophyll-like compounds. Indeed, petroporphyrins are biomarkers derived from chlorophyll.²⁵¹

1.5.2.2.4. Ion source complementarity

Despite the specificity of each ionization source, the combined use of two or three ion sources gives complementary information regarding the complexity of bio-oils. Hertzog et al. combined the use of ESI, APPI, and LDI for the analysis of bio-oils (Figure 1-25). A wide range of unsaturation levels as well as high oxygen atom counts were detected in negative ESI as well as specific sugar derivatives in positive ion ESI.

Furthermore, these authors found that (+) APPI could ionize less polar species (lipids and lignin derivatives) while (–) LDI was restricted to the ionization of lignin derivatives.²⁰⁷ The combination of ionization sources gives information related to the effectiveness of a catalytic hydrotreatment on a bio-oil produced from lignin pyrolysis. In this context, Olcese et al. combined negative ESI and LDI FT-ICR MS analyses to evaluate the catalytic treatment of bio-oils produced by pyrolysis.²⁵² They identified compounds that were catalytically converted and refractory to catalytic treatment by ESI. The former was no longer observed, while ESI still detected the latter. By LDI, they identified after catalytic treatment, more conjugated and less oxygenated species corresponding to the conversion products.²⁵²

Finally, the specificities of each ion source lead to the combination of several of them to carry out a wider non-targeted analysis of such a complex mixture.²⁵³ Combination of ionization sources was also shown to be relevant for other organic complex matrices, such as natural organic matter, whose molecular fingerprint may be close to the bio-oil one.^{254,255} It is well known that part of the NOM comes from the degradation of lignocellulosic materials.

It is a necessary step to understand the fine chemical effect of an upgrading treatment as it was highlighted for bio-oils generated from biomass pyrolysis using different catalysts.¹⁹¹ In the upgrading process of a bio-oil, the need for different ionization sources is related to the important chemical modifications (cracking and deoxygenation), which modify the polarity of its components. However, the non-targeted analysis suffers from some limitations, such as ion suppression or matrix effect, which is the reason why fractionation and/or separation steps prior to such analysis is required.²²³

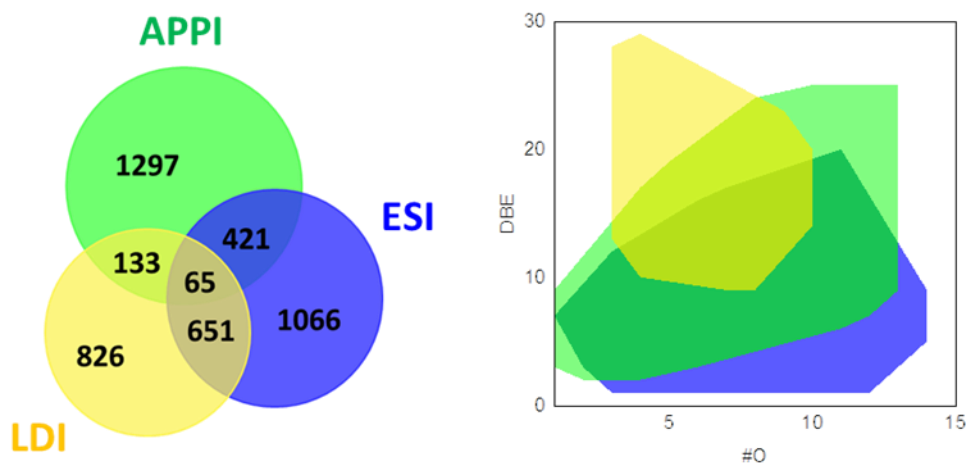


Figure 1-25: Venn diagram (left) and DBE vs. #O (right) of the CHO formulae obtained from ESI, APPI, and LDI FT-ICR MS analyses.²⁵⁶

1.5.3. Chromatographic methods

A solution to overcome ion suppression observed by ESI HRMS, is to implement a separative method prior to the mass spectrometry analysis.

Several studies were performed using different on-line or off-line chromatographic methods, with different detection modes such as refractive index, ultraviolet, and mass spectrometry. A recently published review pointed out such methodological approaches.²²¹ Among the separative methods, there are notably high-performance thin-layer chromatography^{257–259} and gel permeation chromatography.^{260,261} This latter method could be efficiently used for the fractionation of bio-oils^{221,262,263} using different types of columns and could be coupled to FT-ICR MS. Tetrahydrofuran (THF) and dimethylformamide (DMF) are the typically used solvents and low temperatures are usually applied.^{221,261–263} Several studies using GPC on thermochemically produced bio-oils such as fast pyrolysis, catalytic fast pyrolysis, and hydrothermal liquefaction oils showed that this technique could be the most practical method to use for bio-oil fractionation, based on the molecular weight of its components.^{248,261,264}

Liquid chromatography (LC) is also used as part of bio-oil characterization, with different columns such as C18^{262,265} and amide.²⁶⁶ The one-dimensional LC analyses allowed identifying and quantifying some species but with a limited number. Therefore, to increase peak capacity and to separate bio-oil compounds over a larger

polarity range, a two-dimensional LC was carried out, where reversed phase LC (RPLC) was hyphenated to a more polar column.^{263,267,268} Alternatively, size exclusion chromatography can also be used as a first-dimension separation coupled with RPLC with UV and HRMS detection. This method showed almost twice as those detected in 1D RPLC. Thus, it was considered relevant for the analysis of biomass samples.²⁶² Another way to improve separation orthogonality is to hyphenate RPLC to supercritical fluid chromatography (SFC). SFC was already used alone with different detection modes^{269,270} and it allowed observing some isomers.²⁶⁹ Two-dimensional RPLC × SFC analysis was shown to reach a higher peak capacity compared to RPLC × RPLC method, with 560 and 620 peaks, respectively.²⁷⁰

Gas chromatography (GC) is also frequently used to characterize the light bio-oil fraction, which represents a small part of the bio-oil components.²⁷¹ As for LC, studies have been performed by 1D (GC) and 2D (GC × GC), the latter allowing more compounds to be detected.^{272–274}

The next step concerning the characterization of bio-oil with chromatographic methods is to hyphen them with HRMS, in order to take advantage of the high resolution and mass accuracy performances. The main issue is the loss of performances of HRMS instruments at high measurement rate especially for high mass compounds. A few studies have been already performed in which high-performance mass spectrometry was hyphenated to Orbitrap-MS,²⁵⁸ or RPLC to FT-ICR MS.^{265,275} An advantage of the separation step prior to FT-ICR MS was clearly demonstrated with 5500 formulae obtained under the hyphenated method against 2000 in DI-FT-ICR MS.²⁶⁵ This was notably explained by the reduction of the ion suppression caused by the direct infusion mode.

1.5.4. Sample preparation and fractionation

Due to the huge complexity of bio-oils and the fact that the majority of studies are carried out by HRMS (high resolution mass spectrometry) in direct infusion mode, these factors are primarily responsible for the ion suppression phenomena and ionization competition, particularly in electrospray ionization (ESI).²⁷⁶ Less chemicals were found as a consequence. In order to overcome this problem, sample pretreatment was frequently applied in combination with a separative approach prior to mass spectrometry analysis in order to obtain more specifics about the chemical composition of the bio-oil. Fractionation techniques for as well as chromatography may be used. The pretreatment of the samples might alternatively be done using

solvent-based techniques, such as liquid-liquid extraction. In this part, these various methods will be detailed.

1.5.4.1. SARA fractionation

Among the fractionation methods, one is widely used for crude oil or bitumen, samples to separate the compounds into Saturate, Aromatic, Resin, and Asphaltene classes, which gives its name to SARA method.²⁷⁷ It is based on (1) the solubility of oil components in different solvents with different polarities before (2) separation on an alumina column (Figure 1-26). This method is used to separate the component of crude oil into four different classes: saturate (cyclohexane), aromatic (cyclohexane/dichloromethane), resin (methanol/toluene), and asphaltene (n-heptane) before analysis.^{277–281} Overall, it can be stated that SARA fractionation helps to determine the composition of crude oils by dividing them into defined hydrocarbon classes. This fractionation method could be associated with different analytical techniques such as chromatography, NMR,²⁸⁰ or mass spectrometry. Combining SARA with high-resolution MS measurement helps to increase both the number of the detected compounds and the knowledge of their chemical characteristics, leading to provide a better understanding of crude oil.^{282,283}

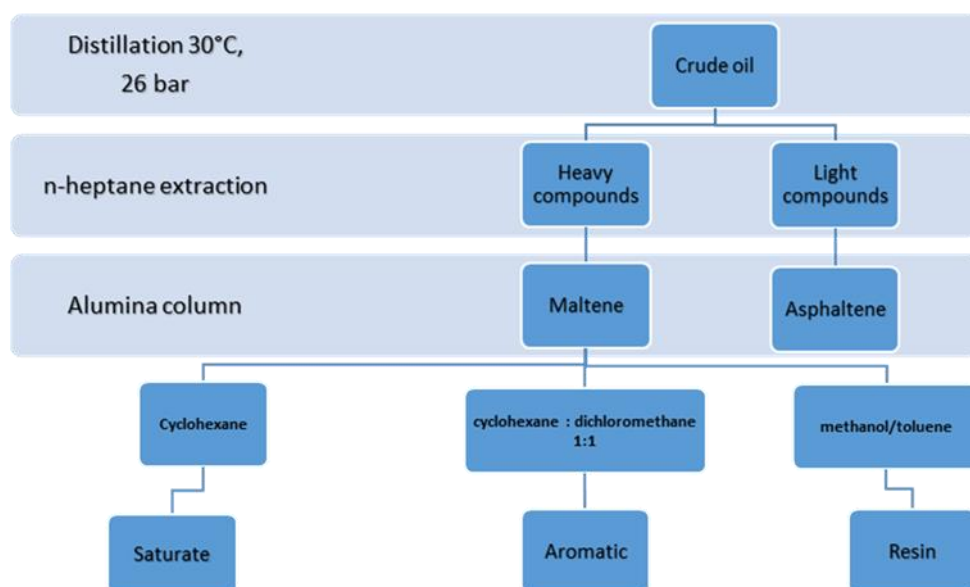


Figure 1-26: Schematic of crude oil saturate, aromatic, resin, and asphaltene (SARA) fractionation.

Cho et al.²⁸³ analyzed the different SARA fractions of heavy crude oil by APPI FT-ICR MS to obtain a detailed characterization. The saturated fraction appeared to

be composed of fewer aromatic molecules with long or multiple alkyl chains, while in the asphaltenes fraction, peri-condensed molecules were observed. The resin fraction combined nitrogen and oxygenated aromatic compounds with short carbon chains.²⁸³ Islam et al.²⁸² used the SARA fractionation followed by APPI FT-ICR MS measurement to analyze weathered and artificially photo-degraded oils. These authors were able to determine the compositional changes at the molecular level by considering the heteroatomic class behavior. In the saturate fraction, the photo-degradation led to the reduction of the S_1 class compounds with a high DBE value. At the same time, the abundance of S_1O_1 class compounds with high DBE values increased in the resin fraction.²⁸²

In addition, a supplementary step to the conventional SARA fractionation can be introduced using ethyl acetate as an additional mobile phase to isolate maltenes and obtain a second resin fraction. Santos et al.²⁷⁷ analyzed this fraction by FT ICR-MS using different ionization techniques. An increase in the number of detected molecular formulas was only found in this fraction two of resin regardless of the ionization technique used. A high aromaticity that was not identified throughout the crude oil analysis was also evidenced in this fraction. However, the overall DBE/C ratios for this fraction did not change significantly compared to the other fractions.²⁷⁷

Furthermore, the modification of SARA fractionation can also be done by integrating separation steps to take into account the chemical properties in addition to the solubility properties.²⁸⁴ This extended-SARA fractionation (E-SARA) allows key functional groups to be identified by fractionating asphaltenes depending on their adsorption at oil-water and oil-solid interfaces (Figure 1-27). These asphaltene subfractions are reported to be a real contribution to the stabilization of a water/oil emulsion.²⁸⁴

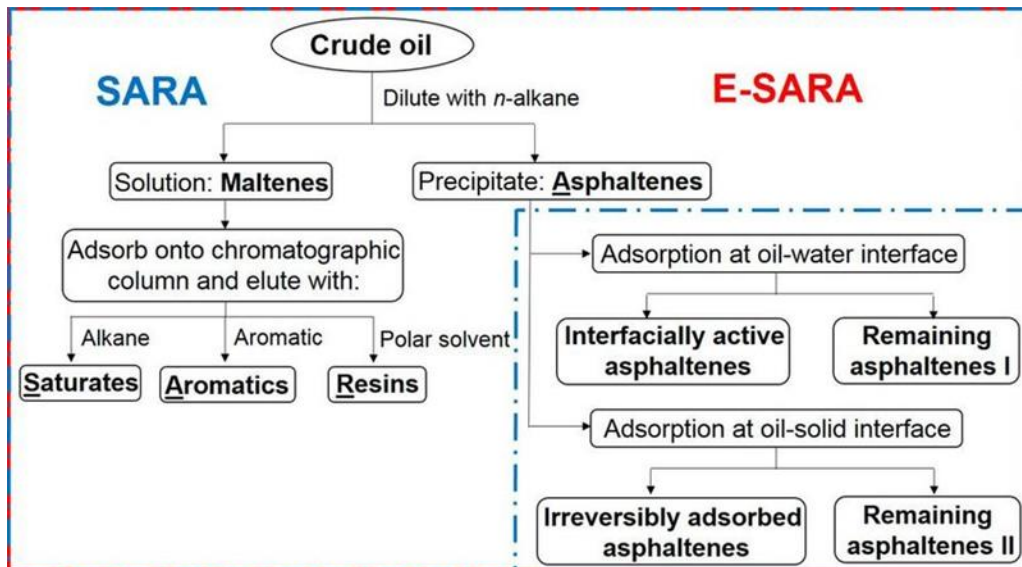


Figure 1-27: Comparison of extended-SARA (E-SARA) analysis with conventional SARA.²⁸⁴

These different SARA fractionation methods were widely used on petrol and could also be applied to bio-oils or formulated materials including bio-oils. Li et al.²⁸⁵ applied this technique for the characterization of aged bitumen modified by bio-oils. These authors studied SARA fractionation on two types of bio-oils: pyrolysis wood PW and co-pyrolysis of wood and rubber CPWR. The latter one showed high aromatic and asphaltene fractions while the former one was dominated by the resin fraction.²⁸⁵ SARA fractionation cannot be directly applied to bio-oil due to the high polarity range of its constituents. Indeed, this method must be adapted to fractionate more efficiently polar compounds with an extended scale of polar solvents.

1.5.4.2. Distillation, Precipitation and Fractionation method (DPF) mass spectrometry.

The distillation, precipitation, and fractionation (DPF) method consist of fractionating oil into six different chemical classes before their analysis by HRMS. The six classes are volatile saturated hydrocarbons, asphaltenes, heavily saturated hydrocarbons, alkyl aromatic hydrocarbons, heteroaromatic compounds, and polar compounds.^{286–288} The DPF procedure is described in Figure 1-28.

The volatile saturated hydrocarbons are obtained using vacuum distillation at room temperature. As in SARA fractionation, asphaltenes are obtained by precipitation using n-heptane. The n-heptane soluble fraction (maltenes) is divided into three compounds classes on a normal-phase silica column with respect to their

elution by *n*-hexane (heavily saturated hydrocarbons and alkyl aromatic hydrocarbons), dichloromethane (heteroaromatic compounds), and finally isopropyl alcohol (polar compounds). The separation of heavily saturated hydrocarbons from alkyl aromatic hydrocarbons is conducted by solid-phase extraction.²⁸⁶

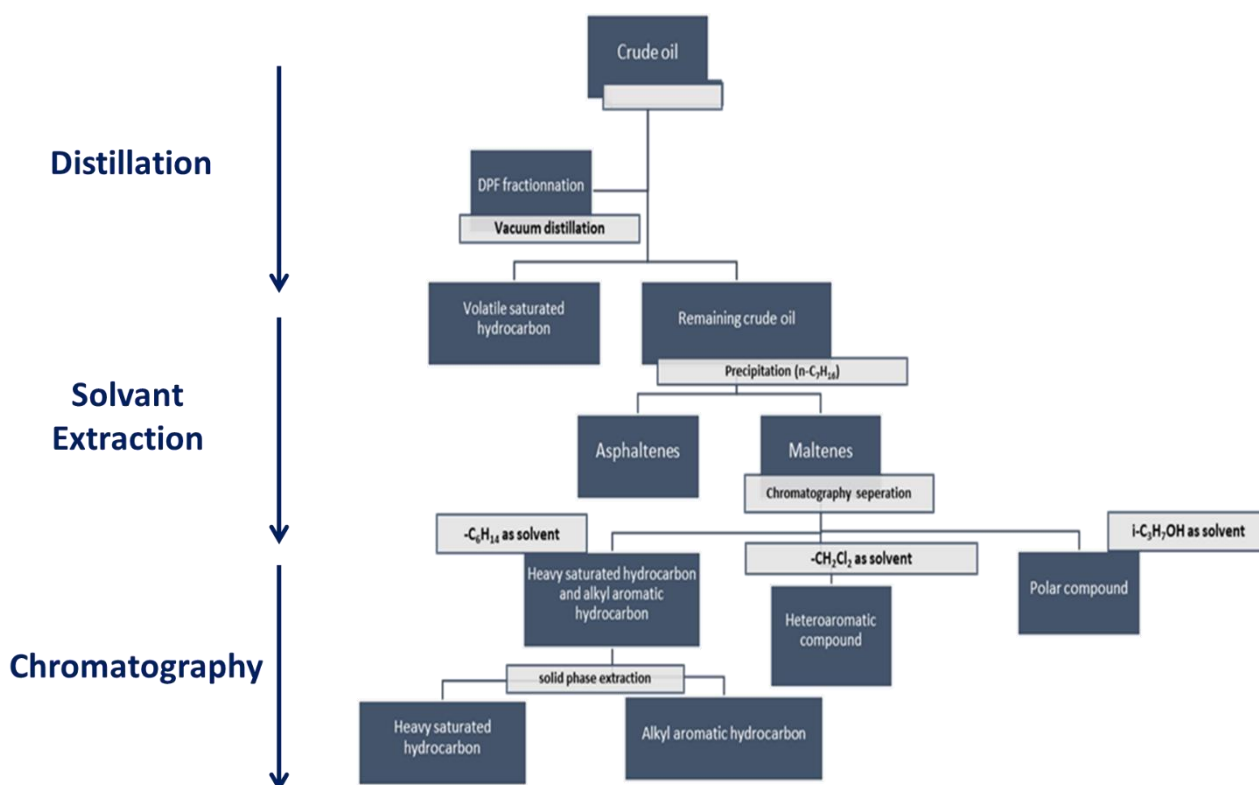


Figure 1-28: DPF fractionation steps adapted from Yerabolu et al.²⁸⁶

In the work of Niyonsaba et al.,²⁸⁹ the six fractions were analyzed by APCI Orbitrap and high-resolution two-dimensional gas chromatography coupled with electron ionization high-resolution time-of-flight mass spectrometer (GC x GC TOF–MS) to achieve the characterization of each fraction at the molecular level.^{287,289} APCI Orbitrap was used in direct infusion for the investigation of the non-volatile fractions in positive ion detection mode whereas volatile saturated hydrocarbons were investigated by GC x GC TOF–MS. Table 1-7 reports the instrumental parameters employed to analyze each of the non-volatile fractions by APCI Orbitrap.^{286,289}

Table 1-7: Sheath and auxiliary gas and solvents used for the analysis of DPF fractions by positive ion APCI.²⁸⁹

DPF Fraction	Sheath and auxiliary gas	Solvent
Asphaltenes	N ₂	CS ₂
Heavy saturated hydrocarbon	O ₂	Hexane
Alkyl aromatic hydrocarbon	N ₂	CS ₂
Heteroaromatic		
Polar compound	N ₂	n-Hexane and methanol

Nitrogen is more frequently used as sheath and auxiliary gas. However, when nitrogen is used, linear saturated hydrocarbons create both $[M]^{+*}$ and $[M-H]^+$ ions and undergo considerable fragmentation. To overcome this problem, some studies showed the usefulness of oxygen. When this latter is applied as sheath and auxiliary gas, only $[M-H]^+$ ions are formed. No ozone neither NO_x formation was reported when O₂ was used.^{290,291} The only thing that should be considered when using O₂ is the temperature, for safety reasons. The results of the DPF MS approach were used to establish some correlation between the chemical compositions of the crude oil samples and their API gravity (American Petroleum Institute gravity).^{286,287,289}

Niyonsaba et al. used DPF MS to determine the chemical compositions of five crude oil samples (two heavy from San Joaquin Valley and California, two medium from Russia and South America, and one light from Illinois) with different API gravities.²⁸⁹ In addition to these methods, Ravikrian et al. used infrared spectroscopy to select tracer compounds representative of each fraction.²⁸⁹ The DPF method excels in providing an accurate analysis of the crude oil (average molecular weight, heteroatom content, etc.) by including the mass balance of each fraction.

The use of this type of approach has not yet been reported in the context of the analysis of bio-oils. However, it awakens interest within the framework of the study of bio-oils improved by catalytic treatment and in that of bio-oils produced by catalytic pyrolysis. Indeed, in these two types of bio-oils, purely hydrocarbon

compounds are present. Being able to distinguish heavily saturated compounds, alkylated aromatic compounds, heteroaromatic compounds, and polar compounds could allow better adaptation to the catalytic conditions to efficiently produce hydrocarbon compounds with higher added value.

1.5.4.3. Flash chromatography

Recently, bio-oil fractionation was performed using a flash chromatography technique with a silica cartridge (Figure 1-29).²⁹² Three eluents (toluene, 90/10 toluene/methanol, 75/25 toluene/methanol, and methanol/water/formic acid) were used to obtain four distinct fractions, which were investigated by gravimetry, chromatography, and FT-ICR MS. Thus, each fraction was characterized by a specific class of compounds (fraction one, low oxygenated and unsaturated compounds; fraction two, more oxygenated unsaturated compounds; fraction three, cellulose and hemicellulose derivatives; and fraction four, the most polar compounds) allowing a better description of the molecular composition of bio-oil.²⁹²

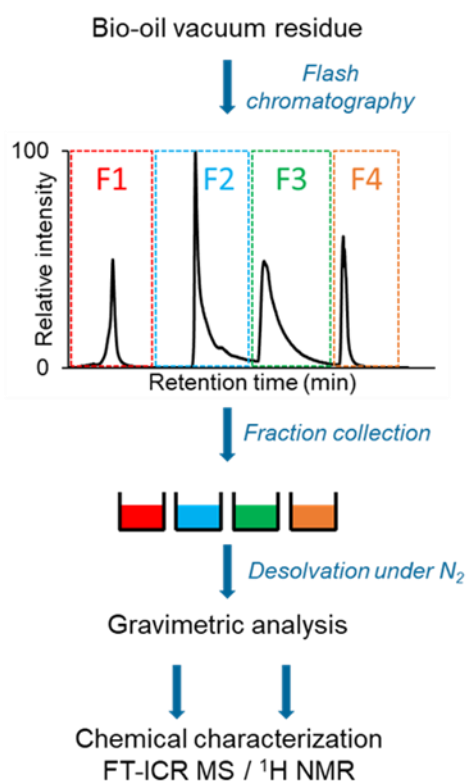


Figure 1-29: Scheme of the experimental workflow from sample fractionation to gravimetric analysis and molecular characterization.²⁹²

1.5.4.4. *Acid/Base/Neutral fractionation*

Acid/base/neutral fractionation could also be used on bio-oils and was applied by Farrapeira et al.²⁹³ This fractionation showed the capacity to obtain four fractions of bio-oils: two acidic, one neutral, and one basic. These fractions were analyzed by 2D GC–TOF-MS. The neutral fraction was mainly composed of aromatics, ketones, ethers, and fatty esters while the basic one was formed of hydrocarbons and alkanes. Among these four fractions, the acidic one was shown to have a similar composition to bio-oil and appeared to contain high concentrations of phenol, catechol, eugenols, and furfural.²⁹³ These results emphasized using bio-oils as a precursor in the chemical industry.²⁹⁴

1.5.4.5. *Adsorption chromatography (AD)*

This separation, sometimes referred to as liquid-solid chromatography or LSC, is used on bio-oil samples before GC analysis to produce fractions with various polarity. The retained chemicals are eluted from the silica chromatographic column using a series of increasing polarity solvents, starting with n-heptane to produce the aliphatic fraction, using toluene to produce the aromatic fractions, methanol, and ether to get the polar and ester portions, respectively.

Gas chromatography coupled to mass spectrometry (GC-MS), Fourier transform infrared (FT-IR), and nuclear magnetic resonance (NMR) spectroscopy will be used to investigate the obtained previous fractions.^{295–298}

1.5.4.6. *Liquid-liquid extraction (LLE)*

In LLE, the bio-oil sample is separated into several fractions according to the solvents employed. Figure I-30 illustrates a polarity-based LLE approach. The sample is divided into fractions that are and are not soluble in water. The former is typically referred to the light fraction and the latter to the heavy fraction.^{299–302} On the aqueous fraction, further extractions using diethyl ether and dichloromethane are carried out. The principal components of the ether-soluble fraction are aldehydes, ketones, and lignin monomers. The short aliphatic hydroxy acids and sugars are related to the ether-insoluble one. Dichloromethane is used to separate the heavy fraction into CH₂Cl₂ soluble (low-molecular mass lignin compounds) and CH₂Cl₂ insoluble (other substances) (high-molecular mass components).^{299–301,303}

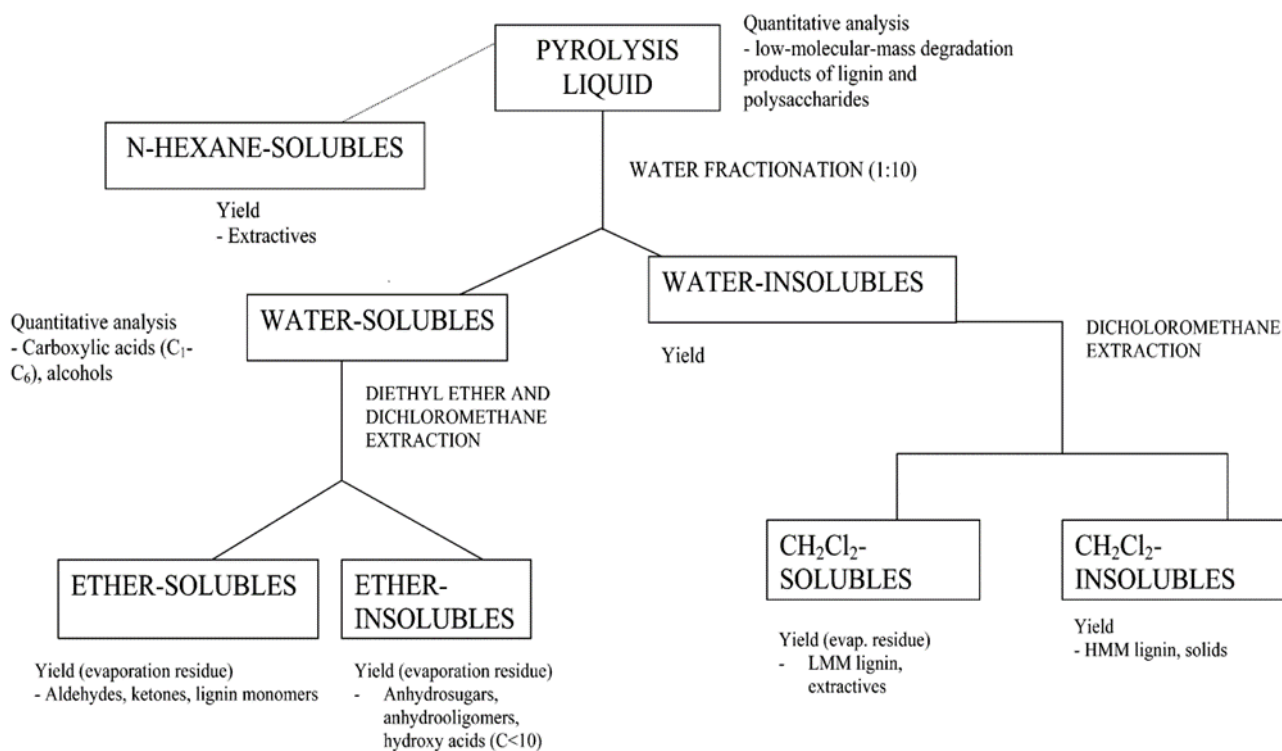


Figure 1-30: Scheme for fractionating bio-oil by polarity (using water-based) LLE.³⁰²

1.5.4.7. Thin layer chromatography

Adsorption serves as the fundamental separation principle in HPTLC, which uses a similar technique and identical physical principles as TLC (adsorption chromatography). Capillary action causes the mobile phase solvent to pass through. Consequently, the components migrate in accordance with their tendency to interact with the adsorbent. It has been shown that high performance thin layer chromatography (HPTLC) can separate anhydrosugars such levoglucosan and cellobiosan from fast pyrolysis oil together with glucose, arabinose, xylose, and cellobiose. Anhydrous dipotassium phosphate/methanol was employed as the eluent solution, and a silica-gel HPTLC plate was utilized.^{304,305}

1.5.4.8. Solid phase extraction SPE

Solid phase extraction, or SPE, is a powerful method for separating certain substances from complex mixtures. Many issues with liquid-liquid extraction, including partial phase separations, less-than-quantitative recoveries, and the disposal of significant amounts of organic solvents, can be solved by SPE.³⁰⁶

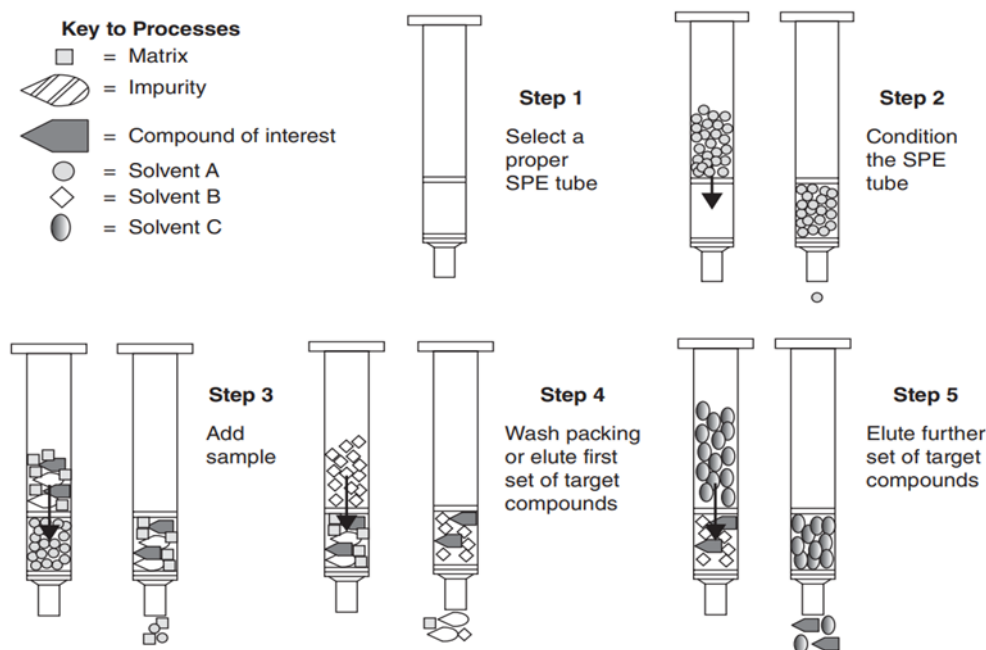


Figure 1-31: Solid phase extraction principle.³⁰⁷

The C18 SPE cartridge was utilized by Brodzinski et al.³⁰⁷ to achieve the bio-oil fractionation. With increasing amounts of methanol added to the water in the eluent, the fractionation was carried out. Acids, furanes, and anhydrosugars are eluted with 100% water. Furan and pyran derivatives, as well as aromatic ketones and aldehydes, are eluted with 15% and 35% of methanol, respectively. Alkyl derivatives of syringol are observed with increasing concentrations of methanol, up to 50%, whereas guaiacol and syringol alkene derivatives need a 100% methanol elution. SPE cartridge with amine-functionalized mesoporous silicas have been used for the extraction/fractionation of bio-oil model compounds and lignin derived bio-oil.³⁰⁶

1.5.5. Getting chemical characteristics beyond the isobaric level: Ion mobility Mass spectrometry IMS

Petroleomics has revealed that species present in complex mixtures such as bio-oils or crude oils present a large diversity of sulfur-, nitrogen-, and oxygen-

containing chemical functions. Therefore, a raw formula, which is the only information obtained by mass spectrometry, can relate to many isomers. In this context, the association of ion mobility with mass spectrometry can be helpful to at least highlight the isomeric diversity and, in the most favorable situations, discriminate these isomers.^{308,309}

Ion mobility spectrometry (IMS) separates the ions through a gas-filled mobility cell under an electric field. Depending on the type of ion mobility technology, the distinction/separation of isomeric/isobaric ions according to their mass, charge, size, and shape can be achieved using different instrumental parameters. The size and shape of an ion are linked to its collision cross-section (CCS). The use of a drift tube ensures the direct correlation of the mobility of an ion with its CCS, which is an intrinsic property. To obtain the ion CCS, the other IM technologies require the use of standard compounds for calibration. The most important issue is to use a standard, in which mobility behavior is close to those of the studied compounds. By comparison of the measured CCS with the CCS calculated by molecular modeling for putative isomers, it is possible to propose detailed structural information about the investigated ion.³¹⁰⁻³¹³ The IMS could be coupled to mass spectrometry IM-MS (ion mobility mass spectrometry). Therefore, before being analyzed by MS, the ions are discriminated according to their mobility in the mobility device. In addition to the m/z and the CCS descriptor, a third one may be used when tandem mass spectrometry (MS/MS) is implemented. Different ion mobility techniques were applied to crude oils. Figure 1-33 gathers a selection of publications dealing with the use of ion mobility mass spectrometry in the field of petroleomics and Figure 1-34 highlights the advantages of the different ion mobility techniques.

Lalli et al.³⁰⁹ combined IM-TOF-MS and MS/MS by collision-induced dissociation (CID) to investigate emulsion interfacial material isolated from Athabasca bitumen and heavy crude oils. These authors focused on the functional isomers from the O_3S_1 heteroatom class³⁰⁹. The results obtained by these authors were compared to the results obtained from the analysis of the same samples by negative ESI FT-ICR MS. It appeared that IM-TOF MS was capable of increasing the description of O_3S_1 heteroatom class isomers, and FT-ICR MS allowed peak assignment to be confirmed.³⁰⁹

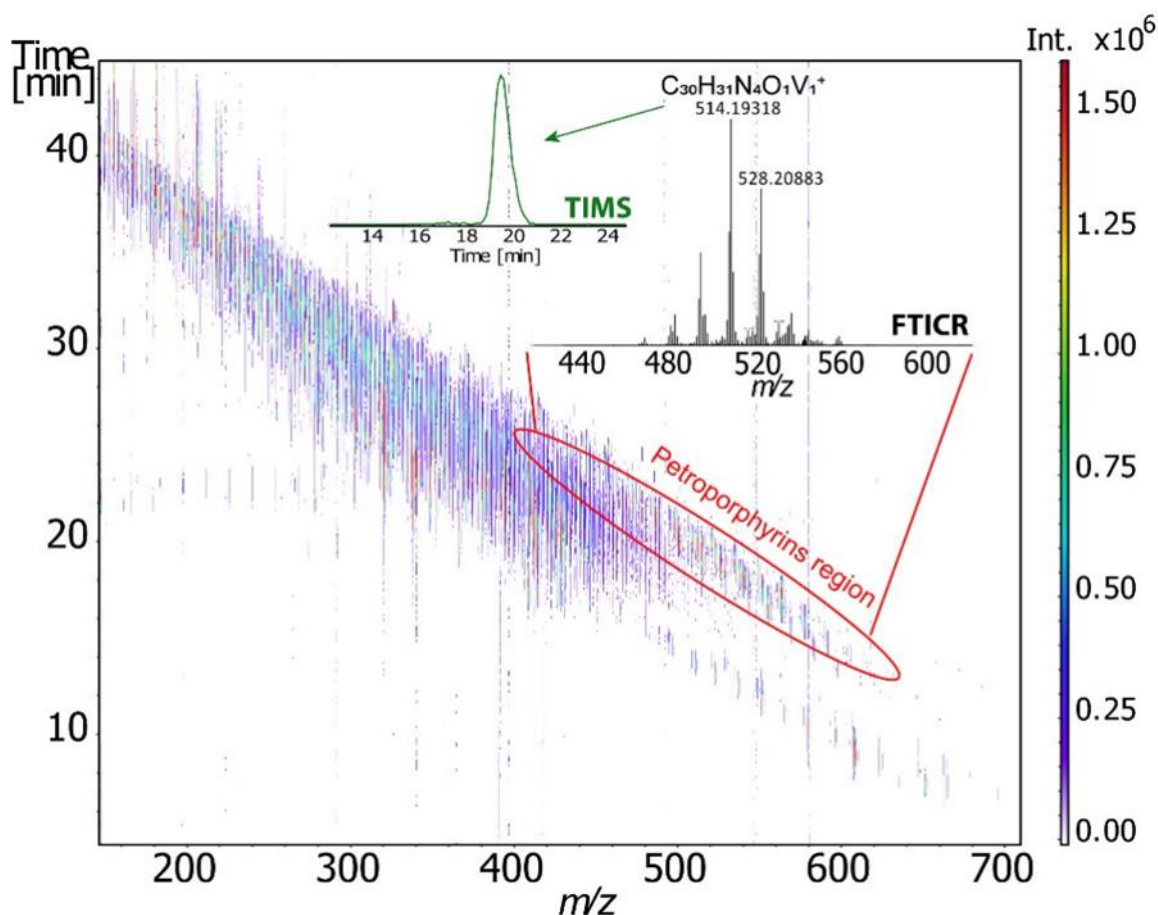


Figure 1-32: 2D TIMS-FT-ICR-MS survey spectra of the Athabasca asphaltene.³¹⁴

More recently, Maillard et al.³¹⁴ used for the first time the combination of trapped ion mobility (TIMS) and FT-ICR MS to obtain information on the structural features and isomeric diversity of vanadium petroporphyrins in heavy petroleum fraction (Figure 1-26).³¹⁴ The determination of the CCS and its correlation with theoretical calculation allowed them to propose some putative structures and the use of the FWHM descriptor ensured the accounting for isomeric diversity.

Regarding IM-MS analysis on bio-oils, a few studies were reported in Figure 1-33. Among these studies, Dhungana et al. applied IM-MS on bio-oils from biomass pyrolysis. As a result of the discovery of oxygen-rich species (one to nine oxygen atoms) with DBEs ranging from 1 to 15, it is anticipated that catalytic upgrading will be necessary if slow-pyrolysis bio-oils are to be used as fuel. IM-MS/MS gives complementary information related especially to isomer separation in addition to the traditionally used HRMS in the analysis of bio-oils.³¹⁵

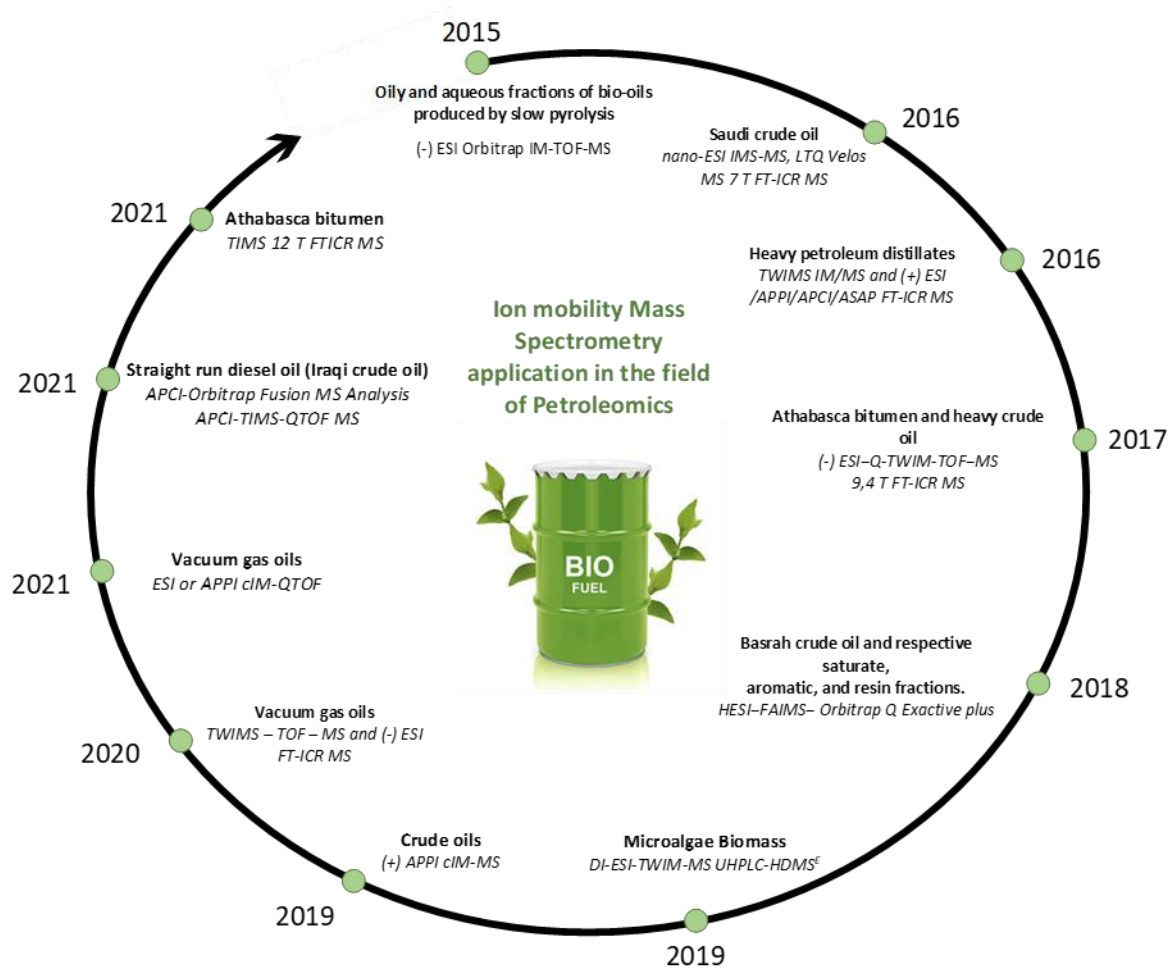


Figure 1-33: Main publications of IM-MS in petroleomics.^{309,314–323}

However, ion mobility spectrometry still suffers from a lack of mobility resolving power. Figure 1-34 highlight the different advantages of IMS technologies. Dodds et al. investigated the correlation between mobility resolving power (mRP), and CCS. These authors demonstrated that the most advanced ion mobility (IM) instruments reach now mRP ($CCS/\Delta CCS$) greater than 300 and are therefore capable of separating compounds with CCS differences as low as 0.5%. Current IM instruments operate across a broad range of separation efficiencies between 50 and 300 mRP. It would take resolving powers on the order of several thousand to resolve the majority of the components in a complex mixture using ion mobility, which is far beyond the capabilities of current instrumentation due to peak broadening limits imposed by ion diffusion.³²⁴

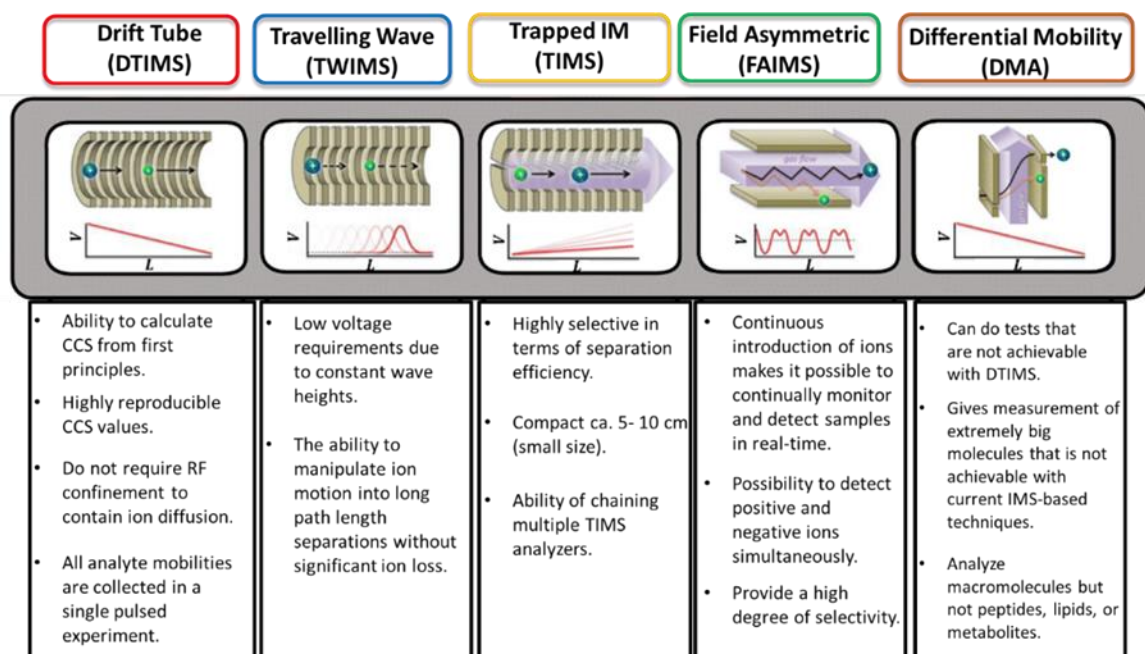


Figure 1-34: Advantages of the different of IMS technology^{312,325–327}.

1.5.6. Tandem Mass Spectrometry

Tandem mass spectrometry is a well-known technique to obtain structural information. Typically, the parent (also named precursor ion) is isolated prior to increasing its internal energy. This leads to the dissociation of part of the chemical bonds to produce fragments also named daughter ions. The activation of the precursor ion may be performed by vibrational excitation through absorption of infrared photons (the so-called infrared multiphoton dissociation (IRMPD)) or by

collision with a gas (collision induced dissociation CID).^{328–335} Alternatively, electronic activation may be performed by the absorption of a UV or VUV photon (UV photodissociation UVPD). Another way to induce the fragmentation of precursor ion is to generate a radical by interaction with an electron observed in electron capture dissociation (ECD), electron transfer dissociation (ETD) and electron induced dissociation (EID) experiments.^{336–338} Although this latter activation method can be applied to singly charged ions, it is mainly used to study multi-charged ions. In petroleomics, the most frequently used activation techniques are CID and IRMPD.

Among the different applications of tandem mass spectrometry in petroleomics, this section will be more specifically dedicated to bio-oils, especially the one produced from lignocellulosic biomass. It is widely known that this raw material is made of biopolymers, namely cellulose, hemicellulose, and lignin, making it a promising source. In order to determine their structure, tandem mass spectrometry has been used, and many investigations are reported.

1.5.6.1. Carbohydrates

The most prevalent kind of carbohydrates in lignocellulosic biomass is cellulose, a glucose polymer and hemicellulose.³³⁹ Hemicellulose is made of C6- (glucose, mannose, galactose) and C5- (xylose and arabinose) carbohydrate units.³⁴⁰ The structural elucidation of isomeric sugars by MS/MS is very challenging. The main part of the investigation by MS/MS conducted on bio-oil carbohydrate component did not lead to a complete structural elucidation but rather to the confirmation of the presence of such compounds in bio-oils. Vinueza et al. demonstrated the use of chloride anion attachment in APCI and ESI tandem mass spectrometry for molecular weight MW measurement and for a partial structural elucidation of various mono-, di-, and oligo-saccharides without sample preparation or derivatization.³⁴¹ Significant HCl loss (chlorine-containing fragment anions) was seen in the collision-induced dissociation CID of the carbohydrate chloride adducts anion. This particular loss was utilized not only to prove that the fragmenting ion was a chloride anion adduct but also it allowed the distinction between carbohydrates containing no free anomeric hydroxyl groups and those that contain them.³⁴¹ In addition, Yu et al. used a similar approach to determine the first reactions and byproducts of fast pyrolysis of xylobiose and xylotriose, model xylan compounds.³⁴² Quantum chemical computations were used by these authors to study the processes of the ring opening and subsequent fragmentations of the reducing end. In particular, it was shown that ring-opening and

coordinated removal of ethenediol from the reducing end of xylobiose were necessary for the synthesis of β -D-xylopyranosylglyceraldehyde (XGRA), the most prevalent fast pyrolysis product of xylobiose and xylotriose. It is claimed that coordinated Maccoll elimination and/or Pinacol ring contraction led to the cleavage of the glycosidic bond and 1,2-dehydration.³⁴²

1.5.6.2. Lignin

Among the biopolymers mentioned previously, lignin is the second largest component of lignocellulosic biomass, accounting for 15% to 30% of the mass, and it is generally considered to be composed of three phenylpropane units.^{343–346} However, tandem mass spectrometry is a promising tool for lignin structural analysis, as fragmentation patterns of model compounds can be extrapolated to identify characteristic moieties in complex samples.³⁴⁷ Zhang et al. applied tandem mass spectrometry on alkali lignin pyrolysis oil after the sequential extraction method. For the raw pyrolysis oil and the subfractions, a peak at m/z 360 with a high relative abundance was observed.³⁴⁸ The precursor of this ion was a dimer connected by a ferulate bond and coniferyl alcohol. Due to the absence of weak binding groups, no further fragmentations were seen in the two other investigated precursor ions.³⁴⁸ In another work, Abdelaziz et al. investigated the first continuous-flow reactor setup for base-catalyzed depolymerization of lignin using sodium hydroxide to create low-molecular-mass aromatics.³⁴⁹ Size exclusion chromatography (SEC), nuclear magnetic resonance spectroscopy (NMR), and supercritical fluid chromatography-diode array detector-tandem mass spectrometry (SFC-MS) were used by these authors to characterize the obtained products (phenolic bio-oil consisting of monomeric/oligomeric aromatic compounds).³⁴⁹ As a result, the aliphatic C-O bonds in the lignin inter-unit structures (β -O-4, β - β , β -1, β -5), were broken under the investigated reaction conditions, providing evidence of efficient lignin depolymerization.³⁴⁹ Moreover, the current lignin depolymerization technique also made it possible to produce partially deoxygenated dimeric and oligomeric fractions for use in liquid fuel applications and other renewable energy sources.³⁴⁹ Recently, Dong et al. used beam-type CID with energy-resolved mass spectrometry (ERMS) to apply previous resonance excitation type CID techniques that identified lignin oligomers containing β -O-4, β -5, and β - β bonds to additionally identify features of 5-5, β -1, and 4-O-5 dimers.³⁴⁷ Overall, the beam-type ERMS provides comprehensive structural data and may eventually help develop instruments for high-throughput lignin dimer detection.³⁴⁷

However, with real bio-oil samples, many mass peaks at each nominal mass render this approach inefficient, mainly due to the low resolution of quadrupole ion precursor isolation for CID. The resolution necessary for the isolation of individual ions can be achieved in the ICR cell by FT-ICR MS, but these measurements are very slow and tricky and involve a decrease in the performance of the instrument due to the gas introduced into the vacuum part for the CID. To overcome this problem, two-dimensional tandem mass spectrometry using FT-ICR MS will be helpful, especially for bio-oils. It enables the creation of two-dimensional maps of precursor ions as well as fragment ions that were activated by infrared or UV photon, or by interaction with an electron (ECD, ETD or EID). The advantage of this modern approach, which is presently employed to study ionized peptides by DIA-ESI, is that it does not require the conventional precursor ion selection step. In order to investigate a complex mixture, it is therefore possible to obtain all the fragmentation spectra of the ions present on a mass spectrum in a reasonable length of time, ranging from a few tens of minutes to a few hours. Several studies were reported on using IRMPD 2DMS for the analysis of polymers^{333,334}, peptides^{335,350} and, agrochemicals.^{331,332}

However, on our knowledge the bio-oil analysis by MS/MS utilizing HRMS is limited at this time, but it may be able to offer structural data on the bio-oil constituents for a deeper characterization (Chapter IV and V).

1.5.7. Specific reactants to chemical functions: derivatization

To go deeper into the description of the structure of oil constituents at the molecular level, some approach has been proposed to evidence by derivatization specific chemical functional groups, as showed in Table 1-8. Most of the derivatization processes have been done with bio-oil due to its wider molecular complexity in terms of chemical functions. Prior to gas and liquid chromatography (GC and LC) examinations and, in some circumstances, for NMR measurements, some chemical functionalities can be derivatized. Targeted analytes in complex mixtures are typically derivatized for a variety of reasons, including (i) ensuring their sensitive detection, (ii) changing the polarity of the analytes to enable GC separation, (iii) increasing the analyte's volatility for GC analyses, and (iv) specifically demonstrating some chemical functions.^{351,352} Primarily, polar molecules are involved (alcohols, amines, acids, etc.).

1.5.7.1. Carbonyls

The bio-oils and the crude oils contain wide amounts of oxygenated compounds that are related to different functional groups.^{248,353} Among these oxygenated functional groups, the carbonyls (aldehydes and ketones) are of major concern because of their significant reactivity and abundance, with up to 20 wt.% in bio-oils³⁵³. There are also well-known carbonyl-specific reactions. The most important ones are the formation of imines by reaction with amines or hydrazone by reaction with the 2,4 dinitrophenylhydrazine (2,4 DNPH) or the Girard T reagent.^{228,354–357}

Hertzog et al.²³⁷ evidenced some carbonyl compounds by ESI positive ion FT–ICR MS in bio-oils, after derivatization with aniline and 3-chloroaniline.²³⁷ The detection of chlorine-containing species, such as $C_xH_yO_zNCl$ and $C_xH_yO_zN_2Cl_2$, allowed these authors to unambiguously define both mono and di-carbonylated $C_xH_yO_z$ compounds. The elemental formula of the original compound corresponding to these carbonyls is obtained by the subtraction of one (or two) $C_6H_4ClNH_2$ and the addition of one (or two) H_2O . This reaction took place in the ESI source itself.²³⁷

In the field of corrosion tests of naphthenic acids, Krajewski et al.³⁵⁸ used an alternative approach. After extraction of the ketones on a strong anion exchange (SAX) cartridge from a corrosion test naphthenic acid commercial sample, they were derivatized by the Amplifex keto reagent. The resulting compounds were analyzed by (–) ESI FT–ICR MS. The N_2O_1 features relative to derivatized O_1 ketone ensured to determine the oxidation products of the naphthenic acids.³⁵⁸

1.5.7.2. Phenols and alcohols

Alcohols, and, more importantly, phenols, are other classes of compounds observed in bio-oils with a great amount (up to 40 wt.%) and to a lesser extent in petroleum. Their abundance is depending on the origin of the oil.³⁵⁹ They can be quantified by gas chromatography mass spectrometry in complex petrochemical samples after derivatization to esters of ferrocene carboxylic acid.³⁶⁰ Indeed, Wasinski and Andersson³⁶⁰ used the esterification reaction between ferrocene carboxylic acid chloride and phenol and alcohol.^{360,361} The introduction of an iron atom by the derivatization reagent may be a very powerful tool for investigating hydroxylated compounds in complex mixtures by MS due to its isotopic pattern.

Another interesting derivatization method of phenol was proposed by Zhu et al.³⁶² who investigated such compounds in jet fuel³⁶². These authors used an

imidazolium-based charged tag (3-(4-(bromomethyl) benzyl)-1-methylimidazolium) that in situ reacted with phenol to produce an ether. This approach significantly increased the sensitivity due to the charged-tagged derivatization. Moreover, it was also demonstrated that thiols may also be derivatized by the same methodology, which ensured the distinction of thiols and thioethers. Nevertheless, classical derivatization techniques could also be applied to derivatize and quantify phenols in complex mixtures such as bio-oils. Among these classical derivatizations, acetylation with acetic anhydride in the presence of pyridine was used and applied by Murwanashyaka et al.³⁶³ GC-MS analysis following this pretreatment (fractionation and acetylation) was applied to monitor the amounts of phenol in the studied samples.³⁶³

Table 1-8: Examples of derivatization reagents used to study oxygenated functional groups in bio-oils.

Functional Group	Derivatization Reagent	Sample	References
Carbonyls	2,4 Dinitophenylhydrazine(2,4 DNPH)	Petroleum resin and Asphaltene	237,354,355
	Girard T		228,357,364
	Quaternary aminoxy (QAO)	Crude oils	357
	Aniline	Bio-oils	237,365
	3-Chloroaniline	Bio-oils	
	Amplifex keto	Naphtenic acids	358
Phenols and alcohol	Ferrocene carboxylic acid chloride	Pyrolysis oil and petrochemical sample	366
	(3-(4-(Bromomethyl) benzyl)-1- methylimidazolium)	Jet fuel	263,360,263,360,361
	Acetic anhydride	One-step and stepwise laboratory batch vacuum pyrolysis of a	362

		mixture of birch bark and birch sapwood	
	Butyl chloroformate	Fuels and engine oils	363
	Pentafluoropyridine	Bio-oils	367
Carboxylic acid	Alkylation (benzyl ester)	oak-maple, pine and straw oils	
	Tetramethyl-p-phenylenediamine (TMPD)		
	2-chloro-1,3,2-dioxaphospholane	Pyrolysis bio-oil	248,368–370
	1,2,3-Dioxaphosphalane		
	2-chloro-4,4,5,5-tetramethyl-1,3,2-dioxaphospholane		
	Diazomethane		
	BF ₃ /methanol	Bio-Oils Derived from Lignocellulosic Biomass	353,371,372 353
	BSTFA		
Tetramethylammonium acetate	Humins		

1.5.7.3. Carboxylic acids

Among the different oxygenated substances that can be present in bio-oils, carboxylic acids are one of the most reactive and concerning compounds. Acidic compounds are responsible for corrosiveness issues and, therefore, storage problems of bio-oils. Moreover, they can also be involved in condensation reactions with other bio-oil compounds, which yield water and decrease the high heating value HHV value of this material and can also lead to the formation of two phases in the bio-oil. For these reasons, carboxylic acid characterization in bio-oil is of major interest, and derivatization is a way to analyze them.

Esterification as benzyl esters is an example of these reagents and was applied by Staš et al. to characterize pyrolysis bio-oil (oak-maple, pine, and straw oils) using GC-MS. These authors showed that the amount of the derivatized acids can be influenced by the type of biomass.^{248,368} However, formic and acetic acid was found to be the majority regardless of the type of biomass. Also, Staš et al. applied another modification by using a phosphitylating agent to characterize and quantify acids of the bio-oils. The phosphitylating agents that have been used are the 2-chloro-4,4,5,5-tetramethyl-1,3,2-dioxaphospholane (TMDP) and 2-chloro-1,3,2-dioxaphospholane.^{248,368,373} The former was shown to provide a better signal than the latter. By employing ³¹P NMR, these P-agents could quantify the acids in bio-oil.^{369,370} Nevertheless, other phosphorylation reagents exist and were applied by Balakshin et al.³⁶⁹ for the analysis of carboxyl groups: 1,2,3-dioxaphosphalane and 2-chloro-4,4,5,5-tetramethyl-1,3,2-dioxaphospholane. As evidenced by the authors, the second result showed a good correlation with those from ¹³C NMR after quantification with ³¹P NMR.^{369,370,373}

Another derivatization reagent exists to modify carboxylic acids such as methylation by esterification reaction using diazomethane or BF₃/methanol and trimethylsilylation using the N,O-bis(trimethylsilyl) trifluoroacetamide (BSTFA).³⁷⁰ These reactions usually happen by replacing the labile hydrogen atom of the carboxylic acids by a methyl or trimethylsilyl group forming carboxylic acids esters and trimethylsilyl ethers, respectively.

1.5.8. Isotope Labelling

Besides the previously described methodologies to obtain structural information of bio-oil composition, another one has emerged recently in the field of petroleomics. It is the hydrogen/deuterium H/D and the $^{16}\text{O}/^{18}\text{O}$ exchanges (Figure 1-35). It is a well-established methodology to investigate a wide range of organic and biological compounds by mass spectrometry. More specifically, H/D exchange (HDX) is used in proteomics to examine the conformation of proteins or in tandem mass spectrometry to confirm and understand the fragmentation pathway. Combined with high-resolution mass spectrometry, the HDX approach ensures the obtaining of chemical and structural information about an individual component of a complex mixture. Isotope labeling was already performed for the analysis of natural complex mixtures.^{374,375} The capabilities of H/D exchange in mass spectrometry have been recently reviewed by Kostyukevich et al.³⁷⁶ Typically, the H/D experiment is performed in solution, and exchangeable hydrogen atoms are only the labile ones. Recently, Nikolaev group developed a new methodology, which ensures the online H/D exchange reaction in the ionization source under atmospheric pressure. In that case, the labile hydrogen atoms are exchanged and part of the less or non-labile ones.³⁷⁷ This approach has been used in various applications and more specifically in the petroleomic field to investigate oils and bio-oils, whatever the atmospheric ionization source (ESI, APCI, and APPI). After the dissolution of a vacuum residue in a mixture of toluene-d₈ and methanol-d₄ and the addition of D₂O and DCOOD to increase the efficiency of HDX, Zhang et al. investigated the compositional variation of the intermediate amine compounds during the heavy petroleum hydrotreatment process for N₁ compounds.³⁷⁸ Depending on the number of exchanged labile hydrogen atoms, they were able to evidence pyridines (N₁D₁), cyclic (N₁D₂), and primary (N₁D₃) amines by FT-ICR and Orbitrap MS. The observation of N₁D₂ (not detected in the feedstock) in the treated heavy petroleum nicely demonstrated the conversion of pyridines into cyclic amines. The application of this methodology to the effluent of four-reactor pilot hydrotreatment plants allowed the authors to compare the efficiency of the HDN. The use of a similar approach by Cho and al. ensured the investigation of the N-containing class compound in crude oils by APPI HDX mass spectrometry. These authors confirmed that the prominent part of N₁ crude oil components was pyridines.³⁷⁹ Moreover, these authors applied this methodology to the resin fractions obtained by the SARA fractionation of two oils. More interestingly, this methodology was employed to study the compositional changes at the molecular level of weathered oils in the context of the Hebei Spirit oil spill.³⁸⁰ The comparison of the resin fraction of the crude oil and the associated weathered oils by APPI HDX mass spectrometry led the authors to understand that secondary and tertiary N₁ amine-containing compounds were preferentially degraded during the early stage of the natural weathering. In the alternative methodology developed by the Nikolaev group, in-ESI source isotope exchange was conducted. The atmosphere was saturated by D₂O vapors in the region between the ESI tip and the inlet of the desolvating

capillary by placing a D_2O drop on a copper plate close to the ESI needle. In these conditions, both labile hydrogen and non-labile hydrogen atoms were exchanged due to gas-phase reactions. The proof of concept of this approach and the mechanism/kinetic description had been extensively described in a recent paper.³⁷⁷ Acter et al.³⁸¹ used a similar methodology to investigate nitrogen-, oxygen- and sulfur-containing compounds in the polar fraction of petroleum samples by in-APPI HDX mass spectrometry. In this work, the D_2O was continuously delivered on a metallic plate in the APPI source. For part of the S_1 compounds, these experiments evidenced the presence of one exchangeable hydrogen atom attached to the sulfur atom (thiol), whereas two H/D exchanges were observed with S_2O_1 . Thus, comparable results were observed using HDX protocols in source APPI HDX mass spectrometry. To go deeper into the structural description of the crude oil components, Kostyukevich used "advanced" isotope exchange in near-critical water using both D_2O and $H_2^{18}O$ ³⁸². H/D or $^{16}O/^{18}O$ may be performed in near-critical water conditions by sealing crude oil with added D_2O or $H_2^{18}O$ in an autoclave at a temperature greater than 573 K and a pressure greater than 30 MPa (the critical temperature and critical pressure of water are 647 K and 22 MPa, respectively). H/D exchange was observed in these experimental conditions for labile hydrogen atoms from functional groups such as $-OH$, $-COOH$, $-NH$, and $-SH$ and, for non-labile hydrogen atoms such as aromatic hydrogens or alpha hydrogens. $^{16}O/^{18}O$ exchange occurred for the oxygen of the carbonyl group. Up to three $^{16}O/^{18}O$ exchanges have been observed in the investigated crude oil.

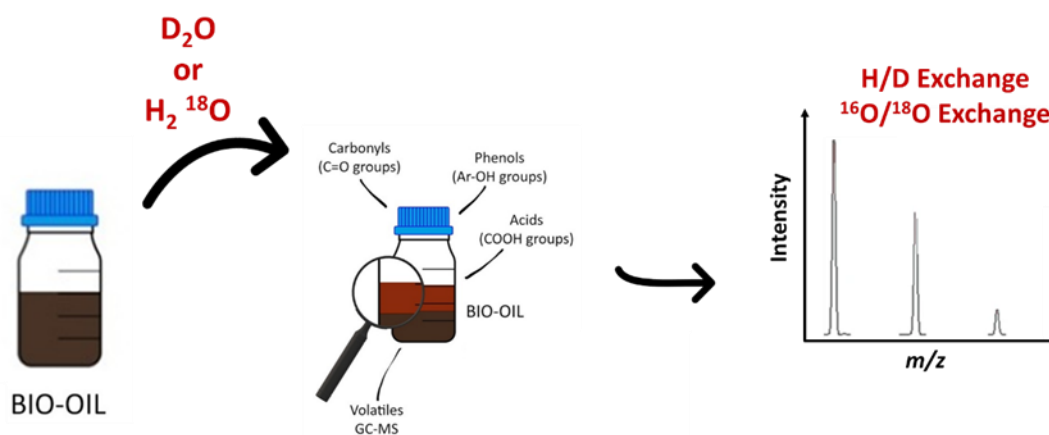


Figure 1-35: The outline for the isotope labelling.

The authors determined that $^{16}O/^{18}O$ exchanges occurred for 276 of the 1500 detected features observed by negative ESI mass spectrometry. The combination of these isotope exchanges with NMR measurements led the authors to propose some putative structures.³⁸³ More recently, the same authors applied H/D or $^{16}O/^{18}O$ isotopic exchange to investigate bio-oils produced by HTL of different raw materials including biomass and food waste.³⁸³ By combining isotope exchange, which gained insights about the presence of functional groups

in an individual molecule, tandem mass spectrometry, and specific software for the data treatment, they proposed a putative structure for close to 350 individual features.

1.5.9. Towards a quantitative approach to petroleomic data

Since ionization efficiency is highly component-dependent, notably for ESI, quantification by untargeted analysis is critical. However, as demonstrated by Son et al.,³⁸⁴ APPI FT-ICR MS measurements of four crude oil samples over 3 months showed very good repeatability, which was the first step for consistent semi-quantitative data. As described in previous sections, ionization competition increases with the complexity of the sample. Some solutions have been proposed in the literature to move towards quantitative data or at least semi-quantitative data. The first consists of reducing sample complexity by using a fractionation or separation step prior to mass spectrometry analysis. For example, Santos et al. used the SARA methodology to obtain light compounds, asphaltene, saturate, aromatic, and two resin fractions before positive ESI or APPI analysis.²⁷⁷ Rodgers et al. used a similar approach by considering the modified aminopropyl silica (MAPS) fractionation of bitumen.³⁸⁵ Lacroix-Andrivet et al. used another methodology by combining high-performance thin-layer chromatography (HPTLC) and laser desorption-ionization (LDI) FT-ICR MS to analyze bitumen.³⁸⁶ The HPTLC of bitumen on cellulose with a heptane/ethanol solvent mixture ensured the separation of maltenes and asphaltenes. The LDI provided the direct analysis of both fractions. The chemical properties of the compounds in the obtained fractions were generally thought to be close enough to reduce the ionization competition phenomenon.

The second approach combined high-resolution mass spectrometry and quantitative comprehensive GCxGC analysis. Guillemant et al. investigated the N₁ compounds of different gas oils by GCxGC nitrogen chemiluminescent detection (NCD) and positive or negative ESI FT-ICR MS.³⁸⁷ The studied gas oils underwent a Flash HPLC pre-fractionation before the analysis to remove the hydrocarbon matrix. The NCD ensured the absolute quantitation of nitrogen compounds. Indeed, the measured signal was directly proportional to the concentration of the nitrogen amounts. The comprehensive GCxGC-NCD led to the efficient separation of basic and neutral N₁ compounds. Moreover, it was possible to distinguish on the 2D chromatogram, for each N₁ class, the compounds with respect to their DBE value. Consequently, the absolute concentration of indoles, carbazoles, tetrahydroquinolines, anilines, pyridines, quinolines, and acridine was obtained. The obtained concentration by GCxGC-NCD did not linearly correlate with the integration of the signal observed by ESI in positive (tetrahydroquinolines, anilines, pyridines DBE 4-5-6, quinolines 7-8-9, and acridine 10-11-12) and negative (indoles DBE 6-7-8, and carbazoles DBE 9-10-11) detection modes. Thus, the ionization competition phenomenon was evidenced. Consequently, the concentration of a given compound and its abundance on the mass spectrum were not simply correlated. The use of multiple linear regression (MLR) ensured the establishment of such correlation. Interestingly this MLR

procedure also ensures the evaluation of the ionization competition phenomenon. Alternatively, Reymond et al. proposed an off-line comprehensive three-dimensional method to quantify polycyclic aromatic hydrocarbons (PAH) in vacuum gas oils.³⁸⁸ After centrifugal partition chromatography (CPC) fractionation, the resulting fractions were analyzed by supercritical fluid chromatography hyphenated to APPI FT-ICR MS. The CPC separation, according to alkylation degree, limited the ion suppression phenomenon. In the used experimental conditions, the MS area of PAH and heavy PAH correlated with their concentration in the investigated gas oils. This approach was validated by spiking the analyzed samples with pyrene-d10. The same authors used this methodology to monitor the evolution of PAH concentration during the hydrotreatment of different vacuum gas oil feedstocks.³⁸⁹

1.6. Conclusion

It is possible to use a variety of thermochemical techniques to produce high added-value chemicals and second-generation biofuels from lignocellulosic biomass. The first method is liquefaction or pyrolysis, which turns solid biomass into a liquid bio-oil. Various paths must be used to upgrade the bio-oil in order to get fuels or chemicals because of its composition.

Nevertheless, a bio-oils complete composition must be known, in order to use it properly. Given the great level of complexity, it is still difficult to describe this substance in full since there is no universal method for this description. Each analytical technique that is utilized does, in fact, have its own originality. To quantify and qualify various functional groups, NMR methods are used. According to their polarity or volatility, some kinds of chemicals can be quantified and identified using chromatographic methods. Additionally, when these methods are combined with MSⁿ, structural information may be acquired.

Petroleomic-based techniques are essential in unraveling the complexity of these products and directing the chemical conversion in order to characterize compounds across a larger mass range. An extensive description of the oligomeric composition of such products at the molecular level is emphasized from the high-resolution mass spectrometry data. To meet the objectives of an accurate control of chemical conversion, it is obvious that there are complex knowledge gaps that must be filled. To fully comprehend the reactivity of the various characteristics indicated by HRMS, access to their chemical properties is very important. Nevertheless, based on what has developed in the petroleum sector, several promising paths to bring some extra data on such complicated mixtures may be drawn. By incorporating fractionation and separation techniques before the mass analysis, recent advancements currently attempt to reduce the experimental restrictions like the selective ionization. Furthermore, many approaches may be used to describe the variety of chemicals that give rise to an MS signal in petroleomic. Although just a few studies have been published on bio-oils, ion mobility mass spectrometry is promising in terms of the isomeric level and offers several

research opportunities. Several new approaches integrate tags of chemical characteristics by classes or more precisely by the functional groups involving derivatization and labelling steps. This aspect is also poorly studied in the field of bio-oil characterization and will be presented in this study.

1.7. References

- (1) Lu, Q.; Li, W.-Z.; Zhu, X.-F. Overview of Fuel Properties of Biomass Fast Pyrolysis Oils. *Energy Convers. Manag.* **2009**, *50* (5), 1376–1383. <https://doi.org/10.1016/j.enconman.2009.01.001>.
- (2) Czernik, S.; Bridgwater, A. V. Overview of Applications of Biomass Fast Pyrolysis Oil. *Energy Fuels* **2004**, *18* (2), 590–598. <https://doi.org/10.1021/ef034067u>.
- (3) Huang, H.; Yuan, X.; Zhu, H.; Li, H.; Liu, Y.; Wang, X.; Zeng, G. Comparative Studies of Thermochemical Liquefaction Characteristics of Microalgae, Lignocellulosic Biomass and Sewage Sludge. *Energy* **2013**, *56*, 52–60. <https://doi.org/10.1016/j.energy.2013.04.065>.
- (4) Azevedo, S. G.; Sequeira, T.; Santos, M.; Mendes, L. Biomass-Related Sustainability: A Review of the Literature and Interpretive Structural Modeling. *Energy* **2019**, *171*, 1107–1125. <https://doi.org/10.1016/j.energy.2019.01.068>.
- (5) Antar, M.; Lyu, D.; Nazari, M.; Shah, A.; Zhou, X.; Smith, D. L. Biomass for a Sustainable Bioeconomy: An Overview of World Biomass Production and Utilization. *Renew. Sustain. Energy Rev.* **2021**, *139*, 110691. <https://doi.org/10.1016/j.rser.2020.110691>.
- (6) Alper, K.; Tekin, K.; Karagöz, S. Pyrolysis of Agricultural Residues for Bio-Oil Production. *Clean Technol. Environ. Policy* **2015**, *17* (1), 211–223. <https://doi.org/10.1007/s10098-014-0778-8>.
- (7) Osman, A. I.; Mehta, N.; Elgarahy, A. M.; Al-Hinai, A.; Al-Muhtaseb, A. H.; Rooney, D. W. Conversion of Biomass to Biofuels and Life Cycle Assessment: A Review. *Environ. Chem. Lett.* **2021**, *19* (6), 4075–4118. <https://doi.org/10.1007/s10311-021-01273-0>.
- (8) Tursi, A. A Review on Biomass: Importance, Chemistry, Classification, and Conversion. *Biofuel Res. J.* **2019**, *6*, 962–979. <https://doi.org/10.18331/BRJ2019.6.2.3>.
- (9) Jin, W.; Pastor-Pérez, L.; Villora-Pico, J. J.; Pastor-Blas, M. M.; Sepúlveda-Escribano, A.; Gu, S.; Charisiou, N. D.; Papageridis, K.; Goula, M. A.; Reina, T. R. Catalytic Conversion of Palm Oil to Bio-Hydrogenated Diesel over Novel N-Doped Activated Carbon Supported Pt Nanoparticles. *Energies* **2020**, *13* (1), 132. <https://doi.org/10.3390/en13010132>.
- (10) Prasad, A.; Sotenko, M.; Blenkinsopp, T.; Coles, S. R. Life Cycle Assessment of Lignocellulosic Biomass Pretreatment Methods in Biofuel Production. *Int. J. Life Cycle Assess.* **2016**, *21* (1), 44–50. <https://doi.org/10.1007/s11367-015-0985-5>.
- (11) Vassilev, S. V.; Baxter, D.; Andersen, L. K.; Vassileva, C. G.; Morgan, T. J. An Overview of the Organic and Inorganic Phase Composition of Biomass. *Fuel* **2012**, *94*, 1–33. <https://doi.org/10.1016/j.fuel.2011.09.030>.
- (12) H. Isikgor, F.; Remzi Becer, C. Lignocellulosic Biomass: A Sustainable Platform for the Production of Bio-Based Chemicals and Polymers. *Polym. Chem.* **2015**, *6* (25), 4497–4559. <https://doi.org/10.1039/C5PY00263J>.

- (13) Wang, F.; Ouyang, D.; Zhou, Z.; Page, S. J.; Liu, D.; Zhao, X. Lignocellulosic Biomass as Sustainable Feedstock and Materials for Power Generation and Energy Storage. *J. Energy Chem.* **2021**, *57*, 247–280. <https://doi.org/10.1016/j.jechem.2020.08.060>.
- (14) Amesho, K. T. T.; Lin, Y.-C.; Mohan, S. V.; Halder, S.; Ponnusamy, V. K.; Jhang, S.-R. Deep Eutectic Solvents in the Transformation of Biomass into Biofuels and Fine Chemicals: A Review. *Environ. Chem. Lett.* **2022**. <https://doi.org/10.1007/s10311-022-01521-x>.
- (15) Alper, K.; Tekin, K.; Karagöz, S.; Ragauskas, A. J. Sustainable Energy and Fuels from Biomass: A Review Focusing on Hydrothermal Biomass Processing. *Sustain. Energy Fuels* **2020**, *4* (9), 4390–4414. <https://doi.org/10.1039/D0SE00784F>.
- (16) Carpenter, D.; Westover, T. L.; Czernik, S.; Jablonski, W. Biomass Feedstocks for Renewable Fuel Production: A Review of the Impacts of Feedstock and Pretreatment on the Yield and Product Distribution of Fast Pyrolysis Bio-Oils and Vapors. *Green Chem.* **2014**, *16* (2), 384–406. <https://doi.org/10.1039/c3gc41631c>.
- (17) Cherubini, F. The Biorefinery Concept: Using Biomass Instead of Oil for Producing Energy and Chemicals. *Energy Convers. Manag.* **2010**, *51* (7), 1412–1421. <https://doi.org/10.1016/j.enconman.2010.01.015>.
- (18) Lourenço, A.; Pereira, H.; Lourenço, A.; Pereira, H. *Compositional Variability of Lignin in Biomass*; IntechOpen, 2017. <https://doi.org/10.5772/intechopen.71208>.
- (19) Sun, R. Lignin Source and Structural Characterization. *ChemSusChem* **2020**, *13* (17), 4385–4393. <https://doi.org/10.1002/cssc.202001324>.
- (20) Chakar, F. S.; Ragauskas, A. J. Review of Current and Future Softwood Kraft Lignin Process Chemistry. *Ind. Crops Prod.* **2004**, *20* (2), 131–141. <https://doi.org/10.1016/j.indcrop.2004.04.016>.
- (21) Barakat, A.; de Vries, H.; Rouau, X. Dry Fractionation Process as an Important Step in Current and Future Lignocellulose Biorefineries: A Review. *Bioresour. Technol.* **2013**, *134*, 362–373. <https://doi.org/10.1016/j.biortech.2013.01.169>.
- (22) Jia, P.; Wang, J.; Zhang, W. Catalytic Hydrothermal Liquefaction of Lignin over Carbon Nanotube Supported Metal Catalysts for Production of Monomeric Phenols. *J. Energy Inst.* **2021**, *94*, 1–10. <https://doi.org/10.1016/j.joei.2020.09.014>.
- (23) Ahlbom, A.; Maschietti, M.; Nielsen, R.; Hasani, M.; Theliander, H. Towards Understanding Kraft Lignin Depolymerisation under Hydrothermal Conditions. *Holzforschung* **2021**, *76* (1), 37–48. <https://doi.org/10.1515/hf-2021-0121>.
- (24) Ragauskas et al. - 2014 - Lignin Valorization Improving Lignin Processing i.Pdf. <https://cellulosicbiomasslab.engr.ucr.edu/sites/default/files/2019-02/Lignin%20Valorization%20improving.pdf> (accessed 2022-11-11).
- (25) Garedew, M.; Lin, F.; Song, B.; DeWinter, T. M.; Jackson, J. E.; Saffron, C. M.; Lam, C. H.; Anastas, P. T. Greener Routes to Biomass Waste Valorization: Lignin Transformation Through Electrocatalysis for Renewable Chemicals and Fuels Production. *ChemSusChem* **2020**, *13* (17), 4214–4237. <https://doi.org/10.1002/cssc.202000987>.
- (26) Klemm, D.; Heublein, B.; Fink, H.-P.; Bohn, A. Cellulose: Fascinating Biopolymer and Sustainable Raw Material. *Angew. Chem. Int. Ed.* **2005**, *44* (22), 3358–3393. <https://doi.org/10.1002/anie.200460587>.
- (27) Klemm, D.; Heinze, T.; Philipp, B.; Wagenknecht, W. New Approaches to Advanced Polymers by Selective Cellulose Functionalization. *Acta Polym.* **1997**, *48* (8), 277–297. <https://doi.org/10.1002/actp.1997.010480801>.

- (28) Sorek, N.; Yeats, T. H.; Szemenyei, H.; Youngs, H.; Somerville, C. R. The Implications of Lignocellulosic Biomass Chemical Composition for the Production of Advanced Biofuels. *BioScience* **2014**, *64* (3), 192–201. <https://doi.org/10.1093/biosci/bit037>.
- (29) Liu, H.; Sun, J.; Chang, J.-S.; Shukla, P. Engineering Microbes for Direct Fermentation of Cellulose to Bioethanol. *Crit. Rev. Biotechnol.* **2018**, *38* (7), 1089–1105. <https://doi.org/10.1080/07388551.2018.1452891>.
- (30) Balat, M.; Balat, H.; Öz, C. Progress in Bioethanol Processing. *Prog. Energy Combust. Sci.* **2008**, *34* (5), 551–573. <https://doi.org/10.1016/j.peccs.2007.11.001>.
- (31) Pulidindi, I. N.; Kimchi, B. B.; Gedanken, A. Can Cellulose Be a Sustainable Feedstock for Bioethanol Production? *Renew. Energy* **2014**, *71*, 77–80. <https://doi.org/10.1016/j.renene.2014.05.032>.
- (32) Scheller, H. V.; Ulvskov, P. Hemicelluloses. *Annu. Rev. Plant Biol.* **2010**, *61* (1), 263–289. <https://doi.org/10.1146/annurev-arplant-042809-112315>.
- (33) Sheldon, R. A. ChemInform Abstract: Green and Sustainable Manufacture of Chemicals from Biomass: State of the Art. *ChemInform* **2014**, *45* (19), no-no. <https://doi.org/10.1002/chin.201419293>.
- (34) Toor, M.; Kumar, S. S.; Malyan, S. K.; Bishnoi, N. R.; Mathimani, T.; Rajendran, K.; Pugazhendhi, A. An Overview on Bioethanol Production from Lignocellulosic Feedstocks. *Chemosphere* **2020**, *242*, 125080. <https://doi.org/10.1016/j.chemosphere.2019.125080>.
- (35) Wettstein, S. G.; Alonso, D. M.; Gürbüz, E. I.; Dumesic, J. A. A Roadmap for Conversion of Lignocellulosic Biomass to Chemicals and Fuels. *Curr. Opin. Chem. Eng.* **2012**, *1* (3), 218–224. <https://doi.org/10.1016/j.coche.2012.04.002>.
- (36) Cantero, D. A. Intensification of Cellulose Hydrolysis Process by Supercritical Water. Obtaining of Added Value Products. **2014**. <https://doi.org/10.13140/2.1.4261.6323>.
- (37) Holliday, R. L.; King, J. W.; List, G. R. Hydrolysis of Vegetable Oils in Sub- and Supercritical Water. *Ind. Eng. Chem. Res.* **1997**, *36* (3), 932–935. <https://doi.org/10.1021/ie960668f>.
- (38) Santori, G.; Di Nicola, G.; Moglie, M.; Polonara, F. A Review Analyzing the Industrial Biodiesel Production Practice Starting from Vegetable Oil Refining. *Appl. Energy* **2012**, *92*, 109–132. <https://doi.org/10.1016/j.apenergy.2011.10.031>.
- (39) Long, F.; Liu, W.; Jiang, X.; Zhai, Q.; Cao, X.; Jiang, J.; Xu, J. State-of-the-Art Technologies for Biofuel Production from Triglycerides: A Review. *Renew. Sustain. Energy Rev.* **2021**, *148*, 111269. <https://doi.org/10.1016/j.rser.2021.111269>.
- (40) Thomas, A.; Müller, S. S.; Frey, H. Beyond Poly(Ethylene Glycol): Linear Polyglycerol as a Multifunctional Polyether for Biomedical and Pharmaceutical Applications. *Biomacromolecules* **2014**, *15* (6), 1935–1954. <https://doi.org/10.1021/bm5002608>.
- (41) Behr, A.; Eilting, J.; Irawadi, K.; Leschinski, J.; Lindner, F. Improved Utilisation of Renewable Resources: New Important Derivatives of Glycerol. *Green Chem* **2008**, *10* (1), 13–30. <https://doi.org/10.1039/B710561D>.
- (42) Besse, X. Conversion catalytique de composés modèles de biomasse en conditions hydrothermales. **2015**, 238.
- (43) Lammens, T. M.; Franssen, M. C. R.; Scott, E. L.; Sanders, J. P. M. Availability of Protein-Derived Amino Acids as Feedstock for the Production of Bio-Based Chemicals. *Biomass Bioenergy* **2012**, *44*, 168–181. <https://doi.org/10.1016/j.biombioe.2012.04.021>.

- (44) Lammens, T. M.; Le Nôtre, J.; Franssen, M. C. R.; Scott, E. L.; Sanders, J. P. M. Synthesis of Biobased Succinonitrile from Glutamic Acid and Glutamine. *ChemSusChem* **2011**, *4* (6), 785–791. <https://doi.org/10.1002/cssc.201100030>.
- (45) *Biomass in the manufacture of industrial products—the use of proteins and amino acids* / SpringerLink. <https://link.springer.com/article/10.1007/s00253-007-0932-x> (accessed 2022-11-11).
- (46) Buchanan, R. A. HYDROCARBON· AND RUBBER-PRODUCING CROPS. 8.
- (47) Bowers, J. E. *Natural Rubber-Producing Plants for the United States*; National Agricultural Library, 1990.
- (48) Thy, P.; Yu, C.; Jenkins, B. M.; Leshner, C. E. Inorganic Composition and Environmental Impact of Biomass Feedstock. *Energy Fuels* **2013**, *27* (7), 3969–3987. <https://doi.org/10.1021/ef400660u>.
- (49) Kumar, R.; Dhurandhar, R.; Chakraborty, S.; Ghosh, A. K. Chapter 12 - Downstream Process: Toward Cost/Energy Effectiveness. In *Handbook of Biofuels*; Sahay, S., Ed.; Academic Press, 2022; pp 249–260. <https://doi.org/10.1016/B978-0-12-822810-4.00012-9>.
- (50) Alalwan, H. A.; Alminshid, A. H.; Aljaafari, H. A. S. Promising Evolution of Biofuel Generations. Subject Review. *Renew. Energy Focus* **2019**, *28*, 127–139. <https://doi.org/10.1016/j.ref.2018.12.006>.
- (51) Naik, S. N.; Goud, V. V.; Rout, P. K.; Dalai, A. K. Production of First and Second Generation Biofuels: A Comprehensive Review. *Renew. Sustain. Energy Rev.* **2010**, *14* (2), 578–597. <https://doi.org/10.1016/j.rser.2009.10.003>.
- (52) Martin, M. A. First Generation Biofuels Compete. *New Biotechnol.* **2010**, *27* (5), 596–608. <https://doi.org/10.1016/j.nbt.2010.06.010>.
- (53) *RFA Publications*. <https://ethanolrfa.org/library/rfa-publications> (accessed 2022-11-12).
- (54) Sánchez, Ó. J.; Cardona, C. A. Trends in Biotechnological Production of Fuel Ethanol from Different Feedstocks. *Bioresour. Technol.* **2008**, *99* (13), 5270–5295. <https://doi.org/10.1016/j.biortech.2007.11.013>.
- (55) Naik, S. N.; Goud, V. V.; Rout, P. K.; Dalai, A. K. Production of First and Second Generation Biofuels: A Comprehensive Review. *Renew. Sustain. Energy Rev.* **2010**, *14* (2), 578–597. <https://doi.org/10.1016/j.rser.2009.10.003>.
- (56) Cirqueira, N.; de Souza Candeco, E.; Barboza, L.; Troyner, F.; Martins Teixeira de Abreu Pietrobél, J.; Bittencourt Sydney, E. Sugarcane First-Generation Bioethanol Units and Advancements in Electric Power and Biogas Production. In *Liquid Biofuels: Bioethanol*; Soccol, C. R., Amarante Guimarães Pereira, G., Dussap, C.-G., Porto de Souza Vandenberghe, L., Eds.; Biofuel and Biorefinery Technologies; Springer International Publishing: Cham, 2022; Vol. 12, pp 85–107. https://doi.org/10.1007/978-3-031-01241-9_5.
- (57) Panella, L. Sugar Beet as an Energy Crop. *Sugar Tech* **2010**, *12* (3–4), 288–293. <https://doi.org/10.1007/s12355-010-0041-5>.
- (58) Waclawovsky, A. J.; Sato, P. M.; Lembke, C. G.; Moore, P. H.; Souza, G. M. Sugarcane for Bioenergy Production: An Assessment of Yield and Regulation of Sucrose Content. *Plant Biotechnol. J.* **2010**, *8* (3), 263–276. <https://doi.org/10.1111/j.1467-7652.2009.00491.x>.
- (59) Claassen, P. A. M.; van Lier, J. B.; Lopez Contreras, A. M.; van Niel, E. W. J.; Sijtsma, L.; Stams, A. J. M.; de Vries, S. S.; Weusthuis, R. A. Utilisation of Biomass for the Supply of

- Energy Carriers. *Appl. Microbiol. Biotechnol.* **1999**, 52 (6), 741–755. <https://doi.org/10.1007/s002530051586>.
- (60) Apar, D. K.; Özbek, B. σ -Amylase Inactivation during Corn Starch Hydrolysis Process. *Process Biochem.* **2004**, 39 (12), 1877–1892. <https://doi.org/10.1016/j.procbio.2003.09.014>.
- (61) Robertson, G. H.; Wong, D. W. S.; Lee, C. C.; Wagschal, K.; Smith, M. R.; Orts, W. J. Native or Raw Starch Digestion: A Key Step in Energy Efficient Biorefining of Grain. *J. Agric. Food Chem.* **2006**, 54 (2), 353–365. <https://doi.org/10.1021/jf051883m>.
- (62) Soni, S. K.; Kaur, A.; Gupta, J. K. A Solid State Fermentation Based Bacterial α -Amylase and Fungal Glucoamylase System and Its Suitability for the Hydrolysis of Wheat Starch. *Process Biochem.* **2003**, 39 (2), 185–192. [https://doi.org/10.1016/S0032-9592\(03\)00058-X](https://doi.org/10.1016/S0032-9592(03)00058-X).
- (63) Pandey, A.; Soccol, C. R.; Mitchell, D. New Developments in Solid State Fermentation: I- Bioprocesses and Products. *Process Biochem.* **2000**, 35 (10), 1153–1169. [https://doi.org/10.1016/S0032-9592\(00\)00152-7](https://doi.org/10.1016/S0032-9592(00)00152-7).
- (64) Menezes, E.; Cataluña, R. Optimization of the ETBE (Ethyl Tert-Butyl Ether) Production Process. *Fuel Process. Technol. - FUEL PROCESS TECHNOL* **2008**, 89, 1148–1152. <https://doi.org/10.1016/j.fuproc.2008.05.006>.
- (65) Croezen, H.; Kampman, B. The Impact of Ethanol and ETBE Blending on Refinery Operations and GHG-Emissions. *Energy Policy* **2009**, 37 (12), 5226–5238. <https://doi.org/10.1016/j.enpol.2009.07.072>.
- (66) Tutak, W. Bioethanol E85 as a Fuel for Dual Fuel Diesel Engine. *Energy Convers. Manag.* **2014**, 86, 39–48. <https://doi.org/10.1016/j.enconman.2014.05.016>.
- (67) Bozbas, K. Biodiesel as an Alternative Motor Fuel: Production and Policies in the European Union. *Renew. Sustain. Energy Rev.* **2008**, 12 (2), 542–552. <https://doi.org/10.1016/j.rser.2005.06.001>.
- (68) F. Ma et M. A. Hanna, « Biodiesel production: a review », *Bioresour. Technol.*, p. 16, 1999.
- (69) *Production | Biofuels.* <https://sites.lafayette.edu/egrs352-sp15-biofuels/benefits/> (accessed 2022-11-16).
- (70) Demirbas, A. Biodiesel Production from Vegetable Oils via Catalytic and Non-Catalytic Supercritical Methanol Transesterification Methods. *Prog. Energy Combust. Sci.* **2005**, 31 (5–6), 466–487. <https://doi.org/10.1016/j.pecc.2005.09.001>.
- (71) Sonntag, N. O. V. Esterification and Interesterification. *J. Am. Oil Chem. Soc.* **1979**, 56 (11Part1), 751A-754A. <https://doi.org/10.1007/BF02667436>.
- (72) Schwab, A. W.; Bagby, M. O.; Freedman, B. Preparation and Properties of Diesel Fuels from Vegetable Oils. *Fuel* **1987**, 66 (10), 1372–1378. [https://doi.org/10.1016/0016-2361\(87\)90184-0](https://doi.org/10.1016/0016-2361(87)90184-0).
- (73) *9.2 The Reaction of Biodiesel: Transesterification | EGEE 439: Alternative Fuels from Biomass Sources.* <https://www.e-education.psu.edu/egee439/node/684> (accessed 2022-11-16).
- (74) Freedman, B.; Butterfield, R. O.; Pryde, E. H. Transesterification Kinetics of Soybean Oil 1. *J. Am. Oil Chem. Soc.* **1986**, 63 (10), 1375–1380. <https://doi.org/10.1007/BF02679606>.

- (75) Freedman, B.; Pryde, E. H.; Mounts, T. L. Variables Affecting the Yields of Fatty Esters from Transesterified Vegetable Oils. *J. Am. Oil Chem. Soc.* **1984**, *61* (10), 1638–1643. <https://doi.org/10.1007/BF02541649>.
- (76) Ma, F.; Hanna, M. A. Biodiesel Production: A Review. *Bioresour. Technol.* **1999**, *16*.
- (77) Ma, F.; Clements, L. D.; Hanna, M. The Effects of Catalyst, Free Fatty Acids, and Water on Transesterification of Beef Tallow. *5*.
- (78) Sprules, F. J. PRODUCTION OF FATTY ESTERS. *6*.
- (79) Huber et al. - 2006 - Synthesis of Transportation Fuels from Biomass Ch.Pdf. https://ncfap.org/documents/biofuels_aviation/Huber%20George%20Biofuels%20Review.pdf (accessed 2022-11-12).
- (80) Wright, H. J.; Segur, J. B.; Clark, H. V.; Coburn, S. K.; Langdon, E. E.; DuPuis, R. N. A Report on Ester Interchange. *Oil Soap* **1944**, *21* (5), 145–148. <https://doi.org/10.1007/BF02549470>.
- (81) Bradshaw, G. B.; Meuly, W. C. UNITED STATES PATENT OFFICE. *8*.
- (82) Huber, G. W.; Iborra, S.; Corma, A. Synthesis of Transportation Fuels from Biomass: Chemistry, Catalysts, and Engineering. *Chem. Rev.* **2006**, *106* (9), 4044–4098. <https://doi.org/10.1021/cr068360d>.
- (83) Smith, M. K. UNITED STATES PATENT OFFICE. *4*.
- (84) López, D. E.; Goodwin, J. G.; Bruce, D. A.; Lotero, E. Transesterification of Triacetin with Methanol on Solid Acid and Base Catalysts. *Appl. Catal. Gen.* **2005**, *295* (2), 97–105. <https://doi.org/10.1016/j.apcata.2005.07.055>.
- (85) Kim, H.-J.; Kang, B.-S.; Kim, M.-J.; Park, Y. M.; Kim, D.-K.; Lee, J.-S.; Lee, K.-Y. Transesterification of Vegetable Oil to Biodiesel Using Heterogeneous Base Catalyst. *Catal. Today* **2004**, *93–95*, 315–320. <https://doi.org/10.1016/j.cattod.2004.06.007>.
- (86) Cantrell, D. G.; Gillie, L. J.; Lee, A. F.; Wilson, K. Structure-Reactivity Correlations in MgAl Hydrotalcite Catalysts for Biodiesel Synthesis. *Appl. Catal. Gen.* **2005**, *287* (2), 183–190. <https://doi.org/10.1016/j.apcata.2005.03.027>.
- (87) Kulkarni, M.; Gopinath, R.; Meher, L. charan; Dalai, A. Solid Acid Catalyzed Biodiesel Production by Simultaneous Esterification and Transesterification. *Green Chem. - GREEN CHEM* **2006**, *8*. <https://doi.org/10.1039/b605713f>.
- (88) Borges, M. E.; Díaz, L. Recent Developments on Heterogeneous Catalysts for Biodiesel Production by Oil Esterification and Transesterification Reactions: A Review. *Renew. Sustain. Energy Rev.* **2012**, *16* (5), 2839–2849. <https://doi.org/10.1016/j.rser.2012.01.071>.
- (89) Mohr, A.; Raman, S. Lessons from First Generation Biofuels and Implications for the Sustainability Appraisal of Second Generation Biofuels. *Energy Policy* **2013**, *63*, 114–122. <https://doi.org/10.1016/j.enpol.2013.08.033>.
- (90) Brown, L. M.; Zeiler, K. G. Aquatic Biomass and Carbon Dioxide Trapping. *Energy Convers. Manag.* **1993**, *34* (9–11), 1005–1013. [https://doi.org/10.1016/0196-8904\(93\)90048-F](https://doi.org/10.1016/0196-8904(93)90048-F).
- (91) Chen, W.-H.; Lin, B.-J.; Huang, M.-Y.; Chang, J.-S. Thermochemical Conversion of Microalgal Biomass into Biofuels: A Review. *Bioresour. Technol.* **2015**, *184*, 314–327. <https://doi.org/10.1016/j.biortech.2014.11.050>.
- (92) Meinita, M. D. N.; Kang, J.-Y.; Jeong, G.-T.; Koo, H. M.; Park, S. M.; Hong, Y.-K. Bioethanol Production from the Acid Hydrolysate of the Carrageenophyte *Kappaphycus Alvarezii*

- (Cottonii). *J. Appl. Phycol.* **2012**, *24* (4), 857–862. <https://doi.org/10.1007/s10811-011-9705-0>.
- (93) Abd-Rahim, F.; Wasoh, H.; Zakaria, M. R.; Ariff, A.; Kapri, R.; Ramli, N.; Siew-Ling, L. Production of High Yield Sugars from *Kappaphycus Alvarezii* Using Combined Methods of Chemical and Enzymatic Hydrolysis. *Food Hydrocoll.* **2014**, *42*, 309–315. <https://doi.org/10.1016/j.foodhyd.2014.05.017>.
- (94) Wei, N.; Quarterman, J.; Jin, Y.-S. Marine Macroalgae: An Untapped Resource for Producing Fuels and Chemicals. *Trends Biotechnol.* **2013**, *31* (2), 70–77. <https://doi.org/10.1016/j.tibtech.2012.10.009>.
- (95) *Transport and sustainability*. Transport and sustainability. <https://www.open.edu/openlearn/science-maths-technology/transport-and-sustainability/science-maths-technology/transport-and-sustainability> (accessed 2022-11-16).
- (96) Sheldon, R. A. ChemInform Abstract: Green and Sustainable Manufacture of Chemicals from Biomass: State of the Art. *ChemInform* **2014**, *45* (19), no-no. <https://doi.org/10.1002/chin.201419293>.
- (97) Karaosmanoğlu, F.; Tetik, E.; Göllü, E. Biofuel Production Using Slow Pyrolysis of the Straw and Stalk of the Rapeseed Plant. *Fuel Process. Technol.* **1999**, *59* (1), 1–12. [https://doi.org/10.1016/S0378-3820\(99\)00004-1](https://doi.org/10.1016/S0378-3820(99)00004-1).
- (98) Chandra, R.; Takeuchi, H.; Hasegawa, T. Methane Production from Lignocellulosic Agricultural Crop Wastes: A Review in Context to Second Generation of Biofuel Production. *Renew. Sustain. Energy Rev.* **2012**, *16* (3), 1462–1476. <https://doi.org/10.1016/j.rser.2011.11.035>.
- (99) Glithero, N. J.; Wilson, P.; Ramsden, S. J. Straw Use and Availability for Second Generation Biofuels in England. *Biomass Bioenergy* **2013**, *55*, 311–321. <https://doi.org/10.1016/j.biombioe.2013.02.033>.
- (100) Pankin, K. E. Estimated Heats of Combustion of Biofuels Based on Wood and Wood-Waste Pyrolysis Products. *Chem. Technol. Fuels Oils* **2016**, *52* (4), 396–401. <https://doi.org/10.1007/s10553-016-0721-2>.
- (101) Cambero, C.; Sowlati, T.; Marinescu, M.; Röser, D. Strategic Optimization of Forest Residues to Bioenergy and Biofuel Supply Chain: Forest Biomass to Bioenergy and Biofuel Supply Chain. *Int. J. Energy Res.* **2015**, *39* (4), 439–452. <https://doi.org/10.1002/er.3233>.
- (102) Sannigrahi, P.; Ragauskas, A. J.; Tuskan, G. A. Poplar as a Feedstock for Biofuels: A Review of Compositional Characteristics. *Biofuels Bioprod. Biorefining* **2010**, *4* (2), 209–226. <https://doi.org/10.1002/bbb.206>.
- (103) Brosse, N.; Dufour, A.; Meng, X.; Sun, Q.; Ragauskas, A. *Miscanthus* : A Fast-Growing Crop for Biofuels and Chemicals Production: A Fast-Growing Crop for Biofuels and Chemicals Production. *Biofuels Bioprod. Biorefining* **2012**, *6* (5), 580–598. <https://doi.org/10.1002/bbb.1353>.
- (104) Xu, J.; Wang, Z.; Cheng, J. J. Bermuda Grass as Feedstock for Biofuel Production: A Review. *Bioresour. Technol.* **2011**, *102* (17), 7613–7620. <https://doi.org/10.1016/j.biortech.2011.05.070>.
- (105) van der Horst, D.; Vermeylen, S. Spatial Scale and Social Impacts of Biofuel Production. *Biomass Bioenergy* **2011**, *35* (6), 2435–2443. <https://doi.org/10.1016/j.biombioe.2010.11.029>.

- (106) Undri, A.; Abou-Zaid, M.; Briens, C.; Berruti, F.; Rosi, L.; Bartoli, M.; Frediani, M.; Frediani, P. Bio-Oil from Pyrolysis of Wood Pellets Using a Microwave Multimode Oven and Different Microwave Absorbers. *Fuel* **2015**, *153*, 464–482. <https://doi.org/10.1016/j.fuel.2015.02.081>.
- (107) Zafar, S. *Biomass Conversion Technologies*. <https://www.cleantechloops.com/biomass-conversion-technologies/> (accessed 2022-11-12).
- (108) Serrano-Ruiz, J. C.; Dumesic, J. A. Catalytic Routes for the Conversion of Biomass into Liquid Hydrocarbon Transportation Fuels. *Energy Env. Sci* **2011**, *4* (1), 83–99. <https://doi.org/10.1039/C0EE00436G>.
- (109) Rocha, L.; Raud, M.; Orupöld, K.; Kikas, T. Second-Generation Bioethanol Production: A Review of Strategies for Waste Valorisation. 18.
- (110) Anwar, Z.; Gulfraz, M.; Irshad, M. Agro-Industrial Lignocellulosic Biomass a Key to Unlock the Future Bio-Energy: A Brief Review. *J. Radiat. Res. Appl. Sci.* **2014**, *7* (2), 163–173. <https://doi.org/10.1016/j.jrras.2014.02.003>.
- (111) Hamelinck, C. N.; Hooijdonk, G. van; Faaij, A. P. Ethanol from Lignocellulosic Biomass: Techno-Economic Performance in Short-, Middle- and Long-Term. *Biomass Bioenergy* **2005**, *28* (4), 384–410. <https://doi.org/10.1016/j.biombioe.2004.09.002>.
- (112) Kabel, M. A.; Bos, G.; Zeevalking, J.; Voragen, A. G. J.; Schols, H. A. Effect of Pretreatment Severity on Xylan Solubility and Enzymatic Breakdown of the Remaining Cellulose from Wheat Straw. *Bioresour. Technol.* **2007**, *98* (10), 2034–2042. <https://doi.org/10.1016/j.biortech.2006.08.006>.
- (113) Zhu, J. Y.; Pan, X. J. Woody Biomass Pretreatment for Cellulosic Ethanol Production: Technology and Energy Consumption Evaluation☆. *Bioresour. Technol.* **2010**, *101* (13), 4992–5002. <https://doi.org/10.1016/j.biortech.2009.11.007>.
- (114) Leibbrandt, N. H.; Aboyade, A. O.; Knoetze, J. H.; Görgens, J. F. Process Efficiency of Biofuel Production via Gasification and Fischer–Tropsch Synthesis. *Fuel* **2013**, *109*, 484–492. <https://doi.org/10.1016/j.fuel.2013.03.013>.
- (115) Luque, R.; Osa, A. R. de la; Manuel Campelo, J.; Angel Romero, A.; Luis Valverde, J.; Sanchez, P. Design and Development of Catalysts for Biomass-To-Liquid-Fischer–Tropsch (BTL-FT) Processes for Biofuels Production. *Energy Environ. Sci.* **2012**, *5* (1), 5186–5202. <https://doi.org/10.1039/C1EE02238E>.
- (116) *Mechanisms of Thermochemical Biomass Conversion Processes. Part 2: Reactions of Gasification: Energy Sources, Part A: Recovery, Utilization, and Environmental Effects: Vol 30, No 7.* <https://www.tandfonline.com/doi/abs/10.1080/10407780600817600?journalCode=ueso20> (accessed 2022-11-12).
- (117) Torres, W.; Pansare, S. S.; Goodwin, J. G. Hot Gas Removal of Tars, Ammonia, and Hydrogen Sulfide from Biomass Gasification Gas. *Catal. Rev.* **2007**, *49* (4), 407–456. <https://doi.org/10.1080/01614940701375134>.
- (118) *Biomass Gasification*. <https://encyclopedia.pub/entry/3648> (accessed 2022-11-12).
- (119) Kan, T.; Strezov, V.; Evans, T. J. Lignocellulosic Biomass Pyrolysis: A Review of Product Properties and Effects of Pyrolysis Parameters. *Renew. Sustain. Energy Rev.* **2016**, *57*, 1126–1140. <https://doi.org/10.1016/j.rser.2015.12.185>.
- (120) Dhyani, V.; Bhaskar, T. A Comprehensive Review on the Pyrolysis of Lignocellulosic Biomass. *Renew. Energy* **2018**, *129*, 695–716. <https://doi.org/10.1016/j.renene.2017.04.035>.

- (121) Wang, G.; Dai, Y.; Yang, H.; Xiong, Q.; Wang, K.; Zhou, J.; Li, Y.; Wang, S. A Review of Recent Advances in Biomass Pyrolysis. *Energy Fuels* **2020**, *34* (12), 15557–15578. <https://doi.org/10.1021/acs.energyfuels.0c03107>.
- (122) Zadeh, Z. E.; Abdulkhani, A.; Aboelazayem, O.; Saha, B. Recent Insights into Lignocellulosic Biomass Pyrolysis: A Critical Review on Pretreatment, Characterization, and Products Upgrading. *Processes* **2020**, *8* (7), 799. <https://doi.org/10.3390/pr8070799>.
- (123) Bridgwater, A. Fast Pyrolysis Processes for Biomass. *Renew. Sustain. Energy Rev.* **2000**, *4* (1), 1–73. [https://doi.org/10.1016/S1364-0321\(99\)00007-6](https://doi.org/10.1016/S1364-0321(99)00007-6).
- (124) Wang, G.; Dai, Y.; Yang, H.; Xiong, Q.; Wang, K.; Zhou, J.; Li, Y.; Wang, S. A Review of Recent Advances in Biomass Pyrolysis. *Energy Fuels* **2020**, *34* (12), 15557–15578. <https://doi.org/10.1021/acs.energyfuels.0c03107>.
- (125) Specialists' Workshop on Fast Pyrolysis of Biomass Proceedings. 405.
- (126) Mohan, D.; Pittman, C. U.; Steele, P. H. Pyrolysis of Wood/Biomass for Bio-Oil: A Critical Review. *Energy Fuels* **2006**, *20* (3), 848–889. <https://doi.org/10.1021/ef0502397>.
- (127) Lu, Q.; Li, W.-Z.; Zhu, X.-F. Overview of Fuel Properties of Biomass Fast Pyrolysis Oils. *Energy Convers. Manag.* **2009**, *50* (5), 1376–1383. <https://doi.org/10.1016/j.enconman.2009.01.001>.
- (128) Bridgwater, A. V. BIOMASS FAST PYROLYSIS. *Therm. Sci.* **2004**, *8* (2), 29.
- (129) Choi, H. S.; Choi, Y. S.; Park, H. C. Fast Pyrolysis Characteristics of Lignocellulosic Biomass with Varying Reaction Conditions. *Renew. Energy* **2012**, *42*, 131–135. <https://doi.org/10.1016/j.renene.2011.08.049>.
- (130) Russell, S. H.; Turrion-Gomez, J. L.; Meredith, W.; Langston, P.; Snape, C. E. Increased Charcoal Yield and Production of Lighter Oils from the Slow Pyrolysis of Biomass. *J. Anal. Appl. Pyrolysis* **2017**, *124*, 536–541. <https://doi.org/10.1016/j.jaap.2017.01.028>.
- (131) Onay, O.; Kockar, O. M. Slow, Fast and Flash Pyrolysis of Rapeseed. *Renew. Energy* **2003**, *28* (15), 2417–2433. [https://doi.org/10.1016/S0960-1481\(03\)00137-X](https://doi.org/10.1016/S0960-1481(03)00137-X).
- (132) Laidy Hernandez-Mena; Arai Pecora; Antonio Beraldo. Slow Pyrolysis of Bamboo Biomass: Analysis of Biochar Properties. *Chem. Eng. Trans.* **2014**, *37*, 115–120. <https://doi.org/10.3303/CET1437020>.
- (133) Williams, P. T.; Besler, S. The Influence of Temperature and Heating Rate on the Slow Pyrolysis of Biomass. *Renew. Energy* **1996**, *7* (3), 233–250. [https://doi.org/10.1016/0960-1481\(96\)00006-7](https://doi.org/10.1016/0960-1481(96)00006-7).
- (134) Horne, P. A.; Williams, P. T. Influence of Temperature on the Products from the Flash Pyrolysis of Biomass. *Fuel* **1996**, *75* (9), 1051–1059. [https://doi.org/10.1016/0016-2361\(96\)00081-6](https://doi.org/10.1016/0016-2361(96)00081-6).
- (135) Scott, D. S.; Piskorz, J. The Continuous Flash Pyrolysis of Biomass. *Can. J. Chem. Eng.* **1984**, *62* (3), 404–412. <https://doi.org/10.1002/cjce.5450620319>.
- (136) Demirbas, A. Effect of Temperature on Pyrolysis Products from Four Nut Shells. *J. Anal. Appl. Pyrolysis* **2006**, *76* (1–2), 285–289. <https://doi.org/10.1016/j.jaap.2005.12.012>.
- (137) Yu, J.; Paterson, N.; Blamey, J.; Millan, M. Cellulose, Xylan and Lignin Interactions during Pyrolysis of Lignocellulosic Biomass. *Fuel* **2017**, *191*, 140–149. <https://doi.org/10.1016/j.fuel.2016.11.057>.
- (138) Bielecki, M.; Zubkova, V. Analysis of Interactions Occurring during the Pyrolysis of Lignocellulosic Biomass. *Molecules* **2023**, *28* (2), 506. <https://doi.org/10.3390/molecules28020506>.

- (139) Kanaujia, P. K.; Sharma, Y. K.; Garg, M. O.; Tripathi, D.; Singh, R. Review of Analytical Strategies in the Production and Upgrading of Bio-Oils Derived from Lignocellulosic Biomass. *J. Anal. Appl. Pyrolysis* **2014**, *105*, 55–74. <https://doi.org/10.1016/j.jaap.2013.10.004>.
- (140) Xue, Y.; Chen, H.; Zhao, W.; Yang, C.; Ma, P.; Han, S. A Review on the Operating Conditions of Producing Bio-Oil from Hydrothermal Liquefaction of Biomass. *Int. J. Energy Res.* **2016**, *40* (7), 865–877. <https://doi.org/10.1002/er.3473>.
- (141) *Effect of process parameters on hydrothermal liquefaction of oil palm biomass for bio-oil production and its life cycle assessment - ScienceDirect.* <https://www.sciencedirect.com/science/article/abs/pii/S0196890415002939> (accessed 2022-11-13).
- (142) Gollakota, A. R. K.; Kishore, N.; Gu, S. A Review on Hydrothermal Liquefaction of Biomass. *Renew. Sustain. Energy Rev.* **2018**, *81*, 1378–1392. <https://doi.org/10.1016/j.rser.2017.05.178>.
- (143) Brand, S.; Susanti, R. F.; Kim, S. K.; Lee, H.; Kim, J.; Sang, B.-I. Supercritical Ethanol as an Enhanced Medium for Lignocellulosic Biomass Liquefaction: Influence of Physical Process Parameters. *Energy* **2013**, *59*, 173–182. <https://doi.org/10.1016/j.energy.2013.06.049>.
- (144) US8492600.Pdf. <https://patentimages.storage.googleapis.com/7f/22/93/e9c344605d610d/US8492600.pdf> (accessed 2022-11-13).
- (145) Dayton, D.; Hlebak, J.; Carpenter, J.; Wang, K.; Mante, O.; Peters, J. Biomass Hydrolysis in a Fluidized Bed Reactor. *Energy Fuels* **2016**, *30*. <https://doi.org/10.1021/acs.energyfuels.6b00373>.
- (146) *Hydrothermal liquefaction of various biomass and waste feedstocks for biocrude production: A state of the art review - ScienceDirect.* <https://www.sciencedirect.com/science/article/abs/pii/S1364032116306347> (accessed 2022-11-13).
- (147) Yao Rachel-Tang, D.; Islam, A.; Hin Taufiq-Yap, Y. Bio-Oil Production via Catalytic Solvolysis of Biomass. *RSC Adv.* **2017**, *7* (13), 7820–7830. <https://doi.org/10.1039/C6RA27824H>.
- (148) Liu, Z.; Zhang, F.-S. Effects of Various Solvents on the Liquefaction of Biomass to Produce Fuels and Chemical Feedstocks. *Energy Convers. Manag.* **2008**, *49* (12), 3498–3504. <https://doi.org/10.1016/j.enconman.2008.08.009>.
- (149) Xue, Y.; Chen, H.; Zhao, W.; Yang, C.; Ma, P.; Han, S. A Review on the Operating Conditions of Producing Bio-Oil from Hydrothermal Liquefaction of Biomass: Producing Bio-Oil from Hydrothermal Liquefaction of Biomass. *Int. J. Energy Res.* **2016**, *40* (7), 865–877. <https://doi.org/10.1002/er.3473>.
- (150) Peterson, A. A.; Vogel, F.; Lachance, R. P.; Fröling, M.; Michael J. Antal, J.; Tester, J. W. Thermochemical Biofuel Production in Hydrothermal Media: A Review of Sub- and Supercritical Water Technologies. *Energy Environ. Sci.* **2008**, *1* (1), 32–65. <https://doi.org/10.1039/B810100K>.
- (151) *Mechanisms of Thermochemical Biomass Conversion Processes. Part 3: Reactions of Liquefaction: Energy Sources, Part A: Recovery, Utilization, and Environmental Effects: Vol 30, No 7.* <https://www.tandfonline.com/doi/abs/10.1080/10407780600817592> (accessed 2022-11-13).

- (152) Jindal, M. K.; Jha, M. K. Hydrothermal Liquefaction of Wood: A Critical Review. *Rev. Chem. Eng.* **2016**, *32* (4), 459–488. <https://doi.org/10.1515/revce-2015-0055>.
- (153) *Biochar: Potential for countering land degradation and for improving agriculture - ScienceDirect.*
<https://www.sciencedirect.com/science/article/abs/pii/S0143622811001780>
(accessed 2022-11-13).
- (154) *Thermochemical liquefaction of high-diversity grassland perennials - ScienceDirect.*
<https://www.sciencedirect.com/science/article/abs/pii/S016523700800123X>
(accessed 2022-11-13).
- (155) Akhtar, J.; Amin, N. A. S. A Review on Process Conditions for Optimum Bio-Oil Yield in Hydrothermal Liquefaction of Biomass. *Renew. Sustain. Energy Rev.* **2011**, *15* (3), 1615–1624. <https://doi.org/10.1016/j.rser.2010.11.054>.
- (156) Yin, S.; Dolan, R.; Harris, M.; Tan, Z. Subcritical Hydrothermal Liquefaction of Cattle Manure to Bio-Oil: Effects of Conversion Parameters on Bio-Oil Yield and Characterization of Bio-Oil. *Bioresour. Technol.* **2010**, *101* (10), 3657–3664. <https://doi.org/10.1016/j.biortech.2009.12.058>.
- (157) *Non-catalytic and catalytic hydrothermal liquefaction of biomass | SpringerLink.*
<https://link.springer.com/article/10.1007/s11164-012-0572-3> (accessed 2022-11-13).
- (158) Singh, A.; Nigam, P. Microbial Biofuels Production; 2014; pp 155–168. <https://doi.org/10.1201/b17587-8>.
- (159) Han, X.; Wang, H.; Zeng, Y.; Liu, J. Advancing the Application of Bio-Oils by Co-Processing with Petroleum Intermediates: A Review. *Energy Convers. Manag. X* **2021**, *10*, 100069. <https://doi.org/10.1016/j.ecmx.2020.100069>.
- (160) Anex, R. P.; Aden, A.; Kazi, F. K.; Fortman, J.; Swanson, R. M.; Wright, M. M.; Satrio, J. A.; Brown, R. C.; Dugaard, D. E.; Platon, A.; Kothandaraman, G.; Hsu, D. D.; Dutta, A. Techno-Economic Comparison of Biomass-to-Transportation Fuels via Pyrolysis, Gasification, and Biochemical Pathways. *Fuel* **2010**, *89*, S29–S35. <https://doi.org/10.1016/j.fuel.2010.07.015>.
- (161) Uddin, M. N.; Techato, K.; Taweekun, J.; Mofijur, M.; Rasul, M. G.; Mahlia, T. M. I.; Ashrafur, S. M. An Overview of Recent Developments in Biomass Pyrolysis Technologies. *Energies* **2018**, *11* (11), 3115. <https://doi.org/10.3390/en11113115>.
- (162) Underwood, G.; Graham, R. G. 54 METHOD OF USING FAST PYROLYSIS LIQUIDS AS LIQUIDSMOKE. 16.
- (163) Hu, X.; Mourant, D.; Gunawan, R.; Wu, L.; Wang, Y.; Lievens, C.; Li, C.-Z. Production of Value-Added Chemicals from Bio-Oil via Acid Catalysis Coupled with Liquid–Liquid Extraction. *RSC Adv.* **2012**, *2* (25), 9366. <https://doi.org/10.1039/c2ra21597g>.
- (164) Lee, R. A.; Lavoie, J.-M. From First- to Third-Generation Biofuels: Challenges of Producing a Commodity from a Biomass of Increasing Complexity. *Anim. Front.* **2013**, *3* (2), 6–11. <https://doi.org/10.2527/af.2013-0010>.
- (165) Paramasivam, B.; Kasimani, R.; Rajamohan, S. Analytical Characterization of the Aegle Marmelos Pyrolysis Products and Investigation on the Suitability of Bio-oil as a Third Generation Bio-fuel for C.I Engine. *Environ. Prog. Sustain. Energy* **2018**, *38*. <https://doi.org/10.1002/ep.13116>.
- (166) Panga, K.; Saranga, V.; Verma, K.; Pooja, K.; Bhagawan, D.; Srilatha, K.; Vurimindi, H. Bio Oil Production from Microalgae via Hydrothermal Liquefaction Technology under

- Subcritical Water Conditions. *J. Microbiol. Methods* **2018**, *153*.
<https://doi.org/10.1016/j.mimet.2018.09.014>.
- (167) de Caprariis, B.; De Filippis, P.; Petrullo, A.; Scarsella, M. Hydrothermal Liquefaction of Biomass: Influence of Temperature and Biomass Composition on the Bio-Oil Production. *Fuel* **2017**, *208*, 618–625. <https://doi.org/10.1016/j.fuel.2017.07.054>.
- (168) Czernik, S.; Bridgwater, A. V. Overview of Applications of Biomass Fast Pyrolysis Oil. *Energy Fuels* **2004**, *18* (2), 590–598. <https://doi.org/10.1021/ef034067u>.
- (169) Yiin, C. L.; Yusup, S.; Udomsap, P.; Yoosuk, B.; Sukkasi, S. Stabilization of Empty Fruit Bunch (EFB) Derived Bio-Oil Using Antioxidants. In *Computer Aided Chemical Engineering*; Elsevier, 2014; Vol. 33, pp 223–228. <https://doi.org/10.1016/B978-0-444-63456-6.50038-7>.
- (170) Oasmaa, A.; Elliott, D. C.; Korhonen, J. Acidity of Biomass Fast Pyrolysis Bio-Oils. *Energy Fuels* **2010**, *24* (12), 6548–6554. <https://doi.org/10.1021/ef100935r>.
- (171) Agblevor, F. A.; Besler, S.; Wiseloge, A. E. Fast Pyrolysis of Stored Biomass Feedstocks. *Energy Fuels* **1995**, *9* (4), 635–640. <https://doi.org/10.1021/ef00052a010>.
- (172) Yu, F.; Deng, S.; Chen, P.; Liu, Y.; Wan, Y.; Olson, A.; Kittelson, D.; Ruan, R. Physical and Chemical Properties of Bio-Oils From Microwave Pyrolysis of Corn Stover. *Appl. Biochem. Biotechnol.* **2007**, *136*, 14.
- (173) Oasmaa, A.; Korhonen, J.; Kuoppala, E. An Approach for Stability Measurement of Wood-Based Fast Pyrolysis Bio-Oils. *Energy Fuels* **2011**, *25* (7), 3307–3313. <https://doi.org/10.1021/ef2006673>.
- (174) Diebold, J. P. *A Review of the Chemical and Physical Mechanisms of the Storage Stability of Fast Pyrolysis Bio-Oils*; NREL/SR-570-27613, 753818; 1999; p NREL/SR-570-27613, 753818. <https://doi.org/10.2172/753818>.
- (175) Czernik, S.; Johnson, D. K.; Black, S. Stability of Wood Fast Pyrolysis Oil. *Biomass Bioenergy* **1994**, *7* (1), 187–192. [https://doi.org/10.1016/0961-9534\(94\)00058-2](https://doi.org/10.1016/0961-9534(94)00058-2).
- (176) Boucher, M. E.; Chaala, A.; Roy, C. Bio-Oils Obtained by Vacuum Pyrolysis of Softwood Bark as a Liquid Fuel for Gas Turbines. Part I: Properties of Bio-Oil and Its Blends with Methanol and a Pyrolytic Aqueous Phase. *Biomass Bioenergy* **2000**, *15*.
- (177) Eboibi, B. E.-O.; Lewis, D. M.; Ashman, P. J.; Chinnasamy, S. Hydrothermal Liquefaction of Microalgae for Biocrude Production: Improving the Biocrude Properties with Vacuum Distillation. *Bioresour. Technol.* **2014**, *174*, 212–221. <https://doi.org/10.1016/j.biortech.2014.10.029>.
- (178) Zhou, D.; Zhang, L.; Zhang, S.; Fu, H.; Chen, J. Hydrothermal Liquefaction of Macroalgae *Enteromorpha Prolifera* to Bio-Oil. *Energy Fuels* **2010**, *24* (7), 4054–4061. <https://doi.org/10.1021/ef100151h>.
- (179) Zhu, Z.; Rosendahl, L.; Toor, S. S.; Yu, D.; Chen, G. Hydrothermal Liquefaction of Barley Straw to Bio-Crude Oil: Effects of Reaction Temperature and Aqueous Phase Recirculation. *Appl. Energy* **2015**, *137*, 183–192. <https://doi.org/10.1016/j.apenergy.2014.10.005>.
- (180) Kim, J.-Y.; Lee, H. W.; Lee, S. M.; Jae, J.; Park, Y.-K. Overview of the Recent Advances in Lignocellulose Liquefaction for Producing Biofuels, Bio-Based Materials and Chemicals. *Bioresour. Technol.* **2019**, *279*, 373–384. <https://doi.org/10.1016/j.biortech.2019.01.055>.

- (181) Adjaye, J. D.; Sharma, R. K.; Bakhshi, N. N. Characterization and Stability Analysis of Wood-Derived Bio-Oil. *Fuel Process. Technol.* **1992**, *31* (3), 241–256. [https://doi.org/10.1016/0378-3820\(92\)90023-J](https://doi.org/10.1016/0378-3820(92)90023-J).
- (182) *Physical and Chemical Stability of Bagasse Biocrude from Liquefaction Stored in Real Conditions* | *Energy & Fuels*. <https://pubs.acs.org/doi/pdf/10.1021/acs.energyfuels.6b02115> (accessed 2022-11-13).
- (183) *Modeling of the thermal decomposition of a treated plywood from thermo-gravimetry and Fourier-transformed infrared spectroscopy experimental analysis* - ScienceDirect. <https://www.sciencedirect.com/science/article/abs/pii/S0165237013000508> (accessed 2022-11-13).
- (184) No, S.-Y. Application of Bio-Oils from Lignocellulosic Biomass to Transportation, Heat and Power Generation—A Review. *Renew. Sustain. Energy Rev.* **2014**, *40*, 1108–1125. <https://doi.org/10.1016/j.rser.2014.07.127>.
- (185) Han, X.; Wang, H.; Zeng, Y.; Liu, J. Advancing the Application of Bio-Oils by Co-Processing with Petroleum Intermediates: A Review. *Energy Convers. Manag. X* **2021**, *10*, 100069. <https://doi.org/10.1016/j.ecmx.2020.100069>.
- (186) Leng, L.; Li, H.; Yuan, X.; Zhou, W.; Huang, H. Bio-Oil Upgrading by Emulsification/Microemulsification: A Review. *Energy* **2018**, *161*, 214–232. <https://doi.org/10.1016/j.energy.2018.07.117>.
- (187) Elkasabi, Y.; Mullen, C. A.; Boateng, A. A. Aqueous Extractive Upgrading of Bio-Oils Created by Tail-Gas Reactive Pyrolysis To Produce Pure Hydrocarbons and Phenols. *ACS Sustain. Chem. Eng.* **2015**, *3* (11), 2809–2816. <https://doi.org/10.1021/acssuschemeng.5b00730>.
- (188) Boscagli, C.; Tomasi Morgano, M.; Raffelt, K.; Leibold, H.; Grunwaldt, J.-D. Influence of Feedstock, Catalyst, Pyrolysis and Hydrotreatment Temperature on the Composition of Upgraded Oils from Intermediate Pyrolysis. *Biomass Bioenergy* **2018**, *116*, 236–248. <https://doi.org/10.1016/j.biombioe.2018.06.022>.
- (189) Maggi, R. E.; Elliott, D. C. Upgrading Overview. In *Developments in Thermochemical Biomass Conversion: Volume 1 / Volume 2*; Bridgwater, A. V., Boocock, D. G. B., Eds.; Springer Netherlands: Dordrecht, 1997; pp 575–588. https://doi.org/10.1007/978-94-009-1559-6_45.
- (190) Chaihad, N.; Karnjanakom, S.; Kurnia, I.; Yoshida, A.; Abudula, A.; Reubroycharoen, P.; Guan, G. Catalytic Upgrading of Bio-Oils over High Alumina Zeolites. *Renew. Energy* **2019**, *136*, 1304–1310. <https://doi.org/10.1016/j.renene.2018.09.102>.
- (191) Hertzog, J.; Carré, V.; Jia, L.; Mackay, C. L.; Pinard, L.; Dufour, A.; Mašek, O.; Aubriet, F. Catalytic Fast Pyrolysis of Biomass over Microporous and Hierarchical Zeolites: Characterization of Heavy Products. *ACS Sustain. Chem. Eng.* **2018**, *6* (4), 4717–4728. <https://doi.org/10.1021/acssuschemeng.7b03837>.
- (192) García, J. R.; Bertero, M.; Falco, M.; Sedran, U. Catalytic Cracking of Bio-Oils Improved by the Formation of Mesopores by Means of Y Zeolite Desilication. *Appl. Catal. Gen.* **2015**, *503*, 1–8. <https://doi.org/10.1016/j.apcata.2014.11.005>.
- (193) *Bio-oils Upgrading for Second Generation Biofuels | Industrial & Engineering Chemistry Research*. <https://pubs.acs.org/doi/pdf/10.1021/ie301714x> (accessed 2022-11-13).
- (194) Elliott, D. C. Historical Developments in Hydroprocessing Bio-Oils. *Energy Fuels* **2007**, *21* (3), 1792–1815. <https://doi.org/10.1021/ef070044u>.

- (195) Nimmanwudipong, T.; Saidi, M.; Samimi, F.; Karimipourfard, D.; Gates, B.; Rahimpour, M. R. Upgrading of Lignin-Derived Bio-Oils by Catalytic Hydrodeoxygenation. *Energy Environ. Sci.* **2013**, *7*, 103–129. <https://doi.org/10.1039/C3EE43081B>.
- (196) Furimsky - 2000 - Catalytic Hydrodeoxygenation.Pdf. <https://www.cae.tntech.edu/~jbiernacki/CHE%204410%202018/HTL%20References/Catalytic%20hydrodeoxygenation.pdf> (accessed 2022-11-13).
- (197) *Hydrotreatment of Fast Pyrolysis Oil Using Heterogeneous Noble-Metal Catalysts | Industrial & Engineering Chemistry Research*. <https://pubs.acs.org/doi/abs/10.1021/ie9006003> (accessed 2022-11-13).
- (198) *Integrated hydropyrolysis and hydroconversion (IH2) for the direct production of gasoline and diesel fuels or blending components from biomass, part 1: Proof of principle testing - Marker - 2012 - Environmental Progress & Sustainable Energy - Wiley Online Library*. https://aiche.onlinelibrary.wiley.com/doi/abs/10.1002/ep.10629?casa_token=zLOEtqgaE2UAAAAA%3A167A09jFKNSmEdQ6oD7wayqJwD5t6qHS2h7ejs1jdTWWyZg3Yd3yX_ixGNw-dcgFYEzgi6MK5iMs2ls (accessed 2022-11-13).
- (199) Melligan, F.; Hayes, M. H. B.; Kwapinski, W.; Leahy, J. J. Hydro-Pyrolysis of Biomass and Online Catalytic Vapor Upgrading with Ni-ZSM-5 and Ni-MCM-41. *Energy Fuels* **2012**, *26* (10), 6080–6090. <https://doi.org/10.1021/ef301244h>.
- (200) Kumar, R.; Strezov, V.; Weldekidan, H.; He, J.; Singh, S.; Kan, T.; Dastjerdi, B. Lignocellulose Biomass Pyrolysis for Bio-Oil Production: A Review of Biomass Pre-Treatment Methods for Production of Drop-in Fuels. *Renew. Sustain. Energy Rev.* **2020**, *123*, 109763. <https://doi.org/10.1016/j.rser.2020.109763>.
- (201) Huang, F.; Pan, S.; Pu, Y.; Ben, H.; Ragauskas, A. J. 19F NMR Spectroscopy for the Quantitative Analysis of Carbonyl Groups in Bio-Oils. *RSC Adv.* **2014**, *4* (34), 17743. <https://doi.org/10.1039/c4ra01293c>.
- (202) Mondal, A.; Ragauskas, A.; Qin, C.; Ni, Y.; Huang, F. PBM • Hydrogenated Pyrolysis Oil Hydrogenation of Pyrolysis Oil from Loblolly Pine Residue PBM • Hydrogenated Pyrolysis Oil. **2020**, *5*, 1–13. <https://doi.org/10.12103/j.issn.2096-2355.2020.01.001>.
- (203) Celikbag, Y.; Via, B. K.; Adhikari, S.; Buschle-Diller, G.; Auad, M. L. The Effect of Ethanol on Hydroxyl and Carbonyl Groups in Biopolyol Produced by Hydrothermal Liquefaction of Loblolly Pine: 31P-NMR and 19F-NMR Analysis. *Bioresour. Technol.* **2016**, *214*, 37–44. <https://doi.org/10.1016/j.biortech.2016.04.066>.
- (204) Schmitt-Kopplin, P.; Kanawati, B. *Fundamentals and Applications of Fourier Transform Mass Spectrometry*; Elsevier, 2019.
- (205) Marshall, A. G.; Rodgers, R. P. Petroleomics: The Next Grand Challenge for Chemical Analysis. *Acc. Chem. Res.* **2004**, *37* (1), 53–59. <https://doi.org/10.1021/ar020177t>.
- (206) Marshall, A. G.; Rodgers, R. P. Petroleomics: Chemistry of the Underworld. *Proc. Natl. Acad. Sci.* **2008**, *105* (47), 18090–18095. <https://doi.org/10.1073/pnas.0805069105>.
- (207) Hertzog, J.; Carré, V.; Le Brech, Y.; Mackay, C. L.; Dufour, A.; Mašek, O.; Aubriet, F. Combination of Electrospray Ionization, Atmospheric Pressure Photoionization and Laser Desorption Ionization Fourier Transform Ion Cyclotron Resonance Mass Spectrometry for the Investigation of Complex Mixtures – Application to the Petroleomic Analysis of Bio-Oils. *Anal. Chim. Acta* **2017**, *969*, 26–34. <https://doi.org/10.1016/j.aca.2017.03.022>.

- (208) Palacio Lozano, D. C.; Thomas, M. J.; Jones, H. E.; Barrow, M. P. Petroleomics: Tools, Challenges, and Developments. *Annu. Rev. Anal. Chem.* **2020**, *13* (1), 405–430. <https://doi.org/10.1146/annurev-anchem-091619-091824>.
- (209) Ryan, D. J.; Qian, K. Laser-Based Ionization: A Review on the Use of Matrix-Assisted Laser Desorption/Ionization and Laser Desorption/Ionization Mass Spectrometry in Petroleum Research. *Energy Fuels* **2020**, *34* (10), 11887–11896. <https://doi.org/10.1021/acs.energyfuels.0c02374>.
- (210) Pereira, I.; de Aguiar, D. V. A.; Vasconcelos, G.; Vaz, B. G. Fourier Transform Mass Spectrometry Applied to Petroleomics. In *Fundamentals and Applications of Fourier Transform Mass Spectrometry*; Elsevier, 2019; pp 509–528. <https://doi.org/10.1016/B978-0-12-814013-0.00016-8>.
- (211) Borisov, R. S.; Kulikova, L. N.; Zaikin, V. G. Mass Spectrometry in Petroleum Chemistry (Petroleomics) (Review). *Pet. Chem.* **2019**, *59* (10), 1055–1076. <https://doi.org/10.1134/S0965544119100025>.
- (212) Niyonsaba, E.; Manheim, J. M.; Yerabolu, R.; Kenttämaa, H. I. Recent Advances in Petroleum Analysis by Mass Spectrometry. *Anal. Chem.* **2019**, *91* (1), 156–177. <https://doi.org/10.1021/acs.analchem.8b05258>.
- (213) Gutiérrez Sama, S.; Farenc, M.; Barrère-Mangote, C.; Lobinski, R.; Afonso, C.; Bouyssière, B.; Giusti, P. Molecular Fingerprints and Speciation of Crude Oils and Heavy Fractions Revealed by Molecular and Elemental Mass Spectrometry: Keystone between Petroleomics, Metallopetroleomics, and Petrointeractomics. *Energy Fuels* **2018**, *32* (4), 4593–4605. <https://doi.org/10.1021/acs.energyfuels.7b03218>.
- (214) *Hydrocarbons, Oils and Lipids: Diversity, Origin, Chemistry and Fate*; Wilkes, H., Ed.; Springer International Publishing: Cham, 2020. <https://doi.org/10.1007/978-3-319-90569-3>.
- (215) Cho, Y.; Ahmed, A.; Islam, A.; Kim, S. Developments in FT-ICR MS Instrumentation, Ionization Techniques, and Data Interpretation Methods for Petroleomics. *Mass Spectrom. Rev.* **2015**, *34* (2), 248–263. <https://doi.org/10.1002/mas.21438>.
- (216) Krajewski, L. C.; Rodgers, R. P.; Marshall, A. G. 126 264 Assigned Chemical Formulas from an Atmospheric Pressure Photoionization 9.4 T Fourier Transform Positive Ion Cyclotron Resonance Mass Spectrum. *Anal. Chem.* **2017**, *89* (21), 11318–11324. <https://doi.org/10.1021/acs.analchem.7b02004>.
- (217) Guigue, J.; Harir, M.; Mathieu, O.; Lucio, M.; Ranjard, L.; Lévêque, J.; Schmitt-Kopplin, P. Ultrahigh-Resolution FT-ICR Mass Spectrometry for Molecular Characterisation of Pressurised Hot Water-Extractable Organic Matter in Soils. *Biogeochemistry* **2016**, *128* (3), 307–326. <https://doi.org/10.1007/s10533-016-0209-5>.
- (218) W, V. K. D. Graphical-Statistical Method for the Study of Structure and Reaction Processes of Coal. *Fuel* **1950**, *29*, 269–284.
- (219) Kim, S.; Kramer, R. W.; Hatcher, P. G. Graphical Method for Analysis of Ultrahigh-Resolution Broadband Mass Spectra of Natural Organic Matter, the Van Krevelen Diagram. *Anal. Chem.* **2003**, *75* (20), 5336–5344. <https://doi.org/10.1021/ac034415p>.
- (220) Kendrick, Edward. A Mass Scale Based on $\text{CH}_2 = 14.0000$ for High Resolution Mass Spectrometry of Organic Compounds. *Anal. Chem.* **1963**, *35* (13), 2146–2154. <https://doi.org/10.1021/ac60206a048>.
- (221) Hertzog, J.; Mase, C.; Hubert-Roux, M.; Afonso, C.; Giusti, P.; Barrère-Mangote, C. Characterization of Heavy Products from Lignocellulosic Biomass Pyrolysis by

- Chromatography and Fourier Transform Mass Spectrometry: A Review. *Energy Fuels* **2021**, *35* (22), 17979–18007. <https://doi.org/10.1021/acs.energyfuels.1c02098>.
- (222) Bi, Y.; Wang, G.; Shi, Q.; Xu, C.; Gao, J. Compositional Changes during Hydrodeoxygenation of Biomass Pyrolysis Oil. *Energy Fuels* **2014**, *28* (4), 2571–2580. <https://doi.org/10.1021/ef4024405>.
- (223) Ruddy, B. M.; Hendrickson, C. L.; Rodgers, R. P.; Marshall, A. G. Positive Ion Electrospray Ionization Suppression in Petroleum and Complex Mixtures. *Energy Fuels* **2018**, *32* (3), 2901–2907. <https://doi.org/10.1021/acs.energyfuels.7b03204>.
- (224) Soares, R.; Franco, C.; Pires, E.; Ventosa, M.; Palhinhos, R.; Koci, K.; Martinho de Almeida, A.; Varela Coelho, A. Mass Spectrometry and Animal Science: Protein Identification Strategies and Particularities of Farm Animal Species. *J. Proteomics* **2012**, *75* (14), 4190–4206. <https://doi.org/10.1016/j.jprot.2012.04.009>.
- (225) Le Maître, J.; Hubert-Roux, M.; Paupy, B.; Marceau, S.; Rüger, C. P.; Afonso, C.; Giusti, P. Structural Analysis of Heavy Oil Fractions after Hydrodenitrogenation by High-Resolution Tandem Mass Spectrometry and Ion Mobility Spectrometry. *Faraday Discuss.* **2019**, *218*, 417–430. <https://doi.org/10.1039/C8FD00239H>.
- (226) *Resolution, Elemental Composition, and Simultaneous Monitoring by Fourier Transform Ion Cyclotron Resonance Mass Spectrometry of Organosulfur Species before and after Diesel Fuel Processing | Analytical Chemistry*. <https://pubs.acs.org/doi/abs/10.1021/ac980487i> (accessed 2022-10-28).
- (227) Qian, K. Molecular Characterization of Heavy Petroleum by Mass Spectrometry and Related Techniques. *Energy Fuels* **2021**, *35* (22), 18008–18018. <https://doi.org/10.1021/acs.energyfuels.1c01783>.
- (228) Shi, Q.; Zhang, Y.; Chung, K. H.; Zhao, S.; Xu, C. Molecular Characterization of Fossil and Alternative Fuels Using Electrospray Ionization Fourier Transform Ion Cyclotron Resonance Mass Spectrometry: Recent Advances and Perspectives. *Energy Fuels* **2021**, *35* (22), 18019–18055. <https://doi.org/10.1021/acs.energyfuels.1c01671>.
- (229) Palacio Lozano, D. C.; Ramírez, C. X.; Sarmiento Chaparro, J. A.; Thomas, M. J.; Gavard, R.; Jones, H. E.; Cabanzo Hernández, R.; Mejia-Ospino, E.; Barrow, M. P. Characterization of Bio-Crude Components Derived from Pyrolysis of Soft Wood and Its Esterified Product by Ultrahigh Resolution Mass Spectrometry and Spectroscopic Techniques. *Fuel* **2020**, *259*, 116085. <https://doi.org/10.1016/j.fuel.2019.116085>.
- (230) Barrow, M. P.; Peru, K. M.; McMartin, D. W.; Headley, J. V. Effects of Extraction PH on the Fourier Transform Ion Cyclotron Resonance Mass Spectrometry Profiles of Athabasca Oil Sands Process Water. *Energy Fuels* **2016**, *30* (5), 3615–3621. <https://doi.org/10.1021/acs.energyfuels.5b02086>.
- (231) Peru, K. M.; Thomas, M. J.; Palacio Lozano, D. C.; McMartin, D. W.; Headley, J. V.; Barrow, M. P. Characterization of Oil Sands Naphthenic Acids by Negative-Ion Electrospray Ionization Mass Spectrometry: Influence of Acidic versus Basic Transfer Solvent. *Chemosphere* **2019**, *222*, 1017–1024. <https://doi.org/10.1016/j.chemosphere.2019.01.162>.
- (232) Mase, C.; Hubert-Roux, M.; Afonso, C.; Giusti, P. Contribution of Atmospheric Pressure Chemical Ionization Mass Spectrometry for the Characterization of Bio-Oils from Lignocellulosic Biomass: Comparison with Electrospray Ionization and Atmospheric Pressure Photoionization. *J. Anal. Appl. Pyrolysis* **2022**, *167*, 105694. <https://doi.org/10.1016/j.jaap.2022.105694>.

- (233) Hertzog, J.; Carré, V.; Aubriet, F. Contribution of Fourier Transform Mass Spectrometry to Bio-Oil Study. In *Fundamentals and Applications of Fourier Transform Mass Spectrometry*; Elsevier, 2019; pp 679–733. <https://doi.org/10.1016/B978-0-12-814013-0.00022-3>.
- (234) Alsbou, E.; Helleur, B. Direct Infusion Mass Spectrometric Analysis of Bio-Oil Using ESI-Ion-Trap MS. *Energy Fuels* **2014**, *28* (1), 578–590. <https://doi.org/10.1021/ef4018288>.
- (235) Lobodin, V. V.; Juyal, P.; McKenna, A. M.; Rodgers, R. P.; Marshall, A. G. Tetramethylammonium Hydroxide as a Reagent for Complex Mixture Analysis by Negative Ion Electrospray Ionization Mass Spectrometry. *Anal. Chem.* **2013**, *85* (16), 7803–7808. <https://doi.org/10.1021/ac401222b>.
- (236) Vasconcelos, G. A.; Pereira, R. C. L.; Santos, C. de F.; Carvalho, V. V.; Tose, L. V.; Romão, W.; Vaz, B. G. Extraction and Fractionation of Basic Nitrogen Compounds in Vacuum Residue by Solid-Phase Extraction and Characterization by Ultra-High Resolution Mass Spectrometry. *Int. J. Mass Spectrom.* **2017**, *418*, 67–72. <https://doi.org/10.1016/j.ijms.2016.11.019>.
- (237) Hertzog, J. Semi-Targeted Analysis of Complex Matrices by ESI FT-ICR MS or How an Experimental Bias May Be Used as an Analytical Tool. 15.
- (238) Lobodin, V. V.; Juyal, P.; McKenna, A. M.; Rodgers, R. P.; Marshall, A. G. Silver Cationization for Rapid Speciation of Sulfur-Containing Species in Crude Oils by Positive Electrospray Ionization Fourier Transform Ion Cyclotron Resonance Mass Spectrometry. *Energy Fuels* **2014**, *28* (1), 447–452. <https://doi.org/10.1021/ef401897p>.
- (239) Zhang, Y.; Huang, C.; Kong, F.; Wang, Y.; Shi, Q.; Zhang, L. Selective Molecular Characterization of Olefins in Hydrocarbon Mixtures by Ag⁺ Complexation ESI High-Resolution Mass Spectrometry. *Fuel* **2022**, *319*, 123760. <https://doi.org/10.1016/j.fuel.2022.123760>.
- (240) Hommerson, P.; Khan, A. M.; de Jong, G. J.; Somsen, G. W. Ionization Techniques in Capillary Electrophoresis-Mass Spectrometry: Principles, Design, and Application. *Mass Spectrom. Rev.* **2011**, *30* (6), 1096–1120. <https://doi.org/10.1002/mas.20313>.
- (241) Raffaelli, A.; Saba, A. Atmospheric Pressure Photoionization Mass Spectrometry. *Mass Spectrom. Rev.* **2003**, *22* (5), 318–331. <https://doi.org/10.1002/mas.10060>.
- (242) Awad, H.; Khamis, M. M.; El-Aneed, A. Mass Spectrometry, Review of the Basics: Ionization. *Appl. Spectrosc. Rev.* **2015**, *50* (2), 158–175. <https://doi.org/10.1080/05704928.2014.954046>.
- (243) Purcell, J. M.; Hendrickson, C. L.; Rodgers, R. P.; Marshall, A. G. Atmospheric Pressure Photoionization Fourier Transform Ion Cyclotron Resonance Mass Spectrometry for Complex Mixture Analysis. *Anal. Chem.* **2006**, *78* (16), 5906–5912. <https://doi.org/10.1021/ac060754h>.
- (244) Alsbou, E.; Helleur, B. Direct Infusion Mass Spectrometric Analysis of Bio-Oil Using ESI-Ion-Trap MS. *Energy Fuels* **2014**, *28* (1), 578–590. <https://doi.org/10.1021/ef4018288>.
- (245) Qi, Y.; Volmer, D. A. Chemical Diversity of Lignin Degradation Products Revealed by Matrix-Optimized MALDI Mass Spectrometry. *Anal. Bioanal. Chem.* **2019**, *411* (23), 6031–6037. <https://doi.org/10.1007/s00216-019-01984-y>.
- (246) Ware, R. L.; Rowland, S. M.; Rodgers, R. P.; Marshall, A. G. Advanced Chemical Characterization of Pyrolysis Oils from Landfill Waste, Recycled Plastics, and Forestry Residue. *Energy Fuels* **2017**, *31* (8), 8210–8216. <https://doi.org/10.1021/acs.energyfuels.7b00865>.

- (247) Jarvis, J. M.; Page-Dumroese, D. S.; Anderson, N. M.; Corilo, Y.; Rodgers, R. P. Characterization of Fast Pyrolysis Products Generated from Several Western USA Woody Species. *Energy Fuels* **2014**, *28* (10), 6438–6446. <https://doi.org/10.1021/ef501714j>.
- (248) Staš, M.; Kubička, D.; Chudoba, J.; Pospíšil, M. Overview of Analytical Methods Used for Chemical Characterization of Pyrolysis Bio-Oil. *Energy Fuels* **2014**, *28* (1), 385–402. <https://doi.org/10.1021/ef402047y>.
- (249) Dalluge, E. A. Bio-Mass for Biomass: Biological Mass Spectrometry Techniques for Biomass Fast Pyrolysis Oils. PhD Thesis, Iowa State University, Digital Repository, 2013. <https://core.ac.uk/download/pdf/38925946.pdf>.
- (250) Smith, E. A.; Lee, Y. J. Petroleomic Analysis of Bio-Oils from the Fast Pyrolysis of Biomass: Laser Desorption Ionization–Linear Ion Trap–Orbitrap Mass Spectrometry Approach. *Energy Fuels* **2010**, *24* (9), 5190–5198. <https://doi.org/10.1021/ef100629a>.
- (251) Giraldo-Dávila, D.; Chacón-Patiño, M. L.; Ramirez-Pradilla, J. S.; Blanco-Tirado, C.; Combariza, M. Y. Selective Ionization by Electron-Transfer MALDI-MS of Vanadyl Porphyrins from Crude Oils. *Fuel* **2018**, *226*, 103–111. <https://doi.org/10.1016/j.fuel.2018.04.016>.
- (252) Olcese, R.; Carré, V.; Aubriet, F.; Dufour, A. Selectivity of Bio-Oils Catalytic Hydrotreatment Assessed by Petroleomic and GC*GC/MS-FID Analysis. *Energy Fuels* **2013**, *27* (4), 2135–2145. <https://doi.org/10.1021/ef302145g>.
- (253) Huba, A. K.; Huba, K.; Gardinali, P. R. Understanding the Atmospheric Pressure Ionization of Petroleum Components: The Effects of Size, Structure, and Presence of Heteroatoms. *Sci. Total Environ.* **2016**, *568*, 1018–1025. <https://doi.org/10.1016/j.scitotenv.2016.06.044>.
- (254) Cao, D.; Huang, H.; Hu, M.; Cui, L.; Geng, F.; Rao, Z.; Niu, H.; Cai, Y.; Kang, Y. Comprehensive Characterization of Natural Organic Matter by MALDI- and ESI-Fourier Transform Ion Cyclotron Resonance Mass Spectrometry. *Anal. Chim. Acta* **2015**, *866*, 48–58. <https://doi.org/10.1016/j.aca.2015.01.051>.
- (255) Hertkorn, N.; Frommberger, M.; Witt, M.; Koch, B. P.; Schmitt-Kopplin, Ph.; Perdue, E. M. Natural Organic Matter and the Event Horizon of Mass Spectrometry. *Anal. Chem.* **2008**, *80* (23), 8908–8919. <https://doi.org/10.1021/ac800464g>.
- (256) Hertzog, J.; Carré, V.; Le Brech, Y.; Mackay, C. L.; Dufour, A.; Mašek, O.; Aubriet, F. Combination of Electrospray Ionization, Atmospheric Pressure Photoionization and Laser Desorption Ionization Fourier Transform Ion Cyclotron Resonance Mass Spectrometry for the Investigation of Complex Mixtures – Application to the Petroleomic Analysis of Bio-Oils. *Anal. Chim. Acta* **2017**, *969*, 26–34. <https://doi.org/10.1016/j.aca.2017.03.022>.
- (257) Tessini, C.; Vega, M.; Müller, N.; Bustamante, L.; von Baer, D.; Berg, A.; Mardones, C. High Performance Thin Layer Chromatography Determination of Cellobiosan and Levoglucosan in Bio-Oil Obtained by Fast Pyrolysis of Sawdust. *J. Chromatogr. A* **2011**, *1218* (24), 3811–3815. <https://doi.org/10.1016/j.chroma.2011.04.037>.
- (258) Undri, A.; Abou-Zaid, M.; Briens, C.; Berruti, F.; Rosi, L.; Bartoli, M.; Frediani, M.; Frediani, P. A Simple Procedure for Chromatographic Analysis of Bio-Oils from Pyrolysis. *J. Anal. Appl. Pyrolysis* **2015**, *114*, 208–221. <https://doi.org/10.1016/j.jaap.2015.05.019>.
- (259) Ferreira, M. F. P.; Oliveira, B. F. H.; Pinheiro, W. B. S.; Correa, N. F.; França, L. F.; Ribeiro, N. F. P. Generation of Biofuels by Slow Pyrolysis of Palm Empty Fruit Bunches:

- Optimization of Process Variables and Characterization of Physical-Chemical Products. *Biomass Bioenergy* **2020**, *140*, 105707. <https://doi.org/10.1016/j.biombioe.2020.105707>.
- (260) Garcia-Perez, M.; Chaala, A.; Pakdel, H.; Kretschmer, D.; Roy, C. Characterization of Bio-Oils in Chemical Families. *Biomass Bioenergy* **2007**, *31* (4), 222–242. <https://doi.org/10.1016/j.biombioe.2006.02.006>.
- (261) Choi, Y. S.; Johnston, P. A.; Brown, R. C.; Shanks, B. H.; Lee, K.-H. Detailed Characterization of Red Oak-Derived Pyrolysis Oil: Integrated Use of GC, HPLC, IC, GPC and Karl-Fischer. *J. Anal. Appl. Pyrolysis* **2014**, *110*, 147–154. <https://doi.org/10.1016/j.jaap.2014.08.016>.
- (262) Dubuis, A.; Le Masle, A.; Chahen, L.; Destandau, E.; Charon, N. Off-Line Comprehensive Size Exclusion Chromatography × Reversed-Phase Liquid Chromatography Coupled to High Resolution Mass Spectrometry for the Analysis of Lignocellulosic Biomass Products. *J. Chromatogr. A* **2020**, *1609*, 460505. <https://doi.org/10.1016/j.chroma.2019.460505>.
- (263) Andersson, T.; Hyötyläinen, T.; Riekkola, M.-L. Analysis of Phenols in Pyrolysis Oils by Gel Permeation Chromatography and Multidimensional Liquid Chromatography. *J. Chromatogr. A* **2000**, *896* (1–2), 343–349. [https://doi.org/10.1016/S0021-9673\(00\)00678-6](https://doi.org/10.1016/S0021-9673(00)00678-6).
- (264) Harman-Ware, A. E.; Ferrell, J. R. Methods and Challenges in the Determination of Molecular Weight Metrics of Bio-Oils. *Energy Fuels* **2018**, *32* (9), 8905–8920. <https://doi.org/10.1021/acs.energyfuels.8b02113>.
- (265) Reymond, C.; Le Masle, A.; Colas, C.; Charon, N. A Rational Strategy Based on Experimental Designs to Optimize Parameters of a Liquid Chromatography-Mass Spectrometry Analysis of Complex Matrices. *Talanta* **2019**, *205*, 120063. <https://doi.org/10.1016/j.talanta.2019.06.063>.
- (266) Meile, K.; Zhurinsh, A.; Viksna, A. Comparison of Photodiode Array, Evaporative Light Scattering, and Single-Quadrupole Mass Spectrometric Detection Methods for the UPLC Analysis of Pyrolysis Liquids. *J. Liq. Chromatogr. Relat. Technol.* **2017**, *40* (7), 369–375. <https://doi.org/10.1080/10826076.2017.1308378>.
- (267) Tomasini, D.; Cacciola, F.; Rigano, F.; Sciarrone, D.; Donato, P.; Beccaria, M.; Caramão, E. B.; Dugo, P.; Mondello, L. Complementary Analytical Liquid Chromatography Methods for the Characterization of Aqueous Phase from Pyrolysis of Lignocellulosic Biomasses. *Anal. Chem.* **2014**, *86* (22), 11255–11262. <https://doi.org/10.1021/ac5038957>.
- (268) Lazzari, E.; Arena, K.; Caramão, E. B.; Dugo, P.; Mondello, L.; Herrero, M. Comprehensive Two-dimensional Liquid Chromatography-based Quali-quantitative Screening of Aqueous Phases from Pyrolysis Bio-oils. *ELECTROPHORESIS* **2021**, *42* (1–2), 58–67. <https://doi.org/10.1002/elps.202000119>.
- (269) Crepier, J.; Le Masle, A.; Charon, N.; Albrieux, F.; Duchene, P.; Heinisch, S. Ultra-High Performance Supercritical Fluid Chromatography Hyphenated to Atmospheric Pressure Chemical Ionization High Resolution Mass Spectrometry for the Characterization of Fast Pyrolysis Bio-Oils. *J. Chromatogr. B* **2018**, *1086*, 38–46. <https://doi.org/10.1016/j.jchromb.2018.04.005>.
- (270) Sarrut, M.; Corgier, A.; Crétier, G.; Le Masle, A.; Dubant, S.; Heinisch, S. Potential and Limitations of On-Line Comprehensive Reversed Phase Liquid

- Chromatography×supercritical Fluid Chromatography for the Separation of Neutral Compounds: An Approach to Separate an Aqueous Extract of Bio-Oil. *J. Chromatogr. A* **2015**, *1402*, 124–133. <https://doi.org/10.1016/j.chroma.2015.05.005>.
- (271) Mohan, D.; Pittman, C. U.; Steele, P. H. Pyrolysis of Wood/Biomass for Bio-Oil: A Critical Review. *Energy Fuels* **2006**, *20* (3), 848–889. <https://doi.org/10.1021/ef0502397>.
- (272) Tessarolo, N. S.; Silva, R. V. S.; Vanini, G.; Casilli, A.; Ximenes, V. L.; Mendes, F. L.; de Rezende Pinho, A.; Romão, W.; de Castro, E. V. R.; Kaiser, C. R.; Azevedo, D. A. Characterization of Thermal and Catalytic Pyrolysis Bio-Oils by High-Resolution Techniques: ¹H NMR, GC×GC-TOFMS and FT-ICR MS. *J. Anal. Appl. Pyrolysis* **2016**, *117*, 257–267. <https://doi.org/10.1016/j.jaap.2015.11.007>.
- (273) Wang, Y.; Han, Y.; Hu, W.; Fu, D.; Wang, G. Analytical Strategies for Chemical Characterization of Bio-oil. *J. Sep. Sci.* **2020**, *43* (1), 360–371. <https://doi.org/10.1002/jssc.201901014>.
- (274) Staš, M.; Auersvald, M.; Vozka, P. Two-Dimensional Gas Chromatography Characterization of Pyrolysis Bio-Oils: A Review. *Energy Fuels* **2021**, *35* (10), 8541–8557. <https://doi.org/10.1021/acs.energyfuels.1c00553>.
- (275) Reymond, C.; Dubuis, A.; Le Masle, A.; Colas, C.; Chahen, L.; Destandau, E.; Charon, N. Characterization of Liquid–Liquid Extraction Fractions from Lignocellulosic Biomass by High Performance Liquid Chromatography Hyphenated to Tandem High-Resolution Mass Spectrometry. *J. Chromatogr. A* **2020**, *1610*, 460569. <https://doi.org/10.1016/j.chroma.2019.460569>.
- (276) Tang, K.; Page, J. S.; Smith, R. D. Charge Competition and the Linear Dynamic Range of Detection in Electrospray Ionization Mass Spectrometry. *J. Am. Soc. Mass Spectrom.* **2004**, *15* (10), 1416–1423. <https://doi.org/10.1016/j.jasms.2004.04.034>.
- (277) Santos, J. M.; Vetere, A.; Wisniewski, A.; Eberlin, M. N.; Schrader, W. Modified SARA Method to Unravel the Complexity of Resin Fraction(s) in Crude Oil. *Energy Fuels* **2020**, *34* (12), 16006–16013. <https://doi.org/10.1021/acs.energyfuels.0c02833>.
- (278) Rezaee, S.; Tavakkoli, M.; Doherty, R.; Vargas, F. M. A New Experimental Method for a Fast and Reliable Quantification of Saturates, Aromatics, Resins, and Asphaltenes in Crude Oils. *Pet. Sci. Technol.* **2020**, *38* (21), 955–961. <https://doi.org/10.1080/10916466.2020.1790598>.
- (279) Gaspar, A.; Zellermann, E.; Lababidi, S.; Reece, J.; Schrader, W. Characterization of Saturates, Aromatics, Resins, and Asphaltenes Heavy Crude Oil Fractions by Atmospheric Pressure Laser Ionization Fourier Transform Ion Cyclotron Resonance Mass Spectrometry. *Energy Fuels* **2012**, *26* (6), 3481–3487. <https://doi.org/10.1021/ef3001407>.
- (280) Verşan K k, M.; Varfolomeev, M. A.; Nurgaliev, D. K. Determination of SARA Fractions of Crude Oils by NMR Technique. *J. Pet. Sci. Eng.* **2019**, *179*, 1–6. <https://doi.org/10.1016/j.petrol.2019.04.026>.
- (281) Klein, G. C.; Angstr m, A.; Rodgers, R. P.; Marshall, A. G. Use of Saturates/Aromatics/Resins/Asphaltenes (SARA) Fractionation To Determine Matrix Effects in Crude Oil Analysis by Electrospray Ionization Fourier Transform Ion Cyclotron Resonance Mass Spectrometry. *Energy Fuels* **2006**, *20* (2), 668–672. <https://doi.org/10.1021/ef050353p>.
- (282) Islam, A.; Cho, Y.; Yim, U. H.; Shim, W. J.; Kim, Y. H.; Kim, S. The Comparison of Naturally Weathered Oil and Artificially Photo-Degraded Oil at the Molecular Level by a

- Combination of SARA Fractionation and FT-ICR MS. *J. Hazard. Mater.* **2013**, *263*, 404–411. <https://doi.org/10.1016/j.jhazmat.2013.09.030>.
- (283) Cho, Y.; Na, J.-G.; Nho, N.-S.; Kim, S.; Kim, S. Application of Saturates, Aromatics, Resins, and Asphaltenes Crude Oil Fractionation for Detailed Chemical Characterization of Heavy Crude Oils by Fourier Transform Ion Cyclotron Resonance Mass Spectrometry Equipped with Atmospheric Pressure Photoionization. *Energy Fuels* **2012**, *26* (5), 2558–2565. <https://doi.org/10.1021/ef201312m>.
- (284) Qiao, P.; Harbottle, D.; Tchoukov, P.; Masliyah, J.; Sjoblom, J.; Liu, Q.; Xu, Z. Fractionation of Asphaltenes in Understanding Their Role in Petroleum Emulsion Stability and Fouling. *Energy Fuels* **2017**, *31* (4), 3330–3337. <https://doi.org/10.1021/acs.energyfuels.6b02401>.
- (285) Li, C.; Rajib, A.; Sarker, M.; Liu, R.; Fini, E. H.; Cai, J. Balancing the Aromatic and Ketone Content of Bio-Oils as Rejuvenators to Enhance Their Efficacy in Restoring Properties of Aged Bitumen. *ACS Sustain. Chem. Eng.* **2021**, *9* (20), 6912–6922. <https://doi.org/10.1021/acssuschemeng.0c09131>.
- (286) Yerabolu, R.; Kotha, R. R.; Niyonsaba, E.; Dong, X.; Manheim, J. M.; Kong, J.; Riedeman, J. S.; Romanczyk, M.; Johnston, C. T.; Kilaz, G.; Kenttämaa, H. I. Molecular Profiling of Crude Oil by Using Distillation Precipitation Fractionation Mass Spectrometry (DPF-MS). *Fuel* **2018**, *234*, 492–501. <https://doi.org/10.1016/j.fuel.2018.07.028>.
- (287) Niyonsaba, E. DEVELOPMENT OF MASS SPECTROMETRIC METHODS FOR FAST IDENTIFICATION OF DRUG METABOLITES AND FOR DETERMINATION OF THE CHEMICAL COMPOSITIONS OF CRUDE OILS OF DIFFERENT API GRAVITIES. thesis, Purdue University Graduate School, 2019. <https://doi.org/10.25394/PGS.8937986.v1>.
- (288) Alzarieni, K. Z.; Zhang, Y.; Niyonsaba, E.; Wehde, K. E.; Johnston, C. T.; Kilaz, G.; Kenttämaa, H. I. Determination of the Chemical Compositions of Condensate-like Oils with Different API Gravities by Using the Distillation, Precipitation, Fractionation Mass Spectrometry (DPF MS) Method. *Energy Fuels* **2021**, *35* (10), 8646–8656. <https://doi.org/10.1021/acs.energyfuels.0c04286>.
- (289) Niyonsaba, E.; Wehde, K. E.; Yerabolu, R.; Kilaz, G.; Kenttämaa, H. I. Determination of the Chemical Compositions of Heavy, Medium, and Light Crude Oils by Using the Distillation, Precipitation, Fractionation Mass Spectrometry (DPF MS) Method. *Fuel* **2019**, *255*, 115852. <https://doi.org/10.1016/j.fuel.2019.115852>.
- (290) Manheim, J.; Zhang, Y.; Viidanoja, J.; Kenttämaa, H. I. An Automated Method for Chemical Composition Analysis of Lubricant Base Oils by Using Atmospheric Pressure Chemical Ionization Mass Spectrometry. *J. Am. Soc. Mass Spectrom.* **2019**, *30* (10), 2014–2021. <https://doi.org/10.1007/s13361-019-02284-6>.
- (291) Jin, C.; Viidanoja, J.; Li, M.; Zhang, Y.; Ikonen, E.; Root, A.; Romanczyk, M.; Manheim, J.; Dziekonski, E.; Kenttämaa, H. I. Comparison of Atmospheric Pressure Chemical Ionization and Field Ionization Mass Spectrometry for the Analysis of Large Saturated Hydrocarbons. *Anal. Chem.* **2016**, *88* (21), 10592–10598. <https://doi.org/10.1021/acs.analchem.6b02789>.
- (292) Hertzog, J.; Garnier, C.; Mase, C.; Mariette, S.; Serve, O.; Hubert-Roux, M.; Afonso, C.; Giusti, P.; Barrère-Mangote, C. Fractionation by Flash Chromatography and Molecular Characterization of Bio-Oil by Ultra-High-Resolution Mass Spectrometry and NMR Spectroscopy. *J. Anal. Appl. Pyrolysis* **2022**, *166*, 105611. <https://doi.org/10.1016/j.jaap.2022.105611>.

- (293) Farrapeira, R. O.; Andrade, Y. B.; Schena, T.; Schneider, J. K.; von Muhlen, C.; Bjerck, T. R.; Krause, L. C.; Caramão, E. B. Characterization by Fast-GC × GC/TOFMS of the Acidic/Basic/Neutral Fractions of Bio-Oils from Fast Pyrolysis of Green Coconut Fibers. *Ind. Eng. Chem. Res.* **2022**, *61* (27), 9567–9574. <https://doi.org/10.1021/acs.iecr.2c00824>.
- (294) Wang, S.; Wang, Y.; Cai, Q.; Wang, X.; Jin, H.; Luo, Z. Multi-Step Separation of Monophenols and Pyrolytic Lignins from the Water-Insoluble Phase of Bio-Oil. *Sep. Purif. Technol.* **2014**, *122*, 248–255. <https://doi.org/10.1016/j.seppur.2013.11.017>.
- (295) Pütün, A. E.; Özcan, A.; Pütün, E. Pyrolysis of Hazelnut Shells in a Fixed-Bed Tubular Reactor: Yields and Structural Analysis of Bio-Oil. *J. Anal. Appl. Pyrolysis* **1999**, *52* (1), 33–49. [https://doi.org/10.1016/S0165-2370\(99\)00044-3](https://doi.org/10.1016/S0165-2370(99)00044-3).
- (296) Özçimen, D.; Karaosmanoğlu, F. Production and Characterization of Bio-Oil and Biochar from Rapeseed Cake. *Renew. Energy* **2004**, *29* (5), 779–787. <https://doi.org/10.1016/j.renene.2003.09.006>.
- (297) Özbay, N.; Uzun, B. B.; Varol, E. A.; Pütün, A. E. Comparative Analysis of Pyrolysis Oils and Its Subfractions under Different Atmospheric Conditions. *Fuel Process. Technol.* **2006**, *87* (11), 1013–1019. <https://doi.org/10.1016/j.fuproc.2006.07.009>.
- (298) Das, P.; Sreelatha, T.; Ganesh, A. Bio Oil from Pyrolysis of Cashew Nut Shell-Characterisation and Related Properties. *Biomass Bioenergy* **2004**, *27* (3), 265–275. <https://doi.org/10.1016/j.biombioe.2003.12.001>.
- (299) Garcia-Perez, M.; Chaala, A.; Pakdel, H.; Kretschmer, D.; Roy, C. Characterization of Bio-Oils in Chemical Families. *Biomass Bioenergy* **2007**, *31* (4), 222–242. <https://doi.org/10.1016/j.biombioe.2006.02.006>.
- (300) Cai, J.; Rahman, Md. M.; Zhang, S.; Sarker, M.; Zhang, X.; Zhang, Y.; Yu, X.; Fini, E. H. Review on Aging of Bio-Oil from Biomass Pyrolysis and Strategy to Slowing Aging. *Energy Fuels* **2021**, *35* (15), 11665–11692. <https://doi.org/10.1021/acs.energyfuels.1c01214>.
- (301) Kanaujia, P. K.; Naik, D. V.; Tripathi, D.; Singh, R.; Poddar, M. K.; Konathala, L. N. S. K.; Sharma, Y. K. Pyrolysis of Jatropha Curcas Seed Cake Followed by Optimization of Liquid-Liquid Extraction Procedure for the Obtained Bio-Oil. *J. Anal. Appl. Pyrolysis* **2016**, *118*, 202–224. <https://doi.org/10.1016/j.jaap.2016.02.005>.
- (302) Oasmaa, A.; Kuoppala, E.; Solantausta, Y. Fast Pyrolysis of Forestry Residue. 2. Physicochemical Composition of Product Liquid. *Energy Fuels* **2003**, *17* (2), 433–443. <https://doi.org/10.1021/ef020206g>.
- (303) Pinheiro Pires, A. P.; Arauzo, J.; Fonts, I.; Domine, M. E.; Fernández Arroyo, A.; Garcia-Perez, M. E.; Montoya, J.; Chejne, F.; Pfromm, P.; Garcia-Perez, M. Challenges and Opportunities for Bio-Oil Refining: A Review. *Energy Fuels* **2019**, *33* (6), 4683–4720. <https://doi.org/10.1021/acs.energyfuels.9b00039>.
- (304) Tessini, C.; Vega, M.; Müller, N.; Bustamante, L.; von Baer, D.; Berg, A.; Mardones, C. High Performance Thin Layer Chromatography Determination of Cellobiosan and Levoglucosan in Bio-Oil Obtained by Fast Pyrolysis of Sawdust. *J. Chromatogr. A* **2011**, *1218* (24), 3811–3815. <https://doi.org/10.1016/j.chroma.2011.04.037>.
- (305) Kanaujia, P. K.; Sharma, Y. K.; Garg, M. O.; Tripathi, D.; Singh, R. Review of Analytical Strategies in the Production and Upgrading of Bio-Oils Derived from Lignocellulosic Biomass. *J. Anal. Appl. Pyrolysis* **2014**, *105*, 55–74. <https://doi.org/10.1016/j.jaap.2013.10.004>.

- (306) Sedai, B.; Zhou, J. L.; Fakhri, N.; Sayari, A.; Baker, R. T. Solid Phase Extraction of Bio-Oil Model Compounds and Lignin-Derived Bio-Oil Using Amine-Functionalized Mesoporous Silicas. *ACS Sustain. Chem. Eng.* **2018**, *6* (8), 9716–9724. <https://doi.org/10.1021/acssuschemeng.8b00747>.
- (307) Meier, D.; Windt, M. Analysis of Bio-Oils. In *Transformation of Biomass*; Hornung, A., Ed.; John Wiley & Sons, Ltd: Chichester, UK, 2014; pp 227–256. <https://doi.org/10.1002/9781118693643.ch13>.
- (308) Lalli, P. M.; Corilo, Y. E.; Rowland, S. M.; Marshall, A. G.; Rodgers, R. P. Isomeric Separation and Structural Characterization of Acids in Petroleum by Ion Mobility Mass Spectrometry. *Energy Fuels* **2015**, *29* (6), 3626–3633. <https://doi.org/10.1021/acs.energyfuels.5b00503>.
- (309) Lalli, P. M.; Jarvis, J. M.; Marshall, A. G.; Rodgers, R. P. Functional Isomers in Petroleum Emulsion Interfacial Material Revealed by Ion Mobility Mass Spectrometry and Collision-Induced Dissociation. *Energy Fuels* **2017**, *31* (1), 311–318. <https://doi.org/10.1021/acs.energyfuels.6b02411>.
- (310) Fernandez-Lima, F. A.; Becker, C.; McKenna, A. M.; Rodgers, R. P.; Marshall, A. G.; Russell, D. H. Petroleum Crude Oil Characterization by IMS-MS and FTICR MS. *Anal. Chem.* **2009**, *81* (24), 9941–9947. <https://doi.org/10.1021/ac901594f>.
- (311) Hernández-Mesa, M.; Ropartz, D.; García-Campaña, A. M.; Rogniaux, H.; Dervilly-Pinel, G.; Le Bizec, B. Ion Mobility Spectrometry in Food Analysis: Principles, Current Applications and Future Trends. *Molecules* **2019**, *24* (15), 2706. <https://doi.org/10.3390/molecules24152706>.
- (312) Gabelica, V.; Marklund, E. Fundamentals of Ion Mobility Spectrometry. *Curr. Opin. Chem. Biol.* **2018**, *42*, 51–59. <https://doi.org/10.1016/j.cbpa.2017.10.022>.
- (313) May, J. C.; McLean, J. A. Ion Mobility-Mass Spectrometry: Time-Dispersive Instrumentation. *Anal. Chem.* **2015**, *87* (3), 1422–1436. <https://doi.org/10.1021/ac504720m>.
- (314) Maillard, J. F.; Le Maître, J.; Rüger, C. P.; Ridgeway, M.; Thompson, C. J.; Paupy, B.; Hubert-Roux, M.; Park, M.; Afonso, C.; Giusti, P. Structural Analysis of Petroporphyrins from Asphaltene by Trapped Ion Mobility Coupled with Fourier Transform Ion Cyclotron Resonance Mass Spectrometry. *The Analyst* **2021**, *146* (13), 4161–4171. <https://doi.org/10.1039/D1AN00140J>.
- (315) Dhungana, B.; Becker, C.; Zekavat, B.; Solouki, T.; Hockaday, W. C.; Chambliss, C. K. Characterization of Slow-Pyrolysis Bio-Oils by High-Resolution Mass Spectrometry and Ion Mobility Spectrometry. *Energy Fuels* **2015**, *29* (2), 744–753. <https://doi.org/10.1021/ef5016389>.
- (316) Farenc, M.; Paupy, B.; Marceau, S.; Riches, E.; Afonso, C.; Giusti, P. Effective Ion Mobility Peak Width as a New Isomeric Descriptor for the Untargeted Analysis of Complex Mixtures Using Ion Mobility-Mass Spectrometry. *J. Am. Soc. Mass Spectrom.* **2017**, *28* (11), 2476–2482. <https://doi.org/10.1007/s13361-017-1749-1>.
- (317) Fasciotti, M.; Souza, G. H. M. F.; Astarita, G.; Costa, I. C. R.; Monteiro, Thays. V. C.; Teixeira, C. M. L. L.; Eberlin, M. N.; Sarpal, A. S. Investigating the Potential of Ion Mobility-Mass Spectrometry for Microalgae Biomass Characterization. *Anal. Chem.* **2019**, *91* (14), 9266–9276. <https://doi.org/10.1021/acs.analchem.9b02172>.
- (318) Le Maître, J.; Paupy, B.; Hubert-Roux, M.; Marceau, S.; Rüger, C.; Afonso, C.; Giusti, P. Structural Analysis of Neutral Nitrogen Compounds Refractory to the

- Hydrodenitrogenation Process of Heavy Oil Fractions by High-Resolution Tandem Mass Spectrometry and Ion Mobility–Mass Spectrometry. *Energy Fuels* **2020**, *34* (8), 9328–9338. <https://doi.org/10.1021/acs.energyfuels.0c01160>.
- (319) Szykuła, K. M.; Wicking, C.; Whitmarsh, S.; Creaser, C. S.; Reynolds, J. C. Characterization of Crude Oil and Its Saturate, Aromatic, and Resin Fractions by High-Field Asymmetric Waveform Ion Mobility Spectrometry–High-Resolution Mass Spectrometry. *Energy Fuels* **2018**, *32* (11), 11310–11316. <https://doi.org/10.1021/acs.energyfuels.8b02718>.
- (320) Maleki, H.; Ghassabi Kondalaji, S.; Khakinejad, M.; Valentine, S. J. Structural Assignments of Sulfur-Containing Compounds in Crude Oil Using Ion Mobility Spectrometry–Mass Spectrometry. *Energy Fuels* **2016**, *30* (11), 9150–9161. <https://doi.org/10.1021/acs.energyfuels.6b01798>.
- (321) Cho, E.; Riches, E.; Palmer, M.; Giles, K.; Ujma, J.; Kim, S. Isolation of Crude Oil Peaks Differing by $m/z \sim 0.1$ via Tandem Mass Spectrometry Using a Cyclic Ion Mobility–Mass Spectrometer. *Anal. Chem.* **2019**, *91* (22), 14268–14274. <https://doi.org/10.1021/acs.analchem.9b02255>.
- (322) Rüger, C. P.; Le Maître, J.; Maillard, J.; Riches, E.; Palmer, M.; Afonso, C.; Giusti, P. Exploring Complex Mixtures by Cyclic Ion Mobility High-Resolution Mass Spectrometry: Application Toward Petroleum. *Anal. Chem.* **2021**, *93* (14), 5872–5881. <https://doi.org/10.1021/acs.analchem.1c00222>.
- (323) Zhang, Y.; Han, Y.; Wu, J.; Wang, Y.; Li, J.; Shi, Q.; Xu, C.; Hsu, C. S. Comprehensive Composition, Structure, and Size Characterization for Thiophene Compounds in Petroleum Using Ultrahigh-Resolution Mass Spectrometry and Trapped Ion Mobility Spectrometry. *Anal. Chem.* **2021**, *93* (12), 5089–5097. <https://doi.org/10.1021/acs.analchem.0c04667>.
- (324) Dodds, J. N.; May, J. C.; McLean, J. A. Correlating Resolving Power, Resolution and Collision Cross Section: Unifying Cross Platform Assessment of Separation Efficiency in Ion Mobility Spectrometry. *Anal. Chem.* **2017**, *89* (22), 12176–12184. <https://doi.org/10.1021/acs.analchem.7b02827>.
- (325) Cumeras, R.; Figueras, E.; Davis, C. E.; Baumbach, J. I.; Gràcia, I. Review on Ion Mobility Spectrometry. Part 1: Current Instrumentation. *The Analyst* **2015**, *140* (5), 1376–1390. <https://doi.org/10.1039/c4an01100g>.
- (326) Dodds, J. N.; Baker, E. S. Ion Mobility Spectrometry: Fundamental Concepts, Instrumentation, Applications, and the Road Ahead. *J. Am. Soc. Mass Spectrom.* **2019**, *30* (11), 2185–2195. <https://doi.org/10.1007/s13361-019-02288-2>.
- (327) Kliman, M.; May, J. C.; McLean, J. A. Lipid Analysis and Lipidomics by Structurally Selective Ion Mobility–Mass Spectrometry. *Biochim. Biophys. Acta* **2011**, *1811* (11), 935–945. <https://doi.org/10.1016/j.bbailip.2011.05.016>.
- (328) Cooks, R. G. Special Feature: Historical. Collision-Induced Dissociation: Readings and Commentary. *J. Mass Spectrom.* **1995**, *30* (9), 1215–1221. <https://doi.org/10.1002/jms.1190300902>.
- (329) van Agthoven, M. A.; Lam, Y. P. Y.; O'Connor, P. B.; Rolando, C.; Delsuc, M.-A. Two-Dimensional Mass Spectrometry: New Perspectives for Tandem Mass Spectrometry. *Eur. Biophys. J.* **2019**, *48* (3), 213–229. <https://doi.org/10.1007/s00249-019-01348-5>.
- (330) Zuber, J.; Rathsack, P.; Otto, M. Structural Characterization of Acidic Compounds in Pyrolysis Liquids Using Collision-Induced Dissociation and Fourier Transform Ion

- Cyclotron Resonance Mass Spectrometry. *Anal. Chem.* **2018**, *90* (21), 12655–12662. <https://doi.org/10.1021/acs.analchem.8b02873>.
- (331) Marzullo, B. P.; Morgan, T. E.; Theisen, A.; Haris, A.; Wootton, C. A.; Perry, S. J.; Saeed, M.; Barrow, M. P.; O'Connor, P. B. Combining Ultraviolet Photodissociation and Two-Dimensional Mass Spectrometry: A Contemporary Approach for Characterizing Singly Charged Agrochemicals. *Anal. Chem.* **2021**, *93* (27), 9462–9470. <https://doi.org/10.1021/acs.analchem.1c01185>.
- (332) Marzullo, B. P.; Morgan, T. E.; Wootton, C. A.; Li, M.; Perry, S. J.; Saeed, M.; Barrow, M. P.; O'Connor, P. B. Comparison of Fragmentation Techniques for the Structural Characterization of Singly Charged Agrochemicals. *Anal. Chem.* **2020**, *92* (4), 3143–3151. <https://doi.org/10.1021/acs.analchem.9b04820>.
- (333) Floris, F.; Vallotto, C.; Chiron, L.; Lynch, A. M.; Barrow, M. P.; Delsuc, M.-A.; O'Connor, P. B. Polymer Analysis in the Second Dimension: Preliminary Studies for the Characterization of Polymers with 2D MS. *Anal. Chem.* **2017**, *89* (18), 9892–9899. <https://doi.org/10.1021/acs.analchem.7b02086>.
- (334) Morgan, T. E.; Wootton, C. A.; Marzullo, B.; Paris, J.; Kerr, A.; Ellacott, S. H.; van Agthoven, M. A.; Barrow, M. P.; Bristow, A. W. T.; Perrier, S.; O'Connor, P. B. Characterization Across a Dispersity: Polymer Mass Spectrometry in the Second Dimension. *J. Am. Soc. Mass Spectrom.* **2021**, *32* (8), 2153–2161. <https://doi.org/10.1021/jasms.1c00106>.
- (335) Paris, J.; Theisen, A.; Marzullo, B. P.; Haris, A.; Morgan, T. E.; Barrow, M. P.; O'Hara, J.; O'Connor, P. B. Multimodal Tandem Mass Spectrometry Techniques for the Analysis of Phosphopeptides. *J. Am. Soc. Mass Spectrom.* **2022**, *33* (7), 1126–1133. <https://doi.org/10.1021/jasms.1c00353>.
- (336) Zhurov, K.; Fornelli, L.; Wodrich, M.; Laskay, U.; Tsybin, Y. ChemInform Abstract: Principles of Electron Capture and Transfer Dissociation Mass Spectrometry Applied to Peptide and Protein Structure Analysis. *Chem. Soc. Rev.* **2013**, *42*. <https://doi.org/10.1039/c3cs35477f>.
- (337) Cooper, H. J.; Håkansson, K.; Marshall, A. G. The Role of Electron Capture Dissociation in Biomolecular Analysis. *Mass Spectrom. Rev.* **2005**, *24* (2), 201–222. <https://doi.org/10.1002/mas.20014>.
- (338) Zhang, H.; Cui, W.; Wen, J.; Blankenship, R. E.; Gross, M. L. Native Electrospray and Electron-Capture Dissociation in FTICR Mass Spectrometry Provide Top-down Sequencing of a Protein Component in an Intact Protein Assembly. *J. Am. Soc. Mass Spectrom.* **2010**, *21* (12), 1966–1968. <https://doi.org/10.1016/j.jasms.2010.08.006>.
- (339) Klemm, D.; Heublein, B.; Fink, H.-P.; Bohn, A. Cellulose: Fascinating Biopolymer and Sustainable Raw Material. *Angew. Chem. Int. Ed.* **2005**, *44* (22), 3358–3393. <https://doi.org/10.1002/anie.200460587>.
- (340) Scheller, H. V.; Ulvskov, P. Hemicelluloses. *Annu. Rev. Plant Biol.* **2010**, *61* (1), 263–289. <https://doi.org/10.1146/annurev-arplant-042809-112315>.
- (341) Vinuesa, N. R.; Gallardo, V. A.; Klimek, J. F.; Carpita, N. C.; Kenttämaa, H. I. Analysis of Carbohydrates by Atmospheric Pressure Chloride Anion Attachment Tandem Mass Spectrometry. *Fuel* **2013**, *105*, 235–246. <https://doi.org/10.1016/j.fuel.2012.08.012>.
- (342) Yu, Z.; Murria, P.; Easton, M. W.; Degenstein, J. C.; Zhu, H.; Xu, L.; Agrawal, R.; Delgass, W. N.; Ribeiro, F. H.; Kenttämaa, H. I. Exploring the Reaction Mechanisms of Fast Pyrolysis of Xylan Model Compounds via Tandem Mass Spectrometry and Quantum

- Chemical Calculations. *J. Phys. Chem. A* **2019**, *123* (42), 9149–9157. <https://doi.org/10.1021/acs.jpca.9b04438>.
- (343) Zeng, J.; Yoo, C. G.; Wang, F.; Pan, X.; Vermerris, W.; Tong, Z. Biomimetic Fenton-Catalyzed Lignin Depolymerization to High-Value Aromatics and Dicarboxylic Acids. *ChemSusChem* **2015**, *8* (5), 861–871. <https://doi.org/10.1002/cssc.201403128>.
- (344) Liu, J.-Y.; Wu, S.; Lou, R. Chemical Structure and Pyrolysis Response of β -O-4 Lignin Model Polymer. *BioResources* **2011**, *6*.
- (345) Calvo-Flores, F. G.; Dobado, J. A. Lignin as Renewable Raw Material. *ChemSusChem* **2010**, *3* (11), 1227–1235. <https://doi.org/10.1002/cssc.201000157>.
- (346) *Theoretical Study of the Remarkably Diverse Linkages in Lignin | The Journal of Physical Chemistry Letters*. <https://pubs.acs.org/doi/full/10.1021/jz201201q> (accessed 2022-10-24).
- (347) Dong, X.; Mayes, H.; Morreel, K.; Katahira, R.; Li, Y.; Ralph, J.; Black, B.; Beckham, G. Energy-Resolved Mass Spectrometry as a Tool for Identification of Lignin Depolymerization Products. *ChemSusChem* *n/a* (n/a). <https://doi.org/10.1002/cssc.202201441>.
- (348) Zhang, X.; Ma, H.; Wu, S.; Wei, W. Sequential Fractionation of Lignin-Derived Pyrolysis Oil via Extraction with a Combination of Water and Organic Solvents. **2019**, *16*.
- (349) Abdelaziz, O. Y.; Li, K.; Tunã, P.; Hulteberg, C. P. Continuous Catalytic Depolymerisation and Conversion of Industrial Kraft Lignin into Low-Molecular-Weight Aromatics. *Biomass Convers. Biorefinery* **2018**, *8* (2), 455–470. <https://doi.org/10.1007/s13399-017-0294-2>.
- (350) Paris, J.; Morgan, T. E.; Wootton, C. A.; Barrow, M. P.; O'Hara, J.; O'Connor, P. B. Facile Determination of Phosphorylation Sites in Peptides Using Two-Dimensional Mass Spectrometry. *Anal. Chem.* **2020**, *92* (10), 6817–6821. <https://doi.org/10.1021/acs.analchem.0c00884>.
- (351) Poole, C. F. Derivatization Reactions for Use with the Electron-Capture Detector. *J. Chromatogr. A* **2013**, *1296*, 15–24. <https://doi.org/10.1016/j.chroma.2013.01.108>.
- (352) Qi, B.-L.; Liu, P.; Wang, Q.-Y.; Cai, W.-J.; Yuan, B.-F.; Feng, Y.-Q. Derivatization for Liquid Chromatography-Mass Spectrometry. *TrAC Trends Anal. Chem.* **2014**, *59*, 121–132. <https://doi.org/10.1016/j.trac.2014.03.013>.
- (353) Kanaujia, P. K.; Sharma, Y. K.; Garg, M. O.; Tripathi, D.; Singh, R. Review of Analytical Strategies in the Production and Upgrading of Bio-Oils Derived from Lignocellulosic Biomass. *J. Anal. Appl. Pyrolysis* **2014**, *105*, 55–74. <https://doi.org/10.1016/j.jaap.2013.10.004>.
- (354) Tessini, C.; Müller, N.; Mardones, C.; Meier, D.; Berg, A.; von Baer, D. Chromatographic Approaches for Determination of Low-Molecular Mass Aldehydes in Bio-Oil. *J. Chromatogr. A* **2012**, *1219*, 154–160. <https://doi.org/10.1016/j.chroma.2011.10.093>.
- (355) Christensen, E. D.; Chupka, G. M.; Luecke, J.; Smurthwaite, T.; Alleman, T. L.; Iisa, K.; Franz, J. A.; Elliott, D. C.; McCormick, R. L. Analysis of Oxygenated Compounds in Hydrotreated Biomass Fast Pyrolysis Oil Distillate Fractions. *Energy Fuels* **2011**, *25* (11), 5462–5471. <https://doi.org/10.1021/ef201357h>.
- (356) Uchiyama, S.; Inaba, Y.; Kunugita, N. Derivatization of Carbonyl Compounds with 2,4-Dinitrophenylhydrazine and Their Subsequent Determination by High-Performance Liquid Chromatography. *J. Chromatogr. B* **2011**, *879* (17), 1282–1289. <https://doi.org/10.1016/j.jchromb.2010.09.028>.

- (357) Alhassan, A.; Andersson, J. T. Ketones in Fossil Materials—A Mass Spectrometric Analysis of a Crude Oil and a Coal Tar. *Energy Fuels* **2013**, *27* (10), 5770–5778. <https://doi.org/10.1021/ef400961d>.
- (358) Krajewski, L. C.; Lobodin, V. V.; Robbins, W. K.; Jin, P.; Bota, G.; Marshall, A. G.; Rodgers, R. P. Method for Isolation and Detection of Ketones Formed from High-Temperature Naphthenic Acid Corrosion. *Energy Fuels* **2017**, *31* (10), 10674–10679. <https://doi.org/10.1021/acs.energyfuels.7b01803>.
- (359) Staš, M.; Chudoba, J.; Kubička, D.; Blažek, J.; Pospíšil, M. Petroleomic Characterization of Pyrolysis Bio-Oils: A Review. *Energy Fuels* **2017**, *31* (10), 10283–10299. <https://doi.org/10.1021/acs.energyfuels.7b00826>.
- (360) Wasinski, F. A. H.; Andersson, J. T. Qualitative Analysis of Phenols and Alcohols in Complex Samples after Derivatization to Esters of Ferrocene Carboxylic Acid by Gas Chromatography with Mass Spectrometric Detection. *J. Chromatogr. A* **2007**, *1157* (1–2), 376–385. <https://doi.org/10.1016/j.chroma.2007.04.060>.
- (361) Rolfes, J.; Andersson, J. T. Determination of Alkylphenols after Derivatization to Ferrocenecarboxylic Acid Esters with Gas Chromatography-Atomic Emission Detection. *Anal. Chem.* **2001**, *73* (13), 3073–3082. <https://doi.org/10.1021/ac001540h>.
- (362) Zhu, H.; Janusson, E.; Luo, J.; Piers, J.; Islam, F.; McGarvey, G. B.; Oliver, A. G.; Granot, O.; McIndoe, J. S. Phenol-Selective Mass Spectrometric Analysis of Jet Fuel. *The Analyst* **2017**, *142* (17), 3278–3284. <https://doi.org/10.1039/C7AN00908A>.
- (363) Murwanashyaka, J. N.; Pakdel, H.; Roy, C. Step-Wise and One-Step Vacuum Pyrolysis of Birch-Derived Biomass to Monitor the Evolution of Phenols. *J. Anal. Appl. Pyrolysis* **2001**, *60* (2), 219–231. [https://doi.org/10.1016/S0165-2370\(00\)00206-0](https://doi.org/10.1016/S0165-2370(00)00206-0).
- (364) Chen, X.; Xu, C.; Zhang, W.; Ma, C.; Liu, X.; Zhao, S.; Shi, Q. Separation and Molecular Characterization of Ketones in a Low-Temperature Coal Tar. *Energy Fuels* **2018**, *32* (4), 4662–4670. <https://doi.org/10.1021/acs.energyfuels.7b03630>.
- (365) Thorn, K. A.; Cox, L. G. Probing the Carbonyl Functionality of a Petroleum Resin and Asphaltene through Oximation and Schiff Base Formation in Conjunction with N-15 NMR. *PLOS ONE* **2015**, *10* (11), e0142452. <https://doi.org/10.1371/journal.pone.0142452>.
- (366) Zaikin, V. G.; Halket, J. M. Derivatization in Mass Spectrometry—8. Soft Ionization Mass Spectrometry of Small Molecules. *Eur. J. Mass Spectrom.* **2006**, *12* (2), 79–115. <https://doi.org/10.1255/ejms.798>.
- (367) Farajzadeh, M. A.; Yadeghari, A.; Khoshmaram, L.; Ghorbanpour, H. Gas Chromatographic Determination of Some Phenolic Compounds in Fuels and Engine Oil after Simultaneous Derivatization and Microextraction: Sample Preparation. *J. Sep. Sci.* **2014**, *37* (20), 2966–2973. <https://doi.org/10.1002/jssc.201400398>.
- (368) Staš, M.; Auersvald, M.; Kejla, L.; Vrtiška, D.; Kroufek, J.; Kubička, D. Quantitative Analysis of Pyrolysis Bio-Oils: A Review. *TrAC Trends Anal. Chem.* **2020**, *126*, 115857. <https://doi.org/10.1016/j.trac.2020.115857>.
- (369) Balakshin, M.; Capanema, E. On the Quantification of Lignin Hydroxyl Groups With ³¹P and ¹³C NMR Spectroscopy. *J. Wood Chem. Technol.* **2015**, *35* (3), 220–237. <https://doi.org/10.1080/02773813.2014.928328>.
- (370) Pu, Y.; Cao, S.; Ragauskas, A. J. Application of Quantitative ³¹P NMR in Biomass Lignin and Biofuel Precursors Characterization. *Energy Environ. Sci.* **2011**, *4* (9), 3154. <https://doi.org/10.1039/c1ee01201k>.

- (371) Ehiosun, K. I.; Grimaud, R.; Lobinski, R. Mass Spectrometric Analysis for Carboxylic Acids as Viable Markers of Petroleum Hydrocarbon Biodegradation. *Trends Environ. Anal. Chem.* **2022**, *35*, e00172. <https://doi.org/10.1016/j.teac.2022.e00172>.
- (372) Grasset, L.; Guignard, C.; Amblès, A. Free and Esterified Aliphatic Carboxylic Acids in Humic and Humic Acids from a Peat Sample as Revealed by Pyrolysis with Tetramethylammonium Hydroxide or Tetraethylammonium Acetate. *Org. Geochem.* **2002**, *33* (3), 181–188. [https://doi.org/10.1016/S0146-6380\(01\)00150-4](https://doi.org/10.1016/S0146-6380(01)00150-4).
- (373) Ben, H.; Ferrell III, J. R. In-Depth Investigation on Quantitative Characterization of Pyrolysis Oil by ^{31}P NMR. *RSC Adv.* **2016**, *6* (21), 17567–17573. <https://doi.org/10.1039/C5RA23939G>.
- (374) York, R.; Bell, N. G. A. Molecular Tagging for the Molecular Characterization of Natural Organic Matter. *Environ. Sci. Technol.* **2020**, *54* (6), 3051–3063. <https://doi.org/10.1021/acs.est.9b04737>.
- (375) Zhrebker, A.; Lechtenfeld, O. J.; Sarycheva, A.; Kostyukevich, Y.; Kharybin, O.; Fedoros, E. I.; Nikolaev, E. N. Refinement of Compound Aromaticity in Complex Organic Mixtures by Stable Isotope Label Assisted Ultrahigh-Resolution Mass Spectrometry. *Anal. Chem.* **2020**, *92* (13), 9032–9038. <https://doi.org/10.1021/acs.analchem.0c01208>.
- (376) Kostyukevich, Y.; Acter, T.; Zhrebker, A.; Ahmed, A.; Kim, S.; Nikolaev, E. Hydrogen/Deuterium Exchange in Mass Spectrometry. *Mass Spectrom. Rev.* **2018**, *37* (6), 811–853. <https://doi.org/10.1002/mas.21565>.
- (377) Kostyukevich, Y.; Kononikhin, A.; Popov, I.; Nikolaev, E. Analytical Description of the H/D Exchange Kinetic of Macromolecule. *Anal. Chem.* **2018**, *90* (8), 5116–5121. <https://doi.org/10.1021/acs.analchem.7b05151>.
- (378) Zhang, Y.; Chen, X.; Zhang, L.; Shi, Q.; Zhao, S.; Xu, C. Specification of Nitrogen Functional Group in Hydrotreated Petroleum Molecule by Hydrogen/Deuterium Exchange Electrospray Ionization High-Resolution Mass Spectrometry. *The Analyst* **2020**, *145*. <https://doi.org/10.1039/D0AN00772B>.
- (379) Cho, Y.; Ahmed, A.; Kim, S. Application of Atmospheric Pressure Photo Ionization Hydrogen/Deuterium Exchange High-Resolution Mass Spectrometry for the Molecular Level Speciation of Nitrogen Compounds in Heavy Crude Oils. *Anal. Chem.* **2013**, *85* (20), 9758–9763. <https://doi.org/10.1021/ac402157r>.
- (380) Islam, A.; Kim, D.; Yim, U. H.; Shim, W. J.; Kim, S. Structure-Dependent Degradation of Polar Compounds in Weathered Oils Observed by Atmospheric Pressure Photo-Ionization Hydrogen/Deuterium Exchange Ultrahigh Resolution Mass Spectrometry. *J. Hazard. Mater.* **2015**, *296*, 93–100. <https://doi.org/10.1016/j.jhazmat.2015.04.042>.
- (381) Acter, T.; Lee, S.; Cho, E.; Jung, M.-J.; Kim, S. Design and Validation of In-Source Atmospheric Pressure Photoionization Hydrogen/Deuterium Exchange Mass Spectrometry with Continuous Feeding of D_2O . *J. Am. Soc. Mass Spectrom.* **2018**, *29* (1), 85–94. <https://doi.org/10.1007/s13361-017-1831-8>.
- (382) Kostyukevich, Y.; Zhrebker, A.; Vlaskin, M. S.; Roznyatovsky, V. A.; Grishin, Y. K.; Nikolaev, E. Speciation of Structural Fragments in Crude Oil by Means of Isotope Exchange in Near-Critical Water and Fourier Transform Mass Spectrometry. *Anal. Bioanal. Chem.* **2019**, *411* (15), 3331–3339. <https://doi.org/10.1007/s00216-019-01802-5>.
- (383) Kostyukevich, Y.; Osipenko, S.; Rindin, K.; Zhrebker, A.; Kovaleva, O.; Rumiantseva, L.; Borisova, L.; Borisova, N.; Vlaskin, M. S.; Nikolaev, E. Analysis of the Bio-Oil Produced by

- the Hydrothermal Liquefaction of Biomass Using High-Resolution Mass Spectrometry and Isotope Exchange. *Energy Fuels* **2021**, *35* (15), 12208–12215. <https://doi.org/10.1021/acs.energyfuels.1c01649>.
- (384) Son, S.; Kim, S.; Yim, Y.-H.; Kim, S. Reproducibility of Crude Oil Spectra Obtained with Ultrahigh Resolution Mass Spectrometry. *Anal. Chem.* **2020**, *92* (14), 9465–9471. <https://doi.org/10.1021/acs.analchem.0c00865>.
- (385) Rodgers, R. P.; Mapolelo, M. M.; Robbins, W. K.; Chacón-Patiño, M. L.; Putman, J. C.; Niles, S. F.; Rowland, S. M.; Marshall, A. G. Combating Selective Ionization in the High Resolution Mass Spectral Characterization of Complex Mixtures. *Faraday Discuss.* **2019**, *218*, 29–51. <https://doi.org/10.1039/C9FD00005D>.
- (386) Lacroix-Andrivet, O.; Hubert-Roux, M.; Mendes Siqueira, A. L.; Bai, Y.; Afonso, C. Comparison of Silica and Cellulose Stationary Phases to Analyze Bitumen by High-Performance Thin-Layer Chromatography Coupled to Laser Desorption Ionization Fourier Transform Ion Cyclotron Resonance Mass Spectrometry. *Energy Fuels* **2020**, *34* (8), 9296–9303. <https://doi.org/10.1021/acs.energyfuels.0c00709>.
- (387) Guillemant, J.; Lacoue-Nègre, M.; Berlioz-Barbier, A.; Albrieux, F.; de Oliveira, L. P.; Joly, J.-F.; Duponchel, L. Towards a New Pseudo-Quantitative Approach to Evaluate the Ionization Response of Nitrogen Compounds in Complex Matrices. *Sci. Rep.* **2021**, *11* (1), 6417. <https://doi.org/10.1038/s41598-021-85854-7>.
- (388) Reymond, C.; Le Masle, A.; Colas, C.; Charon, N. Input of an Off-Line, Comprehensive, Three-Dimensional Method (CPC×SFC/HRMS) to Quantify Polycyclic Aromatic Hydrocarbons in Vacuum Gas Oils. *Anal. Chem.* **2020**, *92* (9), 6684–6692. <https://doi.org/10.1021/acs.analchem.0c00605>.
- (389) A Three-Dimensional Semi-Quantitative Method to Monitor the Evolution of Polycyclic Aromatic Hydrocarbons from Vacuum Gas Oil Feedstocks to Lighter Products. *Fuel* **2021**, *296*, 120175. <https://doi.org/10.1016/j.fuel.2021.120175>.

PART II : MASS SPECTROMETRY AND APPLICATION

CHAPTER 2 : MATERIALS AND METHODS

2.1. Introduction

In this chapter, the description of the production of raw bio-oils used in this study will be given. The studied bio-oil was produced by the GREENER research group at the Reactions and Process Engineering Laboratory (LRGP – UMR CNRS 7274, Nancy, France). Having designed different pyrolysis reactors, this group possesses a strong and deep knowledge of biomass pyrolysis processes. In addition, a multi-technical approach was used by this team to characterize biomass and pyrolysis products.

The main objective of my Ph.D. work is focused on the functional characterization of the raw bio-oil components. The characterization of bio-oils was performed by different petroleomic' approaches requiring high-resolution mass spectrometers as Fourier transform ion cyclotron resonance mass spectrometry (FT-ICR MS). FT-ICR MS can identify thousands of different species by high mass measurement accuracy and high mass resolving power. Additionally, the use of different ionization sources is an advantage to explore in depth the bio-oils components, which present a wide range of molecular weight, boiling point, polarity, and solubility. The used ionization techniques: electrospray ionization (ESI), atmospheric pressure photoionization (APPI) as well as atmospheric pressure chemical ionization (APCI) will be detailed. These ionization sources are coupled to a FT-ICR MS, whose principle will be also stated.

As part of the complex mixture analysis, the bio-oil mass spectrum present tens of thousands of peaks. Different steps of data treatment are required, which include the calibration of the mass spectrum, the assignment of a formulae to each observed ion by means of different and specific software's and the representation of the data. A specific section of this chapter will detail each of these data treatment steps.

The last part of this chapter will briefly describe the principle of tandem mass spectrometry, which has been used for structural analysis.

2.2. Bio-oils produced by pyrolysis

2.2.1. Fast pyrolysis

2.2.1.1. Parameters and reactor

The lab-scale reactor (Figure 2.1) is a quartz micro-fluidized 20 mm x 15 cm (diameter x height) bed reactor.¹ The micro-fluidized bed reactor's (MFBR) gas distributor is made from a sintered plate with a thickness of 5 mm and silica sand particles. For a suitable fluidization regime, silica sand particles between 150 and 300 μm are used as inert bed components. The MFBR is placed inside a homemade electrical furnace with a quartz window to allow the visual control during pyrolysis. Nitrogen gas (99.99%), which enters the reactor simultaneously from above and below, is supplied by two dedicated gas lines. The first one at a constant flow rate of $500 \text{ mL}\cdot\text{min}^{-1}$ is used as fluidizing gas. The flow rate of the second one, used as sweep gas, is fixed at $200 \text{ mL}\cdot\text{min}^{-1}$. The temperature controllers attached to two different thermocouples monitor the temperatures of the micro-fluidized bed and the furnace.

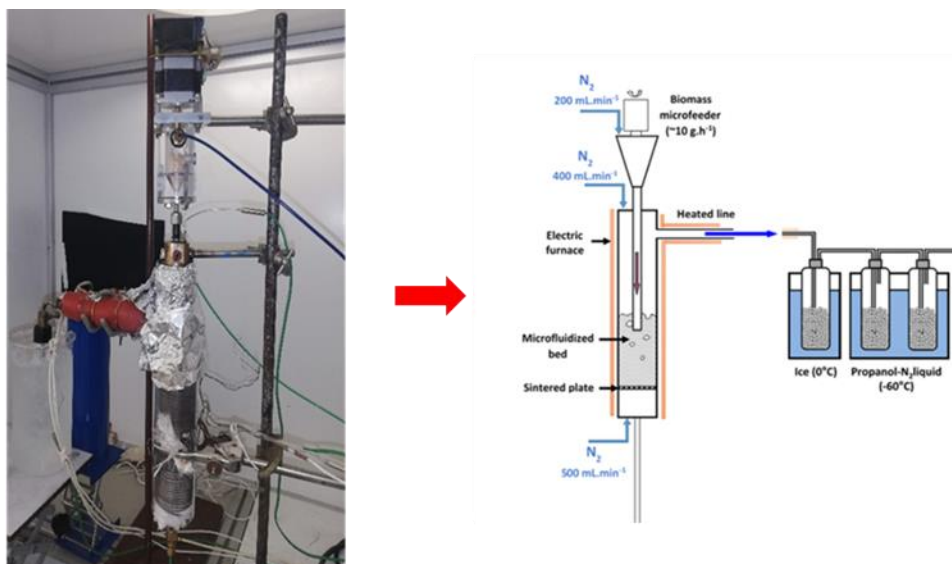


Figure 2-1 : Diagram of the bio-oil collection system and microfluidized bed reactor¹

Adapted from Hertzog et al. thesis.²

The microfluidizer bed is equipped with a micro-feeder that allows the introduction of the biomass in MFBR. This injection could be either done in continuous or stepwise mode. The biomass particles are injected at a flow rate of $10 \text{ g}\cdot\text{h}^{-1}$. N_2 (sweep gas line) is injected to prevent sand from flowing through the injection rod.

2.2.2. Raw Material

In this study, lignocellulosic biomass is oak biomass grounded to powder with particle sizes between 0.8 and 1.7 mm. Commonly, 2 grams of oak biomass were introduced continuously into the micro-fluidized bed.³

2.2.3. Raw bio-oil production

The micro-fluidized bed is maintained at a temperature of 500°C (Figure 2-1). Under these conditions, the gas-phase residence period in the reactor is around 1.2 s. In order to avoid condensation, the generated bio-oil vapors are directed to three cold traps through a heated line set at 350 °C. The first cooler is positioned in an ice bath at 0 °C with the purpose of trapping water and heavier species. Propanol and liquid nitrogen are both present in the second and third coolers, allowing the temperature to be maintained at –60 °C. After the three cryogenic traps, a methanol-filled bubbler is attached to the line. Following the pyrolysis, 20 mL of methanol is used to rinse all of the coolers and pipes in the line in order to collect the condensables. Consequently, a 20 mL solution of bio-oil is produced.

2.3. Petroleomic' methods for characterizing the pyrolysis bio-oils

2.3.1. Introduction

To describe pyrolysis bio-oils, the non-targeted petroleomic technique was used in this work. Marshall developed this technique for high resolution Fourier transform ion cyclotron resonance mass spectrometry's investigation of crude oils.^{4,5} Electrospray ionisation (ESI), atmospheric pressure photoionization (APPI), atmospheric pressure chemical ionization (APCI) and laser desorption/ionisation (LDI) are often used to investigate the different oil components. Due to the huge number of crude oil components, a very high-resolution mass spectrometer must be employed to discriminate and identify the different features observed on a mass spectrum. In the field of petroleomic studies, FT-ICR and FT-Orbitrap mass spectrometry are consequently required.⁶ The petroleomic approach is one of the non-targeted methods, which ensures the assignment of more than 30 000 various elemental formulas when extremely complex mixtures, such as petroleum or bio-oils produced by biomass pyrolysis of are investigated.⁷ Such a methodology is complementary to what can be acquired by liquid or gas chromatography techniques and allows the simultaneous observation of a broad range of substances in terms of chemical functions and molecular weight. Nevertheless, as discussed in Chapter I, no single ionization source can ionize all bio-oil components simultaneously. The specificities of different ionization sources must be used to achieve this result. This work uses ESI, nanoESI, APCI, and APPI ionization to obtain the most complete description of the molecular composition of a bio-oil. It must be kept in mind that non-targeted analysis does not usually allow obtaining a complete characterization of the composition of a highly complex mixture by using a single ionization method. Competitions for ionization are indeed frequent,

especially in ESI. The following sections will develop the fundamental principles of the ionization and mass spectrometry techniques used in my Ph-D work.

2.3.2. Mass Spectrometry: History

"The basic principle of mass spectrometry (MS) is to generate ions from either inorganic or organic compounds by any suitable method, to separate these ions by their mass-to-charge ratio (m/z) and to detect them qualitatively and quantitatively by their respective m/z and abundance. The analyte may be ionized thermally, by electric fields or by impacting energetic electrons, ions or photons. These ions can be single ionized atoms, clusters, molecules or their fragments or associates. Ion separation is affected by static or dynamic electric or magnetic fields."⁸

The beginnings of mass spectrometry can be traced back to work of Wien work in 1898 who showed how ion beams could be bent by passing through superimposed parallel electric and magnetic fields. However, Sir J. J. Thomson, the great-grandfather of modern mass spectrometrists, can be considered the inventor of this technique through his work on the analysis of negatively and positively charged cathode rays using a parabola mass spectrograph at the Cavendish Laboratory of the University of Cambridge.^{9,10} Renowned physicists such as Aston (1919)¹¹, Dempster (1918)¹², Bainbridge (1932)¹³ and, Jordan (1936) continued to advance mass spectrometry throughout the following two decades.

In the 1940s, chemists used mass spectrometry to monitor petroleum refining process after realizing its enormous analytical potential. Through the Consolidated Engineering Corporation, the first mass spectrometer for the industry was made available in 1943. In 1946 and 1949 respectively, the concepts of time-of-flight (ToF) and ion cyclotron resonance (ICR) were introduced.^{14,15}

The development of softer ionization techniques than electron impact (EI) during the 1980s broadened the scope of mass spectrometry "exponentially." including electrospray ionization (ESI) from 1984 to 1988,¹⁶ fast atom bombardment (FAB) in 1981,¹⁷ and matrix-assisted laser desorption/ionization (MALDI) in 1988.¹⁸ The introduction of ESI and MALDI ionization methods has extended the accessible mass range beyond 100kDa and the development of mass spectrometry in biology and life sciences. The 2002 Nobel Prize in Chemistry was awarded to John Fenn for his ESI work and Koichi Tanaka for proving that large molecular weight proteins could be ionized by assisted laser desorption.

Along with advances in ionization techniques, the technological mass analyzer development has made many advances that have improved sensitivity, resolving power, and increased mass range. These developments include high-field magnets for FT-ICR mass spectrometers, the use of high acceleration potentials, electrostatic mirrors, and time lag focusing for ToF instruments. The new century brought instrumental developments, such as two new ion traps: the orbitrap, designed by Alexander Makarov in 2000,¹⁹ and the linear quadrupole ion trap (LIT) by James W. Hager.²⁰

The following section describes the ionization sources used in my work, their underlying mechanisms, and the principle of FT-ICR MS.

2.4. Ionization sources

For mass spectrometry, an analyte must be ionized. In mass spectrometry, ionized molecules (ions, whether cations or anions) are the only detected species. Ionization procedures come in a vast diversity.

2.4.1. Electrospray Ionization ESI

2.4.1.1. Introduction

Zeleny et al. published the first article on electrospray ionization (ESI) in 1917.^{25,26} They showed that generating an electric field between a counter-electrode and a capillary in which a solution is infused, it is possible to create a spray composed of tiny droplets. Later, Malcolm Dole (late 1960s) performed several experiments to establish the conditions necessary for the gas-phase production of large-molecule ion.^{26,27} Finally, in 1984, John Fenn and colleagues introduced electrospray ionization mass spectrometry.^{26,28-30} They first announced the successful coupling of ESI with quadrupole and magnetic sector mass analyzers. ESI has gained popularity as a method for examining a wide range of materials, especially fragile molecules and macromolecules such as peptides, proteins, or polymers. ESI can also generate multi-charged ions, which can be helpful for analysis because it allows the study of large molecules in an m/z range accessible to most instruments and allows the use of alternative activation methods for tandem mass spectrometry.³¹ ESI is considered a "soft ionization" technique because it generally prevents species fragmentation. It is well-suited to investigate polar compounds.

2.4.1.2. Principle

ESI is a desolvation/ionization technique that allows the formation of gas phase ions from species initially in the liquid phase. At atmospheric pressure, the sample solution is infused in the ionization source at a flow rate ranging from 1 to 20 $\mu\text{L}\cdot\text{min}^{-1}$ by a stainless-steel capillary. A potential difference, typically in the 1 to 6 kV range, between the capillary and a counter electrode produces an intense electric field. In the absence of an electric field, the solution forms a meniscus at the exit of the capillary (Figure 2-2). The application of the electric field causes a slight deformation of the meniscus. The increase of the electric field up to the so-called "onset voltage" induces the formation of a Taylor cone, at the end of which tiny droplets are emitted.

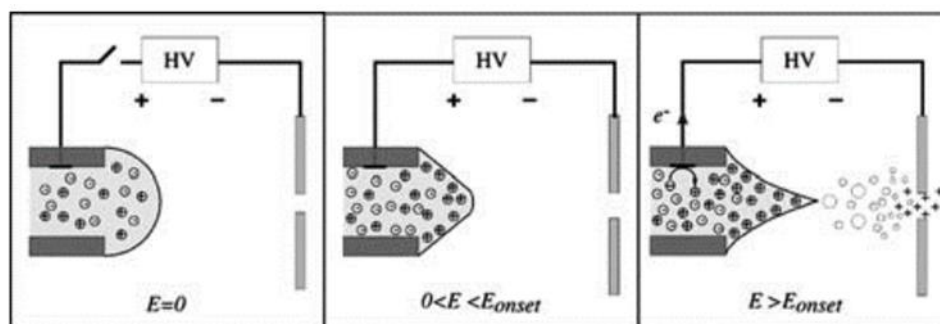


Figure 2-2: Change of the solvent's shape at the output of the capillary in respect with the applied electric field.³²

Due to the electric field ($10^{-6} \text{ V}\cdot\text{m}^{-1}$), charges accumulate at the surface of the meniscus. The nature of these charges depends on the polarity of the potential applied to the capillary. If this potential is positive, the ions at the surface of the meniscus are cations. The electrostatic repulsion between cations and the potential applied on the capillary induces the pinching of the meniscus and the formation of the Taylor cone.³³ When the electric field is greater than E_{onset} , electrostatic forces override surface tension forces, and charged droplets are emitted at the tip of the Taylor cone. Furthermore, as shown in Figure 2-3, an ESI source can be viewed as an electrochemical cell. When operating in the positive ion mode, an oxidation process can occur at the capillary while reduction occurs at the counter electrode.

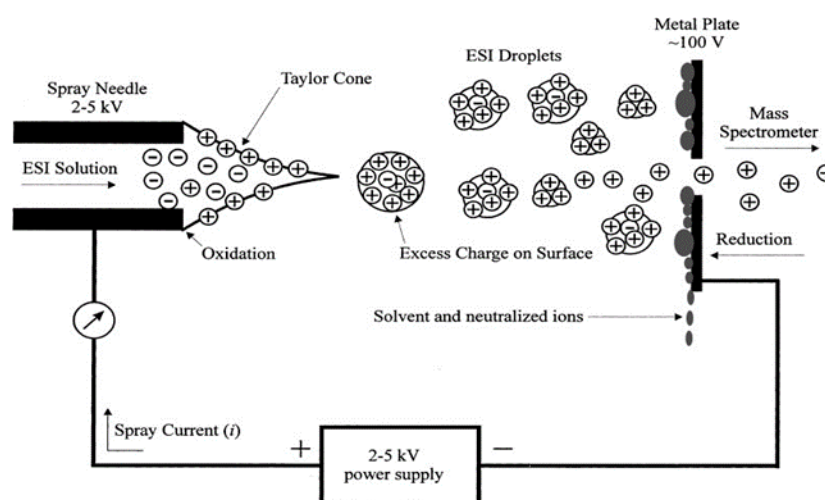


Figure 2-3: The electro spray ionization (ESI) process.³⁴⁻³⁷

After emission, the charged droplets travel from the capillary outlet to the mass spectrometer inlet. The temperature of the ion source (close to the boiling temperature of the solvent used), a hot desolvation gas⁸ (in our case, N_2), and the pressure difference between the ion source and the mass spectrometer induce the evaporation of the solvent in the droplets. Their radius decreases while the number of charges on their surface remains constant. Therefore, the Coulomb repulsion between the charges increases as the density of surface charges increases. When the Coulomb repulsion is greater than the droplet's surface tension,

the Rayleigh limit is reached (Equation 2-1).³⁴⁻³⁶ Droplet fission occurs at this Rayleigh limit (the droplet explodes into several smaller droplets).^{32,37} Each of these smaller droplets undergoes further cycles of evaporation and droplet fission, creating desolvated analyte ions. This phenomenon is referred to Coulomb explosion.

$$Z_{\text{Rayleigh}} \times e = 8\pi r_{\text{max}}^{3/2} \sqrt{\gamma \epsilon_0} \quad \text{Equation 2-1}$$

with Z_{Rayleigh} the charge number, e the elementary charge, r the droplet radius, γ the surface tension, and ϵ_0 the electric permittivity of the surrounding medium.

Figure 2-4 shows the three widely recognized processes for the ultimate step, which leads to the formation of ions, although they are not fully understood and explained.

The ejection of small molecular ion from the droplet is well described by the “ion evaporation model” or “ion ejection model” (IEM) proposed by Iribarne and Thomson.^{37,38} A small “Taylor cone” that can function as an emitter of gas-phase ions appears on the droplet’s surface when a large electric field is applied in the ion source due to the density of charges on the droplet surface. According to the authors, this process is thermodynamically preferable to a series of Coulomb explosions. The second model, known as the “charged-residue model” (CRM), was developed by Dole et al.^{27,37}, and explained how large and folded molecules are ionized. Droplets containing only a single solvated ion are created by repeated Coulomb explosions. As a result, the gas-phase ions are ultimately produced by the evaporation of the last solvent molecules from the droplet.

The two described processes can coexist. The nature of the molecules presents in the sample studied influences the dominance of one process over the other. Unlike CRM, which is better suited to describe the formation of multiply charged species by ESI in the study of large molecules such as proteins, the IEM model is better suited to explain the formation of mono-charged ions of low m/z ratio.³⁹

The last model is known as the “chain ejection model” (CEM). This model describes the ejection of an unfolded ionized protein or polymer from the droplet.

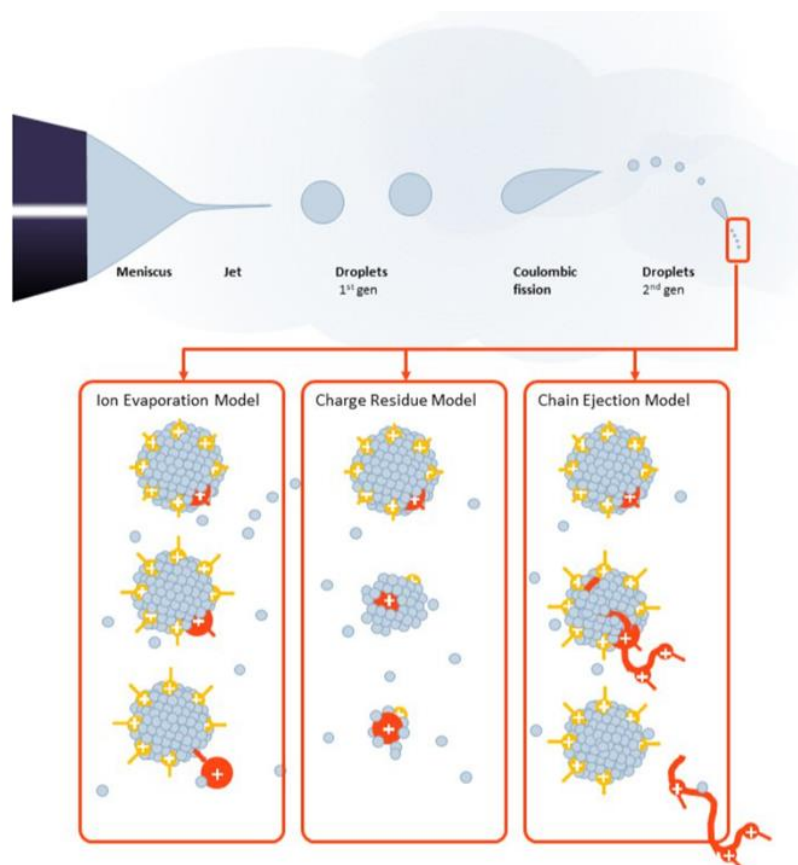


Figure 2-4: Ion ejection model (IEM), charge residue model (CRM), and chain ejection model are shown schematically as part of the ESI ionization process (CEM).⁴⁰

2.4.1.3. Relevant ESI parameters

A wide range of compounds, including low molecular weight compounds as bio-oils components,^{41,42} polymers,⁴³ proteins,⁴⁴ and DNA/RNA⁴⁵ have been investigated by ESI-MS.

As previously mentioned, the pH of the solution is one of the most critical parameters to control. The protonation of basic compounds is favored by a low pH and leads to $[M+H]^+$ cations, while the deprotonation of acidic functional groups occurs in alkaline media and produces $[M-H]^-$ anions. An acid or alkaline solution is classically added to promote these processes to increase the ionization efficiency and, thus, sensitivity. Alternatively, specific dopants such as sodium acetate or ammonium chloride ensure cationization and anionization of the M analyte to form $[M+Na]^+$ or $[M+Cl]^-$ adduct ions, respectively (Chapter 1 section 1.5.2.2). For example, a strong ionic bond is formed for example between an oxygen atom and a cation like sodium or potassium ion through acid/base Lewis reaction. Nevertheless, using some ionic dopant may be responsible of some issues such as the formation of cluster ions in the gas phase or some crystalline at the capillary outlet. Therefore, the concentration of the dopant must be minimal to prevent crystallite formation in the source and cluster ions in the gas phase. Indeed, signal suppression events are frequently observed by the addition of a too-large amount of salt.^{31,46}

Solvent properties are another critical parameter of ESI. Protic solvents are known to favor protonation events. The polarity of the solvent also has an impact on the conformation of the molecule.^{31,44} In the case of macromolecules, solvents that promote their unfolding ensure the increase of accessible ionization sites, resulting in broader charge distribution and higher charge states. The shape of the Taylor cone, and the efficiency of droplet formation depend on the solvent's viscosity and the solvent molecules' ability to form intermolecular bonds. The viscosity of the solvent affects both the flow of the solution and the nature of the ions produced. Charles et al. demonstrated an increase in the size of potassium bromate salt clusters, but not their charge, with increasing solvent viscosity.⁴⁷ In addition, the hydrogen bonds of polar liquids make the droplets more cohesive, which may make the ion generation process less favorable.⁴⁸

The flow rate also influences the ionization efficiency. High flow rates produce larger droplets and lower charge density at their surface, which limits sensitivity. Sensitivity will improve as the flow rate is reduced.⁴⁹

2.4.1.4. ESI configurations

Different ESI source designs have been proposed to improve the efficiency of ion transfer to the mass spectrometer or increase its robustness. They all include a counter-electrode and a metal capillary to produce an intense electric field via a high-voltage supply (Figure 2-5). They also use a heated source and a desolvation (hot) gas at atmospheric pressure to favor ionization. The spray develops in the first pumping stage after passing through a sample cone or a capillary. The ions are then directed to the analyzer while guided through a final skimmer or a lens at a reduced-pressure.

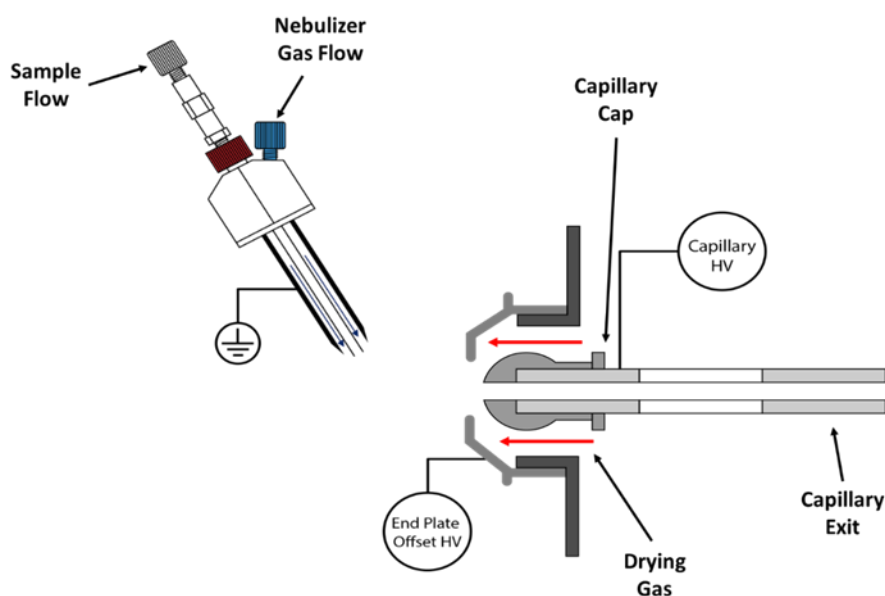


Figure 2-5 : Bruker Solarix ESI source configuration. Adapted from Bruker's FTMS Library.

2.4.2. Nano Electrospray

A version of ESI, known as nano-electrospray ionization (nESI), is performed at very low flow rates (i.e., $\text{nL}\cdot\text{min}^{-1}$). Because the exit orifice of the electrospray capillary tip is much smaller in diameter than the ESI aperture used, the initial droplet size is much smaller (Figure 2-6). These smaller droplets have better ionization efficiency compared to ESI allowing for more sensitive analytical measurements.^{50,51} Because of the lower flow rates, and smaller droplet sizes, lower source temperatures can be used, which is advantageous in some experiments like native protein analysis (to avoid decomposition or unfolding of the analytes of interest). Compared to ESI, the nESI technique is also accomplished at a significantly lower voltage range (e.g., 0.5 - 1.5 kV).⁵² In addition, the nESI allows for a reduction in the consumption of sample solutions. This is advantageous when 2D FTMS experiments are conducted as long infusion times (tens of minutes to some hours) are required.

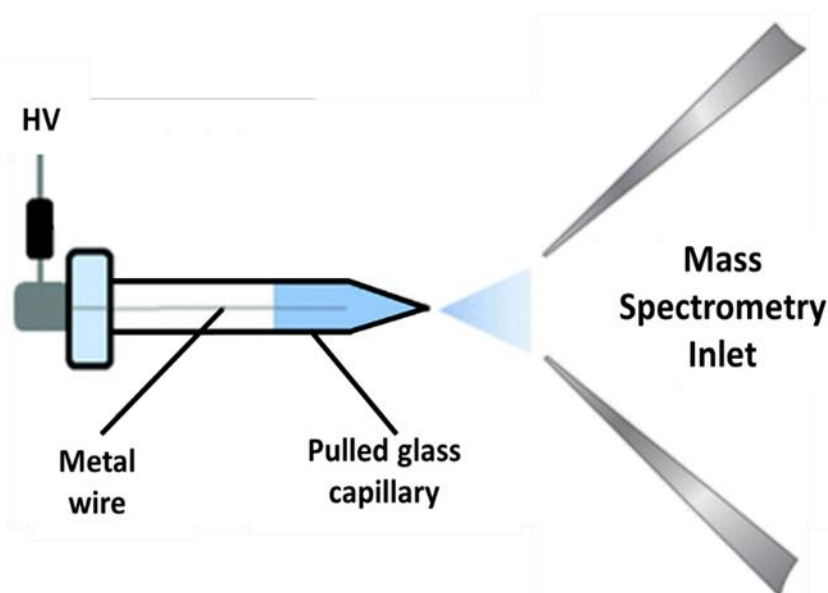


Figure 2-6 : An illustration of a nESI setup design.⁵²

2.4.2.1. Principle

Using a micromanipulator, the nanoESI capillary is positioned at a distance of roughly 1 mm from the counter electrode. To avoid tip crashing or electric discharges during operation, precise ocular control is required during placement. The applied spray voltage ranges from 0.7 to 1.2 kV. To improve the capillary conductivity, gold or another conductive material is sputtered onto the outside of the spray capillaries. Alternatively, wider capillaries with a small metal wire within are also employed (Figure 2-7). When the high voltage is applied, the only force driving the flow of the liquid sample is the capillary force. A moderate gas flow can assist liquid flow. Moreover, a wide range of specialized tips known as nano-electrospray emitters has been proposed.⁵³

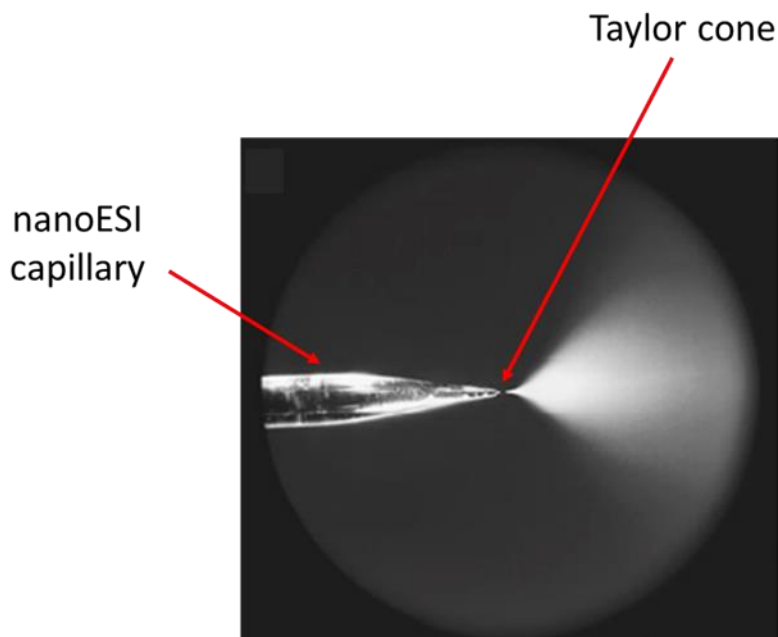


Figure 2-7: Microscopic picture of the nanoESI capillary spray.⁵³

2.4.2.2. Conclusion

ESI is a soft ionization method that restricts the ion fragmentation phenomena, which can be employed for a large variety of applications. The optimization of ESI requires considering many factors. Even though some gas phase phenomena occur, the ionization of the analyte is mainly driven by liquid phase behavior. The moderately polar to ionic compounds with mass ranging from a few tens of Da to MDa are hence the main compounds investigated by ESI.

ESI and nanoESI FT-ICR MS analytical techniques in positive and negative ion detection modes have already been developed to characterize bio-oils.⁵⁴⁻⁵⁶ The work presented in this thesis will show the contribution of ESI in the characterization of different functional groups present in the compounds of a crude bio-oil produced by the pyrolysis of oak.

However, ESI can only partially ionize, if at all, components of pyrolysis bio-oils. Other ionization sources must be used to obtain a complete description of the bio-oil composition. Indeed, atmospheric pressure photoionization (APPI) and atmospheric pressure chemical ionization (APCI) are better suited for analyzing aromatic compounds as well as hydrocarbons because they are less sensitive to analyte polarity.

2.4.3. Atmospheric pressure photoionization APPI

2.4.3.1. Introduction

Atmospheric pressure photoionization (APPI), first used in 2000,⁵⁷ is one of the more recent ionization techniques. The ionization of the analyte occurs in the gas phase and requires the absorption of VUV photons. As a result, a nebulizing probe has to be connected to the VUV light source.

2.4.3.2. APPI principle

Argon, Krypton, or Xenon discharge lamps (Figure 2-9) are frequently used to produce VUV photons. Alternatively, VUV photons from a synchrotron light source can be employed as an alternative to discharge lamps.⁵⁸ The Krypton light is the most popular. A Kr lamp emits photons with an energy of 10.0 and 10.6 eV, lower than the ionization energies of some of the most often used solvents and the primary atmospheric constituents (N₂, O₂, and H₂O). The molecules absorbing at the photon wavelengths, with ionization energy lower than 10 eV can be directly photoionized by the Krypton lamp photon in the gas phase.⁵⁹

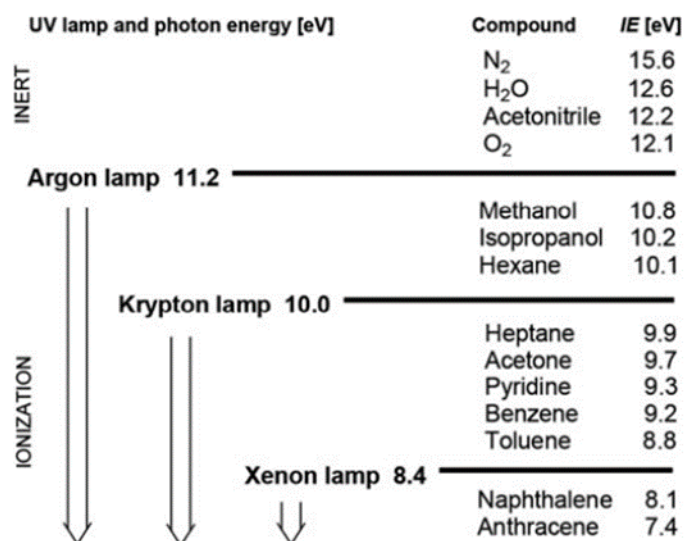


Figure 2-8: Relationship between the ionization energies of common chemicals and the photon energy of UV lamps used for APPI.^{48,58}

The molecules must first undergo nebulization as photoionization process occurs in the gas phase (Figure 2-8). When a molecule containing a UV, chromophore absorbs a photon in the gas phase, distinct reactions are triggered for the molecule of analyte (AB).

- **Photoexcitation:**



Due to the short lifetime of the activated AB^ , it deexcites by several mechanisms.*

- **Photodissociation (non-radiative decay):**



If the photon energy is greater than the AB bound's dissociation energy.

- **Radiative decay:**

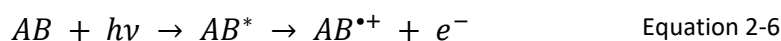


- **Collisional quenching with neutrals (N):**



N is a molecule of analyte, solvent or air

- **Photoionization of the analyte** by ejection of an electron:



However, the photoionization of analyte molecules is neither energetically nor statistically preferred. Moreover, even if $AB^{\bullet+}$ ions are formed, they can be neutralized by recombining with free low energy electrons present in the gas phase (**Recombination**), which makes them disappear:

- **Recombination:**



- **Moderate recombination:**



N is a buffer species that absorbs the extra energy produced by this exothermic process.

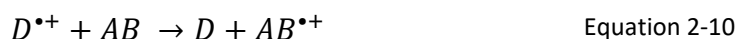
Due to its low concentration, small photoionization cross-section, and low photon density direct photoionization of the analyte AB is nearly ineffective. A UV-absorbing dopant (D) is added to the solution to increase ionization efficiency. A suitable dopant must have ionization energy less than the photon energy and be a good absorber at the wavelength used. Additionally, the corresponding radical cation $D^{\bullet+}$ has to have a low proton affinity and high recombination energy. In this case, ionization may occur by charge transfer from the molecular dopant ion to the AB analyte.

The following processes are involved:

- **Photoionization:**

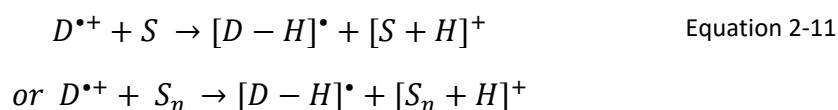


- **Charge transfer:**



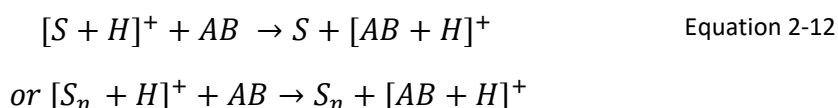
To ensure the formation of a protonated analyte ion, the dopant ions can also cause the creation of solvent reagent ions.

- **Reactant ion formation:**



The AB analyte molecule can be protonated by reaction with $[S+H]^+$ or $[S_n+H]^+$ ions.

- **Proton transfer:**



Direct ionization of a methanol molecule by a krypton lamp is inefficient but adding some acetone as a dopant will make it possible. Toluene, acetone, and aniline are the three most often utilized dopants.^{57,60–63} For instance, one photon from the Krypton lamp ionizes toluene to generate the molecular ion $C_7H_8^{*+}$. A proton may be transferred from this radical cation to a solvent molecule. Methanol and water cannot receive protons from $C_7H_8^{*+}$ because their proton affinities are lower than those of the $C_7H_7^*$ benzyl radical. Consequently, they are not ionized. However, methanol and water clusters have a stronger affinity for protons, which permits the previously mentioned processes.⁶⁴

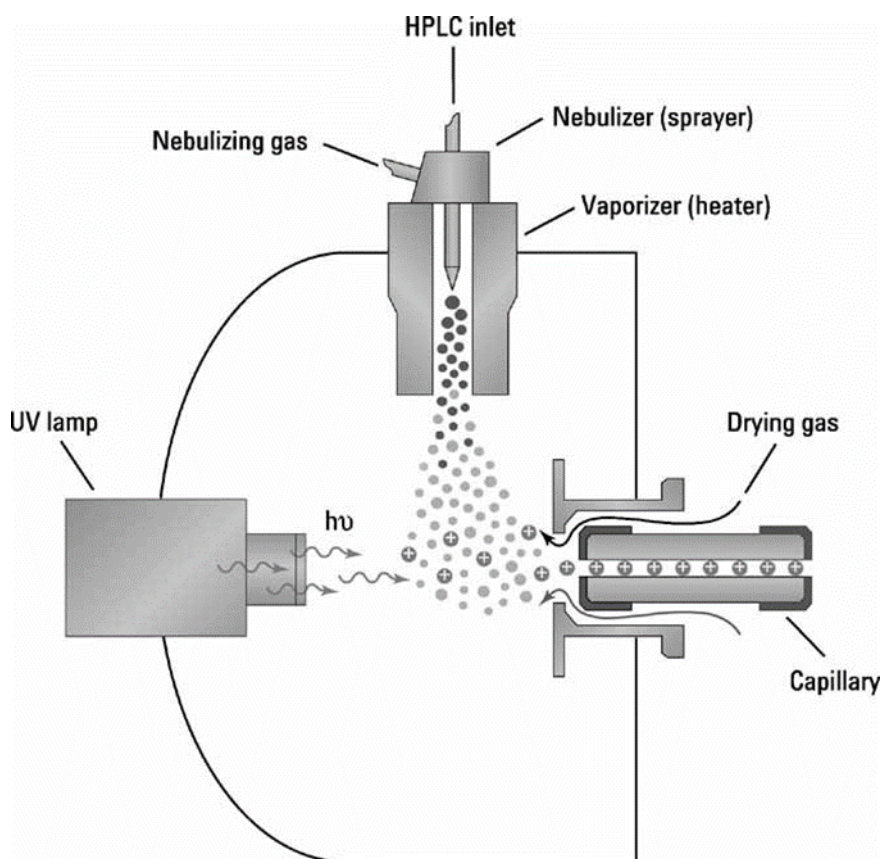


Figure 2-9 : Diagram of a UV APPI source.⁵⁸

2.4.3.3. APPI parameters

The experimental and instrumental parameters used in APPI experiments significantly impact the produced ions and, ultimately, the obtained mass spectrum. In studying a complex mixture, it might be challenging to predict which process (protonation or formation of radical molecular ion) will predominate. Similarly, it can be difficult to predict whether deprotonation or radical anion formation will be observed in negative-ion mode. Generally speaking, molecules with a high proton affinities (PA) tend to generate $[M+H]^+$ ions, whereas nonpolar analytes, especially those with low ionization energies (IE), prefer to create M^{*+} ions.^{60–62} The

acidic compounds readily produce $[M-H]^-$ ions in negative ion mode, whereas high electron affinity (EA) molecules lead to electron capture to produce $M^{\bullet-}$ ions. However, APPI tends to generate both $M^{+\bullet}$ and $[M+H]^+$ (or $M^{\bullet-}$ and $[M-H]^-$) ions, the ratio of which is greatly determined by the dopant.^{63–66,67}

2.4.3.4. APPI configuration

In the experiments reported in this manuscript, APPI was used to investigate raw and fractionated/derivatized bio-oils by APPI 7 T Solarix Bruker FT-ICR MS 2 ω . When heated to 180°C, the Bruker Daltonics APPI source enables the sample vaporization, assisted by a nebulization system that uses N₂ as drying gas. The molecules interact in the gas phase with the photons from the Krypton lamp in the region between the outlet of the infusion pipe and the inlet of the mass spectrometer (Figure 2-10).

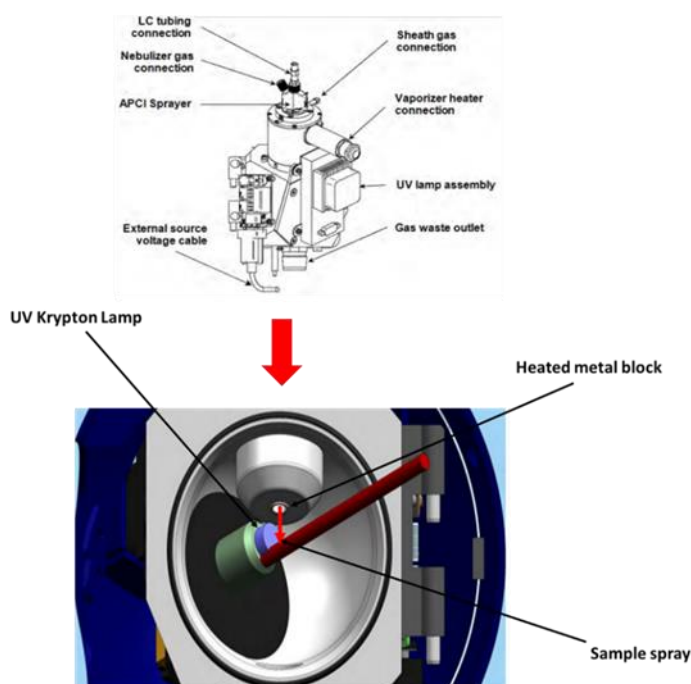


Figure 2-10: (Top) APPI II source components (source housing removed), (Bottom) Interior part of the source. Adapted from Bruker's FTMS Library.

2.4.4. Atmospheric pressure chemical ionization APCI

2.4.4.1. Introduction

In the 1970s, Horning, Carroll, and colleagues at Baylor College of Medicine in Houston, Texas, demonstrated the advantages of coupling liquid and gas chromatography with APCI mass spectrometry.^{68,69} In 1971, the Franklin GNO Corporation commercialized the first equipment incorporating APCI coupled with ion mobility and mass spectrometry.⁷⁰ This apparatus was initially used to analyze trace chemicals and demonstrated high sensitivity. In addition, the mass

spectra obtained were relatively simple with low fragmentation.⁶⁹ In these experiments, the LC eluate was heated to evaporate the sample molecules before ionization. Initially, ionization was performed by electrons from the decay of ^{63}Ni source. Using a radioactive ^{63}Ni source makes it unsuitable for laboratory use because it must be occasionally cleaned with abrasives, which invariably results in radioactive contamination. Thus, in 1975, the Horning group improved APCI source by replacing the ^{63}Ni with a corona discharge.^{71,72} Nowadays, APCI with the corona discharge electrode is the most employed. The corona discharge occurring between the corona tip and the walls of the nebulization chamber, which acts as the counter electrode, ensures the production of electrons. These electrons interact at the atmospheric pressure with the atmospheric gases and solvent to form reagent ions able to ionize the analyte molecules (Figure 2-11). This improved ionization is known as "Atmospheric pressure photoionization (APCI)." In theory, APCI is a variant of "traditional" vacuum chemical ionization. In contrast to conventional chemical ionization (CI), the generation of analyte ions in APCI is done by ion-molecule reactions at atmospheric pressure.

Proton transfer, adduct creation, or charge exchange processes can produce positive ions. On the other hand, proton abstraction, anion attachment, or electron-capture reactions result in the production of negative ions.⁷³

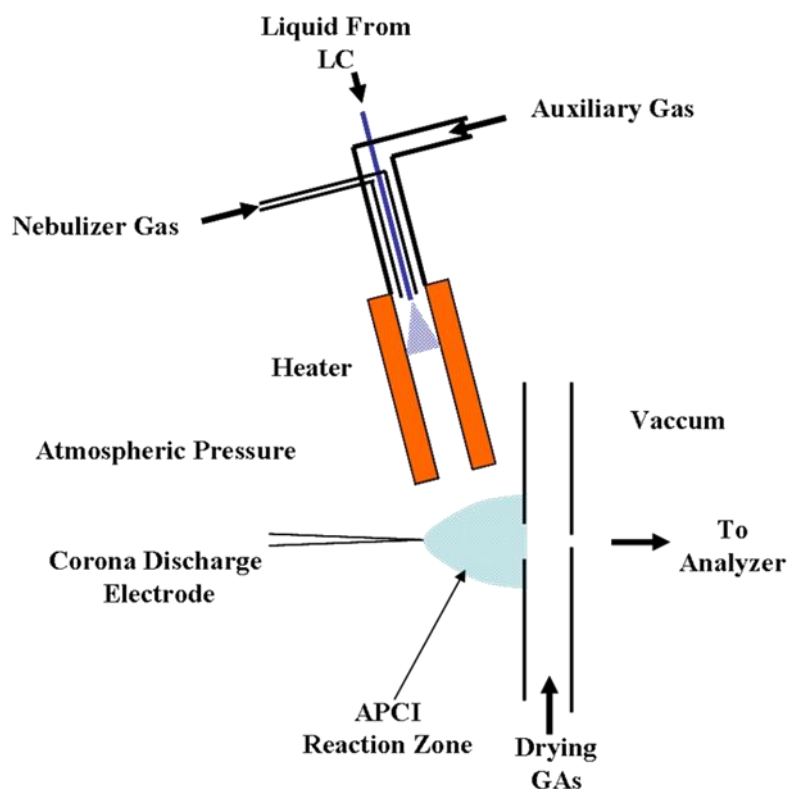
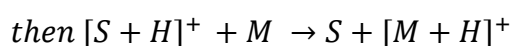
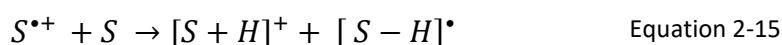


Figure 2-11: APCI source diagram.⁷⁴

2.4.4.2. APCI principle

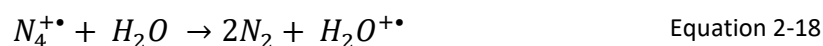
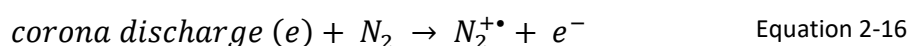
Like ESI and APPI ionization, APCI uses an atmosphere-to-vacuum interface to deliver ions into the mass spectrometer. Modern APCI sources work with a liquid flow rate of 5 to 20 $\mu\text{l}\cdot\text{min}^{-1}$. Typical corona discharge currents are on the order of 10 μA .

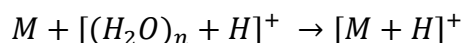
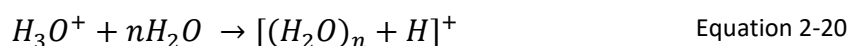
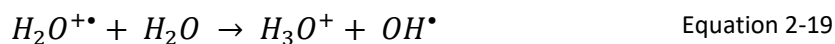
The sample solution is vaporized as the sprayed droplets pass through a heating device. The gas phase analyte molecules are then desolvated before being ionized by species produced by the corona discharge plasma. The electrons produced by the corona discharge ionize the solvent (S) as well as the atmospheric gases to create reactive ions (Equation 2-13), which then ionize the analyte (M) through charge exchange (Equation 2-14) or proton transfer (Equation 2-15):



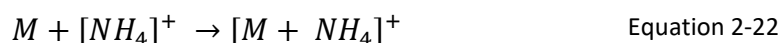
2.4.4.2.1. Processes involving atmospheric gases

For corona discharge current ranging from 1 to 5 μA , atmospheric N_2 are excited and ionized to yield $\text{N}_4^{\bullet\bullet+}$. This ion react with water (atmospheric water or those present in the sample solution) to ultimately generate water cluster ions $\text{H}^+(\text{H}_2\text{O})_n$ (Equations 2-16 to 2-20). The analyte molecules M are then protonated by these water cluster ions (Equation 2-21). An alternative process may be the formation of a $\text{MH}^+(\text{H}_2\text{O})_m$ species. The $\text{MH}^+(\text{H}_2\text{O})_m$ declustering (removal of water molecules) occurs in the high vacuum region of the mass analyzer. The ions that MS detects in analyte molecules are $[\text{M}+\text{H}]^+$ ions.⁷⁵⁻⁷⁷





The $[(H_2O)_n + H]^+$ cluster ion distribution is strongly influenced by the residence time and water content in the environment of the reaction area.⁷⁶ Thus, there can be significant fluctuation in the relative impact of the $[(H_2O)_n + H]^+$ cluster ions on the analyte ion production process. If the used solvent (or its clusters) presents a higher proton affinity than water cluster, proton-transfer processes occur. The APCI of moderately polar substances often leads to ammonium adducts. $[M+NH_4]^+$ ions are observed, for example in the study of oxygen-rich compounds, especially in the absence of basic functional groups:



Ammonium ions can be supplied by the sample solution or originate from smaller amounts of ammonia in the surrounding environment.

2.4.4.3. APCI parameters

Because the solvent, nebulizing gas, and environment contribute to the composition of the plasma generated by the corona discharge, its composition can vary significantly during experiments. Compared to other ionization techniques, APCI has low reproducibility.

The fact that the heating device typically operates at about some hundred °C may give the impression that APCI is a hard ionization technique. However, the exact opposite is true. APCI is even gentler than "traditional" CI. This apparent softness of APCI has several advantages⁷⁸:

- While evaporation is in progress, the aerosol droplets' temperature remains at the solvent's boiling point. As a result, the temperature ranges between 70 and 100°C and only increases to about 150–200°C at exit of the heating device, which slows down the thermal decomposition of the analyte considerably.

- At atmospheric pressure, 10^6 ion-neutral collisions per millisecond ensure that all of the excess energy of produced analyte ions is efficiently dispersed into the surrounding gas.⁷⁶
- Low internal energy decomposition rates are far too slow to allow significant fragmentation in the few milliseconds between nebulization and passage through the interface.

The use of a non-polar solvent is generally an attractive advantage of APCI. Because APCI ionization is governed by gas-phase chemistry, there is no need for special conditions such as polar solvents, high solution conductivity, or specific pH, as required by ESI. APCI spectra, like APPI spectra, often reveal only the ions of the intact molecule.⁵⁷

2.4.4.4. APCI configuration

In the experiments reported in this manuscript, APCI was used to investigate raw and fractionated/derivatized bio-oils by APPI 7 T Solarix Bruker FT-ICR MS 2w. APCI is complement or alternative to APPI source. A corona discharge-powered plasma replaces the UV light source, while the heating device remains the same (Figure 2-12). In addition to the corona needle, using a quartz tube in the APPI to direct the heated vapor to the sample aperture is the essential difference between APCI and APPI.

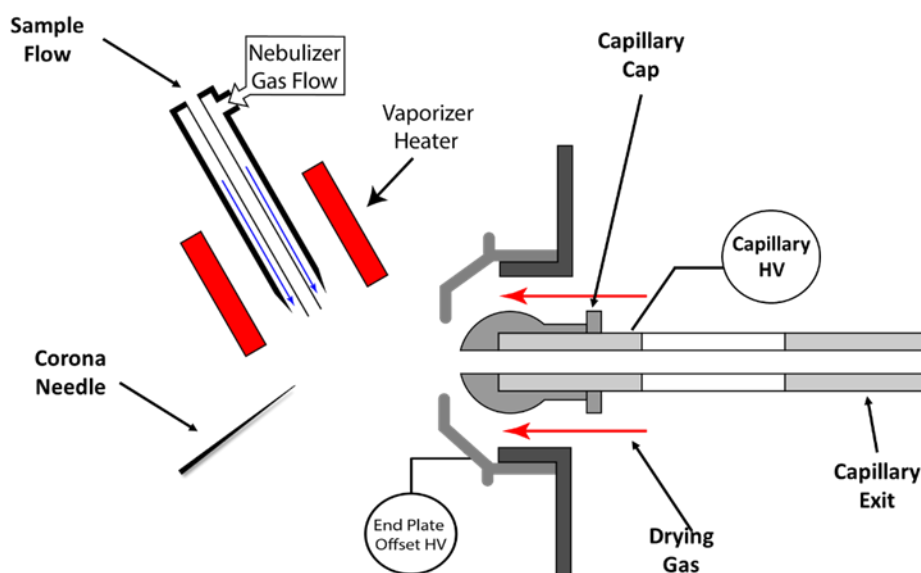


Figure 2-12: Bruker Solarix APCI source configuration. Adapted from Bruker's FTMS Library.

2.4.5. Conclusion

APCI produces ions from neutrals in the gas phase, which gives it a significant advantage over ESI. As a result, APCI allows mass spectrometry to study analytes of low to medium polarity. In the mid-1990s, the use APCI expanded dramatically, likely due to the increased availability of atmospheric-vacuum interfaces with the development of ESI technology. Nowadays, APCI mass spectrometry is used in coupling with LC separation or in direct infusion for analyzing very complex mixtures.

2.5. Mass analyzer

Once the sample molecule has been ionized, the mass spectrometer can analyze and detect them. Applying electric potentials to ion optics causes ions to be transported from the source region via multiple stages of differential pumping to the mass analyzer for their detection and m/z measurement. The mass spectrometer used in this work was a Fourier transform ion cyclotron resonance mass spectrometer.

2.5.1. Fourier Transform Ion Cyclotron Resonance Mass spectrometry

2.5.1.1. Introduction

In 1932, Ernest O. Lawrence used a transverse oscillating electric field orthogonal to a uniform magnetic field to create a particle accelerator, which marked the beginning of the work that led to today's Fourier transform ion cyclotron resonance (FT-ICR) mass spectrometers.^{79,80} This specific accelerator uses cyclotron motion, a circular motion adopted by the ions around the axis of the magnetic field. It has been shown that in ion cyclotron resonance (ICR), the radius of the circular motion of the ions does not affect the angular frequency of the motion. This led to the development of the first ICR mass spectrometers.^{81,82} The use of the Fourier transform by Marshall and Camisarow in 1974 marked the beginning and the significant development of FT-ICR.^{83,84} Since then, the performance of FT-ICR equipment has steadily increased thanks the increase in the strength of the magnetic fields used and the development of electronics, to reaching previously unprecedented levels of resolving power and mass accuracy. These are just a few of the many advantages of FT-ICR, which has been widely used for the study of complex mixtures.⁸⁵⁻⁸⁸ After more than 40 years of development, FT-ICR-MS can now achieve resolving powers of up to 12 million at m/z 400, with a mass accuracy close to 10 ppb, and two 21-Tesla superconducting magnet instrument has been recently built to achieve ultrahigh resolving power with low measurement time and excellent sensitivity.⁸⁹⁻⁹³

2.5.1.2. Cyclotron motion

In an ICR cell, which is immersed in a magnetic field of a permanent superconducting magnet, the ions are trapped in the three directions of space by the joint application of an

electromagnetic field. Ions within the ICR cell experience a force, namely the “Lorentz force”, which is perpendicular to both the magnetic field and the ion’s velocity direction.

$$F = qE + q(v \times B) \quad \text{Equation 2-23}$$

where F is the Lorentz force, q is the charge of the ion, E is the electric field applied, v is the ion’s velocity, and B is the strength of the magnetic field of the magnet. Indeed, due to the Lorentz force, an ion moving at a velocity v and encountering a uniform magnetic field B perpendicular to its direction adopts a circular motion (Figure 2-13).

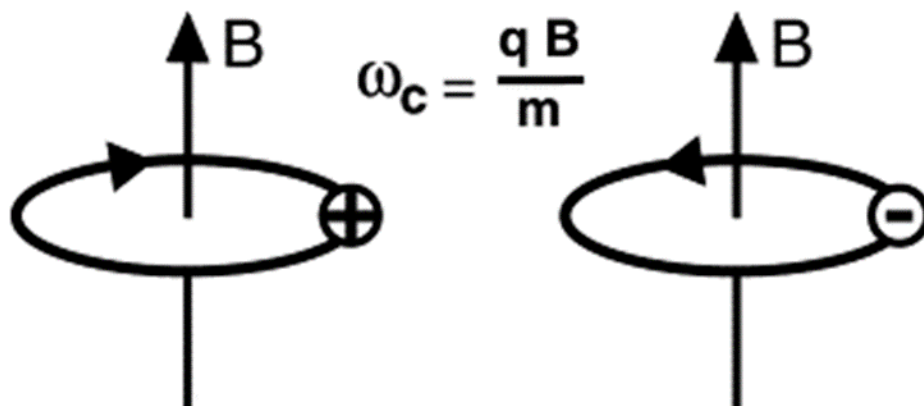


Figure 2-13: Ions moving in a circle in a magnetic field. Positive ions move in a counterclockwise manner when seen along the magnetic field's direction (left), whereas negative ions move in a clockwise direction (right).⁹⁴

Positive and negative ions both move clockwise and counter clockwise, respectively, when considering the direction of the magnetic field. The following equations can be used to calculate the resulting radius, pulsation, and frequency of this "cyclotron motion":

The *radius* r_m of the ions’ circular motion is determined by:

$$r_m = \frac{v}{\omega_c} = \frac{m_i v}{qB} \quad \text{Equation 2-24}$$

The *cyclotron angular frequency* ω_c is derived as a consequence of replacing the velocity v by $r_m \omega_c$:

$$\omega_c = \frac{qB}{m_i} \quad \text{Equation 2-25}$$

and by substituting with the cyclotron frequency, it is obtained:

$$f_c = \frac{\omega_c}{2\pi} = \frac{qB}{2\pi m_i} \quad \text{Equation 2-26}$$

where ω_c is the cyclotron pulsation, m_i is the mass of the ion, and f_c is the cyclotron frequency.

The cyclotron frequency is independent of the initial velocity of the ion but proportional to the magnetic field, the charge of the ion and inversely proportional to its mass (Equation 2-24). According to Equation 2-25, the cyclotron frequency of the ion, and thus its kinetic energy, are independent of each other. Therefore, the kinetic energy dispersion of ions with the same m/z ratio does not alter the mass resolution by broadening the observed peak in the mass spectra, unlike other approaches that are dependent on kinetic energy, such as time of flight mass spectrometers.

An ion with a given m/z value has a constant cyclotron frequency and, therefore, its velocity, or the square root of its kinetic energy, is precisely proportional to the radius of its cyclotron orbit. The following equations illustrate this phenomenon:

$$r = \frac{v}{\omega_c} \quad \text{Equation 2-27}$$

$$v = \sqrt{\frac{2E_k}{m}} \quad \text{Equation 2-28}$$

where r is the radius of the cyclotron orbit, and E_k is the kinetic energy of the ion.

Thus, as shown in Figure 2-14, the magnetic field has an impact on the radius of the ion's orbit. For an ion with a given m/z ratio, the higher the magnetic field, the smaller the radius of the ion's orbit.⁹⁵

With an arbitrary orbital radius of 1 cm and a magnetic field of 7 T, an ion at m/z 500 ion moves with a velocity of $1.40 \times 10^4 \text{ m}\cdot\text{s}^{-1}$ and a kinetic energy of 620 eV. Figure 2-15 illustrates the relationship between the kinetic energy and its orbital radius. This kinetic energy, also called translational energy, can cause the ion to fragment if it collides with gas, and converts part of its external energy (E_k) into internal energy.

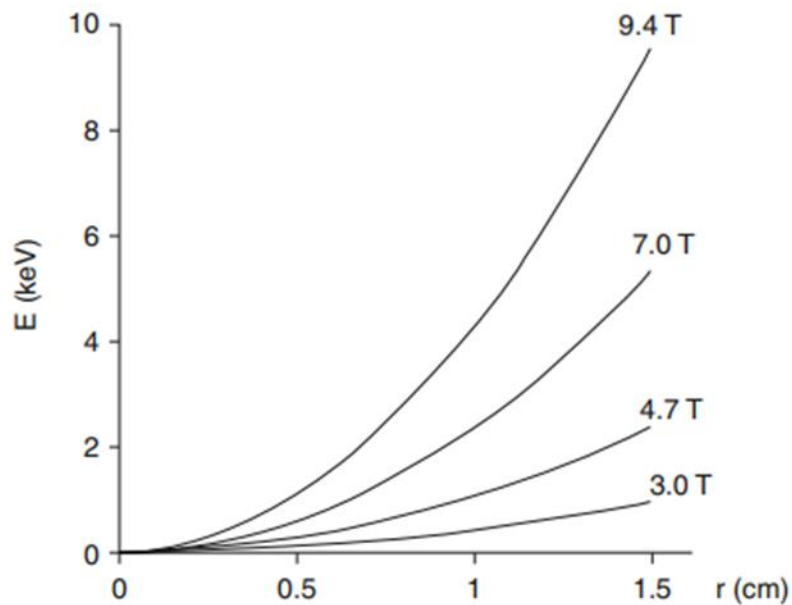


Figure 2-14: Correlation between the mass-to-charge ratio m/z and the ion orbital radius r for different magnetic field.⁷⁹

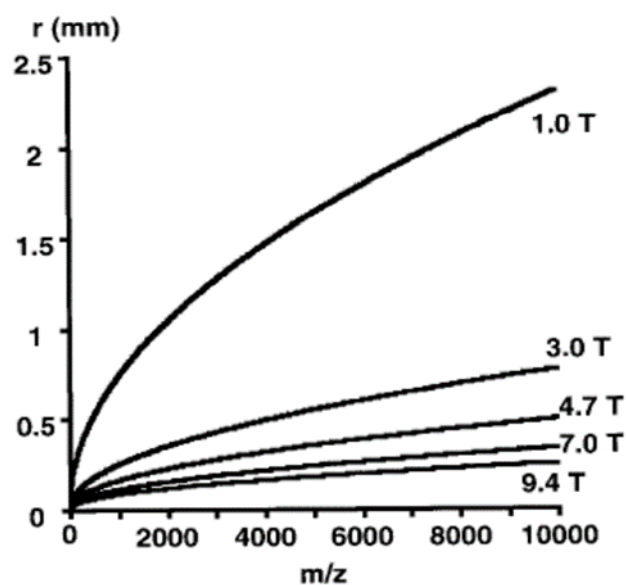


Figure 2-15: Kinetic energy of a $m/z100$ ion in respect with the magnetic field and its orbital radius in an ICR cell.⁹⁵

This allows collision-induced dissociation (CID) experiments to obtain structural information. However, it must be avoided to obtain a mass spectrum free of ion dissociation.

The measurements must be performed under extremely high vacuum, often in the pressure range of 1.33×10^{-8} – 1.33×10^{-9} Pa.

2.5.1.3. Trapping motion basics

The ions are affected by the magnetic field, which limits their motion in the xy plane (perpendicular to the direction of the magnetic field), but not along the magnetic field axis (z axis). Two trapping electrodes (which act perpendicular to the z axis) are placed at the beginning and end of the ICR cell to confine the ions along this axis and thus within the ICR cell (Figure 2-16). These electrodes form a potential well that confines the ions at the center of the ICR cell. This potential well is created by applying a small voltage to these electrodes with the same polarity as the trapped ions.

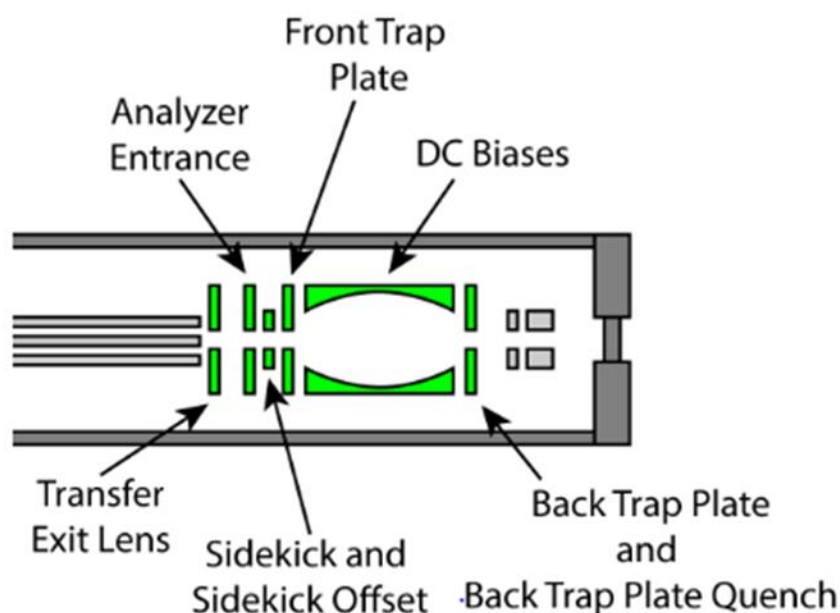


Figure 2-16: Schematic diagram of part of the FTICR mass spectrometry. Ions are contained in an ICR cell, where they are trapped under a magnetic and radio frequency electrostatic field. Adapted from Bruker FTMS Library.

The applied trapping voltage must be greater than the z-component of the kinetic energy of the ion to trap them inside the ICR cell. When confined in the ICR cell, the ions oscillate back and forth along the magnetic field axis. After detection, the ions can be expelled from the cell by lowering the potential applied to either of the trapping plates.

Equation 2-28 gives the frequency of the oscillating motion along the z-axis.⁹⁵

$$f_{trap} = \frac{1}{2\pi} \sqrt{\frac{2 q V_{trap} \alpha}{m a^2}} \quad \text{Equation 2-29}$$

where f_{trap} is the oscillating frequency along the z axis, V_{trap} is the trapping potential, α is the trapping geometry value, and a is the distance between the trapping electrodes.

2.5.1.4. Magnetron motion basics

In addition to the cyclotron motion and the trapping oscillation, the trapped ions undergo a third motion, called magnetron motion.⁸⁹ In addition to the Lorentz force F_L , the curved lines off the electric field near to the trapping plates generate a radially outward force $F_r = qE_{(r)}$ (Equation 2-29)

$$F_r = q E_{(r)} = \frac{q V_{trap} \alpha}{a^2} r \quad \text{Equation 2-30}$$

The magnetic field now affects the trapped ions by converting another circular motion of the radial force component. Thus, the total force acting on an ion is

$$F_{tot} = F_L + F_r = m_i \omega^2 r = qB\omega r - \frac{qV_{trap}\alpha}{a^2} r \quad \text{Equation 2-31}$$

This, when rearranged, shows that it is a quadratic equation in ω

$$\omega^2 - \frac{qB\omega}{m_i} + \frac{qV_{trap}\alpha}{a^2} = 0 \quad \text{Equation 2-32}$$

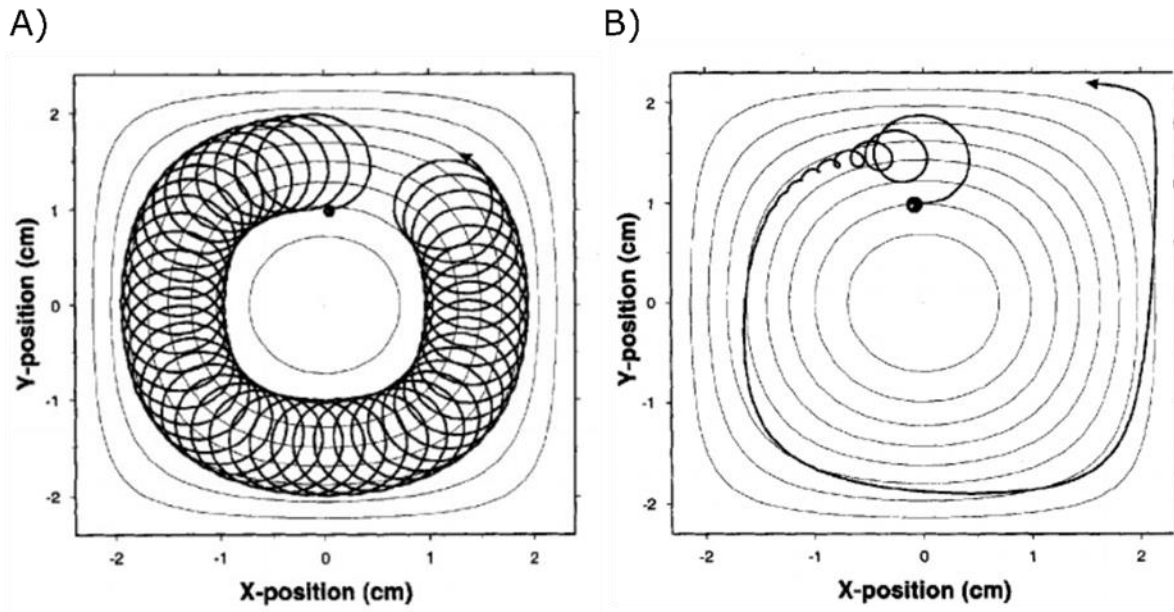


Figure 2-17: Diagram showing the motion of a magnetron and cyclotron within an ICR cell in the absence (A) and presence (B) of collision gas.⁸⁹

This quadratic equation has two solutions, the first representing the reduced cyclotron pulsation ω_+

$$\omega_+ = \frac{\omega_c}{2} + \sqrt{\left(\frac{\omega_c}{2}\right)^2 - \frac{\omega_{trap}^2}{2}} \quad \text{Equation 2-33}$$

where ω_c and ω_{trap} are the cyclotron and the trapping pulsation, respectively.

and the second solution is the magnetron pulsation ω_-

$$\omega_- = \frac{\omega_c}{2} - \sqrt{\left(\frac{\omega_c}{2}\right)^2 - \frac{\omega_{trap}^2}{2}} \quad \text{Equation 2-34}$$

In conclusion, the precession of an ion along the electrostatic field is at the origin of the magnetron motion. In most applications, it is not of crucial importance. It is, however, the cause of the minor and vicinal peaks located either side $\omega_+ \pm k \omega$ of the main peak at ω_+ ,⁹⁵ which may complicate the data treatment of mass spectrum of complex mixtures.

2.5.1.5. Overall motion

The motion of an ion in the ICR cell is the superposition of the three motions mentioned above (cyclotron ω_+ , trapping ω_{trap} , and magnetron motion ω_-). Figure 2-18 shows the overall motion of an ion in an ICR cell.

2.5.1.6. Ion excitation in an ICR cell

Initially, ions of a given m/z ratio orbit randomly at their thermal velocities as a function of their reduced cyclotron frequency f_+ . Their orbital radius is small and close to the ICR cell's center. Moreover, they are out of phase. The radius of the circular motion of these ions must be increased and converted into a coherent motion in the xy direction to be observed on the detection plates. (Figures 2-18 and 2-19). An RF pulse is applied on the excitation plate, the frequencies of which correspond to the reduced frequencies of the trapped ions. The ions resonate with this RF pulse and their kinetic energy increases causing the radius increase of their circular motion (Figure 2-19). This excitation also transforms the incoherent motion of the ion in the xy direction into a coherent motion. Thus, the excitation of the ions within an ICR cell leads to two phenomena:

- The uniform increase in the cyclotron orbit of ions to produce a detectable signal.
- The development of a coherent motion of the excited ions, generating an image current on the detection plate (Figure 2-19).

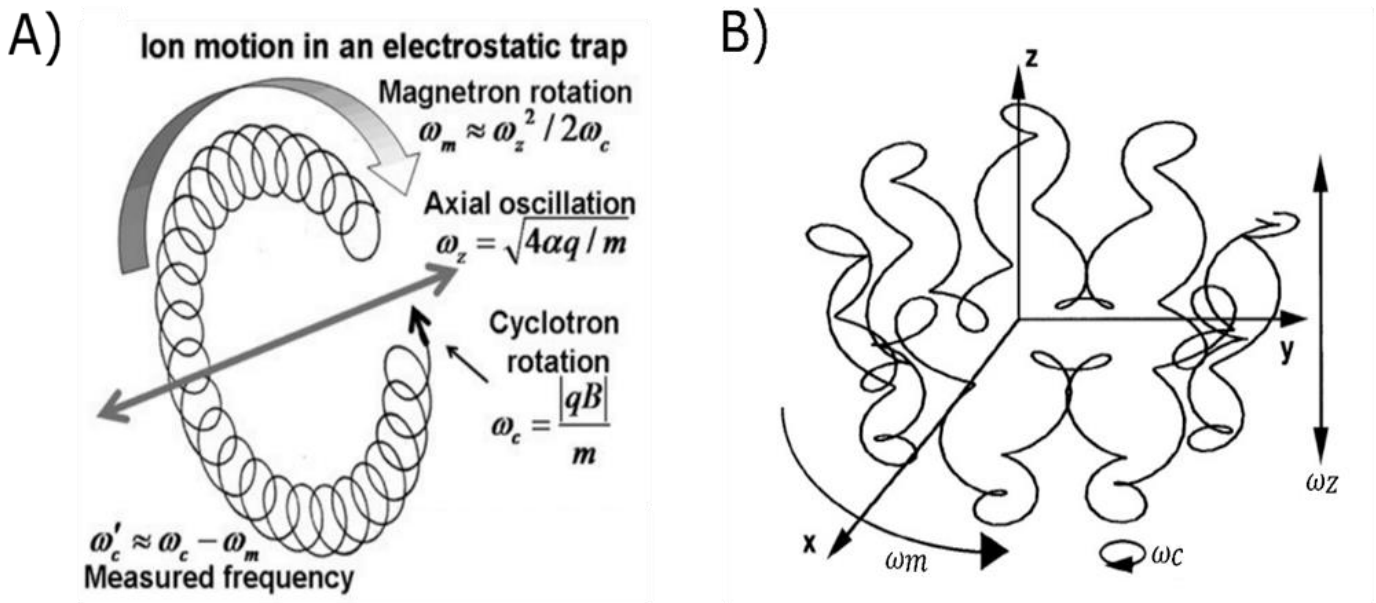


Figure 2-18: (A) representation of the individual ion movements within an ICR cell, and (B) representation of the total ion motion that results. ^{95,96}

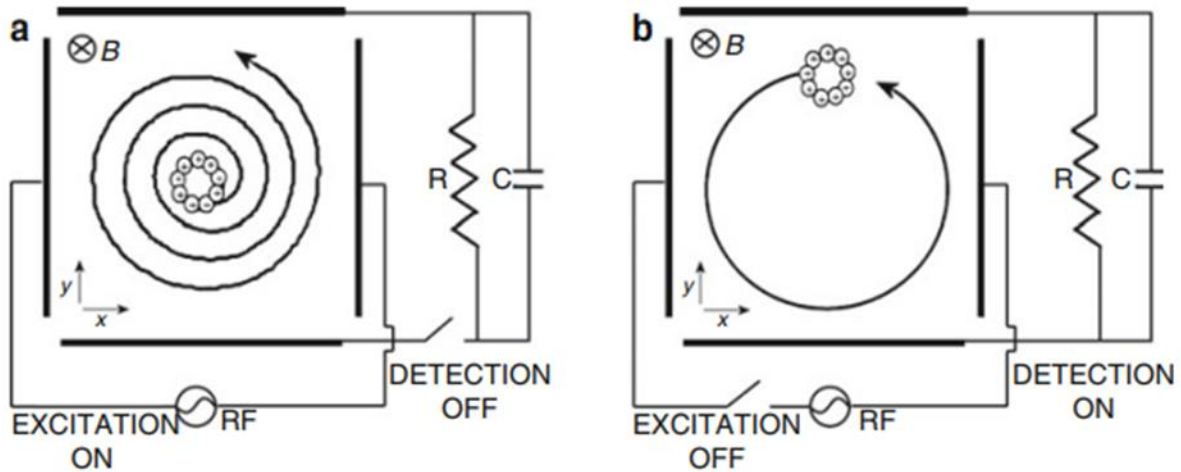


Figure 2-19: The steps involved in ICR-MS's excitation and image current detection. The ion cloud's spiral trajectory is shown in figure (a), which was caused by the ions being excited by an RF electric field that oscillated at the cyclotron resonance frequency. However, the frequency ω_c of circulation is not a function of ion velocity, and the radius is constant throughout detection.⁸⁹

The excitation pulse typically consists of a sine wave with a resonance frequency. To allow broadband detection of ions over a given m/z range, the excitation pulse must sweep across the various frequencies corresponding to the m/z domain of the ions trapped in the ICR cell. Equation 2-34 ensures to determine, as a function of the excitation time, the radius of the ion orbit after excitation.

$$r = \frac{E_0 T_{excite}}{2B} \quad \text{Equation 2-35}$$

where r is the orbit radius, E_0 is the amplitude of the applied excitation waveform (electric field), T_{excite} is the excitation duration, and B is the strength of the magnetic field.

The electric field E_0 is obtained by the application of $+V_0$ and $-V_0$ volts from the two opposite transmitter plates separated by a d distance. Hence, E_0 can be expressed as followed.

$$E_0 = \frac{2V_0}{d} = \frac{2V_{p-p}}{d} \quad \text{Equation 2-36}$$

The parameter V_{p-p} is the peak-to-peak voltage difference between the 2 plates.

By replacing E_0 by $\frac{2V_{p-p}}{d}$ in equation 2-36, it is possible to obtain a new expression of the ion orbital radius of the excited ion.

$$r = \frac{2V_{p-p}T_{excite}}{2dB} \quad \text{Equation 2-37}$$

It is evident from this equation that the final orbit radius does not depend on the m/z but rather increases with the excitation time. All ions achieve the same orbital radius if they are all excited during the same time (T_{excite}).

The different excitation modes in FT-ICR MS

Many excitation modes have been devised. The shape of the excitation waves in the frequency domain makes it easy to distinguish the different approaches (Figure 2-20).⁹⁷⁻¹¹³

The simplest method is to emit a rectangular pulse of a single frequency that exclusively excites the ions at this frequency (Figure 2-20 a). Applying a rectangular pulse to each ion in a mass spectrum is an unrealistic way to produce a mass spectrum according to the required time. In addition, the decrease of the excitation time has an impact on the mass resolution (Figure 2-20 b). As a result, alternatives that use a wide RF bandwidth to simultaneously excite all the ions in the cell have been proposed.⁸⁴

Chirp or *sweep* excitation (Figure 2-20 c) is the first excitation technique used in broadband mode. Marshall first described chirp excitation in 1974.^{83,114} It involves sweeping a wide frequency range to excite ions.¹¹⁴ The excitation amplitudes of the chirp pulses have a disadvantage in that they are not fully uniform. Consequently, the relative intensity of the observed peaks is not strictly the mirror of the relative abundance of the ion in the ICR cell. Ultimately, sweep excitation may induce the ejection of ions if the radius of their orbit overpassed the radius of the ICR cell.

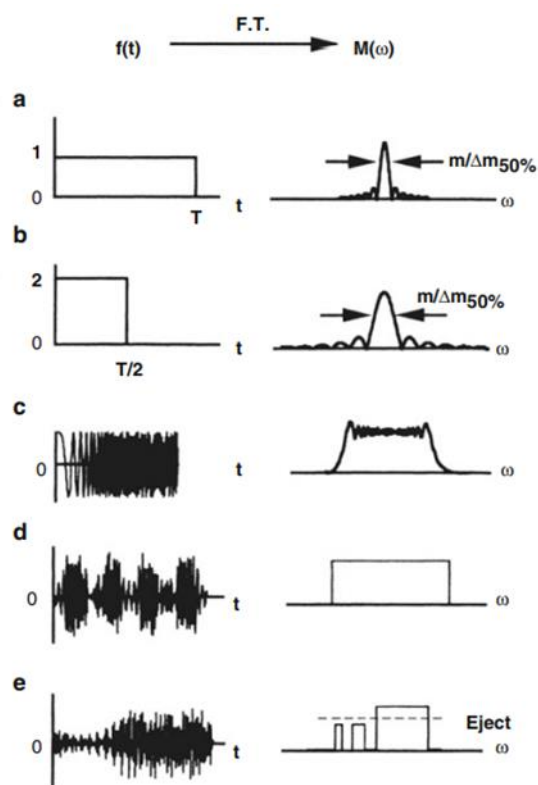


Figure 2-20: Time-domain (left) and frequency-domain (right) excitation waveforms: (a, b) rectangular pulses yield inhomogeneous and rather narrow excitation windows; (c) “chirp” excitation; (d, e) SWIFT excitations, with (e) designed to eject a certain mass range from the cell.⁹⁵

Marshall et al. introduced the “Stored Waveform Inverse Fourier Transform” (SWIFT) excitation in 1985 to overcome the drawbacks of sweep excitation.^{115,116} The SWIFT procedure (Figure 3-20 d) ensures a more homogeneous excitation on a broad range of frequencies. The SWIFT excitation waveform, which must be applied on the excitation plates in the time domain, is calculated by inverse Fourier transform of a given domain of frequencies with the same amplitude (rectangular pulse). Therefore, the ions in a given m/z range – i.e. in a given cyclotron frequency range – are excited in the same manner, and the intensity of the ions observed on the mass spectrum is more representative of their relative abundance. Another benefit of SWIFT is mass resolution is not affected by the excitation time. The excitation shape reported in Figures 3-20 e in the frequency domain allows the non-excitation of ions in a given m/z range or, on the contrary, their over-excitation, which leads to their ejection from the ICR cell. This is helpful for performing MS/MS experiments in the ICR cell.

2.5.1.7. Detection

After excitation, the ions with a coherent motion, are close to the detection electrodes (Figure 2-21). With respect to their polarity, these ions attract (positive ions) or repulse (negative ion) electrons in an RLC circuit. Due to the circular motion of the ions in the ICR cell, the wave created by this alternative passage of electrons from a sensing plate to that diametrically opposite corresponds to the superposition of alternating currents whose frequencies correspond to the cyclotronic frequencies of the ions in the FT-ICR cell. This wave is known as "image current."

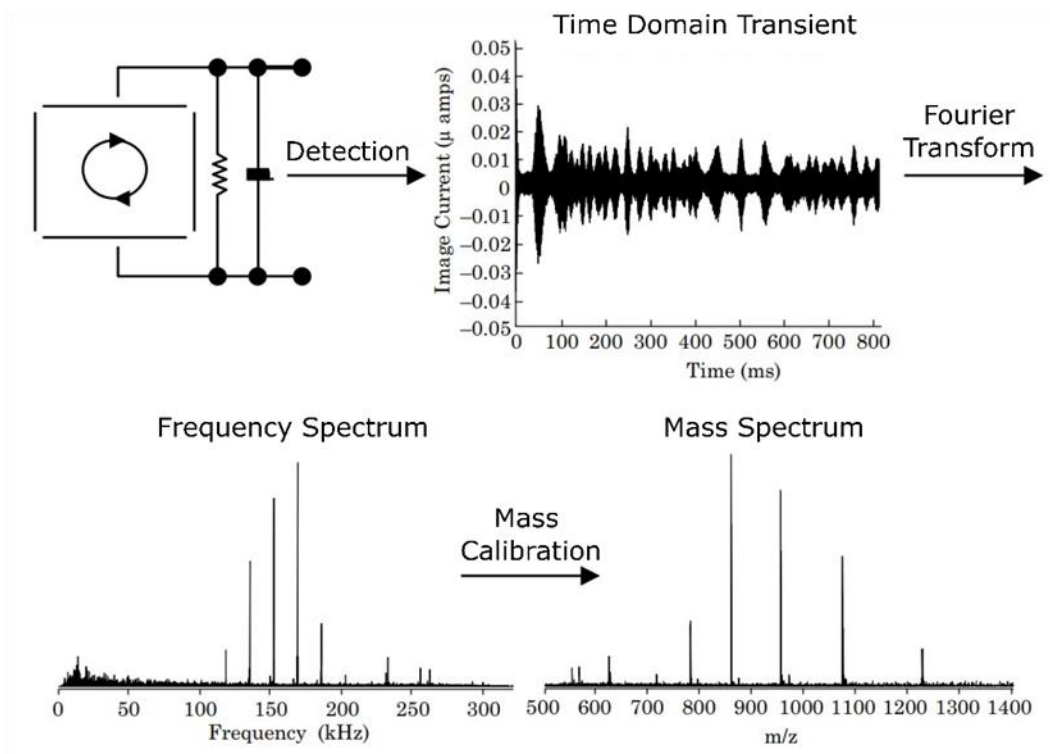


Figure 2-21: The procedure of turning an ion's cyclotron motion into a mass spectrum.¹¹⁷

Then, ions with different m/z values are detected simultaneously. Therefore, the ion current is a composite signal called time-domain transient, which requires the application of fast Fourier transform FFT to define the discrete frequency of each ion, which depends on its m/z ratio (Figure 2-21). Ion excitation and detection are non-destructive events. Consequently, remeasuring experiments are possible on a given ion population. In such an experiment, after detection, the ions are deexcited by the application of an out-of-phase excitation before to be re-excited and detected. This procedure can be reproduced as long as the number of trapped ions is sufficient to generate an ion current and results in an increase in the sensitivity.¹¹⁸ The increase of the sensitivity is also allowed by the amplification of the current ion. The frequency domain spectrum created by FFT is converted into a mass spectrum by the application of the frequency- m/z relationship (Equation 2-25).

2.5.1.8. Apodization

The abrupt truncation at the start and end of the time-domain signal, which covers a finite period T , causes auxiliary wiggles on each side of the frequency peak, as seen in Figure 2-22. These peaks are problematic because they masked smaller “real” peaks. A weight function (apodization function) is applied to the transient for windowing the time-domain waveform to reduce these wiggles. Different apodization functions have been proposed that compel the beginning and end of the time-domain signal to decrease to zero.¹¹⁹ Another mathematic transformation of the time-domain transient is the zero-filling procedure, which consists of adding zeros (equal or twice the number of data points) to increase the length of the transient by two (one-zero-filling) or three (double zero-filling). This procedure results in the increase the number of points per m/z interval (increase of the resolution) and smooths the peak shape.^{120,121}

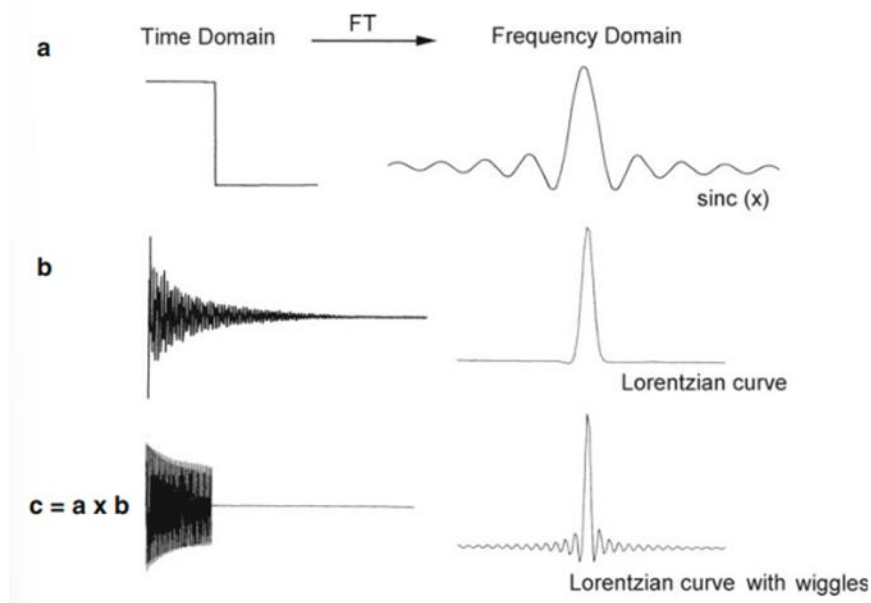


Figure 2-22: Various input signals and how Fourier transformations affect them. (a) A step function is converted to $\text{sinc}(x)$, (b) a fully dampened transient signal containing only one frequency yields a single Lorentzian curve, and (c) when a transient signal is shortened, it may be seen as a mixture of (a) and (b) and produces a Lorentzian curve with “wiggles.”

2.5.1.9. ICR cell

The ICR cells typically have three types of electrodes: trapping, excitation, and detection. The compensation electrodes, that are not systematically added can help the cell's electric field take specific shapes. An ICR cell can be created by assembling these electrodes in different ways. However, the cubic and cylindrical geometries are the most common ICR cell designs (Figure 2-23).¹²²

The shape of the ICR cell, the shape of the trapping potential, and the homogeneity of the magnetic field significantly influence the axial oscillation, the resulting magnetron motion, and disturbances that cause coherence loss, or phase shift. Imperfections in the magnetic and electric fields severely limit the performance of the simple cubic cell (the ICR cell of the pioneers). As a result, several other cell designs offer significantly better performance than the cubic cell have been proposed.^{94,95}

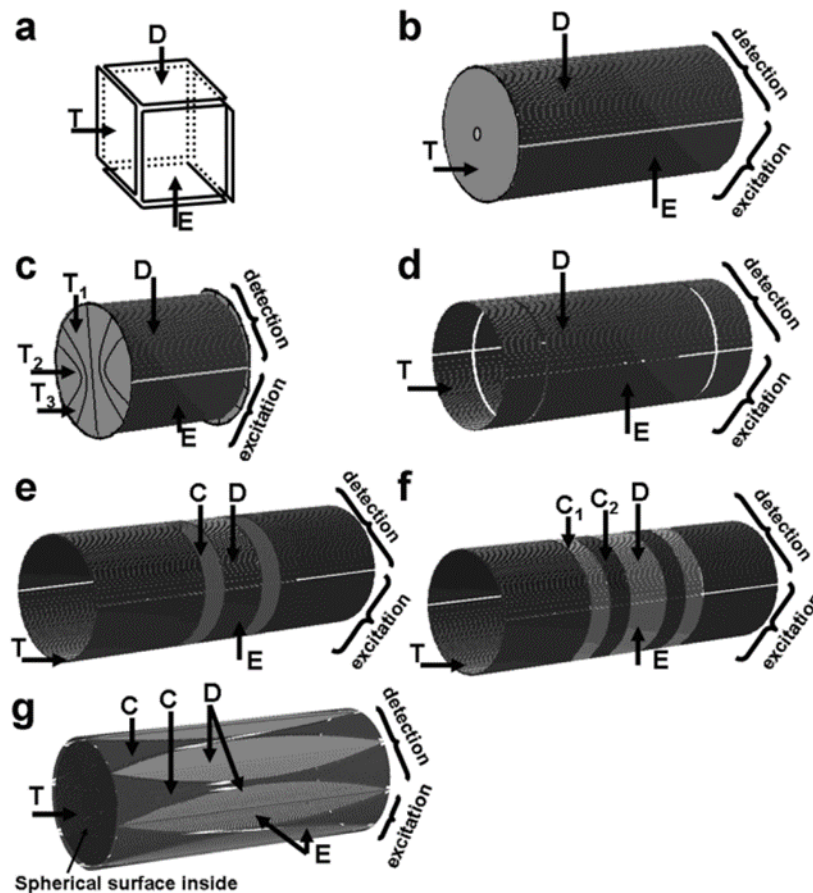


Figure 2-23: Important ICR cell types; A) Cubic cell, B) open-ended cylindrical cell, C) and D) open-ended cylindrical cells with compensation electrodes, E) capped cylindrical cell, F) Infinity cell, and G) dynamically harmonized capped cylindrical cell. The individual electrodes are labelled: excite (E), detect (D), trap (T), and compensation electrode (C).¹²³

Thus, a near-perfect hyperbolic field is produced inside a hyperbolic trap, sometimes called a Penning cell, (Figure 2-23 b). This greatly improves the resolution and accuracy of the m/z ratio measurement compared to a cubic cell. Therefore, optimal working conditions are obtained when a limited number of ions (10 to 10,000) are trapped in the minimal volume of the Penning cell. However, they are unsuitable for analytical work, which requires a cell capable of accepting large populations of ions to provide a high dynamic range and investigate complex mixtures. Distortion of the electric trapping field (bending of the field lines near the trapping

electrodes) can also be avoided by adding auxiliary trapping electrodes to create a triple-segmented cylindrical cell. In this case, the field lines are perfectly parallel for the entire cell length along the magnetic field axis.¹²⁴ The *infinity cell* is an alternative strategy to achieve the same goal by using segmented end caps on a cylindrical cell (Figure 2-23 c).

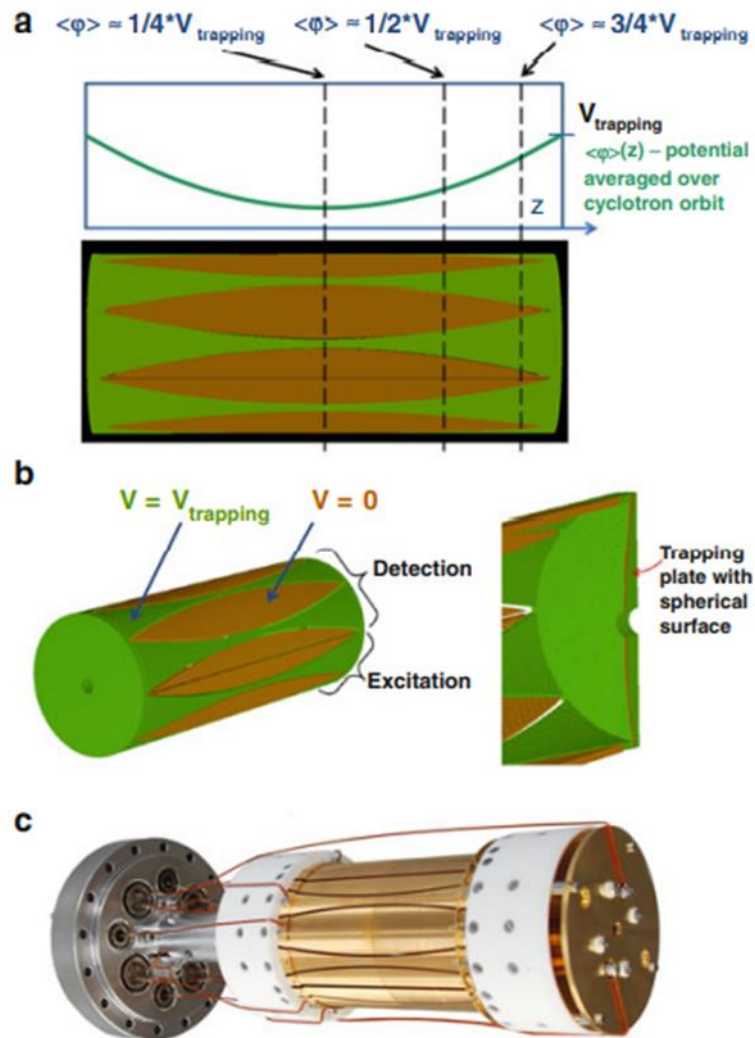


Figure 2-24: Dynamically harmonized ICR cell. (a) Axial cross section showing the segmented cell walls and the hyperbolic trapping potential experienced by ions on average per full cycle. (b) Division into four 90° sections to accomplish excitation and detection plus detail of a trapping plate. (c) Photograph of the Paracell; gold plating is used to minimize electrode oxidation.¹²⁵

E. Nikoleav recently developed a cell that nearly fills the volume of the potential harmonic area. For this purpose, the walls of a long cylindrical cell (150 x 56 mm) are divided into segments that have alternating convex and concave shapes.^{125–127} The convex segments remain grounded while the trapping potential is applied to the concave sections. The form of the trapping plates is nearly spherical. As a result, ions acquire an average harmonic potential during each complete cycle of cyclotron motion (Figure 2-24). For this reason, it is referred to as a *dynamically harmonized ICR cell*. The cylinder is generally divided into four 90° sections for

excitation and detection, with dividing cuts splitting every other convex electrode in half. This design maintains excellent ion capacity and dynamic range while significantly increasing resolving power. Bruker Daltonik markets it under the name *Paracell*.

2.5.1.10. Mass accuracy and Resolving power

The resolving power of a mass spectrometer is one of its essential characteristics. This parameter indicates how well the mass spectrometer can distinguish two ions with a small m/z difference. A mass spectrometer with high resolving power allows narrow peaks to be observed, ensuring an important peak capacity over an m/z range of one Da. This makes it easier to detect many peaks close to each other. The full width at half-maximum resolving power (FWHM) can be calculated by dividing the m/z at the peak apex by the half-maximum width of the peak. It also depends on the magnetic field and the length of the transient and can be estimated by the following equation.^{95,126}

$$R = \frac{m}{\Delta m} = \frac{1.274 \times 10^7 z B T_{acq}}{m} \quad \text{Equation 2-38}$$

where R is the resolution, m is the mass of the ion, Δm is the peak width at half intensity, z is the charge of the ion, B is the strength of the magnetic field, and T_{acq} is the transient length. Equation 2-37 shows that the resolving power increases proportionally with transient length (Figure 2-25). Ultimately, the motion of an ion along the radius of its excited cyclotron orbit can continue indefinitely in a vacuum and in an ideal electric field because collisions with the background gas or adverse ion interactions do not impact it. Then, FT-ICR MS operates at very low pressure (<10⁻¹⁰ mbar) to ensure current image detection over a long time.

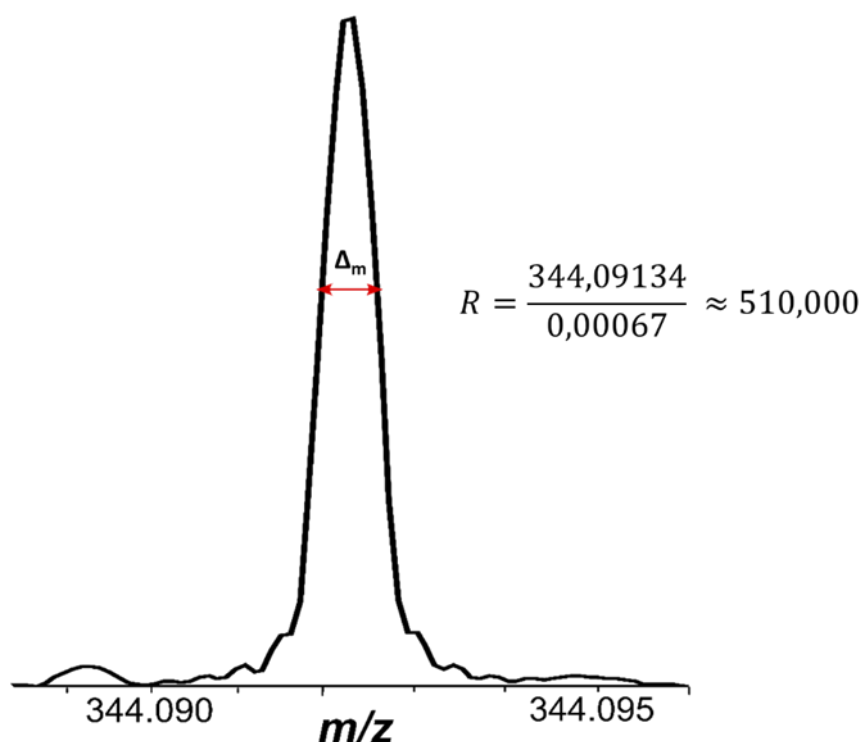


Figure 2-25: Determining a peak's resolution using its peak width and peak center of Oak bio-oil analyzed in (+) ESI FT-ICR MS.

The accuracy of the measured m/z , also known as "mass measurement accuracy," is a crucial feature of a mass analyzer. The resolving power, ion-ion interactions, space charge effects, and the stability of the ion's motion as it oscillates around the cell can impact the accuracy of mass measurement, which is the difference between the actual mass of an ion and its theoretical mass. High accuracy of mass measurements is essential for in-depth analyses, as it increases confidence in the elemental composition assignments.¹²⁸

The Equation 2-38 defines the mass measurement accuracy usually expressed in parts-per-million (ppm).

$$\text{error (ppm)} = \frac{m/z_{\text{measured}} - m/z_{\text{theoretical}}}{m/z_{\text{theoretical}}} \times 10^6 \quad \text{Equation 2-39}$$

where *error (ppm)* is the elemental composition assignment error in ppm, m/z_{measured} is the measured m/z value of the ion, and $m/z_{\text{theoretical}}$ is the exact theoretical mass of the assigned elemental composition.

2.6. Data Acquisition

Superconducting magnets with field strengths of 7, 9.4, and 12 T are the most frequently used in FT-ICR MS. Magnet with 15, 18, and 21 T are less common. There are several advantages to increasing field strengths. For example, resolving power and scanning speed increase linearly with B. Two separate FT-ICR mass spectrometers, a 7 T 2ω FT-ICR MS Bruker Solarix 2XR at the LCP-A2MC in Metz (Figure 2-27) and a 12 T Bruker Solarix at the University of Warwick, were used for this research project. The 7 T mass spectrometer, whose design and associated software are detailed in the next section, served the primary platform for this work. FTMS Control 2.3.0 was used to optimize the different acquisition parameters for both instruments. Bruker DataAnalysis V5.0 was used to analyze and calibrate the obtained mass spectra (Bruker Daltonics). Composer64 (Sierra analytics) was used for peak assignment.

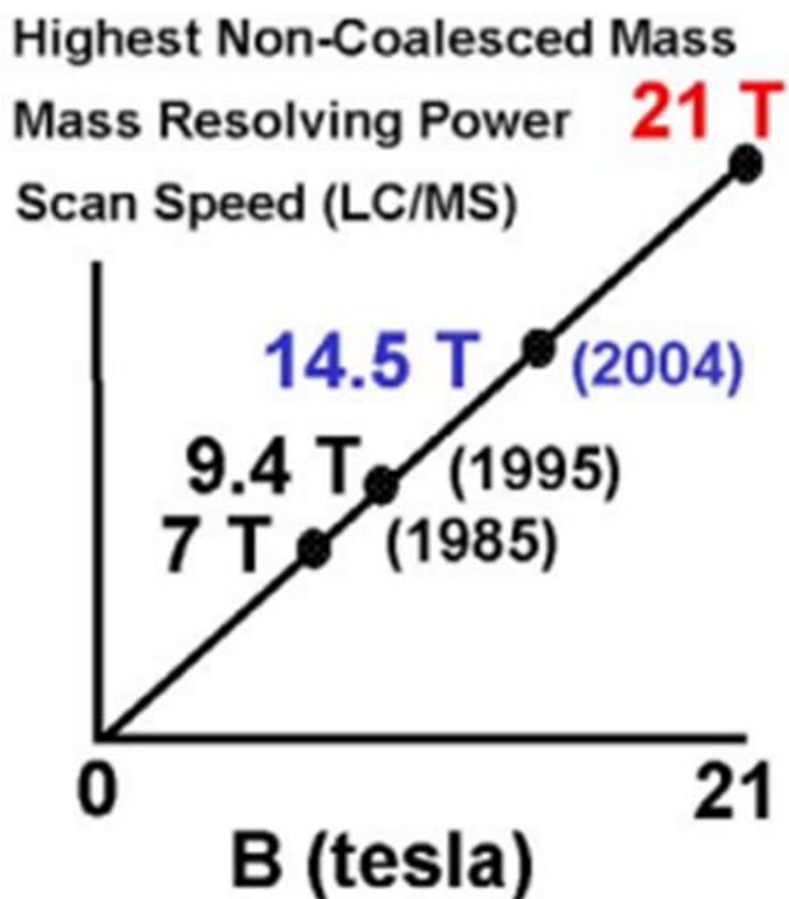


Figure 2-26: Performance of FT-ICR mass spectrometers as a function of the magnetic field.⁹⁵

2.6.1. Acquisition and Analysis

Most ionization techniques used with FT-ICR MS create ions at pressures well above the required pressures for an ideal detection (10^{-10} mbar). These vacuum requirements are met by using levels of differential pumping and conductance limits (usually ion lenses) between each segment to allow pressure drops by reducing gas flow to the next section. In the first vacuum zone, ions produced by the atmospheric pressure ionization sources are inserted orthogonally through the *ionization source* (1). Ions of same polarity are accelerated toward the *ion funnels* (3) by the *deflector plate* (2). The *split octupole* receives the ions from a smaller beam than the ion funnels have focused on (4). The split octupole moves the ions into the *quadrupole* (5), where, depending on the conditions, they can be transmitted, or mass filtered and moved into the *hexapole collision cell* (6), where they are accumulated. In this hexapole, argon gas may be employed as collision gas to activate/induce dissociation (CAD/CID). The accumulated ions (or the fragment ions if a CID experiment is conducted) are then directed to the very low-pressure ICR cell. For separating the higher-pressure zones from the ultra-low-pressure sections, the *beam valve* (7) is particularly helpful. When the beam valve is opened, ions can be directed from the collision/accumulation hexapole into the *ICR cell* (9) by the *transfer hexapole also called ion guide* (8). The ICR cell can also be used for events involving isolation and dissociation. For electron-based dissociation (ExD), the Bruker SolariX has an electron-generating *hollow cathode* (10) as well as optical access for *lasers* (11) to enable photodissociation methods. The instrument further includes a *chemical ionization source* (12) to ensure electron transfer dissociation (ETD) methods.

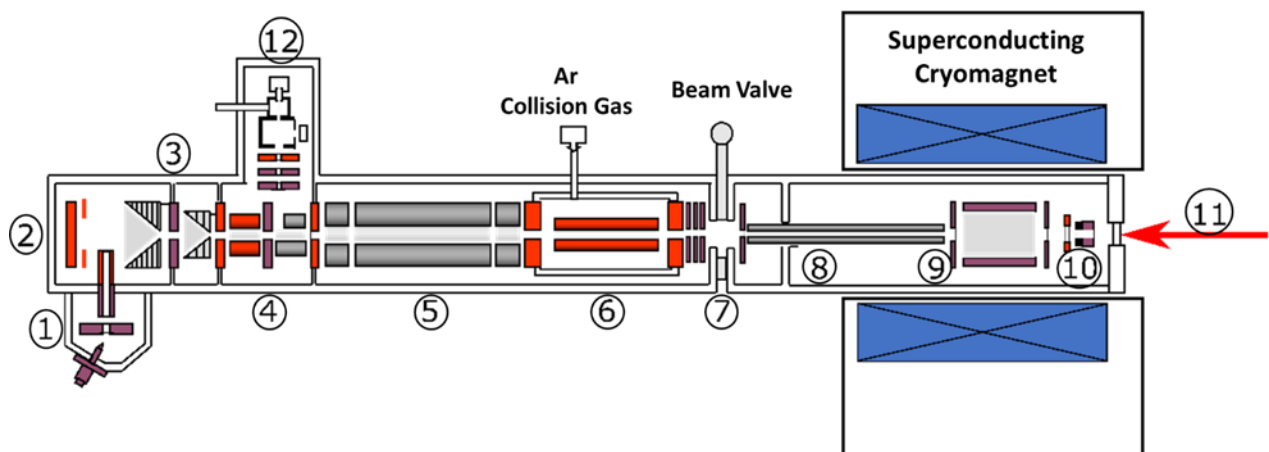


Figure 2-27: Schematic of the 7 T 2ω Bruker SolariX used for the work presented in this thesis. The numbered sections are referred to in the next section. Adapted from Bruker's Instrument diagram.

2.6.2. Summary of FT-ICR Instrumentation

2.6.2.1. Principle Operation

The Lorentz force causes ions moving on a plane perpendicular to the direction of a magnetic field to be propelled into circular orbits. The ion kinetic energy determines the radius of their orbit, while their mass-on-charge ratio determines the oscillation frequency or so-called cyclotron frequency. Ions that are transported into a magnetic field must be stimulated by an RF electric field with a frequency equal to their cyclotron frequency. After being stimulated, ions with the same m/z coherently circulate through the ICR cell on a larger orbit. The detecting plates, which make up roughly half of the inner wall surface of the ICR cell, start to emit image currents as the ion swarms pass by. In order to compute the associated m/z values, the image currents are first recorded in the time domain (for 0.2–20 s), then converted into the frequency domain using the Fourier transformation (FT).

2.6.2.2. Performance characteristics

When it comes to resolving power (10^5 to $>10^6$) and mass measurement accuracy (typically 0.1–2 ppm), FT-ICR instruments are on the most performant mass spectrometers. The level reached is determined by the instrument itself (magnetic field), the transient's duration, and a number of other factors as the number of data points. Modern instruments may be fitted with various ionization methods and offer a large range of tandem-MS capabilities. The investigation of complex mixtures like crude/bio oil or dissolved organic materials is made possible by the remarkable resolving power and mass accuracy.

2.6.2.3. General Considerations

The FT-ICR instruments are large, heavy, and expensive in terms of initial investment and operating costs, mainly due to the requirement to use high-field superconducting magnets and the requirement for ultrahigh vacuum. Although it may be difficult to use an instrument to its full extent, contemporary FT-ICR devices are nonetheless adequate for normal usage. Actually, there are several analytical challenges that FT-ICR-MS alone can resolve.

2.7. - Data Treatment

2.7.1. Calibration

High mass resolution and high mass accuracy are often the goals of high-resolution mass spectrometry (HR-MS). Mass calibration is an important step in order to obtain sub-ppm mass accuracies. Ions with similar m/z values can be separated by resolution, but this does not always indicate where on the m/z axis the individual signals are situated.¹²⁹ In theory, external and internal mass calibration produces the maximum level of mass accuracy. An external calibration can be achieved with the analysis of standard solutions, such as NaTFA for ESI.¹³⁰ This external

calibrant enables the instrument to be tuned for both positive and negative ionization. An internal calibration with well-defined peaks is used to perform the mass spectrum's final calibration. By FT-ICR, internal mass calibration generally provides mass accuracies in the range of 0.1-0.5 ppm. Polyethylene glycol (PEG) calibrant was utilized for APPI and APCI.

2.7.2. Data assignment

A peak list of signals with a signal-to-noise ratio greater than 3 is generated after calibration. The Composer software (Sierra Analytics) uses the following criteria to assign each peak to an elemental formula: $C_{1-100}H_{1-100}N_{0-2}O_{0-25}Na_{0-1}^+$ (positive ion) or $C_{1-100}H_{1-100}N_{0-2}O_{0-25}S_{0-1}^-$ (negative ion). The generated elemental formula must follow two parameters: a double bound equivalent (DBE which is determined by Equation 2-39) in a -0.5 to 40 range, and a mass tolerance error of 3 ppm.

$$DBE = n_C - \frac{n_H}{2} - \frac{n_N}{2} + 1 \quad \text{Equation 2-40}$$

The assigned peaks are reported in the file that composer creates. Each signal is associated with an experimental, theoretical, nominal, and CH₂-based Kendrick mass as well as a mass error, an elemental formula, and a DBE value. All the assignments with an error smaller than 1 ppm are used for recalibration in accordance with Equation 2-40 once these datasets are exported to Excel (Figure 2-28).

$$\frac{m}{z} = \frac{A}{\omega^2} + \frac{B}{\omega} + C \quad \text{(Equation 2-41)}$$

where A , B , and C are constants that are calculated using a quadratic regression,¹³¹ ω the measured pulsation of the ion with a mass m and a charge Z .

Some compound families are marked after assignment. The most prevalent bio-oils are $C_xH_yO_z$, $C_xH_yN_nO_z$, and $C_xH_ySO_z$ (in decreasing order of relative abundance). In (-) ESI, the species are mostly $[M-H]^-$ deprotonated molecules, whereas in (+) ESI, they are predominantly $[M+H]^+$ or $[M+Na]^+$ adduct ions. Compounds can be concurrently detected in LDI and APPI positive ion detection mode as M^{++} and $[M+H]^+$. A pyrolysis bio-oil mass spectrum with an inset at m/z 219 is shown in Figure 2-28. This displays the FT-ICR MS resolving power capabilities and the accuracy of the mass measurement (Figure 2-29).

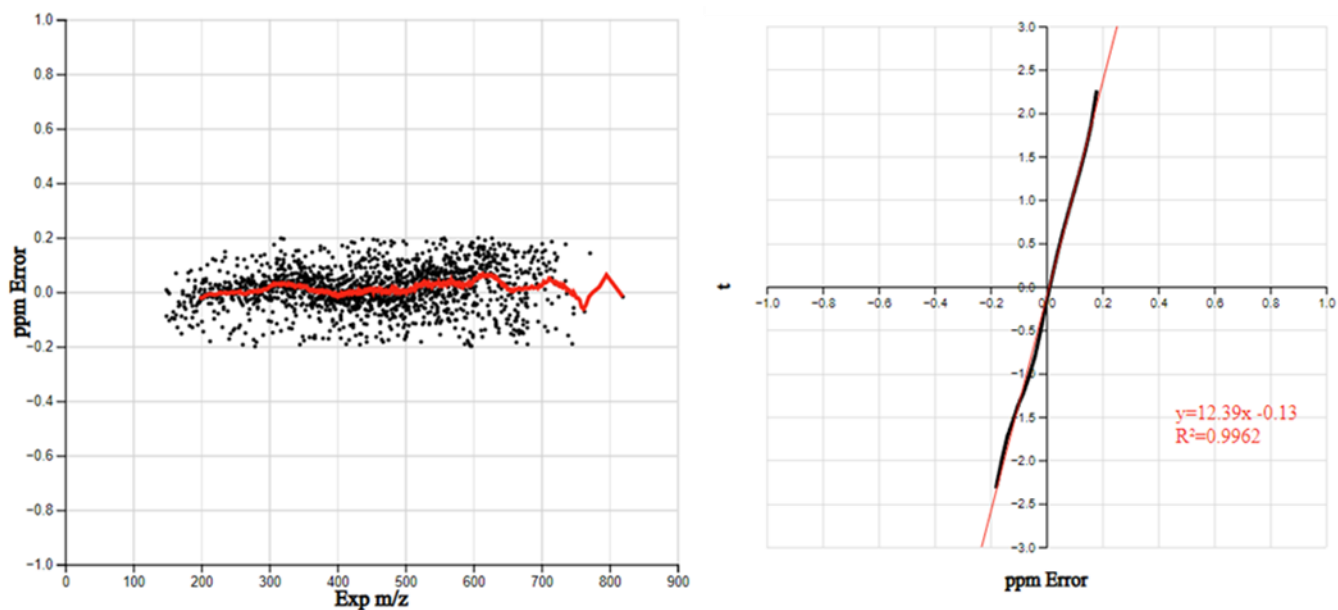


Figure 2-28 : (Right) Mass error (in ppm) vs. m/z for $C_xH_yO_z$ compounds detected in the study of an Oak pyrolysis bio-oil by (-) ESI FT-ICR MS, (Left) Normal probability plot of the errors.

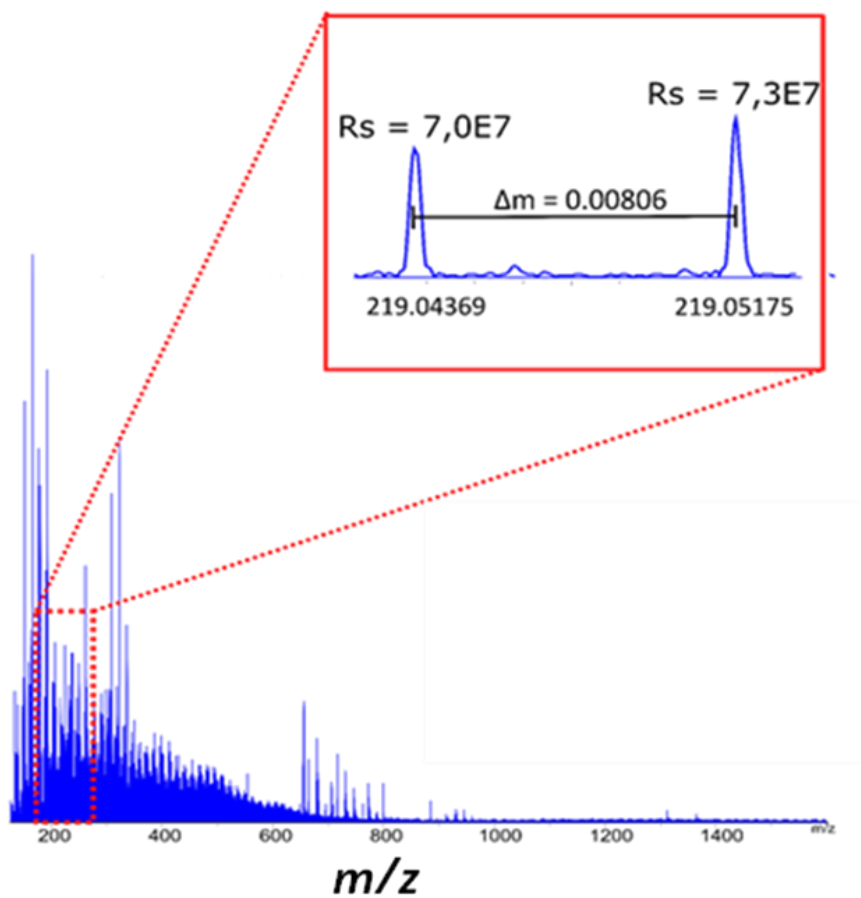


Figure 2-29: (-) ESI FT-ICR mass spectrum of an Oak pyrolysis bio-oil.

2.8. – Graphical Representations

Data processing is necessary to study a complex mixture once datasets are acquired. To analyze the data and provide a raw formula for the different features observed on the mass spectrum of a bio-oil, two software programs are used, the first is Data Analysis (Bruker) and the second is Composer (Sierra Analytics). This data is then graphed in various ways. Part of these graphical representations are discussed in the following sections.

2.8.1. Van Krevelen

Van Krevelen diagrams are commonly used to analyze various complex organic mixtures after they were originally developed to investigate the maturation of coal and oil.^{132–134} The dots plotted on a Van Krevelen diagram represent the detected $C_xH_yO_z$ compounds (Figure 2-30) concerning their O/C (x-coordinate) and H/C (y-coordinate) ratios. This can be applied to hundreds of compounds. The Van Krevelen diagram makes it possible to highlight the major chemical classes of substances, each of which having a unique H/C and O/C ratio.

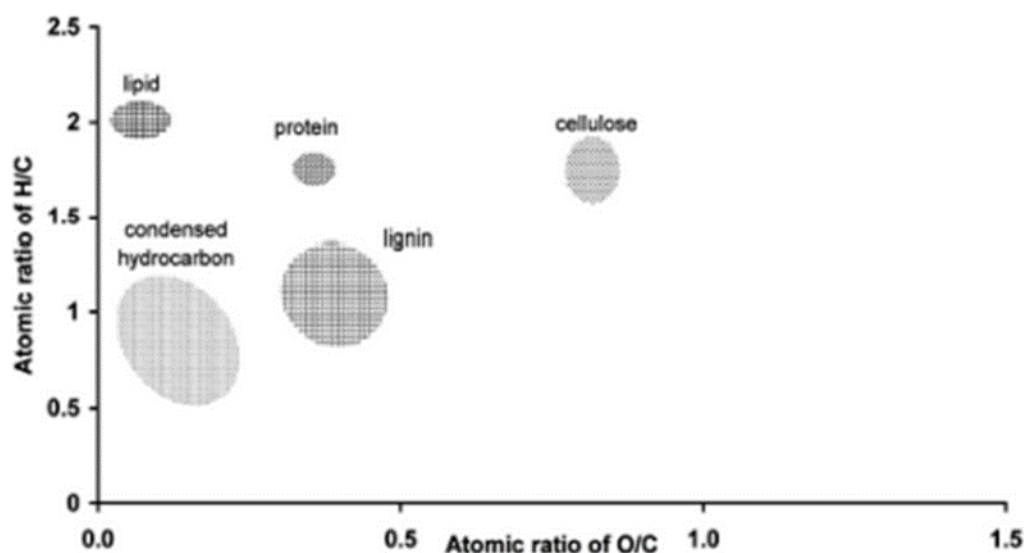


Figure 2-30: Van Krevelen diagram shows certain significant biomolecular parts arranged in various areas.¹³⁴

The illustration of Figure 3-30 makes it possible to highlight the areas of the figure that are specifically for lipids, cellulose/hemicellulose, or lignin derivatives. The N/C and S/C ratios may also be used as x-coordinate to draw diagrams for compounds containing azote and/or sulfur. In addition, oxidation, dehydration, demethylation, decarboxylation, and hydrogenation phenomenon, may also be evidenced in van Krevelen diagrams as lines, as was reviewed by Kim *et al.* in 2003¹³⁴ and Lozano *et al.* in 2021.¹³²

2.8.2. Kendrick Map

Kendrick's mass defect analysis (KMD) is another method to investigate complex organic mixtures easily. This approach involves working with mass defects by changing the mass scale and using a new mass scale reference, such as CH₂. Each detected ion associated with this new "Kendrick's mass" (KM(CH₂)) is represented by its the Kendrick's mass defect (y-coordinate) and its nominal mass (x-coordinate). As a result, compounds that differ by one or more CH₂ units exhibit the same Kendrick's mass defect (Figure 3-31), organizing in a straight horizontal line. It is possible to use different structural units, such as H₂O, H₂, or O, as a reference for the mass scale. Equations 2-41, 2-42, and 2-43 provide the formulas for calculating KM and KMD.

$$KM(CH_2) = IUPAC\ mass_{measured} \times \left[\frac{Nominal\ mass\ CH_2}{IUPAC\ mass\ CH_2} \right] \quad \text{Equation 2-42}$$

$$KM(CH_2) = IUPAC\ mass_{measured} \times \left[\frac{14.00000}{14.01565} \right] \quad \text{Equation 2-43}$$

Where KM is the (exact) Kendrick mass.

$$KMD(CH_2) = nominal\ mass_{measured} - nominal\ KM(CH_2) \quad \text{Equation 2-44}$$

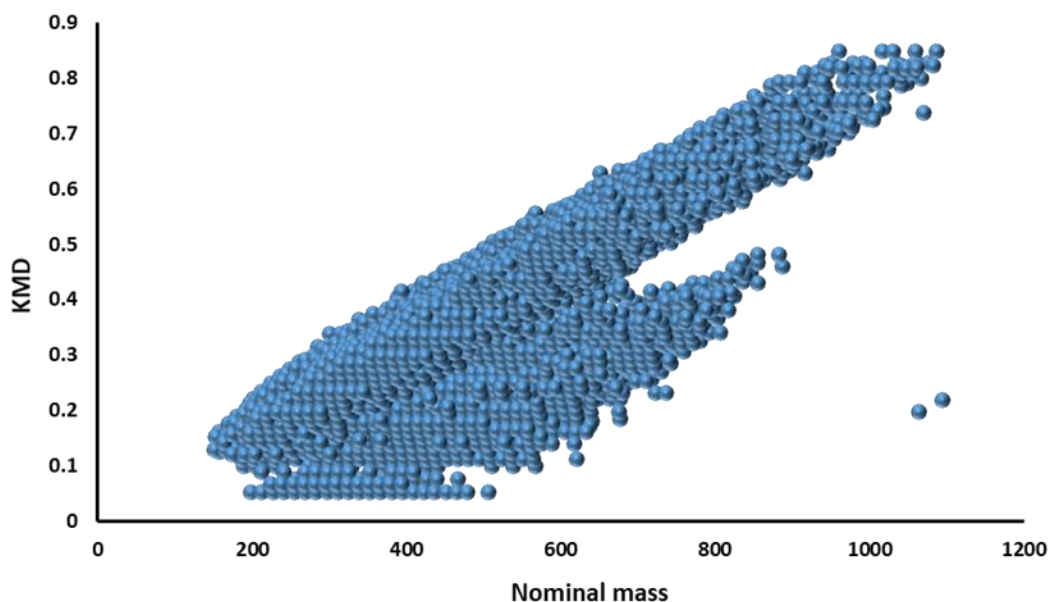


Figure 2-31: Kendrick's map of C_xH_yO_z compounds from Oak pyrolysis bio-oil analyzed by (-) ESI FT-ICR MS.

2.8.3. Other graphical representations

After assignment, the relative abundances of the different chemical families are used to define the global bio-oil composition obtained in a given experimental condition. The heteroatom class distribution e.g., oxygen atom count (Figure 2-32, left bar chart) and, the DBE distribution (Figure 2-32, right bar chart) can be used to gain more knowledge about a given family.

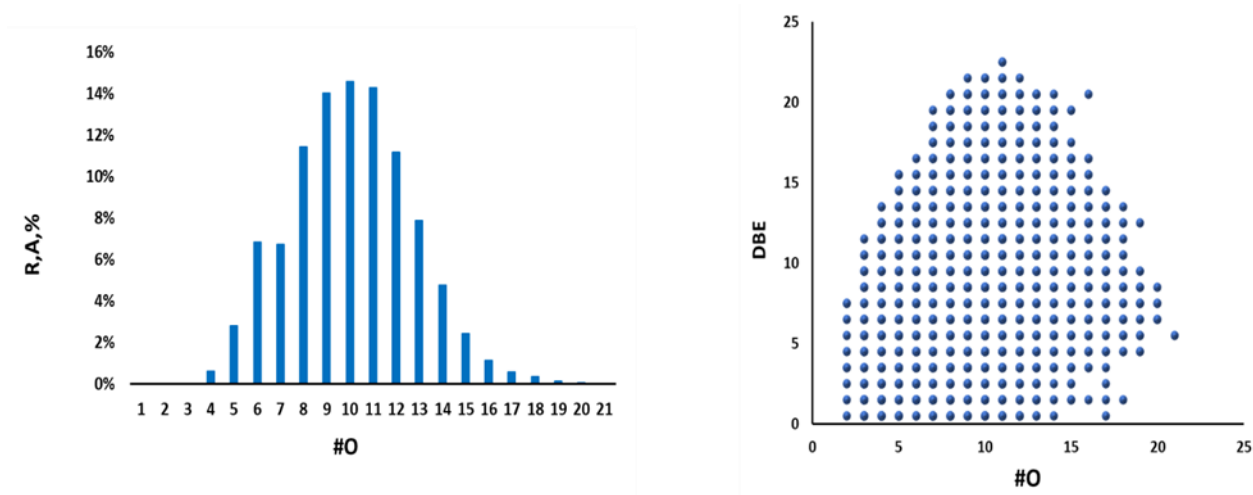


Figure 2-32: Global composition description of an Oak bio-oil obtained by (+) ESI FT-ICR MS analysis. DBE versus oxygen number (right), and relative distribution in respect with the oxygen atom count (left).

2.9. Tandem Mass Spectrometry

2.9.1. Introduction

Determining the m/z of an ion with a high mass-measurement accuracy “only” allows us to define its elemental formula. An additional MS experiment, called tandem mass spectrometry, is required to obtain structural information.^{135,136} A tandem mass spectrometry experiment involves at least two phases of m/z analysis, sometimes referred to as MS^1 and MS^2 . In the first step, a regular mass spectrum is acquired after ionization, followed by selecting a precursor or also-named precursor ion for which structural analysis is needed. In the second step, the activation of the selected ion by different techniques increases its inertial energy, which leads to its dissociation. The final phase of a tandem mass spectrometry experiment consists in the analysis of the fragment ions. Figure 2-33 illustrates the four events needed to complete a simple MS/MS experiment: ionization, precursor isolation, fragmentation and detection.

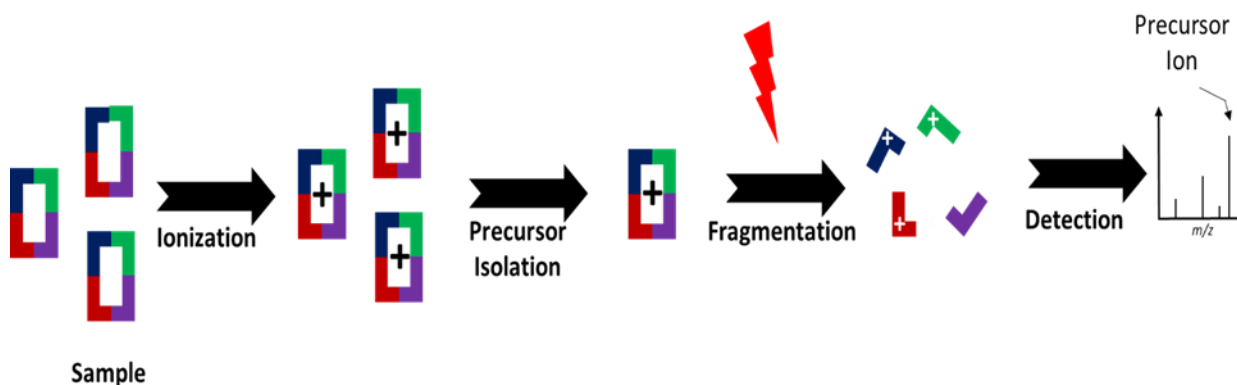


Figure 2-33: Typical steps for performing a tandem MS experiment.

A single precursor ion may break up into various fragment ions created by distinct fragmentation processes, governed by thermodynamic, kinetic, and/or chemical rules. A more intense product ion signal denotes the production of a more stable fragment and/or a higher probability of forming that fragment by a particular fragmentation pathway. In addition to competitive fragmentation events, successive dissociation may be observed.

Different activation methods are available, which use is highly dependent on the employed tandem mass spectrometer and precursor ion properties.¹³⁷ These include electron-based dissociations (ExD), such as electron-capture (ECD), electron-induced (EID), and electron-transfer dissociation (ETD),^{138–140} as well as collision activated/induced dissociation (CAD/CID), infrared multiphoton dissociation (IRMPD),^{141–148} and ultraviolet photodissociation (UVPD).^{149–152}

The next sections will describe to two of them, which has been employed in this study: CID and UVPD.

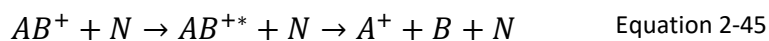
2.9.2. Collision Induced Dissociation CID

Jennings first described collision activated/induced dissociation (CAD/CID) in 1968.¹⁵³ CID is the most used activation method. There are other references to collisional activated dissociation (CAD) and collisional activation (CA), which work in the same way as CID.^{154,155} The activation of ions in the gas phase, by collision with an inert gas, is well-suited for determining the structure of ions with low internal energy, such as those produced by soft ionization techniques.^{156,157}

2.9.2.1. Principle

The selected ion interacts with He, N₂, or Ar (the most commonly used collision gases) to achieve CID fragmentation in a collision cell. The pressure in the collision cell is significantly higher than the high vacuum typically used in mass spectrometry to favor collision events

(Figure 2-34). Such an interaction causes the so-called “*precursor activation*” by increasing the internal energy, which is distributed into the precursor ion’s vibrational and rotational modes. The bond is broken if the final energy in an elongation vibration mode is higher than the dissociation energy, (Equation 2-44). In CID, the dissociation of the weakest bonds is favored.¹⁵⁸



$$E_{AB^{+*}} = E_{AB^+} + Q \quad \text{Equation 2-46}$$

From an energy viewpoint, the final internal energy $E_{AB^{+*}}$ of the precursor ion is the sum of the internal energy E_{AB^+} that it possessed before the collision and the Q energy that was transferred during the collision.^{154,155} The Q energy comes from the partial conversion of the kinetic energy of the ion during the collision events. Therefore, the higher the pressure, the higher the ion kinetic energy, and the higher the mass of the collision gas, the greater the increase Q in internal energy.

Due to the lack of species-specific CID requirements, such as the need for a chromophore as for IRMPD or UVPD this method of activation can be considered universal. Nevertheless, CID suffers from certain restrictions especially linked to not specific dissociation pathways (CO, CO₂, H₂O, NH₃, CH₃OH loss), the inefficient dissociation of the strongest bonds, and its inefficiency for high m/z ions. Therefore, the structural elucidation of aromatic and phenolic compounds can be challenging.

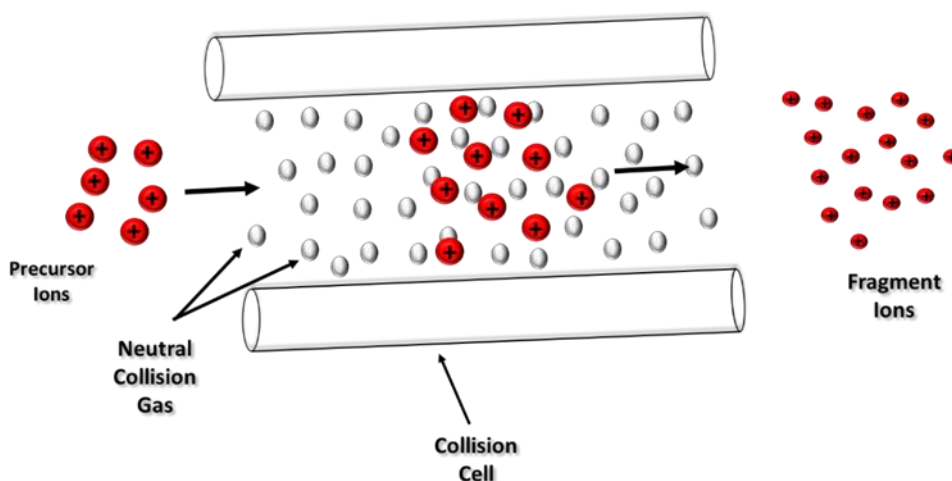


Figure 2-34: A collision cell's representation of the CID fragmentation of precursor ions.

Since the CID is a widely used fragmentation method, some databases are available. These databases may be helpful in identifying the structure of a molecule based on its CID fragmentation data. These databases include Mass Frontier, Pub chem Lite and Metfrag,¹⁵⁹ and *m/z*cloud.¹⁶⁰

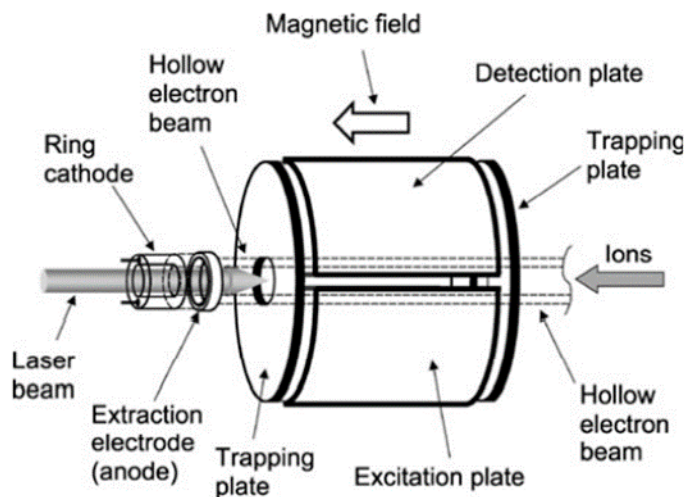


Figure 2-35: UVPD configuration for FT-ICR-MS. Through the center hole of the indirectly heated ring dispenser cathode affixed to the rear trapping plate of an ICR cell, the IR laser is delivered into the cell.¹⁶¹

2.9.3. 4.4- Ultraviolet Photodissociation UVPD

By exposing the precursor ion to UV photons, ultraviolet photodissociation (UVPD) is accomplished. An ion gets excited into a higher electronic excitation state as a result of absorbing a single UV photon, which is followed by its dissociation. This excitation may be accomplished in a single step, i.e., the absorption of one UV photon, unlike IRMPD (Figure 2-36).^{162–164} UV dissociation spectroscopy, which sweeps through wavelengths to identify functional groups, is also made possible by UVPD.^{137,165–169} UVPD requires the precursor ion to have a chromophore to absorb at the wavelength of the photons emitted by the UV laser (193 nm in this study).

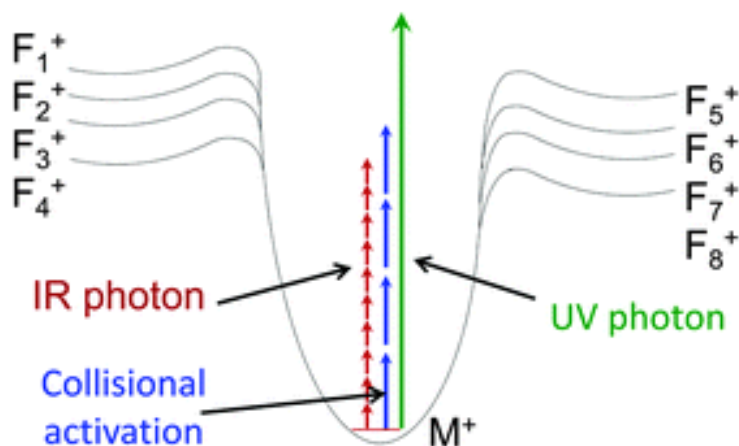


Figure 2-36: Illustration of energy deposition by different fragmentation techniques (CID, IRMPD, and UVPD).¹⁷⁰

It is important to remember that the UV absorption bands might be broad. This is an advantage to conducting UVPD for structural analysis purposes but may be an issue for the active UV spectroscopy of gas phase ion. Without a strong wavelength-specific chromophore, a UVPD event may still occur by decreasing the UV wavelength (increasing the energy per photon) or increasing the laser fluence. Unlike IRMPD and CID, which only excite precursor ions to a vibrational state, UVPD excites them to a higher electronic state.¹³⁷ This allows access to alternative fragmentation pathways. Moreover, part of the fragmentation leads to homolytic bond cleavage to form radical species. The presence of radicals may open the door to non-ergodic dissociation processes. Proteins¹⁶⁵, peptides¹⁷¹, and lipids^{172–174} are parts of the few classes of molecules that have been studied by UVPD. It has been stated that UVPD is a powerful complement to CID and can offer more structural details. The coupling between UVPD and FT-ICR MS is represented in Figure 2-37.

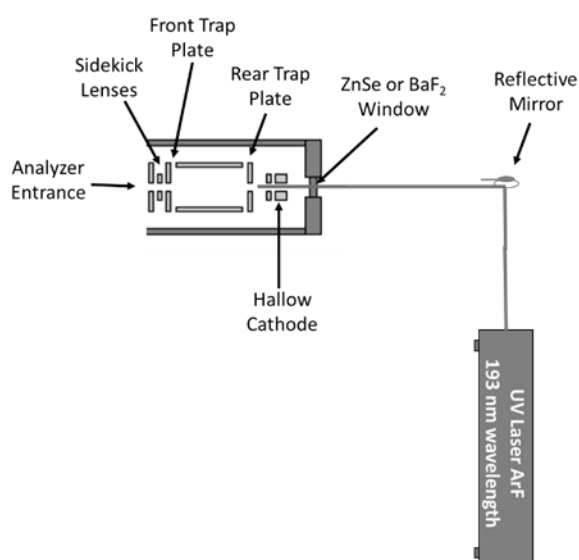


Figure 2-37 : UVPD in FT-ICR MS SolariX.

2.10. Conclusion

The high-resolution mass spectrometers are necessary for the study of raw and derivatized bio-oils. Fourier transform ion cyclotron mass spectrometry was employed in this study, and this chapter detailed how it works and its versatility. This powerful analytical tool can readily identify and assign thousands of distinct species. Due to their capacity to ionize various compounds according to their chemical characteristics (polarity, unsaturation level), ESI, APCI, and APPI sources were employed in the investigation of raw, fractionated, and derivatized bio-oils.

The large amount of data obtained will be graphically represented to facilitate both their interpretation and their comparison. The graphical representations detailed in this chapter, make it simpler to display which compound families are present in the investigated sample. However, these graphs also evaluate the effectiveness of functional derivatization as well as the complementarity of each ionization source. Apart from the functional characterization of bio-oils, tandem mass spectrometry (MS/MS) will also be used for the structural analysis of bio-oils. The last three chapters of this dissertation will describe in detail the obtained results.

2.11. References

- (1) Jia, L.; Le-Brech, Y.; Shrestha, B.; Frowein, M. B.; Ehlert, S.; Mauviel, G.; Zimmermann, R.; Dufour, A. Fast Pyrolysis in a Microfluidized Bed Reactor: Effect of Biomass Properties and Operating Conditions on Volatiles Composition as Analyzed by Online Single Photoionization Mass Spectrometry. *Energy Fuels* **2015**, *29* (11), 7364–7374. <https://doi.org/10.1021/acs.energyfuels.5b01803>.
- (2) Hertzog, J. High Resolution Mass Spectrometry for Molecular Characterization of Bio-Oils Produced by Pyrolysis of Lignocellulosic Biomass. phdthesis, Université de Lorraine, 2017. <https://hal.univ-lorraine.fr/tel-01905674> (accessed 2022-11-08).
- (3) Jia, L.; Buendia-Kandia, F.; Dumarcay, S.; Poirot, H.; Mauviel, G.; Gérardin, P.; Dufour, A. Fast Pyrolysis of Heartwood, Sapwood, and Bark: A Complementary Application of Online Photoionization Mass Spectrometry and Conventional Pyrolysis Gas Chromatography/Mass Spectrometry. *Energy Fuels* **2017**, *31* (4), 4078–4089. <https://doi.org/10.1021/acs.energyfuels.7b00110>.
- (4) Guan, S.; Marshall, A. G.; Scheppele, S. E. Resolution and Chemical Formula Identification of Aromatic Hydrocarbons and Aromatic Compounds Containing Sulfur, Nitrogen, or Oxygen in Petroleum Distillates and Refinery Streams. *Anal. Chem.* **1996**, *68* (1), 46–71. <https://doi.org/10.1021/ac9507855>.
- (5) Marshall, A. G.; Rodgers, R. P. Petroleomics: The Next Grand Challenge for Chemical Analysis. *Acc. Chem. Res.* **2004**, *37* (1), 53–59. <https://doi.org/10.1021/ar020177t>.
- (6) Rodgers, R. P.; McKenna, A. M. Petroleum Analysis. *Anal. Chem.* **2011**, *83* (12), 4665–4687. <https://doi.org/10.1021/ac201080e>.

- (7) Bae, E.; Na, J.-G.; Chung, S. H.; Kim, H. S.; Kim, S. Identification of about 30 000 Chemical Components in Shale Oils by Electrospray Ionization (ESI) and Atmospheric Pressure Photoionization (APPI) Coupled with 15 T Fourier Transform Ion Cyclotron Resonance Mass Spectrometry (FT-ICR MS) and a Comparison to Conventional Oil. *Energy Fuels* **2010**, *24* (4), 2563–2569. <https://doi.org/10.1021/ef100060b>.
- (8) Gross, J. H. Electron Ionization. In *Mass Spectrometry*; Springer Berlin Heidelberg: Berlin, Heidelberg, 2004; pp 193–222. https://doi.org/10.1007/3-540-36756-X_5.
- (9) Thomson1897.Pdf. <https://www.douglas-scott-mcgregor.com/uploads/1/3/3/5/133545016/thomson1897.pdf> (accessed 2022-11-09).
- (10) Thomson, J. J. XLVII. *On Rays of Positive Electricity. The London, Edinburgh, and Dublin Philosophical Magazine and Journal of Science* **1907**, *13* (77), 561–575. <https://doi.org/10.1080/14786440709463633>.
- (11) Aston, F. W. LXXIV. *A Positive Ray Spectrograph. The London, Edinburgh, and Dublin Philosophical Magazine and Journal of Science* **1919**, *38* (228), 707–714. <https://doi.org/10.1080/14786441208636004>.
- (12) Dempster, A. J. A New Method of Positive Ray Analysis. *Phys. Rev.* **1918**, *11* (4), 316–325. <https://doi.org/10.1103/PhysRev.11.316>.
- (13) Bainbridge, K. T. The Isotopic Weight of H 2. *Phys. Rev.* **1932**, *42* (1), 1–10. <https://doi.org/10.1103/PhysRev.42.1>.
- (14) Wolff, M. M.; Stephens, W. E. A Pulsed Mass Spectrometer with Time Dispersion. *Review of Scientific Instruments* **1953**, *24* (8), 616–617. <https://doi.org/10.1063/1.1770801>.
- (15) Sommer, H.; Thomas, H. A.; Hipple, J. A. The Measurement of e M by Cyclotron Resonance. *Phys. Rev.* **1951**, *82* (5), 697–702. <https://doi.org/10.1103/PhysRev.82.697>.
- (16) Fenn, J. B.; Mann, M.; Meng, C. K.; Wong, S. F.; Whitehouse, C. M. Electrospray Ionization for Mass Spectrometry of Large Biomolecules. *Science* **1989**, *246* (4926), 64–71. <https://doi.org/10.1126/science.2675315>.
- (17) Barber, M.; Bordoli, R. S.; Sedgwick, R. D.; Tyler, A. N. Fast Atom Bombardment of Solids (F.A.B.): A New Ion Source for Mass Spectrometry. *J. Chem. Soc., Chem. Commun.* **1981**, No. 7, 325. <https://doi.org/10.1039/c39810000325>.
- (18) Karas, Michael.; Hillenkamp, Franz. Laser Desorption Ionization of Proteins with Molecular Masses Exceeding 10,000 Daltons. *Anal. Chem.* **1988**, *60* (20), 2299–2301. <https://doi.org/10.1021/ac00171a028>.
- (19) Makarov, A. Electrostatic Axially Harmonic Orbital Trapping: A High-Performance Technique of Mass Analysis. *Anal. Chem.* **2000**, *72* (6), 1156–1162. <https://doi.org/10.1021/ac991131p>.
- (20) Hager, J. W. A New Linear Ion Trap Mass Spectrometer. *Rapid Communications in Mass Spectrometry* **2002**, *16* (6), 512–526. <https://doi.org/10.1002/rcm.607>.
- (21) Dass, C. *Fundamentals of Contemporary Mass Spectrometry*; John Wiley & Sons, 2007.
- (22) Covey, T. R.; Huang, E. C.; Henion, J. D. Structural Characterization of Protein Tryptic Peptides via Liquid Chromatography/Mass Spectrometry and Collision-Induced Dissociation of Their Doubly Charged Molecular Ions. *Anal. Chem.* **1991**, *63* (13), 1193–1200. <https://doi.org/10.1021/ac00013a003>.
- (23) Rodrigues, J. A.; Taylor, A. M.; Sumpton, D. P.; Reynolds, J. C.; Pickford, R.; Thomas-Oates, J. Mass Spectrometry of Carbohydrates: Newer Aspects. In *Advances in Carbohydrate Chemistry and Biochemistry*; Elsevier, 2007; Vol. 61, pp 59–141. [https://doi.org/10.1016/S0065-2318\(07\)61003-8](https://doi.org/10.1016/S0065-2318(07)61003-8).

- (24) Whitehouse, C. M.; Dreyer, R. N.; Yamashita, Masamichi.; Fenn, J. B. Electrospray Interface for Liquid Chromatographs and Mass Spectrometers. *Anal. Chem.* **1985**, *57* (3), 675–679. <https://doi.org/10.1021/ac00280a023>.
- (25) J, Z. On the Conditions of Instability of Liquid Drops, with Applications to the Electrical Discharge from Liquid Point. *Phys. Rev.* **1914**, *3*, 69.
- (26) Pramanik, B. N.; Ganguly, A. K.; Gross, M. L. *Applied Electrospray Mass Spectrometry: Practical Spectroscopy Series Volume 32*; CRC Press, 2002.
- (27) Dole, M.; Mack, L. L.; Hines, R. L.; Mobley, R. C.; Ferguson, L. D.; Alice, M. B. Molecular Beams of Macroions. *The Journal of Chemical Physics* **1968**, *49* (5), 2240–2249. <https://doi.org/10.1063/1.1670391>.
- (28) Fenn, J. B.; Mann, M.; Meng, C. K.; Wong, S. F.; Whitehouse, C. M. Electrospray Ionization for Mass Spectrometry of Large Biomolecules. *Science* **1989**, *246* (4926), 64–71. <https://doi.org/10.1126/science.2675315>.
- (29) Fenn, J. Electrospray Ionization Mass Spectrometry: How It All Began. *J Biomol Tech* **2002**, *13* (3), 101–118.
- (30) Yamashita, M.; Fenn, J. B. *Electrospray ion source. Another variation on the free-jet theme*. ACS Publications. <https://doi.org/10.1021/j150664a002>.
- (31) Hendrickson, C. L.; Emmett, M. R. ELECTROSPRAY IONIZATION FOURIER TRANSFORM ION CYCLOTRON RESONANCE MASS SPECTROMETRY. *Annu. Rev. Phys. Chem.* **1999**, *50* (1), 517–536. <https://doi.org/10.1146/annurev.physchem.50.1.517>.
- (32) Rohner, T. C.; Lion, N.; Girault, H. H. Electrochemical and Theoretical Aspects of Electrospray Ionisation. *Phys. Chem. Chem. Phys.* **2004**, *6* (12), 3056. <https://doi.org/10.1039/b316836k>.
- (33) Disintegration of Water Drops in an Electric Field. 18.
- (34) Konermann, L. A Simple Model for the Disintegration of Highly Charged Solvent Droplets during Electrospray Ionization. *J. Am. Soc. Mass Spectrom.* **2009**, *20* (3), 496–506. <https://doi.org/10.1016/j.jasms.2008.11.007>.
- (35) Ahadi, E.; Konermann, L. Surface Charge of Electrosprayed Water Nanodroplets: A Molecular Dynamics Study. *J. Am. Chem. Soc.* **2010**, *132* (32), 11270–11277. <https://doi.org/10.1021/ja1041989>.
- (36) Konermann, L.; Rodriguez, A. D.; Liu, J. On the Formation of Highly Charged Gaseous Ions from Unfolded Proteins by Electrospray Ionization. *Anal. Chem.* **2012**, *84* (15), 6798–6804. <https://doi.org/10.1021/ac301298g>.
- (37) Konermann, L.; Ahadi, E.; Rodriguez, A. D.; Vahidi, S. Unraveling the Mechanism of Electrospray Ionization. *Anal. Chem.* **2013**, *85* (1), 2–9. <https://doi.org/10.1021/ac302789c>.
- (38) Iribarne, J. V. On the Evaporation of Small Ions from Charged Droplets. *J. Chem. Phys.* **1976**, *64* (6), 2287. <https://doi.org/10.1063/1.432536>.
- (39) Cole, R. B. Some Tenets Pertaining to Electrospray Ionization Mass Spectrometry. *Journal of Mass Spectrometry* **2000**, *35* (7), 763–772. [https://doi.org/10.1002/1096-9888\(200007\)35:7<763::AID-JMS16>3.0.CO;2-#](https://doi.org/10.1002/1096-9888(200007)35:7<763::AID-JMS16>3.0.CO;2-#).
- (40) *nano-ElectroSpray Ionization (ESI) FossilonTech*. The nano-electrospray company. <https://www.fossilontech.com/nano-esi> (accessed 2022-10-31).
- (41) Hertzog, J.; Carré, V.; Le Brech, Y.; Mackay, C. L.; Dufour, A.; Mašek, O.; Aubriet, F. Combination of Electrospray Ionization, Atmospheric Pressure Photoionization and Laser Desorption Ionization Fourier Transform Ion Cyclotronic Resonance Mass Spectrometry

- for the Investigation of Complex Mixtures – Application to the Petroleomic Analysis of Bio-Oils. *Analytica Chimica Acta* **2017**, *969*, 26–34. <https://doi.org/10.1016/j.aca.2017.03.022>.
- (42) Mase, C.; Hubert-Roux, M.; Afonso, C.; Giusti, P. Contribution of Atmospheric Pressure Chemical Ionization Mass Spectrometry for the Characterization of Bio-Oils from Lignocellulosic Biomass: Comparison with Electrospray Ionization and Atmospheric Pressure Photoionization. *Journal of Analytical and Applied Pyrolysis* **2022**, *167*, 105694. <https://doi.org/10.1016/j.jaap.2022.105694>.
- (43) Perez Hurtado, P.; Lam, P. Y.; Kilgour, D.; Bristow, A.; McBride, E.; O'Connor, P. B. Use of High Resolution Mass Spectrometry for Analysis of Polymeric Excipients in Drug Delivery Formulations. *Anal. Chem.* **2012**, *84* (20), 8579–8586. <https://doi.org/10.1021/ac301576h>.
- (44) Loo, J. A. Studying Noncovalent Protein Complexes by Electrospray Ionization Mass Spectrometry. *Mass Spectrometry Reviews* **1997**, *16* (1), 1–23. [https://doi.org/10.1002/\(SICI\)1098-2787\(1997\)16:1<1::AID-MAS1>3.0.CO;2-L](https://doi.org/10.1002/(SICI)1098-2787(1997)16:1<1::AID-MAS1>3.0.CO;2-L).
- (45) Chen, Ruidan.; Cheng, Xueheng.; Mitchell, D. W.; Hofstadler, S. A.; Wu, Qinyuan.; Rockwood, A. L.; Sherman, M. G.; Smith, R. D. Trapping, Detection, and Mass Determination of Coliphage T4 DNA Ions by Electrospray Ionization Fourier Transform Ion Cyclotron Resonance Mass Spectrometry. *Anal. Chem.* **1995**, *67* (7), 1159–1163. <https://doi.org/10.1021/ac00103a004>.
- (46) Wilm, M. Principles of Electrospray Ionization. *Molecular & Cellular Proteomics* **2011**, *10* (7), M111.009407. <https://doi.org/10.1074/mcp.M111.009407>.
- (47) Charles, L.; Pépin, D. Electrospray Ion Chromatography–Tandem Mass Spectrometry of Oxyhalides at Sub-Ppb Levels. *Anal. Chem.* **1998**, *70* (2), 353–359. <https://doi.org/10.1021/ac9707186>.
- (48) Gross, J. H. *Mass Spectrometry: A Textbook*; Springer Science & Business Media, 2006.
- (49) Schmidt, A.; Karas, M.; Dülcks, T. Effect of Different Solution Flow Rates on Analyte Ion Signals in Nano-ESI MS, or: When Does ESI Turn into Nano-ESI? *J. Am. Soc. Mass Spectrom.* **2003**, *14* (5), 492–500. [https://doi.org/10.1016/S1044-0305\(03\)00128-4](https://doi.org/10.1016/S1044-0305(03)00128-4).
- (50) Karas, M.; Bahr, U.; Dülcks, T. Nano-Electrospray Ionization Mass Spectrometry: Addressing Analytical Problems beyond Routine. *Fresenius' Journal of Analytical Chemistry* **2000**, *366* (6–7), 669–676. <https://doi.org/10.1007/s002160051561>.
- (51) Wilm, M.; Mann, M. Analytical Properties of the Nanoelectrospray Ion Source. *Anal. Chem.* **1996**, *68* (1), 1–8. <https://doi.org/10.1021/ac9509519>.
- (52) Rahman, M. M.; Chingin, K. Stable and Reproducible Nano-Electrospray Ionization of Aqueous Solutions and Untreated Biological Samples Using Ion Current Limitation Combined with Polarity Reversing. *Anal. Methods* **2019**, *11* (2), 205–212. <https://doi.org/10.1039/C8AY02159G>.
- (53) Gibson, G. T. T.; Mugo, S. M.; Oleschuk, R. D. Nanoelectrospray Emitters: Trends and Perspective. *Mass Spectrometry Reviews* **2009**, *28* (6), 918–936. <https://doi.org/10.1002/mas.20248>.
- (54) Olcese, R.; Carré, V.; Aubriet, F.; Dufour, A. Selectivity of Bio-Oils Catalytic Hydrotreatment Assessed by Petroleomic and GC*GC/MS-FID Analysis. *Energy Fuels* **2013**, *27* (4), 2135–2145. <https://doi.org/10.1021/ef302145g>.
- (55) Hertzog, J.; Carré, V.; Aubriet, F. Contribution of Fourier Transform Mass Spectrometry to Bio-Oil Study. In *Fundamentals and Applications of Fourier Transform Mass*

- Spectrometry*; Elsevier, 2019; pp 679–733. <https://doi.org/10.1016/B978-0-12-814013-0.00022-3>.
- (56) Hertzog, J.; Carré, V.; Le Brech, Y.; Mackay, C. L.; Dufour, A.; Mašek, O.; Aubriet, F. Combination of Electrospray Ionization, Atmospheric Pressure Photoionization and Laser Desorption Ionization Fourier Transform Ion Cyclotron Resonance Mass Spectrometry for the Investigation of Complex Mixtures – Application to the Petroleomic Analysis of Bio-Oils. *Analytica Chimica Acta* **2017**, *969*, 26–34. <https://doi.org/10.1016/j.aca.2017.03.022>.
- (57) Robb, D. B.; Covey, T. R.; Bruins, A. P. Atmospheric Pressure Photoionization: An Ionization Method for Liquid Chromatography–Mass Spectrometry. *Anal. Chem.* **2000**, *72* (15), 3653–3659. <https://doi.org/10.1021/ac0001636>.
- (58) Raffaelli, A.; Saba, A. Atmospheric Pressure Photoionization Mass Spectrometry. *Mass Spectrometry Reviews* **2003**, *22* (5), 318–331. <https://doi.org/10.1002/mas.10060>.
- (59) Ng, C.-Y. V. ACUUM U LTRAVIOLET S PECTROSCOPY AND C HEMISTRY BY P HOTOIONIZATION AND P HOTOELECTRON M ETHODS. *Annu. Rev. Phys. Chem.* **2002**, *53* (1), 101–140. <https://doi.org/10.1146/annurev.physchem.53.082001.144416>.
- (60) Song, L.; Dykstra, A. B.; Yao, H.; Bartmess, J. E. Ionization Mechanism of Negative Ion-Direct Analysis in Real Time: A Comparative Study with Negative Ion-Atmospheric Pressure Photoionization. *J. Am. Soc. Mass Spectrom.* **2009**, *20* (1), 42–50. <https://doi.org/10.1016/j.jasms.2008.09.016>.
- (61) Kauppila, T. J.; Kersten, H.; Benter, T. The Ionization Mechanisms in Direct and Dopant-Assisted Atmospheric Pressure Photoionization and Atmospheric Pressure Laser Ionization. *J. Am. Soc. Mass Spectrom.* **2014**, *25* (11), 1870–1881. <https://doi.org/10.1007/s13361-014-0988-7>.
- (62) Ahmed, A.; Choi, C. H.; Kim, S. Mechanistic Study on Lowering the Sensitivity of Positive Atmospheric Pressure Photoionization Mass Spectrometric Analyses: Size-Dependent Reactivity of Solvent Clusters. *Rapid Communications in Mass Spectrometry* **2015**, *29* (21), 2095–2101. <https://doi.org/10.1002/rcm.7373>.
- (63) Sioud, S.; Kharbatia, N.; Amad, M. H.; Zhu, Z.; Cabanetos, C.; Lesimple, A.; Beaujuge, P. The Formation of [M–H]⁺ Ions in N-Alkyl-Substituted Thieno[3,4-c]-Pyrrole-4,6-Dione Derivatives during Atmospheric Pressure Photoionization Mass Spectrometry. *Rapid Communications in Mass Spectrometry* **2014**, *28* (22), 2389–2397. <https://doi.org/10.1002/rcm.7031>.
- (64) Kauppila, T. J.; Kuuranne, T.; Meurer, E. C.; Eberlin, M. N.; Kotiaho, T.; Kostianen, R. Atmospheric Pressure Photoionization Mass Spectrometry. Ionization Mechanism and the Effect of Solvent on the Ionization of Naphthalenes. *Anal. Chem.* **2002**, *74* (21), 5470–5479. <https://doi.org/10.1021/ac025659x>.
- (65) Kauppila, T. J.; Kostianen, R.; Bruins, A. P. Anisole, a New Dopant for Atmospheric Pressure Photoionization Mass Spectrometry of Low Proton Affinity, Low Ionization Energy Compounds. *Rapid Communications in Mass Spectrometry* **2004**, *18* (7), 808–815. <https://doi.org/10.1002/rcm.1408>.
- (66) Kauppila, T. J.; Kotiaho, T.; Kostianen, R.; Bruins, A. P. Negative Ion-Atmospheric Pressure Photoionization-Mass Spectrometry. *J. Am. Soc. Mass Spectrom.* **2004**, *15* (2), 203–211. <https://doi.org/10.1016/j.jasms.2003.10.012>.

- (67) Fredenhagen, A.; Kühnöl, J. Evaluation of the Optimization Space for Atmospheric Pressure Photoionization (APPI) in Comparison with APCI. *Journal of Mass Spectrometry* **2014**, *49* (8), 727–736. <https://doi.org/10.1002/jms.3401>.
- (68) Horning, E. C.; Horning, M. G.; Carroll, D. I.; Dzidic, I.; Stillwell, R. N. New Picogram Detection System Based on a Mass Spectrometer with an External Ionization Source at Atmospheric Pressure. *Anal. Chem.* **1973**, *45* (6), 936–943. <https://doi.org/10.1021/ac60328a035>.
- (69) Horning, E. C.; Carroll, D. I.; Dzidic, I.; Haegele, K. D.; Horning, M. G.; Stillwell, R. N. Atmospheric Pressure Ionization (API) Mass Spectrometry. Solvent-Mediated Ionization of Samples Introduced in Solution and in a Liquid Chromatograph Effluent Stream. *Journal of Chromatographic Science* **1974**, *12* (11), 725–729. <https://doi.org/10.1093/chromsci/12.11.725>.
- (70) Collins, D.; Lee, M. Developments in Ion Mobility Spectrometry-Mass Spectrometry. *Analytical and bioanalytical chemistry* **2002**, *372*, 66–73. <https://doi.org/10.1007/s00216-001-1195-5>.
- (71) Carroll, D. I.; Dzidic, I.; Stillwell, R. N.; Haegele, K. D.; Horning, E. C. Atmospheric Pressure Ionization Mass Spectrometry. Corona Discharge Ion Source for Use in a Liquid Chromatograph-Mass Spectrometer-Computer Analytical System. *Anal. Chem.* **1975**, *47* (14), 2369–2373. <https://doi.org/10.1021/ac60364a031>.
- (72) Dzidic, I.; Carroll, D. I.; Stillwell, R. N.; Horning, E. C. Comparison of Positive Ions Formed in Nickel-63 and Corona Discharge Ion Sources Using Nitrogen, Argon, Isobutane, Ammonia and Nitric Oxide as Reagents in Atmospheric Pressure Ionization Mass Spectrometry. *Anal. Chem.* **1976**, *48* (12), 1763–1768. <https://doi.org/10.1021/ac50006a035>.
- (73) Niessen, W. M. A.; Tinke, A. P. Liquid Chromatography-Mass Spectrometry General Principles and Instrumentation. *Journal of Chromatography A* **1995**, *703* (1–2), 37–57. [https://doi.org/10.1016/0021-9673\(94\)01198-N](https://doi.org/10.1016/0021-9673(94)01198-N).
- (74) *Interfaces for LCMS*. https://www.shimadzu.co.kr/service-support/technical-support/analysis-basics/fundamental/interfaces_for_lcms.html (accessed 2022-11-07).
- (75) Warscheid, B.; Hoffmann, T. Structural Elucidation of Monoterpene Oxidation Products by Ion Trap Fragmentation Using On-Line Atmospheric Pressure Chemical Ionisation Mass Spectrometry in the Negative Ion Mode. *Rapid Communications in Mass Spectrometry* **2001**, *15* (23), 2259–2272. <https://doi.org/10.1002/rcm.504>.
- (76) Klee, S.; Derpmann, V.; Wißdorf, W.; Klotowski, S.; Kersten, H.; Brockmann, K. J.; Benter, T.; Albrecht, S.; Bruins, A. P.; Dusty, F.; Kauppila, T. J.; Kostianen, R.; O'Brien, R.; Robb, D. B.; Syage, J. A. Are Clusters Important in Understanding the Mechanisms in Atmospheric Pressure Ionization? Part 1: Reagent Ion Generation and Chemical Control of Ion Populations. *J. Am. Soc. Mass Spectrom.* **2014**, *25* (8), 1310–1321. <https://doi.org/10.1007/s13361-014-0891-2>.
- (77) Derpmann, V.; Albrecht, S.; Benter, T. The Role of Ion-Bound Cluster Formation in Negative Ion Mass Spectrometry. *Rapid Communications in Mass Spectrometry* **2012**, *26* (17), 1923–1933. <https://doi.org/10.1002/rcm.6303>.
- (78) Portolés, T.; Mol, J. G. J.; Sancho, J. V.; Hernández, F. Advantages of Atmospheric Pressure Chemical Ionization in Gas Chromatography Tandem Mass Spectrometry: Pyrethroid Insecticides as a Case Study. *Anal. Chem.* **2012**, *84* (22), 9802–9810. <https://doi.org/10.1021/ac301699c>.

- (79) Lawrence, E. O.; Livingston, M. S. The Production of High Speed Light Ions Without the Use of High Voltages. *Phys. Rev.* **1932**, *40* (1), 19–35. <https://doi.org/10.1103/PhysRev.40.19>.
- (80) Comisarow, M. B.; Marshall, A. G. The Early Development of Fourier Transform Ion Cyclotron Resonance (FT-ICR) Spectroscopy. *Journal of Mass Spectrometry* **1996**, *31* (6), 581–585. [https://doi.org/10.1002/\(SICI\)1096-9888\(199606\)31:6<581::AID-JMS369>3.0.CO;2-1](https://doi.org/10.1002/(SICI)1096-9888(199606)31:6<581::AID-JMS369>3.0.CO;2-1).
- (81) Smith, L. G. A New Magnetic Period Mass Spectrometer. *Review of Scientific Instruments* **1951**, *22* (2), 115–116. <https://doi.org/10.1063/1.1745849>.
- (82) Baldeschwieler, J. D. Ion Cyclotron Resonance Spectroscopy: Cyclotron Double Resonance Provides a New Technique for the Study of Ion-Molecule Reaction Mechanisms. *Science* **1968**, *159* (3812), 263–273. <https://doi.org/10.1126/science.159.3812.263>.
- (83) Comisarow, M. B.; Marshall, A. G. Frequency-Sweep Fourier Transform Ion Cyclotron Resonance Spectroscopy. *Chemical Physics Letters* **1974**, *26* (4), 489–490. [https://doi.org/10.1016/0009-2614\(74\)80397-0](https://doi.org/10.1016/0009-2614(74)80397-0).
- (84) Comisarow, M. B.; Marshall, A. G. Fourier Transform Ion Cyclotron Resonance Spectroscopy. *Chemical Physics Letters* **1974**, *25* (2), 282–283. [https://doi.org/10.1016/0009-2614\(74\)89137-2](https://doi.org/10.1016/0009-2614(74)89137-2).
- (85) Ball, A. T.; Prakash, A. S.; Bristow, A. W. T.; Sims, M.; Mosely, J. A. Characterisation of Phosphorylated Nucleotides by Collisional and Electron-Based Tandem Mass Spectrometry. *Rapid Communications in Mass Spectrometry* **2016**, *30* (19), 2155–2163. <https://doi.org/10.1002/rcm.7701>.
- (86) Smith, D. F.; Kiss, A.; Leach, F. E.; Robinson, E. W.; Paša-Tolić, L.; Heeren, R. M. A. High Mass Accuracy and High Mass Resolving Power FT-ICR Secondary Ion Mass Spectrometry for Biological Tissue Imaging. *Anal Bioanal Chem* **2013**, *405* (18), 6069–6076. <https://doi.org/10.1007/s00216-013-7048-1>.
- (87) Lozano, D. C. P.; Gavard, R.; P. Arenas-Diaz, J.; J. Thomas, M.; D. Stranz, D.; Mejía-Ospino, E.; Guzman, A.; F. Spencer, S. E.; Rossell, D.; P. Barrow, M. Pushing the Analytical Limits: New Insights into Complex Mixtures Using Mass Spectra Segments of Constant Ultrahigh Resolving Power. *Chemical Science* **2019**, *10* (29), 6966–6978. <https://doi.org/10.1039/C9SC02903F>.
- (88) Rodgers, R. P.; Marshall, A. G. Petroleomics: Advanced Characterization of Petroleum-Derived Materials by Fourier Transform Ion Cyclotron Resonance Mass Spectrometry (FT-ICR MS). In *Asphaltenes, Heavy Oils, and Petroleomics*; Mullins, O. C., Sheu, E. Y., Hammami, A., Marshall, A. G., Eds.; Springer New York: New York, NY, 2007; pp 63–93. https://doi.org/10.1007/0-387-68903-6_3.
- (89) Amster, I. J. Fourier Transform Mass Spectrometry. *Journal of Mass Spectrometry* **1996**, *31* (12), 1325–1337. [https://doi.org/10.1002/\(SICI\)1096-9888\(199612\)31:12<1325::AID-JMS453>3.0.CO;2-W](https://doi.org/10.1002/(SICI)1096-9888(199612)31:12<1325::AID-JMS453>3.0.CO;2-W).
- (90) Dienes, T.; Pastor, S. J.; Schürch, S.; Scott, J. R.; Yao, J.; Cui, S.; Wilkins, C. L. Fourier Transform Mass Spectrometry—Advancing Years (1992–Mid. 1996). *Mass Spectrometry Reviews* **1996**, *15* (3), 163–211. [https://doi.org/10.1002/\(SICI\)1098-2787\(1996\)15:3<163::AID-MAS2>3.0.CO;2-G](https://doi.org/10.1002/(SICI)1098-2787(1996)15:3<163::AID-MAS2>3.0.CO;2-G).

- (91) Marshall, A. G. Milestones in Fourier Transform Ion Cyclotron Resonance Mass Spectrometry Technique Development. *International Journal of Mass Spectrometry* **2000**, *200* (1–3), 331–356. [https://doi.org/10.1016/S1387-3806\(00\)00324-9](https://doi.org/10.1016/S1387-3806(00)00324-9).
- (92) Smith, R. D. Evolution of Esi–Mass Spectrometry and Fourier Transform Ion Cyclotron Resonance for Proteomics and Other Biological Applications. *International Journal of Mass Spectrometry* **2000**, *200* (1–3), 509–544. [https://doi.org/10.1016/S1387-3806\(00\)00352-3](https://doi.org/10.1016/S1387-3806(00)00352-3).
- (93) Schaub, T. M.; Hendrickson, C. L.; Horning, S.; Quinn, J. P.; Senko, M. W.; Marshall, A. G. High-Performance Mass Spectrometry: Fourier Transform Ion Cyclotron Resonance at 14.5 Tesla. *Anal. Chem.* **2008**, *80* (11), 3985–3990. <https://doi.org/10.1021/ac800386h>.
- (94) Marshall, A. G.; Hendrickson, C. L. Fourier Transform Ion Cyclotron Resonance Detection: Principles and Experimental Configurations. *International Journal of Mass Spectrometry* **2002**, *215* (1–3), 59–75. [https://doi.org/10.1016/S1387-3806\(01\)00588-7](https://doi.org/10.1016/S1387-3806(01)00588-7).
- (95) Marshall, A. G.; Hendrickson, C. L.; Jackson, G. S. Fourier Transform Ion Cyclotron Resonance Mass Spectrometry: A Primer. *Mass Spectrometry Reviews* **1998**, *17* (1), 1–35. [https://doi.org/10.1002/\(SICI\)1098-2787\(1998\)17:1<1::AID-MAS1>3.0.CO;2-K](https://doi.org/10.1002/(SICI)1098-2787(1998)17:1<1::AID-MAS1>3.0.CO;2-K).
- (96) Nikolaev, E. N.; Kostyukevich, Y. I.; Vladimirov, G. N. Fourier Transform Ion Cyclotron Resonance (FT ICR) Mass Spectrometry: Theory and Simulations. *Mass Spectrometry Reviews* **2016**, *35* (2), 219–258. <https://doi.org/10.1002/mas.21422>.
- (97) Hendrickson, C. L.; Quinn, J. P.; Kaiser, N. K.; Smith, D. F.; Blakney, G. T.; Chen, T.; Marshall, A. G.; Weisbrod, C. R.; Beu, S. C. 21 Tesla Fourier Transform Ion Cyclotron Resonance Mass Spectrometer: A National Resource for Ultrahigh Resolution Mass Analysis. *J. Am. Soc. Mass Spectrom.* **2015**, *26* (9), 1626–1632. <https://doi.org/10.1007/s13361-015-1182-2>.
- (98) Marshall, A. G.; Chen, T. 40 Years of Fourier Transform Ion Cyclotron Resonance Mass Spectrometry. *International Journal of Mass Spectrometry* **2015**, *377*, 410–420. <https://doi.org/10.1016/j.ijms.2014.06.034>.
- (99) White, F. M.; Marto, J. A.; Marshall, A. G. An External Source 7 T Fourier Transform Ion Cyclotron Resonance Mass Spectrometer with Electrostatic Ion Guide. *Rapid Communications in Mass Spectrometry* **1996**, *10* (14), 1845–1849. [https://doi.org/10.1002/\(SICI\)1097-0231\(199611\)10:14<1845::AID-RCM749>3.0.CO;2-#](https://doi.org/10.1002/(SICI)1097-0231(199611)10:14<1845::AID-RCM749>3.0.CO;2-#).
- (100) He, F.; Hendrickson, C. L.; Marshall, A. G. Baseline Mass Resolution of Peptide Isobars: A Record for Molecular Mass Resolution. *Anal. Chem.* **2001**, *73* (3), 647–650. <https://doi.org/10.1021/ac000973h>.
- (101) Bossio, R. E.; Marshall, A. G. Baseline Resolution of Isobaric Phosphorylated and Sulfated Peptides and Nucleotides by Electrospray Ionization FTICR MS: Another Step toward Mass Spectrometry-Based Proteomics. *Anal. Chem.* **2002**, *74* (7), 1674–1679. <https://doi.org/10.1021/ac0108461>.
- (102) Smith, R. D. Evolution of Esi–Mass Spectrometry and Fourier Transform Ion Cyclotron Resonance for Proteomics and Other Biological Applications. *International Journal of Mass Spectrometry* **2000**, *200* (1–3), 509–544. [https://doi.org/10.1016/S1387-3806\(00\)00352-3](https://doi.org/10.1016/S1387-3806(00)00352-3).
- (103) Nikolaev, E. N.; Jertz, R.; Grigoryev, A.; Baykut, G. Fine Structure in Isotopic Peak Distributions Measured Using a Dynamically Harmonized Fourier Transform Ion

- Cyclotron Resonance Cell at 7 T. *Anal. Chem.* **2012**, *84* (5), 2275–2283. <https://doi.org/10.1021/ac202804f>.
- (104) Boldin, I. A.; Nikolaev, E. N. Fourier Transform Ion Cyclotron Resonance Cell with Dynamic Harmonization of the Electric Field in the Whole Volume by Shaping of the Excitation and Detection Electrode Assembly. *Rapid Communications in Mass Spectrometry* **2011**, *25* (1), 122–126. <https://doi.org/10.1002/rcm.4838>.
- (105) Marshall, A. G.; Hendrickson, C. L. Fourier Transform Ion Cyclotron Resonance Detection: Principles and Experimental Configurations. *International Journal of Mass Spectrometry* **2002**, *215* (1–3), 59–75. [https://doi.org/10.1016/S1387-3806\(01\)00588-7](https://doi.org/10.1016/S1387-3806(01)00588-7).
- (106) Marshall, A. G.; Grosshans, P. B. FOURIER TRANSFORM ION CYCLOTRON RESONANCE MASS SPECTROMETRY: THE TEENAGE YEARS. *Anal. Chem.* **1991**, *63* (4), 215A–229A. <https://doi.org/10.1021/ac00004a713>.
- (107) Amster, I. J. Fourier Transform Mass Spectrometry. *Journal of Mass Spectrometry* **1996**, *31* (12), 1325–1337. [https://doi.org/10.1002/\(SICI\)1096-9888\(199612\)31:12<1325::AID-JMS453>3.0.CO;2-W](https://doi.org/10.1002/(SICI)1096-9888(199612)31:12<1325::AID-JMS453>3.0.CO;2-W).
- (108) Dienes, T.; Pastor, S. J.; Schürch, S.; Scott, J. R.; Yao, J.; Cui, S.; Wilkins, C. L. Fourier Transform Mass Spectrometry—Advancing Years (1992–Mid. 1996). *Mass Spectrometry Reviews* **1996**, *15* (3), 163–211. [https://doi.org/10.1002/\(SICI\)1098-2787\(1996\)15:3<163::AID-MAS2>3.0.CO;2-G](https://doi.org/10.1002/(SICI)1098-2787(1996)15:3<163::AID-MAS2>3.0.CO;2-G).
- (109) Schaub, T. M.; Hendrickson, C. L.; Horning, S.; Quinn, J. P.; Senko, M. W.; Marshall, A. G. High-Performance Mass Spectrometry: Fourier Transform Ion Cyclotron Resonance at 14.5 Tesla. *Anal. Chem.* **2008**, *80* (11), 3985–3990. <https://doi.org/10.1021/ac800386h>.
- (110) Marshall, A. G. Milestones in Fourier Transform Ion Cyclotron Resonance Mass Spectrometry Technique Development. *International Journal of Mass Spectrometry* **2000**, *200* (1–3), 331–356. [https://doi.org/10.1016/S1387-3806\(00\)00324-9](https://doi.org/10.1016/S1387-3806(00)00324-9).
- (111) MARSHALL, A. G.; HENDRICKSON, C. L.; SHI, S. D.-H. Scaling MS Plateaus with High-Resolution FT-ICRMS. *Anal. Chem. (Wash. DC)* **2002**, *74* (9), 252A–259A.
- (112) Nikolaev, E. N. Some Notes about FT ICR Mass Spectrometry. *International Journal of Mass Spectrometry* **2015**, *377*, 421–431. <https://doi.org/10.1016/j.ijms.2014.07.051>.
- (113) Popov, I.; Nagornov, K.; Vladimirov, G.; Kostyukevich, Y.; Nikolaev, E. (Eugene). Twelve Million Resolving Power on 4.7 T Fourier Transform Ion Cyclotron Resonance Instrument with Dynamically Harmonized Cell-Observation of Fine Structure in Peptide Mass Spectra. *Journal of the American Society for Mass Spectrometry* **2014**, *25*. <https://doi.org/10.1007/s13361-014-0846-7>.
- (114) Marshall, A. G.; Roe, D. C. Theory of Fourier Transform Ion Cyclotron Resonance Mass Spectroscopy: Response to Frequency-sweep Excitation. *The Journal of Chemical Physics* **1980**, *73* (4), 1581–1590. <https://doi.org/10.1063/1.440338>.
- (115) Marshall, A. G.; Wang, T. C. L.; Ricca, T. L. Tailored Excitation for Fourier Transform Ion Cyclotron Mass Spectrometry. *J. Am. Chem. Soc.* **1985**, *107* (26), 7893–7897. <https://doi.org/10.1021/ja00312a015>.
- (116) Guan, S.; Marshall, A. G. Stored Waveform Inverse Fourier Transform (SWIFT) Ion Excitation in Trapped-Ion Mass Spectrometry: Theory and Applications. *International Journal of Mass Spectrometry and Ion Processes* **1996**, *157–158*, 5–37. [https://doi.org/10.1016/S0168-1176\(96\)04461-8](https://doi.org/10.1016/S0168-1176(96)04461-8).
- (117) Walk, T. B.; Trautwein, A. W.; Richter, H.; Jung, G. ESI Fourier Transform Ion Cyclotron Resonance Mass Spectrometry (ESI-FT-ICR-MS): A Rapid High-Resolution Analytical

- Method for Combinatorial Compound Libraries. *Angewandte Chemie International Edition* **1999**, *38* (12), 1763–1765. [https://doi.org/10.1002/\(SICI\)1521-3773\(19990614\)38:12<1763::AID-ANIE1763>3.0.CO;2-#](https://doi.org/10.1002/(SICI)1521-3773(19990614)38:12<1763::AID-ANIE1763>3.0.CO;2-#).
- (118) Pitsenberger, C. C.; Easterling, M. L.; Amster, I. J. Efficient Ion Remeasurement Using Broadband Quadrupolar Excitation FTICR Mass Spectrometry. *Anal. Chem.* **1996**, *68* (21), 3732–3739. <https://doi.org/10.1021/ac960532r>.
- (119) Marshall, A. G.; Verdun, F. R. *Fourier Transforms in NMR, Optical, and Mass Spectrometry: A User's Handbook*; Elsevier, 2016.
- (120) Goodner, K. L.; Milgram, K. E.; Williams, K. R.; Watson, C. H.; Eyler, J. R. Quantitation of Ion Abundances in Fourier Transform Ion Cyclotron Resonance Mass Spectrometry. *J. Am. Soc. Mass Spectrom.* **1998**, *9* (11), 1204–1212. [https://doi.org/10.1016/S1044-0305\(98\)00090-7](https://doi.org/10.1016/S1044-0305(98)00090-7).
- (121) Comisarow, M. B.; Melka, J. D. Error Estimates for Finite Zero-Filling in Fourier Transform Spectrometry. *Anal. Chem.* **1979**, *51* (13), 2198–2203. <https://doi.org/10.1021/ac50049a032>.
- (122) Nikolaev, E.; Lioznov, A. Evaluation of Major Historical ICR Cell Designs Using Electric Field Simulations. *Mass Spectrometry Reviews* **2022**, *41* (2), 262–283. <https://doi.org/10.1002/mas.21671>.
- (123) Nikolaev, E. N.; Kostyukevich, Y. I.; Vladimirov, G. N. Fourier Transform Ion Cyclotron Resonance (FT ICR) Mass Spectrometry: Theory and Simulations. *Mass Spectrometry Reviews* **2016**, *35* (2), 219–258. <https://doi.org/10.1002/mas.21422>.
- (124) Huang, Y.; Li, G.-Z.; Guan, S.; Marshall, A. G. A Combined Linear Ion Trap for Mass Spectrometry. *J. Am. Soc. Mass Spectrom.* **1997**, *8* (9), 962–969. [https://doi.org/10.1016/S1044-0305\(97\)82945-5](https://doi.org/10.1016/S1044-0305(97)82945-5).
- (125) Boldin, I. A.; Nikolaev, E. N. Fourier Transform Ion Cyclotron Resonance Cell with Dynamic Harmonization of the Electric Field in the Whole Volume by Shaping of the Excitation and Detection Electrode Assembly. *Rapid Communications in Mass Spectrometry* **2011**, *25* (1), 122–126. <https://doi.org/10.1002/rcm.4838>.
- (126) Nikolaev, E. N.; Boldin, I. A.; Jertz, R.; Baykut, G. Initial Experimental Characterization of a New Ultra-High Resolution FTICR Cell with Dynamic Harmonization. *J. Am. Soc. Mass Spectrom.* **2011**, *22* (7), 1125–1133. <https://doi.org/10.1007/s13361-011-0125-9>.
- (127) Kostyukevich, Y. I.; Vladimirov, G. N.; Nikolaev, E. N. Dynamically Harmonized FT-ICR Cell with Specially Shaped Electrodes for Compensation of Inhomogeneity of the Magnetic Field. Computer Simulations of the Electric Field and Ion Motion Dynamics. *J. Am. Soc. Mass Spectrom.* **2012**, *23* (12), 2198–2207. <https://doi.org/10.1007/s13361-012-0480-1>.
- (128) *De novo sequencing, peptide composition analysis, and composition-based sequencing: a new strategy employing accurate mass determination by fourier transform ion cyclotron resonance mass spectrometry* - ScienceDirect. <https://www.sciencedirect.com/science/article/pii/S104403050400073X> (accessed 2022-11-08).
- (129) Bristow, A. W. T. Accurate Mass Measurement for the Determination of Elemental Formula—A Tutorial. *Mass Spectrometry Reviews* **2006**, *25* (1), 99–111. <https://doi.org/10.1002/mas.20058>.
- (130) Moini, M.; Jones, B. L.; Rogers, R. M.; Jiang, L. Sodium Trifluoroacetate as a Tune/Calibration Compound for Positive- and Negative-Ion Electrospray Ionization Mass

- Spectrometry in the Mass Range of 100–4000 Da. *Journal of the American Society for Mass Spectrometry* **1998**, *9* (9), 977.
- (131) Ledford, E. B.; Rempel, D. L.; Gross, M. L. Space Charge Effects in Fourier Transform Mass Spectrometry. II. Mass Calibration. *Anal. Chem.* **1984**, *56* (14), 2744–2748. <https://doi.org/10.1021/ac00278a027>.
- (132) Lozano, D. C. P.; E. Jones, H.; Reina, T. R.; Volpe, R.; P. Barrow, M. Unlocking the Potential of Biofuels via Reaction Pathways in van Krevelen Diagrams. *Green Chemistry* **2021**, *23* (22), 8949–8963. <https://doi.org/10.1039/D1GC01796A>.
- (133) Reinhardt, A.; Emmenegger, C.; Gerrits, B.; Panse, C.; Dommen, J.; Baltensperger, U.; Zenobi, R.; Kalberer, M. Ultrahigh Mass Resolution and Accurate Mass Measurements as a Tool To Characterize Oligomers in Secondary Organic Aerosols. *Anal. Chem.* **2007**, *79* (11), 4074–4082. <https://doi.org/10.1021/ac062425v>.
- (134) Kim, S.; Kramer, R. W.; Hatcher, P. G. Graphical Method for Analysis of Ultrahigh-Resolution Broadband Mass Spectra of Natural Organic Matter, the Van Krevelen Diagram. *Anal. Chem.* **2003**, *75* (20), 5336–5344. <https://doi.org/10.1021/ac034415p>.
- (135) McLafferty, F. W. Tandem Mass Spectrometry: From Infancy to Maturity in Twenty-Five Years. *Organic Mass Spectrometry* **1993**, *28* (12), 1403–1406. <https://doi.org/10.1002/oms.1210281208>.
- (136) de Hoffmann, E. Tandem Mass Spectrometry: A Primer. *Journal of Mass Spectrometry* **1996**, *31* (2), 129–137. [https://doi.org/10.1002/\(SICI\)1096-9888\(199602\)31:2<129::AID-JMS305>3.0.CO;2-T](https://doi.org/10.1002/(SICI)1096-9888(199602)31:2<129::AID-JMS305>3.0.CO;2-T).
- (137) Bayat, P.; Lesage, D.; Cole, R. B. TUTORIAL: ION ACTIVATION IN TANDEM MASS SPECTROMETRY USING ULTRA-HIGH RESOLUTION INSTRUMENTATION. *Mass Spec Rev* **2020**, *39* (5–6), 680–702. <https://doi.org/10.1002/mas.21623>.
- (138) Zhurov, K.; Fornelli, L.; Wodrich, M.; Laskay, U.; Tsybin, Y. ChemInform Abstract: Principles of Electron Capture and Transfer Dissociation Mass Spectrometry Applied to Peptide and Protein Structure Analysis. *Chemical Society reviews* **2013**, *42*. <https://doi.org/10.1039/c3cs35477f>.
- (139) Cooper, H. J.; Håkansson, K.; Marshall, A. G. The Role of Electron Capture Dissociation in Biomolecular Analysis. *Mass Spectrometry Reviews* **2005**, *24* (2), 201–222. <https://doi.org/10.1002/mas.20014>.
- (140) Zhang, H.; Cui, W.; Wen, J.; Blankenship, R. E.; Gross, M. L. Native Electrospray and Electron-Capture Dissociation in FTICR Mass Spectrometry Provide Top-down Sequencing of a Protein Component in an Intact Protein Assembly. *J. Am. Soc. Mass Spectrom.* **2010**, *21* (12), 1966–1968. <https://doi.org/10.1016/j.jasms.2010.08.006>.
- (141) Cooks, R. G. Special Feature: Historical. Collision-Induced Dissociation: Readings and Commentary. *J. Mass Spectrom.* **1995**, *30* (9), 1215–1221. <https://doi.org/10.1002/jms.1190300902>.
- (142) van Agthoven, M. A.; Lam, Y. P. Y.; O'Connor, P. B.; Rolando, C.; Delsuc, M.-A. Two-Dimensional Mass Spectrometry: New Perspectives for Tandem Mass Spectrometry. *Eur Biophys J* **2019**, *48* (3), 213–229. <https://doi.org/10.1007/s00249-019-01348-5>.
- (143) Zuber, J.; Rath sack, P.; Otto, M. Structural Characterization of Acidic Compounds in Pyrolysis Liquids Using Collision-Induced Dissociation and Fourier Transform Ion Cyclotron Resonance Mass Spectrometry. *Anal. Chem.* **2018**, *90* (21), 12655–12662. <https://doi.org/10.1021/acs.analchem.8b02873>.

- (144) Marzullo, B. P.; Morgan, T. E.; Theisen, A.; Haris, A.; Wootton, C. A.; Perry, S. J.; Saeed, M.; Barrow, M. P.; O'Connor, P. B. Combining Ultraviolet Photodissociation and Two-Dimensional Mass Spectrometry: A Contemporary Approach for Characterizing Singly Charged Agrochemicals. *Anal. Chem.* **2021**, *93* (27), 9462–9470. <https://doi.org/10.1021/acs.analchem.1c01185>.
- (145) Marzullo, B. P.; Morgan, T. E.; Wootton, C. A.; Li, M.; Perry, S. J.; Saeed, M.; Barrow, M. P.; O'Connor, P. B. Comparison of Fragmentation Techniques for the Structural Characterization of Singly Charged Agrochemicals. *Anal. Chem.* **2020**, *92* (4), 3143–3151. <https://doi.org/10.1021/acs.analchem.9b04820>.
- (146) Floris, F.; Vallotto, C.; Chiron, L.; Lynch, A. M.; Barrow, M. P.; Delsuc, M.-A.; O'Connor, P. B. Polymer Analysis in the Second Dimension: Preliminary Studies for the Characterization of Polymers with 2D MS. *Anal. Chem.* **2017**, *89* (18), 9892–9899. <https://doi.org/10.1021/acs.analchem.7b02086>.
- (147) Morgan, T. E.; Wootton, C. A.; Marzullo, B.; Paris, J.; Kerr, A.; Ellacott, S. H.; van Agthoven, M. A.; Barrow, M. P.; Bristow, A. W. T.; Perrier, S.; O'Connor, P. B. Characterization Across a Dispersity: Polymer Mass Spectrometry in the Second Dimension. *J. Am. Soc. Mass Spectrom.* **2021**, *32* (8), 2153–2161. <https://doi.org/10.1021/jasms.1c00106>.
- (148) Paris, J.; Theisen, A.; Marzullo, B. P.; Haris, A.; Morgan, T. E.; Barrow, M. P.; O'Hara, J.; O'Connor, P. B. Multimodal Tandem Mass Spectrometry Techniques for the Analysis of Phosphopeptides. *J. Am. Soc. Mass Spectrom.* **2022**, *33* (7), 1126–1133. <https://doi.org/10.1021/jasms.1c00353>.
- (149) Ryan, E.; Nguyen, C. Q. N.; Shiea, C.; Reid, G. E. Detailed Structural Characterization of Sphingolipids via 193 Nm Ultraviolet Photodissociation and Ultra High Resolution Tandem Mass Spectrometry. *J. Am. Soc. Mass Spectrom.* **2017**, *28* (7), 1406–1419. <https://doi.org/10.1007/s13361-017-1668-1>.
- (150) Brodbelt, J. S.; Morrison, L. J.; Santos, I. Ultraviolet Photodissociation Mass Spectrometry for Analysis of Biological Molecules. *Chem. Rev.* **2020**, *120* (7), 3328–3380. <https://doi.org/10.1021/acs.chemrev.9b00440>.
- (151) O'Brien, J. P.; Brodbelt, J. S. Structural Characterization of Gangliosides and Glycolipids via Ultraviolet Photodissociation Mass Spectrometry. *Anal Chem* **2013**, *85* (21), 10.1021/ac402379y. <https://doi.org/10.1021/ac402379y>.
- (152) Madsen, J. A.; Cullen, T. W.; Trent, M. S.; Brodbelt, J. S. IR and UV Photodissociation as Analytical Tools for Characterizing Lipid A Structures. *Anal Chem* **2011**, *83* (13), 5107–5113. <https://doi.org/10.1021/ac103271w>.
- (153) Jennings, K. R. Collision-Induced Decompositions of Aromatic Molecular Ions. *International Journal of Mass Spectrometry and Ion Physics* **1968**, *1* (3), 227–235. [https://doi.org/10.1016/0020-7381\(68\)85002-8](https://doi.org/10.1016/0020-7381(68)85002-8).
- (154) McLafferty, F. W.; Bente, P. F.; Kornfeld, Richard.; Tsai, S.-Chuan.; Howe, Ian. Metastable Ion Characteristics. XXII. Collisional Activation Spectra of Organic Ions. *J. Am. Chem. Soc.* **1973**, *95* (7), 2120–2129. <https://doi.org/10.1021/ja00788a007>.
- (155) Levsen, K.; Schwarz, H. Collisional Activation Mass Spectrometry—A New Probe for Determining the Structure of Ions in the Gas Phase. *Angewandte Chemie International Edition in English* **1976**, *15* (9), 509–519. <https://doi.org/10.1002/anie.197605091>.
- (156) Johnson, A. R.; Carlson, E. E. Collision-Induced Dissociation Mass Spectrometry: A Powerful Tool for Natural Product Structure Elucidation. *Anal. Chem.* **2015**, *87* (21), 10668–10678. <https://doi.org/10.1021/acs.analchem.5b01543>.

- (157) Chen, R.; Li, L. Lithium and Transition Metal Ions Enable Low Energy Collision-Induced Dissociation of Polyglycols in Electrospray Ionization Mass Spectrometry. *Journal of the American Society for Mass Spectrometry* **2001**, *12* (7), 832–839. [https://doi.org/10.1016/S1044-0305\(01\)00261-6](https://doi.org/10.1016/S1044-0305(01)00261-6).
- (158) Guevremont, R.; Boyd, R. K. Are Derrick Shifts Real? An Investigation by Tandem Mass Spectrometry. *Rapid Communications in Mass Spectrometry* **1988**, *2* (1), 1–5. <https://doi.org/10.1002/rcm.1290020102>.
- (159) Schymanski, E. L.; Kondić, T.; Neumann, S.; Thiessen, P. A.; Zhang, J.; Bolton, E. E. Empowering Large Chemical Knowledge Bases for Exposomics: PubChemLite Meets MetFrag. *J Cheminform* **2021**, *13* (1), 19. <https://doi.org/10.1186/s13321-021-00489-0>.
- (160) *mzCloud Mass Spectral Library | Thermo Fisher Scientific - FR*. <https://www.thermofisher.com/fr/fr/home/industrial/mass-spectrometry/liquid-chromatography-mass-spectrometry-lc-ms/lc-ms-software/mass-spectral-libraries/mzcloud-mass-spectral-library.html> (accessed 2022-11-09).
- (161) Tsybin, Y. O.; Witt, M.; Baykut, G.; Kjeldsen, F.; Håkansson, P. Combined Infrared Multiphoton Dissociation and Electron Capture Dissociation with a Hollow Electron Beam in Fourier Transform Ion Cyclotron Resonance Mass Spectrometry: Combined IRMPD and ECD in FTICRMS. *Rapid Commun. Mass Spectrom.* **2003**, *17* (15), 1759–1768. <https://doi.org/10.1002/rcm.1118>.
- (162) Holden, D. D.; Sanders, J. D.; Weisbrod, C. R.; Mullen, C.; Schwartz, J. C.; Brodbelt, J. S. Implementation of Fragment Ion Protection (FIP) during Ultraviolet Photodissociation (UVPD) Mass Spectrometry. *Anal. Chem.* **2018**, *90* (14), 8583–8591. <https://doi.org/10.1021/acs.analchem.8b01723>.
- (163) Cannon, J. R.; Cammarata, M. B.; Robotham, S. A.; Cotham, V. C.; Shaw, J. B.; Fellers, R. T.; Early, B. P.; Thomas, P. M.; Kelleher, N. L.; Brodbelt, J. S. Ultraviolet Photodissociation for Characterization of Whole Proteins on a Chromatographic Time Scale. *Anal. Chem.* **2014**, *86* (4), 2185–2192. <https://doi.org/10.1021/ac403859a>.
- (164) B. Cammarata, M.; S. Brodbelt, J. Structural Characterization of Holo- and Apo-Myoglobin in the Gas Phase by Ultraviolet Photodissociation Mass Spectrometry. *Chemical Science* **2015**, *6* (2), 1324–1333. <https://doi.org/10.1039/C4SC03200D>.
- (165) Shaw, J. B.; Robinson, E. W.; Paša-Tolić, L. Vacuum Ultraviolet Photodissociation and Fourier Transform–Ion Cyclotron Resonance (FT-ICR) Mass Spectrometry: Revisited. *Anal. Chem.* **2016**, *88* (6), 3019–3023. <https://doi.org/10.1021/acs.analchem.6b00148>.
- (166) Zhang, L.; Reilly, J. P. Extracting Both Peptide Sequence and Glycan Structural Information by 157 Nm Photodissociation of N-Linked Glycopeptides. *J Proteome Res* **2009**, *8* (2), 734–742. <https://doi.org/10.1021/pr800766f>.
- (167) Cotham, V. C.; Wine, Y.; Brodbelt, J. S. Selective 351 Nm Photodissociation of Cysteine-Containing Peptides for Discrimination of Antigen-Binding Regions of IgG Fragments in Bottom-Up Liquid Chromatography–Tandem Mass Spectrometry Workflows. *Anal. Chem.* **2013**, *85* (11), 5577–5585. <https://doi.org/10.1021/ac400851x>.
- (168) Oh, J. Y.; Moon, J. H.; Kim, M. S. Sequence- and Site-Specific Photodissociation at 266 Nm of Protonated Synthetic Polypeptides Containing a Tryptophanyl Residue. *Rapid Communications in Mass Spectrometry* **2004**, *18* (22), 2706–2712. <https://doi.org/10.1002/rcm.1679>.

- (169) Wilson, J. J.; Brodbelt, J. S. MS/MS Simplification by 355 Nm Ultraviolet Photodissociation of Chromophore-Derivatized Peptides in a Quadrupole Ion Trap. *Anal. Chem.* **2007**, *79* (20), 7883–7892. <https://doi.org/10.1021/ac071241t>.
- (170) Brodbelt, J. S. Photodissociation Mass Spectrometry: New Tools for Characterization of Biological Molecules. *Chem. Soc. Rev.* **2014**, *43* (8), 2757–2783. <https://doi.org/10.1039/C3CS60444F>.
- (171) Greer, S. M.; Bern, M.; Becker, C.; Brodbelt, J. S. Extending Proteome Coverage by Combining MS/MS Methods and a Modified Bioinformatics Platform Adapted for Database Searching of Positive and Negative Polarity 193 Nm Ultraviolet Photodissociation Mass Spectra. *J. Proteome Res.* **2018**, *17* (4), 1340–1347. <https://doi.org/10.1021/acs.jproteome.7b00673>.
- (172) O'Brien, J. P.; Needham, B. D.; Henderson, J. C.; Nowicki, E. M.; Trent, M. S.; Brodbelt, J. S. 193 Nm Ultraviolet Photodissociation Mass Spectrometry for the Structural Elucidation of Lipid A Compounds in Complex Mixtures. *Anal. Chem.* **2014**, *86* (4), 2138–2145. <https://doi.org/10.1021/ac403796n>.
- (173) Ryan, E.; Nguyen, C. Q. N.; Shiea, C.; Reid, G. E. Detailed Structural Characterization of Sphingolipids via 193 Nm Ultraviolet Photodissociation and Ultra High Resolution Tandem Mass Spectrometry. *J. Am. Soc. Mass Spectrom.* **2017**, *28* (7), 1406–1419. <https://doi.org/10.1007/s13361-017-1668-1>.
- (174) KLEIN-DISSERTATION-2019.Pdf. <https://repositories.lib.utexas.edu/bitstream/handle/2152/75171/KLEIN-DISSERTATION-2019.pdf?sequence=1> (accessed 2022-11-09).

PART III : SPECIFIC DERIVATIZATION OF CHEMICAL FUNCTIONAL GROUP

CHAPTER 3 : CHARACTERIZATION OF BIO-OIL AT MOLECULAR LEVEL: SPECIFIC DERIVATIZATION OF CHEMICAL FUNCTIONAL GROUP

3.1. Publication: Characterization of bio-oil at molecular level: specific derivatization of chemical functional group

Anthony ABOU DIB, Vincent CARRÉ, Frédéric AUBRIET

3.2. Introduction

The increasing energy demand in the context of strong tension on fossil resources has caused the urgent need to develop alternative energy sources that are available, greener, and more sustainable. Lignocellulosic biomass resources can contribute to reducing the issues of severe environmental contamination and the lack of fossil fuels.¹⁻³ Valuable molecules, especially bio-oil components, can be generated from lignocellulosic biomass once some chemical bonds of macromolecule components are broken down by digestion or pyrolysis. For this purpose, conversion processes have to be well controlled. Additional up-grading steps are needed to convert bio-oil into a useful mixture of added-value organic compounds to produce a fuel. A complete characterization of the products is required to understand and optimize the efficiency of the catalytic up-grading treatments of raw bio-oils.⁴ Indeed, depending on the nature of the feedstock and the conversion process, bio-oils are composed of hundreds or even thousands of different organic compounds, such as acids, alcohols, ketones, aldehydes, phenols, ethers, esters, carbohydrates, furans, and multifunctional compounds. These functional groups must be identified to determine which catalytic treatments are most effective for upgrading the bio-oils.

Concerning the analysis of the bio-oil composition, analytical methods, such as Fourier transform infrared (FTIR) and nuclear magnetic resonance (NMR) spectroscopy, give global information on the chemical functions of the whole bio-oil components without distinguishing each of their specific contributions.⁵⁻⁹ Therefore, other methods must be employed to describe bio-oils at the molecular level. Stăs et al. reviewed very comprehensively the strategies developed achieving the identification of individual components of bio-oil and their quantification in relation to the characteristic oxygenated functional groups they contain.¹⁰ For each functional group, a specific analytical workflow integrates a pre-sample treatment step, including derivatization and at least one dimension of chromatography before detection by ultraviolet UV or mass spectrometry MS. While gas chromatography (GC) with MS provides relevant information about the molecular formula of the most volatile low-mass compounds, information is missing for polar and heavy constituents.¹¹⁻¹⁵ The bio-oil analysis by high-

resolution mass spectrometry (HRMS) without chromatographic separation can give access to the chemical formulae of all bio-oil components, especially the fraction refractory to the upgrading process.^{16–20} This approach is also called petroleomics.^{21,22} However, although it can give the elemental composition of many components, their structural and chemical diversity is not highlighted.

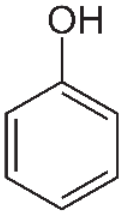
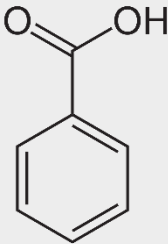
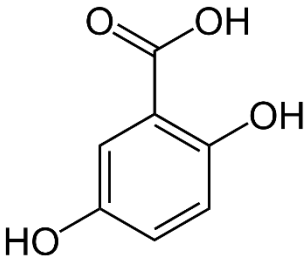
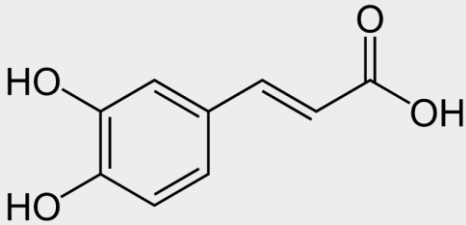
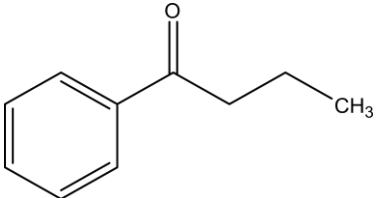
Sample pre-treatment techniques can be employed before HRMS analysis to meet this analytical challenge.²³ Kanaujia et al. suggested exploring the high potentiality of solid-phase extraction (SPE) with different sorbents to split a bio-oil into different fractions corresponding to different chemical families.²⁴ The SPE is an attractive preparation technique because of its selectivity depending on the sorbent, the fast elution profile, and little solvent usage.²⁵ Nevertheless, for bio-oil analyses, SPE is nearly never reported as a fractionation technique,²⁶ except for the use of aminopropyl silica sorbent specifically developed to investigate some compounds by GC.^{27,28} The potential of analyte discrimination by SPE is based on the sorbent/solvent/molecule interactions. It fails, for a given class of compounds (phenolic compounds, for example), to separate poly-chemical functionalized molecules. Depending on the nature and the number of these chemical functions, an additional level of discrimination needs to be considered. This need could be met by tagging chemical functions. The derivatization steps can be applied directly to a mixture such as a bio-oil or combined with fractionation steps. Derivatization by amine-containing reactant has been successfully applied to bio-oil to highlight carbonyl compounds by ESI HRMS.²⁹ In addition, some work has been done on the development of solid phase analytical derivatizations (SPADs) to improve chromatographic analyses.³⁰ For example, carboxylic acids can be derivatized using methyl and ethyl iodides,^{31,32} or N-methyl N-(trimethylsilyl) trifluoroacetamide (MSTFA).³³ on a strong anion-exchange solid phase. The C18 sorbent and copolymer of styrene and divinylbenzene (PS-DVB) help to derivatize phenols with acetic anhydride³⁴ and MSTFA.³³ Additionally, amines on PS-DVB are derivatized using trifluoroacetic anhydride.³⁵

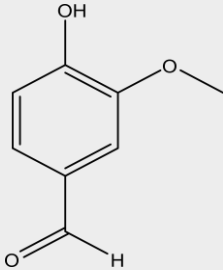
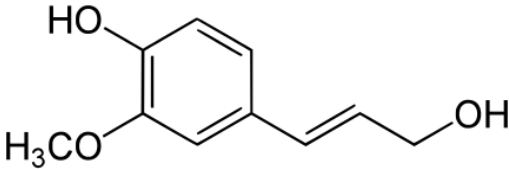
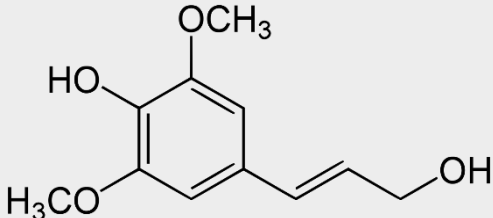
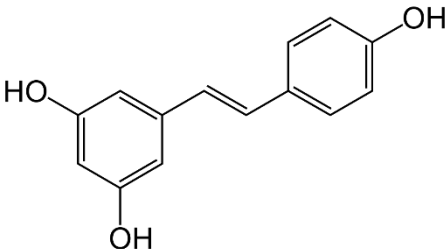
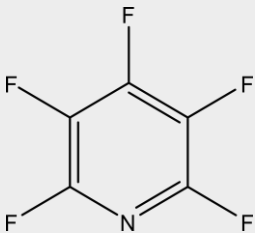
In this work, we will investigate an integrative workflow to reveal the diversity of chemical functions in a pyrolysis bio-oil of lignocellulosic biomass from only a few mg of sample. This study focuses on the lignin-derived, part of which can be refractory to bio-oil catalytic upgrading treatments. The proposed methodology involves different sample preparation steps combining fractionation and derivatization mediated by SPE on a commercial mixed reverse phase/anion-exchange sorbent before analyses by high-resolution mass spectrometry.

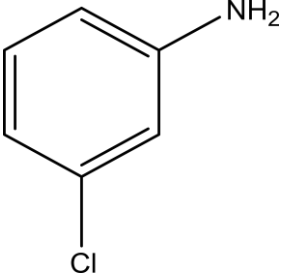
In order to assess the efficiency of the proposed analytical workflow, a mixture of different compounds whose structures and chemical functions are present in the components of pyrolysis lignocellulosic bio-oils was first investigated (Table 3-1). The optimized method was then applied to a real bio-oil sample.

Chapter 3: Characterization of bio-oil at molecular level

Table 3-1: Structure and molecular weight of standards compounds and their derivatization reagent.

Chemicals	Structure	Formula	Monoisotopic mass (Da)
Phenol		C ₆ H ₅ OH	94.0413
Benzoic acid		C ₇ H ₆ O ₂	122.0362
2,5 dihydroxy- benzoic acid (2,5 DHB)		C ₇ H ₆ O ₄	154.0260
3,4 Dihydroxycinnamic acid		C ₉ H ₈ O ₃	164.0467
Butyrophenone		C ₁₀ H ₁₂ O	148.0882

Vanillin		C ₈ H ₈ O ₃	152.0467
Coniferyl alcohol		C ₁₀ H ₁₂ O ₃	180.0780
Sinapyl alcohol		C ₁₁ H ₁₄ O ₄	210.0886
Resveratrol		C ₁₄ H ₁₂ O ₃	228.0780
Pentafluoropyridine (Derivatization reagent)		C ₅ F ₅ N	168.9945

3-chloroaniline (Derivatization reagent)		C_6H_6ClN	127.0183
---	---	-------------	----------

3.3. Materials and Methods

3.3.1. Pyrolysis Bio-oil from lignocellulosic biomass

Bio-oil was produced by heating 2 grams of a powder (particle size from 0.8 to 1.7 mm) of a well-known lignocellulosic biomass (oak) continuously added through a micro-feeder in a micro-fluidized bed reactor at 500°C (the temperature of the sand) for 12 minutes (10 grams/hour). The equipment was developed at LRGF Nancy. The bio-oil is collected at -60°C and recovered in methanol ("bio-oil solution") and stored at -20 °C before analysis.

3.3.2. Reagents and chemicals

LCMS grade methanol (VWR–Prolabo), phenol (99%, Aldrich), resveratrol (99%, Aldrich), vanillin (97%, Aldrich), butyrophenone (99%, Aldrich), 2,5 dihydroxybenzoic acid (98%, Aldrich), 3,4 dihydroxycinnamic acid (97%, Aldrich) and lignin standards: coniferyl alcohol (98%, Aldrich), and sinapyl alcohol (98%, Aldrich), were used as supplied. Standard compounds (Table 1) were solubilized in methanol at a final concentration of 10^{-3} mol.L⁻¹. Pentafluoropyridine (≥99%), and 3-chloroaniline (99%, Alfa Aesar) purchased from sigma Aldrich, were used as derivatization reagent.

3.3.3. FT-ICR MS Analysis

The different standards and oak bio-oil samples were analyzed by high-resolution mass spectrometry. A Solarix 7T 2XR FTMS spectrometer (Bruker) equipped with a 7 T superconducting magnet and of three ionization sources (ESI, APCI and APPI) was used in positive and negative ion detection mode. For the ESI, the capillary was set to +4200 V, the source temperature was maintained at 200 °C and a sample flow rate was fixed to 2 μL.min⁻¹. For the APPI experiment, the capillary was set to +700 V, the vaporizer temperature was maintained at 400°C and the source temperature at 195°C and direct infusion was performed at a flow rate of 15 μL.min⁻¹. For APPI analysis, 0.1% of toluene was used as dopant. The used APPI was fitted with a Kr discharged lamp delivering photons with an energy of 10.0 and 10.6 eV. For APCI, the source parameters were than for APPI experiments, the current of the corona needle was fixed to 3500 nA. The ions were accumulated in the RF hexapole for 0.050 seconds

before being transferred to the FT ICR cell. FT-ICR mass spectra were acquired from m/z 140 to 1000 with a transient size of 4 Mwords resulting in a 710,000 resolving power at m/z 229.0683. A sum of 500 individual transients was accumulated to produce a mass spectrum.

For the MS/MS analysis on the standards, an isolation window of 3 Da was applied, the neutral gas used is Argon and the applied collision voltage was between 13 and 18 eV.

3.3.4. Data processing

Data analysis, and visualization were performed using Data Analysis 5.0 (Bruker), and Composer64 (Sierra analytics) software's. Different graphical representations were used. The double bond equivalent number (DBE)³⁶ with respect to the carbon atom count representation was used to evidence the number unsaturation (Chapter II). The heteroatom (CH, CHO, CHON...) class distribution and the van Krevelen diagram ensured the depiction of the molecular assignments. The Van Krevelen diagram represents the different compounds by dots whose x and y coordinates are the ratios O/C and H/C, respectively and allows to distinguish chemical families such as lipids, unsaturated hydrocarbons, phenolics, and carbohydrates (Chapter II).³⁷

3.3.5. Solid phase extraction and derivatization on solid phase

A combination of stepwise solid phase extraction and chemical-derivatization workflow was developed to discriminate the bio-oil components with respect to their functional groups. For that purpose, a mixed-mode polymeric sorbent including reversed-phase and anion-exchange functionalities was used (Oasis MAX cartridge 6 ml, 500 mg, LP from Waters France). The SPE procedure was performed on a HyperSep™ Glass Block vacuum manifold system (ThermoFisher Scientific, France). The used workflow integrating different derivatization procedures is shown Figure 3-1. First, the cartridge was successively conditioned by 2.5 ml of MeOH, 2.5 mL of water, and 2.5 mL of a 0,1M NaOH solution. Secondly, the sample (mixture of standard compounds or bio-oil) was diluted to 1 mg.mL⁻¹ in 1M of NaOH and 1mL was loaded onto the column. Three successive fractions were collected in respect with the used effluent.

After the addition of 2.5 mL of the MeOH/H₂O mixture (90/10) followed by 2.5 mL of MeOH (washing step), the first fraction was collected. This fraction corresponds to the compounds which are non-retained by the mixed cartridge phase. This fraction was acidified by 1% of formic acid before MS analysis. The solid phase was then dried under vacuum for 15 min. Two milliliters of a pentafluoropyridine (PFP) solution in acetonitrile (10% V/V) were then added. After 15 min, the time required to ensure the derivatization took place, 4 mL of acetonitrile were added to eluate the phenolic compounds derivatized by PFP. This constituted the fraction 2. The volatility of the PFP allowed the excess derivatization agent to be eliminated by keeping this fraction in the open air. The cartridge was left to dry for 10 min under vacuum. The third fraction was then obtained by adding 2mL of 1% formic acid (FA) in a 90:10 MeOH/H₂O (V/V) solution and eluting the compounds twice with 2 mL of MeOH. The three fractions were

divided into two aliquots. In one, 0.1% V/V of 3-chloroaniline (CIA) was added to lead to three additional fractions (fraction 1 – CIA, fraction 2 – CIA, fraction 3 – CIA) in which carbonyl functions were derived.

3.3.6. NMR analysis

Complementary ^{19}F NMR measurements were performed to confirm the formation of tetrafluoropyridyl bi-aryl ether and the derivatization of the phenolic compounds. The ^{19}F NMR measurements were performed with a 400 MHz spectrometer Avance NEO (Bruker) within the organic synthesis group of the Environmental and Sustainable Chemistry Team (LCP–A2MC – Metz). For the ^{19}F analysis, the derivatization was accomplished in deuterated solvents.

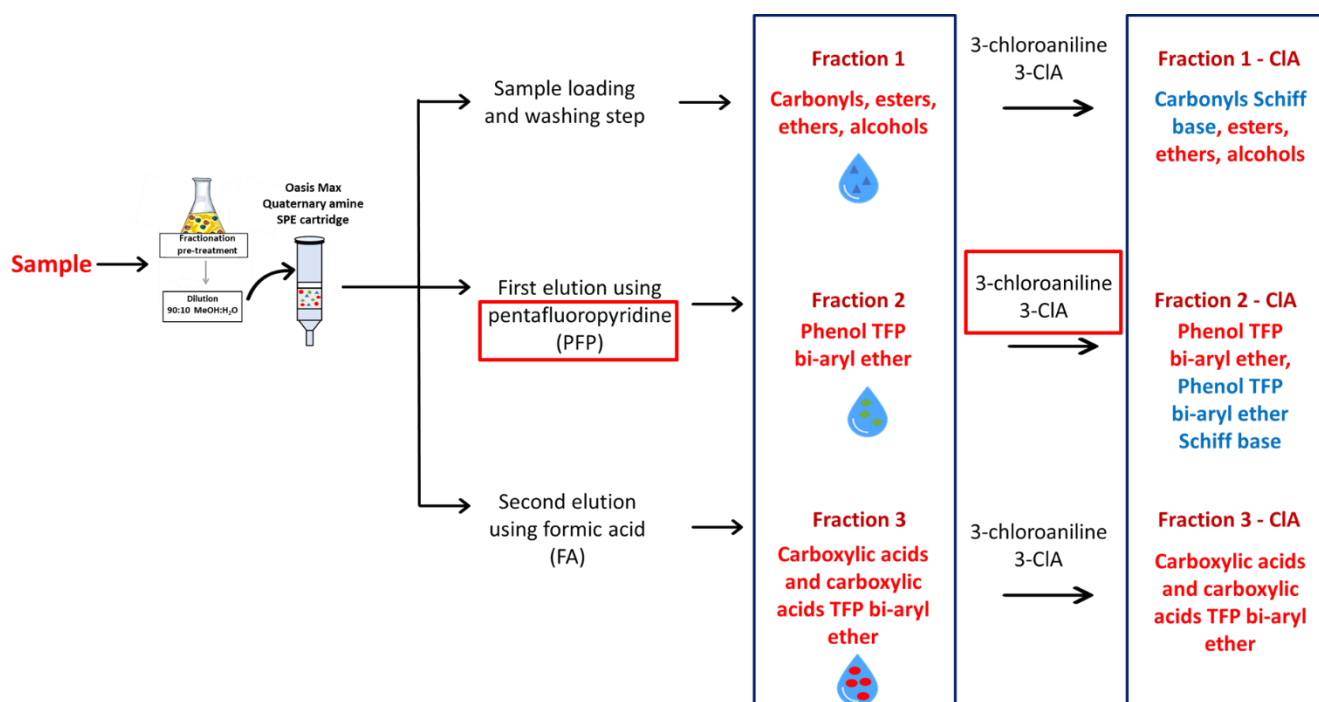


Figure 3-1: Scheme of the experimental workflow from sample fractionation to derivatization and functional characterization.

3.4. Results and Discussion

3.4.1. Rationalization of the used workflow

The work aims to provide an extensive molecular description of bio-oil mono- and poly-functionalized components to optimize their valorization process by catalytic deoxygenation. The most interesting ones are compounds derived from lignin that contain chemical functions carbonyl, phenol, ether, carboxylic acid, and alcohol, some of which are refractory to catalytic treatment. In an alkaline medium, some of these chemical functions are negatively charged,

resulting in their immobilization on an anion-exchange sorbent. They can thus be separated from the neutral components of bio-oils. In the first step of the proposed workflow, the phenolates and carboxylates remain attached to the anionic sorbent while compounds with only ether and/or carbonyl and/or alcohol groups are eluted by the methanol/water solvent to yield fraction 1. Since the bio-oils are acidic (pH around 5), it is necessary to increase the pH to 12 by adding sodium hydroxide to deprotonate carboxylic acids and phenolic compounds before putting the bio-oil sample on the SPE cartridge. At this step, the bio-oil compounds, which possess at least one phenolic group, or one carboxylic acid function are retained on the cartridge. Adding PFP ensures the derivatization of the phenolic group and release from the sorbent (fraction 2). The final addition of an acidic solution allows the attached carboxylates to be converted into their corresponding carboxylic acid and eluted to yield fraction 3. A large number of bio-oil components, especially the oligomeric ones, are polyfunctional. Consequently, each fraction is a mixture of compounds with different functional groups. The final addition of 3-chloroaniline ensures the derivatization of the carbonyls, which increase the structural description of some of the oxygenated bio-oil compounds. The selection of the derivatization reagents is based on, first their specific and quick reaction with a given chemical function, and second the introduction of atoms, which are not initially present in biomass pyrolysis bio-oil (fluorine and chlorine). This labeling by stable isotope facilitates tracking the derivatized species on the obtained mass spectrum. For carbonyls, the specific isotopic pattern of chlorine eases the final data treatment.

3.4.1.1. Carbonyls:

The carbonyls are known to react specifically and rapidly with primary amine forming the Schiff base in acidic medium. Hertzog et al. demonstrated that it is possible to derivatize carbonyl in the electrospray ionization source by adding amine reagent in the investigated bio-oil sample, and identify them by mass spectrometry.²⁹ Indeed, the imines formed were detected in the form of iminium ions (Figure 3-2). The 3-chloroaniline was chosen as an efficient primary amine for the derivatization of carbonyl groups. The other investigated chloro-aniline isomers were less reactive. In the proposed work-flow, carbonyl compounds may be found in each fraction. Consequently, the derivatization by 3-chloroaniline was systematically employed before the analysis by ESI-MS.

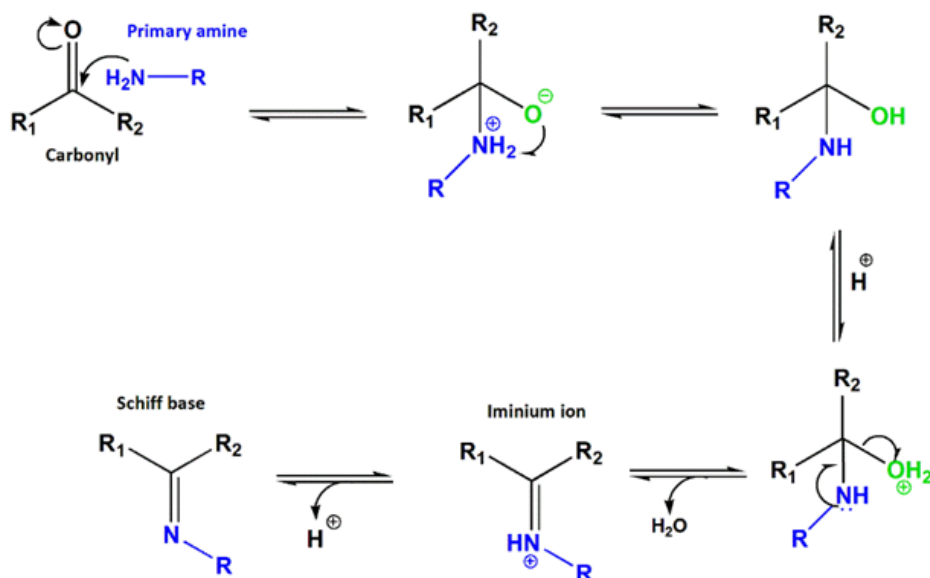


Figure 3-2: Mechanism of the reaction leading to the Schiff base formation from primary amine.

3.4.1.2. Phenols:

In the bio-oils produced by pyrolysis of lignocellulosic biomass, phenolic compounds contribute significantly to oxygen-containing compounds in monomeric and polymeric forms.¹² After the first step of the fractionation process, phenolic compounds, in form of phenolate, are retained by the anion exchange sorbent. Therefore, their elution and labeling steps were combined by a derivatization agent able to react and neutralize phenolate. At room temperature, pentafluoropyridine (PFP) demonstrates its ability to react rapidly with a wide range of phenolic compounds to form the tetrafluoropyridyl ethers in an alkaline medium through an S_NAr reaction (Figure 3-3).^{38,39} PFP is a good candidate as a specific reactant and eluant to recover phenolic compounds labeled with C₅F₄N on each phenol group. To demonstrate the efficiency and specificity of this solid-phase analytical derivatization step, phenol like compounds were investigated according to different protocols using or not including an immobilization step on the SPE sorbent. Firstly, a 1/1 (V/V) PFP and phenol mixture was stirred for 16 hours at 50°C in presence of potassium carbonate (pH 11.5) according to a published protocol.³⁹ The obtained solution was analyzed by (+) APPI FT-ICR MS and demonstrated the reaction of the PFP molecule with three phenols. The three ortho and para sites of the PFP molecule were thought to react with phenol. Secondly, a 1 mL phenol solution was investigated according to the described workflow. No compounds were detected by MS of the fraction 1. The analysis of the second fraction 2 evidenced only one compound corresponding to the reaction of one PFP molecule with only one phenol. This result demonstrated the specific one-to-one reaction between PFP and a phenolic compound. This is important in the bio-oil investigation, since bio-oil contains large amounts of a significant variety of phenolic compounds. Thus, an anion exchange SPE step is needed to avoid the multiple reactions of PFP with three (possibly different) phenolic compounds.

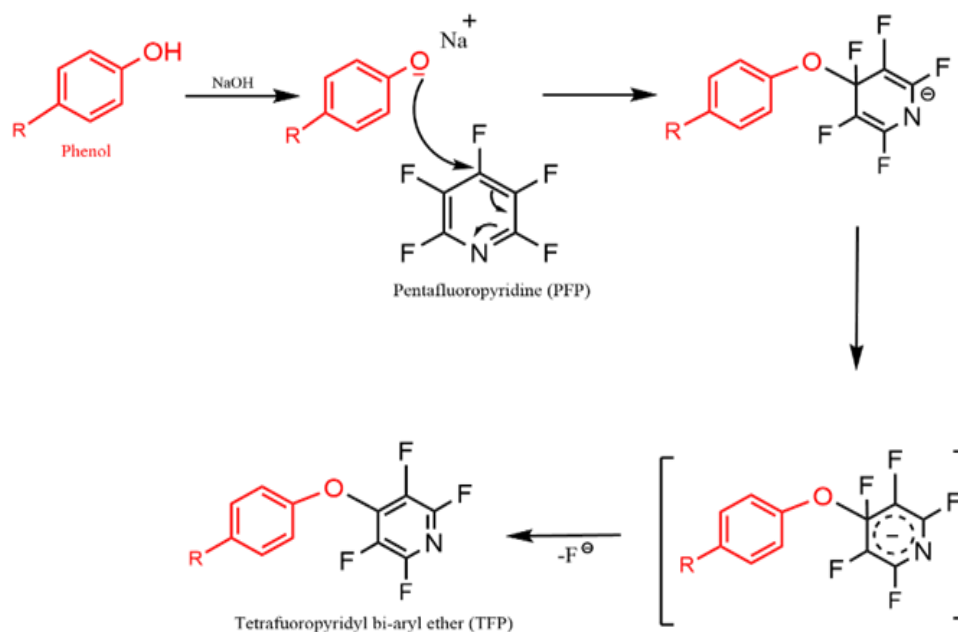


Figure 3-3: Mechanism of the reaction leading to the tetrafluoropyridyl bi-aryl ether formation from the reaction between phenol and pentafluoropyridine.

3.4.1.3. Carboxylic acids:

Bio-oil compounds containing at least one carboxylic acid group were attached to the sorbent as carboxylates. Only last step allowed their elution by neutralization using weakly acidic medium. They were gathered into the fraction 3.

3.4.2. Method application to representative compounds of bio-oils

Before applying the fractionation and derivatization protocol to a real bio-oil sample, the mixture of the selected standard compounds (Table 3-1) was studied to validate its usefulness and robustness. Their selection was based on the presence of structure and functional groups commonly found in lignin bio-oils. Each standard was investigated separately before adding it to the mixture. After applying the derivatization method on the standard mixture, a blank analysis on the same used SPE cartridge was conducted to verify that all the compounds were eluted. The used ionization techniques were selected with respect to the chemical properties of the labeled and not-labeled compounds in each fraction. To overcome the formation of sodium clusters, APCI (+) was used to analyze fraction 1 and fraction 3 while the fraction 2 was analyzed by APPI (+) since the tetrafluoropyridyl bi-aryl ether formed is non-polar and is not efficiently ionized by ESI.

3.4.2.1. Fraction F1

that Fraction 1 was expected to contain only butyrophenone, the solely non-phenolic and non-acidic compound in the mixture. The mass spectrum obtained by (+) ESI and (+) APCI FT-ICR MS presented only one peak at m/z 149.0958, corresponding to the protonated butyrophenone. By ESI, an additional mass peak was observed at m/z 171.0780, relative to the Na^+ adduct of butyrophenone as well as sodium formate cluster ions. These latter resulted from the acidification of the fraction by adding formic acid.

The addition of 3-chloroaniline in fraction 1 led to the derivatization of butyrophenone by the 3-chloro-aniline, which was detected by (+) ESI-MS at m/z 258.1041 (^{35}Cl contribution) as $[\text{M}+\text{H}]^+$. The obtained isotopic pattern was those of a compound containing only one chlorine atom (Figure 3-4). The formation of the Schiff base by the reaction of the primary amine with carbonyl group of butyrophenone was confirmed by collision induced dissociation (CID) tandem mass spectrometry (Table 3-2). The ion fragments observed were identical to those obtained by Hertzog et al. on the same Schiff base.²⁹ These results also demonstrated that neither phenolic nor carboxylic compounds were collected in the fraction 1.

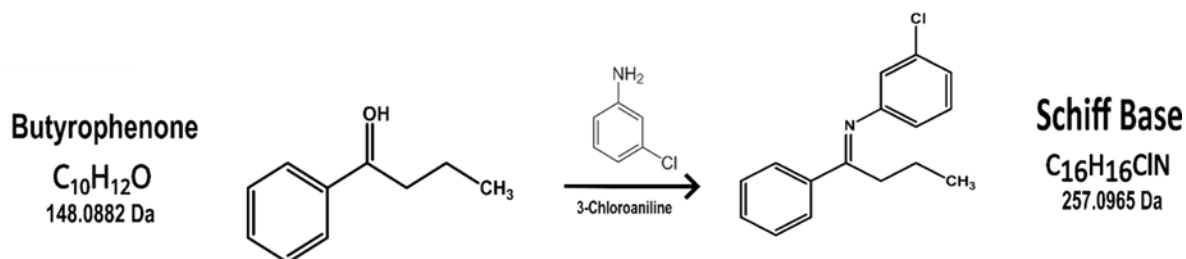


Figure 3-4: Structure of the butyrophenone obtained in fraction 1 and its corresponding derivatization using the primary amine.

Table 3-2: Tandem mass spectrometry analysis of the butyrophenone and its corresponding imine compound.

Name	MS	Collision voltage	MS ²	
			m/z	-Loss (abundance %)
Butyrophénone	[C ₁₀ H ₁₂ O+H] ⁺ m/z149,09586	-12	131,0853	- H ₂ O (29)
			121,0646	-C ₂ H ₄ (36)
			107,0490	- C ₃ H ₆ (100)
			105,0697	-C ₂ H ₄ O (24)
Butyrophénone - chloroaniline Schiff base	[C ₁₆ H ₁₆ N ³⁵ Cl+H] ⁺ m/z258,10413	-12	229,0650	-C ₂ H ₅ (39)
			216,0572	- C ₃ H ₆ (100)
			180,0573	- C ₆ H ₆ (35)
			131,0854	- C ₆ H ₄ ³⁵ CINH ₂ (40)
	[C ₁₆ H ₁₆ N ³⁷ Cl+H] ⁺ m/z260,12005	-12	231,0809	-C ₂ H ₅ (39)
			218,0731	- C ₃ H ₆ (100)
			182,0731	- C ₆ H ₆ (35)
			131,0856	- C ₆ H ₄ ³⁷ CINH ₂ (39)

3.4.2.2. Fraction F2

Phenolic compounds not containing carboxylic acid function were expected to be in fraction 2 resulting from the elution of PFP- derivatized compounds. These compounds are phenol, (Figure 3-5), which form tetrafluoropyridyl bi-aryl ethers by reaction with PFP.³⁹ The analysis by (+) APPI was the most-suited ion source to sensitively detect them. The mass spectrum obtained in the study of the fraction 2, evidenced the molecular M⁺• ion of each of the five PFP-derivatized phenolic compound as well as an ion relative to unreacted PFP. It was observed peaks at m/z243.0301 (C₁₁H₅F₄NO⁺•), 301.0356 (C₁₃H₈F₄NO₃⁺•), 329.0669 (C₁₅H₁₁F₄NO₃⁺•), 359.0775 (C₁₆H₁₃F₄NO₄⁺•), and 675.0446 (C₂₉H₉F₁₂N₃O₃⁺•) corresponding to the PFP mono-derivatization of phenol, vanillin, coniferyl alcohol, sinapyl alcohol and the PFP tri-derivatization of resveratrol, respectively. No peaks relative to the non-derivatized phenolic compounds were observed.

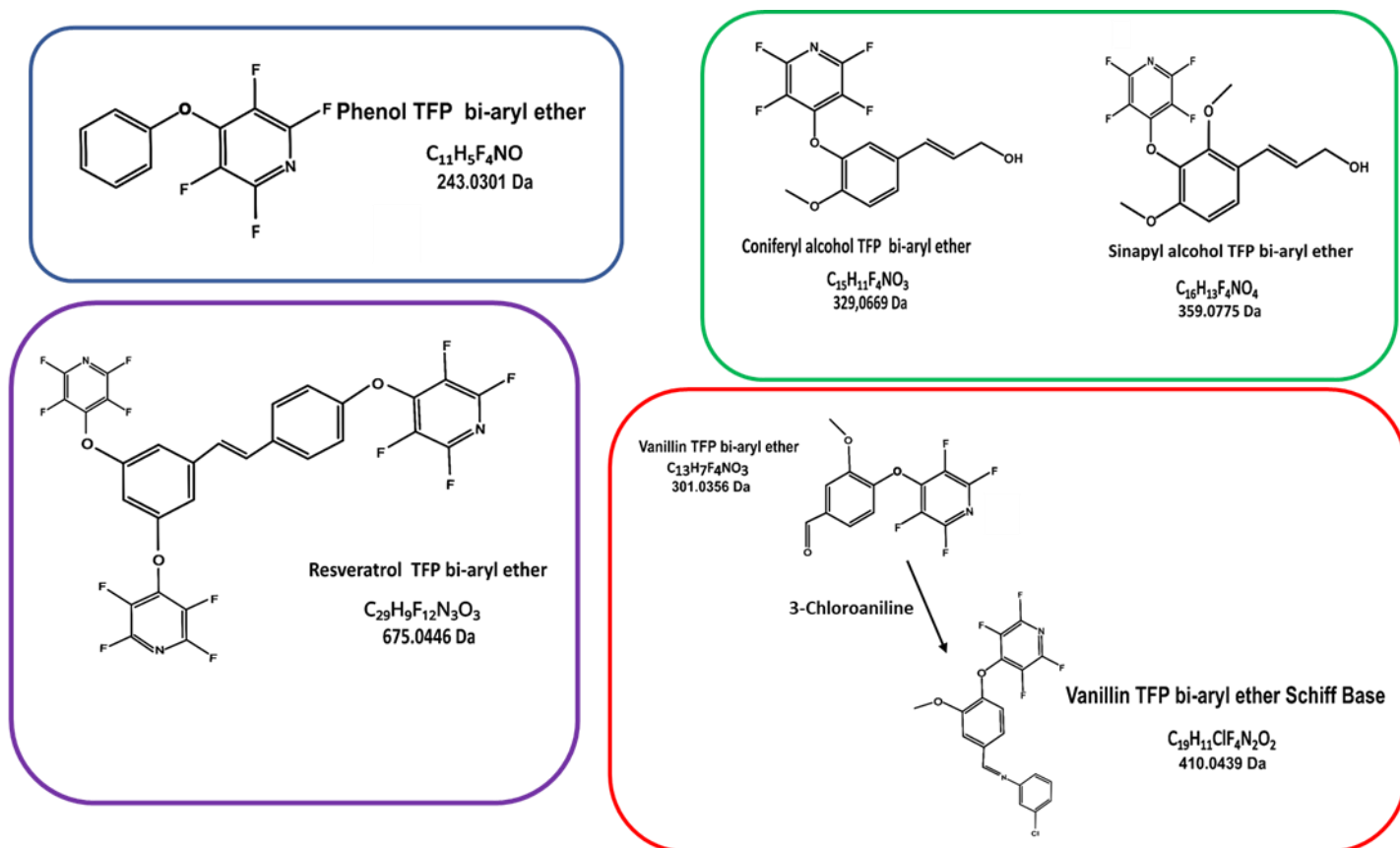


Figure 3-5: Structure of the four compounds obtained in fraction 2 after derivatization using the PFP and the primary amine.

To confirm the structure of the TFP bi-aryl ethers of standard compounds, tandem mass spectrometry experiments were conducted on each $M^{+\bullet}$ PFP-derivatized phenolic compound molecular ion. For derivatized phenol, the loss of a fluorine radical and CNF were observed. This highlighted that bond cleavage only occurred on the TFP moiety. The NMR ^{19}F spectrum (Figure 3-6 A) obtained in the study of phenol-PFP-derivate showed two peaks at -92 and -157 ppm, whereas three peaks were observed at -90 , -135 and -164 ppm for PFP (Figure 3-6 B). Consequently, the formation of the ether by S_NAr involved the para position of the PFP. The MS/MS of the vanillin-PFP derivate led to the main losses typically observed in the study of the vanillin.²⁹ Indeed, the main fragment ions relative to the elimination CO, and $\bullet OCH_3$ were observed at $m/z273.0407$ and $m/z270.0173$, respectively. In addition, the loss of $C_5F_4NO^{+\bullet}$ leading to the fragment ion at $m/z135.0806$ confirmed the formation of the ether bond between the tetrafluoropyridine moiety and vanillin. A similar behavior was observed, when MS/MS experiments were performed on the molecular ion of the derivatized coniferyl and sinapyl alcohol (Table 3-3). For these latter compounds, the other fragmentations observed, were from the elimination of water relative to the propenyl alcohol, those of $\bullet OCH_3$ from the methoxy group and linked to opening of the aromatic ring rearrangements (Table 3-3).

Interestingly, the polyphenolic resveratrol compound, led solely to the observation of an ion at m/z 675.0446, which implicated that each of the phenolic group were derivatized by PFP. The MS/MS of the derivate product led to the observation of the m/z 509.0532 and m/z 273.0617 ion related to the loss of one or two oxy tetrafluoropyridine radical ($\bullet\text{O}-\text{C}_5\text{F}_4\text{N}$), respectively.

The second derivatization step, by 3-chloroaniline, allowed to label the carbonyl group if present in the investigated phenolic compound. The (+) APPI FTICRMS analysis ensured to only observe the protonated $[\text{C}_{19}\text{H}_{11}\text{Cl}_1\text{F}_4\text{N}_2\text{O}_2+\text{H}]^+$ double-derivatized (by PFP and 3-chloroaniline) vanillin at m/z 411.0517. This ion was associated with the expected Schiff base showing of the TFP bi-aryl ether of vanillin. This behavior confirmed that carbonyl group did not react with the PFP. In addition, the absence of reaction products of 3-chloro-aniline with the other PFP derivates demonstrated the orthogonality of the two derivatization procedures. The structure of the double-derivatized vanillin ion was confirmed by MS/MS experiment of $[\text{C}_{19}\text{H}_{11}\text{Cl}_1\text{F}_4\text{N}_2\text{O}_2+\text{H}]^+$ (Table 3-3). Both fragmentation pathways evidenced in the study of vanillin tetrafluoropyridyl bi-aryl ether and vanillin-chloro-aniline base Schiff reported by Hertzog et al.²⁹ were observed.

On a data treatment point of view, to define the nature of the phenolic components of bio-oils in fraction 2, the examination of the elemental formulae of the ion detected by (+) APPI is of interest. The ions assign to chemical formula containing a F_4N motif or a multiple of this motif provides information on the number of phenolic groups. The subtraction of $\text{C}_5\text{F}_4\text{N}$ and the addition of one H retrieve the non-derivatized elemental formulae. A similar procedure is used to define the nature of the compound derivatized by 3-chloroaniline.

No ions relative to benzoic acid, 2.5 DHB, and 3.4 dihydroxycinnamic acid were observed on the obtained mass spectrum of the fraction 2, even though they included a phenolic moiety.

This well-demonstrated that carboxylic compounds were retained on the SPE sorbent by interaction with the carboxylate function.

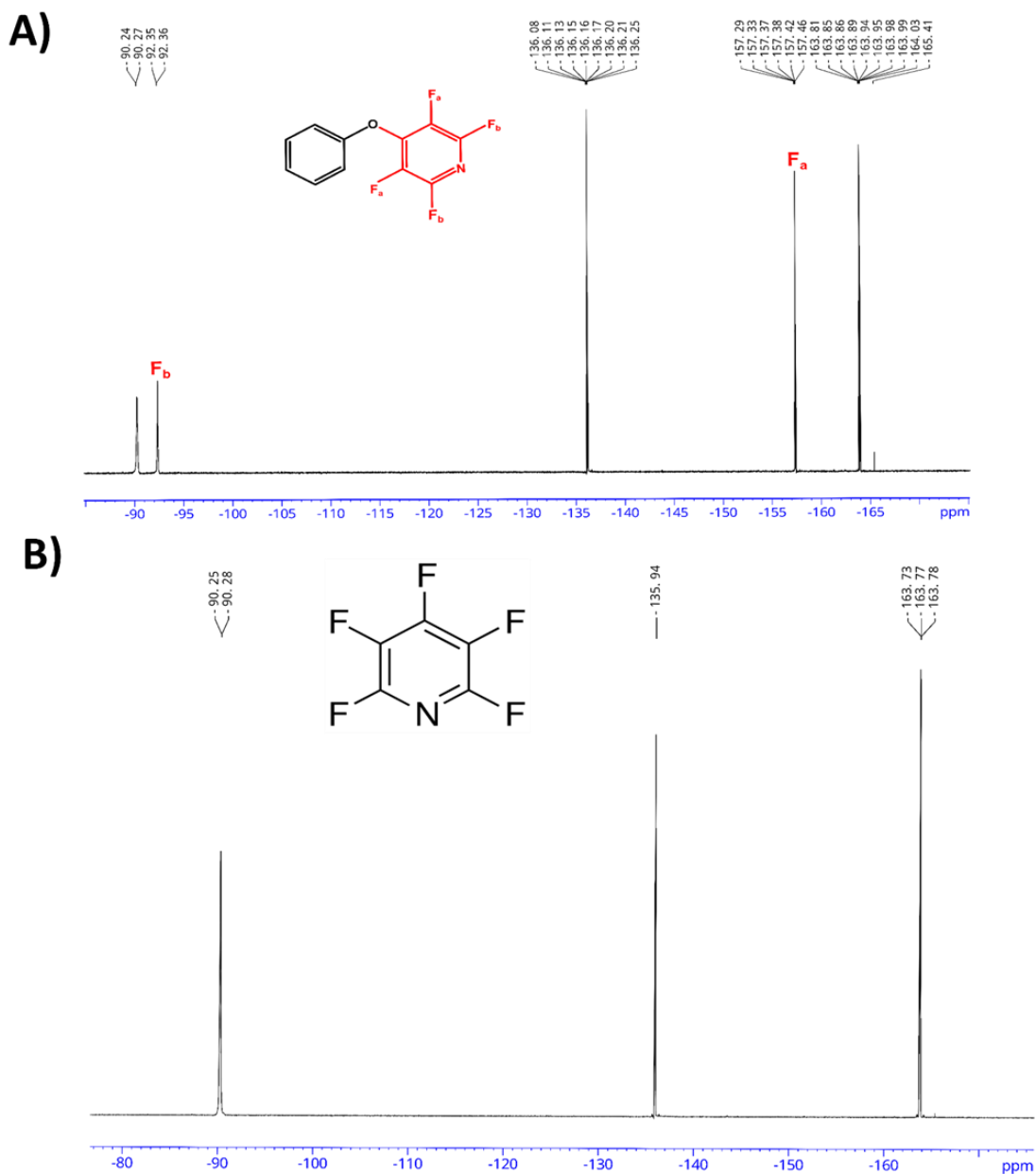


Figure 3-6: ^{19}F NMR spectrum (Top) ^{19}F NMR of the obtained product "Tetrafluoropyridyl bi-aryl ether" after derivatization of the standard phenol on the SPE cartridge. F_a corresponds to the fluorine in the meta position and F_b corresponds to that the fluorine in the ortho position. (Bottom) ^{19}F NMR of the pentafluoropyridine

Chapter 3: Characterization of bio-oil at molecular level

Table 3-3: Tandem mass spectrometry analysis of the derivatized standard eluted using the pentafluoropyridine PFP as derivatization agent.

Name	MS	Collision voltage (V)	MS ²	
			m/z	-Loss (abundance %)
Phenol - PFP	C ₁₁ H ₅ F ₄ NO ₁ ⁺ m/z243,0301	-12	224,0314	-F (90)
			198,0284	-CFN (100)
Vanillin - PFP	C ₁₃ H ₇ F ₄ NO ₃ ⁺ m/z301,03566	-12	286.048608	-CH ₃ [•] (100)
			273,04074	-CO (39)
			272,0329	-CHO (14)
			270,01734	-CH ₃ O [•] (13)
			135,08064	-C ₅ F ₄ NO [•] (7)
Vanillin - PFP – 3-chloroanilin	[C ₁₉ H ₁₁ ³⁵ Cl ₁ F ₄ N ₂ O ₂ +H] ⁺ m/z411,0517	-12	379,0256	-CH ₃ OH (12)
			375,0751	-H ³⁵ Cl (1)
			274,0488	-C ₇ H ₄ ClN (11)
			244,0526	-C ₅ HF ₄ NO (17)
			138,0108	-C ₁₂ H ₇ F ₄ NO ₂ (100)
	[C ₁₉ H ₁₁ ³⁷ Cl ₁ F ₄ N ₂ O ₂ +H] ⁺ m/z413,0674	-12	381,0412	-CH ₃ OH (12)
			375,0751	-H ³⁷ Cl (1)
			274,0488	-C ₇ H ₄ ClN (11)
			246,0680	-C ₅ HF ₄ NO (17)
			140,0261	-C ₁₂ H ₇ F ₄ NO ₂ (100)
Sinapyl Alcohol + PFP	C ₁₆ H ₁₃ F ₄ NO ₄ ⁺ m/z359.0775	-12	340.0592	-H ₂ O (1)
			331.0827	-CO (100)
			328,0592	-CH ₃ O [•] (1)
			316,0592	-C ₂ H ₃ O (4)
			303.0513	-C ₃ H ₄ O (5)
			298,0485	-C ₂ H ₅ O ₂ (1)
			192.0786	-C ₅ HF ₄ NO (3)
			175.0757	-H ₂ O, -C ₅ F ₄ NO [•] (1)
			161.0600	-OCH ₃ , -C ₅ HF ₄ NO (1)
Coniferyl Alcohol + PFP	C ₁₅ H ₁₁ F ₄ NO ₃ ⁺ m/z329.0669	-12	311.05615	-H ₂ O (1)
			301.0720	-CO (100)
			298,04863	-CH ₃ O [•] (1)
			286,0483	-C ₂ H ₃ O (24)
			273.0407	-C ₃ H ₄ O (6)
			163,075228	-C ₅ HF ₄ NO (5)
Resveratrol + PFP	C ₂₉ H ₉ F ₁₂ N ₃ O ₃ ⁺ m/z675.0446	-12	655.0316	-HF (1)
			635.0316	-2*HF (1)
			509.0532	-C ₅ F ₄ NO [•] (6)
			359.0571	-C ₅ F ₄ N [•] , -C ₅ F ₄ NO [•] (1)
			273.0407	-2* C ₅ F ₄ NO [•] (100)

3.4.2.3. Fraction F3

After acidification by formic acid and elution, it was expected that fraction 3 contain the remaining compounds mainly those with a carboxylic acid group due to the protonation of the

carboxylate. The protonated benzoic acid and 2,5 DHB twice derivatized by PFP were observed by (+) APCI, and (+) ESI FT-ICR MS. The molecular ion from the twice PFP-derivatized 3,4 dihydroxycinnamic acid was observed by (+) APCI FT-ICR MS. Indeed, the (+) APCI Fraction 3 spectrum led to the observation of the $[C_{17}H_4F_8N_2O_4 + H]^+$ and the $[C_{19}H_6F_8N_2O_4 + H]^+$ at m/z 453.0116 and 479.0272, respectively (Figure 3-7). The PFP derivatization of the phenolic groups of 2,5 DHB and the 3,4 dihydroxycinnamic acid occurred during the second step of this workflow. Interestingly, the number of the PFP was indicative of the number of phenolic group and PFP derivatization did not require that the phenolate absorbed on the sorbent to be efficiently derivatized.

Tandem mass spectrometry was conducted on the both derivatized 2,5 DHB and the 3,4 dihydroxycinnamic acids. The loss of CO_2 (m/z 409.0218 and 435.0374) and water (m/z 435.0010 and 461.0167) were observed for both compounds (Table 3-4). This result indicated that PFP did not react with the acidic group. The loss of TFP-OH for the protonated 2,5 DHB and 3,4 dihydroxycinnamic acid were also observed. Surprisingly, a twice oxy-tetrafluoropyridin unit loss was not observed, in contrast to what observed for polyphenolic compounds of the fraction 2. This specific behavior is still under investigation.

Finally, the protonated $[C_7H_6O_2 + H]^+$ benzoic acid was observed, as expected, at 123.0440 (no phenolic group). By MS/MS, only one major fragment was detected and related to the loss of CO_2 .

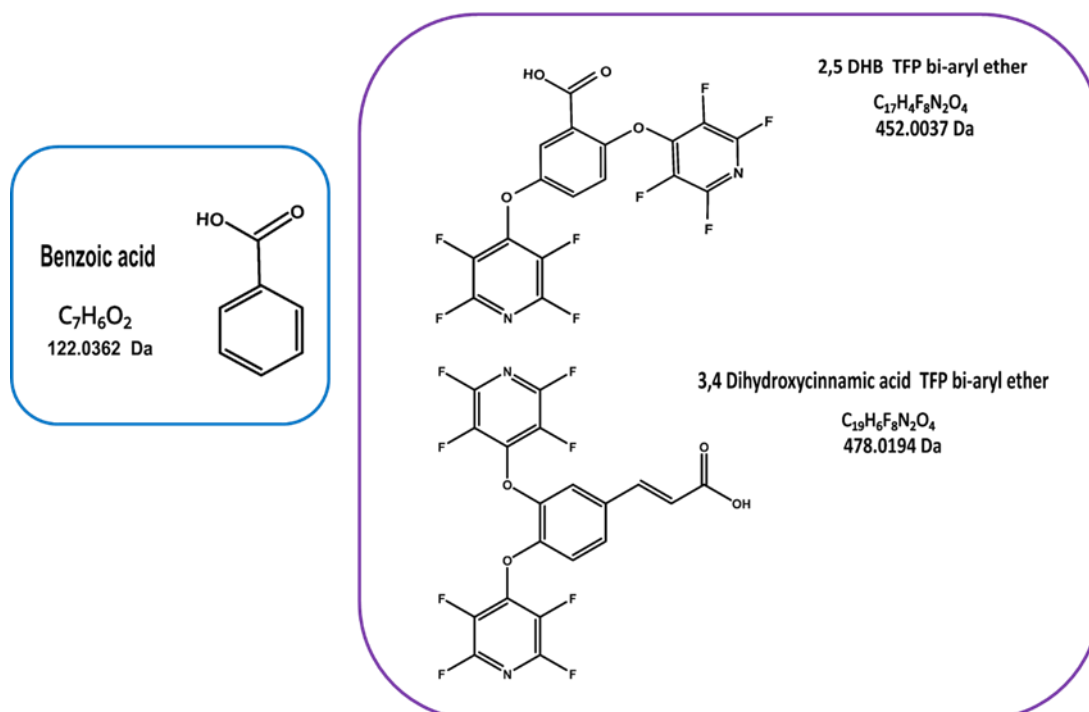


Figure 3-7: Structure of the four compounds obtained in fraction 3 and its corresponding derivatization using the PFP.

Table 3-4: Tandem mass spectrometry analysis of the derivatized standard eluted using the formic acid after derivatization by pentafluoropyridine.

Name	MS	Collision voltage (V)	MS ²	
			m/z	-Loss (abundance %)
2.5 DHB + PFP	$[C_{17}H_4F_8N_2O_4 + H]^+$ m/z453.0116	-12	435.0010	-H ₂ O (2)
			433.0539	-F (24)
			409.0218	-CO ₂ (100)
			286.0122	-C ₅ HF ₄ N (54)
			243.0302	-C ₅ F ₄ NO [•] , -CO ₂ (84)
3.4 dihydroxycinnamic acid + PFP	$[C_{19}H_6F_8N_2O_4 + H]^+$ m/z479.0272	-12	461.0167	-OH (77)
			435.0374	-CO ₂ (6)
			328.0228	-C ₅ F ₄ N [•] (17)
			312.0278	-C ₅ F ₄ NO [•] (100)
			295.0251	-C ₅ F ₄ NO [•] , -H ₂ O (30)
			268.0380	-C ₅ F ₄ NO [•] , -CO ₂ (3)
			243.0302	-C ₅ F ₄ NO [•] , -C ₃ H ₂ O ₂ (35)

Then, the sample fractionation and derivation steps applied on a mixture of representative molecules of lignocellulosic bio-oil allow to reveal different classes of oxygen-containing compounds depending on their functional groups and their number at the molecular level. Fraction 1 gathers the non-acid and non-phenolic compounds in which carbonyl function can be tagged. Fraction 2 recovers the phenolic compounds for which each phenolic chemical function and carbonyl are highlighted. The Fraction 3 groups the acidic compounds for which each phenolic group and carbonyl are labeled.

3.5. Application to Bio-oils

The integrative fractionation/derivatization method was applied on a lignocellulosic bio-oil obtained by fast-pyrolysis of oak. For comparison, bio-oil was first analyzed by (+) ESI, (-) ESI (+) APCI and (+) APPI FT ICR-MS. Numerous oxygen-containing compounds were detected as displayed in the Figure 3-8. Different zones were highlighted on the van Krevelen diagrams: lignin derivatives for which $0.5 < H/C < 1.5$ and $0.2 < O/C < 0.6$, lipid-like compounds in the $0.06 < O/C < 0.2$ and $1.8 < H/C < 2.2$ area while the carbohydrate-like compounds are seen at $1.5 < H/C < 2$ and $O/C < 0.5$. It was observed that the highest density of the oxygen-containing compounds was found in the lignin derivative area.

After the sample bio-oil fractionation/derivation steps, the six fractions were analyzed by FTICRMS with the most suited ionization technique for sensitively detecting the compounds in each of the three fractions. Hundreds and even thousands of signals were typically observed in the different mass spectra (Figure 3-9). These mass spectra were processed by assigning

signals to CHO elemental formula, including N, Cl and F to highlight the labeled carbonyl components, and the derivatized phenolic compounds, respectively.

Elemental composition of the original $C_xH_yO_z$ bio-oil constituents can be derived from the formulae of the neutrals linked to the detected ions (remove of a proton for $[M+H]^+$ cation addition of a proton for $[M-H]^-$ anions, and addition of an electron for $M^{+\bullet}$ molecular ion):

$-C_{(x+6n)}H_{(y+(6-2)n)}O_{(z-n)}N_nCl_n$ for compounds with n carbonyl groups.

$-C_{(x+5m)}H_{(y-m)}O_zF_{4m}N_m$ for phenolic compounds with m phenolic groups.

$-C_{(x+6n+5m)}H_{(y+4n-m)}O_{(z-n)}F_{4m}N_{m+n}Cl_n$ for phenolic compounds with m phenol groups and n carbonyls.

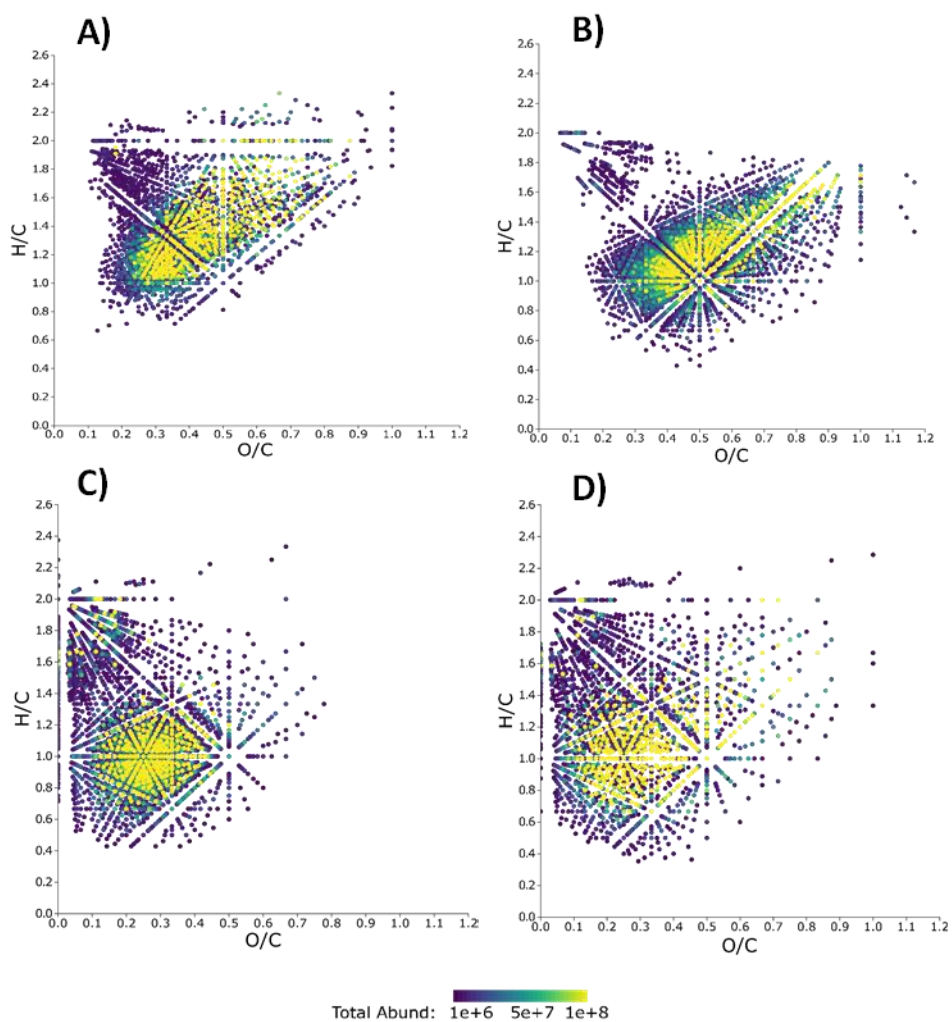


Figure 3-8: Van Krevelen diagrams of Oak raw bio-oil analyzed by FT ICR-MS with (+) ESI (A), (-) ESI (B), (+) APPI (C), and (+) APCI (D). Representations done using the in-house "Punc'data" data treatment software.

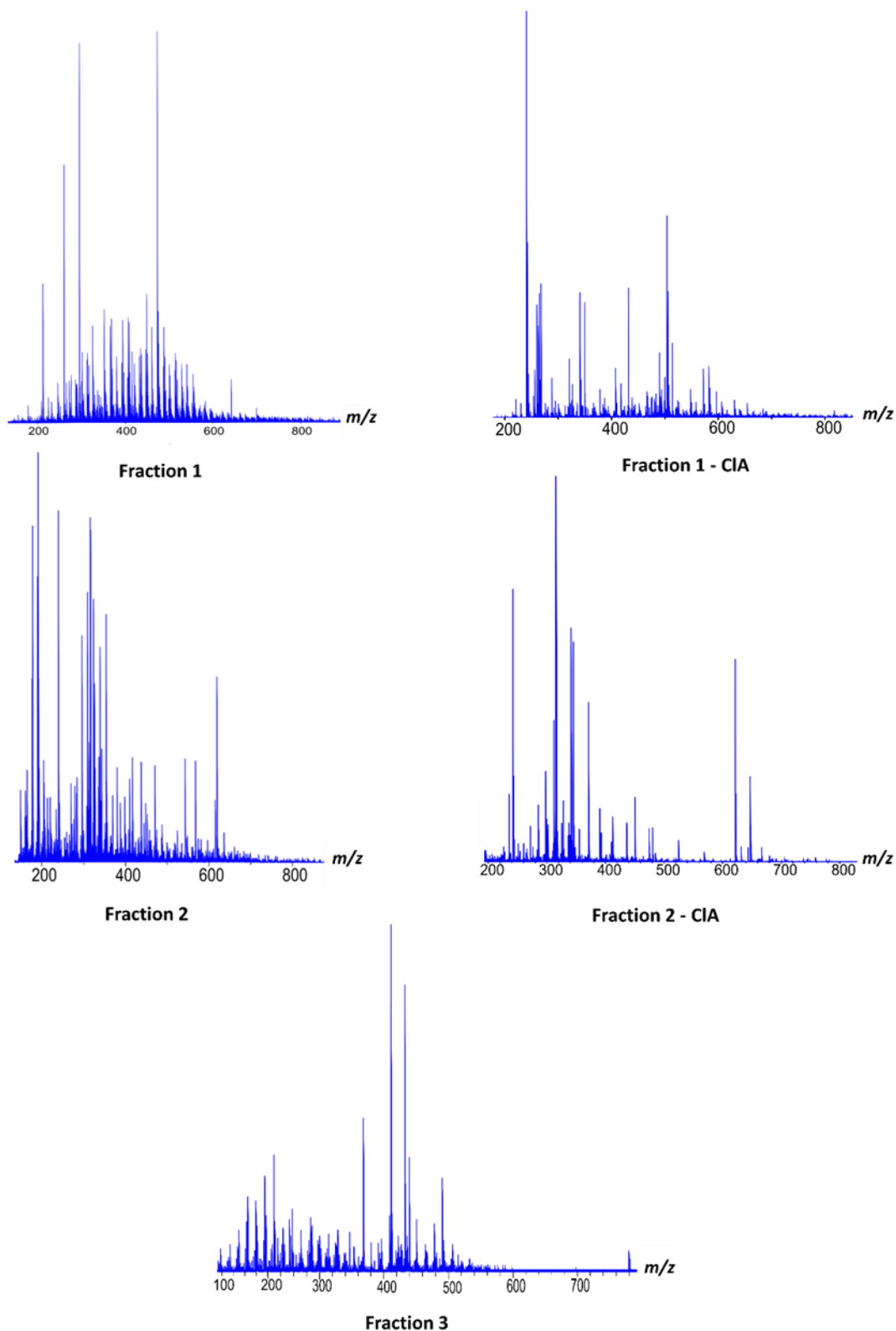


Figure 3-9: Mass spectrum obtained after the analysis of each fraction. (Top left) Mass spectrum by APCI (+) of the fraction 1 before adding the primary amine, (Top right) Mass spectrum by APCI (+) of the fraction 1- CIA after adding the primary amine, (Middle left) Mass spectrum by APPI (+) of the fraction 2 before adding the primary amine, (Middle right) Mass spectrum by APPI (+) of the fraction2- CIA after adding the primary amine, and (Bottom) Mass spectrum by APCI (+) of the fraction 3.

According to the established protocol, the compounds in fraction 1 are esters, ethers, furans, ketones, aldehydes and aliphatic alcohol. Van Krevelen diagram of the fraction 1 analyzed by (+) APCI FT-ICR MS is given in Figure 3-10A. Around 1400 elemental formulas were assigned to oxygen-containing compounds. They had a high diversity of elemental composition those H/C and O/C ratios covered the area of the lignin and carbohydrate derivatives. Specific markers of the cellulose pyrolysis such as levoglucosan ($C_6H_{10}O_5$, H/C = 1.666 and O/C = 0.833), and cellobiosan ($C_{12}H_{22}O_{11}$, H/C = 1.833 and O/C = 0.9166) were clearly observed.

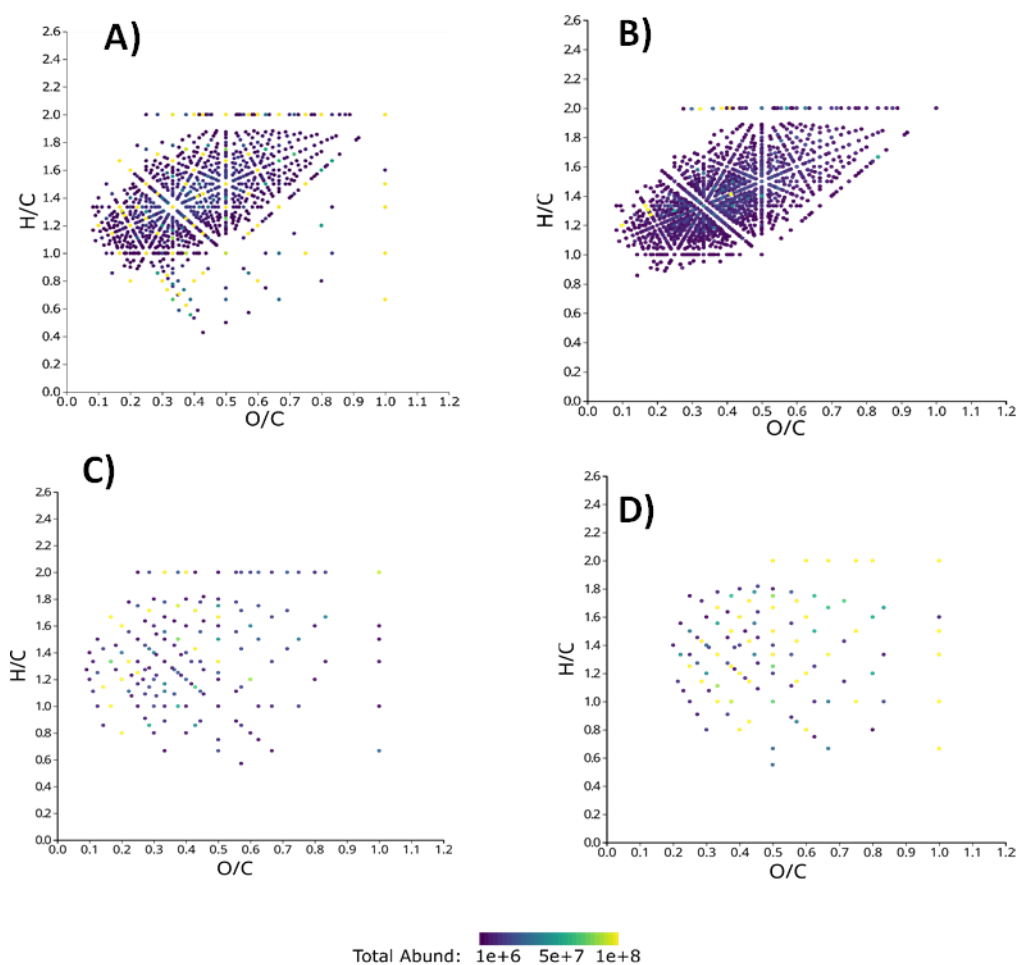


Figure 3-10: Van Krevelen diagram of: A- fraction 1 analyzed by (+) APCI FT-ICR MS B,C,D- fraction 1 – CIA analyzed by (+) ESI FT-ICR MS for compounds that remain non-derivatized (B), are derivatized once (C), and are derivatized twice (D) by 3-chloroaniline.

Distinction of the carbonyl families from the fraction 1 was done by adding 3-chloroaniline (Fraction 1-CIA). Three van Krevelen diagrams of the fraction 1-CIA are given Figure 3-10. Figure 3-10 B displays the non-carbonyl compounds, Figure 3-10 C the compounds that have one carbonyl group, and Figure 3-10 D the compounds that have two carbonyl groups. First, it has to be noticed that the sum of number of elemental compositions of these 3 classes reaches more than 3500 increasing by a factor 2.5 the number of detected compounds,

compared to what observed in Figure 3-10A in the absence of 3-chloroaniline derivation. From all of these non-phenolic and non-acidic compounds, 2/3 are non-carbonylated, around 1/4 have one carbonyl group and the remained compounds have two carbonyl groups. Interestingly, for these three classes, their distribution according to the number of O atoms is quite similar but as the number of carbonyl group increases, a decrease of their distribution in regard to the number of C atom is observed (Figure 3-11).

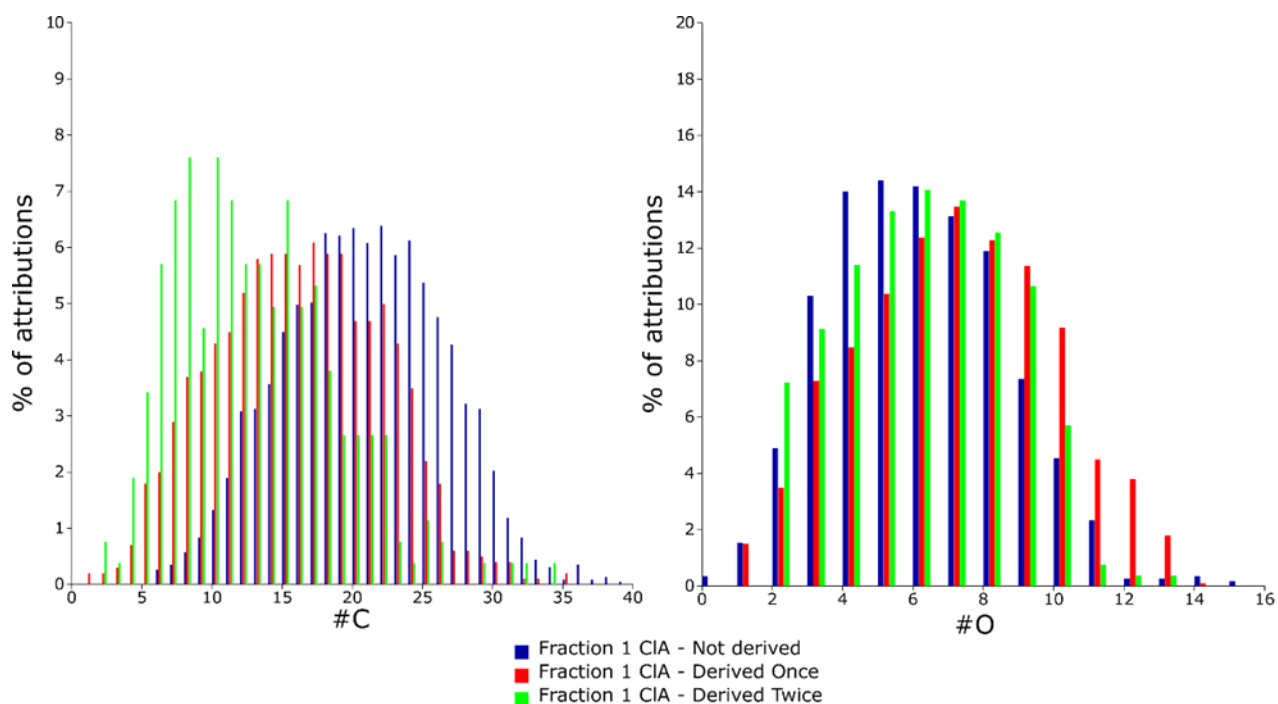


Figure 3-11: Relative distribution in respect with the carbon atom count (left) and with the oxygen atom count (right) for the fraction 1 analyzed by (+) APCI after adding the 3-chloroaniline.

Indeed, very low mass species were observed for twice carbonylated compounds such as glyoxal. This effect was related to the optimal mass measurement range that was considered in these experiments, which was in the 114 - 1000 m/z range. Each derivatization by 3-chloroaniline implied a mass shift of 109 Da giving accessible the detection of low mass compounds but decreasing the sensitivity for the detection of high mass compounds, which m/z became greater than 1000. This behavior is well illustrated by the DBE distribution with respect to the carbon and oxygen numbers (Figure 3-12) and the range class compound distribution in respect with the carbon and oxygen count (Figure 3-11). The higher the oxygen count, the carbon count, and the DBE, the higher the mass of the bio-oil component. Consequently, the heaviest compounds, which can be derivatized several times were out of the optimized m/z range used to ensure the transfer of the ion into the ICR cell. Therefore, the high mass species are mainly associated with the once derived and even the non-derivatized compounds. Moreover, adding the 3-chloroaniline to this fraction did not only allow the distinction between no carbonyl species and carbonyl species (reacted once or twice with the

primary amine) but also allowed the distinction between carbohydrates containing no free anomeric hydroxyl groups (anomeric carbon) and those that contain them. Sugars exist in equilibrium between these two configurations. In the open-chain form, the anomeric carbon is the carbon of the carbonyl group, which is either an aldehyde or ketone, depending on the nature of the sugar. Once the sugar exists in this configuration, the carbonyl site is active, and the Schiff base could be formed explaining the carbohydrate zone highlighted in the Van Krevelen diagram (Figure 3-10 C) of the compounds who reacted once or not with amine.

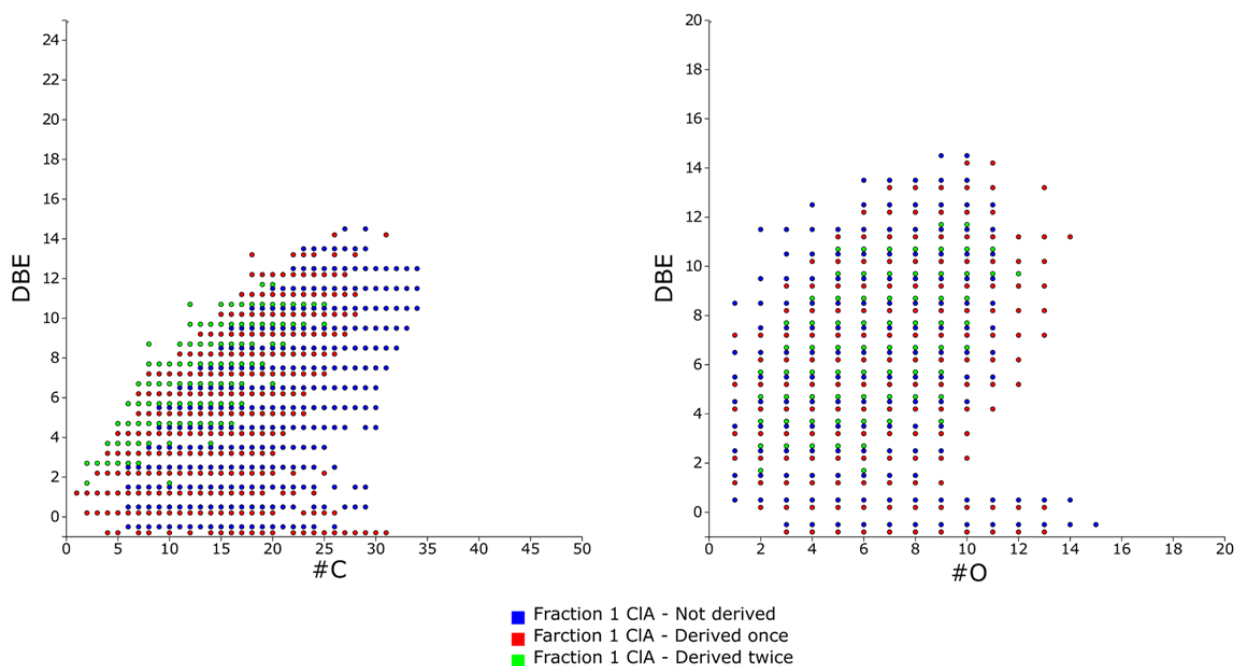


Figure 3-12: DBE versus #C and #O for the fraction 1 CIA analyzed by APPI (+), (blue) not derivatized by the 3-chloroaniline, (red) derived once, and (green) derived twice with PFP.

The distinction of the carbonyl families (with primary amine) was also used to evidence methoxy and dimethoxy phenol derivatives of the fraction 2. The Van Krevelen diagrams (Figure 3-13) of the compounds derivatized by PFP and both by PFP and 3-chloro-aniline highlight only the zone that matches with the lignin derivatives. As a result, these lignin-linked species are mono and polyphenolic species with a restricted number (one, two or three) of phenolic chemical functions since these compounds were once (Figure 3-13 A), twice (Figure 3-13 B) and thrice (Figure 3-13 C) derivatized by the PFP, as was seen on the resveratrol standard. Nevertheless, it has also be kept in bear, that each derivatization by a PFP molecule increases the mass of the compounds by 149 Da. Consequently, the compounds which underwent an important number of PFP derivatization were out of the optimized m/z range, which did not allow their sensitive detection. The same behavior may explain the poor contribution of compounds, which can be derivatized several times by PFP and 3-chloroaniline (Figure 3-14). Thus, the few species which have both phenolic and carbonyl sites were low mass compounds. They were evidenced in the lignin zone (Figure 3-15) of the van Krevelen diagram. The Figure 3-

15 shows the representation of the DBE with respect of the oxygen and carbon number. Basically, the DBE and consequently the level of unsaturation increases when the H/C decrease but is primary not correlated with the number of oxygen atoms. The presence of at least a phenolic group (a six-membered aromatic ring) requires a DBE value equal at least to 4.

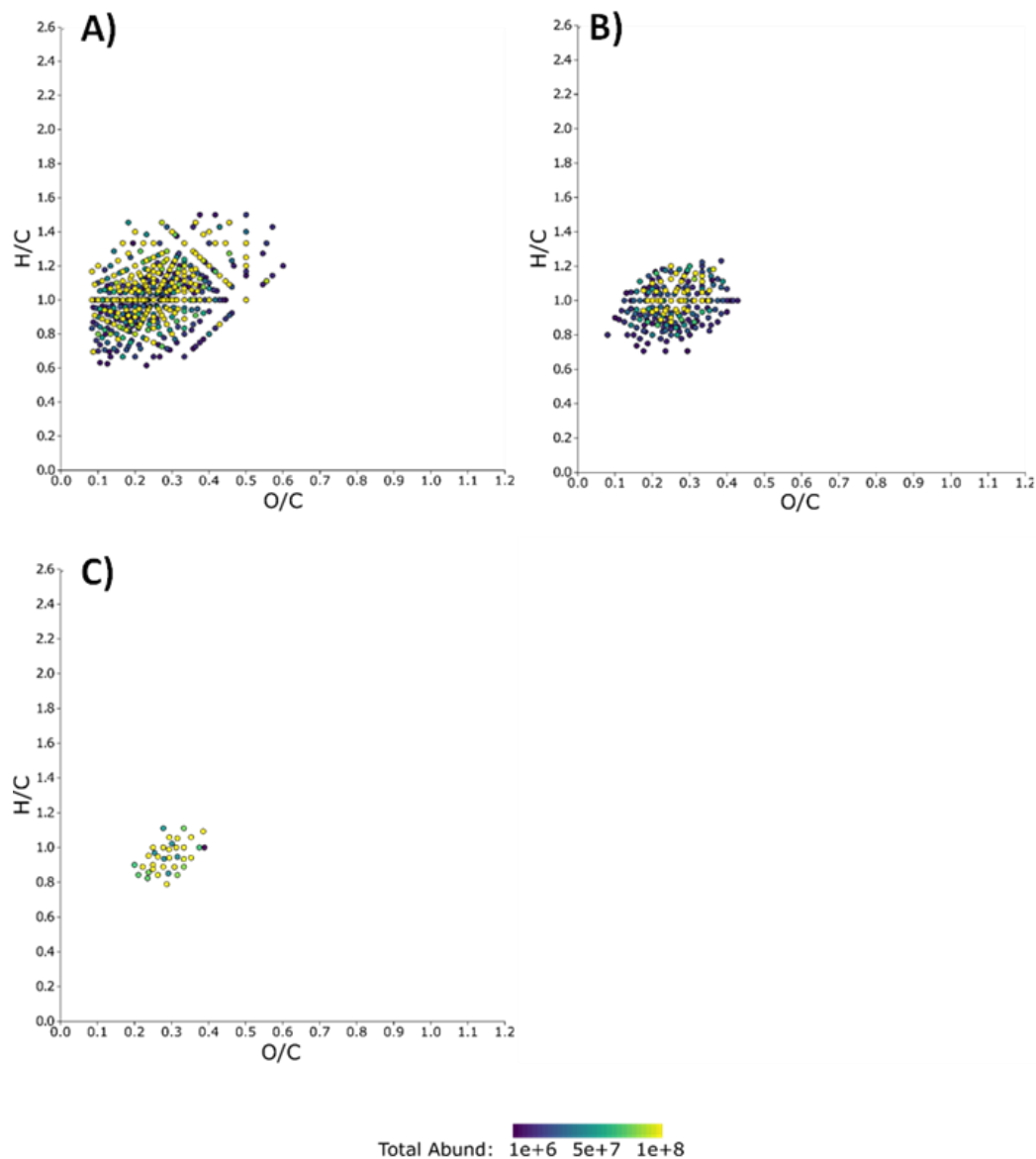


Figure 3-13: (Top Left) Van Krevelen diagram of the fraction 2 analyzed by APPI (+) and derived once with PFP, (Top right) Van Krevelen diagram of the fraction 2 derived twice with PFP, and (Bottom left) Van Krevelen diagram of the fraction 2 derived thrice with PFP.

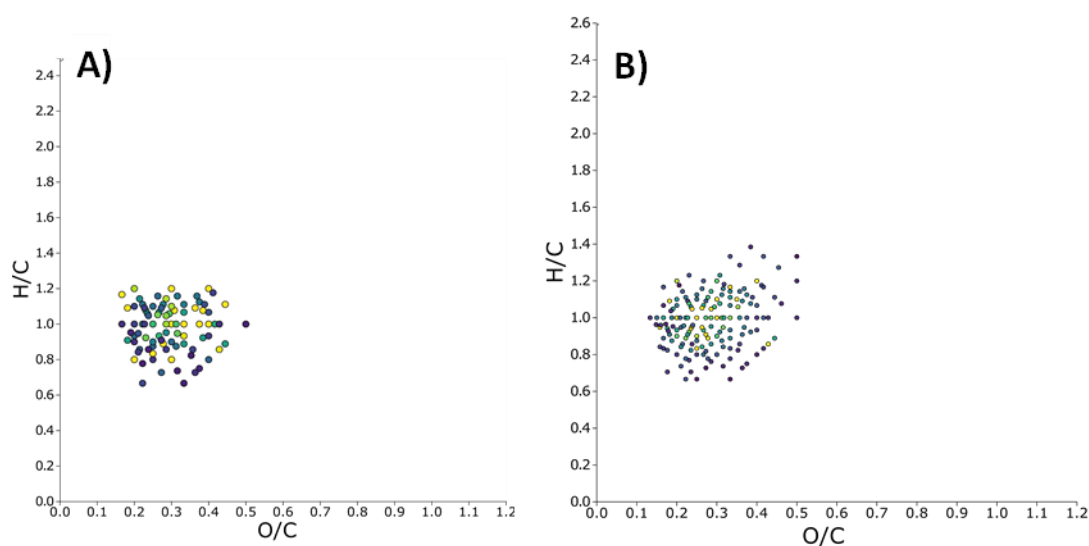


Figure 3-14: (Left) Van Krevelen diagram of the fraction 2 CIA analyzed by APPI (+) and derived once with PFP and the primary amine, and (Right) Van Krevelen diagram of the fraction 2 CIA derived only once with PFP.

The phenolic compounds, which were once derivatized by PFP, present a DBE value ranging from 4 to 18 (Figure 3-15 A), which means that a large part of them (low DBE value) only contain a phenolic ring decorated by poorly unsaturated substituents such as guaiacol, cresol, creosol. Nevertheless, a significant number of once PFP derivates includes lignin-like oligomer for which the number of poly-phenolic character is mainly from the presence of methoxy functions (coniferyl and synapyl units). The phenolic compounds derived twice with PFP (Figure 3-15 B) are compounds with at least 10 carbon atoms and a DBE greater than 6. Part of them is relative to monophenolic compounds with two phenol function but the majority of them are polyphenolic ones (Figure 3-16). For the compounds that were derivatized once with PFP and once with the 3-chloroaniline (Figure 3-17), they have a number of carbons >6 and DBE values ≥ 5 . According to their similar distribution to the monophenolic compounds, the only difference is made by the presence of a carbonyl group leading to an increase of 1 the value of the DBE and the number of carbon and oxygen atoms.

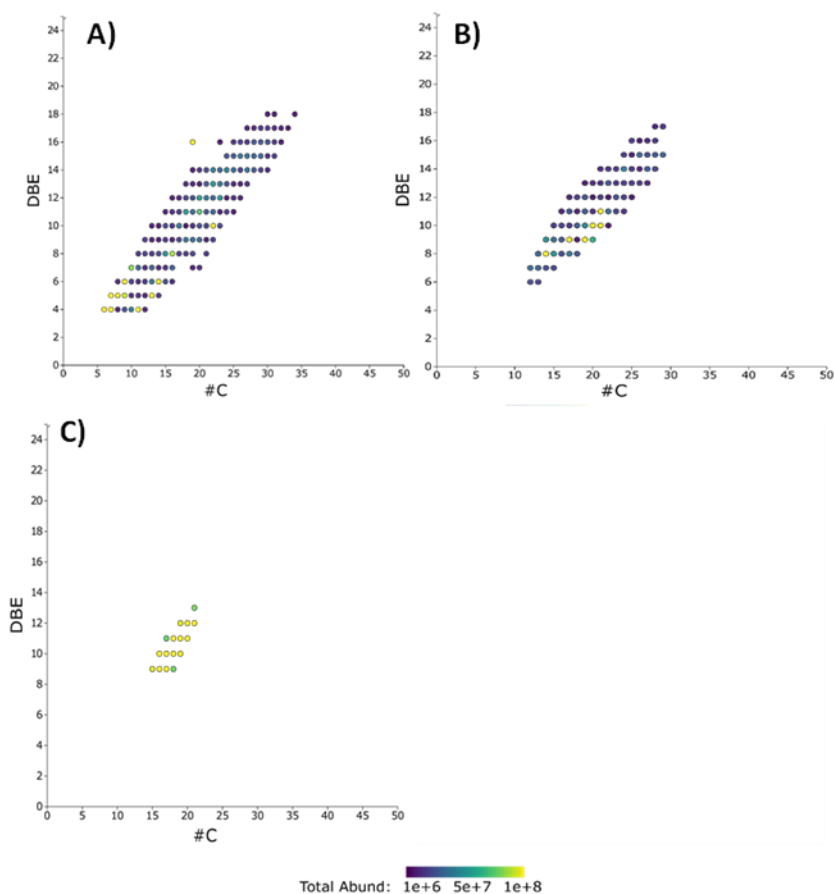


Figure 3-15: DBE versus #C for the compounds obtained in fraction 2 after subtraction of the derivatization reagent analyzed by APCI (+). (Upper left, A) DBE versus #C for the compounds once derived with the PFP, (Upper right, B) DBE versus #C for the compounds twice derived with the PFP, and (Bottom C) DBE versus #C for the compounds derived thrice with the PFP.

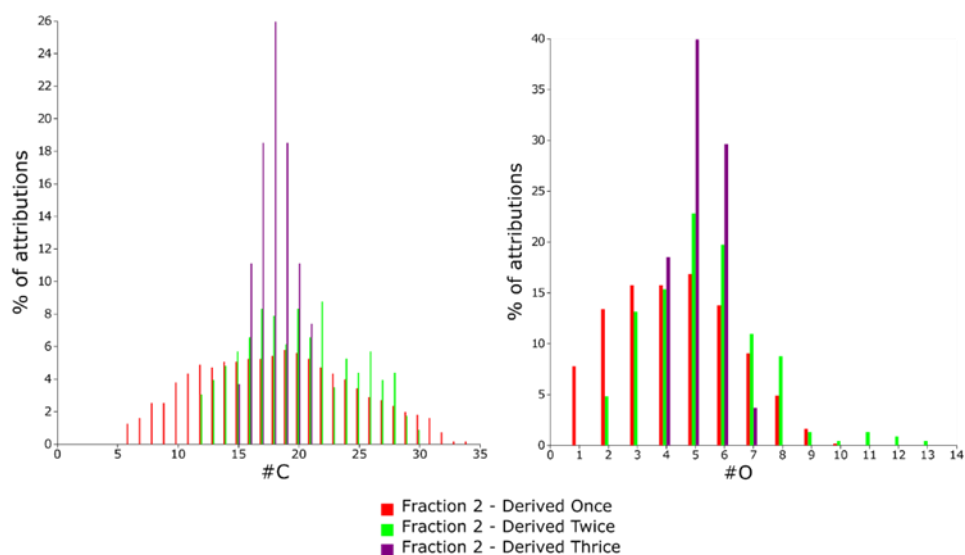


Figure 3-16: Relative distribution in respect with the carbon atom count (left) and with the oxygen atom count (right) for the different compounds obtained in fraction 2.

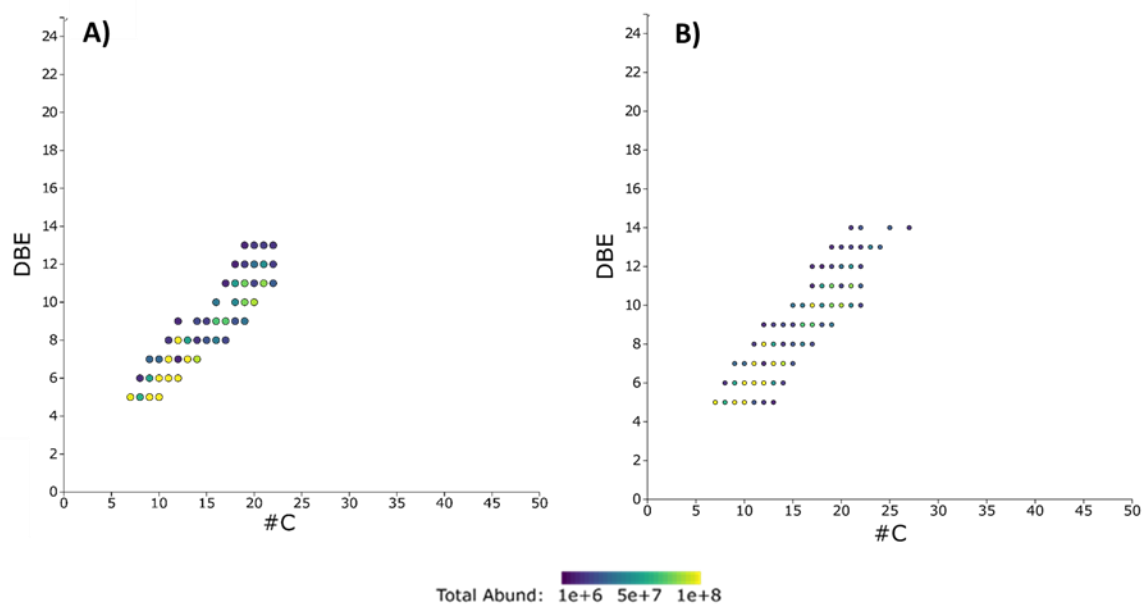


Figure 3-17: DBE versus #C for the compounds obtained in fraction 2 – CIA after subtraction of the derivatization reagent analyzed by APCI (+). (Left, A) DBE versus #C for the compounds once derived with the PFP and once with the primary amine, (Right, B) DBE versus #C for the compounds derived only with PFP and not derived with primary amine.

Fraction 3 was analyzed by (+) APCI FT-ICR MS. According to the established protocol, it brings together the compounds having at least one carboxylic acid group. More than 710 elemental formulae correspond to these acids some of which are also derived by PFP (Figure 3-18). Lipidic compounds are mainly highlighted in the van Krevelen diagram of the compounds that were not derived with pentafluoropyridine even if another portion of compounds is in the carbohydrate and lignin zones of (Figure 3-18 A). It's clear that these compounds are mainly monofunctional acid (lipids) and are also highlighted in the representation of their DBE with respect to their carbon number (Figure 3-20). The species with high number of carbon and low value of DBE are known to be fatty acids emphasizing the fact that the compounds in this zone are monofunctional acids and correspond to the non-, mono-, or poly unsaturated lipids. The other distribution is mainly relative to the presence of one aromatic ring, with possible 1 to 5 oxygen atoms coming from alkoxy groups, ether, O-heterocyclic and/or saturated alcohol moieties. The Van Krevelen diagram (Figure 3-18 B and C) of the compounds that were derived once or twice with the PFP are concentrated in the lignin zone. Indeed, these compounds are multifunctional having at least one or two phenol site and one acidic site. However, the density distribution of these compounds (Figure 3-19) shows clearly a high density concentrated at $0.5 < H/C < 1.5$ and $0.2 < O/C < 0.6$.

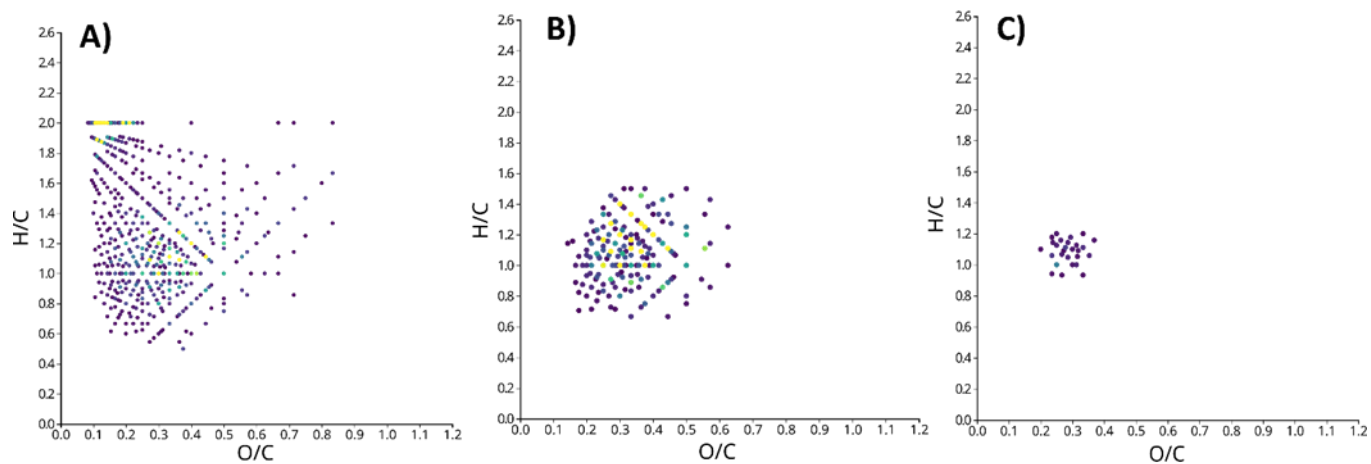


Figure 3-18: Van Krevelen of the fraction 3 analyzed by APCI (+), (left, A) not derived by the pentafluoropyridine, (middle, B) derived once by the pentafluoropyridine, and (right, C) derived twice by the pentafluoropyridine.

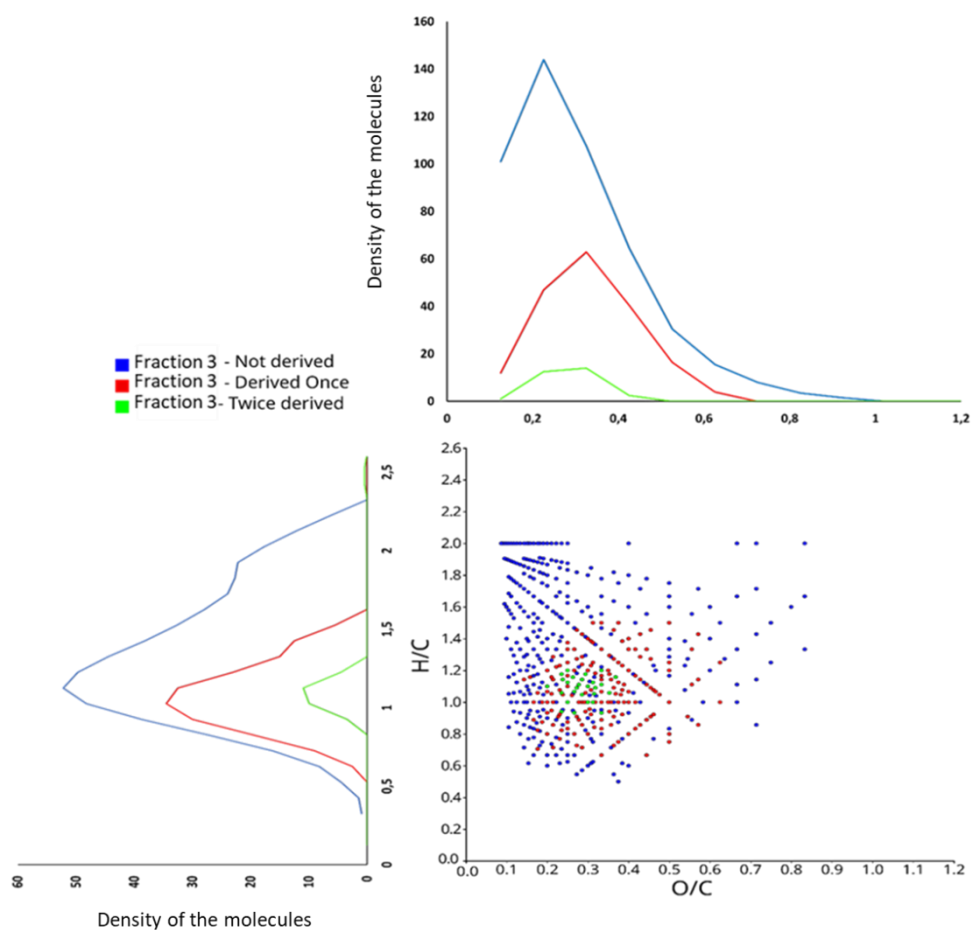


Figure 3-19: The density of molecules distributed along the H/C and O/C ratio for the fraction 3 analyzed by APPI (+) FT-ICR MS.

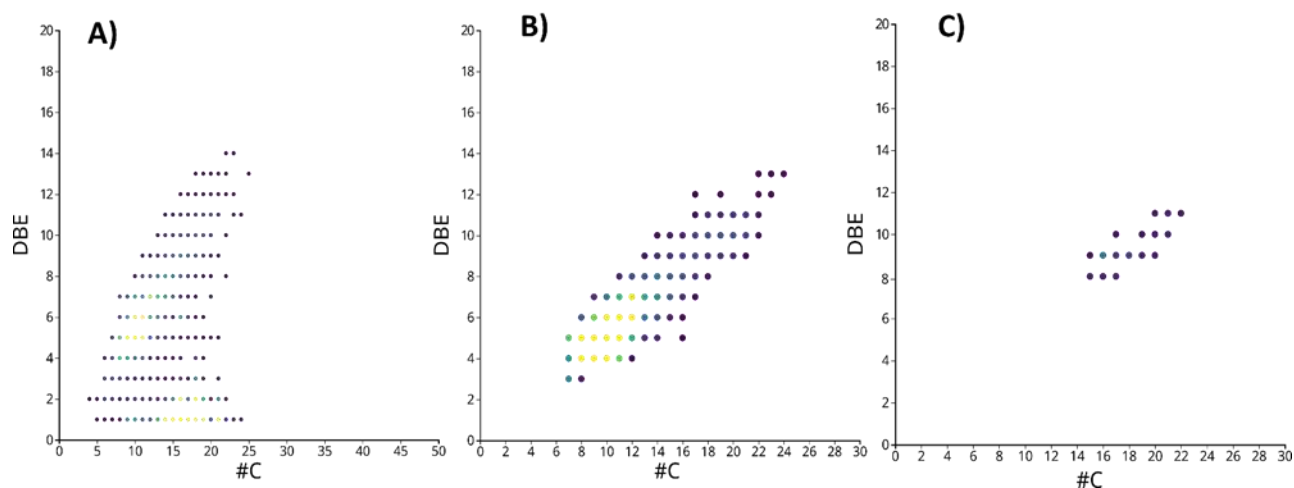


Figure 3-20: DBE versus carbon number of the compounds obtained in fraction 3 analyzed by APCI (+), (top) not derived, (middle) derived once, and (bottom) derived twice.

According to the DBE distribution, it is interesting to note that the presence of at one phenol group for these acids does not switch the DBE distribution to higher values. It means that no more than one aromatic ring is present in their structures substituted by at least one hydroxyl and other groups. For polyphenolic acids, from DBE=9 and #C >13, the number of attributions is very high meaning that these compounds have clearly two phenol rings (Figure 3-21 and 3-22).

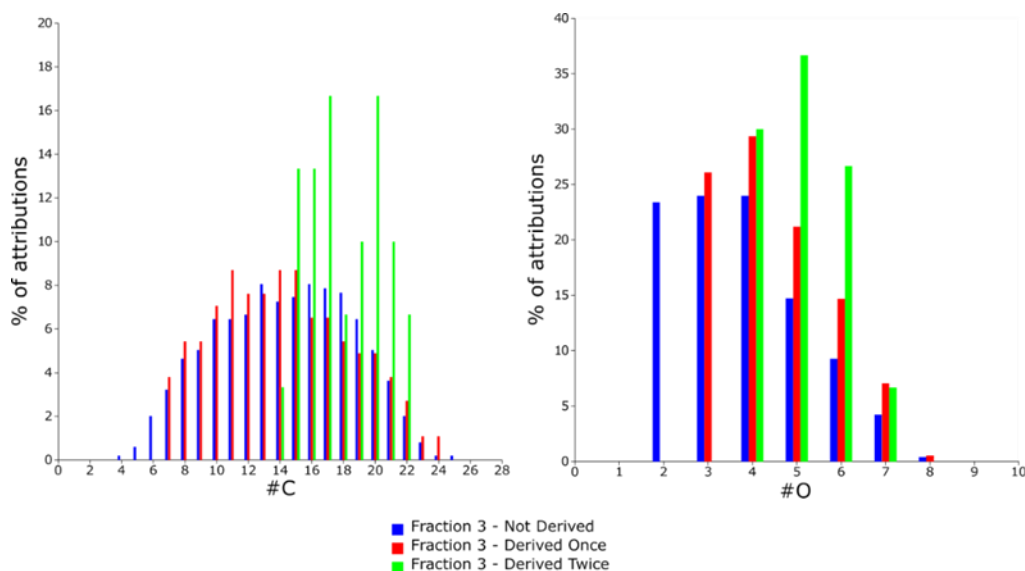


Figure 3-21: Relative distribution in respect with the carbon atom count (left) and with the oxygen atom count (right) for the different compounds obtained in fraction 3 analyzed by APCI (+).

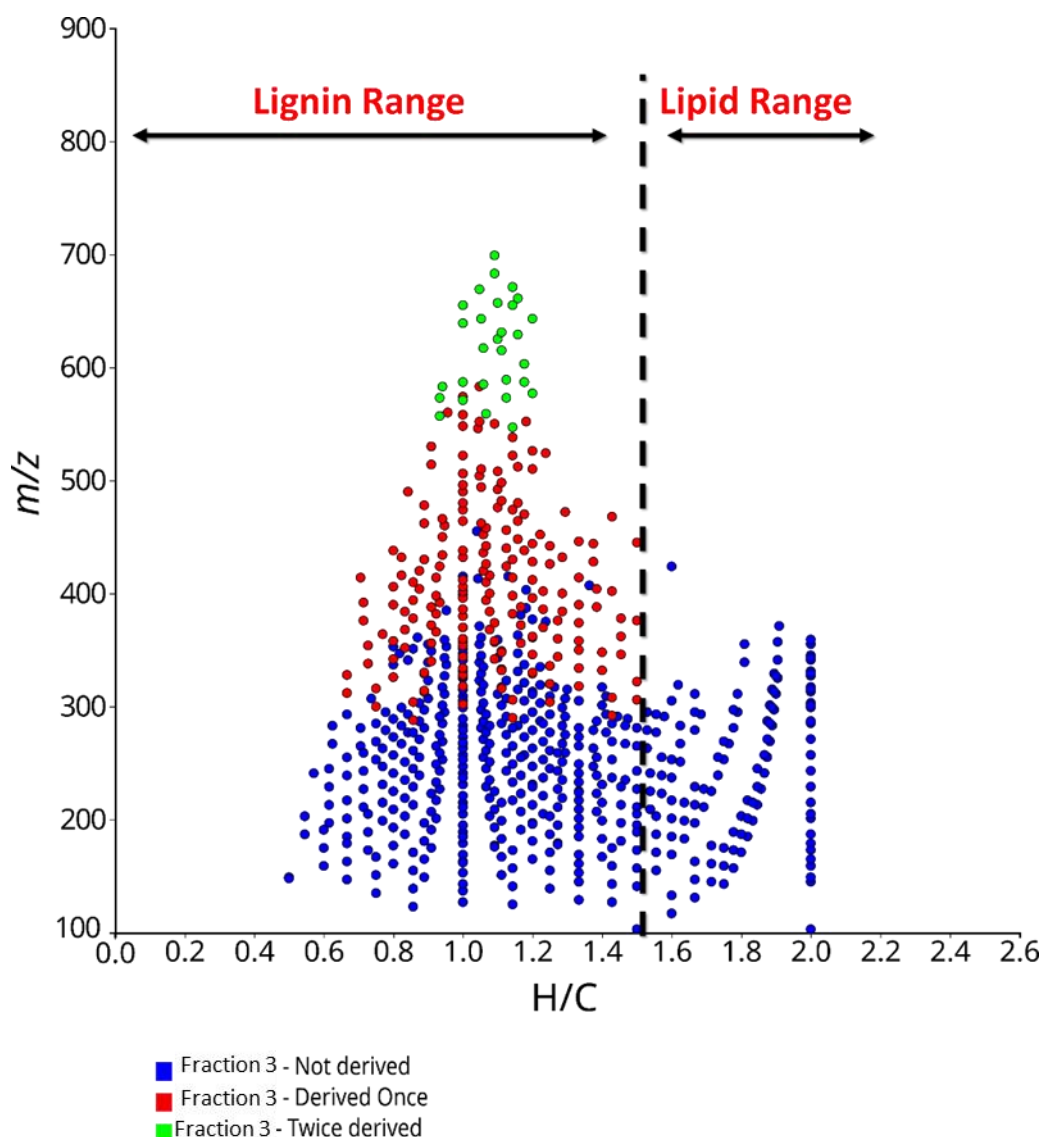


Figure 3-22: m/z ratio versus H/C ratio showing that the derivatized compounds in the fraction 3 analyzed by APCI (+).

Figure 3-22 shows the distribution of H/C ratio in function of m/z for the compounds obtained in the fraction 3. The compounds that were not derivatized with PFP fully cover the mass range from m/z 200 to 450. Based on the H/C ratio, these compounds could be divided into two classes. The first one gathers compounds with H/C ratio < 1.4 and are related to pyrolytic lignin while the second-class groups the compounds with H/C ratio > 1.5 and they are in majority lipidic species. This second class emphasize the previous observation obtained on the DBE distribution which highlights that these compounds are fatty acids with no phenolic site. The van Krevelen diagram (Figure 3-22) shows that the compounds derived once and twice with the PFP have H/C comprised between 0.8 and 1.4, and O/C comprised between 0.2 and 0.6 (Figure 3-18). These compounds cover a restricted range of m/z and H/C , from 300 to 700 which highlights that these compounds are high mass species and more concentrated in the van Krevelen plot in the zone related to lignin.

3.6. Conclusion

Using the pentafluoropyridine and the 3-chloroaniline as specific derivatization reagents, we were able to develop an efficient derivatization method using solid-phase extraction with anion-exchange sorbent. By applying this method to a standard mixture and a real bio-oil sample, we were able to show that different class of functional groups are well identified for O-containing compounds. It allows to generate three fractions from one sample divided as follow: the fraction 1 groups non-acid and non-phenolic components with additional identification of carbonyl compounds if present, the fraction 2 distinguishes mono and polyphenolic compounds and identifies of carbonyl group if present and the fraction 3 includes acidic components for which phenolic and/or carbonyl moieties can be highlighted if present. As a result, it is clearly demonstrated the capability of this integrative approach to direct the petroleomic analysis of a complex sample on the diversity of its functional groups.

3.7. References

- (1) Lu, Q.; Li, W.-Z.; Zhu, X.-F. Overview of Fuel Properties of Biomass Fast Pyrolysis Oils. *Energy Convers. Manag.* **2009**, *50* (5), 1376–1383. <https://doi.org/10.1016/j.enconman.2009.01.001>.
- (2) Czernik, S.; Bridgwater, A. V. Overview of Applications of Biomass Fast Pyrolysis Oil. *Energy Fuels* **2004**, *18* (2), 590–598. <https://doi.org/10.1021/ef034067u>.
- (3) Huang, H.; Yuan, X.; Zhu, H.; Li, H.; Liu, Y.; Wang, X.; Zeng, G. Comparative Studies of Thermochemical Liquefaction Characteristics of Microalgae, Lignocellulosic Biomass and Sewage Sludge. *Energy* **2013**, *56*, 52–60. <https://doi.org/10.1016/j.energy.2013.04.065>.
- (4) Wang, W.; Lemaire, R.; Bensakhria, A.; Luart, D. Review on the Catalytic Effects of Alkali and Alkaline Earth Metals (AAEMs) Including Sodium, Potassium, Calcium and Magnesium on the Pyrolysis of Lignocellulosic Biomass and on the Co-Pyrolysis of Coal with Biomass. *J. Anal. Appl. Pyrolysis* **2022**, *163*, 105479. <https://doi.org/10.1016/j.jaap.2022.105479>.
- (5) Joseph, J.; Baker, C.; Mukkamala, S.; Beis, S. H.; Wheeler, M. C.; DeSisto, W. J.; Jensen, B. L.; Frederick, B. G. Chemical Shifts and Lifetimes for Nuclear Magnetic Resonance (NMR) Analysis of Biofuels. *Energy Fuels* **2010**, *24* (9), 5153–5162. <https://doi.org/10.1021/ef100504d>.
- (6) Fortin, M.; Mohadjer Beromi, M.; Lai, A.; Tarves, P. C.; Mullen, C. A.; Boateng, A. A.; West, N. M. Structural Analysis of Pyrolytic Lignins Isolated from Switchgrass Fast-Pyrolysis Oil. *Energy Fuels* **2015**, *29* (12), 8017–8026. <https://doi.org/10.1021/acs.energyfuels.5b01726>.
- (7) Nanda, S.; Mohanty, P.; Kozinski, J. A.; Dalai, A. K. Physico-Chemical Properties of Bio-Oils from Pyrolysis of Lignocellulosic Biomass with High and Slow Heating Rate. *Energy Environ. Res.* **2014**, *4* (3), p21. <https://doi.org/10.5539/eer.v4n3p21>.
- (8) Yu, Y.; Chua, Y. W.; Wu, H. Characterization of Pyrolytic Sugars in Bio-Oil Produced from Biomass Fast Pyrolysis. *Energy Fuels* **2016**, *30* (5), 4145–4149. <https://doi.org/10.1021/acs.energyfuels.6b00464>.
- (9) Pérez-Ramírez, J.; Callén, M. S. Determining Bio-Oil Composition via Chemometric Tools Based on Infrared Spectroscopy.

- (10) Staš, M.; Auersvald, M.; Kejla, L.; Vrliška, D.; Kroufek, J.; Kubička, D. Quantitative Analysis of Pyrolysis Bio-Oils: A Review. *TrAC Trends Anal. Chem.* **2020**, *126*, 115857. <https://doi.org/10.1016/j.trac.2020.115857>.
- (11) Djokic, M. R.; Dijkmans, T.; Yildiz, G.; Prins, W.; Van Geem, K. M. Quantitative Analysis of Crude and Stabilized Bio-Oils by Comprehensive Two-Dimensional Gas-Chromatography. *J. Chromatogr. A* **2012**, *1257*, 131–140. <https://doi.org/10.1016/j.chroma.2012.07.035>.
- (12) Tessarolo, N. S.; Silva, R. C.; Vanini, G.; Pinho, A.; Romão, W.; de Castro, E. V. R.; Azevedo, D. A. Assessing the Chemical Composition of Bio-Oils Using FT-ICR Mass Spectrometry and Comprehensive Two-Dimensional Gas Chromatography with Time-of-Flight Mass Spectrometry. *Microchem. J.* **2014**, *117*, 68–76. <https://doi.org/10.1016/j.microc.2014.06.006>.
- (13) Bartoli, M.; Rosi, L.; Frediani, M.; Frediani, P. A Simple Protocol for Quantitative Analysis of Bio-Oils through Gas-Chromatography/Mass Spectrometry. *Eur. J. Mass Spectrom.* **2016**, *22* (4), 199–212. <https://doi.org/10.1255/ejms.1432>.
- (14) Palacio Lozano, D. C.; Jones, H. E.; Gavard, R.; Thomas, M. J.; Ramírez, C. X.; Wootton, C. A.; Sarmiento Chaparro, J. A.; O'Connor, P. B.; Spencer, S. E. F.; Rossell, D.; Mejia-Ospino, E.; Witt, M.; Barrow, M. P. Revealing the Reactivity of Individual Chemical Entities in Complex Mixtures: The Chemistry Behind Bio-Oil Upgrading. *Anal. Chem.* **2022**, *94* (21), 7536–7544. <https://doi.org/10.1021/acs.analchem.2c00261>.
- (15) Charon, N.; Ponthus, J.; Espinat, D.; Broust, F.; Volle, G.; Valette, J.; Meier, D. Multi-Technique Characterization of Fast Pyrolysis Oils. *J. Anal. Appl. Pyrolysis* **2015**, *116*, 18–26. <https://doi.org/10.1016/j.jaap.2015.10.012>.
- (16) Hertzog, J.; Mase, C.; Hubert-Roux, M.; Afonso, C.; Giusti, P.; Barrère-Mangote, C. Characterization of Heavy Products from Lignocellulosic Biomass Pyrolysis by Chromatography and Fourier Transform Mass Spectrometry: A Review. *Energy Fuels* **2021**, *35* (22), 17979–18007. <https://doi.org/10.1021/acs.energyfuels.1c02098>.
- (17) Hertzog, J.; Carré, V.; Le Brech, Y.; Mackay, C. L.; Dufour, A.; Mašek, O.; Aubriet, F. Combination of Electrospray Ionization, Atmospheric Pressure Photoionization and Laser Desorption Ionization Fourier Transform Ion Cyclotron Resonance Mass Spectrometry for the Investigation of Complex Mixtures – Application to the Petroleomic Analysis of Bio-Oils. *Anal. Chim. Acta* **2017**, *969*, 26–34. <https://doi.org/10.1016/j.aca.2017.03.022>.
- (18) Staš, M.; Chudoba, J.; Kubička, D.; Blažek, J.; Pospíšil, M. Petroleomic Characterization of Pyrolysis Bio-Oils: A Review. *Energy Fuels* **2017**, *31* (10), 10283–10299. <https://doi.org/10.1021/acs.energyfuels.7b00826>.
- (19) Harman-Ware, A. E.; Ferrell, J. R. Methods and Challenges in the Determination of Molecular Weight Metrics of Bio-Oils. *Energy Fuels* **2018**, *32* (9), 8905–8920. <https://doi.org/10.1021/acs.energyfuels.8b02113>.
- (20) Hertzog, J.; Carré, V.; Aubriet, F. Contribution of Fourier Transform Mass Spectrometry to Bio-Oil Study. In *Fundamentals and Applications of Fourier Transform Mass Spectrometry*; Elsevier, 2019; pp 679–733. <https://doi.org/10.1016/B978-0-12-814013-0.00022-3>.
- (21) Hughey, C. A.; Rodgers, R. P.; Marshall, A. G. Resolution of 11 000 Compositionally Distinct Components in a Single Electrospray Ionization Fourier Transform Ion Cyclotron Resonance Mass Spectrum of Crude Oil. *Anal. Chem.* **2002**, *74* (16), 4145–4149. <https://doi.org/10.1021/ac020146b>.

- (22) Marshall, A. G.; Rodgers, R. P. Petroleomics: The Next Grand Challenge for Chemical Analysis. *Acc. Chem. Res.* **2004**, *37* (1), 53–59. <https://doi.org/10.1021/ar020177t>.
- (23) Abou-Dib, A.; Aubriet, F.; Hertzog, J.; Vernex-Loiset, L.; Schramm, S.; Carré, V. Next Challenges for the Comprehensive Molecular Characterization of Complex Organic Mixtures in the Field of Sustainable Energy. *Molecules* **2022**, *27* (24), 8889. <https://doi.org/10.3390/molecules27248889>.
- (24) Kanaujia, P. K.; Sharma, Y. K.; Garg, M. O.; Tripathi, D.; Singh, R. Review of Analytical Strategies in the Production and Upgrading of Bio-Oils Derived from Lignocellulosic Biomass. *J. Anal. Appl. Pyrolysis* **2014**, *105*, 55–74. <https://doi.org/10.1016/j.jaap.2013.10.004>.
- (25) Faraji, M.; Yamini, Y.; Gholami, M. Recent Advances and Trends in Applications of Solid-Phase Extraction Techniques in Food and Environmental Analysis. *Chromatographia* **2019**, *82* (8), 1207–1249. <https://doi.org/10.1007/s10337-019-03726-9>.
- (26) Meier, D.; Windt, M. Analysis of Bio-Oils. In *Transformation of Biomass*; Hornung, A., Ed.; John Wiley & Sons, Ltd: Chichester, UK, 2014; pp 227–256. <https://doi.org/10.1002/9781118693643.ch13>.
- (27) Sedai, B.; Zhou, J. L.; Fakhri, N.; Sayari, A.; Baker, R. T. Solid Phase Extraction of Bio-Oil Model Compounds and Lignin-Derived Bio-Oil Using Amine-Functionalized Mesoporous Silicas. *ACS Sustain. Chem. Eng.* **2018**, *6* (8), 9716–9724. <https://doi.org/10.1021/acssuschemeng.8b00747>.
- (28) Barks_hannah_l_201005_mast.Pdf. https://smartech.gatech.edu/bitstream/handle/1853/33953/barks_hannah_l_201005_mast.pdf (accessed 2022-11-10).
- (29) Hertzog, J. Semi-Targeted Analysis of Complex Matrices by ESI FT-ICR MS or How an Experimental Bias May Be Used as an Analytical. *Journal of The American Society for Mass Spectrometry*, **2018**, *29*(3), 543-557.
- (30) Atapattu, S. N.; Rosenfeld, J. M. Micro Scale Analytical Derivatizations on Solid Phase. *TrAC Trends Anal. Chem.* **2019**, *113*, 351–356. <https://doi.org/10.1016/j.trac.2018.10.028>.
- (31) Field, J. A.; Monohan, Keith. In-Vial Derivatization and Empore Disk Elution for the Quantitative Determination of the Carboxylic Acid Metabolites of Dacthal in Groundwater. *Anal. Chem.* **1995**, *67* (18), 3357–3362. <https://doi.org/10.1021/ac00114a037>.
- (32) Chatfield, S. N.; Croft, M. Y.; Dang, T.; Murby, E. J.; Yu, G. Y. F.; Wells, R. J. Simultaneous Extraction and Methylation of Acidic Analytes Adsorbed onto Ion Exchange Resins Using Supercritical Carbon Dioxide Containing Methyl Iodide. *Anal. Chem.* **1995**, *67* (5), 945–951. <https://doi.org/10.1021/ac00101a023>.
- (33) Ng, L.-K.; Lafontaine, P.; Harnois, J. Gas Chromatographic–Mass Spectrometric Analysis of Acids and Phenols in Distilled Alcohol Beverages. *J. Chromatogr. A* **2000**, *873* (1), 29–38. [https://doi.org/10.1016/S0021-9673\(99\)01100-0](https://doi.org/10.1016/S0021-9673(99)01100-0).
- (34) Tang, P. H.-T.; Ho, J. S. Liquid–Solid Disk Extraction Followed by Supercritical Fluid Elution and Gas Chromatography of Phenols from Water. *J. High Resolut. Chromatogr.* **1994**, *17* (7), 509–518. <https://doi.org/10.1002/jhrc.1240170702>.
- (35) Brede, C.; Skjevraak, I.; Herikstad, H. Determination of Primary Aromatic Amines in Water Food Simulant Using Solid-Phase Analytical Derivatization Followed by Gas

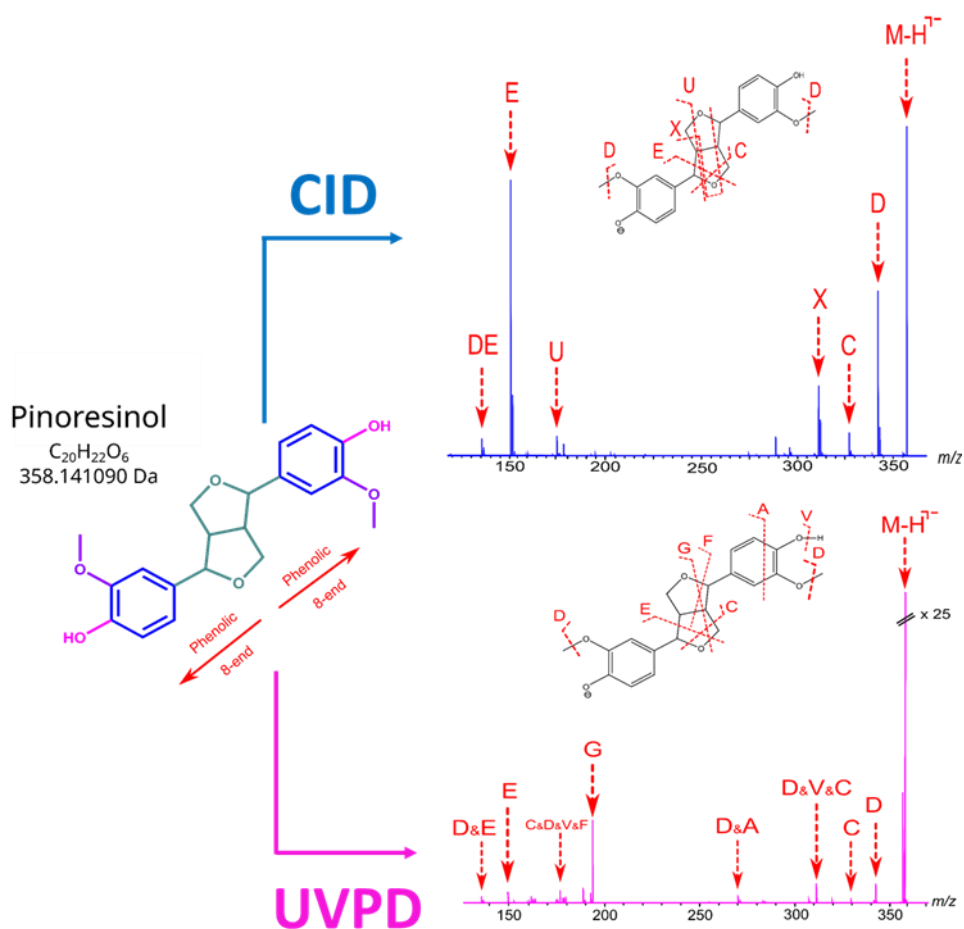
- Chromatography Coupled with Mass Spectrometry. *J. Chromatogr. A* **2003**, *983* (1–2), 35–42. [https://doi.org/10.1016/S0021-9673\(02\)01652-7](https://doi.org/10.1016/S0021-9673(02)01652-7).
- (36) Marshall, A. G.; Rodgers, R. P. Petroleomics: Chemistry of the Underworld. *Proc. Natl. Acad. Sci.* **2008**, *105* (47), 18090–18095. <https://doi.org/10.1073/pnas.0805069105>.
- (37) Kim, S.; Kramer, R. W.; Hatcher, P. G. Graphical Method for Analysis of Ultrahigh-Resolution Broadband Mass Spectra of Natural Organic Matter, the Van Krevelen Diagram. *Anal. Chem.* **2003**, *75* (20), 5336–5344. <https://doi.org/10.1021/ac034415p>.
- (38) Gautam, R.; Geniza, I.; Iacono, S. T.; Friesen, C. M.; Jennings, A. R. Perfluoropyridine: Discovery, Chemistry, and Applications in Polymers and Material Science. *Molecules* **2022**, *27* (5), 1616. <https://doi.org/10.3390/molecules27051616>.
- (39) G. Brittain, W. D.; L. Cobb, S. Tetrafluoropyridyl (TFP): A General Phenol Protecting Group Readily Cleaved under Mild Conditions. *Org. Biomol. Chem.* **2019**, *17* (8), 2110–2115. <https://doi.org/10.1039/C8OB02899K>.

PART IV : TANDEM MASS SPECTROMETRY: STRUCTURAL ANALYSIS OF CHEMICAL FUNCTIONAL GROUPS

CHAPTER 4 : UVPD vs CID: POTENTIAL TOOL FOR STRUCTURAL ANALYSIS OF BIO-OILS COMPONENTS

4.1. Publication: UVPD vs CID potential tool for structural analysis of bio-oil components

Anthony ABOU DIB, Bryan MARZULLO, Vincent CARRÉ, Jasmine HERTZOG, Mark Barrow, Peter O'CONNOR, Frédéric AUBRIET



4.2. Abstract

The compounds produced by pyrolysis or hydrothermal liquefaction of lignocellulosic biomass can be sustainable substitutes for those from fossil resources. Indeed, many chemicals in the generated bio-oils may be helpful to fuels or chemical building blocks. Nevertheless, these bio-oils must be upgraded by deoxygenation or cracking catalytic treatments before being employed. A satisfactory structural elucidation and characterization of the functional groups are required. This remains a significant analytical challenge. This is precisely the case for lignin derivatives, which part of them is refractory to upgrading treatment.

Mass spectrometry and tandem mass spectrometry (MS/MS) are helpful in this context. However, the traditional collisional activation (CID) does not always lead to significant structural information due to no specific fragmentation. Alternative activation techniques have to be used as ultraviolet photodissociation (UVPD). Herein, the complementarity between UVPD and CID MS/MS for the structural analysis of lignin-derived compounds illustrates the utility of UV activation in the study of bio-oil components. In this study, six lignin model compounds that efficiently absorb UV photons: the 2,5-dihydroxybenzoic acid and vanillin, known to be in pyrolysis bio-oils, coniferyl, and sinapyl alcohol, two elementary units of lignin, and two lignin dimers (pinoresinol and guaiacylglycerol- β -guaiacylolether GGE) were investigated. Tandem mass spectrometry measurements on each standard compound deprotonated ion resulted in fingerprint fragment ions unique to each analyte. Although just a small selection of compounds was discussed for this study, UVPD was more effective at providing structural details on a few bio-oil components generated by the pyrolysis of lignocellulosic biomass. The result of this work opens the path for the "2D FTMS" to systematically elucidate the structures of lignin-derived chemicals in bio-oils.

4.3. Introduction

To fight global warming and the emission of greenhouse gases, alternatives to fossil fuels such as natural gas, oil, or coal have to be found. The use of biomass is an exciting and sustainable solution. Thus, bioethanol and biodiesel production led to the development of first-generation biofuels. These biofuels have the disadvantage of competing with human and animal food and using dedicated crops leading to significant deforestation, pesticides, and fertilizers. The production of second-generation biofuels (from the conversion of lignocellulosic biomass) and third-generation (from algae) can have a less environmental impact and do not compete with the agri-food sector. Thus, converting lignocellulosic biomass may produce valuable chemicals and cleaner energy. One conversion method is pyrolysis, which produces gases, condensates (bio-oils), and char. The bio-oils have a promising future as sources of valuable chemicals or biofuel.^{1,2} The significant amounts of oxygen in bio-oil components have various undesirable effects that limit their usage.³ They are poorly chemical and thermo-oxidative stable, possess an excessively acidic behavior (corrosive characteristics), and present immiscibility with conventional petroleum fuels.³ An appropriate upgrading is therefore required before using bio-oils as biofuels. Such upgrading processes include catalytic hydrodeoxygenation and cracking treatment. Consequently, an adequate knowledge of the chemical components of bio-oils in detail is required to optimize such upgrading procedures.

For the past three decades, scientists worldwide have concentrated on producing bio-oils from lignocellulosic biomass (especially by pyrolysis) as a potential substitute for petroleum⁴⁻⁶ to achieve their characterization from a molecular viewpoint. The comprehensive study of bio-oil is very challenging since it may contain hundreds to thousands of different products resulting from the thermal conversion of the three main components of the lignocellulosic biomass (cellulose, hemicellulose, and lignin).⁷⁻⁹ The bio-oil components present a wide range of molecular weight, boiling point, polarity, and solubility. Traditionally, gas chromatography GC, 2D gas chromatography GCxGC,¹⁰⁻¹³ gel permeation chromatography GPC,^{14,15} high-performance liquid chromatography HPLC,¹⁶⁻¹⁸ Fourier-transform infrared FTIR^{19,20}, and nuclear magnetic resonance spectroscopy NMR²¹⁻²⁴ technologies have been used to

characterize the chemical composition of bio-oils. FTIR and NMR give global information on chemical groups' distribution in bio-oil components. Targeted approaches combining GC or GCxGC with mass spectrometry (MS) have been used to investigate many volatile and semi-volatile bio-oil compounds. However, throughout the past few decades, only a restricted number of works have been performed to study the structure of nonvolatile and high-molecular-weight bio-oil molecules.^{20,25–29}

In contrast, many investigations deal with the untargeted petroleomic analysis of bio-oil. Petroleomics requires using ultrahigh-resolution mass spectrometry (UHRMS), such as Fourier transform ion cyclotron resonance mass spectrometry (FT-ICR MS), to provide high confidence in the assignment of an elemental formula to each detected feature.^{30–33} Such an approach is limited to the identification of different class compounds concerning the number of oxygen or carbon atoms or the number of unsaturation, the so-called double bond equivalent (DBE). Despite its limitation (no structural information), petroleomics ensures to follow up the global efficiency of upgrading processes by modifying class compound distribution, typically eliminating the most oxygenated compounds. Nevertheless, identifying the structure of molecules refractory to upgrading treatment is needed to improve the bio-oil compound conversion.

Consequently, tandem mass spectrometry (MS/MS) is required to investigate the structure and functional groups present in the refractory species, mainly from the lignin thermal conversion. Different activation techniques are available to perform MS/MS, including collision activated/induced dissociation (CAD/CID),^{27,34,35} infrared multiphoton dissociation (IRMPD),^{36–38} and ultraviolet photodissociation (UVPD),^{39–41}. CID is the most widely used, especially to investigate organic compounds. IRMPD and UVPD are mainly employed to study biomolecules as peptides or proteins.^{42,43,44} In CID, the precursor ion is accelerated into a cloud of neutral gas, such as argon or nitrogen ensuring the conversion of part of its kinetic energy into internal energy. As a result, the excess of internal energy is distributed in the vibrational and rotational modes of the precursor ion, and the weaker bonds dissociate. Such an activation process may lead to dissociation events that are not always very informative (loss of water, carbon monoxide, or carbon dioxide), especially for aromatic or condensed organic compounds. Thus, the structural MS/MS characterization of bio-oil components refractory to upgrading treatment, is a significant issue because these compounds are mainly lignin derivatives. Alternative activation techniques have to be used. Since the aromatic molecules absorb UV photons efficiently, UVPD may be an exciting alternative to CID for the structural investigation of lignin derivative compounds. UVPD is still poorly employed for organic compounds but used to investigate polymers,^{45,46} and agrochemicals.^{39,45,47} By absorbing one or two high-energy UV photons, the UVPD ion-activation process occurs. Ions are then excited by their electronic state, giving access to more energetic dissociation pathways than collisional activation. Being a gas-less activation technique, UVPD is also of significant interest in FT-ICR MS.

To investigate, in this study, the capability of UVPD to obtain structural information of model compounds associated with bio-oil components. Six compounds have been studied. The two formers are 2.5 dihydroxybenzoic acid and vanillin, known to be in pyrolysis bio-oils. Coniferyl and sinapyl alcohol, two elementary units of lignin, and two lignin dimers (pinoresinol and guaiacylglycerol- β -guaiacylether GGE) were also considered. The choice of these molecules was made to cover the diversity of chemical groups (phenol, carboxylic acid, carbonyl, aromatic) present in bio-oil components, which are refractory to the upgrading

process. UVPD and CID MS/MS experiments were performed to demonstrate the usefulness of UV activation and their potential complementarity.

4.4. Materials and methods

4.4.1. Chemicals

LCMS grade methanol (VWR–Prolabo), as well as the used multi-functional standards, vanillin (97%, Aldrich), 2,5 dihydroxybenzoic acid (98%, Aldrich), and lignin standards such as coniferyl alcohol (98%, Aldrich), sinapyl alcohol (98%, Aldrich), guaiacylglycerol- β -guaiacylether (Aldrich), and pinoresinol ($\geq 95\%$, Aldrich), which structure is given in Figure 4-1, were used as supplied. Standard compounds were solubilized in methanol at a final concentration of 1 mg. mL⁻¹.

4.4.2. Mass spectrometry analysis

All samples were ionized using a home-built nano-electrospray ion source (nESI), and analyzed at the University of Warwick, Coventry, England, using a 12 T Bruker solarix FT-ICR mass spectrometer (Bruker Daltonik, GmbH, Bremen, Germany). 10 to 15 μ L of the sample solution was loaded into a pulled glass capillary tip using a Sutter P-97 Flaming/Brown micropipette puller (Sutter Instrument Co., Novato, CA, USA), and a nichrome wire was placed inside the tip, which served as the electrical connection. The capillary was set to -800V, and the nebulizing gas was maintained at 0.8 bar. The collision gas for the CID-based fragmentation investigations was argon. To isolate the deprotonated species a 3 Da isolation window was used. This window was chosen to select the whole isotope envelope and preserve sufficient precursor intensity for CID or UVPD fragmentation. For CID studies, an optimized collision potential (13–18 eV) was applied to the selected ions into the collision cell to promote fragmentation. The fragment ions were detected in the infinite ICR cell. For UVPD, the deprotonated species were exposed in the ICR cell to radiation from a 193 nm ArF excimer laser (ExciStar XS, Coherent) shot with a pulse energy and time duration of 1.8 mJ, and 7–10 ns, respectively. Each photon in the UV pulse had an energy of 6.4 eV. One hundred mass spectra were averaged to increase signal-to-noise ratios (S/N). Mass spectrum was acquired at 4 M. For both MS/MS methodologies, the precursor ion was accumulated for 2 seconds in the collision cell before being transferred to the Infinity ICR cell after (CID) or before (UVPD) activation.

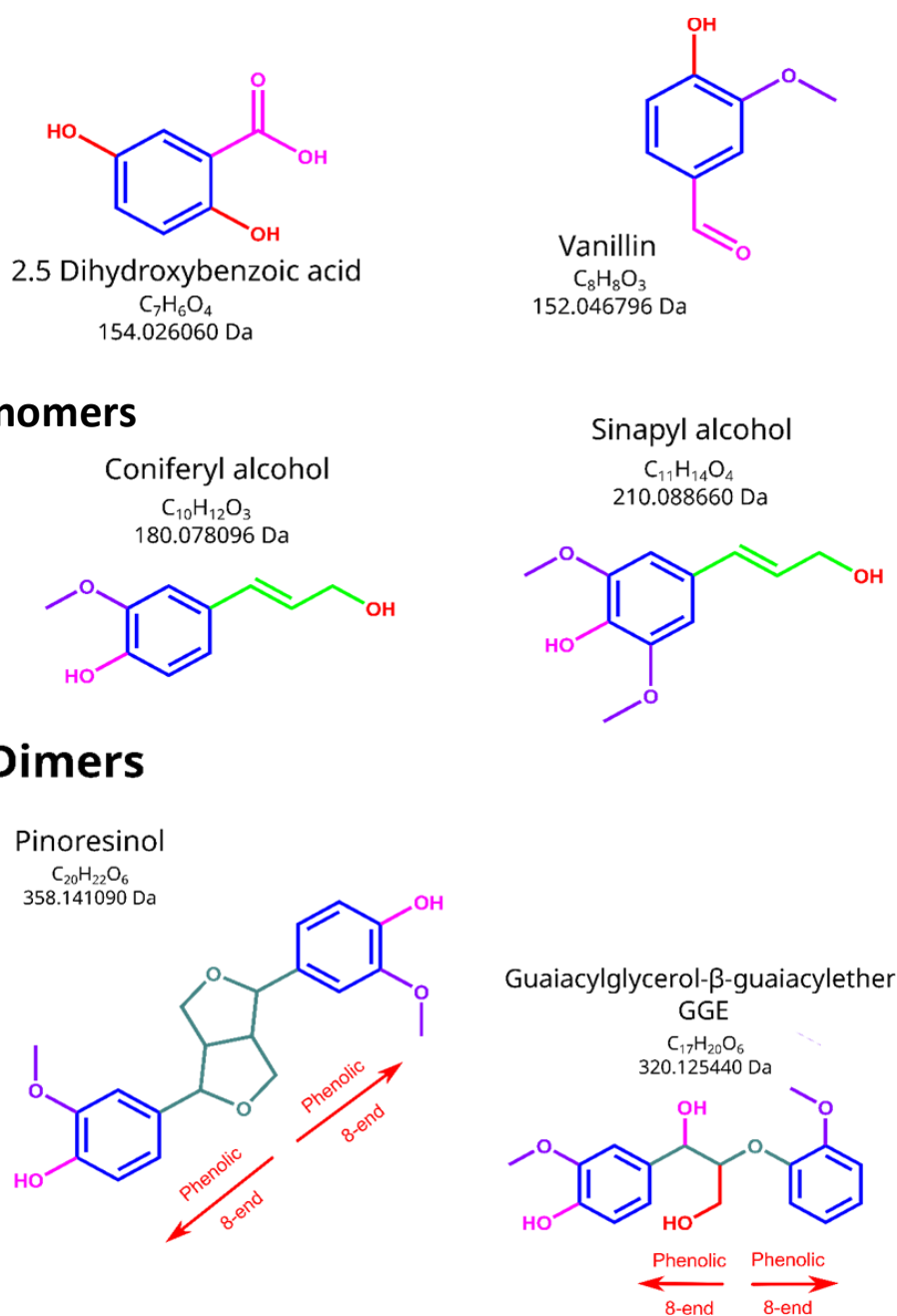


Figure 4-1: Structures of the six bio-oils standards that were investigated in this study. The various moieties in each compound are highlighted by the color coding of the structures.

4.5. Results and discussion

The direct infusion was used to analyze by (–) nESI MS the six bio-oil standards. CID and UVPD at 193nm were used to fragment the deprotonated molecular ion. The ultra-high mass resolution FT-ICR MS instrument employed in this study allowed the identification of fragment losses by very accurate *m/z* measurement and enabled the determination of a single elemental composition for each fragment ion. The putative fragmentation mechanisms were

systematically proposed and reported. When available, the fragmentation mechanisms were discussed and compared to previously published works performed by collisional activation.

4.5.1. Monoaromatic bio-oil components' MS/MS behavior

Tandem mass spectrometry first investigated some monoaromatic bio-oil components' MS/MS behavior. The MS/MS results of the 2,5 DHB by CID and UVPD, and vanillin is reported in this section.

4.5.1.1. 2,5 dihydroxybenzoic acid (2,5 DHB) CID and UVPD behavior

For 2,5 DHB, the decarboxylation was the prominent observed phenomenon and led to the formation of m/z 109.0291 ion, whatever the used activation method. It is a well know fragmentation pathway observed in the study of hydroxy and methoxy benzoate anion and led to the elimination of CO_2 .⁴⁸ The UV activation led mainly to eliminating a hydroxyl radical and forming an m/z 136.0174 ion. The easy absorption of UV photons by the aromatic ring induced this process, which produced a distonic radical anion whose stability was increased by delocalization. The fragmentation mechanisms are given in Figure 4-2. The peak list, and relative intensity of the fragment from the CID and UVPD of 2,5 DHB are highlighted in Table 4-1.

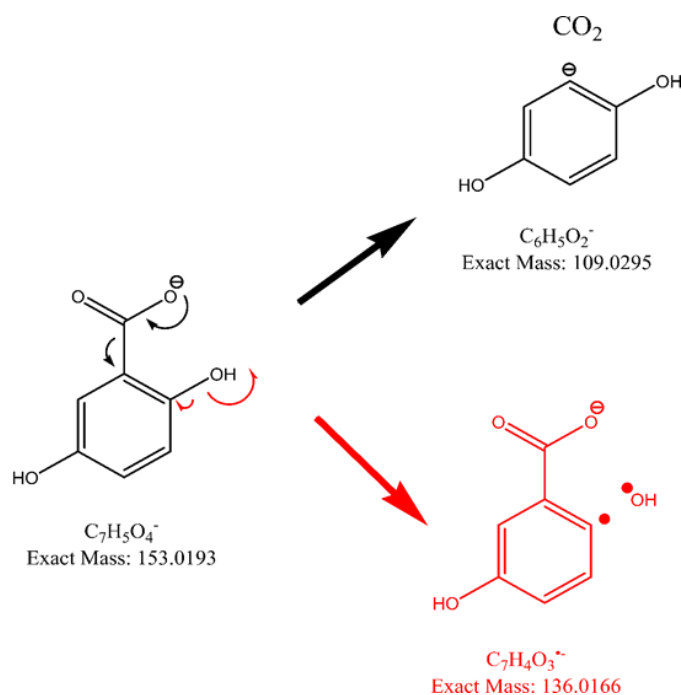


Figure 4-2: Proposed (black) and UVPD (black) of 2,5 dihydroxy benzoic

Table 4-1: Peak list and fragments from CID and

mechanism of CID (black and red) fragmentation acid.

relative intensity of the UVP of 2,5 DHB.

Name	MS [M-H] ⁻	Activation Mode	MS ²		
			Collision voltage	<i>m/z</i>	-Loss (abundance) %
2,5-Dihydroxybenzoic acid	C ₇ H ₅ O ₄ ⁻	CID	-13	109.0291	-CO ₂ (100)
				136.0174	-OH [•] (100)
	<i>m/z</i> 153.0182	UVPD		109.0291	-CO ₂ (34)

4.5.1.2. Vanillin CID and UVPD behavior

The [M-H]⁻ vanillin ion at *m/z*151.0385 was found to be the result of the deprotonation of the phenol. Figure 4-3 present the spectra of the fragmentation in both CID and UVPD.

Whatever the activation (collisional or UV absorption), one significant fragmentation pathway was the elimination of a methyl radical from the homolytic cleavage of the methoxy bound to form a quinone-like distonic radical anion at *m/z*136.0168. The elimination of carbon monoxide followed this fragmentation process to yield a 5-membered ring associated with the C₆H₄O₂^{•-} radical ion at *m/z*108.0218. By CID, a poor abundant *m/z*123.0453 fragment, relative to the elimination of CO, was also formed by a similar process from the deprotonated vanillin ion. UVPD did not yield this ion. All proposed CID fragmentation pathways are supported by previously published work and are presented in Figure 4-4.⁴⁹⁻⁵³ Two specific fragments were observed on the vanillin UVPD MS/MS spectrum. The former was relative to the elimination of the [•]CHO radical, and the second was the loss of C₂H₂O. Both of these mechanisms were considered to be initiated by the efficient absorption of a UV photon by the aromatic moiety. The formation of [M-H-[•]CHO]^{•-} came from the homolytic cleavage of the carbon-carbon bond relative to the aldehyde function. The delocalization of the radical on the aromatic ring favored the stabilization of the resulting ion, which was detected at *m/z*122.0362. The *m/z*109.0284 ion resulted from the loss of an ethynol unit from the phenolic ring to lead to the formation of disubstituted cyclobutadiene. This process required the prior migration of a proton from the methyl of the methoxy group to produce a primary carbanion. The ring size reduction was thought to result from homolytic-bound cleavage initiated by the

absorption of a UV photon. The peak list, and relative intensity of the fragment from the CID and UVPD of vanillin are highlighted in Table 4-2.

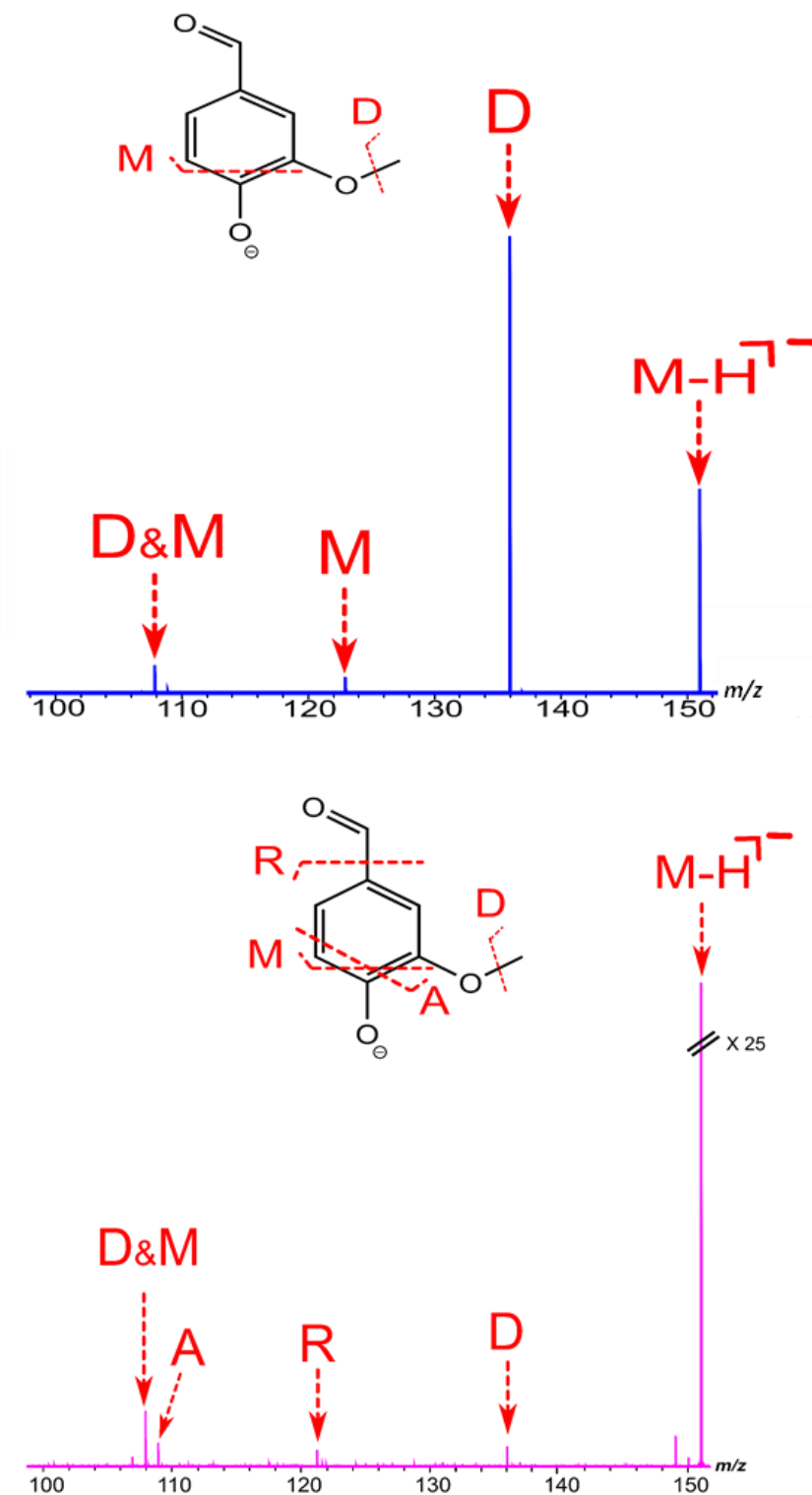


Figure 4-3:(Top) CID MS/MS spectrum of the deprotonated vanillin molecule, along with its corresponding cleavage diagram. (Bottom) UVPD MS/MS spectrum of vanillin along with its cleavage diagram.

Table 4-2: Peak list and relative intensity of the fragments from the CID and UVPD of vanillin.

Name	MS [M-H] ⁻	Activation Mode	MS ²			
			Collision voltage	m/z	-Loss (abundance) %	Assignment
Vanillin	C ₈ H ₇ O ₃ ⁻ m/z151.0389	CID	-13	136.0168	-CH ₃ [•] (100)	D
				123.0453	-CO (1)	M
				108.0218	-CO, -CH ₃ [•] (1)	D&M
		UVPD	136.0168	-CH ₃ [•] (39)	D	
			122.0362	-CHO [•] (5)	R	
			109.0284	-C ₂ H ₂ O (10)	A	
			108.0218	-CO, -CH ₃ [•] (100)	D&M	

4.5.2. Lignin monomer CID and UVPD behavior

Coniferyl (G) and sinapyl (S) alcohol were investigated as lignin monomers. The sole difference between these compounds is an additional methoxy group on the phenolic unit. Consequently, the deprotonated coniferyl alcohol and sinapyl alcohol ions led to a mass difference equal to CH₂O (30.011 Da). It was also the case for fragment ions resulting from the dissociation process involving the hydroxy propenyl moiety. This behavior is advantageous to identify the involved fragmentation process. The fragmentation spectra of the both monomers are represented in Figure 4-5 and 4-6 as well as the fragmentation mechanisms are given in Figures 5-7, and 5-8. The peak list, and relative intensity of the fragment from the CID and UVPD of both monomers are highlighted in Table 4-3, and Table 4-4.

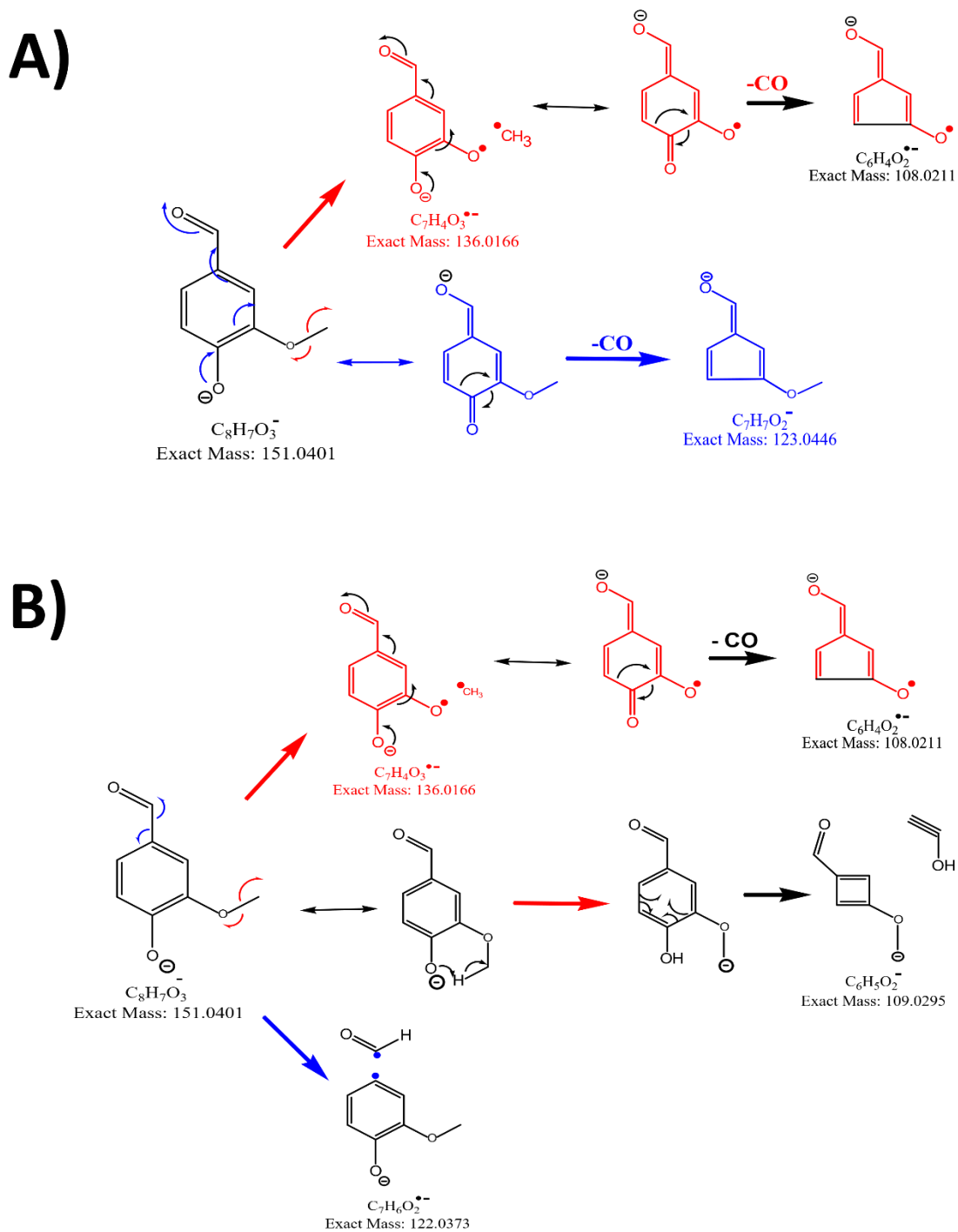


Figure 4-4:(Top) Proposed mechanisms of CID fragmentation of vanillin, (Bottom) Proposed mechanism of UVPD fragmentation of vanillin.

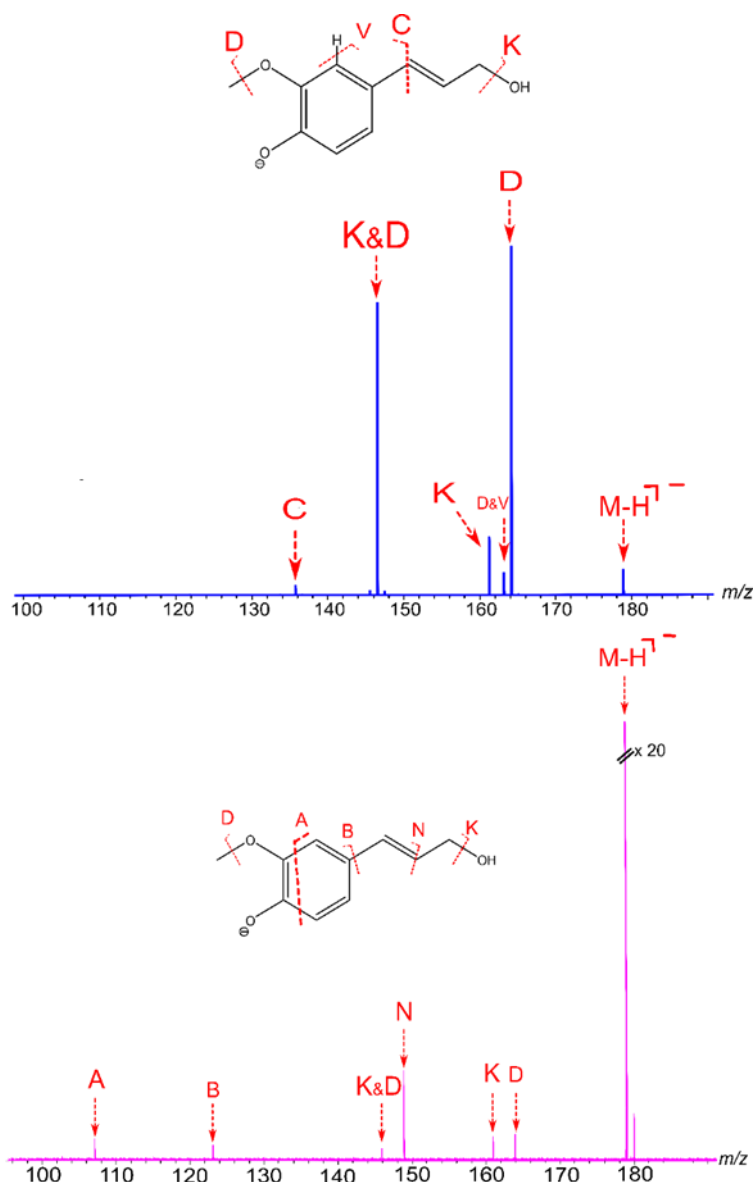


Figure 4-5: (Top) CID MS/MS spectrum of the deprotonated coniferyl alcohol molecule, along with its corresponding cleavage diagram. (Bottom) UVPD MS/MS spectrum of coniferyl alcohol along with its cleavage diagram.

By collisional activation of deprotonated coniferyl alcohol (m/z 179.0702) and sinapyl alcohol, (m/z 209.0823) ion, methyl radical (m/z 164.0469 and 194.0584), water (m/z 161.0596 and 191.0713), $\bullet\text{CH}_3 + \text{H}_2\text{O}$ (m/z 146.0362 and 176.0478) and $\text{C}_2\text{H}_4\text{O}$ (m/z 135.0444 and 165.0552) losses were observed. The elimination of $\bullet\text{CH}_3$ radical result from a process (red mechanism) identical to what it described for vanillin and led to forming a distonic radical anion. The elimination of water implied the hydroxy propenyl and led to the formation of a disubstituted deprotonated indene ion. This latter mechanism is supported by Zhang et al. who investigated the MS² behavior of coniferyl alcohol after H/D exchange of the allyl alcohol.⁴⁹ The subsequent elimination of a $\bullet\text{CH}_3$ radical led to m/z 146.0362 and 176.0478 from

G and S lignin monomers, respectively. Alternatively, these fragment ions were formed by the subsequent elimination of water after deprotonated G and S ions released a $\bullet\text{CH}_3$ radical.

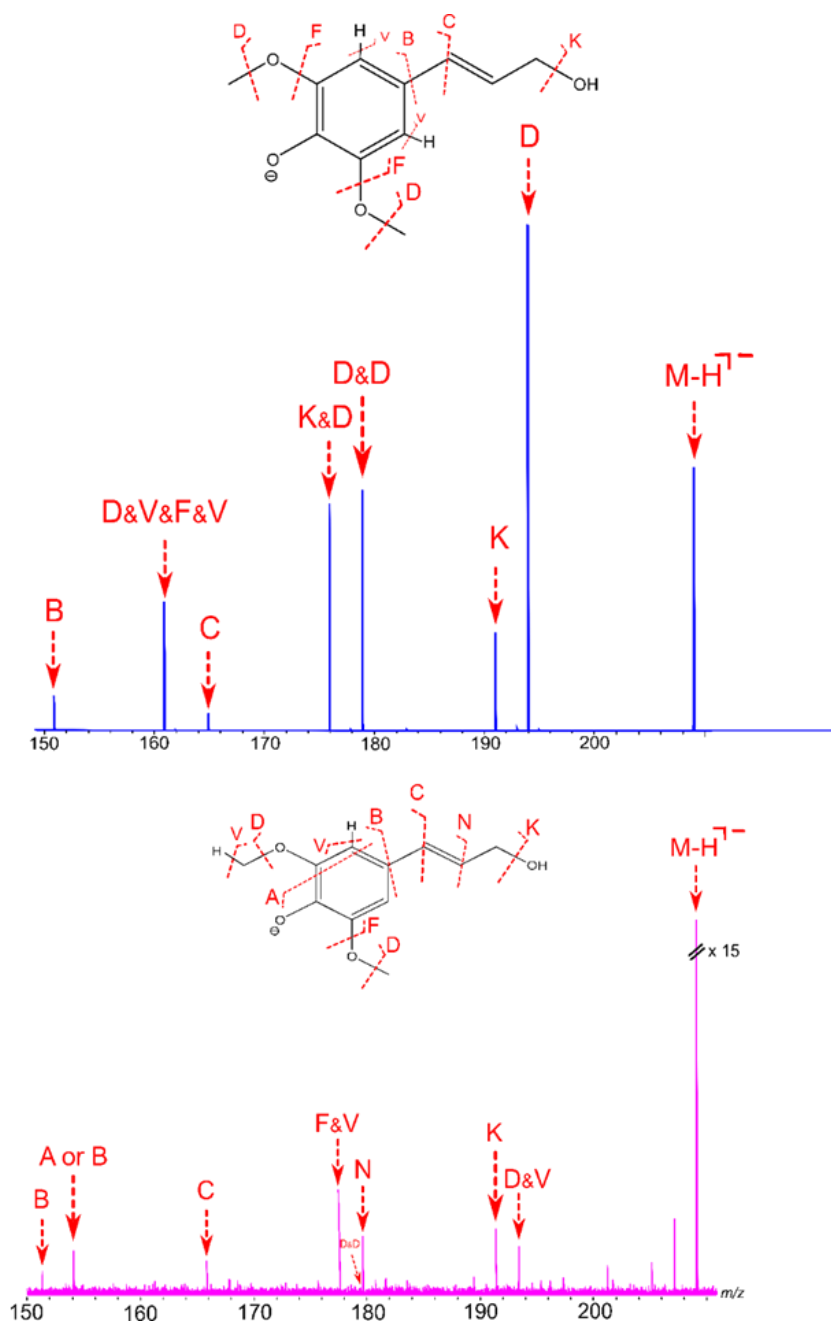


Figure 4-6: (Top) CID MS/MS spectrum of the deprotonated sinapyl alcohol molecule, along with its corresponding cleavage diagram. (Bottom) UVPD MS/MS spectrum of sinapyl alcohol along with its cleavage diagram.

Chapter 4: UVPD vs CID: Potential tool for structural analysis of bio-oils components

Table 4-3: Peak list, relative intensity of the fragments, and assignments from the CID and UVP of coniferyl alcohol.

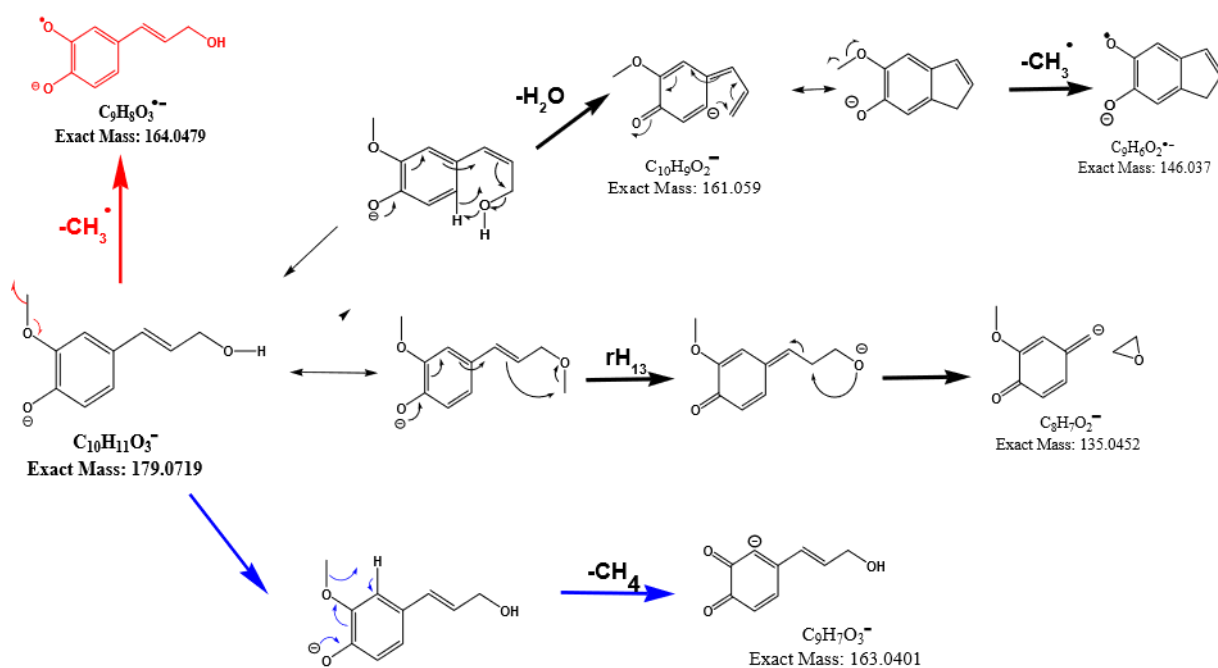
Name	MS [M-H] ⁻	Activation Mode	MS ²		Assignment			
			Collision voltage	-Loss (abundance) m/z %				
Coniferyl alcohol	C ₁₀ H ₁₁ O ₃ ⁻ m/z179.0702	CID	-13	164.0469	-CH ₃ [•] (100)	D		
				163.0389	-CH ₄ (7)	D&V		
				161.0596	-H ₂ O (2)	K		
				146.0362	-H ₂ O, -CH ₃ [•] (88)	K&D		
				135.0444	- C ₂ H ₄ O (3)	C		
				164.0469	-CH ₃ [•] (36)	D		
		UVPD				161.0596	-H ₂ O (35)	K
						149.0598	-CH ₂ O (100)	N
						146.0362	-H ₂ O, -CH ₃ [•] (33)	K&D
						123.0444	-C ₃ H ₄ O (28)	B
						107.0485	- C ₃ H ₄ O ₂ (29)	A

Chapter 4: UVPD vs CID: Potential tool for structural analysis of bio-oils components

Table 4-4: Peak list, relative intensity of the fragments, and assignment from the CID and UVP of sinapyl alcohol.

Name	MS [M-H] ⁻	Activation Mode	MS ²			Assignment		
			Collision voltage	m/z	-Loss (abundance) %			
Sinapyl alcohol	C ₁₁ H ₁₃ O ₄ ⁻ m/z209.0808	CID	-15	194.0584	-CH ₃ [•] (100)	D		
				191.0713	-H ₂ O (10)	K		
				179.0341	-CH ₃ * 2 (23)	D&D		
				176.0478	-H ₂ O, -CH ₃ [•] (22)	K&D		
				165.0552	C ₂ H ₄ O (2)	C		
				161.0244	-CH ₃ OH, CH ₄ (13)	D&V&F&V		
				151.0401	-C ₃ H ₆ O (3)	B		
				193.0498	-CH ₄ (74)	D&V		
				191.0713	-H ₂ O (81)	K		
		UVPD				179.0714	-CH ₂ O (75)	N
						179.0341	-CH ₃ * 2 (37)	D&D
						177.0548	-CH ₃ OH (100)	F&V
						165.0552	-C ₂ H ₄ O (38)	C
						153.0552	-C ₃ H ₄ O (66)	A or B
						151.0401	-C ₃ H ₆ O (27)	B

A)



B)

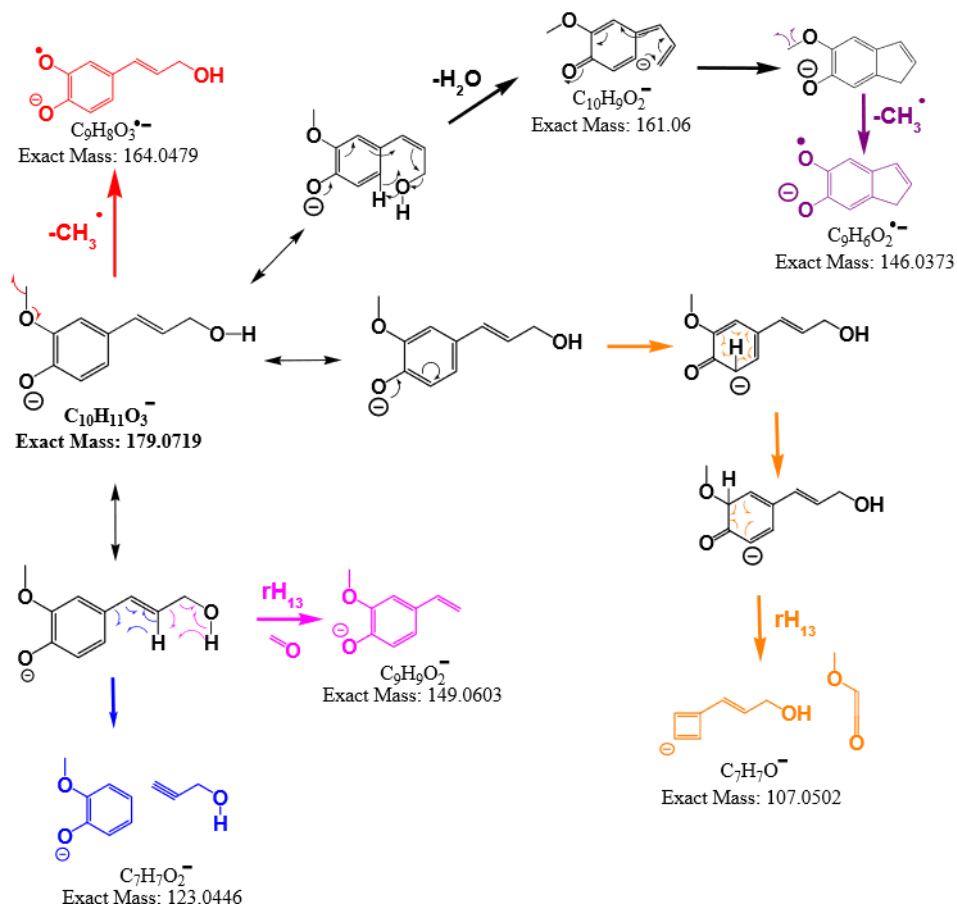


Figure 4-7: (Top) Proposed mechanisms of CID fragmentation of coniferyl alcohol, (Bottom) Proposed mechanism of UVPD fragmentation of coniferyl alcohol.

The elimination of C_2H_4O from G and S $[M-H]^-$ ion was thought to result from the elimination of the ethylene oxide molecule and the formation of a tropylium-like anion stabilized by resonance. Such a process was first initiated by the charge migration from the phenolate to the hydroxy propenyl, inducing the rH_{13} proton transfer from the alcohol. For coniferyl alcohol, the elimination of methane was also clearly observed, which was associated with one mesomeric form of the phenolate and the concerted elimination of the methyl group and a proton in its ortho position. Such a process was also observed with sinapyl alcohol. Indeed, a tiny abundant ion was detected at m/z 193.0498. For the sinapyl alcohol, three additional fragment ions were observed at m/z 179.0341, 161.0244, and 151.0401. The two former ones resulted from fragmentation involving the two methoxy groups. The m/z 179.035 ion was formed by the successive elimination of two $\bullet CH_3$ radicals, and the m/z 161.0244 one by the consecutive elimination of methane and methanol. Alternatively, m/z 161.0244 was formed by the elimination of a $\bullet CH_3$ radical from the m/z 176.0478, which led to an indene-quinone-like anion. This mechanism is supported by MS^3 experiments performed by Hauptert et al.⁵⁰ It was thought that methane loss occurred first due to observing of the small abundant ion at m/z 193.0495. The associated fragmentation processes are reported in Figure 4-8 and Figure 4-9 and implicated the last hydrogen on the aromatic ring. The m/z 151.0401 fragment ion corresponded to the elimination of the hydroxy propenyl after the rH_{13} transfer of a proton from the aromatic ring to the hydroxy propenyl. The different mechanisms proposed are supported by a significant number of previously published works.⁵⁰⁻⁵⁵

At this exception of the C_2H_4O elimination by the deprotonated coniferyl alcohol ion, the fragment ions obtained by collisional activation of both studied lignin monomers were also observed by UVPD. Nevertheless, UVPD led to the formation of specific fragments involving homolytic bond cleavage. The main UVPD deprotonated coniferyl alcohol ion fragment was relative to the loss of formaldehyde, which implied the alcohol function and a rH_{13} transfer of its hydrogen atom to lead to the m/z 149.0598 ion. A similar process occurred for sinapyl alcohol and yielded the m/z 179.0714 ion, which FT-ICR MS easily distinguished from the m/z 179.0341 ion described previously and corresponded to the successive elimination of two $\bullet CH_3$ radicals. A close process was involved in explaining the elimination of the hydroxy propenyl from both $[M-H]^-$ lignin monomers anion. The UV activation ensured the rH_{13} migration of the C_8 hydrogen atom to the phenolate and the concomitant homolytic dissociation of the C_6-C_8 bond to yield the m/z 123.0444 and 153.0552 for coniferyl and sinapyl deprotonated ion, respectively. Finally, a fragment ion was observed for coniferyl alcohol at m/z 107.048 and for sinapyl alcohol at m/z 153.0552, corresponding to the $C_3H_4O_2$ loss. It was thought that the involved process led to the opening of the aromatic ring with the rH_{13} transfer of the hydrogen in the meta position of the methoxy. Specifically, sinapyl deprotonated ion led to the elimination of a methanol molecule and the formation of the m/z 177.0548 ion corresponding to the main fragment produced by UVPD. The fragmentation process is still under investigation. It is not yet fully understood why the such process did not occur for coniferyl alcohol. One possible explanation is the involvement of the two methoxy groups and the formation of a fused bicyclic ion. Finally, the m/z 151.0401 fragment formation required the rH_{13} transfer of two hydrogen atoms by homolytic cleavage before eliminating propanol radical to yield the distonic $C_8H_6O_3^{\bullet-}$ ion.

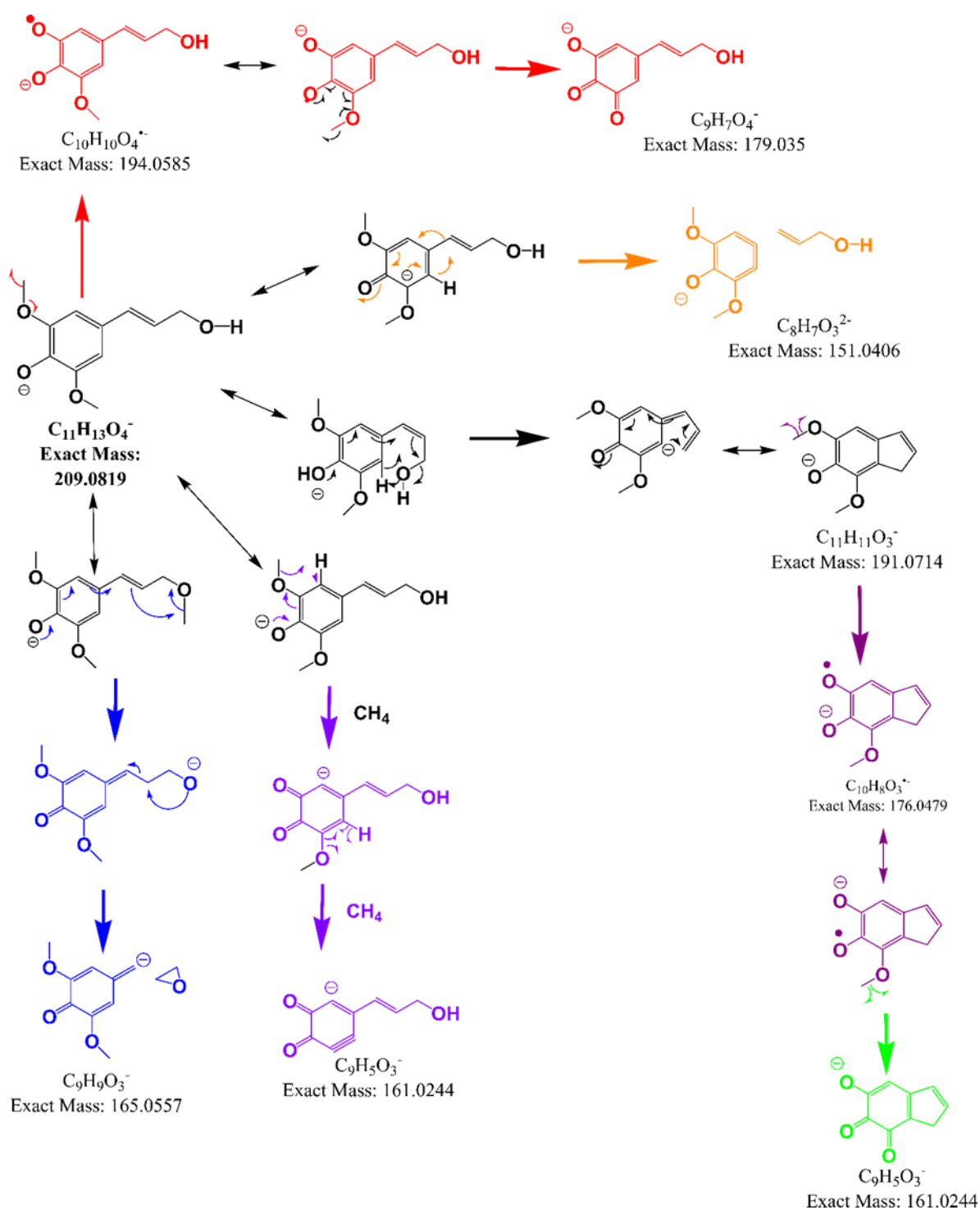


Figure 4-8: Proposed mechanisms of CID fragmentation of sinapyl alcohol.

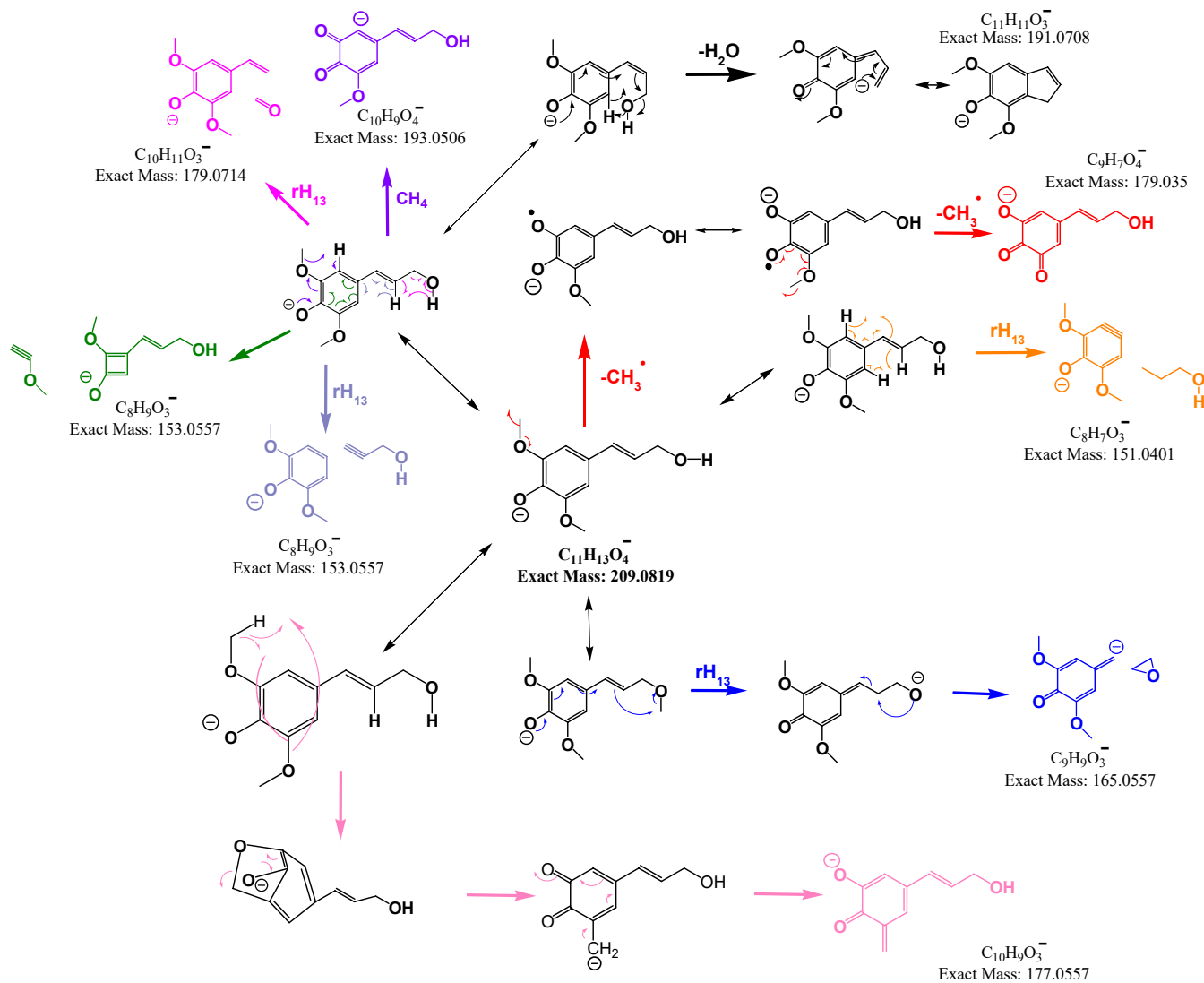


Figure 4-9: Proposed mechanisms of UVPD fragmentation of sinapyl alcohol

4.5.3. Lignin dimers CID and UVPD behavior

Pinoresinol and guaiacylglycerol- β -guaiacyl ether (GGE) were the two dimers investigated in this work since they are known to be the major bonding structure in lignin. Pinoresinol is formed through a β - β linkage between two coniferyl alcohol monomers, while guaiacylglycerol- β -guaiacyl ether is formed by a β -O-4 link between a hydroxylated coniferyl alcohol and a guaiacol unit (G'). The $[M-H]^-$ deprotonated pinoresinol and GGE at m/z 357.134 and 319.118 were investigated by CID and UVPD.

4.5.3.1. Pinoresinol CID and UVPD behavior

Due to the association of two coniferyl alcohol units, part of the observed losses was identical to what was described in the previous section. Indeed, the $[M - H - CH_3]^{\bullet -}$ was observed corresponding to one (CID and UVPD) methyl radical loss. Due to β - β linkage between the two propenyl alcohol moieties, most of the fragmentations for the coniferyl alcohol cannot occur for pinoresinol. However, a phenoxide-quinone methide conversion (Figure 4-10, in blue) occurred in which the 8-O-8' ether bond was broken following a charge-driven process. This phenomenon was the driving force to explain most of the processes which led to the fragmentation of the pinoresinol (Figure 4-12, and 4-13). The fragmentation spectra of the $[M-H]^-$ pinoresinol ion for both CID and UVPD fragmentation is presented in Figure 4-11.

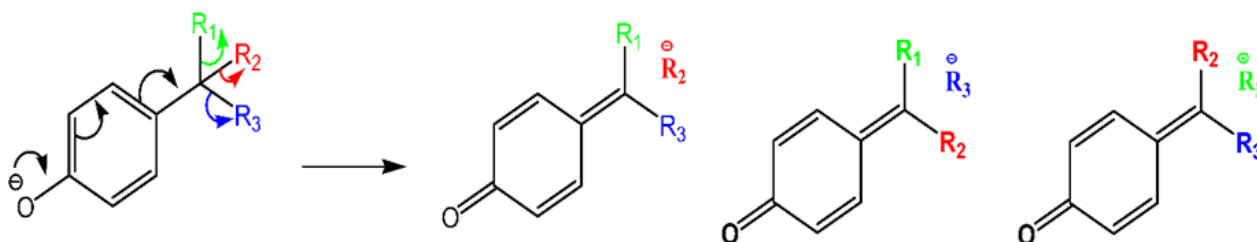


Figure 4-10: Phenoxide/ quinone methide conversion.⁶² Two pathways should be considered: (1) anion/neutral complex-mediated proton abstraction leading to the loss of the H₂O in β -O-4 linkage, (2) secondary fragmentation leading to a charge-driven cleavage except H₂O.

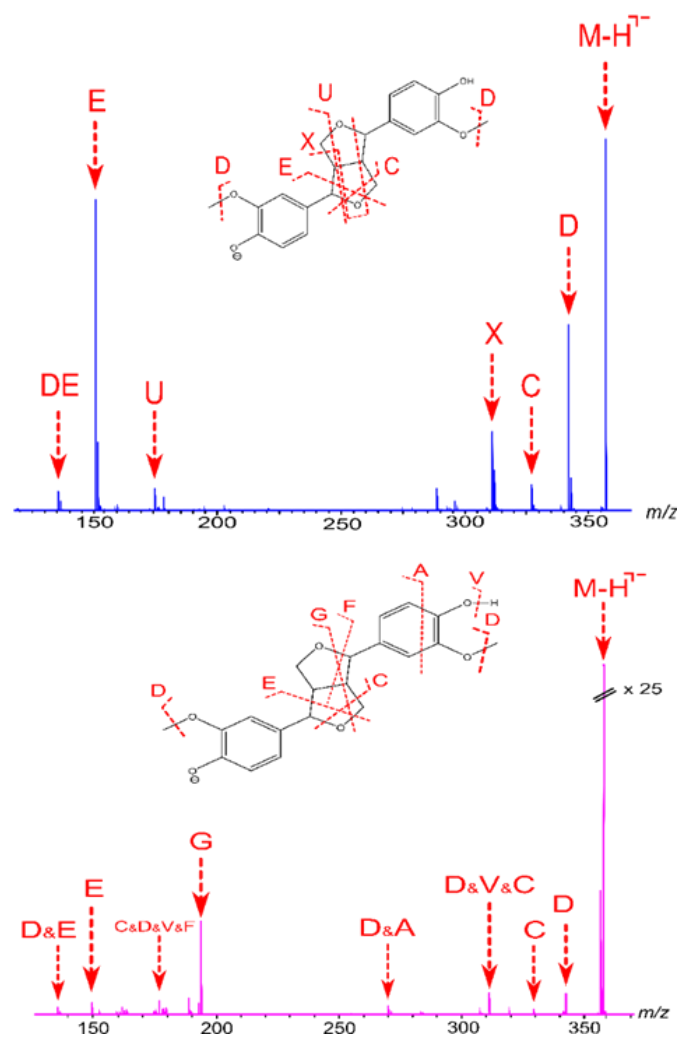


Figure 4-11: (Top) CID MS/MS spectrum of the deprotonated pinosresinol molecule, along with its corresponding cleavage diagram. (Bottom) UVPD MS/MS spectrum of the deprotonated pinosresinol molecule along with its cleavage diagram.

According to the opening of the five-membered-ring, the formed ion was an alcoholate or a primary carbanion. The subsequent activation of the carbanion led to the opening of the second five membered-ring and the concomitant elimination of butadiene and 3-hydroxy-4-methoxybenzaldehyde to yield a deprotonated 3-hydroxy-4-methoxybenzaldehyde anion observed at m/z 151.0391, which lost a methyl radical to form the m/z 136.0157 anion. Alternatively, this latter ion could be formed by a similar process the $[M - H - CH_3]^-$ fragment ion underwent. The m/z 175.0753 and 311.1277 fragment ion corresponded to the fragmentation of the alcoholate intermediate by eliminating 4-hydroxy-3-methoxybenzyl alcohol methanoate ester and formic acid, respectively. Both of these fragment ions required the formation a disubstituted 1,3 dioxane through the nucleophile substitution of one of the carbon atoms in the alpha position of the oxygen atom. Then, an opening of the aromatic ring mechanism led to the elimination of formic acid ion or 4-hydroxy-3-methoxybenzyl alcohol methanolate ester. The proposed mechanisms of the pinosresinol deprotonated specie are supported by previously published MS/MS and MS³ works.^{51,56-59} At the exception of m/z 175.0753, the fragment ions observed by collisional activation were also observed by UVPD. However, the UVPD fragmentation spectra showed additional fragments. The first one, at m/z 311.0915, corresponded to the loss of methane from the m/z 327.1227 ion and forming of a quinone moiety. Alternatively, m/z 327.1227 underwent an opening of the aromatic ring

rearrangement to lose a methoxy ethynol and formed the m/z 270.0889 ion corresponding to the contraction of the 2-methoxy-phenolic group into cyclobutadienyl one. The rH_{13} migration of a hydrogen atom in the alpha position of the alcoholate ensured the elimination from the m/z 311.0918 ion of a substituted quinone and the formation of the $C_{10}H_9O_3^-$ anion, which one of the mesomeric forms was the deprotonated coniferyl aldehyde ion observed at m/z 177.0547. The last fragment ion produced by UV activation was observed at m/z 194.0574 and was found to be relative to an oxidized form of the deprotonated coniferyl aldehyde anion. Its formation resulted from a homolytic cleavage of one O-CH₂ bound, which induced the homolytic break of the shared carbon-carbon bound of the two five-membered-ring. The rH_{14} migration of the hydrogen atom in the alpha of the alkoxy towards the second oxygen atom leads to the extension of the conjugation domain, to the formation of the hydroxy propenyl chain, and to the elimination of the eugenol radical.

The fragment ion produced by CID of the pinoresinol deprotonated molecule did not reveal the opening of one of the aromatic rings. Consequently, it would be challenging to establish the position of the substituents on the phenolic rings. Nevertheless, observing fragments associated with the phenolic nuclei ensured identifying of the number and the nature of the aromatic ring substituents. By UVPD, a cross-ring cleavage occurred and ensured to define that hydroxyl and methoxy groups were on two adjacent positions of the phenolic ring.

The peak list, and relative intensity of the fragment from the CID and UVPD of pinoresinol are gathered in Table 4-5.

Chapter 4: UVPD vs CID: Potential tool for structural analysis of bio-oils components

Table 4-5: Peak list, relative intensity of the fragments, and assignment from the CID and UVPD of Pinoresinol.

Name	MS [M-H] ⁻	Activation Mode	MS ²		Assignment	
			Collision voltage	m/z		-Loss (abundance) %
Pinoresinol	C ₂₀ H ₂₁ O ₆ ⁻ m/z357.1332	CID	-15	342.1097	- CH ₃ [•] (30)	D
				327.1227	-CH ₂ O (2)	C
				311.1277	- HCOOH (5)	X
				175.0753	-C ₉ H ₁₀ O ₄ (2)	U
				151.0391	-C ₁₂ H ₁₄ O ₃ (100)	E
				136.0157	- C ₁₃ H ₁₇ O ₃ [•] (15)	D&E
		UVPD	342.1097	- CH ₃ [•] (15)	D	
			327.1227	- CH ₂ O (1)	C	
			311.0918	-CH ₄ , -CH ₂ O (3)	D&V&C	
			270.0889	- C ₃ H ₄ O ₂ , -CH ₃ [•] (3)	D&A	
			194.0574	-C ₁₀ H ₁₁ O ₂ [•] (100)	G	
			177.0547	-CH ₂ O, -CH ₄ , - C ₈ H ₆ O ₂ (9)	C&D&V&F	
			150.0331	- C ₁₂ H ₁₅ O ₃ [•] (9)	E	
			136.0157	- C ₁₃ H ₁₆ O ₃ [•] (8)	D&E	

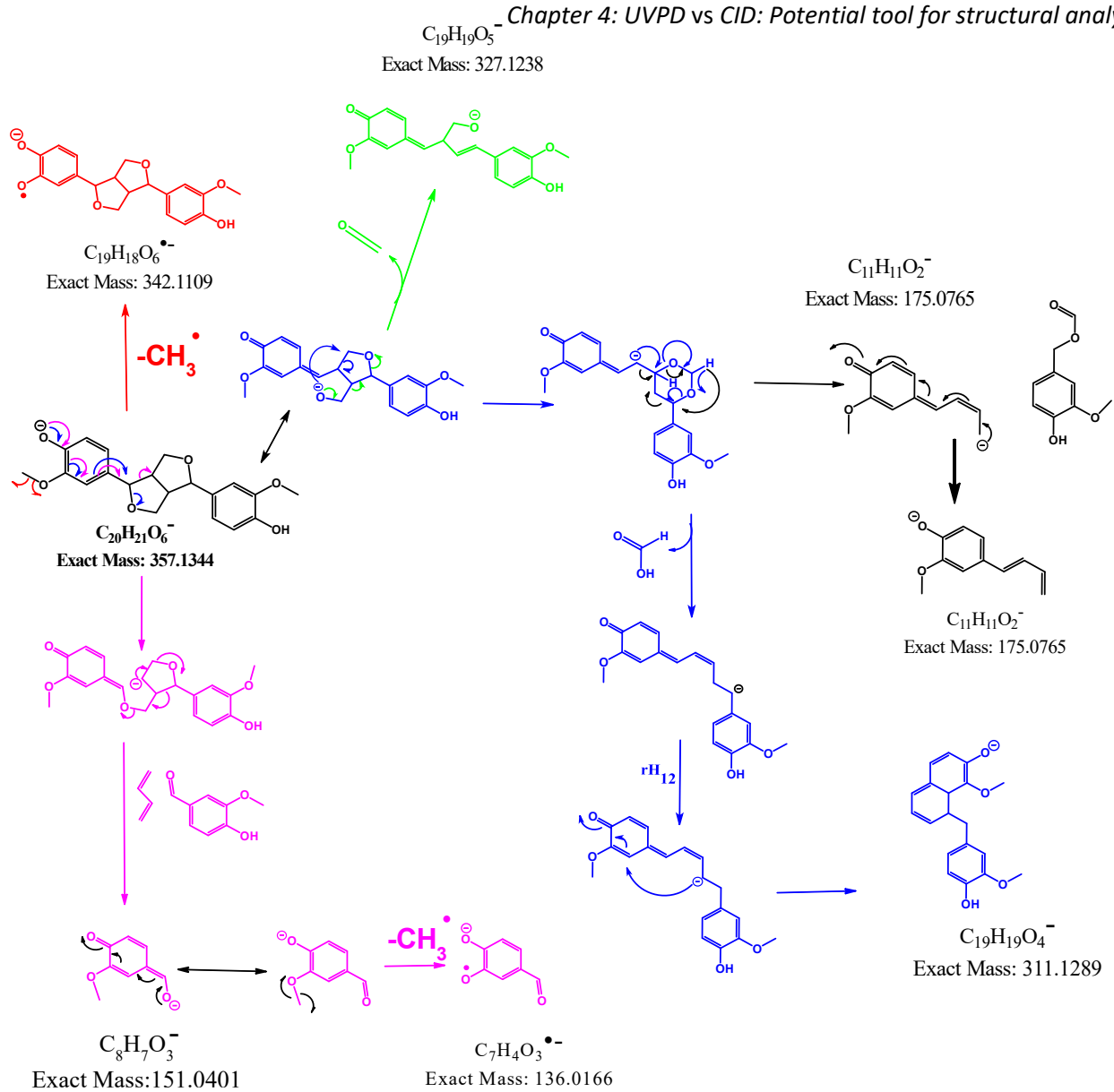


Figure 4-12: Proposed mechanisms of CID fragmentation of pinoresinol.

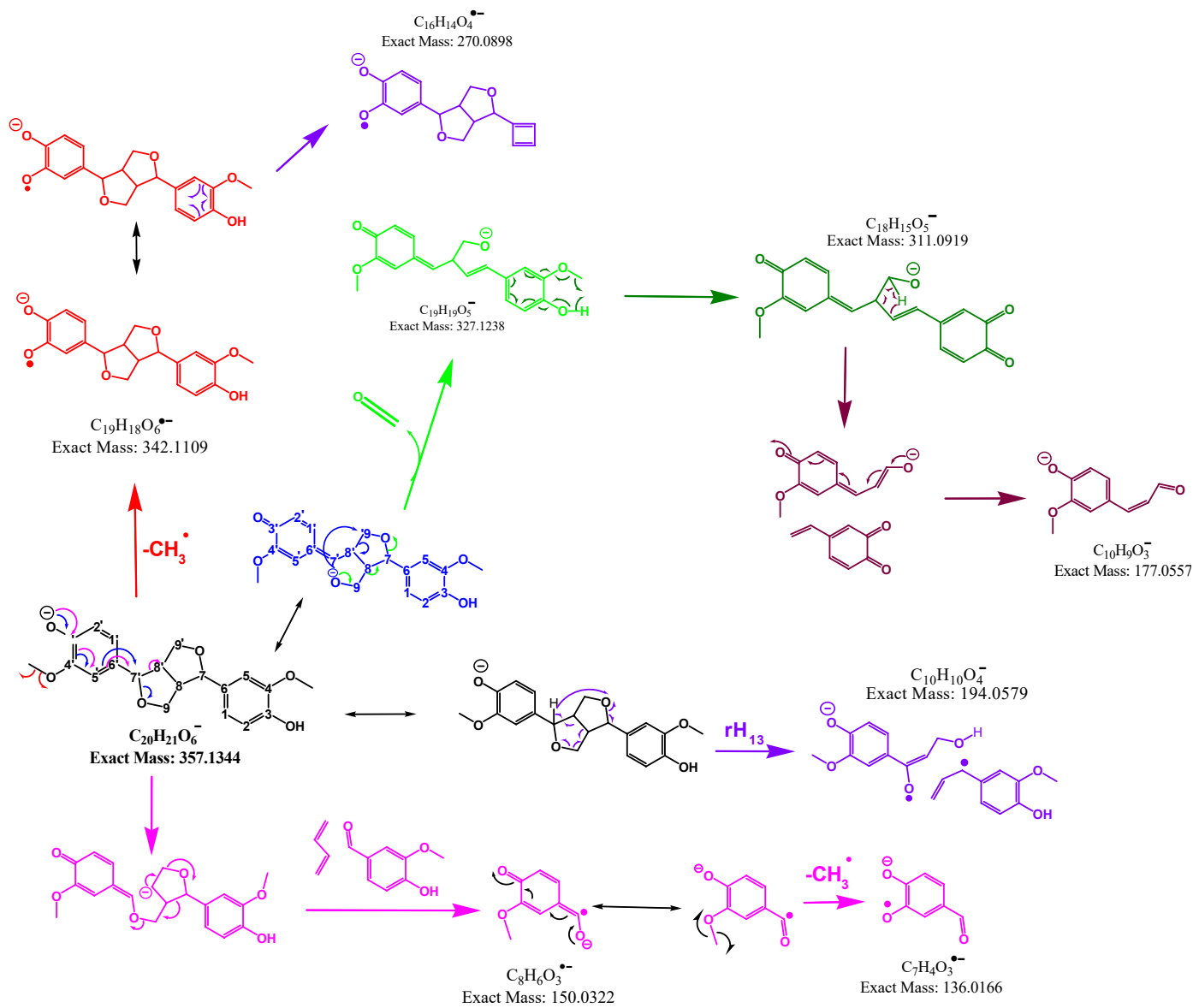


Figure 4-13: Proposed mechanisms of UVPD fragmentation of pinoresinol.

4.5.3.2. Guaiacylglycerol- β -guaiacyl ether GGE CID and UVPD behavior

Guaiacylglycerol- β -guaiacyl ether is formed by a β -O-4 linkage (the most often linkage in lignin monomer) between a hydroxylated coniferyl alcohol and a guaiacol unit. The fragmentation spectra of the GGE for both CID and UVPD fragmentation is presented in Figure 4-14. The cleavage of the β -O-4 linkage was one of the driving forces leading to most of the observed fragments. The second one involved the hydroxyl group on the coniferyl unit. Only one poor abundant fragment ion was found to be specific to UVPD. It corresponded to $C_9H_9O_2^-$ anion and was detected at m/z 149.0595.

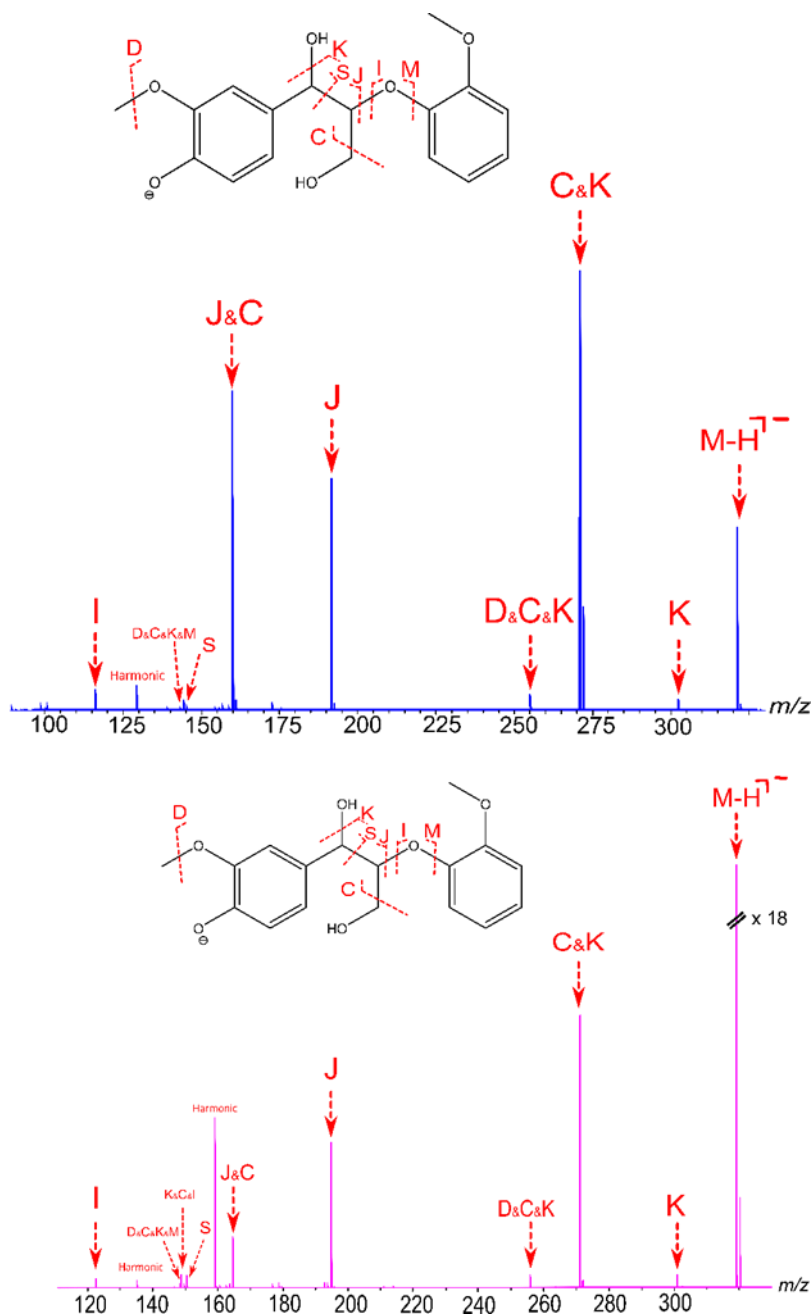


Figure 4-14: (Top) CID MS/MS spectrum of the deprotonated GGE molecule, along with its corresponding cleavage diagram. (Bottom) UVPD MS/MS spectrum of GGE along with its cleavage diagram.

GGE has been extensively investigated by tandem mass spectrometry. The proposed fragmentation mechanism is displayed in Figure 4-15, and Figure 4-16. The most abundant fragment observed in this study has still been reported.^{53,54,56,60,61} The three high mass ion fragments observed at m/z 301.1071, 271.0978, and 256.0741 resulted from the successive elimination of water, formaldehyde, and methyl radical from the GGE deprotonated ion to lead to $[M - H - H_2O]^-$, $[M - H - H_2O - CH_2O]^-$, and $[M - H - H_2O - CH_2O - CH_3]^-$. The charge migration from the phenolate ensured the formation of a quinonic unit and the elimination of water by releasing the α -hydroxy function after a rH_{15} transfer of the proton from the second hydroxyl. The easy elimination of formaldehyde to yield the m/z 271.0978 ion ensured the quinone-phenolate equilibrium to be displaced to the phenolate. The $[M - H - H_2O - CH_2O]^-$ was the most abundant detected fragment ion, whatever the used activation technique. The subsequent elimination of the CH_3^\bullet led to the formation of a pseudo-quinolinic radical anion, which was observed at m/z 256.0741. An alternative to the elimination of water was the formation of a quinone methide ion at m/z 195.0655 through the elimination of guaiacol allowed by the rH_{13} migration to the oxygen of the ether function and the subsequent dissociation of the β -O-4 linkage or the formation of the guaiacol deprotonated ion (m/z 123.0452) by an inductive cleavage of the β -O-4 linkage. The conversion of the quinone methide ion at m/z 195.066 into its alcoholate form ensured the elimination of formaldehyde and the formation of the deprotonated ion of 1-(4-hydroxy-3-methoxyphenyl) ethenol, which was thought to be in equilibrium with 1-(4-hydroxy-3-methoxyphenyl) ethenone at m/z 165.0550. In addition to these ions produced by CID and UVPD of deprotonated GGE anions, two tiny fragment ions deserve some attention.

They were observed at m/z 149. The former one ($C_8H_5O_3^-$) at m/z 149.0233 was formed whatever the used activation technique. It resulted from methoxyphenyl radical elimination from m/z 256.0741 ion to lead to a furan-like quinone. The second one, at m/z 149.0595, was specifically observed by UVPD. It was produced by 1,3 benzodioxole elimination from the $[M - H - H_2O - CH_2O]^-$ allowed by the $rH_{1,5}$ migration of one hydrogen atom of the guaiacyl methyl and the homolytic cleavage of the β -O-4 linkage.

In contrast to what was observed in the pinoresinol study, neither CID nor UVPD led to RDA-like ring opening. Nevertheless, structural details on the core branched alkyl chain between both phenolic units were provided. In addition, specific ions were ensured to identify the formula of the monomer unit, guaiacol (m/z 123.0452) and hydroxy coniferyl alcohol (m/z 195.065). In that case, the fragmentation process has to be regarded as a depolymerization phenomenon.

The peak list, and relative intensity of the fragments from the CID and UVPD of the GGE are displayed in Table 4-6.

Chapter 4: UVPD vs CID: Potential tool for structural analysis of bio-oils components

Table 4-6: Peak list, relative intensity of the fragments, and assignment from the CID and UVPD of GGE.

Name	MS [M-H] ⁻	Activation Mode	MS ²		Assignment			
			Collision voltage	m/z				
GGE	C ₁₇ H ₁₉ O ₆ ⁻ m/z319.1176	CID	-15	301.1071	-H ₂ O (2)	K		
				271.0978	-H ₂ O, -CH ₂ O (100)	C&K		
				256.0741	-H ₂ O, -CH ₂ O, -CH ₃ (3)	D&C&K		
				195.0655	-C ₇ H ₈ O ₂ (13)	J		
				165.0550	-C ₇ H ₈ O ₂ , -CH ₂ O (20)	J&C		
				151.0388	-C ₉ H ₁₂ O ₃ (1)	S		
				149.0233	-C ₇ H ₇ O, -CH ₂ O, -H ₂ O, -CH ₃ (2)	D&C&K&M		
				123.0452	-C ₁₀ H ₁₂ O ₄ (7)	I		
		UVPD				301.1071	-H ₂ O (1)	K
						271.0978	-H ₂ O, -CH ₂ O (100)	C&K
						256.0741	-H ₂ O, -CH ₂ O, -CH ₃ (1)	D&C&K
						195.0655	-C ₇ H ₈ O ₂ (15)	J
						165.0550	-C ₇ H ₈ O ₂ , -CH ₂ O (5)	J&C
						151.0388	-C ₉ H ₁₂ O ₃ (1)	S
						149.0595	-C ₇ H ₆ O ₂ , -H ₂ O, -CH ₂ O (2)	K&C&I
						149.0233	-C ₇ H ₇ O, -CH ₂ O, -H ₂ O, -CH ₃ (1)	D&C&K&M
				123.0452	-C ₁₀ H ₁₂ O ₄ (1)	I		

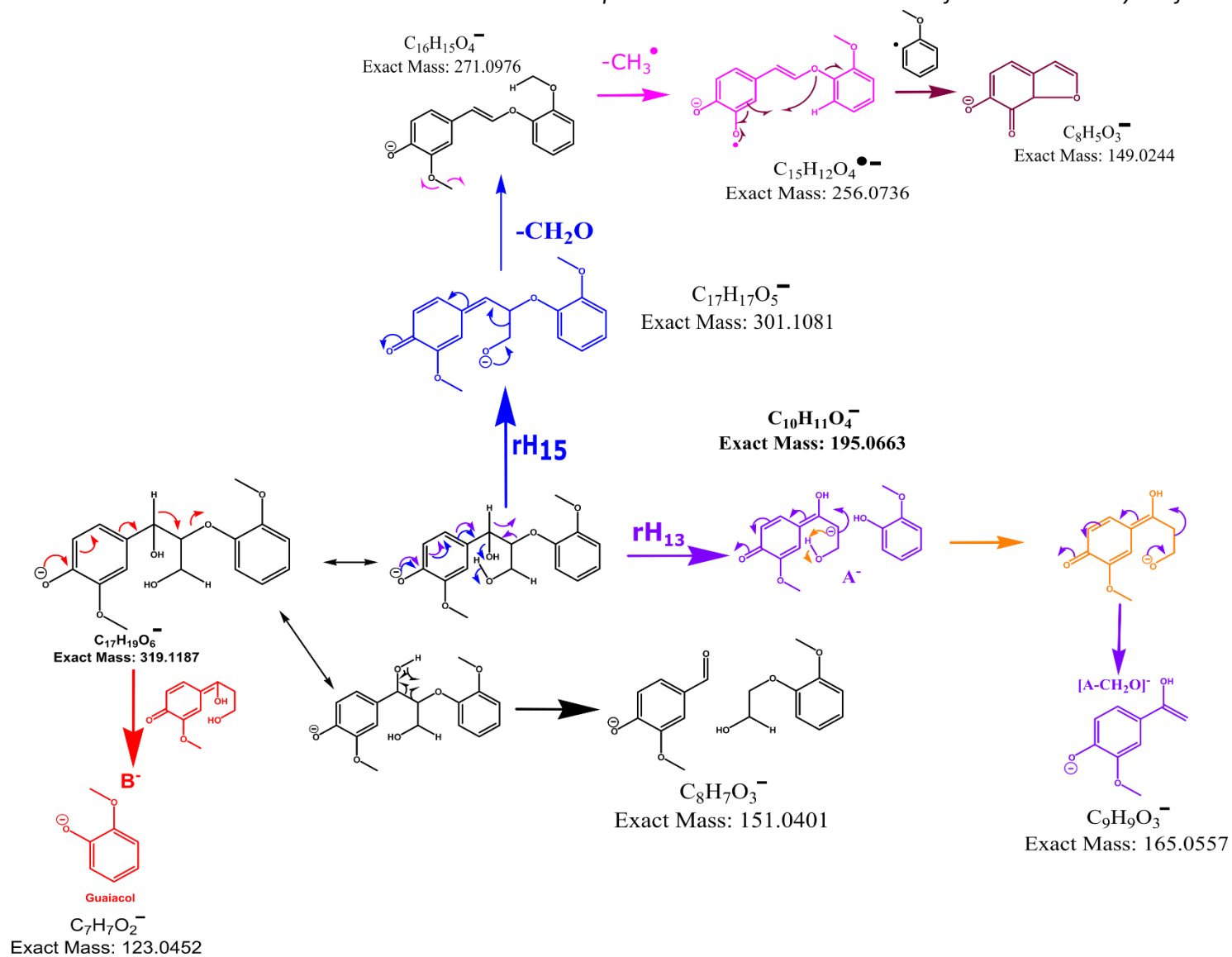


Figure 4-15: Proposed mechanisms of CID fragmentation of GGE.

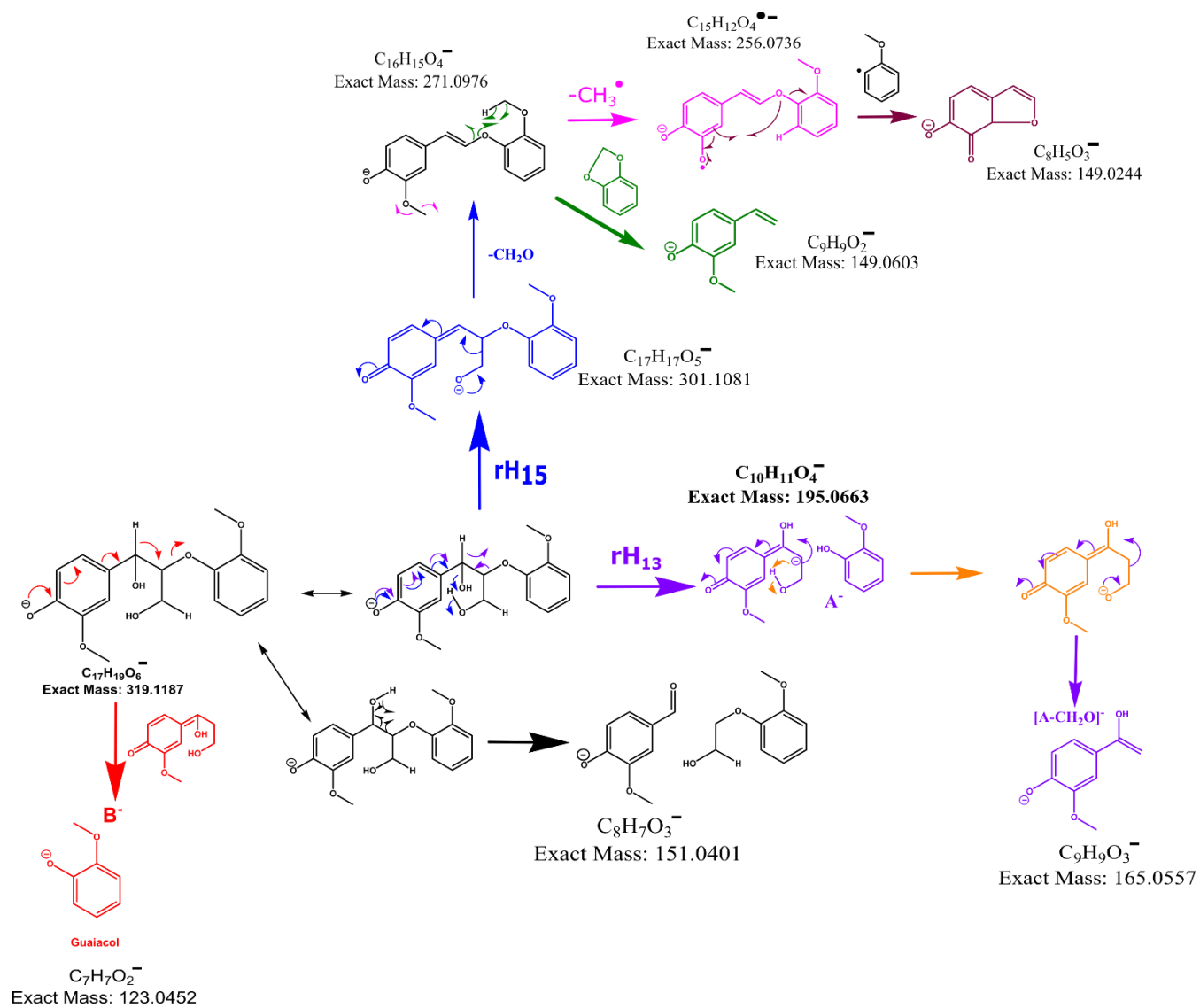


Figure 4-16: Proposed mechanisms of UVPD fragmentation of GGE.

4.5.4. Comparison of CID and UVPD for bio-oil standard link to lignin.

The different moieties –e.g., functional groups– found by MS/MS investigation of the six investigated bio-oil standards are reported in Table 4-7. Figure 4-1 highlights with different colors the different functional groups present in each studied compound. CID MS/MS appeared less efficient than UVPD fragmentation in obtaining information on the functional groups in the investigated compounds. UVPD demonstrated its ability to give insights into all functional groups for five of the six examined standards. To ensure a graphical and easy comparison of the results obtained by CID and UVPD, Figure 4-17 displays the double bond equivalent (DBE) vs. carbon number map of the different fragment ions for each of the six investigated standards.

Table 4-7: For each bio-oil standard, moieties found by the two fragmentation techniques.

Sample	Number of Moieties	
	CID	UVPD
2,5 Dihydroxybenzoic acid	1/4	2/4
Vanillin	2/4	4/4
Coniferyl Alcohol	3/5	5/5
Sinapyl Alcohol	3/5	5/5
Pinoresinol	3/4	4/4
GGE	5/5	5/5

In addition to an easy comparison of UVPD and CID tandem mass spectra, this graphical representation highlights general trends observed after collisional or photon activation of the precursor ions. The increase of the DBE by an integer corresponds to eliminating of a neutral, whereas the rise by a half-integer is relative to the elimination of a radical. For lignin oligomers and dimers, fragment ions are gathered into two series. The former is relative to fragment ions with a DBE equal to or greater than the DBE of the precursor ion. An increase in the DBE reveals the extension of the conjugation domain by processes such as dealkylation or dehydration upon CID and UVPD. The second series observed in the study of lignin monomers and dimers demonstrates the partial or complete elimination of the hydroxy propenyl moiety or one of the lignin monomers, respectively. This second group of fragment ions also includes species formed by the opening of one of the six-membered phenolic units by UVPD.

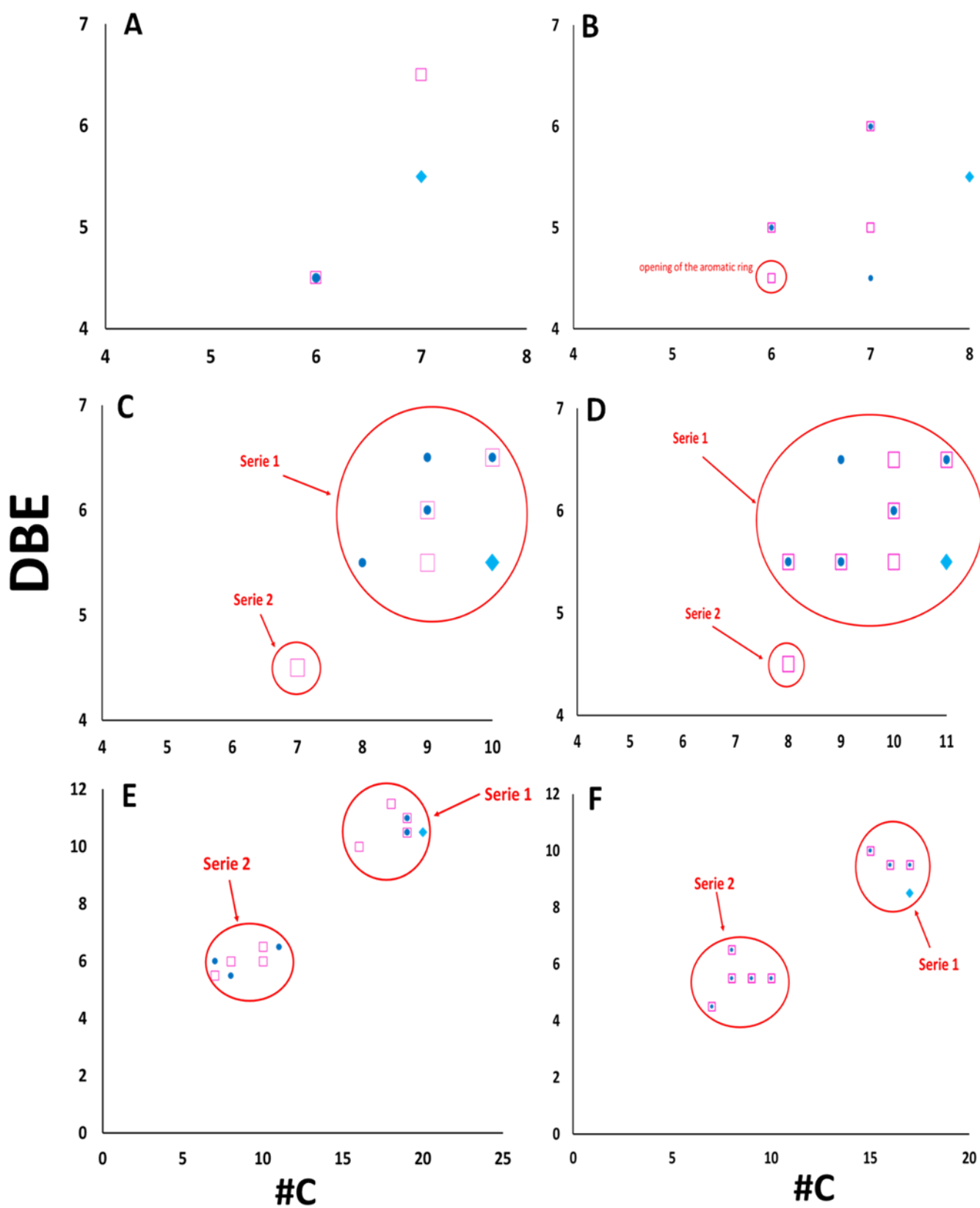


Figure 4-17: DBE versus number of carbons of CID (dark blue) and UVPD (light purple) for the six bio-oil standards. The precursor ion is in light blue. (A) DHB, (B) Vanillin, (C) Coniferyl alcohol, (D) Sinapyl alcohol, (E) Pinoresinol, and (F) GGE.

Indeed, a large number of fragments are positioned lower to the left of the graphic, indicating that significant losses of DBE and #C result from the photon activation. For instance, the pinoresinol behavior is mostly due to the loss of the aromaticity following an opening of the aromatic ring fragmentation or the cleavage of the β - β lignin bond. Compared to CID, UVPD exhibits more fragments at lower levels of DBE, indicating that highly aromatic compounds are more resistant to activation by CID than UVPD. The specificity of both used fragmentation techniques may well explain this. By collisional activation, the dissociation is driven by the charge on the one hand and by the strength of the bond on the other hand. Indeed, the vibrational activation by CID leads to the distribution of the energy into the different degrees of freedom of the precursor ion. Only dissociation processes involving the breaking of the weakest bonds are observed.

Activation by UV photons at 193 nm involves the excited electronic levels of the precursor ion. It requires an efficient absorption of the incident photons, which is allowed by the phenolic groups, and induces the homolytic dissociation of the bonds near the chromophores responsible for the absorption. The dissociation processes are no longer directed by the charge but by the presence of the formed radicals. Thus, non-ergodic fragmentations can sometimes occur at a significant distance from the charge. These can lead to the opening of aromatic rings or the breaking of stronger bonds. Therefore, UVPD-specific fragmentations are often more informative than fragmentation observed by CID. The specific UVPD loss of the OH hydroxy group by 2.5 DHB highlights the phenol function and that of the HCO radical, which allows the identification of the aldehyde function of vanillin. The opening of the aromatic rings leads to information on the position of the substituent groups of the phenolic ring of vanillin, lignin oligomers, and dimers. In addition, in the context of the study of lignin dimers, the depolymerization processes are significantly more important in UVPD than CID. These processes are exciting to more easily identify the monomers that constitute these dimers and, more broadly, lignin oligomers.

4.6. Conclusion

In this chapter, six standards proven to be present in bio-oils and comparable in structure to bio-oil components were subjected to CID and UVPD fragmentation techniques. For most of the standards examined, UVPD fragmentation generated a greater diversity of fragments, allowing the identification of more functional groups than CID. Overall, UVPD provided more important structural details than CID for most of the compounds studied, allowing the identification of more functional groups. Thus, most of the phenolic compounds led to the opening of the aromatic ring rearrangement enabling the localization of the position of some substituents of the phenolic group and the cleavage of bonds associated with the formation of lignin dimers. Although a limited number of compounds were studied for these experiments, UVPD demonstrated its superior ability to provide structural information on some components of bio-oils produced by the pyrolysis of lignocellulosic biomass.

Furthermore, by combining CID and UVPD, we produced complementary fragment ions. This study paves the way for systematic structural elucidation of lignin-derived compounds in bio-oils by so-called "2D FTMS". Indeed, bio-oils produced by biomass pyrolysis contain several thousands of compounds that cannot be studied systematically and individually by the usual tandem mass spectrometry methods. On the contrary, the 2D FTMS allows without isolating each precursor ion to obtain structural information using gas-free activation methods like UVPD.

4.7. References

- (1) Raffelt, K.; Henrich, E.; Koegel, A.; Stahl, R.; Steinhardt, J.; Weirich, F. The BTL2 Process of Biomass Utilization Entrained-Flow Gasification of Pyrolyzed Biomass Slurries. In *Twenty-Seventh Symposium on Biotechnology for Fuels and Chemicals*; McMillan, J. D., Adney, W. S., Mielenz, J. R., Klasson, K. T., Eds.; Humana Press: Totowa, NJ, 2006; pp 153–164. https://doi.org/10.1007/978-1-59745-268-7_11.
- (2) Badger, P. C.; Fransham, P. Use of Mobile Fast Pyrolysis Plants to Densify Biomass and Reduce Biomass Handling Costs—A Preliminary Assessment. *Biomass Bioenergy* **2006**, *30* (4), 321–325. <https://doi.org/10.1016/j.biombioe.2005.07.011>.
- (3) Oasmaa, A.; Meier, D. Characterization, Analysis, Norms and Standards; 2005; pp 19–59.
- (4) Czernik, S.; Bridgwater, A. V. Overview of Applications of Biomass Fast Pyrolysis Oil. *Energy Fuels* **2004**, *18* (2), 590–598. <https://doi.org/10.1021/ef034067u>.
- (5) Bridgwater, A. V. Review of Fast Pyrolysis of Biomass and Product Upgrading. *Biomass Bioenergy* **2012**, *38*, 68–94. <https://doi.org/10.1016/j.biombioe.2011.01.048>.
- (6) Venderbosch, R.; Prins, W. Fast Pyrolysis Technology Development. *Biofuels Bioprod. Biorefining* **2010**, *4* (2), 178–208. <https://doi.org/10.1002/bbb.205>.
- (7) Shen, D. K.; Gu, S. The Mechanism for Thermal Decomposition of Cellulose and Its Main Products. *Bioresour. Technol.* **2009**, *100* (24), 6496–6504. <https://doi.org/10.1016/j.biortech.2009.06.095>.
- (8) Kanaujia, P. K.; Sharma, Y. K.; Garg, M. O.; Tripathi, D.; Singh, R. Review of Analytical Strategies in the Production and Upgrading of Bio-Oils Derived from Lignocellulosic Biomass. *J. Anal. Appl. Pyrolysis* **2014**, *105*, 55–74. <https://doi.org/10.1016/j.jaap.2013.10.004>.
- (9) Mohan, D.; Pittman, C. U. Jr.; Steele, P. H. Pyrolysis of Wood/Biomass for Bio-Oil: A Critical Review. *Energy Fuels* **2006**, *20* (3), 848–889. <https://doi.org/10.1021/ef0502397>.
- (10) Auersvald, M.; Kejla, L.; Eschenbacher, A.; Thi, H. D.; Van Geem, K. M.; Šimáček, P. Detailed Characterization of Sulfur Compounds in Fast Pyrolysis Bio-Oils Using GC × GC-SCD and GC-MS. *J. Anal. Appl. Pyrolysis* **2021**, *159*, 105288. <https://doi.org/10.1016/j.jaap.2021.105288>.
- (11) Amarasekara, A. S.; Reyes, C. D. G. Acidic Ionic Liquid Catalyzed Liquefactions of Corn Cobs and Switchgrass in Acetone: Analysis of Bio-Oils Using LC-MS and GC-MS. *J. Anal. Appl. Pyrolysis* **2020**, *145*, 104752. <https://doi.org/10.1016/j.jaap.2019.104752>.

- (12) Olcese, R.; Carré, V.; Aubriet, F.; Dufour, A. Selectivity of Bio-Oils Catalytic Hydrotreatment Assessed by Petroleomic and GC*GC/MS-FID Analysis. *Energy Fuels* **2013**, *27* (4), 2135–2145. <https://doi.org/10.1021/ef302145g>.
- (13) Staš, M.; Auersvald, M.; Vozka, P. Two-Dimensional Gas Chromatography Characterization of Pyrolysis Bio-Oils: A Review. *Energy Fuels* **2021**, *35* (10), 8541–8557. <https://doi.org/10.1021/acs.energyfuels.1c00553>.
- (14) Garcia-Perez, M.; Chaala, A.; Pakdel, H.; Kretschmer, D.; Roy, C. Characterization of Bio-Oils in Chemical Families. *Biomass Bioenergy* **2007**, *31* (4), 222–242. <https://doi.org/10.1016/j.biombioe.2006.02.006>.
- (15) Harman-Ware, A. E.; Ferrell, J. R. Methods and Challenges in the Determination of Molecular Weight Metrics of Bio-Oils. *Energy Fuels* **2018**, *32* (9), 8905–8920. <https://doi.org/10.1021/acs.energyfuels.8b02113>.
- (16) Staš, M.; Auersvald, M.; Kejla, L.; Vrtilška, D.; Kroufek, J.; Kubička, D. Quantitative Analysis of Pyrolysis Bio-Oils: A Review. *TrAC Trends Anal. Chem.* **2020**, *126*, 115857. <https://doi.org/10.1016/j.trac.2020.115857>.
- (17) Lang, X.; Dalai, A. K.; Bakhshi, N. N.; Reaney, M. J.; Hertz, P. B. Preparation and Characterization of Bio-Diesels from Various Bio-Oils. *Bioresour. Technol.* **2001**, *11*.
- (18) Undri, A.; Abou-Zaid, M.; Briens, C.; Berruti, F.; Rosi, L.; Bartoli, M.; Frediani, M.; Frediani, P. A Simple Procedure for Chromatographic Analysis of Bio-Oils from Pyrolysis. *J. Anal. Appl. Pyrolysis* **2015**, *114*, 208–221. <https://doi.org/10.1016/j.jaap.2015.05.019>.
- (19) Lievens, C.; Mourant, D.; He, M.; Gunawan, R.; Li, X.; Li, C.-Z. An FT-IR Spectroscopic Study of Carbonyl Functionalities in Bio-Oils. *Fuel* **2011**, *90* (11), 3417–3423. <https://doi.org/10.1016/j.fuel.2011.06.001>.
- (20) Qian, Y.; Zuo, C.; Tan, J.; He, J. Structural Analysis of Bio-Oils from Sub-and Supercritical Water Liquefaction of Woody Biomass. *Energy* **2007**, *32* (3), 196–202. <https://doi.org/10.1016/j.energy.2006.03.027>.
- (21) David, K.; Kosa, M.; Williams, A.; Mayor, R.; Realff, M.; Muzzy, J.; Ragauskas, A. ³¹P-NMR Analysis of Bio-Oils Obtained from the Pyrolysis of Biomass. *Biofuels* **2010**, *1* (6), 839–845. <https://doi.org/10.4155/bfs.10.57>.
- (22) Huang, F.; Pan, S.; Pu, Y.; Ben, H.; Ragauskas, A. J. ¹⁹F NMR Spectroscopy for the Quantitative Analysis of Carbonyl Groups in Bio-Oils. *RSC Adv.* **2014**, *4* (34), 17743. <https://doi.org/10.1039/c4ra01293c>.
- (23) Meier, D.; Windt, M. Analysis of Bio-Oils. In *Transformation of Biomass*; Hornung, A., Ed.; John Wiley & Sons, Ltd: Chichester, UK, 2014; pp 227–256. <https://doi.org/10.1002/9781118693643.ch13>.
- (24) Mullen, C. A.; Strahan, G. D.; Boateng, A. A. Characterization of Various Fast-Pyrolysis Bio-Oils by NMR Spectroscopy †. *Energy Fuels* **2009**, *23* (5), 2707–2718. <https://doi.org/10.1021/ef801048b>.
- (25) Ong, H. C.; Yu, K. L.; Chen, W.-H.; Pillejera, M. K.; Bi, X.; Tran, K.-Q.; Pétrissans, A.; Pétrissans, M. Variation of Lignocellulosic Biomass Structure from Torrefaction: A Critical Review. *Renew. Sustain. Energy Rev.* **2021**, *152*, 111698. <https://doi.org/10.1016/j.rser.2021.111698>.
- (26) Mu, W.; Ben, H.; Newalkar, G.; Ragauskas, A.; Qiu, D.; Deng, Y. Structure Analysis of Pine Bark-, Residue-, and Stem-Derived Light Oil and Its Hydrodeoxygenation Products. *Ind. Eng. Chem. Res.* **2014**, *53* (28), 11269–11275. <https://doi.org/10.1021/ie500541p>.

- (27) Zuber, J.; Rathsack, P.; Otto, M. Structural Characterization of Acidic Compounds in Pyrolysis Liquids Using Collision-Induced Dissociation and Fourier Transform Ion Cyclotron Resonance Mass Spectrometry. *Anal. Chem.* **2018**, *90* (21), 12655–12662. <https://doi.org/10.1021/acs.analchem.8b02873>.
- (28) Bayerbach, R.; Meier, D. Characterization of the Water-Insoluble Fraction from Fast Pyrolysis Liquids (Pyrolytic Lignin). Part IV: Structure Elucidation of Oligomeric Molecules. *J. Anal. Appl. Pyrolysis* **2009**, *85* (1–2), 98–107. <https://doi.org/10.1016/j.jaap.2008.10.021>.
- (29) Staš, M.; Chudoba, J.; Kubička, D.; Blažek, J.; Pospíšil, M. Petroleomic Characterization of Pyrolysis Bio-Oils: A Review. *Energy Fuels* **2017**, *31* (10), 10283–10299. <https://doi.org/10.1021/acs.energyfuels.7b00826>.
- (30) Hertzog, J.; Carré, V.; Le Brech, Y.; Dufour, A.; Aubriet, F. Toward Controlled Ionization Conditions for ESI-FT-ICR-MS Analysis of Bio-Oils from Lignocellulosic Material. *Energy Fuels* **2016**, *30* (7), 5729–5739. <https://doi.org/10.1021/acs.energyfuels.6b00655>.
- (31) Tessarolo, N. S.; Silva, R. C.; Vanini, G.; Pinho, A.; Romão, W.; de Castro, E. V. R.; Azevedo, D. A. Assessing the Chemical Composition of Bio-Oils Using FT-ICR Mass Spectrometry and Comprehensive Two-Dimensional Gas Chromatography with Time-of-Flight Mass Spectrometry. *Microchem. J.* **2014**, *117*, 68–76. <https://doi.org/10.1016/j.microc.2014.06.006>.
- (32) Tessarolo, N. S.; Silva, R. V. S.; Vanini, G.; Casilli, A.; Ximenes, V. L.; Mendes, F. L.; de Rezende Pinho, A.; Romão, W.; de Castro, E. V. R.; Kaiser, C. R.; Azevedo, D. A. Characterization of Thermal and Catalytic Pyrolysis Bio-Oils by High-Resolution Techniques: ¹H NMR, GC × GC-TOFMS and FT-ICR MS. *J. Anal. Appl. Pyrolysis* **2016**, *117*, 257–267. <https://doi.org/10.1016/j.jaap.2015.11.007>.
- (33) Hertzog, J.; Carré, V.; Le Brech, Y.; Mackay, C. L.; Dufour, A.; Mašek, O.; Aubriet, F. Combination of Electrospray Ionization, Atmospheric Pressure Photoionization and Laser Desorption Ionization Fourier Transform Ion Cyclotronic Resonance Mass Spectrometry for the Investigation of Complex Mixtures – Application to the Petroleomic Analysis of Bio-Oils. *Anal. Chim. Acta* **2017**, *969*, 26–34. <https://doi.org/10.1016/j.aca.2017.03.022>.
- (34) Dhungana, B.; Becker, C.; Zekavat, B.; Solouki, T.; Hockaday, W. C.; Chambliss, C. K. Characterization of Slow-Pyrolysis Bio-Oils by High-Resolution Mass Spectrometry and Ion Mobility Spectrometry. *Energy Fuels* **2015**, *29* (2), 744–753. <https://doi.org/10.1021/ef5016389>.
- (35) Johnson, A. R.; Carlson, E. E. Collision-Induced Dissociation Mass Spectrometry: A Powerful Tool for Natural Product Structure Elucidation. *Anal. Chem.* **2015**, *87* (21), 10668–10678. <https://doi.org/10.1021/acs.analchem.5b01543>.
- (36) Yoo, H. J.; Liu, H.; Håkansson, K. Infrared Multiphoton Dissociation and Electron-Induced Dissociation as Alternative MS/MS Strategies for Metabolite Identification. *Anal. Chem.* **2007**, *79* (20), 7858–7866. <https://doi.org/10.1021/ac071139w>.
- (37) Paris, J.; Morgan, T. E.; Marzullo, B. P.; Wootton, C. A.; Barrow, M. P.; O'Hara, J.; O'Connor, P. B. Two-Dimensional Mass Spectrometry Analysis of IgG1 Antibodies. *J. Am. Soc. Mass Spectrom.* **2021**, *32* (7), 1716–1724. <https://doi.org/10.1021/jasms.1c00096>.
- (38) Marzullo, B. P.; Morgan, T. E.; Wootton, C. A.; Perry, S. J.; Saeed, M.; Barrow, M. P.; O'Connor, P. B. Advantages of Two-Dimensional Electron-Induced Dissociation and Infrared Multiphoton Dissociation Mass Spectrometry for the Analysis of

- Agrochemicals. *Anal. Chem.* **2020**, *92* (17), 11687–11695. <https://doi.org/10.1021/acs.analchem.0c01585>.
- (39) Marzullo, B. P.; Morgan, T. E.; Theisen, A.; Haris, A.; Wootton, C. A.; Perry, S. J.; Saeed, M.; Barrow, M. P.; O'Connor, P. B. Combining Ultraviolet Photodissociation and Two-Dimensional Mass Spectrometry: A Contemporary Approach for Characterizing Singly Charged Agrochemicals. *Anal. Chem.* **2021**, *93* (27), 9462–9470. <https://doi.org/10.1021/acs.analchem.1c01185>.
- (40) Feider, C. L.; Macias, L. A.; Brodbelt, J. S.; Eberlin, L. S. Double Bond Characterization of Free Fatty Acids Directly from Biological Tissues by Ultraviolet Photodissociation. *Anal. Chem.* **2020**, *92* (12), 8386–8395. <https://doi.org/10.1021/acs.analchem.0c00970>.
- (41) Brodbelt, J. S.; Morrison, L. J.; Santos, I. Ultraviolet Photodissociation Mass Spectrometry for Analysis of Biological Molecules. *Chem. Rev.* **2020**, *120* (7), 3328–3380. <https://doi.org/10.1021/acs.chemrev.9b00440>.
- (42) Brodbelt, J. S. Photodissociation Mass Spectrometry: New Tools for Characterization of Biological Molecules. *Chem Soc Rev* **2014**, *43* (8), 2757–2783. <https://doi.org/10.1039/C3CS60444F>.
- (43) Paris, J.; Theisen, A.; Marzullo, B. P.; Haris, A.; Morgan, T. E.; Barrow, M. P.; O'Hara, J.; O'Connor, P. B. Multimodal Tandem Mass Spectrometry Techniques for the Analysis of Phosphopeptides. *J. Am. Soc. Mass Spectrom.* **2022**, *33* (7), 1126–1133. <https://doi.org/10.1021/jasms.1c00353>.
- (44) Theisen, A.; Wootton, C. A.; Haris, A.; Morgan, T. E.; Lam, Y. P. Y.; Barrow, M. P.; O'Connor, P. B. Enhancing Biomolecule Analysis and 2DMS Experiments by Implementation of (Activated Ion) 193 Nm UVPD on a FT-ICR Mass Spectrometer. *Anal. Chem.* **2022**, *94* (45), 15631–15638. <https://doi.org/10.1021/acs.analchem.2c02354>.
- (45) Morgan, T. E.; Wootton, C. A.; Marzullo, B.; Paris, J.; Kerr, A.; Ellacott, S. H.; van Agthoven, M. A.; Barrow, M. P.; Bristow, A. W. T.; Perrier, S.; O'Connor, P. B. Characterization Across a Dispersity: Polymer Mass Spectrometry in the Second Dimension. *J. Am. Soc. Mass Spectrom.* **2021**, *32* (8), 2153–2161. <https://doi.org/10.1021/jasms.1c00106>.
- (46) Floris, F.; Vallotto, C.; Chiron, L.; Lynch, A. M.; Barrow, M. P.; Delsuc, M.-A.; O'Connor, P. B. Polymer Analysis in the Second Dimension: Preliminary Studies for the Characterization of Polymers with 2D MS. *Anal. Chem.* **2017**, *89* (18), 9892–9899. <https://doi.org/10.1021/acs.analchem.7b02086>.
- (47) Marzullo, B. P.; Morgan, T. E.; Wootton, C. A.; Li, M.; Perry, S. J.; Saeed, M.; Barrow, M. P.; O'Connor, P. B. Comparison of Fragmentation Techniques for the Structural Characterization of Singly Charged Agrochemicals. *Anal. Chem.* **2020**, *92* (4), 3143–3151. <https://doi.org/10.1021/acs.analchem.9b04820>.
- (48) Marcum, C. L.; Jarrell, T. M.; Zhu, H.; Owen, B. C.; Hauptert, L. J.; Easton, M.; Hosseinaei, O.; Bozell, J.; Nash, J. J.; Kenttämaa, H. I. A Fundamental Tandem Mass Spectrometry Study of the Collision-Activated Dissociation of Small Deprotonated Molecules Related to Lignin. *ChemSusChem* **2016**, *9* (24), 3513–3526. <https://doi.org/10.1002/cssc.201600678>.
- (49) Zhang, J.; Feng, E.; Li, W.; Sheng, H.; Milton, J. R.; Easterling, L. F.; Nash, J. J.; Kenttämaa, H. I. Studies of the Fragmentation Mechanisms of Deprotonated Lignin Model Compounds in Tandem Mass Spectrometry. *Anal. Chem.* **2020**, *92* (17), 11895–11903. <https://doi.org/10.1021/acs.analchem.0c02275>.

- (50) Hauptert, L. J.; Owen, B. C.; Marcum, C. L.; Jarrell, T. M.; Pulliam, C. J.; Amundson, L. M.; Narra, P.; Aqueel, M. S.; Parsell, T. H.; Abu-Omar, M. M.; Kenttämaa, H. I. Characterization of Model Compounds of Processed Lignin and the Lignome by Using Atmospheric Pressure Ionization Tandem Mass Spectrometry. *Fuel* **2012**, *95*, 634–641. <https://doi.org/10.1016/j.fuel.2011.12.015>.
- (51) Kiyota, E.; Mazzafera, P.; Sawaya, A. C. H. F. Analysis of Soluble Lignin in Sugarcane by Ultrahigh Performance Liquid Chromatography–Tandem Mass Spectrometry with a Do-It-Yourself Oligomer Database. *Anal. Chem.* **2012**, *84* (16), 7015–7020. <https://doi.org/10.1021/ac301112y>.
- (52) Prothmann, J.; Sun, M.; Spégel, P.; Sandahl, M.; Turner, C. Ultra-High-Performance Supercritical Fluid Chromatography with Quadrupole-Time-of-Flight Mass Spectrometry (UHPSFC/QTOF-MS) for Analysis of Lignin-Derived Monomeric Compounds in Processed Lignin Samples. *Anal. Bioanal. Chem.* **2017**, *409* (30), 7049–7061. <https://doi.org/10.1007/s00216-017-0663-5>.
- (53) Owen, B. C.; Hauptert, L. J.; Jarrell, T. M.; Marcum, C. L.; Parsell, T. H.; Abu-Omar, M. M.; Bozell, J. J.; Black, S. K.; Kenttämaa, H. I. High-Performance Liquid Chromatography/High-Resolution Multiple Stage Tandem Mass Spectrometry Using Negative-Ion-Mode Hydroxide-Doped Electrospray Ionization for the Characterization of Lignin Degradation Products. *Anal. Chem.* **2012**, *84* (14), 6000–6007. <https://doi.org/10.1021/ac300762y>.
- (54) Sheng, H.; Murria, P.; Degenstein, J. C.; Tang, W.; Riedeman, J. S.; Hurt, M. R.; Dow, A.; Klein, I.; Zhu, H.; Nash, J. J.; Abu-Omar, M.; Agrawal, R.; Delgass, W. N.; Ribeiro, F. H.; Kenttämaa, H. I. Initial Products and Reaction Mechanisms for Fast Pyrolysis of Synthetic G-Lignin Oligomers with B-O-4 Linkages via On-Line Mass Spectrometry and Quantum Chemical Calculations. *ChemistrySelect* **2017**, *2* (24), 7185–7193. <https://doi.org/10.1002/slct.201700582>.
- (55) Xu, L.; Ma, X.; Murria, P.; Talpade, A.; Sheng, H.; Meilan, R.; Chapple, C.; Agrawal, R.; Delgass, W. N.; Ribeiro, F. H.; Kenttämaa, H. I. Fast Determination of the Lignin Monomer Compositions of Genetic Variants of Poplar via Fast Pyrolysis/Atmospheric Pressure Chemical Ionization Mass Spectrometry. *J. Am. Soc. Mass Spectrom.* **2021**. <https://doi.org/10.1021/jasms.1c00186>.
- (56) Morreel, K.; Kim, H.; Lu, F.; Dima, O.; Akiyama, T.; Vanholme, R.; Niculaes, C.; Goeminne, G.; Inzé, D.; Messens, E.; Ralph, J.; Boerjan, W. Mass Spectrometry-Based Fragmentation as an Identification Tool in Lignomics. *Anal. Chem.* **2010**, *82* (19), 8095–8105. <https://doi.org/10.1021/ac100968g>.
- (57) Milder, I. E. J.; Arts, I. C. W.; Venema, D. P.; Lasaroms, J. J. P.; Wähälä, K.; Hollman, P. C. H. Optimization of a Liquid Chromatography–Tandem Mass Spectrometry Method for Quantification of the Plant Lignans Secoisolariciresinol, Matairesinol, Lariciresinol, and Pinosesinol in Foods. *J. Agric. Food Chem.* **2004**, *52* (15), 4643–4651. <https://doi.org/10.1021/jf0497556>.
- (58) Eklund, P. C.; Backman, M. J.; Kronberg, L. Å.; Smeds, A. I.; Sjöholm, R. E. Identification of Lignans by Liquid Chromatography–Electrospray Ionization Ion-Trap Mass Spectrometry. *J. Mass Spectrom.* **2007**, *43* (1), 97–107. <https://doi.org/10.1002/jms.1276>.
- (59) Jarrell, T. M.; Marcum, C. L.; Sheng, H.; Owen, B. C.; O’Lenick, C. J.; Maraun, H.; Bozell, J. J.; Kenttämaa, H. I. Characterization of Organosolv Switchgrass Lignin by Using High

- Performance Liquid Chromatography/High Resolution Tandem Mass Spectrometry Using Hydroxide-Doped Negative-Ion Mode Electrospray Ionization. *Green Chem* **2014**, *16* (5), 2713–2727. <https://doi.org/10.1039/C3GC42355G>.
- (60) Boes, K. S.; Narron, R. H.; Chen, Y.; Park, S.; Vinueza, N. R. Characterization of Biofuel Refinery Byproduct via Selective Electrospray Ionization Tandem Mass Spectrometry. *Fuel* **2017**, *188*, 190–196. <https://doi.org/10.1016/j.fuel.2016.10.016>.
- (61) Sheng, H.; Tang, W.; Gao, J.; Riedeman, J. S.; Li, G.; Jarrell, T. M.; Hurt, M. R.; Yang, L.; Murria, P.; Ma, X.; Nash, J. J.; Kenttämä, H. I. (-)ESI/CAD MSⁿ Procedure for Sequencing Lignin Oligomers Based on a Study of Synthetic Model Compounds with β -O-4 and 5-5 Linkages. *Anal. Chem.* **2017**, *89* (24), 13089–13096. <https://doi.org/10.1021/acs.analchem.7b01911>.
- (62) Morreel, K.; Dima, O.; Kim, H.; Lu, F.; Niculaes, C.; Vanholme, R.; Dauwe, R.; Goeminne, G.; Inzé, D.; Messens, E.; Ralph, J.; Boerjan, W. Mass Spectrometry-Based Sequencing of Lignin Oligomers. *Plant Physiol.* **2010**, *153* (4), 1464–1478. <https://doi.org/10.1104/pp.110.156489>.

CHAPTER 5 : PRINCIPLE OF THE TWO-DIMENSIONAL MASS SPECTROMETRY 2D FTMS AND APPLICATION ON BIO-OIL

5.1. Introduction

In classical tandem mass spectrometry, the precursor ion selection is necessary. This step can be facilitated by using chromatography. In this case, the complexity of the sample is less than when the entire sample is fed into the ion source to conduct flow injection analysis (FIA). An attractive alternative for analyzing components of a complex mixture by MS/MS, is a data-independent analysis (DIA) approach used in a two-dimensional mass spectrometry (2DMS) experiment. In this case the isolation of precursor ion is not required. Before the MS/MS event, the ion trajectory manipulation in the ICR cell, and thus the modulation in fragmentation efficiency, enables the correlation of the fragment ions to their matching precursor ions.

5.2. 2D-FTMS principle

The reversibility of resonant excitation inside the ICR cell was shown in 1984 by Marshall et al.¹ A single frequency resonant stimulation with constant amplitude and extending duration was used to excite ions of a given m/z in a preliminary experiment.² The intensity of the corresponding peak in the mass spectrum increased as the ion radius increased until the ion radius exceeded the radius of the ICR cell. A second experiment reversed the sign of the applied voltage after 1 ms to switch the phase of the resonant excitation by 180°, resulting in a decrease of the peak intensity. Based on these results, Pfändler et al. suggested a pulse sequence for two-dimensional mass spectrometry in 1987.³ The Gäumann pulse sequence, a pulse-delay-pulse sequence, is frequently used in FT-ICR MS to obtain 2DMS.^{3,4} The Gäumann pulse sequence and associated ion paths within the ICR cell are shown in Figure 5-1.

The following events occur during each iteration of Gäumann pulse sequence (Figure 5-1 a) in a 2D FT-ICR MS experiment:^{3,4}

- Ionization, external ion accumulation in the storage hexapole, and ion transfer to the ICR cell.
- P_1 - t_1 - P_2 sequence.
- Fragmentation (τ_m).
- P_3 excitation for detection
- Transient acquisition (t_2).

1. **P₁**: after the ionization event, all the produced ions are transferred into the ICR cell and are excited by the initial pulse P₁ to increase their orbital radii r₁. Thanks to this pulse, the ions of the same m/z value circulate in the ICR cell in the form of a coherent packet of ions.
2. **t₁ Delay**: after the initial activation, the delay (t₁) allows the ions to gain phase and spatial separation. ω_{ICR} , the cyclotron motion of the ions increases by $\omega_{ICR} \times t_1$, increasing the phase of the motion of the ions.
3. **P₂**: the P₂ pulse (identical the P₁ pulse) is applied after t₁.

Two phenomena occur:

- 1- if the ions are out of phase with the RF of the pulse, they are de-excited, the radius of their orbit decreases up to be close to the center of the ICR cell.
 - 2- If the ions are in phase with the RF of the pulse, their orbit still increases.
4. **τ_m** : after the de-excitation of part of the ions to the center of the ICR cell and the additional excitation of the others. The “de-excited ions” are activated by UV or IR photons from a laser whose pathway is located close to the ICR cell's center during the τ_m time. Consequently, for a given t₁ time, only a restricted part of the ions trapped in the cell undergo fragmentation processes. The modification of the t₁ time between P₁ and P₂ pulse changes the population of ions, whose undergo photon activation.
 5. **P₃**: after fragmentation, the third pulse P₃, is used to excite the fragment ions and their precursor ions for their detection. The ions, which were in phase with the P₂ pulse are stepwise excited by P₁ + P₂ + P₃ pulses on an orbit which radius is greater than the radius of the ICR cell and are ejected.
 6. **t₂**: is the time used for the detection of the fragment and precursors ions.

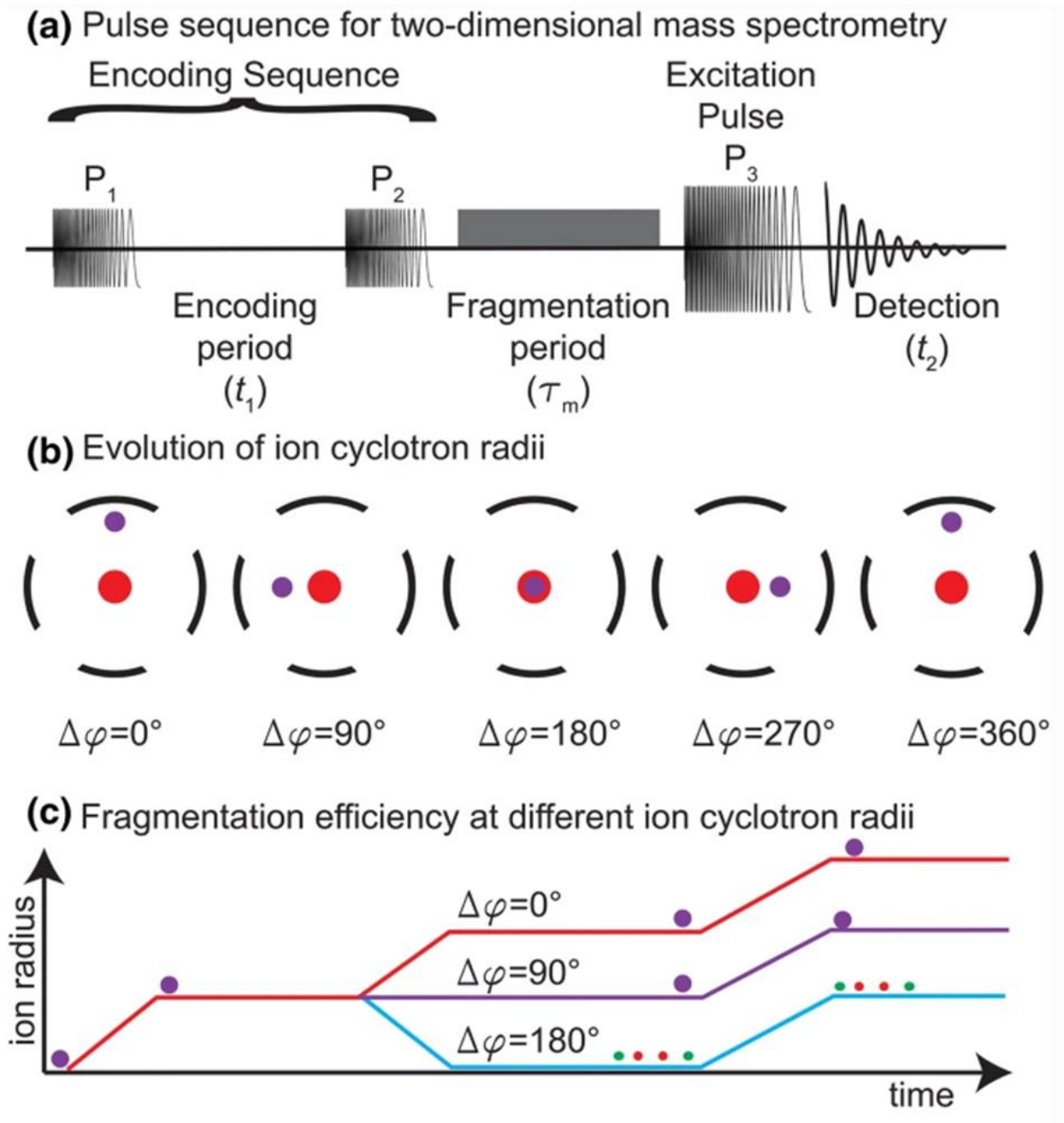


Figure 5-1: A common Gäumann FT-ICR 2DMS pulse sequence is shown in (A). (B) How the pulse sequence affected the ions' orbital radii. (C) The impact of the ion's circling radius on fragmentation efficiency. It is important to keep in mind that the ion is totally in-phase with the second excitation pulse for $\Delta\varphi = 0^\circ$, while it is fully out-of-phase for $\Delta\varphi = 180^\circ$. Most ions will settle within these two limits in the majority of scans. Ions with lower orbital energies will fragment more easily than ions with greater radii (orange line) (red and purple).^{4,5}

After the application of the first Gäumann pulse sequence, the ions are expelled from the cell using a quench pulse and a new batch of ions are injected. The Gäumann pulse sequence cycle is looped, and the delay time (t_1) is increased to ensure the activation of another precursor ion population. Each cycle's detection event generates a transient, which is added to a list; hence, the transients are not averaged together but rather maintained apart for processing. The number of cycles/scans performed, which is typically 2^n (2^n is the number of scans, where n is an integer, in order to benefit from the speed advantage of the fast Fourier transform.) can lead to huge data file size as well important data acquisition time. In this context, FIA, which ensure the continuously infused of the sample into the ionization source of the mass spectrometer is well suited.

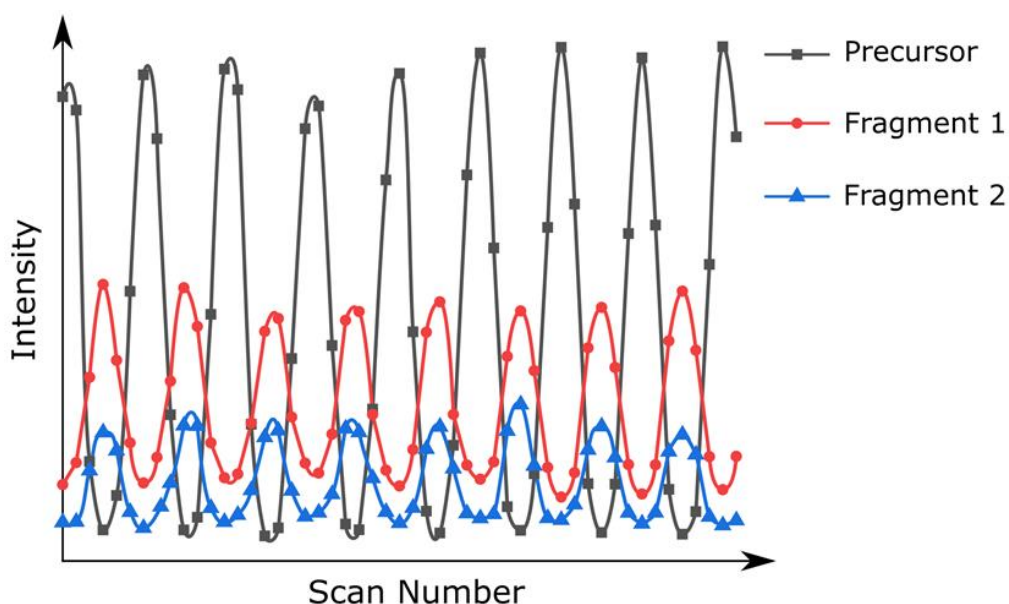


Figure 5-2: Graph showing the fluctuation in intensity between the precursor ions (black) and matching fragment ions (red and blue).⁵

The intensity of the product ions formed, and thus the fragmentation efficiency, is dependent on the precursor ion's orbiting radius. The intensity of the precursor and the product ions will vary at the same frequency from scan to scan; this can be seen in figure 5-2, where the intensity of the product ions modulates at the same frequency as the intensity of the precursor ion but fully out-of-phase.⁵

5.3. Data processing and representation

The 2DMS data, which size is in the Gbytes range, must be processed. An efficient two-dimensional Fourier transform (2D-FFT) can be used to accomplish this. Consequently, the product ions will be correlated with the relevant precursor ions. The "SPIKE" (Spectroscopy

Processing Innovative Kernel) Python script is capable of carrying out this kind of data-processing.⁶ SPIKE can use denoising techniques in addition to the 2D-FFT to try to eliminate the noise streaks that are often seen in 2DMS spectra.⁷⁻⁹ After processing, the data acquired from the 2DMS experiment is constituted of intensity (z-axis), fragment m/z (x-axis), and precursor m/z (y-axis), generating a 3D data set that is often shown as a xy contour plot. The precursor m/z axis derives from the frequency of the ion's intensity modulation, whereas the fragment m/z axis derives from the observed reduced cyclotron frequencies of the ions. Several features could be considered from the 2DMS contour plot presented in Figure 5-3.⁵

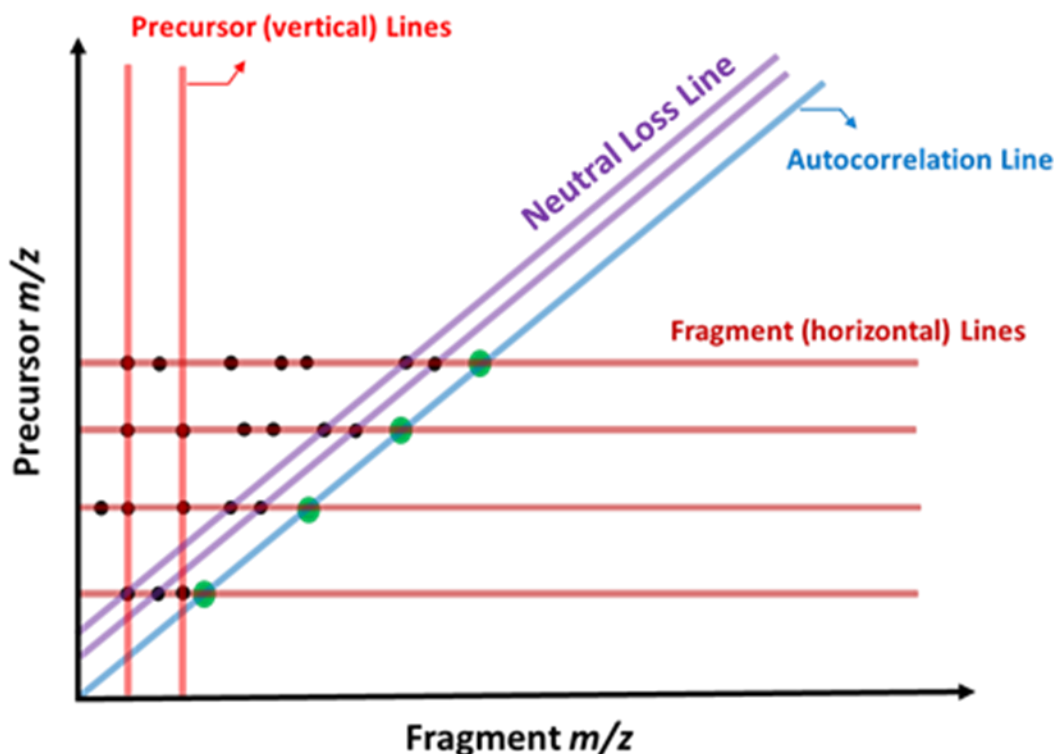


Figure 5-3: A 2DMS contour plot is represented and labelled with the numerous lines that may be seen to analyze the data.⁵

Autocorrelation line:

The autocorrelation line, an important component of a 2DMS spectrum, is shown as the $y = x$ diagonal line. This line gives the m/z of all precursor ions. Though having a slightly modified connection between ions and the observed intensity, this line may be viewed as a reflection of the MS^1 mass spectrum. Note that the ions which does not undergo dissociation are absent from the autocorrelation line.

Fragment lines:

The fragment ions of a given precursor are obtained by considering the horizontal line at the precursor ion's m/z value. Consequently, fragment line relative to a precursor ion is similar to its classical MS/MS spectrum.

Precursor lines:

The vertical lines are named precursor lines and gathered all the precursor ions, which lead to a specific fragment ion. As a result, the information obtained is “similar” to what is received in a traditional precursor ion scan experiment when the MS/MS is carried out with a triple quadrupole.

Neutral loss lines:

The diagonal lines parallel to the autocorrelation line are used to depict neutral loss lines. The neutral loss line will be matched by all species that lose the same neutral. The results obtained may be compared to the classical neutral loss scan obtained by triple quadrupole tandem mass spectrometry.

5.4. 2D-FTMS advantages

The advantages of the two-dimensional mass spectrometry are:³⁻⁵

- Ions that are in the ICR cell are fragmented without selection and yield a MS/MS spectrum. The fragment ions may be linked to their respective precursor ion because they inherit its intensity modulation frequency. This is accomplished in just one experimental cycle.
- Based on the previous benefit, 2D FTMS is a genuine tandem mass spectrometry method applicable for analyzing complex mixtures in a reasonable time (some tens of minutes).
- In the field of this study, offline fractionation can be done before to apply 2D FTMS experiments on each fraction, which reduces the complexity/peak density of the 3D contour plot and, consequently, the difficulty of data processing.

The main disadvantages of the 2D FTMS analysis are limited resolving power, lower signal-to-noise ratio than traditional MS/MS, and a low sensitivity. Nevertheless, some of these issues may be overcome by increasing the measurement time, which also leads to an increase of sample consumption, and data size.

5.1. Application on bio-oil

5.1.1. *Publication: Two-dimensional Fourier transform ion cyclotron mass spectrometry applied to bio-oil: a step beyond molecular formula for complex mixture characterization.*

Anthony Abou-Dib, Bryan P. Marzullo, Diana Catalina Palacio Lozano, Jasmine Hertzog, Peter B. O'Connor, Mark P. Barrow, Vincent Carré, Frédéric Aubriet

5.1.2. Introduction

Lignocellulosic biomass is regarded as a sustainable and renewable resource for carbon material. It is mainly composed of cellulose and hemicellulose, which are both carbohydrate polymers, and lignin, which is a supramolecular structure made of phenolic moieties.¹⁰ The thermochemical conversion of this raw material notably leads to a liquid material, namely bio-oil, that can be upgraded into second-generation biofuel or value-added chemicals. However, bio-oil is considered as a complex mixture comprising tens of thousands of species of different chemical functions and covering a wide mass and polarity range. Thus, bio-oils are characterized by a high oxygen content responsible for a low heating value and a high acidity compared to fossil fuels.^{11,12} These properties are not compatible with actual thermal engines, therefore bio-oils must undergo upgrading treatments such as deoxygenation and cracking treatments to reach physicochemical characteristics similar as those of petroleum-based oils.¹³ The optimization of both the conversion and upgrading processes requires the most accurate as possible description of the bio-oil sample composition before and after treatment. Several analytical techniques have been applied for bio-oil characterization but non-targeted ultra-high-resolution mass spectrometry (UHRMS) is considered as the preferred method.^{14–16} In fact, this analytical technique, and more particularly Fourier transform ion cyclotron resonance (FT-ICR), provides the highest resolution and mass accuracy to decipher the molecular complexity of such organic matrixes.^{17–20} FT-ICR MS enables to detect and assign up to hundreds of thousands molecular formulae,²¹ but neither chemical functions nor structural information is provided, which are required for a better understanding of the upgrading processes and identifying refractory bio-oil components.²² To overcome these limitations, tandem mass spectrometry (MS/MS) is one of the solutions. However, it is impossible to perform a classical MS/MS experiment on each of the thousands of ions observed on the mass spectrum of a bio-oil. The time required is considerable, and the presence at a given nominal mass of several isobaric contributions does not allow for achieving the optimal and unique selection of the precursor ion. As part of FT-ICR MS, two-dimensional MS (2DMS) was developed,²³ which enables tandem mass spectrometry to be performed without precursor ion isolation, and this over a given m/z range. By this way, it is possible to trace simultaneously, the fragmentation pattern of different precursor ions.²⁴ Some studies have been carried out by 2D FT-ICR MS with different fragmentation methods. Thus, agrochemicals^{25,26}, and peptides²⁷ were characterized by 2D FT-ICR MS using electron induced

dissociation (EID), ultraviolet photodissociation (UVPD), infrared multiphoton dissociation (IRMPD), and electron capture dissociation (ECD). In this paper, UVPD 2D FT-ICR MS was applied for the first time to pyrolysis bio-oil. This activation method was used because of the high energy of UV photons, which provides new fragmentation pathways that are not accessible through conventional collisional activation. The achieved fragmentation mass spectra, especially from pyrolysis lignin derivatives, allowed increasing our knowledge on the chemical functions and structure of the bio-oil compounds. This study also demonstrated the capacity of 2DMS to be a data-independent analysis method and an effective technique for the structural characterization of complex mixtures such as bio-oils in a single experiment.

5.1.3. Materials and Methods

5.1.3.1. Oak Pyrolysis Bio-oil

Bio-oil was obtained at the LRGP laboratory (Nancy, France) by pyrolysis of 2 grams of oak powder (0.8 to 1.7 mm) continuously added through a micro-feeder (10 grams/hour) in a micro-fluidized bed reactor heated at 500°C for 12 minutes. The bio-oil was recovered in methanol ("bio-oil solution") and stored at -20 °C before analysis.²⁸ The bio-oil was diluted in methanol at a 100 µL/mL final concentration for the 2DMS analysis.

5.1.3.2. Sample Preparation

LCMS grade methanol (VWR–Prolabo), lignin standards as coniferyl alcohol (98%, Aldrich), guaiacylglycerol-β-guaiacylether (GGE) (Aldrich), and pinoresinol (≥95%, Aldrich) were used. These standard compounds were chosen due to their presence in bio-oil^{29–31} and their chromophore group (Figure 1) that absorb at 193 nm, i.e., the UV laser wavelength used in this study. They were solubilized in methanol at a final concentration of 1mg.mL⁻¹.

5.1.3.3. FT-ICR MS Analysis

The samples were analyzed using a 12T Bruker Solarix FT-ICR mass spectrometer (Bruker Daltonik, GmbH, Bremen, Germany), equipped with an Infinity ICR cell. Fragmentation was performed with a Coherent ExciStar XS, ArF excimer laser that emits 193 nm UV photon with a pulse energy of 1.8 mJ and a pulse duration of 7-10 ns.

Each standard was first subject to one-dimension analysis (classical MS/MS). This was performed by electrospray ionization (ESI) in negative-ion mode using a home-built nano-ESI source, as detailed by Zhao *et al.*³² The capillary voltage was set to -800 V, the nebulizing gas was maintained at 0.8 bar, and the drying gas was controlled at a temperature of 150°C with a flow rate of 2 L.min⁻¹. The precursor ions were accumulated for 2 seconds in a hexapole before being transferred to the ICR cell and irradiated by one laser shot. Mass spectra were acquired with a 4 M time-domain and resulted from the accumulation of one hundred scans. A resolving power of ~472,000 was obtained at m/z 179.0702.

For the 2DMS experiments, the diluted bio-oil and the mixture of standards were injected using a 10 mL syringe and subjected to independent analysis. Samples were infused with a flow rate of 60 $\mu\text{L}\cdot\text{h}^{-1}$ in the ESI source, working in negative-ion mode, with a capillary voltage set at -5000 V, the nebulizing gas was maintained at 1 bar, and the drying gas was set at 220°C with a flow rate of 4 $\text{L}\cdot\text{min}^{-1}$. The ions were accumulated for 0.5 s before being transferred to the ICR cell to be fragmented by the UV laser beam. The 2DMS experiments were done by applying the Gäumann pulse sequence.^{3,4} The delay between the first excitation pulse (P_1) and the second pulse (P_2) was 4.5×10^{-7} s with a P_1 width equals to 1 μs . To produce the 2DMS data set, 1 M resolution on the x-axis (2^{20} , fragment m/z) and 8k (8192 single scans) scan lines on the y-axis (precursor m/z) were used (m/z range 143-500). This resulted to a resolving power of $\sim 170,000$ at m/z 179.0702. The 2D-UVPD-MS experiment lasted for three hours and thirty minutes.

5.1.3.4. Data treatment and graphical representations

The data achieved in 1DMS were treated by Data Analysis 5.0 software (Bruker, Bremen, Germany). Fragmentation mass spectra of each standard were calibrated by using the precursor ion as a "lock mass" and the resulting fragments.

For the 2DMS, SPIKE³³ was used to process the data to produce a 2D FFT, digital demodulation, and urQRd³⁴ de-noising. For both standards and bio-oil, a de-noise rank of 25 was used as it was found to be the best compromise in eliminating the noise streaks, frequently present in a 2DMS spectra, and conserving the peaks. In-house T2D LabView-based software was employed to analyze the 2DMS maps. This software was also used to calibrate the 2DMS data based on the previously identified fragment ions obtained in the 1D experiments. Mass accuracy values lower than 1 ppm were obtained. For the 2DMS analysis, a 2DMS contour plot is obtained and is labelled with the various lines that can be observed for the interpretation of the data (section 5.3). Among these lines, we have the autocorrelation line, a key feature of a 2DMS spectrum, the neutral loss line highlighting all the species that have common neutral losses, and the horizontal line also known as fragment line.

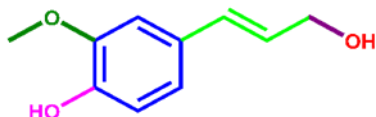
Some graphical representations were employed to plot the achieved molecular assignments. For instance, double bond equivalent (DBE) vs. carbon number graph was employed. DBE represents the unsaturation degree of a molecule and is calculated according to this equation the $DBE = c - (h/2) + (n/2) + 1$.³⁵ Molecular formulae were also represented according to their O/C and H/C values, which resulted to a van Krevelen diagram. This latter graph allows distinguishing biochemical families such as lipids, unsaturated hydrocarbons, phenolics from lignin, and carbohydrates.^{36,37}

Furthermore, the moiety coverage of each molecule was determined by counting the different molecular moieties observed after fragmentation and comparing it to the total number previously set based on the structure. The fragmentation efficiency (FE - Equation 5-1) allows to determine the efficiency of dissociation of the applied technique.

Monomers

Coniferyl alcohol

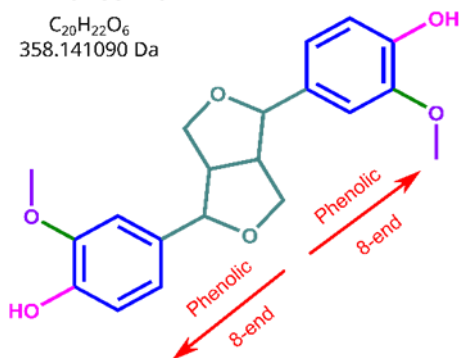
$C_{10}H_{12}O_3$
180.078096 Da



Dimers

Pinoresinol

$C_{20}H_{22}O_6$
358.141090 Da



Guaiacylglycerol- β -guaiacylether
(GGE)

$C_{17}H_{20}O_6$
320.125440 Da

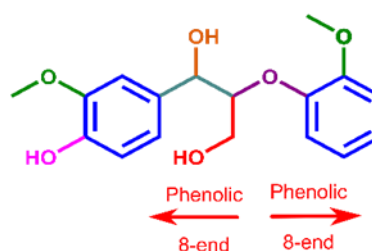


Figure 5-4: Structures of the three lignin standards employed in this study. The various moieties found in each compound are highlighted by the color-coding of the structures.

The structures present in Figure 5-4 are color-coded, highlighting the different moieties present in each compound. For instance, coniferyl alcohol comprises 6 different moieties. Its fragmentation led to three moieties (H_2O moiety in red, CH_3 moiety in green, and formaldehyde moiety in purple).

$$FE\% = \frac{\text{Sum of all product ion intensities}}{\text{Sum of all product ion intensities} + \text{Precursor ion intensity}} \times 100 \quad \text{Equation 5-1}$$

For the FE calculation, the intensity of the radical fragment ions (odd-electron anions), the fragment ions (even-electron ions) and the $[M-H]^-$ deprotonated species were taken into consideration.

In order to have an insight on the fragmentation pattern (if the ion has lost a neutral or a radical), calculation of the percentage of the even- and odd-electron fragments was used by applying the Equations 5-2 and 5-3 in which for all product ion intensities, the odd and the even electron fragment ions were considered.

$$\% \text{odd electron ions} = \frac{\text{Sum of all odd electron ion intensities}}{\text{Sum of all product ion intensities} + \text{Precursor ion intensity}} \times 100 \quad \text{Equation 5-2}$$

$$\% \text{even electron ions} = \frac{\text{Sum of all even electron ion intensities}}{\text{Sum of all product ion intensities} + \text{Precursor ion intensity}} \times 100 \quad \text{Equation 5-3}$$

These different calculations were used to compare the results obtained by 1D and 2DMS of the standards. For the comparison of 2DMS on the standards with the 2DMS of bio-oils, an extraction of the horizontal line with m/z values similar to the standard ones was used.

5.1.4. Results and discussion

5.1.4.1. 1D and 2DMS on individual and mixture of lignin standards

Fragmentation efficiencies (FE) and moiety coverage obtained from the three phenolic standards in 1D and 2D experiments were reported in Table 5-1. In 1DMS, the deprotonated standard was isolated and fragmented whereas in 2DMS experiments, the fragmentation pattern of the mix of the three standards was investigated. These latter analyses were showed to be successful as the 3 standards fragmented, as evidenced by the autocorrelation line ($y = x$) extracted from the 2D map (Figures 5-5 A and B) as well as the horizontal line for each standard.

The three standards had fragmentation patterns that were similar to those of their respective 1DMS spectra (Chapter IV), however certain cleavages were missed in the 2D experiment. The 1DMS experiment of the coniferyl alcohol led to the loss of methyl radical (m/z 164.047), water (m/z 161.0605), and formaldehyde (m/z 149.0605) (Table 5-2), and to a moiety coverage of 50% (Table 5-1). For the 2DMS of the standard mixture, neutral losses from coniferyl alcohol were formaldehyde, which was also observed in 1DMS, and specific fragments (Table 5-3).

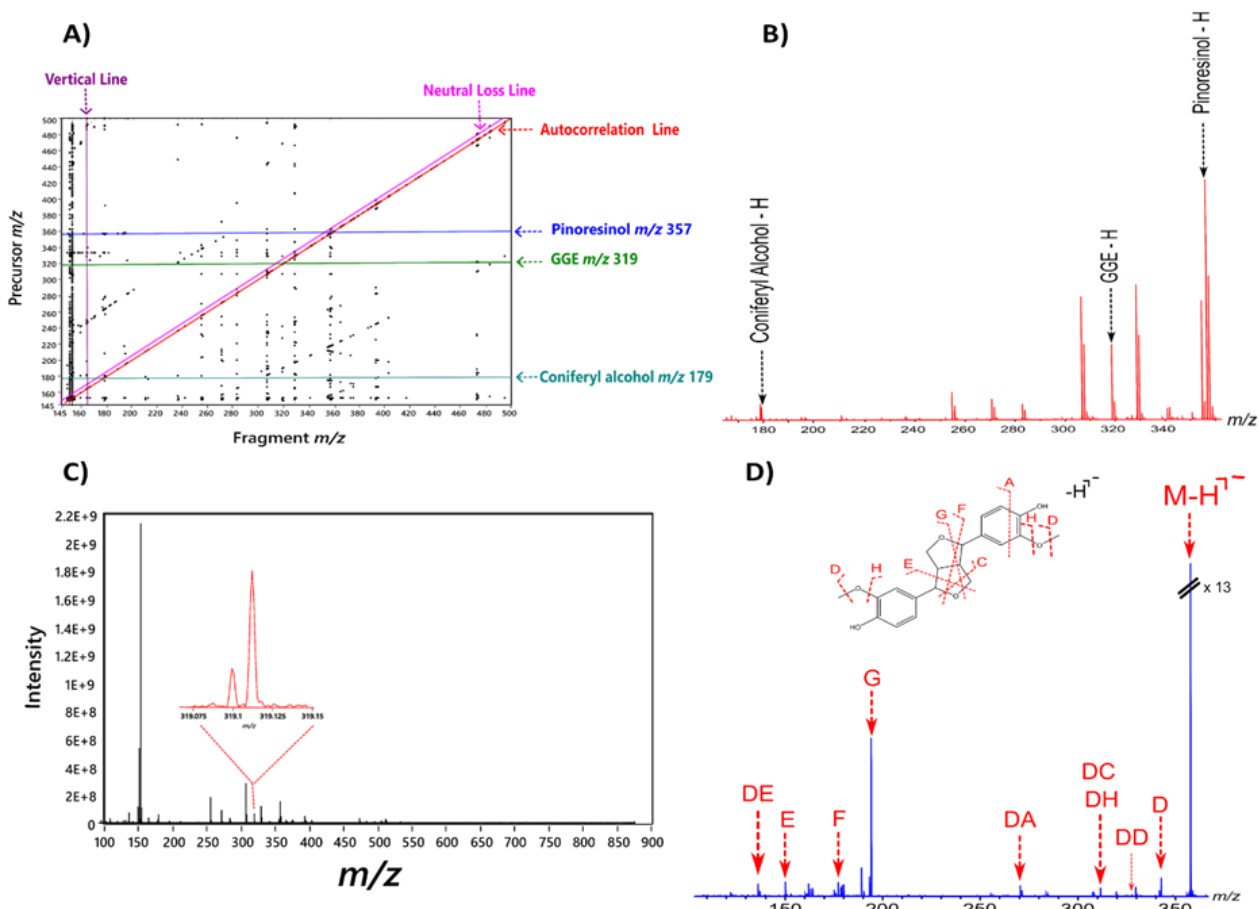


Figure 5-5: (A) 2D-UVPD-MS map for the three standards mixtures, (B) the extracted autocorrelation line, (C) the extracted neutral loss line of m/z 124 (guaiacol), and (D) the extracted horizontal line at m/z 357.

Table 5-1: Fragmentation efficiency percentages (FE (%)) and moiety coverage (%) in the 1D and 2D experiments for each Investigated lignin standard.

	1D- UVPD MS		2D-UVPD MS	
	FE %	Moiety coverage %	FE %	Moiety coverage %
Coniferyl alcohol	3	50	1	67
GGE	2	56	1	56
Pinoresinol	4	67	5	67

Table 5-2: Peak list, relative intensity of the fragment, and assignment from the 1DMS of the standard coniferyl alcohol.

Name	MS [M-H] ⁻	Activation Mode	MS ²	
			m/z	Loss (abundance %)
Coniferyl alcohol	C ₁₀ H ₁₁ O ₃ ⁻ m/z179.0702	UVPD	164.0476	-CH ₃ (64)
			161.0605	-H ₂ O (100)
			149.0605	-CH ₂ O (85)

Table 5-3: Peak list, relative intensity of the fragment, and assignment from the 2DMS of coniferyl alcohol in the standard mixture after a denoise rank of 25.

Name	MS [M-H] ⁻	Activation Mode	MS ²	
			m/z	Loss (abundance %)
Coniferyl alcohol	C ₁₀ H ₁₁ O ₃ ⁻ m/z179.0702	UVPD	163.0405	-CH ₄ (100)
			149.0599	-CH ₂ O (4)
			123.0445	-C ₃ H ₄ O (5)
			107.0485	-C ₃ H ₄ O ₂ (5)

A cross-ring cleavage relative to the opening of the aromatic ring (m/z 107.0485) helped to localize the substitutions on the aromatic ring and increased the number of identifiable moieties (67%). In addition, the homolytic dissociation of the carbon-carbon bond between the phenolic ring and the hydroxy propenyl (m/z 123.0445), as well as the elimination of methane (m/z 163.0405) were observed.

The two phenolic dimers studied in this work were pinoresinol and guaiacylglycerol- β -guaiacyl ether (GGE), which are known to constitute the primary bonding structure in lignin.³⁸ For the pinoresinol, similar fragments were produced by 1DMS (Table 5-4) and 2DMS experiments (Table 5-5), and led to a similar moiety coverage.

Table 5-4: Peak list, relative intensity of the fragment, and assignment from the 1DMS of the standard pinosresinol.

Name	MS [M-H] ⁻	Activation Mode	MS ²	
			m/z	Loss (abundance %)
Pinosresinol	C ₂₀ H ₂₁ O ₆ ⁻ m/z357.1343	UVPD	342.1097	- CH ₃ (73)
			327.1227	- CH ₂ O (2)
			311.0918	-CH ₄ , -CH ₂ O (2)
			270.0889	- C ₃ H ₄ O ₂ , -CH ₃ (3)
			194.0574	-C ₁₀ H ₁₁ O ₂ (100)
			177.0547	-CH ₂ O, -CH ₄ , -C ₈ H ₆ O ₂ (16)
			151.0391	- C ₁₂ H ₁₄ O ₃ (84)
			136.0157	- C ₁₃ H ₁₇ O ₃ (32)

Table 5-5: Peak list, relative intensity of the fragment, and assignment from the 2DMS of pinosresinol in the standard mixture after a denoise rank of 25.

Name	MS [M-H] ⁻	Activation Mode	MS ²	
			m/z	Loss (abundance %)
Pinosresinol	C ₂₀ H ₂₁ O ₆ ⁻ m/z357.1343	UVPD	342.1097	- CH ₃ (11)
			311.0918	-CH ₄ , -CH ₂ O (3)
			270.0889	- C ₃ H ₄ O ₂ , -CH ₃ (3)
			194.0574	-C ₁₀ H ₁₁ O ₂ (100)
			177.0547	CH ₂ O, -CH ₄ , -C ₈ H ₆ O ₂ (9)
			150.0311	- C ₁₂ H ₁₅ O ₃ (9)
			137.0233	- C ₁₃ H ₁₆ O ₃ (3)

For GGE, more fragments were identified by 2DMS (Table 5-7) than by 1DMS experiments (Table 5-6), including guaiacol (*m/z*123.0452) and 2-methoxy-4-vinylphenol (*m/z*149.0595). Although more fragments were highlighted, GGE still achieved a similar moiety coverage but 2DMS remains more informative, compared to 1DMS, due to a higher number of fragments. Overall, 1D and 2DMS of GGE and pinosresinol revealed close dissociation trends, including •OCH₃, formaldehyde, CH₄, •CH₃, H₂O, and neutral monomer

loss such as guaiacol (124.0518 Da) for GGE and coniferyl alcohol (180.0780 Da) in the case of pinoresinol. These neutral monomer losses were characteristic of the right phenolic 8-end of each of these dimers. They were also evidenced by the extraction of the neutral loss line (peak related to the GGE precursor when the neutral loss line of 124.0518 Da was extracted (Figure 5-5 C).²⁶ In addition to that, the GGE standard is characterized by the incorporation of an extra water molecule during the formation of a β -O-4 link between monomers increasing the mass of the lignin molecule by 18 Da. Therefore, the β -O-4 linkage has a specific neutral loss of 18 Da (water) and 48 Da (loss of water and formaldehyde). Consequently, compounds that present a β -O-4 linkage can be gained by extracting the neutral loss line at 18 and 48 Da.

Table 5-6: Peak list, relative intensity of the fragment, and assignment from the 1DMS of the standard GGE.

Name	MS [M-H] ⁻	Activation Mode	MS ²	
			m/z	Loss (abundance %)
GGE	C ₁₇ H ₁₉ O ₆ ⁻ m/z319.1187	UVPD	301.1081	-H ₂ O (1)
			271.0972	-H ₂ O, -CH ₂ O (100)
			256.0736	- H ₂ O, -CH ₂ O, -CH ₃ (1)
			195.0655	-C ₇ H ₈ O ₂ (15)
			165.0549	-C ₇ H ₈ O ₂ , -CH ₂ O (5)
			151.0392	-C ₉ H ₁₂ O ₃ (1)

Table 5-7: Peak list, relative intensity of the fragment, and assignment from the 2DMS of GGE in the standard mixture after a denoise rank of 25.

Name	MS [M-H] ⁻	Activation Mode	MS ²	
			m/z	Loss (abundance %)
GGE	C ₁₇ H ₁₉ O ₆ ⁻ m/z319.1187	UVPD	301.1081	-H ₂ O (100)
			271.0972	-H ₂ O, -CH ₂ O (18)
			256.0736	- H ₂ O, -CH ₂ O, -CH ₃ (4)
			165.0549	-C ₇ H ₈ O ₂ , -CH ₂ O (5)
			151.0392	-C ₉ H ₁₂ O ₃ (13)
			149.0595	-C ₇ H ₇ O, -CH ₂ O, -H ₂ O, -CH ₃ (2)
			123.0452	-C ₁₀ H ₁₂ O ₄ (4)

Table 5-1 reports the UVPD fragmentation efficiency for the three standards in both 1D and 2DMS analyses. A greater fragmentation efficiency was seen for the pinoresinol in 2DMS than that obtained by 1DMS. Unlike the UVPD fragmentation for GGE and coniferyl alcohol, where the fragmentation efficiency dropped from 1D to 2DMS (2% to 1% and from 3% to 1%, respectively). These differences of behavior are still unclear. They may be linked with the differences of absorption properties of the deprotonated molecule in the gas phase. Unfortunately, no data were available. Nevertheless, the absorption of pinoresinol in liquid phase is higher at 193 nm than those of GGE and coniferyl alcohol ($A = 0.7552$ a.u. for pinoresinol, $A = 0.6946$ a.u. for GGE, and $A = 0.6921$ a.u. Figure 5-6). Despite having a putative low absorbance at $\lambda = 193$ nm, the deprotonated molecule of the three standards were able to fragment, highlighting the advantage of the activation by UV irradiation.

The differences observed between the 1D and 2D fragmentation experiments concerning both the fragmentation efficiency and moiety coverage could be tentatively rationalized. These can be explained by the UV pulse hitting the ions throughout the 2D experiment and the scan lines (100 accumulated scans in 1D and 8192 single scans in 2D). Moreover, the overlapping between the precursor ion cloud and the laser beam during the pulse sequence employed in 2D experiments might be the cause of the observed difference in the fragmentation efficiency.

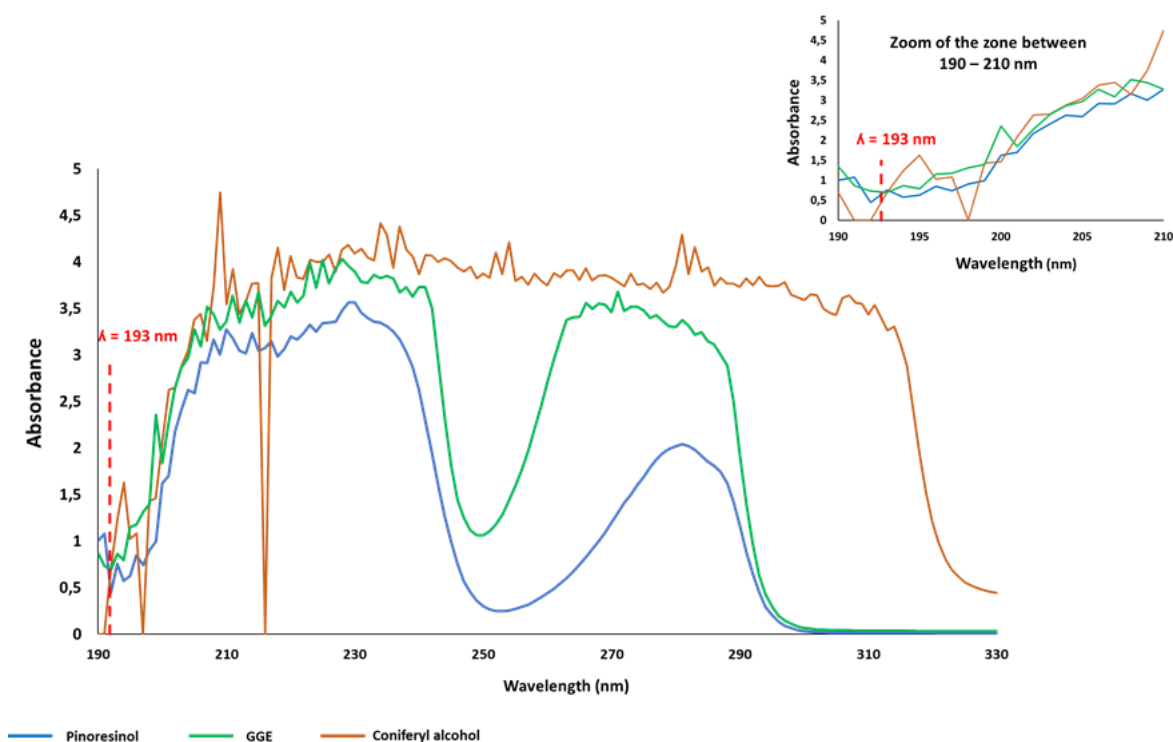


Figure 5-6: UV spectra of the used three standards with a concentration of $1 \text{ mg}\cdot\text{mL}^{-1}$ in methanol. The UV analysis was conducted at the chemistry department of the University of Lorraine in Metz. A UV/Vis thermo scientific Evolution 201 was the used spectrophotometer and the data were obtained using thermo insight software.

The nature of the observed fragment ions (even- or odd-electron ions) as well as their relative abundance appeared to be compound-dependent and in a lesser extent dependent of the used MS/MS method (Table 5-8). Thus, pinoresinol led to more abundant odd-electron fragments especially by 2DMS, than the two other standards, which mainly or quasi-exclusively (2DMS) formed even-electron daughter ions. Some variations in the ratios of both types of fragment ions under the two MS/MS conditions were observed. Part of these differences can be explained by the variation of the laser energy throughout the long duration (several tens of minutes) of the 2D experiment. Consequently, the laser fluence may be significantly different from 1D to 2D experiments, which led to open or close some fragmentation pathways. Moreover, pinoresinol is the standard compound, which present in solution the higher absorption at the 193 nm wavelength. It is also the standard, which led to the higher amount of odd-electron fragment, which required homolytic bond cleavage. Both of these behaviors have to be correlated.

Table 5-8: Different fragment ions collected from 1D and 2D-UPVD-MS of the standard mixture were distributed between odd and even-electron ion.

	1D-UVPD-MS		2D-UVPD-MS	
	Odd e ⁻ ions %	Even e ⁻ ions %	Odd e ⁻ ions %	Even e ⁻ ions %
Coniferyl alcohol	26	74	0	100
GGE	4	96	3	97
Pinoresinol	67	33	89	11

Part of the previously observed differences may also be linked to the amounts of ions transfer to the ICR cell before UV activation. Higher amounts of precursor ions were used in 1DMS ($\sim 10^{10}$) than by 2DMS ($\sim 10^7$) due to (i) a longer accumulation time for the isolation before fragmentation in 1D, (ii) a higher number of averaged scans, (iii) and a longer transient (a transient duration of 1.05 seconds for 4 MW and 0.26 seconds for 1MW). Nevertheless, the pulse sequence (experiment timings) in 2DMS ensured that a given deprotonated molecule was activated during different scans. Indeed, each time the delay between the pulse P1 and P2 corresponded to the time necessary for this ion to travel a half-integer number of orbits, it was out of phase and deexcited. Consequently, its MS/MS spectrum was acquired several times, which ensured a sensitivity increase.

5.1.4.2. 2DMS on bio-oil

For the 2DMS analysis of the bio-oil, two data set were used. The first one with a de-noise rank of 25 and the second one without de-noise, for both, comparable resolving power was obtained. Without the use of de-noising, the autocorrelation line appeared, as well as some harmonics and scintillation noise (Figure 5-7).³⁹ As a result, the spectrum becomes more challenging to interpret even if it is more insightful. To overcome this complexity in 2DMS contour plot of bio-oil, the de-noise rank 25 was privileged.

The 2D contour plot of the bio-oils was used to extract the auto-correlation line (Figure 5-8).

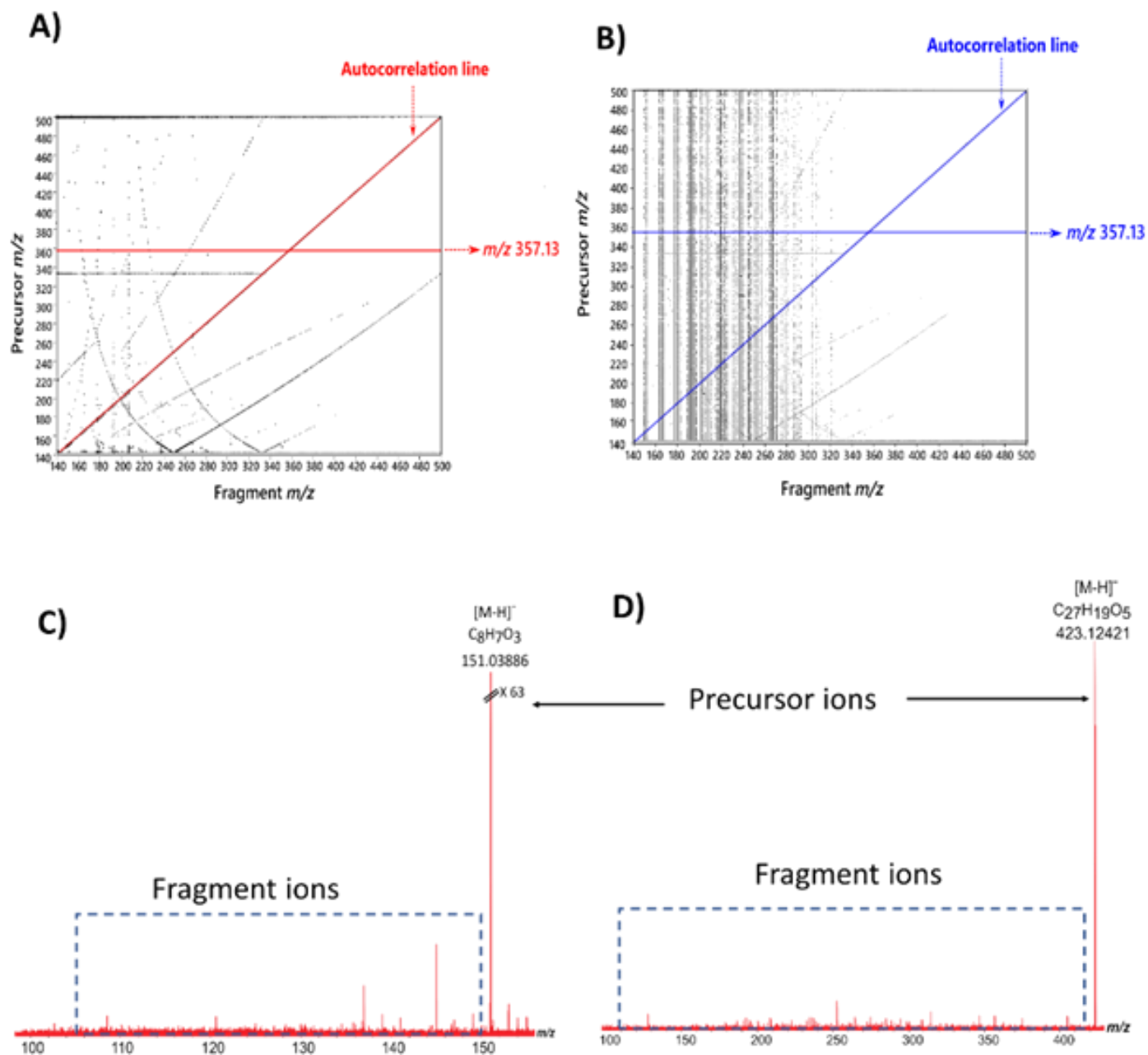


Figure 5-7: 2D contour plot of a bio-oil. (Left) 2D contour plot with a de-noise rank 25, (Right) 2D contour plot without de-noise. (C) Mass spectrum corresponding to the autocorrelation line extracted from the 2D map at a low m/z value, and (D) Mass spectrum corresponding to the autocorrelation line extracted from the 2D map at a high m/z value.

Most of the ion observed by bio-oil direct infusion (–) ESI FT-ICR MS were also found on the autocorrelation precursor ion lines obtained by 2DMS. This shows that 2DMS conserves the main part of the information. Van Krevelen diagram of the precursor ions extracted from the auto-correlation line indicates they are pyrolytic lignin compounds (Figure 5-9 A). In addition, the DBE distribution vs. carbon number graph of the precursor species evidences compounds with DBE higher than 3 with more than 6 carbon atoms (Figure 5-9 B). These characteristics suggest the presence of at least one benzene ring (a phenolic ring) that can absorb a 193 nm photon. This is also the reason why no carbohydrate, neither lipidic compounds were evidenced on the Van Krevelen diagram from the autocorrelation line. Due to a poor absorption of lipids and carbohydrates to the laser wavelength, their activation by 193 nm photons is nearly inefficient. Therefore, the nearly 4000 compounds that are not present on the autocorrelation line are mainly non-lignin derivatives

To have a better insight into the chemical functions and molecular moiety of some lignin derivatives, specific neutral loss lines were extracted from the 2D contour plot, which correspond to typical chemical functions or lignin moiety. Table 5-9 gathers the functional groups and lignin monomers by neutral loss masses. Their amounts are given relative to the full number of precursors. The percentage of precursors was calculated based on the division of total number of the total losses by the total number of precursors.

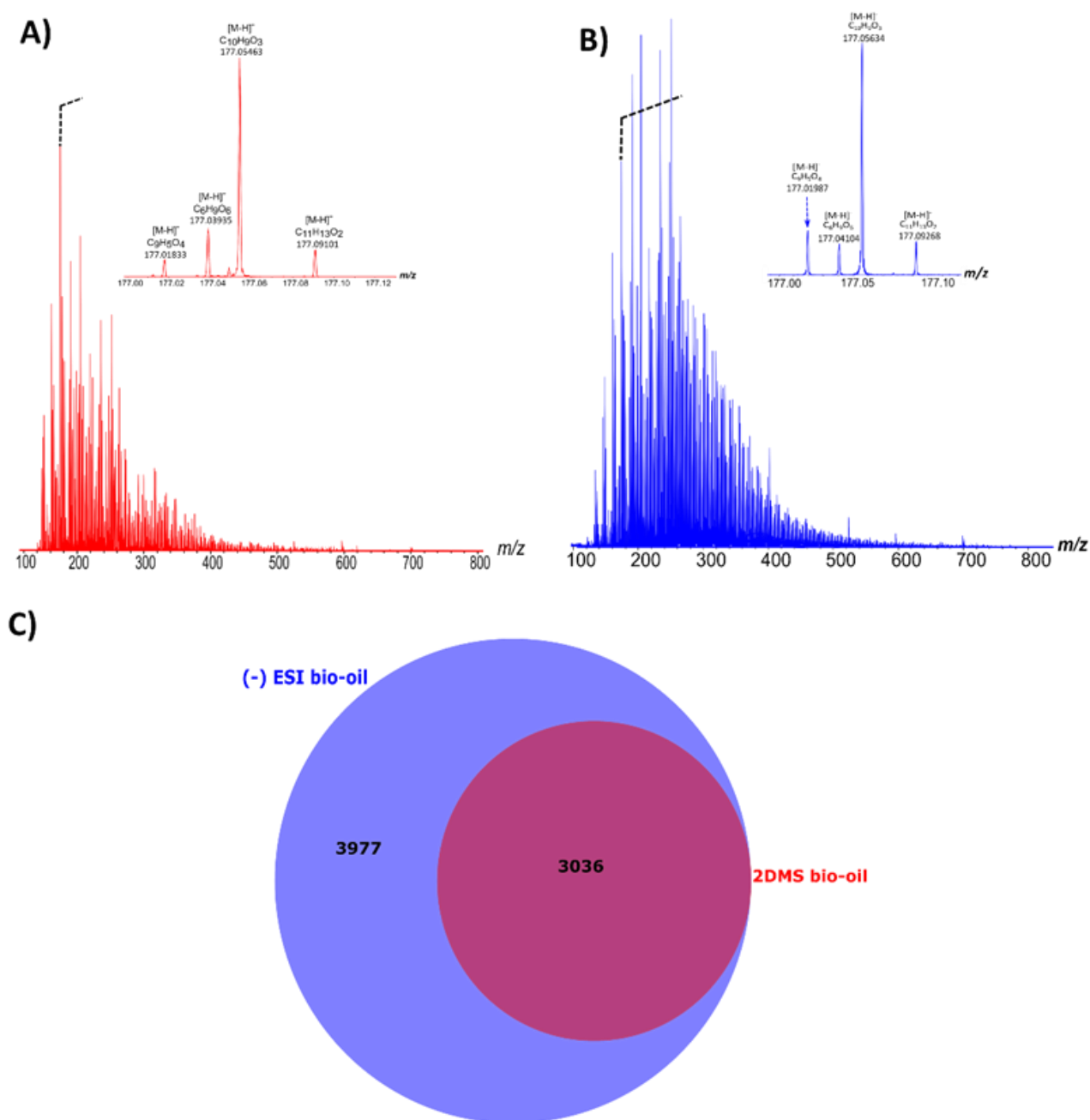


Figure 5-8: (A) Mass spectrum corresponding to the autocorrelation line extracted from the 2D map with a denoise rank of 25, (B) Mass spectrum of a raw bio-oil analyzed by negative electrospray (C) Venn Diagram highlighting that no significant loss between 2DMS on bio-oil and the FTMS analysis of raw bi-oil in (-) ESI.

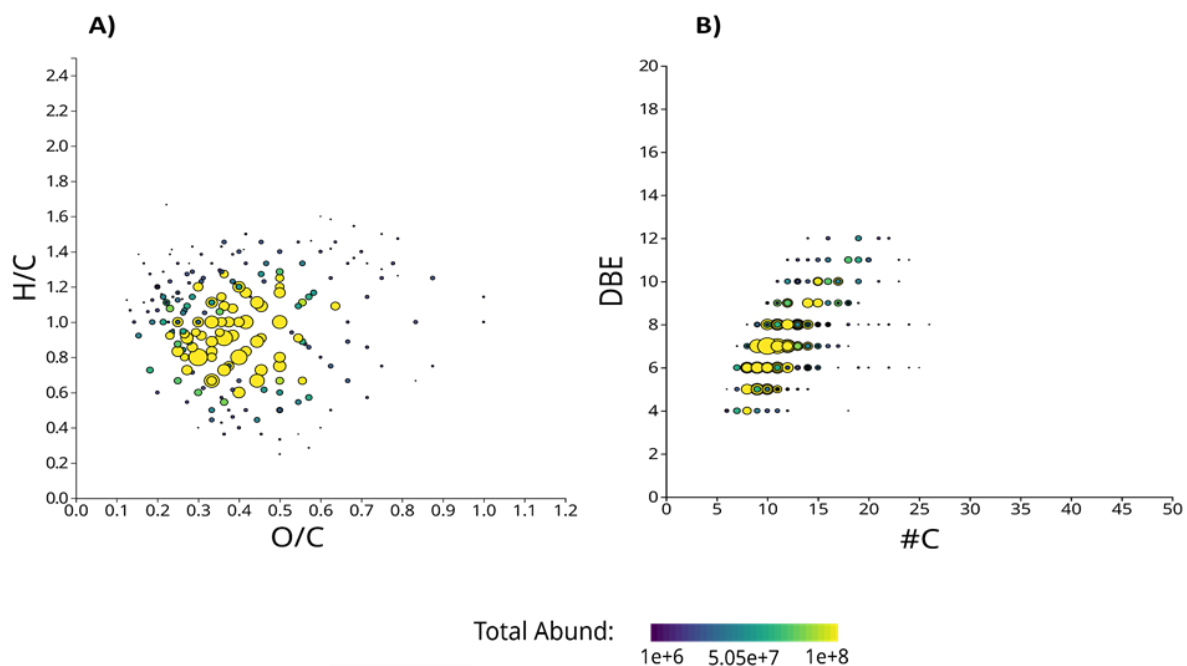


Figure 5-9: (A) Van Krevelen diagram of the extracted autocorrelation line from the 2D map in negative ESI, (B) DBE versus the number of carbons of the precursor present in the autocorrelation line. The graphical representation was done by using in house developed software.

Table 5-9: Classification of functional groups and lignin monomers by neutral loss masses and percentage of precursors.^{29,40}

	Neutral losses	Neutral losses masses	Percentage of precursors
Functional groups	Alcohols (-H ₂ O)	18 Da	11%
	Carbonyls* (-CO)	28 Da	4%
	Carboxylic acid (-CO ₂)	44 Da	5%
Lignin monomers	Phenol (-C ₆ H ₆ O)	94.0413 Da	10%
	Cresol (-C ₇ H ₈ O)	108.0569 Da	11%
	Guaiacol (-C ₇ H ₈ O ₂)	124.0518 Da	11%
	Creosol (-C ₈ H ₁₀ O ₂)	138.0675 Da	10%

*Carbonyl includes ketones and aldehydes.

Thus, neutral losses of H₂O and CO₂ were observed for several precursors suggesting that lignin derivatives bear alcohol and carboxylic acids functions, respectively. The CO loss must be associated to the well-known contraction of a six-membered ring into a five-membered ring, when a phenolic group or a quinone is present in the precursor ion. Moreover, neutral loss lines of some lignin monomers were also extracted, which evidenced some phenolic moiety such as phenol and guaiacol within bio-oil compounds. Concerning these species, one suggests that they have the same fragmentation pattern as the standards investigated in the previous section. Such fragmentation behavior may be helpful to define

the nature of the lignin monomer unit present on the 8-end position. Both phenol and cresol losses are indicative of a p-coumaryl unit, whereas guaiacol and creosol are produced by fragmentation of coniferyl unit. It is expected that sinapyl unit on an 8-end position leads to dimethoxy-phenol ($C_8H_{10}O_3$) and dimethoxy-hydroxytoluene ($C_9H_{12}O_3$) losses. No neutral loss corresponding to these compounds were significantly observed. Consequently, it is reasonable to conclude that no sinapyl unit is in 8-end position of the oligomeric lignin derivatives in the pyrolysis bio-oil.

The horizontal lines obtained in 2DMS of precursor ions at m/z 179.0702, 319.1187, and 357.1343, corresponding to the m/z values of the standard ions previously investigated, were extracted and compared with the results obtained from 2DMS analysis of the standard mixture. For the bio-oil precursor at m/z 179.0702, the fragment at m/z 107.0485 attributed to cross-ring cleavage was not observed in the study of the bio-oil but a fragment at m/z 161.0605 relative to the loss of H_2O was obtained (Table 5-10).

The experiments carried out on the coniferyl alcohol, observed at m/z 179.0702, did not exhibit the loss of water. The m/z 123.0445 ion relative to the elimination of the propenyl alcohol moieties seems to indicate that phenolic moiety is a guaicyl unit. Consequently, the m/z 179.0702 ion observed in the study of the bio-oil sample was thought to be a coniferyl alcohol isomer for which the alcohol was in position 2 and not in position 3 of the propenyl. In that case, the elimination of a water molecule is easy. The dissociation of the m/z 357.1343 observed in the study of the bio-oil is an isomer of pinosresinol. Indeed, neither the loss of formaldehyde nor that of a methyl radical (one of the most favorable dissociation pathways obtained by pinosresinol UVPD) were evidenced (Table 5-10). By contrast other fragment ions were obtained. The m/z 137.0233, 151.0399 and 177.0553 may be relative to the fragmentation involving a coniferyl alcohol unit (both latter fragment ions were also observed in the study of GGE dimer), nevertheless, it is difficult to go deeper in the interpretation to propose a putative structure.

Concerning the m/z 319.1187 (Table 5-10), the sole difference is the absence of the fragment associated to the guaiacol at m/z 123.0452, which was a low abundant fragment obtained in the investigated of the standard mixture. For the bio-oil m/z 319.1187 ion, similar moiety coverage to those of the 2DMS on the standard mixture was obtained (Tables 5-1 and 5-11). The calculation of the fragmentation efficiency was done by extracting the same fragments as those achieved with the GGE standard. As a result, similar fragmentation efficiencies and characterized moieties, as those obtained with the standard compound, were observed with bio-oil compounds in 2DMS. This suggests that GGE is likely present in bio-oil.

Differences observed between the data achieved on the standards and on the bio-oil compounds can be explained by isomeric compounds with other fragmentation patterns.

Another reason explaining the differences in fragmentation pattern is that the targeted peak corresponding to the precursor ion, may not be very well resolved in 1M data acquisition

and may overlap with other precursor ions. Then, when the fragment line is extracted, it frequently includes many precursors and their related fragments, which occasionally results in a miscorrelation.

Table 5-10: Peak list, relative intensity of the fragment, and assignment from the 2DMS of the candidate compound at m/z 179, 357, and 319 in bio-oil after a denoise rank of 25.

Putative compound	Activation Mode	MS ²	
		m/z	Loss (abundance %)
Coniferyl alcohol m/z 179.0702	UVPD	163.0390	-CH ₄ (28)
		161.0605	-H ₂ O (23)
		149.0599	-CH ₂ O (100)
		123.0445	-C ₃ H ₄ O (12)
Pinoresinol m/z 357.1343	UVPD	271.0940	- C ₃ H ₃ O ₂ , -CH ₃ (15)
		195.0657	-C ₁₀ H ₁₀ O ₂ (29)
		179.0701	-C ₁₀ H ₁₀ O ₃ (100)
		177.0553	-CH ₂ O, -CH ₄ , -C ₈ H ₆ O ₂ (73)
		151.0399	- C ₁₂ H ₁₄ O ₃ (21)
		137.0233	- C ₁₃ H ₁₇ O ₃ (15)
GGE m/z 319.1187	UVPD	301.1075	-H ₂ O (23)
		271.0820	-H ₂ O, -CH ₂ O (39)
		257.0817	- CH ₃ O, CH ₃ O (100)
		195.0655	-C ₇ H ₈ O ₂ (42)
		165.0549	-C ₈ H ₁₀ O ₃ (36)
		151.0397	-C ₉ H ₁₂ O ₃ (39)
		149.0595	-C ₈ H ₁₀ O ₄ (25)

Table 5-11: Fragmentation efficiency percentages (FE (%)) and moiety coverage (%) in 2D experiments on bio-oils.

	FE %	Moiety coverage %
<i>m/z</i> 179.070	1	67
<i>m/z</i> 319.118	1	56
<i>m/z</i> 357.134	3	44

5.1.5. Conclusion

In this work, lignin standard mixture and pyrolysis bio-oil were analyzed for the first time by one- and two-dimensional mass spectrometry with the application of UVPD as activation mode. The data-independent analysis (DIA) performed as part of the 2DMS analysis has been demonstrated to be a successful technique for the structural elucidation of complex mixtures, which is not possible by direct infusion FT-ICR MS. From the 2DMS data, it was possible to have an insight into fragmentation patterns of standards, which were compared to bio-oil compounds. Similar fragmentation efficiency and molecular moieties were obtained between standards and bio-oil compounds, which helped to have higher confidence in compound assignment. In addition, bio-oil compounds were able to be *m/z*-grouped into classes of monomers and chemical functional groups. This information offers a paramount insight into the structure of the molecule for a better molecular description of the bio-oil composition. Moreover, this can also be relevant for the monitoring of some upgrading treatments.

5.2. References

- (1) Marshall, A. G.; Lin Wang, T.-C.; Lebatuan Ricca, T. Ion Cyclotron Resonance Excitatio/de-Excitation: A Basis for Stochastic Fourier Transform Ion Cyclotron Mass Spectrometry. *Chem. Phys. Lett.* **1984**, *105* (2), 233–236. [https://doi.org/10.1016/0009-2614\(84\)85657-2](https://doi.org/10.1016/0009-2614(84)85657-2).
- (2) Marshall, A. G.; Lin Wang, T.-C.; Lebatuan Ricca, T. Ion Cyclotron Resonance Excitatio/de-Excitation: A Basis for Stochastic Fourier Transform Ion Cyclotron Mass Spectrometry. *Chem. Phys. Lett.* **1984**, *105* (2), 233–236. [https://doi.org/10.1016/0009-2614\(84\)85657-2](https://doi.org/10.1016/0009-2614(84)85657-2).
- (3) Pfändler, P.; Bodenhausen, G.; Rapin, J.; Houriet, R.; Gäumann, T. Two-Dimensional Fourier Transform Ion Cyclotron Resonance Mass Spectrometry. *Chem. Phys. Lett.* **1987**, *138* (2–3), 195–200. [https://doi.org/10.1016/0009-2614\(87\)80367-6](https://doi.org/10.1016/0009-2614(87)80367-6).
- (4) van Agthoven, M. A.; Lam, Y. P. Y.; O'Connor, P. B.; Rolando, C.; Delsuc, M.-A. Two-Dimensional Mass Spectrometry: New Perspectives for Tandem Mass Spectrometry. *Eur. Biophys. J.* **2019**, *48* (3), 213–229. <https://doi.org/10.1007/s00249-019-01348-5>.
- (5) Marzullo, B. P.; Morgan, T. E.; Wootton, C. A.; Perry, S. J.; Saeed, M.; Barrow, M. P.; O'Connor, P. B. Advantages of Two-Dimensional Electron-Induced Dissociation and Infrared Multiphoton Dissociation Mass Spectrometry for the Analysis of Agrochemicals. *Anal. Chem.* **2020**, *92* (17), 11687–11695. <https://doi.org/10.1021/acs.analchem.0c01585>.

- (6) Chiron, L.; Coutouly, M.-A.; Starck, J.-P.; Rolando, C.; Delsuc, M.-A. SPIKE a Processing Software Dedicated to Fourier Spectroscopies. arXiv August 24, 2016. <http://arxiv.org/abs/1608.06777> (accessed 2022-11-09).
- (7) Chiron, L.; van Agthoven, M. A.; Kieffer, B.; Rolando, C.; Delsuc, M.-A. Efficient Denoising Algorithms for Large Experimental Datasets and Their Applications in Fourier Transform Ion Cyclotron Resonance Mass Spectrometry. *Proc. Natl. Acad. Sci.* **2014**, *111* (4), 1385–1390. <https://doi.org/10.1073/pnas.1306700111>.
- (8) Bray, F.; Bouclon, J.; Chiron, L.; Witt, M.; Delsuc, M.-A.; Rolando, C. Nonuniform Sampling Acquisition of Two-Dimensional Fourier Transform Ion Cyclotron Resonance Mass Spectrometry for Increased Mass Resolution of Tandem Mass Spectrometry Precursor Ions. *Anal. Chem.* **2017**, *89* (17), 8589–8593. <https://doi.org/10.1021/acs.analchem.7b01850>.
- (9) Halper, M.; Delsuc, M.-A.; Breuker, K.; van Agthoven, M. A. Narrowband Modulation Two-Dimensional Mass Spectrometry and Label-Free Relative Quantification of Histone Peptides. *Anal. Chem.* **2020**, *92* (20), 13945–13952. <https://doi.org/10.1021/acs.analchem.0c02843>.
- (10) Carpenter, D.; Westover, T. L.; Czernik, S.; Jablonski, W. Biomass Feedstocks for Renewable Fuel Production: A Review of the Impacts of Feedstock and Pretreatment on the Yield and Product Distribution of Fast Pyrolysis Bio-Oils and Vapors. *Green Chem.* **2014**, *16* (2), 384–406. <https://doi.org/10.1039/c3gc41631c>.
- (11) Volpe, R.; Messineo, A.; Millan, M.; Volpe, M.; Kandiyoti, R. Assessment of Olive Wastes as Energy Source: Pyrolysis, Torrefaction and the Key Role of H Loss in Thermal Breakdown. *Energy* **2015**, *82*, 119–127. <https://doi.org/10.1016/j.energy.2015.01.011>.
- (12) Dhungana, B.; Becker, C.; Zekavat, B.; Solouki, T.; Hockaday, W. C.; Chambliss, C. K. Characterization of Slow-Pyrolysis Bio-Oils by High-Resolution Mass Spectrometry and Ion Mobility Spectrometry. *Energy Fuels* **2015**, *29* (2), 744–753. <https://doi.org/10.1021/ef5016389>.
- (13) Adams, P.; Bridgwater, T.; Lea-Langton, A.; Ross, A.; Watson, I. Chapter 8 - Biomass Conversion Technologies. In *Greenhouse Gas Balances of Bioenergy Systems*; Thornley, P., Adams, P., Eds.; Academic Press, 2018; pp 107–139. <https://doi.org/10.1016/B978-0-08-101036-5.00008-2>.
- (14) Abou-Dib, A.; Aubriet, F.; Hertzog, J.; Vernex-Loset, L.; Schramm, S.; Carré, V. Next Challenges for the Comprehensive Molecular Characterization of Complex Organic Mixtures in the Field of Sustainable Energy. *Molecules* **2022**, *27* (24), 8889. <https://doi.org/10.3390/molecules27248889>.
- (15) Staš, M.; Chudoba, J.; Kubička, D.; Blažek, J.; Pospíšil, M. Petroleomic Characterization of Pyrolysis Bio-Oils: A Review. *Energy Fuels* **2017**, *31* (10), 10283–10299. <https://doi.org/10.1021/acs.energyfuels.7b00826>.
- (16) Garcia-Perez, M.; Chaala, A.; Pakdel, H.; Kretschmer, D.; Roy, C. Characterization of Bio-Oils in Chemical Families. *Biomass Bioenergy* **2007**, *31* (4), 222–242. <https://doi.org/10.1016/j.biombioe.2006.02.006>.
- (17) Hsu, C. S.; Hendrickson, C. L.; Rodgers, R. P.; McKenna, A. M.; Marshall, A. G. Petroleomics: Advanced Molecular Probe for Petroleum Heavy Ends. *J. Mass Spectrom.* **2011**, *46* (4), 337–343. <https://doi.org/10.1002/jms.1893>.
- (18) Zhurov, K. O.; Kozhinov, A. N.; Tsybin, Y. O. Evaluation of High-Field Orbitrap Fourier Transform Mass Spectrometer for Petroleomics. *Energy Fuels* **2013**, *27* (6), 2974–2983. <https://doi.org/10.1021/ef400203g>.

- (19) Marshall, A. G.; Hendrickson, C. L. High-Resolution Mass Spectrometers. *Annu. Rev. Anal. Chem.* **2008**, *1* (1), 579–599. <https://doi.org/10.1146/annurev.anchem.1.031207.112945>.
- (20) Hsu, C. S. Mass Resolving Power Requirement for Molecular Formula Determination of Fossil Oils. *Energy Fuels* **2012**, *26* (2), 1169–1177. <https://doi.org/10.1021/ef201848k>.
- (21) Krajewski, L. C.; Rodgers, R. P.; Marshall, A. G. 126 264 Assigned Chemical Formulas from an Atmospheric Pressure Photoionization 9.4 T Fourier Transform Positive Ion Cyclotron Resonance Mass Spectrum. *Anal. Chem.* **2017**, *89* (21), 11318–11324. <https://doi.org/10.1021/acs.analchem.7b02004>.
- (22) Le Maître, J.; Hubert-Roux, M.; Paupy, B.; Marceau, S.; Rüger, C. P.; Afonso, C.; Giusti, P. Structural Analysis of Heavy Oil Fractions after Hydrodenitrogenation by High-Resolution Tandem Mass Spectrometry and Ion Mobility Spectrometry. *Faraday Discuss.* **2019**, *218*, 417–430. <https://doi.org/10.1039/C8FD00239H>.
- (23) Pfändler, P.; Bodenhausen, G.; Rapin, J.; Houriet, R.; Gäumann, T. Two-Dimensional Fourier Transform Ion Cyclotron Resonance Mass Spectrometry. *Chem. Phys. Lett.* **1987**, *138* (2–3), 195–200. [https://doi.org/10.1016/0009-2614\(87\)80367-6](https://doi.org/10.1016/0009-2614(87)80367-6).
- (24) Ross, C. W.; Guan, S.; Grosshans, P. B.; Ricca, T. L.; Marshall, A. G.; Ricca, T. L.; Marshall, A. G. Two-Dimensional Fourier Transform Ion Cyclotron Resonance Mass Spectrometry/Mass Spectrometry with Stored-Waveform Ion Radius Modulation. *J. Am. Chem. Soc.* **1993**, *115* (17), 7854–7861. <https://doi.org/10.1021/ja00070a035>.
- (25) Marzullo, B. P.; Morgan, T. E.; Wootton, C. A.; Perry, S. J.; Saeed, M.; Barrow, M. P.; O'Connor, P. B. Advantages of Two-Dimensional Electron-Induced Dissociation and Infrared Multiphoton Dissociation Mass Spectrometry for the Analysis of Agrochemicals. *Anal. Chem.* **2020**, *92* (17), 11687–11695. <https://doi.org/10.1021/acs.analchem.0c01585>.
- (26) Marzullo, B. P.; Morgan, T. E.; Theisen, A.; Haris, A.; Wootton, C. A.; Perry, S. J.; Saeed, M.; Barrow, M. P.; O'Connor, P. B. Combining Ultraviolet Photodissociation and Two-Dimensional Mass Spectrometry: A Contemporary Approach for Characterizing Singly Charged Agrochemicals. *Anal. Chem.* **2021**, *93* (27), 9462–9470. <https://doi.org/10.1021/acs.analchem.1c01185>.
- (27) van Agthoven, M. A.; Chiron, L.; Coutouly, M.-A.; Delsuc, M.-A.; Rolando, C. Two-Dimensional ECD FT-ICR Mass Spectrometry of Peptides and Glycopeptides. *Anal. Chem.* **2012**, *84* (13), 5589–5595. <https://doi.org/10.1021/ac3004874>.
- (28) Jia, L.; Le-Brech, Y.; Shrestha, B.; Frowein, M. B.; Ehlert, S.; Mauviel, G.; Zimmermann, R.; Dufour, A. Fast Pyrolysis in a Microfluidized Bed Reactor: Effect of Biomass Properties and Operating Conditions on Volatiles Composition as Analyzed by Online Single Photoionization Mass Spectrometry. *Energy Fuels* **2015**, *29* (11), 7364–7374. <https://doi.org/10.1021/acs.energyfuels.5b01803>.
- (29) Staš, M.; Kubička, D.; Chudoba, J.; Pospíšil, M. Overview of Analytical Methods Used for Chemical Characterization of Pyrolysis Bio-Oil. *Energy Fuels* **2014**, *28* (1), 385–402. <https://doi.org/10.1021/ef402047y>.
- (30) Kanaujia, P. K.; Sharma, Y. K.; Garg, M. O.; Tripathi, D.; Singh, R. Review of Analytical Strategies in the Production and Upgrading of Bio-Oils Derived from Lignocellulosic Biomass. *J. Anal. Appl. Pyrolysis* **2014**, *105*, 55–74. <https://doi.org/10.1016/j.jaap.2013.10.004>.

- (31) Bai, X.; Kim, K. H.; Brown, R. C.; Dalluge, E.; Hutchinson, C.; Lee, Y. J.; Dalluge, D. Formation of Phenolic Oligomers during Fast Pyrolysis of Lignin. *Fuel* **2014**, *128*, 170–179. <https://doi.org/10.1016/j.fuel.2014.03.013>.
- (32) Zhao, C.; Sethuraman, M.; Clavreul, N.; Kaur, P.; Cohen, R. A.; O'Connor, P. B. A Detailed Map of Oxidative Post-Translational Modifications of Human P21ras Sing Fourier Transform Mass Spectrometry. *Anal. Chem.* **2006**, *78* (14), 5134–5142. <https://doi.org/10.1021/ac060525v>.
- (33) Chiron, L.; Coutouly, M.-A.; Starck, J.-P.; Rolando, C.; Delsuc, M.-A. SPIKE a Processing Software Dedicated to Fourier Spectroscopies. arXiv August 24, 2016. <http://arxiv.org/abs/1608.06777> (accessed 2023-01-12).
- (34) Chiron, L.; van Agthoven, M. A.; Kieffer, B.; Rolando, C.; Delsuc, M.-A. Efficient Denoising Algorithms for Large Experimental Datasets and Their Applications in Fourier Transform Ion Cyclotron Resonance Mass Spectrometry. *Proc. Natl. Acad. Sci.* **2014**, *111* (4), 1385–1390. <https://doi.org/10.1073/pnas.1306700111>.
- (35) Marshall, A. G.; Rodgers, R. P. Petroleomics: Chemistry of the Underworld. *Proc. Natl. Acad. Sci.* **2008**, *105* (47), 18090–18095. <https://doi.org/10.1073/pnas.0805069105>.
- (36) Kim, S.; Kramer, R. W.; Hatcher, P. G. Graphical Method for Analysis of Ultrahigh-Resolution Broadband Mass Spectra of Natural Organic Matter, the Van Krevelen Diagram. *Anal. Chem.* **2003**, *75* (20), 5336–5344. <https://doi.org/10.1021/ac034415p>.
- (37) Lozano, D. C. P.; E. Jones, H.; Reina, T. R.; Volpe, R.; P. Barrow, M. Unlocking the Potential of Biofuels via Reaction Pathways in van Krevelen Diagrams. *Green Chem.* **2021**, *23* (22), 8949–8963. <https://doi.org/10.1039/D1GC01796A>.
- (38) Chakar, F. S.; Ragauskas, A. J. Review of Current and Future Softwood Kraft Lignin Process Chemistry. *Ind. Crops Prod.* **2004**, *20* (2), 131–141. <https://doi.org/10.1016/j.indcrop.2004.04.016>.
- (39) van Agthoven, M. A.; Lam, Y. P. Y.; O'Connor, P. B.; Rolando, C.; Delsuc, M.-A. Two-Dimensional Mass Spectrometry: New Perspectives for Tandem Mass Spectrometry. *Eur. Biophys. J.* **2019**, *48* (3), 213–229. <https://doi.org/10.1007/s00249-019-01348-5>.
- (40) Lehto, J.; Oasmaa, A.; Solantausta, Y.; Kytö, M.; Chiaramonti, D. *Fuel Oil Quality and Combustion of Fast Pyrolysis Bio-Oils*; 2018. <https://doi.org/10.13140/RG.2.2.15925.99042>.

GENERAL CONCLUSION AND PERSPECTIVES

In this Ph.D. thesis, two strategies were developed to obtain information on the structure of some thousands of species that have been evidenced in the bio-oils and, as a result, to have a better characterization to enhance the pyrolysis and the up-grading catalytic processes. The experiments were carried out by a 7T 2 ω FT-ICR mass spectrometry with different ionization sources to evidence the bio-oil components on a broad range of polarity and mass. The Solarix spectrometer used benefits from the most recent technological improvements and making possible to obtain very high performances. This instrument ensures the simultaneous measurement of tens of thousands of species with a mass measurement accuracy equivalent to a few percent of the mass of an electron for a molecule of a hundred atoms and with an extremely high resolution.

The work of this Ph.D. was divided into two approaches. The first to identify the variety of chemical functions in the components of a bio-oil produced by pyrolysis of lignocellulosic biomass. Emphasis was placed on lignin derivatives, which some of them resist to up-grading catalytic treatments. Before performing a high-resolution mass spectrometry analysis, the first approach involves different sample preparation steps, including **fractionation** and **derivatization**. The fractionation and part of the derivation steps were performed on an "Oasis Max" solid-phase extraction cartridge using a sorbent combining a reverse phase and an anionic phase. The proposed analytical procedure was first applied to a range of standard compounds derived from the pyrolysis of lignin, which have been selected based on their structures and the chemical functions usually found in the constituents of lignocellulosic bio-oil to evaluate its effectiveness. The analytical methodology was then applied to a real sample of bio-oil.

Different derivatization agents were chosen based on the targeted functional group. These agents systematically present at least one atom, which is not present in bio-oil components to differentiate the derivatized molecules from the non-derivatized bio-oil components as pentafluoropyridine PFP and 3-chloroaniline. The isotopic signature of chlorine also facilitated the data post-treatment. The 3-chloroaniline was used to evidence carbonyl groups and the pentafluoropyridine (PFP) to react rapidly, specifically, and effectively with phenolic compounds to produce tetrafluoropyridyl biaryl ethers via an S_NAr reaction.

The proposed methodology leads to the production of three fractions:

- The first fraction contains the bio-oil compounds not retained by the stationary phase of the cartridge. These are compounds that are neither phenolic nor acidic. These are mainly carbonyls (ketones and aldehydes), esters, ethers, and sugar derivatives. Carbonyls are evidenced by reaction with 3-chloroaniline and the formation of Schiff bases.
- The second fraction obtained by elution with PFP consists of the phenolic components of the bio-oil (phenol, polyphenols, alkoxy-phenols, alkoxy-polyphenols ...), which not contain carboxylic acid function. For polyphenolic compounds, the reaction with PFP takes place for each phenolic group, which determines the number of phenolic groups for a given phenolic compound. 3-chloroaniline is also added to label the carbonyl groups if the evidenced phenolic compounds also present aldehydic or ketonic chemical functions.
- The final fraction, obtained by elution with formic acid, corresponds to bio-oil compounds with at least one carboxylic acid group. Such a compound, which also has one or several phenolic functions, is observed as a mono- or poly-PFP derived compound. The addition of 3-chloroaniline ensures to evidence carbonyls.

The application of this method to a pyrolysis bio-oil, led to the observation of hundreds or even thousands of signals for the three obtained fractions. Fraction 1 contained lignin, carbohydrate derivatives, and a small proportion of lipid compounds. After adding 3-chloroaniline, it was possible to highlight that part of the lignin and carbohydrate derivatives involved one carbonyl function. The compounds with two carbonyls were associated to lignin-linked compounds. In the second fraction, only a few compounds were found to present two phenol groups. Indeed, the majority were derived once by PFP. These two classes of compounds were of course in the area of lignin derivatives on the Van Krevelen diagram. Consequently, the main part of the lignin-derivates oak bio-oil components are relative to sinapyl and coniferyl units and in a very restricted amount to p-coumaryl units. Two classes of compounds were observed in the last fraction. The former were free fatty acids and were not derivatized by PFP, while the latter included phenolic lignin derivatives with a carboxylic acid chemical function and were observed as once and twice PFP-derivates.

As part of the characterization of bio-oils, it was thus possible to demonstrate the full potential of attaching a chemical function involving one or more atoms with a specific isotopic profile, such as chlorine or which are not present in bio-oil such as fluorine, to carry out semi-directed non-targeted analyses. The first approach and the classical petroleomic analysis ensured the specific analysis and distinction of different oxygenated classes of bio-oil components.

The second part of this Ph.D. focused on the capabilities of tandem mass spectrometry to obtain a structural analysis of bio-oil components. To achieve this goal, two problems had

to be overcome. The first was the impossibility of conducting "conventional" tandem mass spectrometry experiments on such a complex matrix in a reasonable time. The second was to obtain relevant information on the bio-oil components by MS/MS and to avoid observing mostly non-specific losses (water, monoxide or carbon dioxide, formaldehyde, ...). The 2D-FTMS approach was well-suited to overcome the first issue and to save important experimental time. To limit the non-specific fragmentation favored by ergolic-activation methods, it was chosen to use the alternative and still little used UVPD dissociation method. To study the main UVPD fragmentation pathways, six standards were first selected to address the large variety of chemical groups (phenol, carboxylic acid, carbonyl, aromatic) of bio-oil compounds. Emphasis has been made on lignin derivatives according to their sometimes-inefficient conversion by catalytic up-grading treatment. The obtained results were compared to the well-established CID activation. The CID and UVPD activation fragmentation scheme of each selected compound was highlighted. Each standard had at least one (even more) UVPD-specific fragmentation often leading to one of the most abundant fragment ions. For most of the six examined compounds, UVPD gave more significant structural information than CID, enabling the identification of more functional groups. Most of the investigated phenolic compounds led to the opening of the aromatic ring rearrangement, which ensured the localization of certain phenolic group substituents.

These results pave the way for the systematic "2D FTMS" structural elucidation of lignin-derived chemicals in bio-oils. The first results of this new approach have been detailed in the last chapter of this thesis manuscript. 2D FTMS exploited the particularities of data-independent analysis (DIA) to perform tandem mass spectrometry experiments without preliminary precursor ion selection and was able to get insights into the fragmentation patterns observed in the study of, first, a standard mixture of standards and, second, a pyrolysis bio-oil. While comparing standards and bio-oil compounds results, similar fragmentation efficiency and molecular moieties were found, which increased confidence in the compound assignment. Moreover, 2D FTMS analysis was able to categorize bio-oil components into different class compounds in respect with the observed losses. Such information may be of significance in the follow-up of bio-oil up-grading process.

In addition to the functional and the structural characterization of bio-oil which were the scope of this work, several supplementary investigations may be of interest in order to understand more about the composition of bio-oils and try to address some of the limitations of the currently employed non-targeted methods.

In the first approach, two limitations could be addressed. One of them is the loss of data resulting from the shift in the m/z value for the derivatized compounds, and the second one is that, unlike the phenolic and carbonyl functions, we have no information of the number of carboxylic acid functions. To each of these limitations, we propose an alternative perspective. A last step for the derivatization of carboxylic acid function by deuterated reactant might be added, and the m/z range could be optimized to be able to identify high

mass species. Due to the lack of a chromophore that absorbs at 193 nm, the second approach was unable to provide structural information on lipids and carbohydrates. Before performing this study, a derivatization procedure that allows UV photon absorption might be used. Further data processing and analysis of a 2D contour plot may also be beneficial.

Furthermore, the derivatization/fractionation method has shown its effectiveness in identifying the functional groups of bio-oils. The ion mobility can be exploited for studying these fractions to obtain additional information, mainly to differentiate the isomeric compounds. In the same spirit, combining the two approaches developed in this work can be of significant interest. Indeed, derivatization/fractionation makes it possible to identify the nature of chemical groups, while 2D FTMS ensures their localization from a molecular structural point of view. These developments have still been initiated in collaboration with Bryan Marzullo, Mark Barrow and Peter O'Connor at the University of Warwick.

Finally, the liquid or gas chromatography technique before FT-ICR MS analysis of the different fractions obtained by the method developed in this study may be helpful for the distinction of isomer compounds. However, this would reduce the complexity of mass spectra at the expense of resolution. We recently initiated a study of this type by GC FT-ICR MS with Diana Lozano from the University of Warwick.

LIST OF PUBLICATIONS AND COMMUNICATIONS

PUBLICATIONS

Title: Next Challenges for the Comprehensive Molecular Characterization of Complex Organic Mixtures in the Field of Sustainable Energy: A review

Anthony Abou-Dib, Frédéric Aubriet, Jasmine Hertzog, Lionel Vernex-Loiset, Sébastien Schramm and Vincent Carré.

Published in Molecules journal, DOI: 10.3390/molecules27248889

ORAL COMMUNICATIONS

Authors: Anthony ABOU DIB, Vincent CARRÉ, and Frédéric AUBRIET

Title: « Pushing the capacity of FT ICR MS for the analysis of bio-oils to a higher level»

Congress: Scientific Journey - Meetings of the Young Club of the French Society of Mass Spectrometry - remotely, 12 December 2020

Authors: Anthony ABOU DIB, Vincent CARRÉ, and Frédéric AUBRIET

Title: « Pushing the capacity of FT ICR MS for the analysis of bio-oils to a higher level»

Congress: EU FT-ICR MS – Second advanced User school – Prague – Czech Republic, from 26 September 2021 till 31 September 2021

Authors: Anthony ABOU DIB, Vincent CARRÉ, and Frédéric AUBRIET

Title: « Characterization of bio-oil by specific derivatization of chemical functional group»

Congress: LCP-A2MC Young Researchers Day – Metz, July 8, 2021

Authors: Anthony ABOU DIB, Vincent CARRÉ, and Frédéric AUBRIET

Title: « Methodological development in FT-ICR MS for the analysis of bio-oil produced by pyrolysis of lignocellulosic biomass»

Congress: LCP-A2MC Young Researchers Day – Metz, June 28, 2022

POSTER COMMUNICATIONS

Authors: Anthony ABOU DIB, Vincent CARRÉ, and Frédéric AUBRIET

Title: « Pushing the capacity of FT ICR MS for the analysis of bio-oils to a higher level»

Congress: Seminar of the C2MP doctoral school – Nancy, June 16, 2022

Authors: Anthony ABOU DIB, Vincent CARRÉ, and Frédéric AUBRIET

Title: « Characterization of bio-oil by specific derivatization of chemical functional group»

Congress: Mass spectrometry international conference - Maastricht - The Netherlands, August 2022

Authors: Anthony ABOU DIB, Vincent CARRÉ, and Frédéric AUBRIET

Title: « Characterization of bio-oil at molecular level: Specific derivatization of chemical functional group»

Congress: Analytics 2022 – Nantes, 5-8 September 2022

AWARDS

Award: Nico Nibbering Travel Award

Congress: Mass spectrometry international conference - Maastricht - The Netherlands, August 2022

COLLABORATION AND SCHOLARSHIP

Scholarship: DrEAMS scholarship – Université de Lorraine Université d'excellence

Collaboration: ICR warwick lab – University of Warwick – United Kingdom from 01 March 2022 till 01 June 2022

TEACHING MISSIONS

Academic year 2020 – 2021 (48 HETD)

Practical work on "Chemistry of solutions" – Bachelor year 1 Life Sciences - Bridoux Campus - University of Lorraine

Academic year 2021 – 2022 (48 HETD)

Practical work on "Chemistry of solutions" – Bachelor year 1 Life Sciences - Bridoux Campus - University of Lorraine

LAB RESPONSIBILITIES

Elected doctoral student representative in the LCP-A2MC council since March 2021

Elected representative of doctoral students at the doctoral school since December 2020

Elected representative member of the Lorraine college of the doctoral school since January 2021

RESUME EN FRANÇAIS DE LA THESE



Doctoral School C2MP

Laboratory LCP-A2MC

Résumé en Français de la thèse

**Développement Méthodologique en FT-ICR MS pour
l'analyse des bio-huiles issues de la pyrolyse de la
biomasse lignocellulosique**

Soutenue le 03 Mai 2023 à Metz

En vue de l'obtention du grade de

DOCTEUR EN CHIMIE DE L'UNIVERSITÉ DE LORRAINE

Présenté par

Anthony N. ABOU DIB

Sous la direction de Pr. Frédéric AUBRIET et Dr. Vincent CARRÉ

INTRODUCTION

En raison de l'augmentation de la population mondiale et de la demande en énergie, l'utilisation des énergies fossiles telles que le pétrole, le gaz et le charbon, stockées pendant plusieurs millions d'années, posent un problème lié à leur rareté et à l'épuisement de leur gisement. La disponibilité décroissante de ces ressources est à l'origine d'une partie des crises géopolitiques et économiques actuelles. L'utilisation de combustibles fossiles est également à l'origine de problèmes environnementaux croissants en particulier liés au réchauffement climatique et à la pollution de l'environnement. C'est pourquoi, il est nécessaire de développer d'autres ressources énergétiques plus respectueuse de l'environnement et plus durables.¹

La biomasse peut être une alternative aux énergies fossiles dans la mesure où sa conversion notamment par pyrolyse peut conduire à des composés à haute valeur ajoutée. La biomasse est définie comme la matière organique produite par tous les végétaux et animaux.^{2,3} La conversion de cette matière organique donne accès notamment à des biocarburants dit de deuxième génération s'il s'agit de biomasse de type lignocellulosique. Celle-ci est largement disponible et provient des secteurs agricole et forestier voire de cultures dédiées.⁴

La nature des biocarburants et des composés valorisables qui peuvent être produits à partir de la biomasse dépend de sa nature et des processus de conversion/transformation utilisés.^{5,6} Le biodiesel, le bioéthanol et le biogaz sont les biocarburants de première génération les plus utilisés.⁷ La transestérification des triglycérides des plantes oléagineuses et huiles végétales produit du biodiesel, tandis que la fermentation des sucres et des amidons produit du bioéthanol. Le biogaz est produit à partir de la digestion anaérobie des déchets animaux ou végétaux pouvant être produits par des cultures dédiées.⁷ Le principal problème des biocarburants de première génération est l'utilisation de produits comestibles pour l'alimentation humaine et animale.

Pour surmonter ce problème, les biocarburants de deuxième génération sont en cours de développement et se distinguent des biocarburants de première génération du fait qu'elles sont produites à partir de matière première qui n'interfère pas avec l'alimentation humaine et animale.⁸ Ces biocarburants sont produits à partir de la biomasse lignocellulosique provenant du bois et de résidus agricoles tel que la paille.^{8,9} Les principaux constituants de la biomasse lignocellulosique (Figure 1) sont :

- La cellulose : polymère de glucose, représente 40 à 80 % de la biomasse. C'est l'homopolymère organique le plus répandu sur Terre.¹⁰
- L'hémicellulose : plus complexe que la cellulose, elle constitue le deuxième composé le plus abondant dans la biomasse (15 à 30%). Elle est constituée d'un

ensemble de cinq monosaccharides : le glucose (C₆), la xylose (C₅), le mannose (C₆), le galactose (C₆) et l'arabinose (C₅) qui sont des pentoses et des hexoses.¹¹

- La lignine : hétéropolymère amorphe composé de motifs phénoliques par des liaisons chimiques. Sa proportion dans la biomasse lignocellulosique est comprise entre 10 à 25 %.¹²

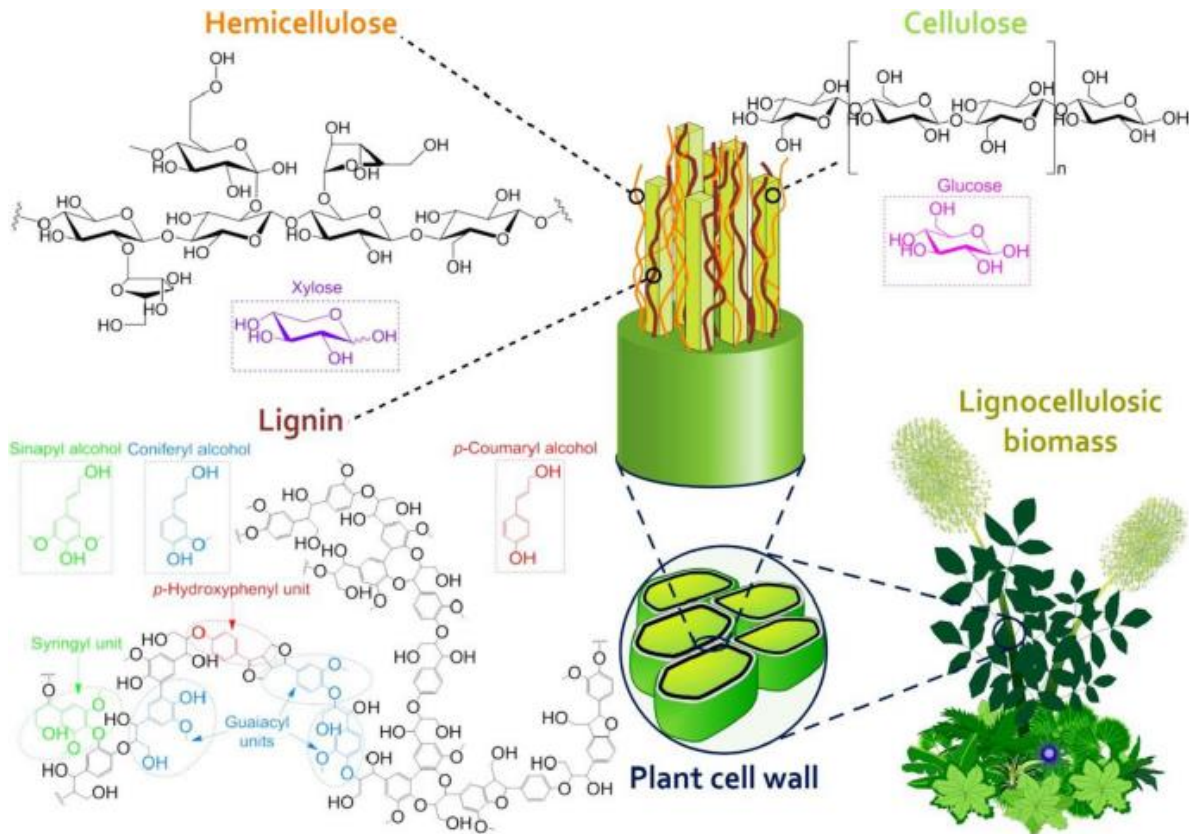


Figure 10: Compositions de la biomasse.¹³⁻¹⁵

La conversion de cette biomasse lignocellulosique en bio-huiles mènent à la production de biocarburants de deuxième génération par deux voies principales de conversion. La première voie est biochimique et consiste à convertir la cellulose, l'hémicellulose et plus spécialement l'amidon de la biomasse en sucres simples en utilisant des enzymes et des micro-organismes, puis en les transformant en alcool par fermentation.¹⁶ La deuxième est la conversion thermochimique, qui implique la pyrolyse, la liquéfaction ou la gazéification de tous les composants de la biomasse lignocellulosique.^{17,18,19} Dans ces procédés, la biomasse est convertie, à haute température (pyrolyse/gazéification) ou à haute pression (liquéfaction), en présence ou non d'oxygène, en biogaz, biochar et bio-huiles.²⁰ Du fait de leur potentiel de valorisation et leur composition moléculaire très complexes, les bio-huiles suscitent un intérêt croissant, conduisant à l'appellation "pétrole verte".²¹ Les bio-huiles obtenues ont une teneur élevée en oxygène, et donc une acidité et une réactivité élevée rendant son utilisation directe impossible (problèmes de corrosivité et de stockage).^{22,23} Pour surmonter ces problèmes, il est nécessaire de développer des traitements catalytique de désoxygénation ou de craquage le plus souvent en utilisant de catalyseurs pour réduire leur

teneur en d'oxygène.^{24,25} Ces procédés catalytiques doivent également permettre le craquage des composés les plus lourds.²⁵

Afin de déterminer quels sont les traitements catalytiques les mieux adaptés, la connaissance aussi précise que possible de la composition de ces bio-huiles est requise. Des travaux ont été réalisés sur la caractérisation des bio-huiles en utilisant différentes techniques analytiques (GC/MS, 2D GC/MS, FTIR et NMR). Cependant, ces méthodes n'ont pas encore permis de caractériser finement la composition moléculaire des bio-huiles.^{26,27} La combinaison de plusieurs techniques est nécessaire pour atteindre cet objectif. Deux approches sont généralement utilisées pour étudier les mélanges complexes. La première permette de caractériser et de quantifier un nombre donné de composés ou de familles de composés connus au moyen de techniques analytiques spécifiques. On parle alors d'analyse ciblée. Parmi les techniques utilisés pour ce type d'analyse, on peut citer la spectroscopie infrarouge (IR) et par résonance magnétique nucléaire (RMN)^{23,26} ainsi que la chromatographie en phase gazeuse (GC) ou liquide (HPLC) associée éventuellement à une analyse moléculaire (spectrométrie de masse) ou structurale (spectrométrie de masse en tandem). Le principal inconvénient des techniques ciblées est que seule une liste préétablie de composés, généralement de faible poids moléculaire, est examinée et ne représente qu'une très petite fraction des constituants des bio-huiles.^{26,28}

Marshall et al. ont développé une approche non ciblée en l'appliquant initialement à l'étude de pétroles bruts pour étudier les centaines voire les milliers de composés présents dans ce type d'échantillon.²⁹ Elle peut également être employée dans le cadre de l'étude de bio-huile et est appelée pétroléomique. Cette approche est typiquement basée sur l'infusion directe de l'échantillon de bio-huile dans la source d'ionisation du spectromètre de masse et vise à décrire tous les composés de bio-huiles détectés à l'échelle moléculaire.^{30,31} En raison de la grande complexité moléculaire des pétroles bruts ou des bio-huiles, un spectromètre de masse à haute résolution (HRMS), comme le spectromètre de masse à résonance cyclotronique des ions à transformée de Fourier (FT-ICR MS), est nécessaire.^{29,32} En outre, l'utilisation de différentes sources d'ionisation peut être un avantage pour explorer d'une façon exhaustive les bio-huiles.³³

De manière synthétique, l'objectif de cette étude est de développer deux méthodes d'analyse pétroléomique des bio-huiles de pyrolyse de la biomasse. La première est basée sur des procédures de dérivation et de fractionnement spécifiques, et la seconde sur la spectrométrie de masse en tandem. Le but de ces deux approches est d'obtenir des informations structurales sur plus de six milles espèces déjà observées dans les bio-huiles. Ces développements ont été menés par spectrométrie de masse à résonance cyclotronique des ions à transformée de Fourier (7T FT-ICR MS). Les sources d'ionisation par électronebulisation (ESI), photoionisation à pression atmosphérique (APPI) et l'ionisation chimique à pression atmosphérique (APCI) ont été utilisées en raison de leur capacité à ioniser

des composés de polarité différente. Cela permet d'avoir une description de la diversité moléculaire de ces bio-huiles aussi importante que possible.

PRINCIPE DE L'APPROCHE PETROLEOMIQUE

Marshall *et al.* ont été les premiers à appliqué l'approche pétroléomique pour la caractérisation des pétrole.³⁴ En raison de la complexité de ce type d'échantillons, des spectromètres de masse à haute résolution sont nécessaires. Le grand pouvoir résolutif fourni par ces appareils ($> 1\,000\,000$) rend possible la distinction des espèces isobares. Plusieurs dizaines de milliers de pics peuvent être observés sur un seul spectre de masse, comme le montre la figure 2. A chaque pic est attribué une formule unique $C_xH_yN_nO_z$ avec une très grande précision de mesure de masse ($< 0,2$ ppm). Avec cette méthode, il est possible d'analyser l'échantillon à une échelle "globale". Cependant, le grand nombre de données produites rend l'interprétation difficile, et l'absence de séparation en amont peut entraîner des compétitions à l'ionisation. Enfin, il est impossible de distinguer les isomères en utilisant cette méthode.

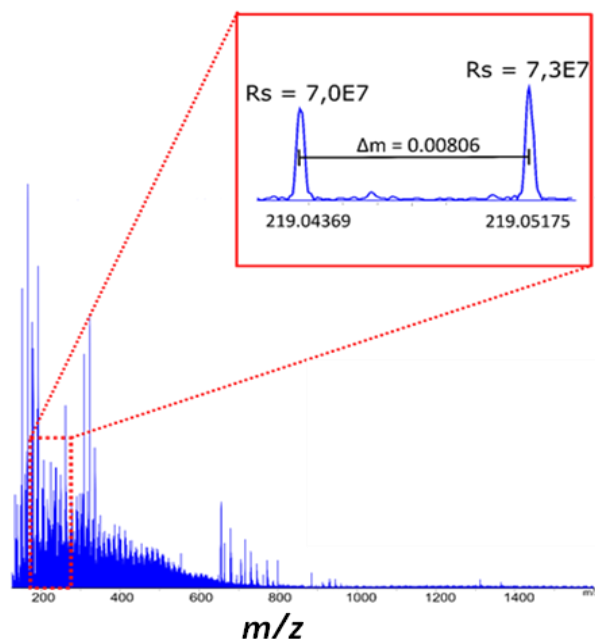


Figure 11: Spectre de masse d'une bio-huile de pyrolyse de chêne obtenu par (-) ESI FT-ICR MS.

La très grande quantité d'informations obtenue nécessite des représentations graphiques pour faciliter l'interprétation et la comparaison inter-échantillon. Parmi ces représentations, on peut citer les diagrammes de Van Krevelen (Figure 3), qui représentent les différents composés $C_xH_yO_z$ par des points dont les coordonnées x et y sont les rapports O/C et H/C, respectivement. Cette représentation permet de mettre en évidence des zones spécifiques du diagramme pour les lipides, les dérivés de cellulose et d'hémicellulose

(carbohydrates) ou les dérivés de lignine. Pour les composés contenant des atomes d'azote et/ou du soufre, les rapports N/C et S/C peuvent également être utilisés pour tracer des diagrammes similaires.

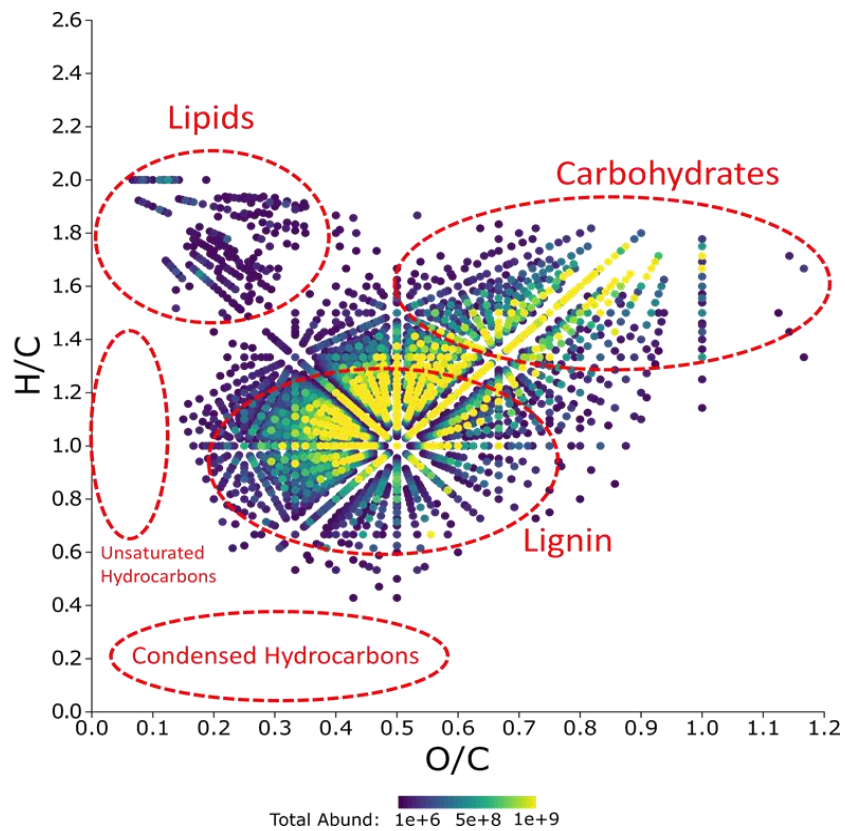


Figure 12: Diagramme de van Krevelen représentant les principaux constituants d'une bio-huile produite par pyrolyse de biomasse.³⁵

En calculant, pour une molécule, son équivalent en double liaison appelée DBE (Double Bound Equivalent), il est possible de représenter son degré d'insaturation et d'aromaticité. La DBE est facilement obtenue à l'aide de l'équation suivante :

$$DBE = n_C - \frac{n_H}{2} - \frac{n_N}{2} + 1 \quad \text{Équation 1}$$

La FT-ICR MS

Le principe de fonctionnement fondamental du FT-ICR repose sur la capacité d'un ion à adopter une trajectoire circulaire et uniforme lorsqu'il est positionné dans un champ magnétique uniforme (B_0), à condition qu'il soit initialement animé d'une vitesse perpendiculaire au champ magnétique. Ce mouvement est connu sous le nom de mouvement cyclotronique, et sa fréquence est donnée par :³⁶

$$\omega_c = \frac{1}{2\pi} \frac{qB}{m_i} \text{ Avec } q = z x e \quad \text{Équation 2}$$

La fréquence mesurée est donc inversement proportionnelle au rapport m/z . Dans le but de piéger les ions afin d'en assurer la détection, il est nécessaire qu'un potentiel de l'ordre du volt soit appliqué aux plaques, dites de piégeages, afin de créer un puits de potentiel pour piéger les ions dans la dimension perpendiculaire au champ magnétique B_0 . Le mouvement initial des ions ayant un même rapport m/z au centre de la cellule ICR est incohérent. La fréquence associée à ce mouvement sont comprises entre quelques dizaines de kHz pour les molécules les plus lourdes à quelques dizaines de MHz pour les molécules les plus légères. Ces valeurs sont bien entendu dépendant de valeur de B_0 .³⁷

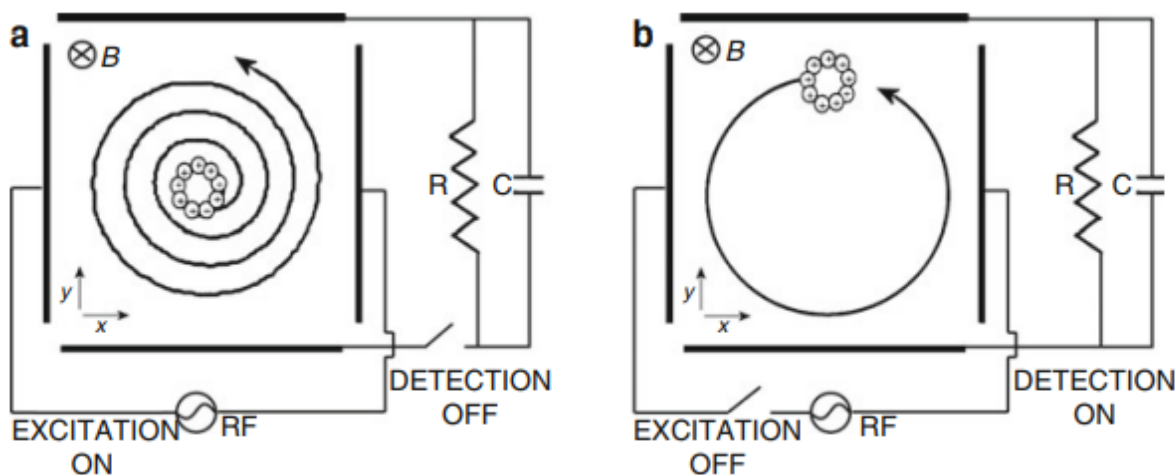


Figure 13: Mouvement cyclotronique d'un d'ion dans un champ magnétique B dans une cellule d'analyse ICR.³⁸

La cellule ICR dans laquelle les ions sont piégés est composée d'électrodes de piégeage, d'électrodes d'excitation et d'électrodes de détection. L'énergie cinétique des ions augmente en appliquant un champ de radiofréquence aux plaques d'excitation constitué de la superposition de fréquences comprises entre quelques kHz et quelques MHz. Le rayon de leur trajectoire cyclotronique augmente (Figure 4). Ce comportement a pour conséquence de rendre le mouvement des ions cohérent. Après l'arrêt de l'excitation radiofréquence, le mouvement des ions se stabilise sur une orbite haute, près des plaques de piégeage. Ainsi, ils peuvent passer à proximité des plaques de détection, sur lesquelles ils produisent un courant alternatif à une fréquence égale à la fréquence de leur mouvement du cyclotronique.³⁷

La figure 5 montre le processus d'acquisition et de traitement d'un spectre de masse à l'intérieur d'une cellule FT-ICR. Dans la configuration la plus simple, il y a deux électrodes pour chaque fonction. Les ions sont piégés radialement par le champ magnétique et axialement par les électrodes de piégeage. Les paquets d'ions à proximité d'une plaque de détection interagissent avec les électrons de cette plaque. Le courant entre les deux plaques de détection, appelé courant miroir, est amplifié, converti en tension et mesuré à intervalles de temps réguliers. On obtient ainsi un signal transitoire qui est convertit par transformée de Fourier en spectre de fréquence. Les fréquences peuvent ensuite être converties en rapports m/z .³⁹

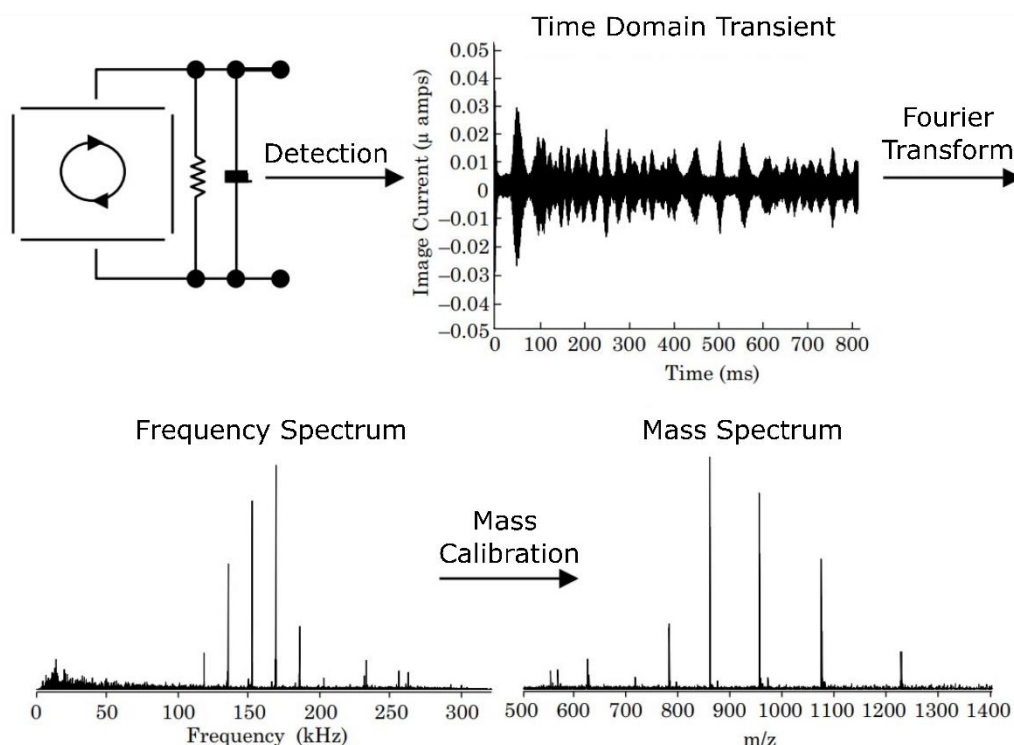


Figure 14: La procédure de transformation d'un mouvement cyclotronique ionique en un spectre de masse.³⁹

Les sources d'ionisation

Dans une source d'ionisation, les molécules sont vaporisées et ionisées. Les ions peuvent être de polarité positive ou négative. Plusieurs sources d'ionisation existent et sont utilisées en fonction des propriétés physico-chimiques, notamment la polarité et la masse des molécules étudiées. Les sources d'ionisations utilisées dans le cadre de cette étude sont l'électronébulisation (ESI), la photoionisation à pression atmosphérique (APPI), et l'ionisation chimique à pression atmosphérique (APCI).

L'ESI permet d'observer en particulier, des ions $[M+H]^+$ associés à la protonation, ou $[M-H]^-$ à la déprotonation des constituants de l'échantillon. Elle permet l'ionisation

préférentielle des composés possédant une polarité moyenne à élevée. A pression atmosphérique, l'échantillon est introduit dans la source d'ionisation à travers un capillaire en acier inoxydable à un débit de 1 à 10 $\mu\text{l}\cdot\text{min}^{-1}$. Un potentiel de 2 à 4 kV est appliqué sur la pointe du capillaire. Un champ électrique intense est créé entre le capillaire et une contre-électrode. La conséquence de ce champ électrique fort est que la solution qui émerge du capillaire voit des charges électriques soit positives ou négatives (en fonction de la polarité du champ créé) se concentrer à sa surface. Des gouttelettes se détachent du capillaire et présentent à leur surface une forte concentration d'ions de charges positives ou négatives. Sous l'effet de la température qui règne dans la source d'ionisation mais aussi d'un flux de gaz de séchage le solvant contenu dans ces gouttelettes s'évapore ce qui conduit à leur explosion (compétition des forces de cohésion et des répulsions coulombienne) et de manière ultime à la libération d'ion en phase gazeuse (Figure 6).⁴⁰ Les facteurs influençant le procédé d'ionisation par ESI sont la température de la source, la nature du solvant et la présence d'agents favorisant les processus de cationisation, d'anionisation, de protonation ou de déprotonation.⁴¹

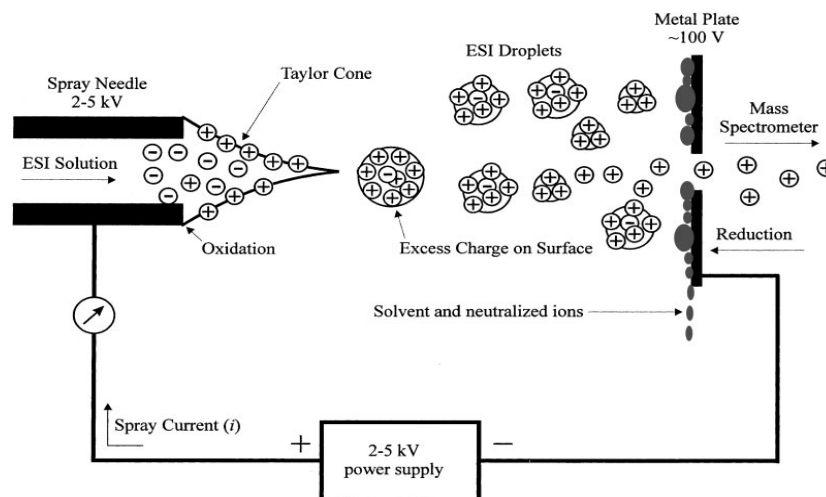


Figure 15: Processus d'ionisation en ESI. ⁴²⁻⁴⁵

La photo ionisation à pression atmosphérique (APPI) est un procédé d'ionisation à pression atmosphérique. C'est une méthode d'ionisation douce pour l'analyse de molécules peu polaires à moyennement polaires. L'APPI est une méthode d'ionisation dans laquelle l'échantillon est ionisé par une lampe ultraviolette. Ces photons UV sont généralement émis par une lampe à décharge d'Argon, de Xénon ou de Krypton. Cette dernière est la plus courante et présentant l'avantage d'émettre des photons de 10,0 et 10,6 eV (énergie plus faible que l'énergie d'ionisation des principaux composants de l'air). Le principe de l'APPI se base sur le pouvoir de photo-ioniser sélectivement et directement les analytes d'un effluent liquide vaporisé. Les molécules doivent être en phase gazeuse à travers l'étape de nébulisation. L'interaction d'un photon d'énergie $h\nu$ et d'une molécule AB conduit à son excitation. Et si l'énergie d'ionisation de l'échantillon est plus basse que l'énergie du photon absorbé, la molécule excitée est ionisée sous forme d'un radical cation. D'autres processus

impliquant des molécule de solvant peuvent conduire au transfert de proton et à la formation d'ions $[M+H]^+$.⁴⁶

Afin d'augmenter l'efficacité d'ionisation, l'ajout d'un dopant à la solution contenant l'échantillon est nécessaire. Cet ajout permet aussi d'augmenter le rendement d'ionisation de l'analyte. Un dopant approprié doit être un bon absorbant à la longueur d'onde utilisée et présenté une énergie d'ionisation inférieure à l'énergie des photon utilisés. Le dopant couramment utilisé est le toluène. En se basant sur les réactions impliquées dans les processus APPI, des ions radicalaire M^+ et protonés $[M+H]^+$ ou deprotonés $[M-H]^-$ peut être observés pour un analyte donné suivant le mode de détection choisi.⁴⁷⁻⁵¹

Comme les modes d'ionisation ESI et APPI, APCI utilise une interface atmosphère-vide pour délivrer des ions dans le spectromètre de masse. Les sources APCI modernes fonctionnent avec un débit de 5 à 20 $\mu\text{l}\cdot\text{min}^{-1}$. Les courants de décharge corona typiques sont de l'ordre de 10 μA . La solution d'échantillon est vaporisée en passant au travers d'une chambre de nébulisation maintenue température élevée. La désolvatation des molécules d'analyte de phase gazeuse a lieu avant que les molécules soient ionisées par les espèces produites par le plasma de décharge corona. Les électrons produits par la décharge corona ionisent le solvant (S) ainsi que les gaz atmosphériques pour créer des ions réactifs qui ionisent ensuite l'analyte (M) par échange de charge ou transfert de protons.⁵²

Le solvant, le gaz de nébulisation et l'environnement contribuent à la composition du plasma généré par la décharge corona. Sa composition peut varier considérablement au cours des expériences. Comparé à d'autres techniques d'ionisation, l'APCI a une faible reproductibilité. Le fait que le dispositif de chauffage fonctionne typiquement à une centaine de degré Celsius peut donner l'impression que l'APCI est une technique d'ionisation dure. Cependant, c'est tout le contraire. L'APCI est encore plus doux que l'ionisation chimique "traditionnelle".⁵³

MATERIELS ET METHODES

Spectromètres de masse à résonance cyclotronique de ions à transformée de Fourier

Le spectromètre Solarix qui a été utilisé dans cette étude est un spectromètre 7T 2XR FTMS (Bruker) au *Laboratoire de Chimie et Physique Approche Multi-échelles des Milieux Complexes*, à Metz. Cet instrument est équipé des sources d'ionisation ESI, APPI et APCI et il bénéficie des améliorations technologiques les plus récentes qui permettent d'obtenir des performances jusqu'alors inégalées (Figure 7).

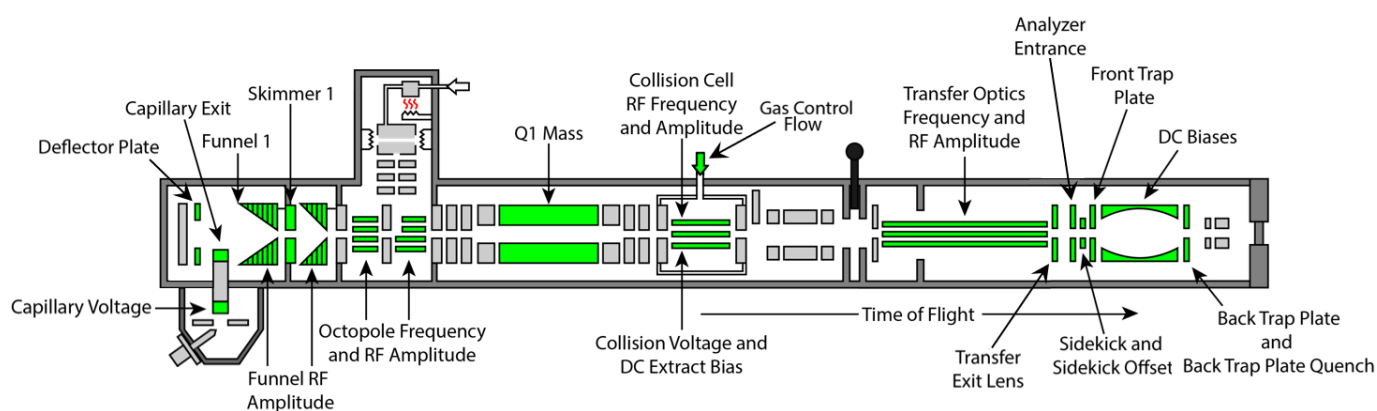


Figure 16: Représentation schématique du spectromètre de masse FTICR Solarix 7T 2XR FTMS. Copyright 2019 Bruker Daltonics.

Cet instrument assure la mesure simultanée de dizaine de milliers d'espèces avec une précision sur la mesure de masse équivalente à quelques pourcents de la masse d'un électron pour une molécule d'une centaine d'atomes et avec une résolution extrêmement élevée (> 2 000 000).

L'analyse structurale en spectrométrie de masse en tandem ont été effectuées à l'Université de Warwick, dans le cadre de la bourse DrEAMS avec un appareil FT-ICR MS de 12 T (Bruker Solarix) équipé de la source ESI (Bruker Daltonics).

Production du bio-huile

La bio-huile examinée dans le cadre de cette étude a été produite au sein du groupe de recherche GREENER au *Laboratoire Réactions et Génie des Procédés* (UMR CNRS 7274) de Nancy. La biomasse lignocellulosique employée est une biomasse de chêne en poudre dont la taille des particules varie entre 0,8 et 1,7 mm. La biomasse de chêne (2 g) est introduit en continu dans le lit micro-fluidisé.

Le lit micro-fluidisé est maintenu à une température de 500°C (Figure 8). Dans ces conditions, la durée de séjour de la phase gazeuse dans le réacteur est d'environ 1,2 s. Afin d'éviter la condensation, les vapeurs de bio-huile générées sont dirigées vers trois pièges froids via une ligne chauffée réglée à 350°C. Le premier refroidisseur est positionné dans un bain de glace à 0°C dans le but de piéger l'eau et les espèces plus lourdes. Le propanol et l'azote liquide sont tous les deux présents dans le deuxième et le troisième refroidisseur, permettant de maintenir la température à -60 °C. Après les trois pièges cryogéniques, un barboteur rempli de méthanol est fixé à la ligne. A l'issue de la pyrolyse, 20 mL de méthanol sont utilisés pour rincer l'ensemble des refroidisseurs et canalisations de la ligne afin de récupérer les condensables.⁵⁴

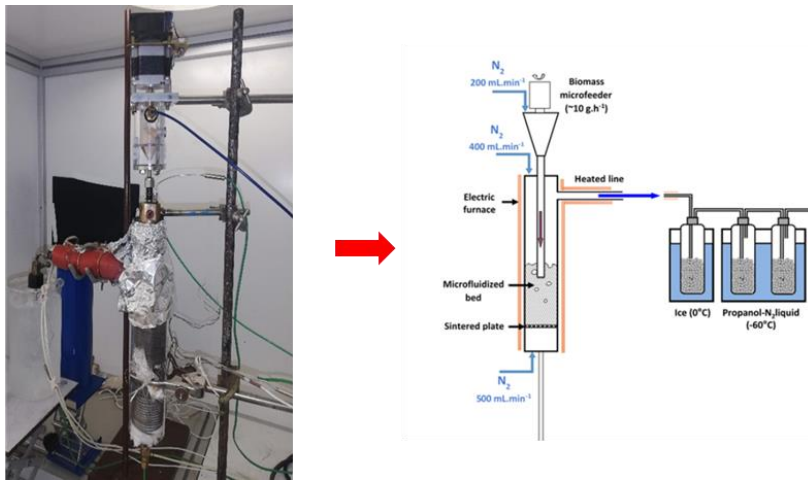


Figure 17: Réacteur à micro-lit fluidisé et pièges cryogéniques utilisés pour la production et la collecte de bio-huiles de pyrolyse.⁵⁵

PREMIERE APPROCHE : DERIVATION SPECIFIQUE DES FONCTIONS CHIMIQUES

Cette approche vise à identifier la variété des fonctions chimiques présentes dans les composés d'une bio-huile produite par pyrolyse de la biomasse lignocellulosique. L'accent a été mis sur les dérivés de la lignine, dont certains résistent aux traitements catalytiques d'upgrading. Avant d'effectuer une analyse par spectrométrie de masse à haute résolution, la première approche implique différentes étapes de préparation des échantillons, incluant des étapes de fractionnement et de dérivation. Les étapes de fractionnement et une partie des étapes de dérivation ont été réalisées sur une cartouche d'extraction en phase solide « Oasis Max » à l'aide d'une résine échangeuse d'anion. La procédure analytique proposée a d'abord été appliquée à une gamme de composés standards issus de la pyrolyse de la lignine, qui ont été sélectionnés en fonction de leurs structures et des fonctions chimiques habituellement présentes dans les constituants de la bio-huile lignocellulosique pour évaluer son efficacité. La méthodologie analytique a ensuite été appliquée à un échantillon réel de bio-huile. La figure 9 présente le schéma global de la fractionnement/dérivation.

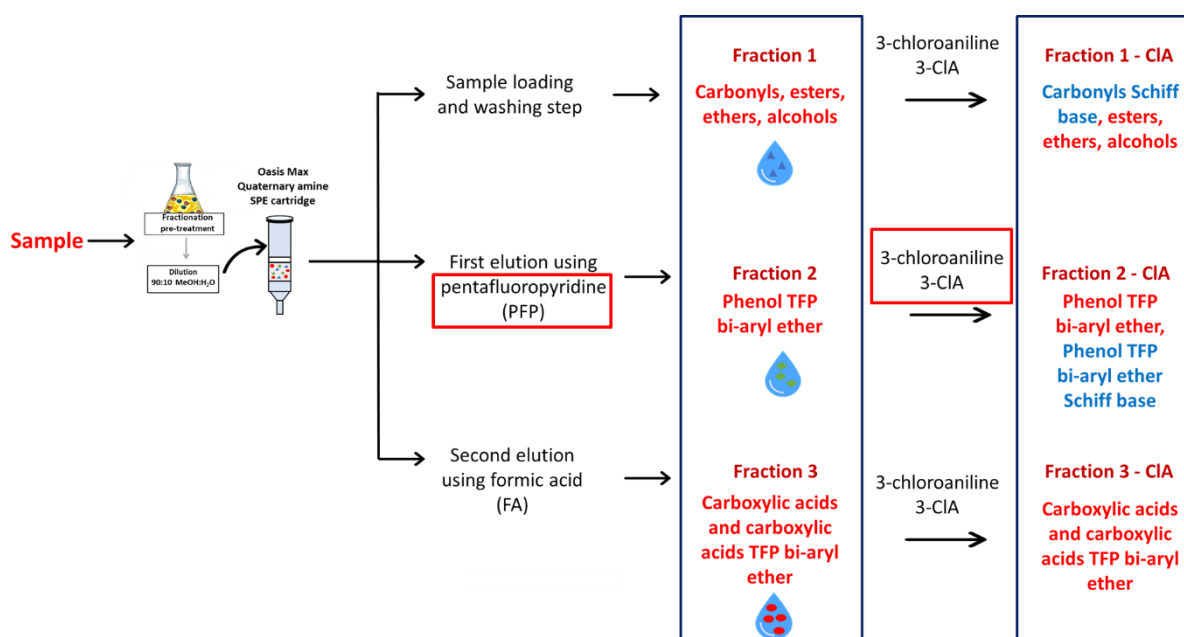


Figure 18: Le schéma global de la procédure de fractionnement et de dérivation.

Différents agents de dérivation ont été choisis en fonction du groupe fonctionnel ciblé. Ces agents présentent systématiquement au moins un atome, qui n'est pas présent dans les composants de bio-huile pour différencier les molécules dérivées des composants de bio-huile non dérivés comme la pentafluoropyridine PFP et la 3-chloroaniline. La signature isotopique du chlore a également facilité le post-traitement des données. La 3-chloroaniline a été utilisée pour mettre en évidence les groupes carbonyles et la pentafluoropyridine (PFP) pour réagir

rapidement, spécifiquement et efficacement avec les composés phénoliques pour produire des tétrafluoropyridyle bi-aryle éthers via une réaction S_NAr .

La méthodologie proposée conduit à la production de trois fractions :

- La première fraction contient les composés de bio-huile non retenus par la phase stationnaire de la cartouche en milieu basique. Ce sont des composés qui ne sont ni phénoliques ni acides. Ce sont principalement des carbonyles (cétones et aldéhydes), des esters, des éthers et des dérivés de sucres. Les carbonyles sont mis en évidence par réaction avec la 3-chloroaniline et la formation de bases de Schiff.

- La seconde fraction obtenue par élution avec la PFP est constituée des composants phénoliques de la bio-huile (phénol, polyphénols, alkoxy-phénols, alkoxy-polyphénols...), qui ne contiennent pas de fonction acide carboxylique. Pour les composés poly-phénoliques, la réaction avec le PFP a lieu pour chaque groupe phénol, ce qui détermine le nombre de groupes phénols pour un composé donné. La 3-chloroaniline est également ajoutée pour marquer les groupements carbonyles si les composés phénoliques présentent également des fonctions aldéhydes ou cétones.

- La fraction finale, obtenue par élution avec l'acide formique, correspond aux composés de bio-huile possédant au moins un groupement acide carboxylique. Un tel composé, s'il possède également une ou plusieurs fonctions phénols, est observé comme un composé dérivé mono- ou poly-PFP. L'ajout de 3-chloroaniline assure la mise en évidence des carbonyles.

L'application de cette méthode à une bio-huile de pyrolyse, a conduit à l'observation de centaines voire de milliers de signaux pour les trois fractions obtenues. La fraction 1 contenait des dérivés de la lignine, des sucres et une petite proportion de composés lipidiques (Figure 10). Après ajout de 3-chloroaniline, il a été possible de mettre en évidence qu'une partie des dérivés de la lignine et des sucres impliquait une fonction carbonyle. Les composés à deux carbonyles sont associés à des composés dérivés de la lignine.

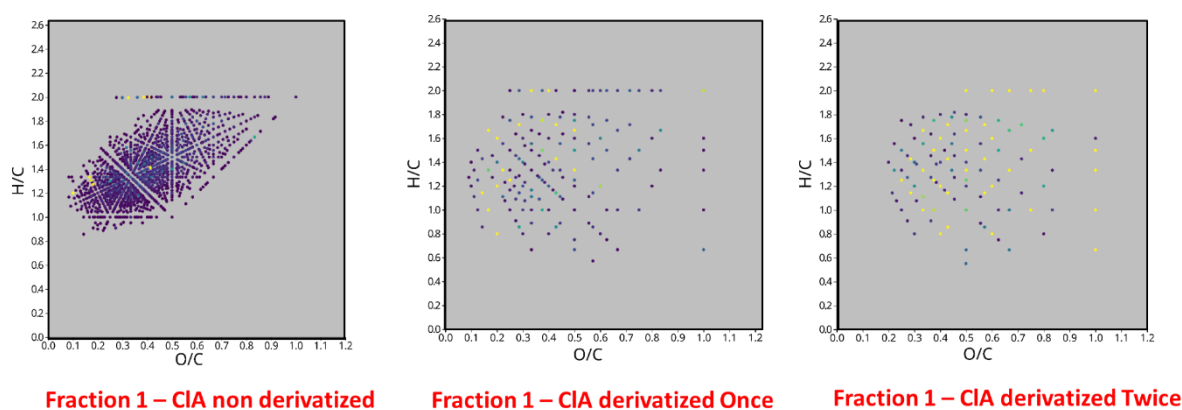


Figure 19: Diagramme de Van Krevelen de la fraction 1 après ajout de 3-chloroaniline.

Dans la deuxième fraction, seuls quelques composés se sont avérés présenter deux voire trois groupes phénols. En effet, la majorité a été dérivée une fois par PFP. Ces deux classes de composés relevaient bien sûr du domaine des dérivés de la lignine sur le diagramme de Van Krevelen (Figure 11).

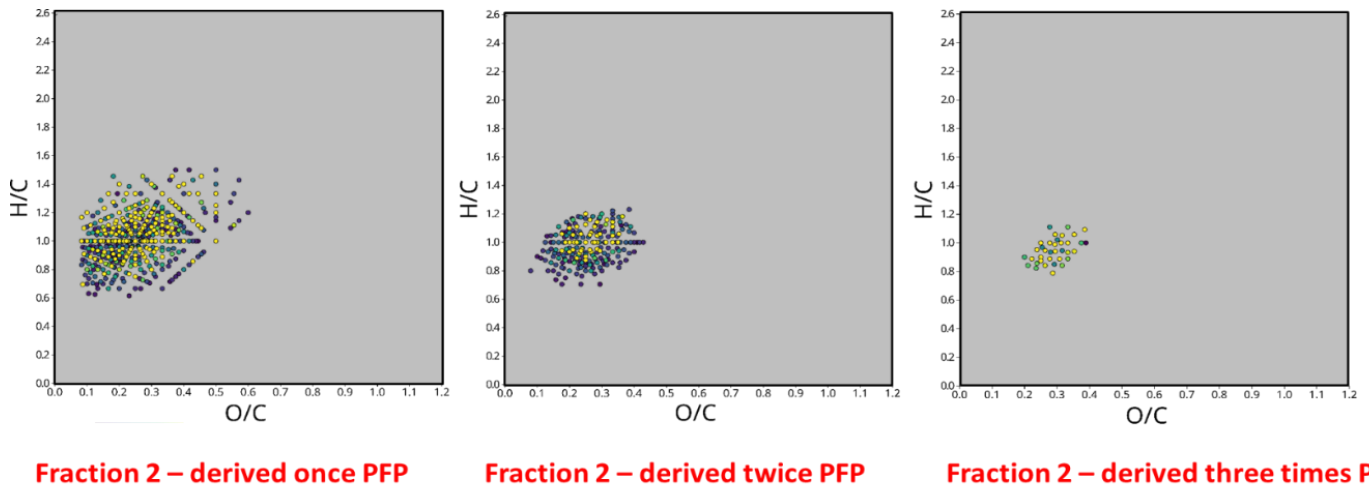


Figure 20: Diagramme de Van Krevelen de la fraction 2 après ajout de la PFP.

Deux classes de composés ont été observées dans la dernière fraction. Les premiers sont des acides gras libres et n'ont pas été dérivés par la PFP, tandis que les seconds comprennent des dérivés de lignine phénolique avec une fonction chimique d'acide carboxylique et ont été observés une fois et deux fois dérivés par la PFP (Figure 12). Aucun composé présent dans cette dernière fraction n'a réagi avec la 3-chloroaniline.

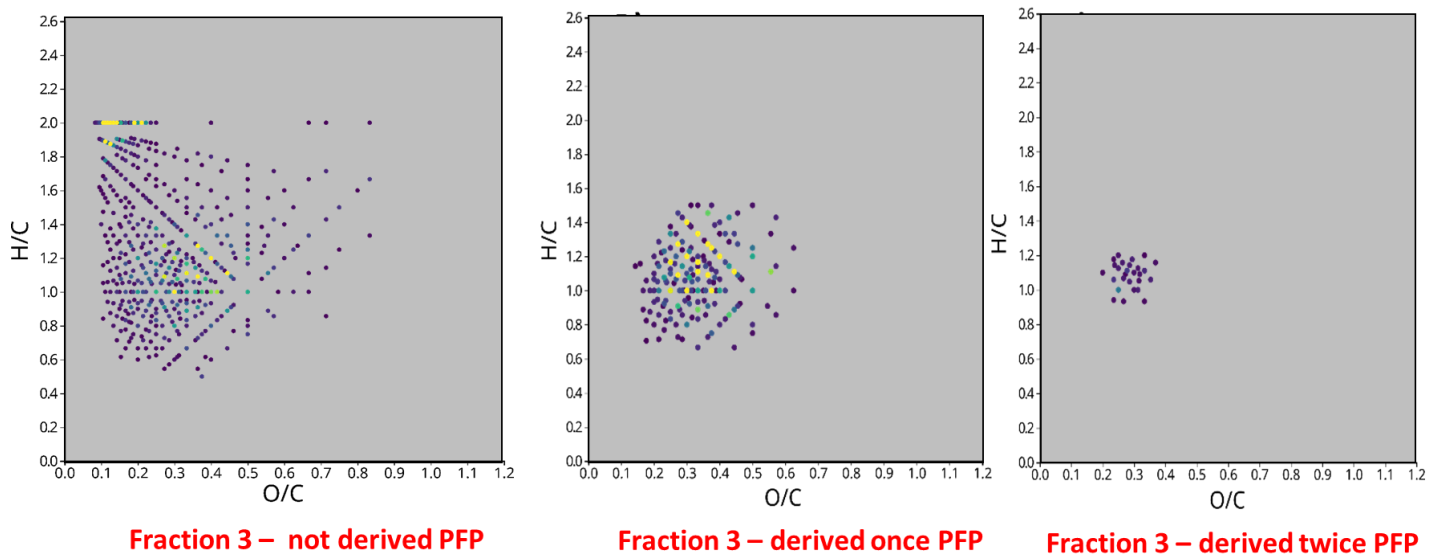


Figure 21: Diagramme de Van Krevelen de la fraction 3 après ajout de l'acide formique.

Dans le cadre de la caractérisation des bio-huiles, il a ainsi été possible de démontrer tout le potentiel de fixer une fonction chimique faisant intervenir un ou plusieurs atomes avec un profil isotopique particulier, comme le chlore ou qui ne sont pas présents dans la bio-huile comme le fluor pour réaliser des analyses non ciblées semi-dirigées. La première approche et l'analyse pétroliomique classique ont assuré l'analyse spécifique et la distinction des différentes classes oxygénées des composants de la bio-huile.

DEUXIEME APPROCHE : SPECTROMETRIE DE MASSE EN TANDEM : ANALYSE STRUCTURELLE

La spectrométrie de masse en tandem

La spectrométrie de masse en tandem est nécessaire pour obtenir des informations structurales. Elle implique deux étapes d'analyse, appelées MS^1 et MS^2 . Dans la première étape, un spectre de masse classique est obtenu après ionisation. La sélection d'un ion précurseur encore nommé ion parent pour lequel une analyse structurale est nécessaire est alors réalisée. Dans la deuxième étape, l'activation de l'ion sélectionné par différentes techniques augmente son énergie interne, ce qui conduit à sa dissociation. La phase finale d'une expérience de spectrométrie de masse en tandem consiste en l'analyse des fragments d'ions. La figure 13 illustre les quatre événements nécessaires pour mener à bien une expérience MS/MS : ionisation, isolation des précurseurs, fragmentation et détection.^{56,57}

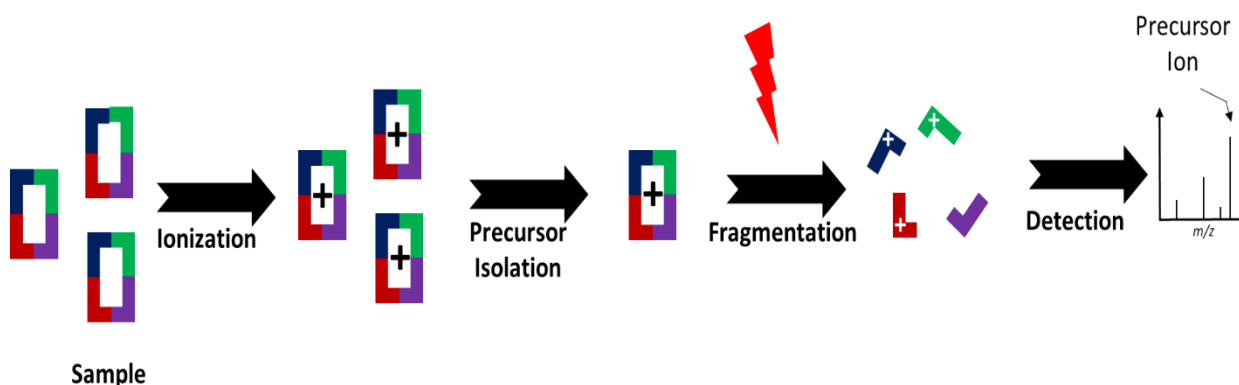


Figure 22: Les différentes étapes pour effectuer une expérience MS en tandem.

Différentes méthodes d'activation existent, dont l'utilisation dépend fortement du spectromètre de masse en tandem utilisé et des propriétés des ions parents. Dans notre étude, on s'intéresse à utiliser la dissociation induite par collision CID et la photodissociation ultraviolette UVPD.

En CID, l'ion sélectionné entre en collision avec un gaz neutre tel que He, N₂ ou Ar (les gaz de collision les plus couramment utilisés) pour assurer sa fragmentation qui aura lieu dans la cellule de collision. Afin de favoriser les événements de collision, la pression dans la cellule de collision est significativement plus élevée que le vide poussé généralement utilisé en spectrométrie de masse. L'interaction entre l'ion précurseur et le gaz neutre provoque ce que l'on appelle « l'activation de l'ion précurseur » conduisant à l'augmentation de son énergie interne par conversion au cours de la collision d'une partie de son énergie cinétique. Cette énergie interne est distribuée dans les modes vibrationnels et rotationnels de l'ion parent. En CID, la dissociation des liaisons les plus faibles est favorisée.⁵⁸

L'UVPD a lieu en exposant l'ion précurseur à des photons UV. A la suite de l'absorption d'un seul photon UV, l'ion est excité dans un état électronique supérieur et se dissocie. Du fait qu'un seul photon UV est absorbé, cette excitation peut être réalisée en une seule étape, contrairement à l'IRMPD (Figure 14).⁵⁹⁻⁶¹ L'UVPD nécessite que l'ion précurseur possède un chromophore pour absorber à la longueur d'onde des photons émis par le laser UV (193 nm dans cette étude).

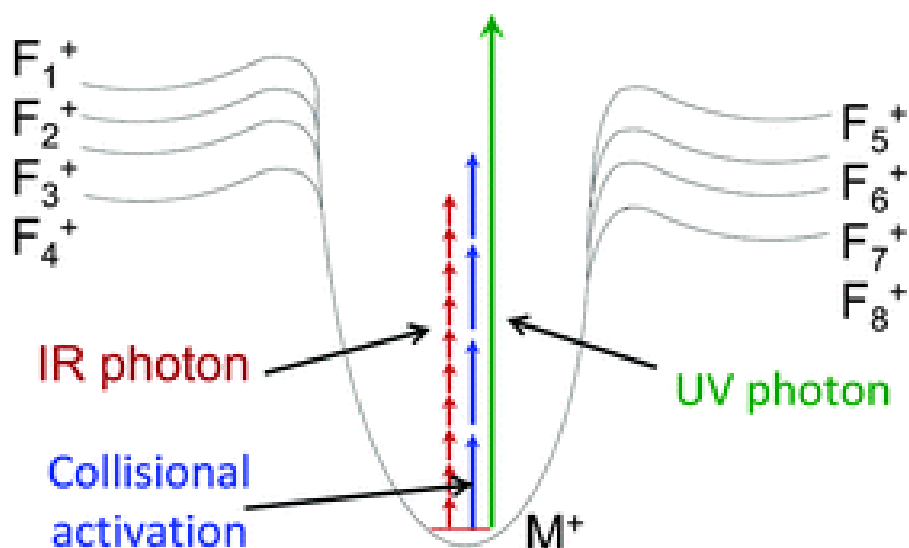


Figure 23: Illustration des différentes techniques de fragmentation (CID, IRMPD et UVPD).⁶²

La spectrométrie de masse bidimensionnelle 2D FTMS

La 2D FTMS se base sur la séquence d'impulsions de Gäumann. C'est une séquence **impulsion-délai-impulsion**, qui est fréquemment utilisée. La séquence d'impulsions de Gäumann est divisé en 5 étapes :^{63,64}

- Ionisation, accumulation externe des ions dans l'hexapôle et transfert des ions vers la cellule ICR.

- Séquence $P_1-t_1-P_2$: tous les ions transférés dans la cellule ICR sont excités par l'impulsion initiale P_1 pour augmenter leurs rayons orbitaux r_1 . Après l'activation initiale, le délai (t_1) permet aux ions de gagner en phase et d'être séparé spatialement. L'impulsion P_2 (identique à l'impulsion P_1) est appliquée après t_1 .

- Fragmentation (τ_m) : La fragmentation aura lieu après la désexcitation d'une partie des ions (ceux en opposition de phase par rapport à l'impulsion P_2) au centre de la cellule ICR. Les autres voient leur rayon orbital augmenter.

- Excitation P_3 pour la détection : Après fragmentation, la troisième impulsion P_3 , sert à exciter les ions fragments et leurs ions précurseurs pour en assurer la détection.

- Acquisition du transient (t_2) : T_2 est le temps utilisé pour la détection des ions fragment et précurseurs.

Après traitement, les données obtenues sont présentées sous la forme d'une carte 2D dont les coordonnées x et y sont les axes m/z des fragments et des précurseurs, respectivement (Figure 15). Cette carte 2D présente la ligne d'autocorrélation (contient tous les ions précurseurs qui ont été fragmentés), des lignes horizontales regroupant un ion précurseur et ses fragments, des lignes verticales qui rassemblent tous les ions précurseurs conduisant à un même ion fragment et des lignes de pertes des neutres qui groupent tous les ions précurseurs qui perdent le même neutre.

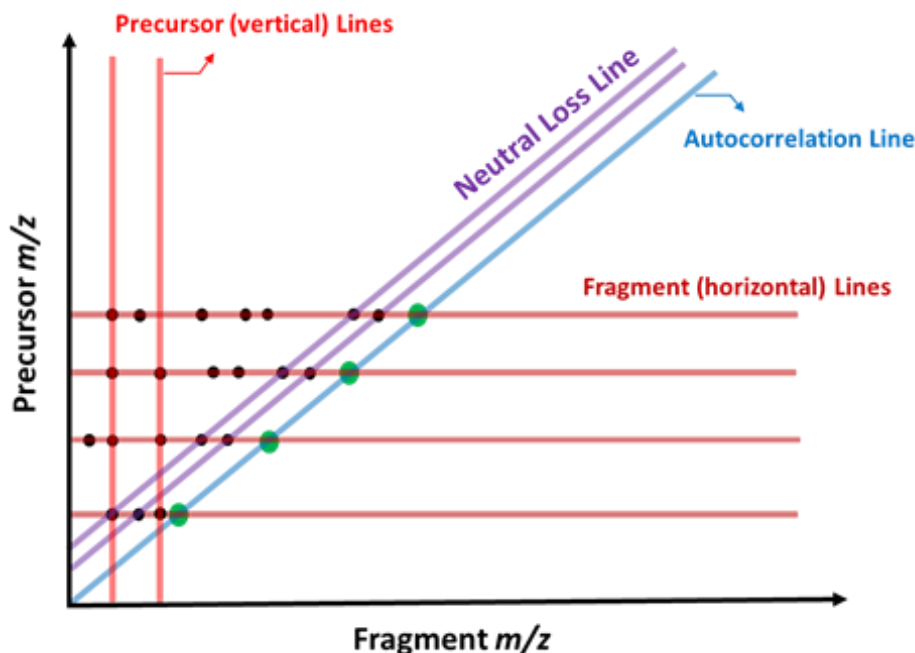


Figure 24: Une carte 2DMS représente les nombreuses lignes qui peuvent être extraite pour le traitement des données.

CID vs UVPD

Cette partie du travail de thèse est axée sur les capacités de la spectrométrie de masse en tandem en mode pour obtenir une analyse structurale des composants de la bio-huile. Pour atteindre cet objectif, deux problèmes ont dû être surmontés. Le premier était l'impossibilité de mener des expériences de spectrométrie de masse en tandem "classiques" sur une matrice aussi complexe en un temps raisonnable. La seconde était d'obtenir des informations pertinentes sur les composants de la bio-huile par MS/MS et d'éviter d'observer des pertes majoritairement non spécifiques (eau, monoxyde ou dioxyde de carbone, formaldéhyde, ...). L'approche 2D-FTMS était bien adaptée pour surmonter le premier problème et pour gagner un temps expérimental important. Pour limiter la fragmentation non spécifique favorisée par les méthodes d'activation ergodique, il a été choisi d'utiliser la méthode alternative et encore peu utilisée de dissociation de petites molécules organique, l'UVPD. Pour étudier les principales voies de fragmentation de l'UVPD, six standards ont d'abord été sélectionnés pour répondre à la grande variété de groupes chimiques (phénol, acide carboxylique, carbonyle, aromatique) des composés de bio-huile. L'accent a été mis sur les dérivés de la lignine en raison de leur conversion parfois inefficace par traitement de valorisation catalytique. L'ESI (-) FT-ICR MS 12T a été utilisé pour ioniser ces composés. Les résultats obtenus ont été comparés à l'activation CID. Le schéma de fragmentation d'activation CID et UVPD de chacun des composés sélectionnés a été mis en évidence (présenter dans la partie 4 de ce manuscrit).

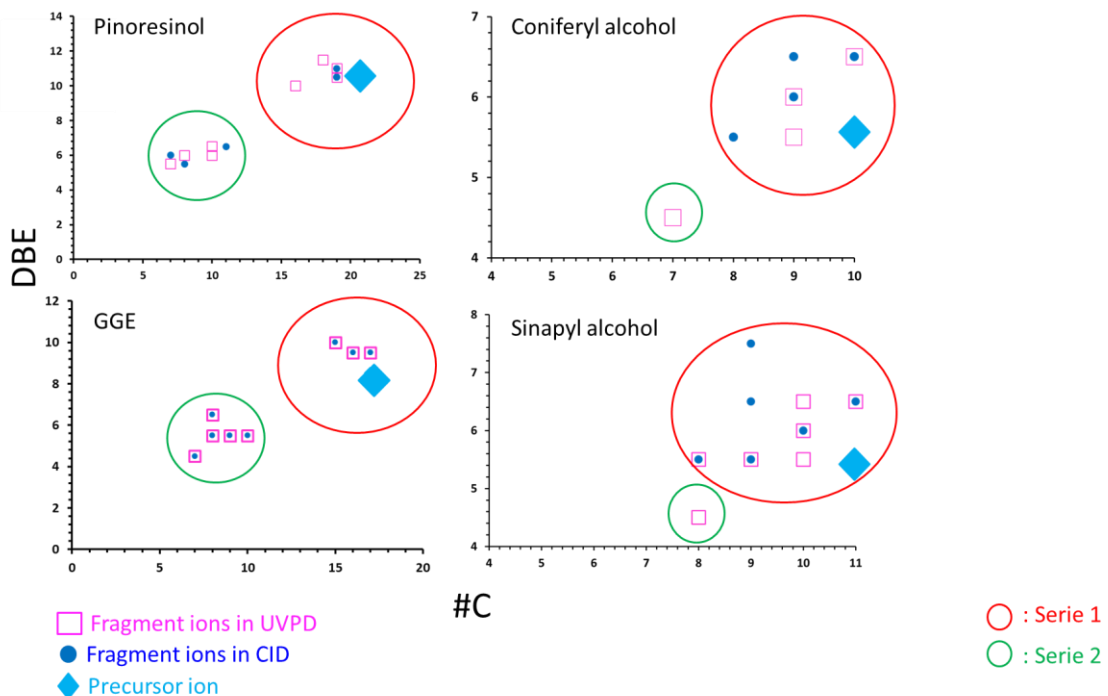


Figure 25: Représentation du DBE en fonction du nombre d'atome de carbone des différents standards utilisés.

La représentation de la DBE en fonction du nombre d'atome de carbone a été utilisée pour permettre la comparaison des modes d'activation collisionnelle ou photonique des ions parents. Par comparaison avec l'activation CID, l'UVPD conduit à plus de fragments à des niveaux inférieurs de DBE, ce qui indique que les composés hautement aromatiques sont plus résistants à l'activation CID qu'à l'UVPD. La spécificité des deux techniques de fragmentation a été utilisées pour rationaliser cette observation.

L'activation par les photons UV à 193 nm implique les niveaux électroniques excités de l'ion parent. Elle nécessite une absorption efficace des photons incidents, assuré par les groupements phénoliques, et induit la dissociation homolytique des liaisons à proximité des chromophores responsables de l'absorption. Les processus de dissociation ne sont plus dirigés par la charge mais par la présence des radicaux formés. Ainsi, des fragmentations non ergodiques peuvent parfois se produire à une distance significative de la charge. Ceux-ci peuvent conduire à l'ouverture de cycles aromatiques ou à la rupture de liaisons plus fortes. Chaque standard avait au moins une (voire plus) fragmentation spécifique à l'UVPD conduisant souvent à l'un des ions fragments les plus abondants. Pour la plupart des six composés examinés, UVPD a donné des informations structurales plus importantes que CID, permettant l'identification de groupes plus fonctionnels (Tableau 1). La plupart des composés phénoliques étudiés ont conduit à des ouvertures de cycles aromatiques, ce qui a permis la localisation de certains substituants du groupe phénolique.

Fragmentation	UVPD	CID
Opening of the aromatic cycle	✓	✗
C-C bond	✓	✓
β-β lignin bond	✓	✓
CO ₂	✓	✓
OH•	✓	✗
H ₂ O	✓	✓
CH ₃ •	✓	✓
Formaldehyde	✓	✓
H ₂ O	✓	✓
CH ₄	✓	✗
C ₃ H ₄ O	✓	✗
Coniferyl unit	✓	✗
Guaiacol	✓	✗

Tableau 1: Exemples des fragments spécifiques obtenues dans les deux méthodes d'activation utilisés.

Les fragmentations spécifiques à l'UVPD sont souvent plus informatives que la fragmentation observée par CID (Tableau 1). La perte UVPD spécifique du groupe hydroxy •OH de la 2,5 DHB met en évidence la fonction phénol et celle du radical HCO• permet l'identification de la fonction aldéhyde de la vanilline. Le processus impliquant l'ouverture de cycles aromatiques, conduit à des informations sur la position des groupes substituants du cycle phénolique de la vanilline, des oligomères de lignine et des dimères. De plus, dans le cadre de l'étude des dimères de lignine, les processus de dépolymérisation sont significativement plus importants en UVPD qu'en CID. Ces processus sont avantageux pour identifier plus facilement les monomères qui constituent ces dimères et, plus largement, les oligomères de lignine.

La spectrométrie de masse bidimensionnelle

L'UVPD 2D FT-ICR MS a été appliqué pour la première fois à l'étude d'une bio-huile de pyrolyse. Les spectres de masse de fragmentation obtenus, en particulier à partir de dérivés de la lignine par pyrolyse, ont permis d'accroître nos connaissances sur les fonctions chimiques et la structure des composés de la bio-huile. Les échantillons ont été analysés à l'aide d'un spectromètre de masse 12T Bruker Solarix FT-ICR (Bruker Daltonik, GmbH, Brême, Allemagne), équipé d'une Infinity cell ICR. La fragmentation a été réalisée avec un laser excimère Coherent ExciStar XS, ArF qui émet des photons UV de 193 nm avec une énergie d'impulsion de 1,8 mJ et une durée d'impulsion de 7 à 10 ns. Chaque standard a d'abord fait l'objet d'une analyse en 1D (MS/MS classique). Le mélange de ces standards ainsi qu'un échantillon réel de bio-huile ont subi l'analyse 2D.

1D et 2DMS sur les standards

Pour la comparaison entre 1D et 2D, l'efficacité de la fragmentation FE ainsi que la fraction de couverture de fonctions chimiques ont été calculées. Pour l'alcool coniférylique, en plus de la perte de neutres liée au formaldéhyde, qui a également été observée en 1D et 2DMS, des fragments spécifiques n'ont été observés en 2DMS. Ces fragments sont liés au clivage du cycle benzénique entraînant l'ouverture du cycle aromatique permettant la localisation des substitutions sur ce cycle, la dissociation homolytique de la liaison carbone-carbone entre le cycle phénolique et l'hydroxypropényle est également observé. Ces fragments supplémentaires ont conduit à une augmentation de la fraction de couverture de fonctions chimiques de 50 % en 1D à 67 % en 2D. Pour le pinorésinol, un dimère phénolique, des fragments similaires ont été produits par 1D et 2DMS, et ont conduit à une fraction de couverture de fonctions chimiques similaire.

Une autre différence a été observée entre 1D et 2DMS sur les standards. Cette différence est liée à la nature des ions fragments observés (ions déprotonés ou radicalaires). Le pinorésinol a conduit à des fragments radicalaires plus abondants, en particulier par 2DMS, que les deux autres standards, qui formaient principalement en 2DMS, des ions fils non radicalaires. Une augmentation de la %FE a été obtenue pour les ions radicalaires (pinorésinol)

tandis qu'une diminution du %FE a été observée pour les ions déprotonés ce qui montre que la FE évolue dans le même sens de la formation des ions fils radicalaires ou non-radicalaires.

2DMS sur la bio-huile

Une grande parties des ions observés par infusion directe de bio-huile (-) ESI FT-ICR MS ont également été observés sur la ligne d'autocorrélation obtenues par 2DMS. Le diagramme de Van Krevelen des ions précurseurs extraits de cette ligne indique qu'il s'agit de composés pyrolytiques de lignine (Figure 17-A). De plus, le graphique de la distribution DBE en fonction du nombre de carbone des espèces précurseurs met en évidence des composés avec un DBE supérieur à 3 et plus de 6 atomes de carbone (Figure 17-B). Ces caractéristiques suggèrent la présence d'au moins un cycle aromatique (un cycle phénolique) capable d'absorber un photon à 193 nm. C'est aussi la raison pour laquelle aucun sucre, ni composé lipidique n'a été mis en évidence sur le diagramme de Van Krevelen à partir de la ligne d'autocorrélation.

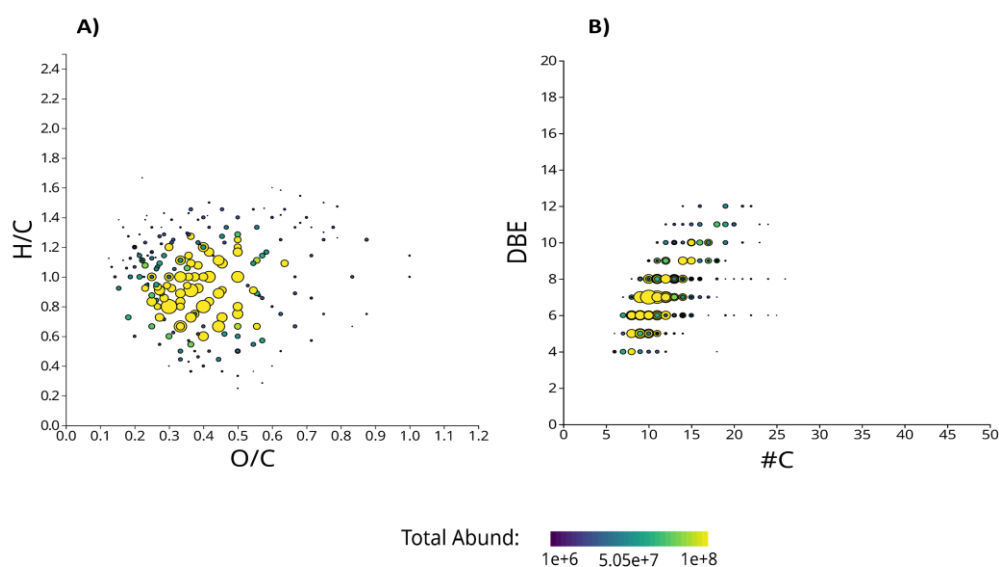


Figure 26: (A) Diagramme de Van Krevelen de la ligne d'autocorrélation extraite de la carte 2D en ESI négatif, (B) DBE en fonction du nombre de carbones du précurseur présent sur la ligne d'autocorrélation.

En appliquant la 2DMS, on a pu obtenir des informations sur les fonctions chimiques et la fraction moléculaire de certains dérivés de la lignine, et cela par extraction de la ligne des pertes des neutres du tracé de la contour 2D. Ces lignes des neutres extraites correspondent soit à des fonctions chimiques typiques tel que la perte d'eau lié à la fonction alcool et la perte de dioxyde de carbone lié à la fonction acide carboxylique, soit à la fraction de la lignine.

Cette dernière permet de mettre en évidence certaines fractions phénoliques telles que le phénol et le gaïacol au sein des composés de la bio-huile. Concernant ces espèces, on suggère qu'elles ont le même schéma de fragmentation que les standards étudiés dans la section précédente. Un tel comportement de fragmentation peut être utile pour définir la nature de l'unité monomère de lignine présente sur la position « 8-end ». Les pertes de phénol

et de crésol indiquent une unité p-coumaryl, tandis que le gaïacol et le crésol sont produits par fragmentation de l'unité coniferyl.

Comparaison entre 2DMS sur les standards et la bio-huile

Pour cette comparaison, les lignes horizontales obtenues en 2DMS à m/z 179,0702, 319,1187 et 357,1343, correspondant aux valeurs m/z des ions standards précédemment étudiés, ont été extraites et comparées aux résultats obtenus à partir de l'analyse 2DMS du mélange de standards. Par exemple, pour le précurseur de la bio-huile à m/z 179,0702, le fragment attribué au clivage du cycle aromatique n'a pas été observé dans l'étude de la bio-huile mais un fragment relatif à la perte d'eau a été obtenu. L'ion relatif à l'élimination des fractions d'alcool propénylique observé sur les deux échantillons semble indiquer que la fraction phénolique est une unité guaiacyl. Par conséquent, l'ion à m/z 179,0702 observé dans l'étude de l'échantillon de bio-huile a été considéré comme un isomère de l'alcool coniférylique pour lequel l'alcool était en position 2 et non en position 3 du propényle. Dans ce cas, l'élimination d'une molécule d'eau est en effet plus facile.

Pour ces trois composés, des efficacités de la fragmentations FE ainsi que des fractions de couverture de fonctions chimiques similaires à celles obtenus avec les composés standards ont été observés avec des composés de bio-huile en 2DMS. Cela suggère qu'ils sont probablement présents dans la bio-huile. Les légères différences observées entre les données obtenues sur les standards et sur les composés de la bio-huile peuvent s'expliquer par la présence de composés isomères avec d'autres schémas de fragmentation ou lorsque la ligne des fragments est extraite, elle comprend fréquemment de nombreux précurseurs et leurs fragments associés, ce qui conduit parfois à de mauvaises corrélations.

CONCLUSION

La conversion de la biomasse lignocellulosique en une bio-huile est réalisée par différentes procédés et plus spécialement par pyrolyse rapide. En raison de la complexité de la bio-huile obtenue, cette dernière doit être améliorée par différentes voies pour en connaître sa composition. Cette caractérisation des bio-huiles par approche pétroléomique nécessite des spectromètres de masse à haute résolution d'où la nécessité d'utiliser la spectrométrie de masse à résonance cyclotronique des ions à transformés de Fourier FT-ICR MS. Cet instrument permet d'identifier des milliers d'espèces différentes. De plus, l'utilisation de différentes sources d'ionisation peut être un avantage pour explorer en profondeur ces bio-huiles.

Cette étude a permis de mettre en place et d'optimiser deux approches pour une caractérisation détaillée de bio-huiles issues de pyrolyse de biomasse lignocellulosique. En utilisant la pentafluoropyridine et la 3-chloroaniline comme réactifs de dérivation spécifique,

nous avons pu développer une méthode de dérivation efficace utilisant une extraction en phase solide avec une résine échangeuse d'anions. En appliquant cette méthode à un mélange standard et à un véritable échantillon de bio-huile, nous avons pu montrer que différentes classes de groupes fonctionnels sont bien identifiées pour les composés contenant de l'oxygène.

L'analyse structurale constitue la deuxième approche de cette étude. L'UVPD a fourni des informations structurales plus importants qu'en CID pour la plupart des composés étudiés. Ainsi, la plupart des composés phénoliques ont conduit à des ouvertures de cycles aromatiques permettant la localisation de la position de certains substituants du groupement phénolique et le clivage de liaisons associées à la formation de dimères de lignine. Bien qu'un nombre limité de composés aient été étudiés pour ces expériences, l'UVPD a démontré sa haute capacité à fournir des informations structurales sur certains composants des bio-huiles produites par la pyrolyse de la biomasse lignocellulosique.

Cette étude ouvre le chemin à une élucidation structurale des composés dérivés de la lignine dans les bio-huiles par ce que l'on appelle la "2D FTMS". La FTMS 2D a exploité dans l'étude d'un mélange de standards et d'une bio-huile de pyrolyse.

CHAPTER 6 : REFERENCES

- (1) Bracmort, K. Biomass: Comparison of Definitions in Legislation. 20.
- (2) Perea-Moreno, M.-A.; Samerón-Manzano, E.; Perea-Moreno, A.-J. Biomass as Renewable Energy: Worldwide Research Trends. *Sustainability* **2019**, *11* (3), 863. <https://doi.org/10.3390/su11030863>.
- (3) Contescu, C.; Adhikari, S.; Gallego, N.; Evans, N.; Biss, B. Activated Carbons Derived from High-Temperature Pyrolysis of Lignocellulosic Biomass. *C* **2018**, *4* (3), 51. <https://doi.org/10.3390/c4030051>.
- (4) Li, Y.; Rezgui, Y.; Zhu, H. District Heating and Cooling Optimization and Enhancement – Towards Integration of Renewables, Storage and Smart Grid. *Renew. Sustain. Energy Rev.* **2017**, *72*, 281–294. <https://doi.org/10.1016/j.rser.2017.01.061>.
- (5) McKendry, P. Energy Production from Biomass (Part 2): Conversion Technologies. *Bioresour. Technol.* **2002**, *83* (1), 47–54. [https://doi.org/10.1016/S0960-8524\(01\)00119-5](https://doi.org/10.1016/S0960-8524(01)00119-5).
- (6) Huber, G. W.; Iborra, S.; Corma, A. Synthesis of Transportation Fuels from Biomass: Chemistry, Catalysts, and Engineering. *Chem. Rev.* **2006**, *106* (9), 4044–4098. <https://doi.org/10.1021/cr068360d>.
- (7) Naik, S. N.; Goud, V. V.; Rout, P. K.; Dalai, A. K. Production of First and Second Generation Biofuels: A Comprehensive Review. *Renew. Sustain. Energy Rev.* **2010**, *14* (2), 578–597. <https://doi.org/10.1016/j.rser.2009.10.003>.
- (8) Callegari, A.; Bolognesi, S.; Cecconet, D.; Capodaglio, A. G. Production Technologies, Current Role, and Future Prospects of Biofuels Feedstocks: A State-of-the-Art Review.

- Crit. Rev. Environ. Sci. Technol.* **2020**, *50* (4), 384–436. <https://doi.org/10.1080/10643389.2019.1629801>.
- (9) Dutta, K.; Daverey, A.; Lin, J.-G. Evolution Retrospective for Alternative Fuels: First to Fourth Generation. *Renew. Energy* **2014**, *69*, 114–122. <https://doi.org/10.1016/j.renene.2014.02.044>.
- (10) Klemm, D.; Heublein, B.; Fink, H.-P.; Bohn, A. Cellulose: Fascinating Biopolymer and Sustainable Raw Material. *Angew. Chem. Int. Ed.* **2005**, *44* (22), 3358–3393. <https://doi.org/10.1002/anie.200460587>.
- (11) Scheller, H. V.; Ulvskov, P. Hemicelluloses. *Annu. Rev. Plant Biol.* **2010**, *61* (1), 263–289. <https://doi.org/10.1146/annurev-arplant-042809-112315>.
- (12) *The biorefinery concept: Using biomass instead of oil for producing energy and chemicals* | Elsevier Enhanced Reader. <https://doi.org/10.1016/j.enconman.2010.01.015>.
- (13) H. Isikgor, F.; Remzi Becer, C. Lignocellulosic Biomass: A Sustainable Platform for the Production of Bio-Based Chemicals and Polymers. *Polym. Chem.* **2015**, *6* (25), 4497–4559. <https://doi.org/10.1039/C5PY00263J>.
- (14) Wang, F.; Ouyang, D.; Zhou, Z.; Page, S. J.; Liu, D.; Zhao, X. Lignocellulosic Biomass as Sustainable Feedstock and Materials for Power Generation and Energy Storage. *J. Energy Chem.* **2021**, *57*, 247–280. <https://doi.org/10.1016/j.jechem.2020.08.060>.
- (15) Amesho, K. T. T.; Lin, Y.-C.; Mohan, S. V.; Halder, S.; Ponnusamy, V. K.; Jhang, S.-R. Deep Eutectic Solvents in the Transformation of Biomass into Biofuels and Fine Chemicals: A Review. *Environ. Chem. Lett.* **2022**. <https://doi.org/10.1007/s10311-022-01521-x>.
- (16) Sivamohan Reddy, N. Pathways of Lignocellulosic Biomass Conversion to Renewable Fuels. *Biomass Convers. Biorefinery* **2013**.
- (17) Dhyani, V.; Bhaskar, T. A Comprehensive Review on the Pyrolysis of Lignocellulosic Biomass. *Renew. Energy* **2018**, *129*, 695–716. <https://doi.org/10.1016/j.renene.2017.04.035>.
- (18) van Rossum, G.; Zhao, W.; Castellvi Barnes, M.; Lange, J.-P.; Kersten, S. R. A. Liquefaction of Lignocellulosic Biomass: Solvent, Process Parameter, and Recycle Oil Screening. *ChemSusChem* **2014**, *7* (1), 253–259. <https://doi.org/10.1002/cssc.201300297>.
- (19) Jindal, M. K.; Jha, M. K. Hydrothermal Liquefaction of Wood: A Critical Review. *Rev. Chem. Eng.* **2016**, *32* (4), 459–488. <https://doi.org/10.1515/revce-2015-0055>.
- (20) Wu, Y.; Wang, H.; Li, H.; Han, X.; Zhang, M.; Sun, Y.; Fan, X.; Tu, R.; Zeng, Y.; Xu, C. C.; Xu, X. Applications of Catalysts in Thermochemical Conversion of Biomass (Pyrolysis, Hydrothermal Liquefaction and Gasification): A Critical Review. *Renew. Energy* **2022**, *196*, 462–481. <https://doi.org/10.1016/j.renene.2022.07.031>.
- (21) No, S.-Y. Application of Bio-Oils from Lignocellulosic Biomass to Transportation, Heat and Power Generation—A Review. *Renew. Sustain. Energy Rev.* **2014**, *40*, 1108–1125. <https://doi.org/10.1016/j.rser.2014.07.127>.
- (22) Stöcker, M. Biofuels and Biomass-To-Liquid Fuels in the Biorefinery: Catalytic Conversion of Lignocellulosic Biomass Using Porous Materials. *Angew. Chem. Int. Ed.* **2008**, *47* (48), 9200–9211. <https://doi.org/10.1002/anie.200801476>.
- (23) Staš, M.; Auersvald, M.; Kejla, L.; Vrtiška, D.; Kroufek, J.; Kubička, D. Quantitative Analysis of Pyrolysis Bio-Oils: A Review. *TrAC Trends Anal. Chem.* **2020**, *126*, 115857. <https://doi.org/10.1016/j.trac.2020.115857>.

- (24) Xiu, S.; Shahbazi, A. Bio-Oil Production and Upgrading Research: A Review. *Renew. Sustain. Energy Rev.* **2012**, *16* (7), 4406–4414. <https://doi.org/10.1016/j.rser.2012.04.028>.
- (25) Lian, X.; Xue, Y.; Zhao, Z.; Xu, G.; Han, S.; Yu, H. Progress on Upgrading Methods of Bio-Oil: A Review: Upgrading Progress of Bio-Oil. *Int. J. Energy Res.* **2017**, *41* (13), 1798–1816. <https://doi.org/10.1002/er.3726>.
- (26) Michailof, C. M.; Kalogiannis, K. G.; Sfetsas, T.; Patiaka, D. T.; Lappas, A. A. Advanced Analytical Techniques for Bio-Oil Characterization. *WIREs Energy Environ.* **2016**, *5* (6), 614–639. <https://doi.org/10.1002/wene.208>.
- (27) Wang, Y.; Han, Y.; Hu, W.; Fu, D.; Wang, G. Analytical Strategies for Chemical Characterization of Bio-Oil. *J. Sep. Sci.* **2020**, *43* (1), 360–371. <https://doi.org/10.1002/jssc.201901014>.
- (28) Djokic, M. R.; Dijkmans, T.; Yildiz, G.; Prins, W.; Van Geem, K. M. Quantitative Analysis of Crude and Stabilized Bio-Oils by Comprehensive Two-Dimensional Gas-Chromatography. *J. Chromatogr. A* **2012**, *1257*, 131–140. <https://doi.org/10.1016/j.chroma.2012.07.035>.
- (29) Marshall, A. G.; Rodgers, R. P. Petroleomics: The Next Grand Challenge for Chemical Analysis. *Acc. Chem. Res.* **2004**, *37* (1), 53–59. <https://doi.org/10.1021/ar020177t>.
- (30) Marshall, A. G.; Rodgers, R. P. Petroleomics: The Next Grand Challenge for Chemical Analysis. *Acc. Chem. Res.* **2004**, *37* (1), 53–59. <https://doi.org/10.1021/ar020177t>.
- (31) Marshall, A. G.; Rodgers, R. P. Petroleomics: Chemistry of the Underworld. *Proc. Natl. Acad. Sci.* **2008**, *105* (47), 18090–18095. <https://doi.org/10.1073/pnas.0805069105>.
- (32) Abdelnur, P. V.; Vaz, B. G.; Rocha, J. D.; de Almeida, M. B. B.; Teixeira, M. A. G.; Pereira, R. C. L. Characterization of Bio-Oils from Different Pyrolysis Process Steps and Biomass Using High-Resolution Mass Spectrometry. *Energy Fuels* **2013**, *27* (11), 6646–6654. <https://doi.org/10.1021/ef400788v>.
- (33) Cho, Y.; Ahmed, A.; Islam, A.; Kim, S. Developments in FT-ICR MS Instrumentation, Ionization Techniques, and Data Interpretation Methods for Petroleomics: METHODS FOR PETROLEOMICS. *Mass Spectrom. Rev.* **2015**, *34* (2), 248–263. <https://doi.org/10.1002/mas.21438>.
- (34) Marshall, A. G.; Rodgers, R. P. Petroleomics: The Next Grand Challenge for Chemical Analysis. *Acc. Chem. Res.* **2004**, *37* (1), 53–59. <https://doi.org/10.1021/ar020177t>.
- (35) Kim, S.; Kramer, R. W.; Hatcher, P. G. Graphical Method for Analysis of Ultrahigh-Resolution Broadband Mass Spectra of Natural Organic Matter, the Van Krevelen Diagram. *Anal. Chem.* **2003**, *75* (20), 5336–5344. <https://doi.org/10.1021/ac034415p>.
- (36) Lawrence, E. O.; Livingston, M. S. The Production of High Speed Light Ions Without the Use of High Voltages. *Phys. Rev.* **1932**, *40* (1), 19–35. <https://doi.org/10.1103/PhysRev.40.19>.
- (37) Marshall, A. G.; Hendrickson, C. L.; Jackson, G. S. Fourier Transform Ion Cyclotron Resonance Mass Spectrometry: A Primer. *Mass Spectrom. Rev.* **1998**, *17* (1), 1–35. [https://doi.org/10.1002/\(SICI\)1098-2787\(1998\)17:1<1::AID-MAS1>3.0.CO;2-K](https://doi.org/10.1002/(SICI)1098-2787(1998)17:1<1::AID-MAS1>3.0.CO;2-K).
- (38) Amster, I. J. Fourier Transform Mass Spectrometry. *J. Mass Spectrom.* **1996**, *31* (12), 1325–1337. [https://doi.org/10.1002/\(SICI\)1096-9888\(199612\)31:12<1325::AID-JMS453>3.0.CO;2-W](https://doi.org/10.1002/(SICI)1096-9888(199612)31:12<1325::AID-JMS453>3.0.CO;2-W).
- (39) Walk, T. B.; Trautwein, A. W.; Richter, H.; Jung, G. ESI Fourier Transform Ion Cyclotron Resonance Mass Spectrometry (ESI-FT-ICR-MS): A Rapid High-Resolution Analytical Method for Combinatorial Compound Libraries. *Angew. Chem. Int. Ed.* **1999**, *38* (12),

- 1763–1765. [https://doi.org/10.1002/\(SICI\)1521-3773\(19990614\)38:12<1763::AID-ANIE1763>3.0.CO;2-#](https://doi.org/10.1002/(SICI)1521-3773(19990614)38:12<1763::AID-ANIE1763>3.0.CO;2-#).
- (40) Disintegration of Water Drops in an Electric Field. 18.
- (41) Banerjee, S.; Mazumdar, S. Electrospray Ionization Mass Spectrometry: A Technique to Access the Information beyond the Molecular Weight of the Analyte. *Int. J. Anal. Chem.* **2012**, 1–40. <https://doi.org/10.1155/2012/282574>.
- (42) Banerjee, S.; Mazumdar, S. Electrospray Ionization Mass Spectrometry: A Technique to Access the Information beyond the Molecular Weight of the Analyte. *Int. J. Anal. Chem.* **2012**, 2012, 1–40. <https://doi.org/10.1155/2012/282574>.
- (43) Kebarle, P.; Tang, L. From Ions in Solution to Ions in the Gas Phase - the Mechanism of Electrospray Mass Spectrometry. *Anal. Chem.* **1993**, 65 (22), 972A-986A. <https://doi.org/10.1021/ac00070a001>.
- (44) Gross, J. H. *Mass Spectrometry: A Textbook*; Springer Science & Business Media, 2006.
- (45) Eriksson, V. Concentration Dependent Response of Phospholipids in Electrospray Ionization Mass Spectrometry. 51.
- (46) Ng, C.-Y. VACUUM ULTRAVIOLET SPECTROSCOPY AND CHEMISTRY BY PHOTOIONIZATION AND PHOTOELECTRON METHODS. *Annu. Rev. Phys. Chem.* **2002**, 53 (1), 101–140. <https://doi.org/10.1146/annurev.physchem.53.082001.144416>.
- (47) Robb, D. B.; Covey, T. R.; Bruins, A. P. Atmospheric Pressure Photoionization: An Ionization Method for Liquid Chromatography–Mass Spectrometry. *Anal. Chem.* **2000**, 72 (15), 3653–3659. <https://doi.org/10.1021/ac0001636>.
- (48) Song, L.; Dykstra, A. B.; Yao, H.; Bartmess, J. E. Ionization Mechanism of Negative Ion-Direct Analysis in Real Time: A Comparative Study with Negative Ion-Atmospheric Pressure Photoionization. *J. Am. Soc. Mass Spectrom.* **2009**, 20 (1), 42–50. <https://doi.org/10.1016/j.jasms.2008.09.016>.
- (49) Kauppila, T. J.; Kersten, H.; Benter, T. The Ionization Mechanisms in Direct and Dopant-Assisted Atmospheric Pressure Photoionization and Atmospheric Pressure Laser Ionization. *J. Am. Soc. Mass Spectrom.* **2014**, 25 (11), 1870–1881. <https://doi.org/10.1007/s13361-014-0988-7>.
- (50) Ahmed, A.; Choi, C. H.; Kim, S. Mechanistic Study on Lowering the Sensitivity of Positive Atmospheric Pressure Photoionization Mass Spectrometric Analyses: Size-Dependent Reactivity of Solvent Clusters. *Rapid Commun. Mass Spectrom.* **2015**, 29 (21), 2095–2101. <https://doi.org/10.1002/rcm.7373>.
- (51) Sioud, S.; Kharbatia, N.; Amad, M. H.; Zhu, Z.; Cabanetos, C.; Lesimple, A.; Beaujuge, P. The Formation of [M–H]⁺ Ions in N-Alkyl-Substituted Thieno[3,4-c]-Pyrrole-4,6-Dione Derivatives during Atmospheric Pressure Photoionization Mass Spectrometry. *Rapid Commun. Mass Spectrom.* **2014**, 28 (22), 2389–2397. <https://doi.org/10.1002/rcm.7031>.
- (52) Andrade, F. J.; Shelley, J. T.; Wetzel, W. C.; Webb, M. R.; Gamez, G.; Ray, S. J.; Hieftje, G. M. Atmospheric Pressure Chemical Ionization Source. 1. Ionization of Compounds in the Gas Phase. *Anal. Chem.* **2008**, 80 (8), 2646–2653. <https://doi.org/10.1021/ac800156y>.
- (53) Portolés, T.; Mol, J. G. J.; Sancho, J. V.; Hernández, F. Advantages of Atmospheric Pressure Chemical Ionization in Gas Chromatography Tandem Mass Spectrometry: Pyrethroid Insecticides as a Case Study. *Anal. Chem.* **2012**, 84 (22), 9802–9810. <https://doi.org/10.1021/ac301699c>.
- (54) Jia, L.; Le-Brech, Y.; Shrestha, B.; Frowein, M. B.; Ehlert, S.; Mauviel, G.; Zimmermann, R.; Dufour, A. Fast Pyrolysis in a Microfluidized Bed Reactor: Effect of Biomass

- Properties and Operating Conditions on Volatiles Composition as Analyzed by Online Single Photoionization Mass Spectrometry. *Energy Fuels* **2015**, *29* (11), 7364–7374. <https://doi.org/10.1021/acs.energyfuels.5b01803>.
- (55) Hertzog, J. High Resolution Mass Spectrometry for Molecular Characterization of Bio-Oils Produced by Pyrolysis of Lignocellulosic Biomass. phdthesis, Université de Lorraine, 2017. <https://hal.univ-lorraine.fr/tel-01905674> (accessed 2022-11-08).
- (56) McLafferty, F. W. Tandem Mass Spectrometry: From Infancy to Maturity in Twenty-Five Years. *Org. Mass Spectrom.* **1993**, *28* (12), 1403–1406. <https://doi.org/10.1002/oms.1210281208>.
- (57) de Hoffmann, E. Tandem Mass Spectrometry: A Primer. *J. Mass Spectrom.* **1996**, *31* (2), 129–137. [https://doi.org/10.1002/\(SICI\)1096-9888\(199602\)31:2<129::AID-JMS305>3.0.CO;2-T](https://doi.org/10.1002/(SICI)1096-9888(199602)31:2<129::AID-JMS305>3.0.CO;2-T).
- (58) Guevremont, R.; Boyd, R. K. Are Derrick Shifts Real? An Investigation by Tandem Mass Spectrometry. *Rapid Commun. Mass Spectrom.* **1988**, *2* (1), 1–5. <https://doi.org/10.1002/rcm.1290020102>.
- (59) Holden, D. D.; Sanders, J. D.; Weisbrod, C. R.; Mullen, C.; Schwartz, J. C.; Brodbelt, J. S. Implementation of Fragment Ion Protection (FIP) during Ultraviolet Photodissociation (UVPD) Mass Spectrometry. *Anal. Chem.* **2018**, *90* (14), 8583–8591. <https://doi.org/10.1021/acs.analchem.8b01723>.
- (60) Cannon, J. R.; Cammarata, M. B.; Robotham, S. A.; Cotham, V. C.; Shaw, J. B.; Fellers, R. T.; Early, B. P.; Thomas, P. M.; Kelleher, N. L.; Brodbelt, J. S. Ultraviolet Photodissociation for Characterization of Whole Proteins on a Chromatographic Time Scale. *Anal. Chem.* **2014**, *86* (4), 2185–2192. <https://doi.org/10.1021/ac403859a>.
- (61) B. Cammarata, M.; S. Brodbelt, J. Structural Characterization of Holo- and Apo-Myoglobin in the Gas Phase by Ultraviolet Photodissociation Mass Spectrometry. *Chem. Sci.* **2015**, *6* (2), 1324–1333. <https://doi.org/10.1039/C4SC03200D>.
- (62) Brodbelt, J. S. Photodissociation Mass Spectrometry: New Tools for Characterization of Biological Molecules. *Chem Soc Rev* **2014**, *43* (8), 2757–2783. <https://doi.org/10.1039/C3CS60444F>.
- (63) Pfändler, P.; Bodenhausen, G.; Rapin, J.; Houriet, R.; Gäumann, T. Two-Dimensional Fourier Transform Ion Cyclotron Resonance Mass Spectrometry. *Chem. Phys. Lett.* **1987**, *138* (2–3), 195–200. [https://doi.org/10.1016/0009-2614\(87\)80367-6](https://doi.org/10.1016/0009-2614(87)80367-6).
- (64) van Agthoven, M. A.; Lam, Y. P. Y.; O'Connor, P. B.; Rolando, C.; Delsuc, M.-A. Two-Dimensional Mass Spectrometry: New Perspectives for Tandem Mass Spectrometry. *Eur. Biophys. J.* **2019**, *48* (3), 213–229. <https://doi.org/10.1007/s00249-019-01348-5>.

**Methodological developments in FT-ICR MS for the analysis
of bio-oils produced by pyrolysis of lignocellulosic biomass****Abstract**

Bio-oils from lignocellulosic biomass are promising source for producing biofuels and high-added-value chemicals. Different processes such as pyrolysis, allow the conversion of lignocellulosic biomass into bio-oils. The composition of these bio-oils is complex and contains highly oxygenated compounds, which limits their use. Therefore, these bio-oils must be upgraded by catalytic deoxygenation and/or cracking treatments. To determine the effectiveness of the catalytic treatments, a thorough knowledge of the chemical composition of bio-oils is required. A high-resolution mass spectrometer, such as Fourier Transform Ion Cyclotron Resonance (FT-ICR MS) coupled with ESI, APPI, and APCI, allow for in-depth study of the composition of the generated bio-oil at the molecular level. To evaluate the chemical characteristics of these compounds, the research conducted in this Ph.D. thesis focuses on two aspects. The first is based on developing an analytical fractionation/derivatization method to label oxygen-containing compounds according to their functional groups. Combining solid-phase extraction (SPE) with an anion exchange sorbent and derivatization with stable isotope-labeled agents demonstrated, the identification of several oxygenated classes of bio-oil constituents by FT-ICR MS analyses. The second aspect is applied for the first time to bio-oil analysis. It uses two-dimensional ultra-violet photodissociation mass spectrometry UVPD-MS for structural analysis of the bio-oil components. Without using the conventional precursor ion isolation and fragmentation for MS/MS experiment, 2D-UVPD-MS has proven to be a powerful tool for performing tandem mass spectrometry experiments on such a complex system. 2D-UVPD-MS has proved to efficient fragment small, single-charged molecules and produce fragment ions various chemical species, such as bio-oil components, thus providing useful structural information.

Keywords: *Bio-oils, pyrolysis, Fourier transform ion cyclotron resonance mass spectrometry, SPE, fractionation, derivatization, two-dimensional mass spectrometry 2DMS, UVPD, petroleomic approach.*

Résumé

La biomasse lignocellulosique est considérée comme une source importante pour produire des bio-huiles, une ressource prometteuse pour obtenir des biocarburants et des produits chimiques biosourcés à haute valeur ajoutée. La conversion de la biomasse lignocellulosique est réalisée par différents procédés tels que la pyrolyse. La composition de ces bio-huiles est complexe avec de nombreux composés oxygénés. Par conséquent, il est nécessaire de faire subir à ces bio-huiles des traitements catalytiques de désoxygénation et/ou de craquage. Afin de déterminer quels sont les traitements catalytiques les mieux adaptés, une connaissance aussi précise que possible de la composition de ces bio-huiles est nécessaire. Un spectromètre de masse à haute résolution, tel que le spectromètre de masse à résonance cyclotronique des ions à transformée de Fourier (FT-ICR MS) couplé à l'ESI, l'APPI et l'APCI, a été utilisé pour permettre une étude approfondie de la composition élémentaire de ces bio-huiles. La recherche menée dans le cadre de cette thèse de doctorat porte sur deux approches. La première était basée sur le développement d'une méthode analytique de fractionnement/dérivation de différents groupes fonctionnels présents dans les constituants d'une bio-huile en utilisant une cartouche SPE et trois réactifs de dérivation. En combinant le fractionnement et la dérivation par des composés marqués avec des isotopes stables, l'identification de plusieurs classes de composés oxygénés de la bio-huile a été réalisée. La pentafluoropyridine s'est avérée être spécifique des composés phénoliques sans réagir avec les fonction acides et alcools et la 5-chloroanalyne a démontré sa spécificité pour les carbonyles (cétones et aldéhydes). Le deuxième aspect a été appliqué pour la première fois à l'étude structurale des constituants d'une bio-huile et consiste à utiliser la spectrométrie de masse bidimensionnelle couplée à photodissociation ultraviolette UVPD-MS. Sans utiliser la méthode conventionnelle d'isolation et d'activation des ions parents, la 2D-UVPD-MS s'est avérée efficace pour fragmenter les petites molécules à charge unique et produire des ions fragments à partir de diverses espèces chimiques, telles que les composants de la bio-huile, fournissant ainsi des informations structurelles utiles.

Mots-clés : *Bio-huiles, pyrolyse, spectrométrie de masse à résonance cyclotronique des ions à transformée de Fourier, SPE, fractionnement, dérivation, spectrométrie de masse bidimensionnelle 2DMS, 2D-UVPD-MS, approche pétroléomique.*